

# Structure and Solvation of Iron(II) Schiff Base Complexes and Other Ions

A Thesis submitted for the Degree of  
Doctor of Philosophy

by

Diane Lesley Elvidge

in the

Faculty of Science

of the

Department of Chemistry

at the

University of Leicester

FEBRUARY 1988

UMI Number: U527040

All rights reserved

INFORMATION TO ALL USERS

The quality of this reproduction is dependent upon the quality of the copy submitted.

In the unlikely event that the author did not send a complete manuscript and there are missing pages, these will be noted. Also, if material had to be removed, a note will indicate the deletion.



UMI U527040

Published by ProQuest LLC 2015. Copyright in the Dissertation held by the Author.  
Microform Edition © ProQuest LLC.

All rights reserved. This work is protected against  
unauthorized copying under Title 17, United States Code.

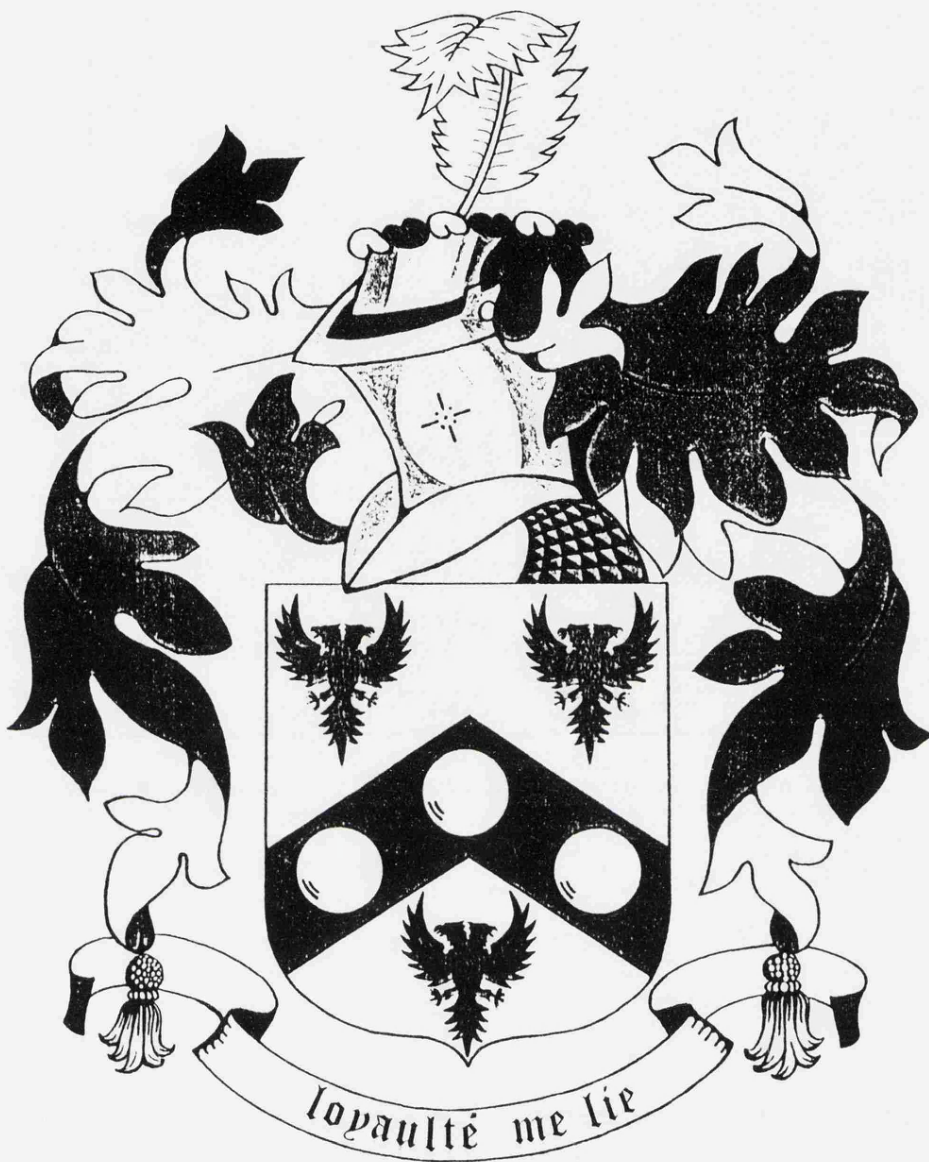


ProQuest LLC  
789 East Eisenhower Parkway  
P.O. Box 1346  
Ann Arbor, MI 48106-1346

To Mum and Peter  
with love and thanks



Handwritten text, possibly a signature or name, located in the upper right quadrant of the page.



Marching on together,  
We're going to see you win.....

## ACKNOWLEDGEMENTS

I am indebted to my supervisor, Dr. John Burgess, for his continual help, guidance and encouragement during my research. Many thanks go also to Dr. Mike J. Blandamer and Dr. David L. Turner for their much appreciated words of wisdom. I am very grateful to Miss Vikki Wright for her skillful typing of the manuscript and to Mrs. Ann Crane who so expertly drew the diagrams.

I acknowledge the receipt of an SERC award.

Finally, I would like to thank my family and my friends, particularly Barbara, Christina, Ann and Julie, who were always there when needed and, last but not least, my baby godson, Thomas, and my team, Leeds United - champions both.

STATEMENT

The accompanying thesis submitted for the degree of Ph.D. and entitled "Structure and Solvation of Iron(II) Schiff Base Complexes and Other Ions" is based on work conducted by the author in the Department of Chemistry of the University of Leicester mainly during the period between October 1983 and October 1986.

All the work recorded in this thesis is original unless otherwise acknowledged in the text or by references.

None of the work has been submitted for another degree in this or any other University.

Date: 6th June 1988 Signed: D. Eridge

## LIST OF CONTENTS

	<u>Page No.</u>
<u>CHAPTER 1 - INTRODUCTION</u>	
1.1 - General	1
1.2 - Transfer chemical potentials	2
1.3 - Low-spin iron(II) di-imine complexes	4
1.3.1 General	4
1.3.2 Schiff base ligands	7
1.3.3 Stereoisomers	8
1.3.4 Ligand notation of iron(II) Schiff base complexes	13
REFERENCES	16
<u>CHAPTER 2 - EXPERIMENTAL</u>	
2.1 - Introduction	18
2.2 - Preparation of iron(II) Schiff base complexes	18
2.2.1 General	18
2.2.2 General method of preparation	20
2.2.3 Preparative method involving the use of hydroxylamine hydrochloride	21
2.3 - Collection and analysis of kinetic data	23
2.3.1 First-order rate constants	23
2.3.2 Analysis of absorbance/time data	26
2.3.3 Spectrophotometric apparatus	28
2.4 - <sup>1</sup> H nuclear magnetic resonance spectra	29
2.5 - Solubilities of salts of iron(II) complexes	29
2.6 - Solubility of KIO <sub>3</sub> in water + ethanol mixtures	30
REFERENCES	33
<u>CHAPTER 3 - SOLVATION OF IONS IN WATER + ETHANOL MIXTURES</u>	
3.1 - Introduction	34
3.1.1 Background	34
3.1.2 Extrathermodynamic assumptions	36
3.1.3 Methods used by other authors	37
3.1.4 Ion solvation in binary aqueous mixtures	40
3.2 - Method	45
3.2.1 Description of the system and definitions of standard states	45
3.2.2 Calculation of transfer chemical potentials for salts	46
3.2.3 Application of the TATB assumption	48
3.2.4 Derivation of single-ion transfer parameters	49
3.2.5 Accuracy of results	51

LIST OF CONTENTS (Continued) ....

Page No.

3.3 - Results and Discussion	54
3.3.1 Introduction	54
3.3.2 Transfer chemical potentials for ions in aqueous ethanol mixtures	56
3.3.3 General solvation pattern in aqueous ethanol mixtures	87
3.3.4 Comparison of solvation patterns in aqueous alcohols and aqueous acetone mixtures	100
REFERENCES	106

CHAPTER 4 - SOLVATION OF IONS IN WATER + ETHYLENE GLYCOL AND WATER + GLYCEROL MIXTURES

4.1 - Introduction	110
4.1.1 General	110
4.1.2 Methods used by other authors	111
4.1.3 Structure of aqueous ethylene glycol and aqueous glycerol mixtures	113
4.2 - Method	115
4.2.1 Calculation of transfer chemical potentials for salts	115
4.2.2 Calculation of single-ion transfer chemical potentials	117
4.3 - Results	118
4.3.1 Introduction	118
4.3.2 Derivation of single-ion transfer parameters for aqueous ethylene glycol mixtures	118
4.3.3 Derivation of single-ion transfer parameters for aqueous glycerol mixtures	125
4.4 - Discussion	130
4.4.1 General solvation pattern in aqueous ethylene glycol mixtures	130
4.4.2 General solvation pattern in aqueous glycerol mixtures	141
4.4.3 Comparison of solvation of ions in aqueous alcohol, aqueous ethylene glycol and aqueous glycerol mixtures	146
REFERENCES	154

CHAPTER 5 - KINETIC INVESTIGATION INTO THE EXISTENCE OF GEOMETRICAL ISOMERS OF LOW-SPIN IRON(II) SCHIFF BASE DI-IMINE COMPLEXES

5.1 - Introduction	156
5.1.1 Background	156
5.1.2 Kinetics	159

LIST OF CONTENTS (Continued) ....

Page No.

5.2 - Experimental	160
5.2.1 Preparation of complexes	160
5.2.2 Kinetics	161
5.3 - Results and Discussion	162
5.3.1 Observed trends in $k_{obs}$	162
5.3.2 Re-analysis of kinetic data	170
5.3.3 Ultraviolet/visible absorption spectra	189
5.3.4 The effect of modified synthetic methods	191
5.3.5 Isomers in samples of related complexes	195
5.4 - Conclusion	211
REFERENCES	224

CHAPTER 6 -  $^1\text{H}$  NMR STUDY OF LOW-SPIN IRON(II) SCHIFF BASE DI-IMINE COMPLEXES

6.1 - Introduction	225
6.2 - Experimental	228
6.3 - Results and Discussion	230
6.3.1 Assignment of spectra measured in $\text{d}_3$ -acetonitrile at 298 K	230
6.3.1.1 General	230
6.3.1.2 Tris-(bidentate) complexes	235
6.3.1.3 Bis-(terdentate) and mono-(hexadentate) complexes	249
6.3.2 Further observations	255
6.3.2.1 General	255
6.3.2.2 Temperature effects	257
6.3.2.3 Two-dimensional spectrum of complex N	260
6.3.3 The occurrence and nature of the diastereoisomeric forms	262
REFERENCES	287

CHAPTER 7 - IRON(II) SCHIFF BASE DI-IMINE COMPLEXES: FURTHER STUDIES

7.1 - <u>General Introduction</u>	288
7.2 - <u>Bis-(terdentate) iron(II) Schiff base complexes</u>	288
7.2.1 Introduction	288
7.2.2 Experimental	290
7.2.2.1 Preparation of complexes	290
7.2.2.2 Solubility measurements	290
7.2.2.3 Kinetics	291
7.2.3 Results and Discussion	292
7.2.3.1 Transfer chemical potentials	292
7.2.3.2 Reaction with acid	297
7.2.3.3 Reaction with hydroxide	302

LIST OF CONTENTS (Continued) ....

Page No.

7.3 - <u>Crystal structure of a mono-(hexadentate) iron(II) Schiff base complex: a comparative study</u>	310
7.3.1 Introduction	310
7.3.2 Experimental	310
7.3.3 Results and Discussion	310
7.4 - <u>Reaction of iron(II) with Schiff base ketoxime ligands</u>	325
7.4.1 Introduction	325
7.4.2 Experimental	328
7.4.2.1 General	328
7.4.2.2 Generation of complex species in acidic and alkaline aqueous solutions	329
7.4.2.3 Generation of complex species in water + amine mixtures	329
7.4.3 Results and Discussion	331
7.4.3.1 Complex species formed in acidic and alkaline aqueous solutions	331
7.4.3.2 Complex species formed in water + amine mixtures	339
REFERENCES	346
APPENDIX A	348
APPENDIX B	356

## GLOSSARY

### (i) Ligand, ion and solvent abbreviations

aq	-	water
A2S	-	anthraquinone-2-sulphonate
bipy	-	2,2'-bipyridyl
bsb	-	bidentate Schiff base
Bu <sup>t</sup> OH	-	t-butyl alcohol
cit	-	citrate
EG	-	ethylene glycol (ethane-1,2-diol)
en	-	ethylenediamine (ethane-1,2-diamine)
EtOH	-	ethanol
Fic	-	iron(III)dicyclopentadienyl
Foc	-	iron(II)dicyclopentadienyl (ferrocene)
G	-	glycerol (propane-1,2,3-triol)
hsb	-	hexadentate Schiff base
i	-	ion
L	-	ligand
MeOH	-	methanol
N2S	-	naphthalene- $\beta$ -sulphonate
OAc	-	acetate
ox	-	oxalate
phen	-	1,10-phenanthroline
Pic	-	picrate
Pr <sup>i</sup> OH	-	isopropanol
S	-	solvent
sb *	-	Schiff base
TA	-	tetraphenylarsonium
TAB	-	triisoamyl-n-butylammonium (tris[3-methylbutyl]butylammonium)
tart	-	tartrate
TB	-	tetraphenylboronate
terpy	-	2,2'; 6', 2''-terpyridyl
TP	-	tetraphenylphosphonium
tsb	-	terdentate Schiff base
W	-	water

---

\* Abbreviations used to denote specific Schiff base ligands are given in Section 1.3.4.

(ii) Principal symbols

- [A] - concentration of A  
[A]<sub>0</sub> concentration of A at t=0  
[A]<sub>t</sub> concentration of A at time t
- c - concentration (scale)
- c<sub>r</sub> - reference molarity
- eq - equilibrium
- E<sup>⊖</sup> - standard electrode potential  
E<sub>c</sub><sup>⊖</sup> standard electrode potential on concentration scale  
E<sub>m</sub><sup>⊖</sup> standard electrode potential on molal scale  
E<sub>x</sub><sup>⊖</sup> standard electrode potential on mole fraction scale
- f<sub>x</sub> - activity coefficient on mole fraction scale
- F - Faraday's constant
- G - Gibbs free energy  
ΔG<sub>t</sub><sup>0</sup> standard Gibbs free energy of transfer
- H - enthalpy  
H<sup>E</sup> excess enthalpy of mixing
- I - ionic strength
- I - intensity of light  
I<sub>0</sub> intensity of incident light  
I<sub>t</sub> intensity of transmitted light
- J - coupling constant (nmr)
- k - rate constant  
k<sub>f</sub> rate constant for faster reacting isomer  
k<sub>n</sub> n<sup>th</sup>-order rate constant  
k<sub>obs</sub> observed rate constant  
k<sub>s</sub> rate constant for slower reacting isomer  
k<sub>1</sub> first-order rate constant
- K<sub>sp</sub> - solubility product
- l - pathlength
- ln - logarithm to base e
- log - logarithm to base 10
- m - molal (scale)
- M - molarity
- M<sup>n+</sup> - metal ion of charge n+
- M<sub>x</sub> - relative molar mass of x

Continued ....

- nmr - nuclear magnetic resonance  
 $n_x$  - number of moles of x  
p - pressure  
ppm - parts per million (nmr)  
P - absorbance  
     $P_i$  initial absorbance  
     $P_0$  absorbance at  $t=0$   
     $P_t$  absorbance at time t  
     $P_{t_{1/2}}$  absorbance after one half-life  
     $P_\infty$  absorbance at  $t=\infty$   
     $P'$  absorbance  $\times 10^3$   
R - molar gas constant  
soly - solubility  
S - entropy  
     $S^E$  excess entropy of mixing  
t - time  
 $t_{1/2}$  - half-life  
T - absolute temperature  
TABTB - triisooamyl-n-butylammonium tetraphenylboronate (assumption)  
TATB - tetraphenylarsonium tetraphenylboronate (assumption)  
TMS - tetramethylsilane  
TPTB - tetraphenylphosphonium tetraphenylboronate (assumption)  
vol % - volume percentage (co-solvent)  
wt % - weight percentage (co-solvent)  
x - mole fraction (scale)

- 
- $\gamma$  - activity coefficient on concentration scale  
 $\log_m \gamma_{\pm}^2$  - medium effect of electrolyte  
 $\epsilon$  - extinction coefficient  
     $\epsilon_\lambda$  extinction coefficient at wavelength  $\lambda$   
 $\lambda$  - wavelength  
     $\lambda_{max}$  wavelength of maximum absorbance  
 $\mu$  - chemical potential  
     $\mu_x$  chemical potential of x  
     $\mu^\ominus$  standard chemical potential

Continued ....

$\delta_m \mu^\ominus$  standard transfer chemical potential

$\mu_x^*(l)$  chemical potential of pure liquid x

$\nu$  - stoichiometric factor (number of moles of ions formed from 1 mole of electrolyte)

$\rho$  - density



# CHAPTER 1

**Introduction**

## 1.1 GENERAL

This thesis is concerned with aspects of the structure, the solvation and the reactivity of ions. Obviously, these phenomena are intimately related. The characteristics of solvation of an ion are largely attributable to its structure. In turn, the nature and extent of these ion-solvent interactions have a profound effect on the rates of reactions in which the ion may then take a part. Ion solvation can be studied experimentally from several aspects, by certain thermodynamic, kinetic, spectroscopic and structural methods. These techniques yield information needed to characterise ion solvation such as solvation numbers, the sizes of solvated ions, the distances between ions and adjacent solvent molecules and thermodynamic and other measures of ion-solvent interactions. Qualitative indications as to the nature of ion-solvent interactions and the effect of the ions on solvent-solvent interactions may be obtained from such data. Some of these techniques can be used to obtain single-ion parameters directly. These include nmr spectroscopy in slow solvent exchange situations, ultraviolet/visible spectra and X-ray diffraction. In the case of thermodynamic studies, however, measurements are made for whole salts so that thermodynamic data cannot be obtained directly for individual ions. The splitting of such measured values for whole salts into ionic components requires the introduction of at least one assumption. Once a satisfactory method for effecting this split has been established, then thermodynamic measurement of ion-solvent interactions can be obtained using such quantities as Gibbs free energies, enthalpies, entropies, volumes and heat capacities involved in solvation processes. In terms of comparing ion-solvent interactions for a given ion in different solvents, the change in these thermodynamic parameters when the solvent is varied is of particular

interest. Transfer parameters of these thermodynamic functions provide a measure of such changes. One such quantity is the transfer chemical potential of an ion.

## 1.2 TRANSFER CHEMICAL POTENTIALS

The standard transfer chemical potential of an ion,  $\delta_m \mu^\ominus$ , is defined as the difference in the standard chemical potentials of the ion in a solvent W,  $\mu_w^\ominus$ , and in a solvent S,  $\mu_s^\ominus$ , as shown in equation 1.1 where  $\delta_m$

$$\delta_m \mu_{w \rightarrow s}^\ominus = \mu_s^\ominus - \mu_w^\ominus \quad \dots [1.1]$$

is a solvent operator symbolizing the transference process involved.

Transfer chemical potentials for salts can be obtained directly from solubility and electrochemical measurements. By splitting transfer chemical potentials of salts into their ionic components, lists of single-ion transfer chemical potentials from a reference solvent into other solvents can be used to obtain information concerning the nature of solute-solvent and solvent-solvent interactions in the systems. The effects on these interactions of ionic size, ionic charge and, for complex ions, the nature of ligands may be explored. In terms of the solvents, factors such as basicity, H-bonding ability and structure can be examined.

The calculation of single-ion transfer parameters requires no small degree of care as the procedure is beset with difficulties. Descriptions of systems involved and definitions of standard states of components therein must be thermodynamically valid and adhered to throughout the procedure. This problematic area was discussed in detail by Blandamer et al.<sup>1</sup> The method of splitting transfer chemical potentials for salts into their ionic components also raises problems. Such splitting can be achieved only by the introduction of an extrathermodynamic assumption. A number of extrathermodynamic assumptions have been used,<sup>2-6</sup> the choice

of which affects the outcome of the analysis. As a result, the relative merits of the different assumptions have been discussed at length in the literature.<sup>7-9</sup> Thus, different authors favouring different assumptions have produced sets of single-ion values the use of which, in terms of comparing sets of values, is limited. Much more useful and informative would be lists of single-ion transfer parameters derived using the same extrathermodynamic assumption. The choice of solute composition scale (molar, molal or mole fraction) also affects the results, the conversion of single-ion values given on one scale to another scale being tedious rather than difficult. If the solvent S is a binary mixture, the possible use of different solvent composition scales (volume percentages, weight percentages or mole fractions of one of the solvents) also complicates any attempted comparisons of quoted values.

Thus, it can be seen that in order to make full use of relevant data available in the literature, derivation of single-ion transfer parameters using a single extrathermodynamic assumption and given on the same solute and solvent composition scale is required. This is attempted in Chapters 3 and 4 in which transfer chemical potentials for single ions in three binary aqueous solvent mixtures, water + ethanol mixtures, water + ethylene glycol (ethane-1,2-diol) mixtures and water + glycerol (propane-1,2,3-triol) mixtures are calculated. Single-ion transfer parameters from water into these binary aqueous solvent mixtures are calculated from solubility and electrochemical data for salts. The extrathermodynamic assumption used is the tetraphenylarsonium tetraphenylboronate (TATB) assumption<sup>10</sup> and values are all given on the same solute composition scale (molar) and the same solvent composition scale (weight percentage co-solvent in the solvent mixture). In addition to discussion of the results in terms of ion solvation (in these and other

binary aqueous mixtures), comparisons between values derived using different extrathermodynamic assumptions (but given on the same solute and solvent composition scale) are made.

### 1.3 LOW-SPIN IRON(II) DI-IMINE COMPLEXES

#### 1.3.1 General

Ion solvation is one of several aspects from which a series of low-spin iron(II) complexes, termed iron(II) di-imine complexes, have been studied.<sup>1,11-13</sup>

Crystal field theory states that in an octahedral ligand field the degeneracy of the d orbitals containing the valence shell electrons of a transition metal ion is removed. The five d orbitals are split into a group of three orbitals,  $t_{2g}$ , and a group of two orbitals,  $e_g$ . The energy of the  $e_g$  set (i.e. the  $d_{z^2}$  and the  $d_{x^2-y^2}$  orbitals) is higher than that of the  $t_{2g}$  set (i.e. the  $d_{xy}$ ,  $d_{xz}$  and  $d_{yz}$  orbitals). The degree of splitting between the two sets,  $\Delta$ , is dependent on the field strength of the ligand [see Fig. 1.1]. For a metal ion such as  $Fe^{2+}$

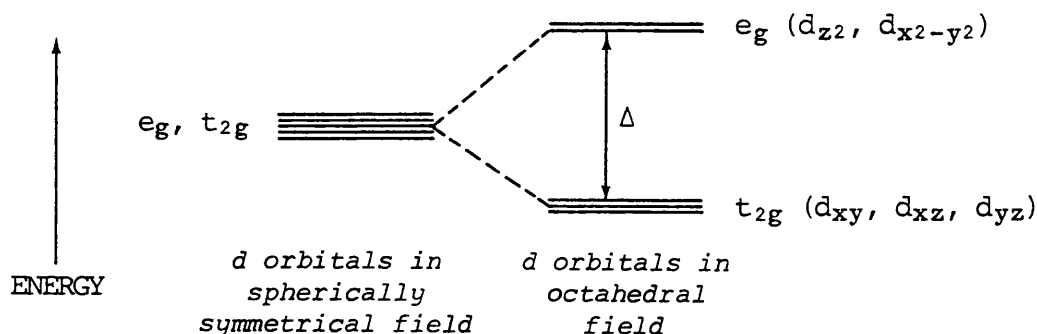
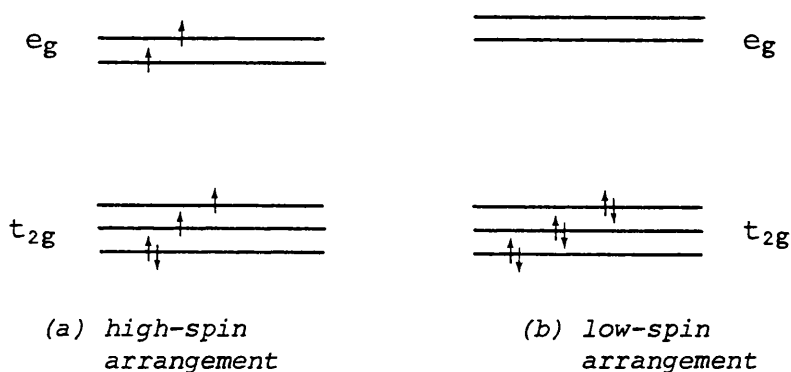


FIGURE 1.1

Crystal field splitting diagram for an octahedral complex.

possessing a  $d^6$  configuration there are two ways in which the non-bonding electrons can be distributed amongst the  $e_g$  and  $t_{2g}$  levels [see Fig. 1.2]. If the pairing energy for the electrons,  $P$ , is larger than  $\Delta$ , the electrons

will be distributed as in Fig. 1.2(a) with the maximum number of unpaired spins. If  $\Delta > P$ , the electrons pair in the  $t_{2g}$  orbitals as far as possible as shown in Fig. 1.2(b). Thus, strong field ligands (high  $\Delta$ ) will result in complexes having the low-spin arrangement while weak field ligands (low  $\Delta$ ) will result in complexes having the high-spin arrangement. The majority of iron(II) complexes are high-spin ( $t_{2g}^4 e_g^2$ ) but complexes containing ligands which have a large crystal field effect are low-spin ( $t_{2g}^6$ ) and are kinetically inert. Such low-spin complexes of iron(II) include  $[\text{Fe}(\text{CN})_6]^{4-}$  and a large class of pseudo-octahedral compounds known as low-spin iron(II) di-imine complexes.

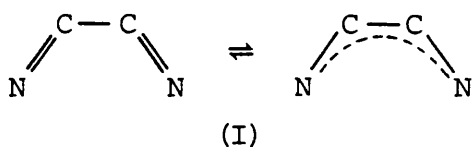


**FIGURE 1.2**

Ligand field diagrams showing the ground state electron occupancy for octahedral complexes of transition metal ions possessing a  $d^6$  configuration.

Low-spin iron(II) di-imine complexes all contain the di-imine moiety

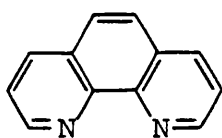
(I). The existence of low-spin compounds such as  $[\text{Fe}(\text{phen})_3]^{2+}$  and



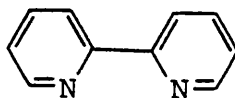
$[\text{Fe}(\text{bipy})_3]^{2+}$  where phen is 1,10-phenanthroline (II) and bipy is

2,2'-bipyridyl (III) has been known for almost a century.<sup>14,15</sup> Since

that time the preparation of many low-spin iron(II) complexes of ligands

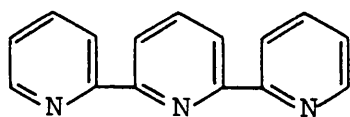


(II)

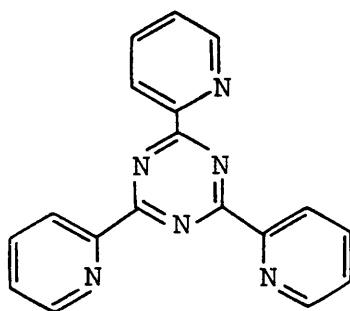


(III)

containing the di-imine chelating unit have been reported.<sup>16-19</sup> Such ligands are by no means all bidentate as are phen and bipy. Ligands such as 2,2'; 6',2''-terpyridyl (IV)<sup>20</sup> and 2,4,6-tris(2-pyridyl)-1,3,5-triazine (V),<sup>21</sup> form low-spin bis-(terdentate) iron(II) complexes. 1,8-

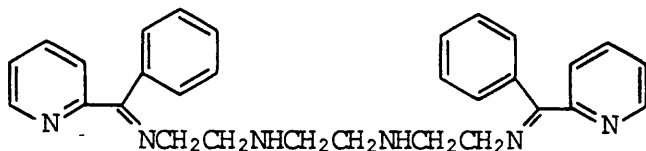


(IV)



(V)

bis-[phenyl(2-pyridyl)methyleneamino]-3,6-diazaoctane (VI)<sup>22</sup> is one of several hexadentate ligands (ligands containing six donor atoms) which form low-spin iron(II) complexes. Quadridentate and quinquedentate



(VI)

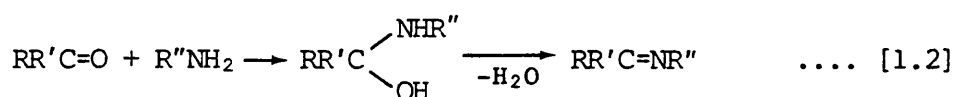
di-imine ligands, with four and five donor atoms respectively, forming low-spin iron(II) complexes have also been reported.<sup>19,23</sup>

Low-spin iron(II) di-imine complexes have intense colours. This is believed to be a result of electron transfer from the filled  $t_{2g}$  orbitals on the metal ion to the lowest lying vacant  $\pi^*$  orbitals on the ligands. These transitions occur in the visible region and lead to stabilization of the complexes.

The kinetics of a number of reactions of low-spin iron(II) di-imine complexes have been studied over the years. For reactions involving either the appearance or the disappearance of complexes of this type, changes in the absorption in the visible region for the reaction mixtures are dramatic. As, in the majority of reactions, the absorbances due to species other than the di-imine complexes in the reaction mixtures at  $\lambda_{\max}$  of the complexes in this region are negligible, then rates of reactions can be conveniently measured spectrophotometrically. In such a way, the kinetics of reactions of low-spin iron(II) di-imine complexes such as their reactions with acid,<sup>22,24</sup> alkali,<sup>25,26</sup> cyanide,<sup>27</sup> peroxydisulphate<sup>28</sup> and hydrogen peroxide<sup>29</sup> have been studied. The effects of solvents,<sup>30</sup> substituents<sup>31</sup> and added salts<sup>32</sup> on rates of reactions have also been probed.

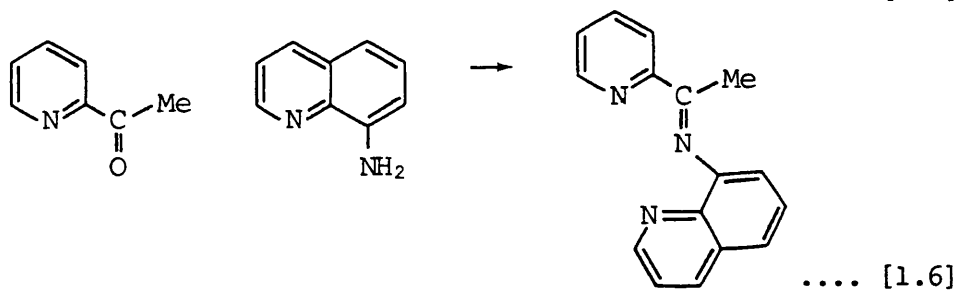
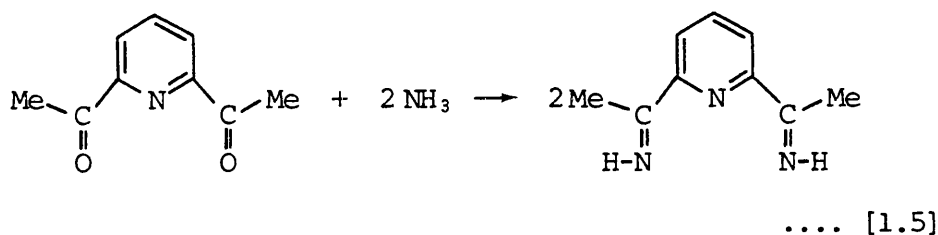
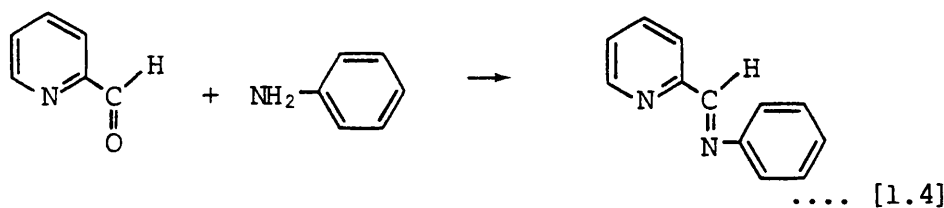
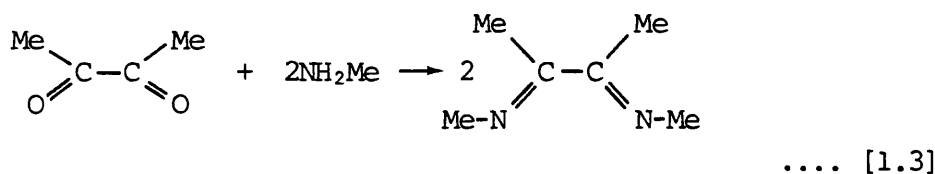
### 1.3.2 Schiff base ligands

An extensive series of multidentate ligands containing the di-imine moiety, termed Schiff base ligands, which form low-spin complexes with iron(II) exists.<sup>19,26,29</sup> These ligands are synthesised by combination of an appropriate carbonyl compound and a primary amine. Strictly, the term 'Schiff base' refers to the imino product (a species containing a carbon-nitrogen double bond) of the reaction of an aldehyde or ketone with a primary amine. Such a reaction involves initial addition of the reactants followed by dehydration [equation 1.2]. The same fundamental



reaction is involved also in the formation of a Schiff base ligand. In this case, however, the nature of the carbonyl compound is such that the reaction leads to the formation of a di-imine moiety (or sometimes

more than one) in the product. Examples of some such Schiff base ligands, and the reactants involved in their formation, are shown in equations 1.3, 1.4, 1.5 and 1.6. All the resulting ligands contain the



di-imine moiety. Those in equations 1.3 and 1.4 are bidentate ligands each containing one di-imine group (N=C-C=N). The ligands shown in equations 1.5 and 1.6 are examples of terdentate ligands, each formally containing one di-imine group but having in addition a second chelate ring fused on the di-imine group.

### 1.3.3 Stereoisomers

It can be seen that the Schiff base di-imine ligands shown in equations 1.3 and 1.5 are symmetrical whereas those shown in equations

1.4 and 1.6 are unsymmetrical. The nature of such unsymmetrical ligands means that iron(II) complexes containing these ligands may theoretically exist in more than one stereoisomeric form.

For tris-(bidentate) iron(II) complexes containing unsymmetrical ligands there are four possible stereoisomers. The configurations of these isomeric forms are shown in Fig. 1.3.

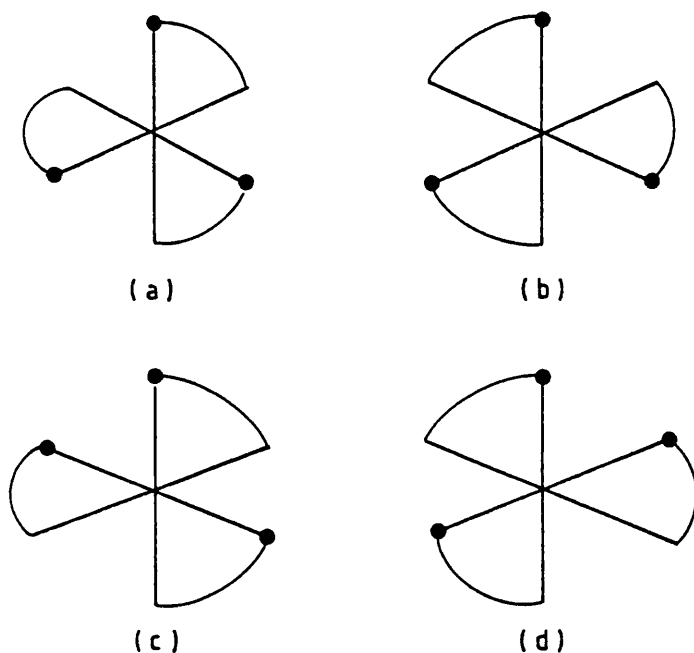


FIGURE 1.3

Possible stereoisomeric forms of a complex of the type  $[\text{Fe}(\text{LL}')_3]^{2+}$  where  $\text{LL}'$  is an unsymmetrical bidentate ligand.

In forms (a) and (b), the identical ends of the three ligands lie in a single face of the octahedron. This configuration is termed the 'fac' isomeric form. In forms (c) and (d), two of the three identical ends of the ligands bear a meridional relationship to each other. This configuration is termed the 'mer' isomeric form. It can be seen that the 'fac' isomers each possess a three-fold rotation axis of symmetry which is absent from the 'mer' isomeric forms. Forms (a) and (b) are non-superimposable mirror images and are therefore enantiomers.

Enantiomers have identical physical properties except for the direction of rotation of the plane of polarized light. They also have identical chemical properties except towards optically active reagents. Forms (c) and (d) also constitute a pair of enantiomers. The stereoisomeric relationship between the pair of 'mer' isomers and the pair of 'fac' isomers is that of diastereoisomers. Diastereoisomers have similar, though not identical, chemical properties and have different physical properties. In principle then, at least, diastereoisomers can be separated from each other by fractional distillation, fractional crystallization or chromatography.

For bis-(terdentate)iron(II) complexes containing unsymmetrical ligands, the existence of diastereoisomeric forms of a complex will be dependent of whether the terdentate ligands are necessarily planar. If the ligands are planar then the only possible stereoisomeric forms that can exist are a pair of enantiomers depicted in Fig. 1.4(a) and (b). If, however, the ligand may be either 'bent' or co-planar then six stereoisomeric forms may exist, the three pairs of enantiomers depicted in (a) and (b) and in (c) and (d) and in (e) and (f). The former two pairs of enantiomers each possess a two-fold rotation axis of symmetry which is lacking in the latter pair. It is generally believed that for complexes of this type the constituent ligands are indeed planar.<sup>33</sup>

For the mono-(hexadentate)iron(II) complexes of this type there are several ways in which the ligand may be wrapped around the central iron atom. Consider the case where the two halves of the hexadentate ligand are identical, i.e. the ligand is of the type NRNR'NR''R''NR'NRN. For an iron(II) complex containing this ligand, eight stereoisomeric forms are possible, i.e. four pairs of enantiomers. These are shown in Fig. 1.5.

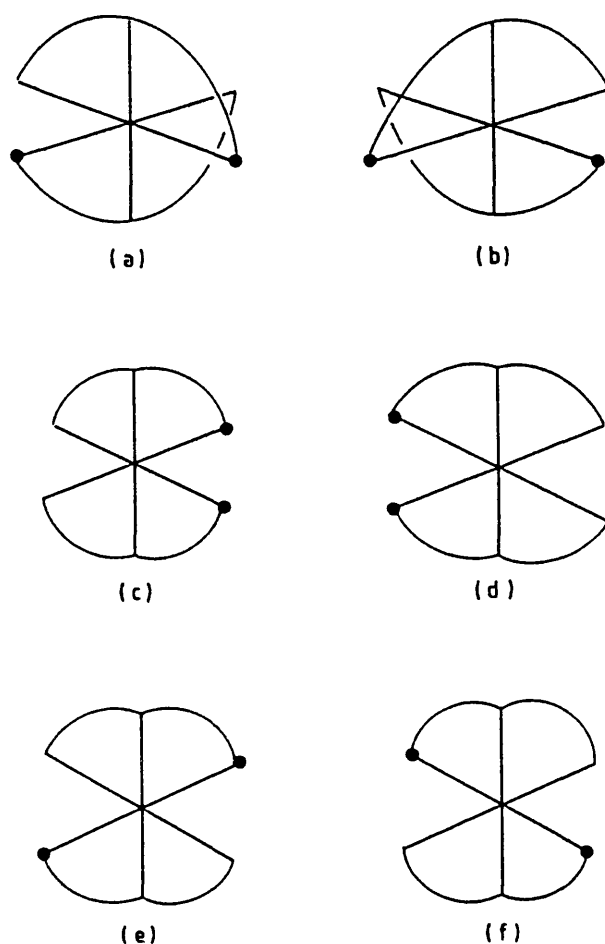
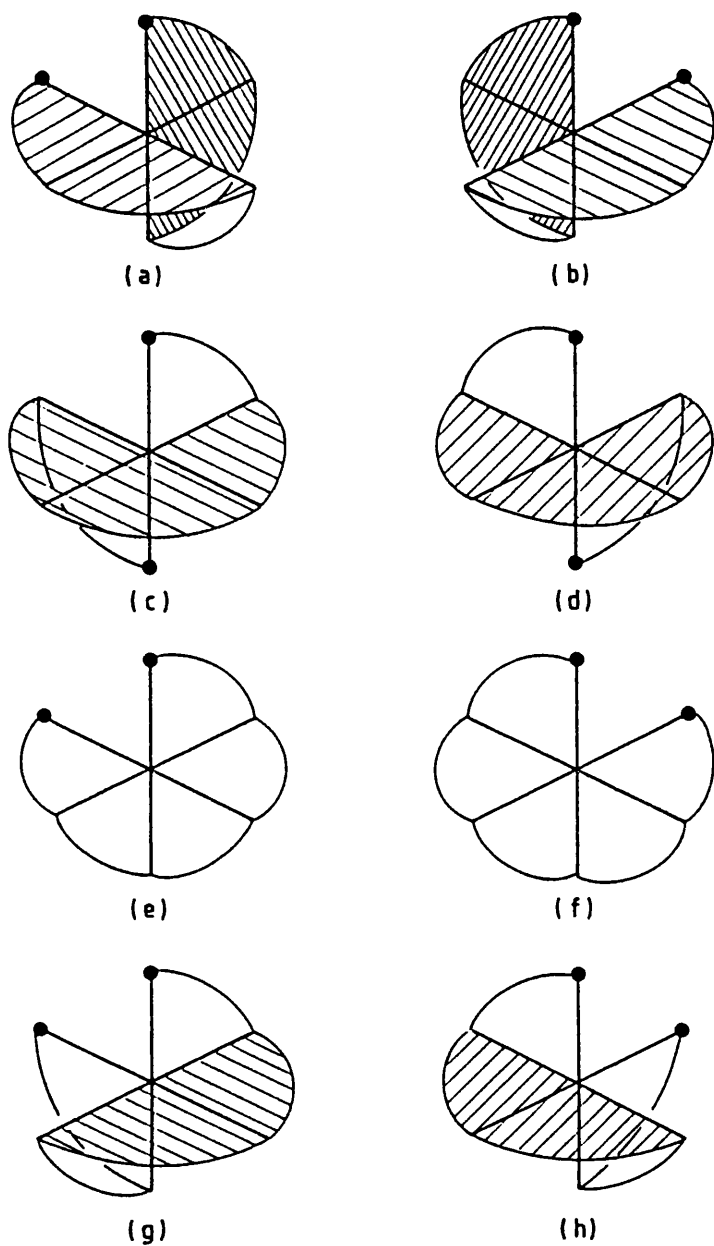


FIGURE 1.4

Possible stereoisomeric forms of a complex of the type  $[\text{FeL}_2]^{2+}$  where L is an unsymmetrical terdentate ligand.

In this figure, (a) and (b) are enantiomers, as are (c) and (d), as are (e) and (f) and as are (g) and (h). With the exception of (g) and (h) all the stereoisomeric forms possess a two-fold rotation axis of symmetry.

The possible existence of stereoisomeric forms of iron(II) complexes containing unsymmetrical, multidentate Schiff base di-imine ligands forms the basis of Chapters 5 and 6. Attempted detection of isomeric forms of the complexes concerns the existence of diastereoisomers only. The presence of enantiomeric forms of the complexes cannot be detected



**FIGURE 1.5**

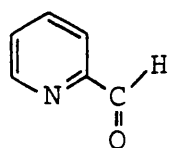
Possible stereoisomeric forms of a complex of the type  $[\text{FeL}]^{2+}$  where L is a hexadentate ligand  $\text{NRNR}'\text{NR}''\text{R}'''\text{NR}'\text{NRN}$ .

by the techniques employed under the observed conditions. In Chapter 5, the likelihood of previously obtained inconsistent results of kinetic studies involving complexes of this type<sup>34</sup> being the result of the presence of isomers of the complexes is explored. The kinetics of alkali (hydroxide) fission of a series of iron(II) Schiff base di-imine

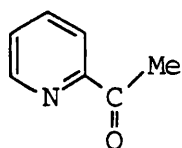
complexes containing unsymmetrical ligands are studied. Possible isomeric detection rests on the supposition that the analogous rate constants for the reactions of diastereoisomeric forms of a complex will be sufficiently different to allow detection. In Chapter 6, the presence of isomeric forms in samples of low-spin iron(II) Schiff base complexes containing unsymmetrical ligands is investigated using the  $^1\text{H}$  nmr technique. In this case the possibility of detection of isomers stems from the differing symmetries of diastereoisomeric forms. Results of further studies (kinetic, spectroscopic and X-ray crystallographic) probing the reactivity, structure and solvation of some iron(II) Schiff base di-imine complexes are discussed in Chapter 7.

#### 1.3.4 Ligand notation of iron(II) Schiff base complexes

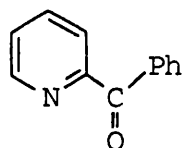
Throughout Chapters 3, 4, 5, 6 and 7 the following system for abbreviating the names of Schiff base ligands is used. The ligands were all made by combination of one of three carbonyl compounds, pyridine-2-carboxaldehyde (VII), 2-acetyl pyridine (VIII) or 2-benzoyl pyridine (IX) and a primary amine. The abbreviated names of these



(VII)



(VIII)



(IX)

ligands contain three parts, x, y and z given in the form (x, y, z). The first part, x, denotes the denticity of the ligand. Thus, for bidentate, terdentate and hexadentate ligands, x is bsb, tsb and hsb respectively. The second part of the abbreviated ligand name, y, indicates the carbonyl compound used in the synthesis of the ligand. Thus, for ligands made using pyridine-2-carboxaldehyde, 2-acetyl pyridine

or 2-benzoyl pyridine, y is H, Me or Ph respectively. The third part of the ligand notation, z, relates to the primary amine used in the preparation of the ligand. The amines used in the preparations of the complexes and the abbreviation for each amine are shown in Table 1.1. Thus, for example, (bsb,H,Me) is the bidentate Schiff base di-imine ligand derived using pyridine-2-carboxaldehyde and methylamine; (hsb,Ph, trien) is the hexadentate Schiff base ligand derived using 2-benzoyl pyridine and triethylenetetramine. The low-spin iron(II) tris-(bidentate) complex  $[\text{Fe}(\text{gmi})_3]^{2+}$  referred to in Chapter 4 contains the bidentate ligand derived from glyoxal and methylamine.

TABLE 1.1

Primary amines used in the preparation of iron(II) Schiff base complexes and their abbreviations, z.

PRIMARY AMINE	Z
methylamine	Me
aniline	Ph
<u>m</u> -toluidine (3-methylaniline)	Ph: <u>m</u> -Me
<u>p</u> -toluidine (4-methylaniline)	Ph: <u>p</u> -Me
3,4-dimethylaniline	Ph: 3,4-Me <sub>2</sub>
<u>m</u> -anisidine ( <u>m</u> -methoxyaniline)	Ph: <u>m</u> -OMe
<u>p</u> -anisidine ( <u>p</u> -methoxyaniline)	Ph: <u>p</u> -OMe
benzylamine (phenylmethylamine)	CH <sub>2</sub> Ph
α-phenylethylamine (α-methylbenzylamine)	MeCHPh
hydroxylamine hydrochloride	OH
taurine (2-aminoethanesulphonic acid)	CH <sub>2</sub> CH <sub>2</sub> SO <sub>3</sub> <sup>-</sup>
triethylenetetramine (1,4,7,10-tetraaza-n-decane)	trien
tris(2-aminoethyl)amine	t2a
8-aminoquinoline	8amq
2-picolylamine (2-[aminomethyl]pyridine)	2pa

## REFERENCES FOR CHAPTER 1

1. M. J. Blandamer, J. Burgess, B. Clark, P. P. Duce, A. W. Hakin, N. Gosal, S. Radulovic, P. Guardado, F. Sanchez, C. D. Hubbard and E. A. Abu-Gharib, J. Chem. Soc., Faraday Trans. I, 1986, 82, 1471.
2. B. Case, N. S. Hush, R. Parsons and M. E. Peover, J. Electroanal. Chem., 1965, 10, 360.
3. R. Alexander, A. J. Parker, J. H. Sharp and W. E. Waghorne, J. Am. Chem. Soc., 1972, 94, 1148.
4. C. L. de Ligny, H. J. M. Denessen and M. Alfenaar, Rec. Trav. Chim., 1971, 90, 1265.
5. C. F. Wells, Trans. Faraday Soc., 1965, 61, 2194.
6. E. Grunwald, G. Baughman and G. Kohnstam, J. Am. Chem. Soc., 1960, 82, 5801.
7. Y. Marcus, "Ion Solvation", Wiley, Chichester, 1985.
8. A. J. Parker, Chem. Rev., 1969, 69, 1.
9. O. Popovych, Crit. Rev. Anal. Chem., 1970, 1, 73.
10. R. Alexander and A. J. Parker, J. Am. Chem. Soc., 1967, 89, 5549.
11. J. Burgess, J. Chem. Soc. (A), 1968, 2728.
12. J. Burgess, J. Chem. Soc. (A), 1969, 1899.
13. M. J. Blandamer, J. Burgess, P. P. Duce and R. I. Haines, J. Chem. Soc., Dalton Trans., 1980, 2442.
14. F. Blau, Chem. Ber., 1888, 21, 1077.
15. F. Blau, Monatsh., 1889, 10, 375; 1898, 19, 647.
16. P. Krumholz, J. Am. Chem. Soc., 1953, 75, 2163.
17. F. Lions and K. V. Martin, J. Am. Chem. Soc., 1957, 79, 2733.
18. F. H. Case, J. Chem. Eng. Data, 1976, 21, 124.
19. M. J. Blandamer, J. Burgess, R. I. Haines, F. M. Mekhail and P. Askalani, J. Chem. Soc., Dalton Trans., 1978, 1001.
20. G. T. Morgan and F. H. Burstall, J. Chem. Soc., 1932, 20.
21. F. H. Case and E. Croft, J. Am. Chem. Soc., 1959, 81, 905.
22. E. R. Gardner, F. M. Mekhail and J. Burgess, Int. J. Chem. Kinetics, 1974, 6, 133.
23. V. L. Goedken, J. J. Pluth, Shie-Ming Peng and B. Bursten, J. Am. Chem. Soc., 1976, 98, 8014.
24. J. Burgess and R. H. Prince, J. Chem. Soc., 1963, 5752.
25. J. Burgess and R. H. Prince, J. Chem. Soc., 1965, 4697.
26. M. J. Blandamer, J. Burgess, P. Cookson, D. L. Roberts, P. Wellings, F. M. Mekhail and P. Askalani, J. Chem. Soc., Dalton Trans., 1978, 996.

REFERENCES (Continued) ....

27. J. Burgess, Inorg. Chim. Acta, 1971, 5, 133.
28. J. Burgess and R. H. Prince, J. Chem. Soc. (A), 1966, 1772.
29. J. Burgess, J. Chem. Soc. (A), 1967, 955.
30. G. Wada, K. Takahashi and M. Isobe, Bull. Chem. Soc. Jpn., 1981, 54, 3739.
31. J. Burgess, J. Chem. Soc. (A), 1967, 431.
32. N. F. Ashford, M. J. Blandamer, J. Burgess, D. Laycock, M. Waters, P. Wellings, R. Woodhead and F. M. Mekhail, J. Chem. Soc., Dalton Trans., 1979, 869.
33. R. H. Holyer, C. D. Hubbard, S. F. A. Kettle and R. G. Wilkins, Inorg. Chem., 1966, 5, 622.
34. J. Burgess, personal communication.



# CHAPTER 2

**Experimental**

## 2.1 INTRODUCTION

Details of experimental procedures are presented in this chapter. Methods by which salts of iron(II) Schiff base complexes were prepared are described as are the experimental techniques by which these complexes were studied. For kinetic determinations the computer-driven analysis of the collected data for first-order rate constants is described. Measurement of the solubilities of potassium iodate in water + ethanol mixtures by titrimetric analysis, used in Chapter 3, is also described.

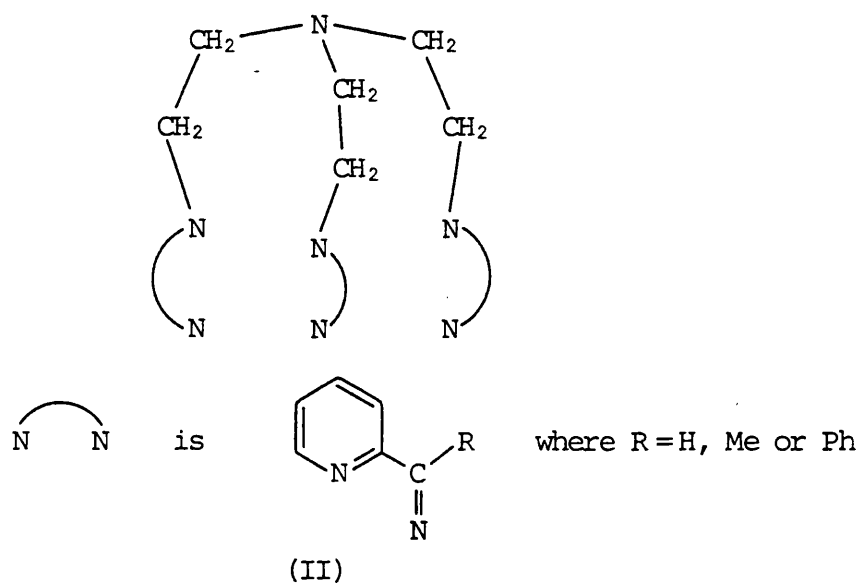
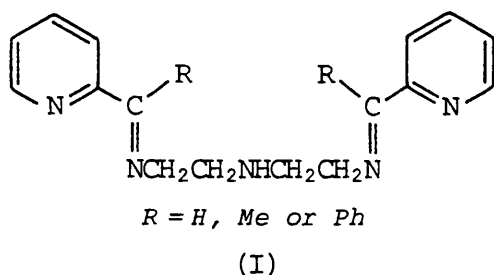
## 2.2 PREPARATION OF IRON(II) SCHIFF BASE COMPLEXES

### 2.2.1 General

All the preparations of the iron(II) Schiff base complexes used in this study involved the generation of a Schiff base ligand, be it bidentate, terdentate or hexadentate, by the reaction of a carbonyl compound with a primary amine. The carbonyl compound used in the syntheses was one of three, pyridine-2-carboxaldehyde, 2-acetyl pyridine or 2-benzoyl pyridine. By reference to the primary amine, preparation of the iron(II) complexes can be split into two categories. Firstly, are the complexes in which the primary amine used in the syntheses was hydroxylamine hydrochloride. In these cases the Schiff base ligand was prepared in solution, isolated in its solid form and re-crystallized before its reaction with  $\text{Fe}^{2+}$  to form the complex. Secondly, are the iron(II) Schiff base complexes whose preparation involved all the other primary amines. In these cases, solutions of the three reactants,  $\text{Fe}^{2+}$ , the carbonyl compound and the amine, were mixed together to generate the complex species without previous isolation and purification of the Schiff base ligand in its solid form. This latter method of preparation, being

the most frequently used synthetic procedure, is termed the 'general method of preparation' and is outlined below in Section 2.2.2.

In all preparations, stoichiometric amounts of reactants were used. Thus, for the bidentate and terdentate Schiff base ligands, the appropriate amines and carbonyl compounds were combined in the ratio of 1:1 in each case. For the hexadentate Schiff base ligands (hsb,R, trien), shown in (I), and (hsb,R,t2a), shown in (II), where R=H, Me or Ph, the appropriate amines and carbonyl compounds were combined in the ratios of 1:2 and 1:3 respectively. In the preparations of tris-(bidentate) iron(II) complexes, bis-(terdentate) iron(II) complexes and mono-(hexadentate) iron(II) complexes, metal to ligand ratios of 1:3, 1:2 and 1:1 respectively were used.



When solutions of salts of the complexes in binary aqueous solvent mixtures were prepared, the solvent mixtures were made up by combination of known volumes of water and the co-solvent. Solvent composition is described in terms of the volume percentage of the co-solvent in the solvent mixture, x vol % co-solvent, i.e. if y was the volume of co-solvent and z the volume of water before mixing, then  $x = [y/(y+z)] \times 100$  vol % co-solvent. For example, a 40 vol % MeOH solvent mixture was prepared by the combination of 40 cm<sup>3</sup> of methanol and 60 cm<sup>3</sup> of water.

Solutions of complexes to be used in kinetic studies were made up so that the initial absorbances of the reaction mixtures were approximately 1 (thus, the initial concentrations of the complexes in the reaction mixtures were in the region of 10<sup>-4</sup> M).

#### 2.2.2 General method of preparation

Salts of iron(II) Schiff base di-imine complexes, whose preparations involved a primary amine other than hydroxylamine hydrochloride, were first prepared by the same general method using stoichiometric amounts of iron(II) chloride tetrahydrate, amine and carbonyl compound.

Methanolic solutions of the appropriate amine and carbonyl compound were mixed together and allowed to stand for at least 10 minutes in order to generate the 'in situ' Schiff base ligand. This solution was then added to a solution of iron(II) chloride tetrahydrate which contained a couple of drops of glacial acetic acid. A microspatula of sodium dithionite was added and the intensely coloured solution was allowed to stand for about 1 hour at room temperature. After filtering through 'celite filter-aid' most of the solvent was evaporated off and the residue was taken up in water. The solution was filtered through 'celite

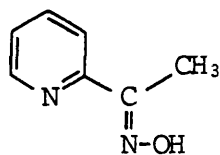
filter-aid' again. The perchlorate, hexafluorophosphate, thiocyanate or iodide salts of the iron(II) complex species were precipitated by the addition of saturated aqueous solutions of sodium perchlorate, potassium hexafluorophosphate, ammonium thiocyanate or potassium iodide respectively. The chloride salt was obtained by evaporation of the solution until precipitation occurred. The filtered solid was washed thoroughly with water, ethanol and ether and dried in vacuo at room temperature over phosphorus pentoxide. In cases where the quantity or quality of the product was low, the procedure was repeated under an inert atmosphere of nitrogen.

Modifications to this general method of preparation are detailed in the chapters where they are used. Modified methods of preparation were used either in an attempt to produce samples of complexes containing differing proportions of isomers or to obtain the most satisfactory  $^1\text{H}$  nmr spectra. Such modifications include a change in the order of mixing of the reactants and changes in the time scale of the preparation of the salts. The order of mixing of reactants has been found, in some cases, to be important. For example, in the preparation of  $[\text{Fe}(\text{gmi})_3]^{2+}$ , where gmi is the bidentate Schiff base ligand derived from glyoxal and methylamine, the complex is generated in solution only if the solutions of  $\text{Fe}^{2+}$  and methylamine are combined first, with subsequent addition of the solution of glyoxal. Samples of the complex cannot be obtained when the 'in situ' Schiff base ligand is generated in solution first, the ligand being formed only in very low yield in this case.

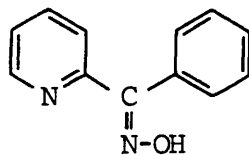
### 2.2.3 Preparative method involving the use of hydroxylamine hydrochloride

When the primary amine used in the synthesis of a complex was hydroxylamine hydrochloride, the Schiff base ligand was prepared, isolated and purified before being combined with  $\text{Fe}^{2+}$  to form the complex in solution.

Methyl-2-pyridyl ketoxime (III) and phenyl-2-pyridyl ketoxime (IV) were prepared by the reaction of hydroxylamine hydrochloride with 2-acetyl pyridine or 2-benzoyl pyridine respectively. 0.5g of hydroxylamine



(III)



(IV)

hydrochloride was dissolved in 3 cm<sup>3</sup> of water to which solution was added 6 cm<sup>3</sup> of 10% Na<sub>2</sub>CO<sub>3</sub>.10 H<sub>2</sub>O solution. 0.2g of the carbonyl compound was added with just sufficient methanol to produce a clear solution. The mixture was heated on a water bath for 10 minutes and then cooled in ice. Precipitation of the white crystalline product was induced by scratching the side of the vessel with a glass rod. The filtered product was re-crystallized from hot ethanol.

In the preparations of the iron(II) complexes using the ketoxime Schiff base ligands and iron(II)chloride tetrahydrate, stoichiometric amounts of the two reactants were used. The iron(II) salt was dissolved in water and a microspatula of sodium dithionite was added. The solution was made acidic by the addition of drops of dilute sulphuric acid (until the pH of the solution, as measured using universal indicator paper, was approximately 3). A stoichiometric amount of the ketoxime ligand was added. In the case of methyl-2-pyridyl ketoxime the solid was added, when phenyl-2-pyridyl ketoxime was used a solution of the ketoxime in ethanol was added. In the former case, the reaction mixture was stirred until the solid had dissolved, in the latter case, the solution was stirred for 10 minutes. The reaction mixture was then filtered using 'celite filter-aid' and the perchlorate salt of the complex was precipitated by the addition of a saturated aqueous solution of sodium perchlorate. The precipitate was washed with water, ethanol and ether and dried in vacuo

over phosphorus pentoxide.

## 2.3 COLLECTION AND ANALYSIS OF KINETIC DATA

### 2.3.1 First-order rate constants

The rate of a reaction may be defined in terms of the rate of disappearance of a reactant (equation 2.1). For a first-order process

$$\text{rate} = \frac{-d[\text{reactant}]}{dt} \quad \dots [2.1]$$

in which a species A reacts to form a product P the rate law takes the form shown in equation 2.2 where  $k_1$  is the first-order rate constant for the reaction. Integration of equation 2.2 yields equation 2.3

$$\frac{-d[A]}{dt} = k_1 [A] \quad \dots [2.2]$$

which can be rewritten as shown in equation 2.4.  $[A]_0$  and  $[A]_t$  are the concentrations of species A at time  $t=0$  and at time  $t$  respectively.

$$\ln\left(\frac{[A]_0}{[A]_t}\right) = k_1 t \quad \dots [2.3]$$

$$[A]_t = [A]_0 \exp(-k_1 t) \quad \dots [2.4]$$

The latter equation shows that the concentration of A falls exponentially with time with a rate determined by  $k_1$ .

The half-life of a chemical reaction,  $t_{\frac{1}{2}}$ , is defined as the time taken for the concentration of a reactant to fall to half its initial value.

For the case in question the half-life is the time taken for the concentration of A to fall from  $[A]_0$  to  $\frac{1}{2}[A]_0$ . Thus, from equation 2.3 the half-life and rate constant for a first-order reaction are related as shown in equation 2.5. It can be seen that for such a reaction the half-

$$t_{\frac{1}{2}} = \frac{\ln 2}{k_1} \quad \dots [2.5]$$

life is independent of concentration.

For second-order reactions following the type of rate law shown in equation 2.6 the rate law can be simplified using the 'isolation method'. In equation 2.6 species A and B react together to form a

$$\frac{-d[A]}{dt} = k_2 [A][B] \quad \dots [2.6]$$

product P.  $k_2$  is the second-order rate constant for the reaction. If species B is present in such great excess that its concentration does not change significantly during the course of the reaction, then [B] may be absorbed into the rate constant to give a new rate constant  $k_{obs}$  which is first-order (equation 2.7). Thus the rate law simplifies to that

$$k_{obs} = k_2 [B] \quad \dots [2.7]$$

shown in equation 2.8. This is a pseudo-first-order rate law. Thus, when  $[B] \gg [A]$  the second-order reaction obeys a first-order rate law and

$$\frac{-d[A]}{dt} = k_{obs} [A] \quad \dots [2.8]$$

as such can be treated in the manner shown earlier.

The kinetics of reactions of many low-spin iron(II) di-imine complexes having reaction orders greater than one have been investigated using the isolation method. For example, hydroxide attack at low spin tris-(bidentate)iron(II) complexes has, in general, been shown to follow the rate law given in equation 2.9.  $k_1$ ,  $k_2$ ,  $k_3$  and  $k_4$  are first-, second-,

$$\frac{-d[\text{complex}]}{dt} = (k_1 + k_2[\text{OH}^-] + k_3[\text{OH}^-]^2 + k_4[\text{OH}^-]^3) \times [\text{complex}] \quad \dots [2.9]$$

third- and fourth-order rate constants respectively. The  $k_3$  and  $k_4$  terms are generally only significant for certain complexes at high concentrations of nucleophile.  $k_4$  may be simply a reflection of specific ion effects. Irrespective of the relative significance of such terms, under conditions where  $[\text{OH}^-] \gg [\text{complex}]$  then an overall first-order rate constant for the reaction,  $k_{obs}$ , can be measured (equation 2.8). Thus

if, for a given complex, the kinetics of alkali fission follow a rate law in which the  $k_3$  and  $k_4$  terms are negligible, then under the conditions  $[\text{OH}^-] \gg [\text{complex}]$ ,  $k_{\text{obs}} = k_1 + k_2[\text{OH}^-]$ . If only the  $k_4$  term is insignificant then  $k_{\text{obs}} = k_1 + k_2[\text{OH}^-] + k_3[\text{OH}^-]^2$ , etc.

Observation of the rate of decrease in the concentration of a reactant can be accomplished spectrophotometrically by measuring the change in absorbance of the reactant with time. The absorbance,  $P$ , of a single species  $A$  in dilute solution in monochromatic light of wavelength  $\lambda$  is related to the concentration of  $A$  by the Beer-Lambert Law (equation 2.10).  $I_0$  and  $I_t$  are the intensities of the incident and transmitted

$$P = \log_{10} \left( \frac{I_0}{I_t} \right) = \epsilon_{\lambda} [A] \ell \quad \dots [2.10]$$

light respectively at wavelength  $\lambda$ ,  $\epsilon_{\lambda}$  is the molar extinction coefficient of  $A$  at wavelength  $\lambda$ ,  $[A]$  is the concentration of species  $A$  and  $\ell$  is the pathlength. The total absorbance of a solution at wavelength  $\lambda$  is equal to the sum of the absorbances at that wavelength of all the components of the solution (equation 2.11).  $\epsilon_A$  and  $\epsilon_B$  are the molar

$$P = \epsilon_A [A] \ell + \epsilon_B [B] \ell + \dots \quad \dots [2.11]$$

extinction coefficients of species  $A$  and  $B$  in the solution at wavelength  $\lambda$ .

For a first-order reaction monitored by observing the change in absorption of a species  $A$  at the wavelength of its absorption maximum,  $\lambda_{\text{max}}$ , combination of equations 2.3 and 2.10 yields equation 2.12.  $P_0$  is the initial absorbance of  $A$ , i.e. at  $t=0$ ,  $P_t$  is the absorbance of  $A$  at time  $t$  and  $P_{\infty}$  is the absorbance of  $A$  when the reaction is complete, i.e. at  $t=\infty$ . This equation provides a means of calculating first-order

$$\ln \left( \frac{[A]_0}{[A]_t} \right) = \ln \left[ \frac{(P_0 - P_{\infty})}{(P_t - P_{\infty})} \right] = k_1 t \quad \dots [2.12]$$

rate constants from sets of experimentally observed absorbance/time data.

For low-spin iron(II) di-imine complexes the dramatic changes in P at their absorption maxima in the ultraviolet/visible region as the complexes undergo reactions makes spectrophotometric monitoring of the reactions of these complexes a particularly useful way of studying their reaction kinetics.

### 2.3.2 Analysis of absorbance/time data

Experimentally observed absorbance/time data were analysed by the minicomputer (see Section 2.3.3) for first-order rate constants using the non-linear least squares procedure described by Moore.<sup>1</sup> Rearrangement of equation 2.12 yields an expression for the absorbance at time t, P<sub>t</sub> (equation 2.13). Thus P<sub>t</sub> is defined by three independent

$$P_t = (P_0 - P_\infty) \exp(-k_1 t) + P_\infty \quad \dots [2.13]$$

variables, P<sub>0</sub>, P<sub>∞</sub> and k<sub>1</sub> (equation 2.14). The general differential

$$P_t = P_t [P_0, P_\infty, k_1] \quad \dots [2.14]$$

of equation 2.14 is given by equation 2.15.

$$dP_t = \left( \frac{\partial P_t}{\partial P_0} \right)_{P_\infty, k_1} dP_0 + \left( \frac{\partial P_t}{\partial P_\infty} \right)_{P_0, k_1} dP_\infty + \left( \frac{\partial P_t}{\partial k_1} \right)_{P_0, P_\infty} dk_1 \quad \dots [2.15]$$

From equation 2.13, the partial differentials in equation 2.15 are given in equations 2.16, 2.17 and 2.18.

$$\frac{\partial P_t}{\partial P_0} = \exp(-k_1 t) = \alpha_1 \quad \dots [2.16]$$

$$\frac{\partial P_t}{\partial P_\infty} = 1 - \exp(-k_1 t) = \alpha_2 \quad \dots [2.17]$$

$$\frac{\partial P_t}{\partial k_1} = -t (P_0 - P_\infty) \exp(-k_1 t) = \alpha_3 \quad \dots [2.18]$$

Equation 2.15 can be written to give equation 2.19.

$$dP_t = \alpha_1 dP_0 + \alpha_2 dP_\infty + \alpha_3 dk_1 \quad \dots [2.19]$$

The analysis is initiated using estimates of  $P_0$ ,  $P_\infty$  and  $k_1$  entered into the minicomputer at the beginning of the run. From these estimates, absorbances  $P_t(\text{calc})$  at each time  $t$  are calculated and the differences between observed and calculated  $P_t$  at each data point are obtained, i.e.  $dP_t = P_t(\text{obs}) - P_t(\text{calc})$ . In order to improve the fit,  $\alpha_1$ ,  $\alpha_2$  and  $\alpha_3$  are calculated from equations 2.16, 2.17 and 2.18 at each time step  $t$  and the quantity  $Q$  defined in equation 2.20 is minimized.

$$Q = \sum (dP_t - \alpha_1 dP_0 - \alpha_2 dP_\infty - \alpha_3 dk_1)^2 \quad \dots [2.20]$$

When  $Q$  is at a minimum then  $dQ/dX = 0$ .

$$dQ/dP_0 = \sum \alpha_1^2 dP_0 + \sum \alpha_1 \alpha_2 dP_\infty + \sum \alpha_1 \alpha_3 dk_1 - \sum \alpha_1 dP_t = 0 \quad \dots [2.21]$$

$$dQ/dP_\infty = \sum \alpha_2 \alpha_1 dP_0 + \sum \alpha_2^2 dP_\infty + \sum \alpha_2 \alpha_3 dk_1 - \sum \alpha_2 dP_t = 0 \quad \dots [2.22]$$

$$dQ/dk_1 = \sum \alpha_3 \alpha_1 dP_0 + \sum \alpha_3 \alpha_2 dP_\infty + \sum \alpha_3^2 dk_1 - \sum \alpha_3 dP_t = 0 \quad \dots [2.23]$$

This information can be arranged in matrix form:

$$\begin{array}{ccc|c|c} \left| \begin{array}{ccc} \sum \alpha_1^2 & \sum \alpha_2 \alpha_1 & \sum \alpha_3 \alpha_1 \\ \sum \alpha_2 \alpha_1 & \sum \alpha_2^2 & \sum \alpha_2 \alpha_3 \\ \sum \alpha_3 \alpha_1 & \sum \alpha_2 \alpha_3 & \sum \alpha_3^2 \end{array} \right| & \left| \begin{array}{c} dP_0 \\ dP_\infty \\ dk_1 \end{array} \right| & \left| \begin{array}{c} \sum \alpha_1 dP_t \\ \sum \alpha_2 dP_t \\ \sum \alpha_3 dP_t \end{array} \right| \\ X & \beta & Y \end{array}$$

$$\text{Thus, } Y = \beta X \quad \dots [2.24]$$

Calculated parameters  $\alpha_1$ ,  $\alpha_2$  and  $\alpha_3$  are placed in array  $X$  and equation 2.24 and solved for  $\beta$  (i.e. for  $dP_0$ ,  $dP_\infty$  and  $dk_1$ ) using a linear least squares method.<sup>2</sup> The computed correctors improved estimates of  $P_0$ ,  $P_\infty$  and  $k_1$ , i.e.  $P_0(\text{improved}) = P_0(\text{previous}) + dP_0$ . Improved  $P_t(\text{calc})$  at time  $t$  is obtained from equation 2.13 and compared to the observed absorbance  $P_t(\text{obs})$ . If the agreement between  $P_t(\text{calc})$  and  $P_t(\text{obs})$  is poor, the cycle is repeated until either  $\sum [P_t(\text{obs}) - P_t(\text{calc})]^2$  is at a minimum or is comparable to the magnitude of the estimated experimental precision. The analysis is complete and estimates of  $P_0$ ,

$P_{\infty}$  and  $k_1$  together with their standard errors are obtained.

### 2.3.3 Spectrophotometric apparatus

The Pye Unicam SP 800 spectrophotometer monitored the absorbances of solutions in the ultraviolet/visible region (200-750 nm). The spectrophotometer was capable of measuring the change in absorbance with time over a pre-set range of up to 400 nm. Such repeat wavelength scans provided information concerning  $\lambda_{\max}$  useful in subsequent kinetic analysis using the SP 1800 spectrophotometer. They also provided a useful check that the reactions went to completion and allowed detection of the existence of isosbestic points. The cell compartments were thermostatted by circulating water at constant temperature. This was achieved by means of a water bath with a contact thermometer and relay-controlled heater.

The Pye Unicam SP 1800 ultraviolet/visible spectrophotometer measured the change in absorbance with time of solutions at a single wavelength in the region 190-820 nm. It was capable of handling up to three sample cells and three reference cells. The sample cells were housed in an insulated copper cell block cooled by circulating water and thermostatted by means of a heater coil and platinum resistance thermometer connected to a Wheatstone bridge. The electronically controlled thermostat unit was linked to a digital thermometer which gave readings from the temperature probe in the cell carriage to an accuracy of  $\pm 0.005$  K. The spectrophotometer was connected to a Microprocessor Instrumentation of Kinetic Experiments interface which was in turn connected to a Hewlett-Packard 9825A (24 K) minicomputer via a digital voltmeter. The minicomputer was also connected to a Hewlett-Packard 7245A plotter. The Hewlett-Packard BASIC program written by Dr. M. J. Blandamer controlling the complete system required certain information before initiation of a

kinetic run. This information included estimated values of the initial and final absorbance readings and rate constant, the number of readings before calculation of a rate constant and the number of readings between consecutive calculations. During a kinetic run, absorbance and time data for each cell were stored in the computer's memory and printed out by a thermal printer. After monitoring each cell for at least 2.5 half lives the minicomputer calculated the final values of the first-order rate constant, initial and final absorbance readings using a non-linear least squares procedure. First-order plots were obtained at the end of each analysis from the plotter connected to the minicomputer.

#### 2.4 <sup>1</sup>H NUCLEAR MAGNETIC RESONANCE SPECTRA

The iron(II) Schiff base complexes prepared especially for use in the <sup>1</sup>H nmr study were obtained as the hexafluorophosphate salts of the complexes. These salts were obtained using a modified version of the general method of preparation, modified method (V), which is described in Chapter 6 (Section 6.2). This choice of anion reflected the increased solubilities of the PF<sub>6</sub><sup>-</sup> salts of the complexes in d<sub>3</sub>-acetonitrile. The samples of the complexes in d<sub>3</sub>-acetonitrile were made as concentrated as possible. <sup>1</sup>H nmr spectra were first obtained using a Varian EM 390 (90 MHz) spectrometer with tetramethylsilane (TMS) as the internal reference. Where appropriate, <sup>1</sup>H nmr spectra of the samples were then obtained using a Bruker AM 300 (300 MHz) spectrometer. All spectra, unless otherwise stated, were measured at room temperature.

#### 2.5 SOLUBILITIES OF SALTS OF IRON(II) COMPLEXES

Measurements of solubilities were made using the Pye Unicam SP8 100

spectrophotometer.

Solubilities of salts were measured by the preparation of saturated solutions of the salts in solvents of given composition (for binary aqueous solvent mixtures, solvent compositions were described in terms of x vol % co-solvent, see Section 2.2.1) and subsequent spectrophotometric estimation of the absorbances of the solutions at values of  $\lambda_{\max}$  in the visible region. Saturated solutions were prepared by agitation of an excess of solid with the solvent in a thermostatted vessel for several hours. An aliquot of the saturated solution was removed, diluted when necessary to give an absorbance reading of approximately 1, and its absorbance at  $\lambda_{\max}$  measured. In cases where all the excess solid in the vessel containing the saturated solution was not settled on the bottom of the vessel, the solution was centrifuged. Solubility measurements were made at 298.2 K.

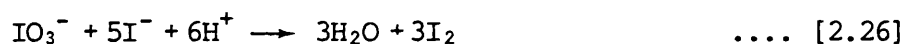
The absorbance of a single substance A in dilute solution at wavelength  $\lambda$  is related to the concentration of A, [A] given in  $\text{mol dm}^{-3}$ , by the Beer-Lambert Law, see equation 2.25, where  $\epsilon_{\lambda}$  is the extinction

$$P = \epsilon_{\lambda} \ell [A] \quad \dots [2.25]$$

coefficient of A at wavelength  $\lambda$ , given in  $\text{mol}^{-1} \text{dm}^3 \text{cm}^{-1}$ , and  $\ell$  is the pathlength in cm.

## 2.6 SOLUBILITY OF KIO<sub>3</sub> IN WATER + ETHANOL MIXTURES

The solubility of potassium iodate in water + ethanol mixtures was determined by volumetric analysis. Free iodine liberated by the reaction of potassium iodate with an excess of potassium iodide in acidified solution (equation 2.26) was titrated with standard sodium thiosulphate solutions (equation 2.27). The indicator used in the



titrations was starch solution. With free iodine, starch solution produces a deep blue colouration, the blue colour disappearing as soon as sufficient sodium thiosulphate has been added to react with all the iodine.

Saturated solutions of potassium iodate in water + ethanol mixtures were prepared by agitating excess of the solid with the appropriate solvent mixture in a darkened, thermostatted vessel. The solvent composition scale used was volume percentage of ethanol in the solvent mixture, x vol % EtOH. The definition of x vol % EtOH was given in Section 2.2.1. Starch indicator was prepared by mixing 1g of starch with water to form a thin paste. The paste was poured into about 250 cm<sup>3</sup> of boiling water, boiled for 2 or 3 minutes and then cooled for use. Each titrimetric run was carried out as follows. Ensuring that the undissolved solid was settled on the bottom of the vessel, 2 cm<sup>3</sup> of the saturated KIO<sub>3</sub> solution was removed by pipette and diluted to 25 cm<sup>3</sup>. Excess potassium iodide was added and the solution was acidified with dilute sulphuric acid (see equation 2.26). The sodium thiosulphate solution was run into the potassium iodate solution from a burette until the colour of the latter changed to pale yellow. Then a few drops of starch solution were added producing a blue colouration. Further drop-by-drop addition of the thiosulphate solution was continued until the blue colouration disappeared.

Before the solubility of potassium iodate in water + ethanol mixtures was determined by titration, a preliminary titrimetric investigation was undertaken. A reported value of the solubility of KIO<sub>3</sub> in water was used to estimate the required molarity of a sodium thiosulphate solution that would result in the use of 25 cm<sup>3</sup> of the solution when it was titrated with 2 cm<sup>3</sup> of the saturated aqueous KIO<sub>3</sub> solution. Preliminary

titrations were carried out using a sodium thiosulphate solution of this molarity (0.1934 M) to ascertain the approximate volumes of the solution used in titrations with 2 cm<sup>3</sup> of saturated solutions of potassium iodate in the water + ethanol mixtures. From these measurements the molarities of sodium thiosulphate solutions needed to result in the use of 25 cm<sup>3</sup> titres of the solutions when they were titrated against 2 cm<sup>3</sup> of the saturated solutions of KIO<sub>3</sub> in water + ethanol mixtures were estimated.

Values for the solubility of potassium iodate in water + ethanol mixtures obtained were the average of least four titrimetric runs. The accuracy of the analysis procedure had been checked by titration of solutions of known concentration of KIO<sub>3</sub> in varying water + ethanol mixtures against standardized sodium thiosulphate solutions. Sodium thiosulphate solutions had been standardized by titration with potassium permanganate. The error involved was less than 1%.

REFERENCES FOR CHAPTER 2

1. P. Moore, J. Chem. Soc., Faraday Trans. I, 1972, 68, 1890.
2. D. Z. Arbritton and A. L. Schmeltekoft, "Modern Spectroscopy, Modern Research II", ed. K. N. Rao, Academic Press, New York, 1976.



# CHAPTER 3

**Solvation of Ions in Water  
+ Ethanol Mixtures**

### 3.1 INTRODUCTION

#### 3.1.1 Background

There is much work in the literature concerned with the investigation of the solvation characteristics of inorganic ions in binary aqueous mixtures by means of studying the transfer chemical potentials of ions in these systems. In these cases the transfer chemical potential of an ion,  $\delta_{ml}^{\ominus}$ , is the change in its chemical potential upon transference from water to a water + co-solvent mixture. Therefore it would not seem to be, at first sight, a difficult task to bring together the available data for any one binary solvent system in order to produce a comprehensive study comparing the solvation characteristics of ions in that system. This, however, is not the case. A closer inspection reveals a diversity in the methods of measurement and subsequent calculation of the transfer parameters for single ions such that casual comparison of the reported values could be at best misleading and at worst meaningless.

The majority of the relevant work in the literature is based on solubility and electrochemical data for salts from which the transfer parameters of the salts can be calculated. The derivation of single-ion transfer parameters from those calculated for salts can be achieved only by the introduction of an extrathermodynamic assumption. [This is in contrast to certain other techniques such as nmr spectroscopy which, under certain conditions, yield single-ion transfer properties.] There are over 20 such extrathermodynamic assumptions quoted in the literature and agreement between estimates for a given ion derived using different extrathermodynamic assumptions ranges from good to poor. That the single-ion values obtained depend on the assumption used has meant that the comparative worths of the different assumptions have been a hotly

disputed subject of discussion. The failure, as yet, to prove unequivocally the superiority of one or more of the methods over the rest means that the comparison of single-ion values derived using different extrathermodynamic assumptions is undesirable and, indeed, uninformative at anything other than a very superficial level. [It should be remembered that the differences between  $\delta_{m\mu}^{\ominus}$  (ion) values for ions of identical charge are independent of single-ion assumptions.]

Even in cases where authors have incorporated the same extrathermodynamic assumption into their analysis the problem is not entirely eliminated. Reported transfer parameters may be on the molal, molar or mole fraction scale depending on the composition scale used when the concentration of the salt was measured. These solute composition scales are used variously by different authors depending on the use to which the data are to be put. For thermodynamic treatments the molal rather than the molar scale is preferable to avoid concentration being a function of T and p. For treatments linking thermodynamic and kinetic data the molar scale is favoured. In the present case, standard transfer parameters on the molar scale are most apt as they provide a direct measure of the interaction of the solute with the solvent. This is because they are devoid of any contribution from the translational degree of freedom of the solute.<sup>1</sup> Conversion between these scales is fairly straightforward but tedious. This also applies to the binary aqueous solvent composition scale which can be measured in terms of weight percentage, volume percentage or mole fraction of co-solvent. Methods used by different authors to describe a given solution also differ.

It would seem, therefore, that the soundest way of producing a useful study of the solvation of ions in a given binary solvent system using

the data available in the literature would be to calculate single-ion transfer parameters from the basic solubility and electrochemical measurements for salts given therein using the same solute composition scale, solvent composition scale and extrathermodynamic assumption throughout.

This is what has been attempted here for a range of simple and complex ions in water + ethanol mixtures. Transfer chemical potentials were calculated on the molar composition scale for solutes and the weight percentage ethanol composition scale for the mixed solvents. The extrathermodynamic assumption used in the analysis was the tetraphenylarsonium tetraphenylboronate (TATB) assumption.

### 3.1.2 Extrathermodynamic assumptions

The many methods which have been proposed for splitting transfer parameters for salts into their ionic contributions all require the use of extrathermodynamic assumptions. These methods and the assumptions they involve have been reviewed by several authors.<sup>2,3,4,5</sup> Some of the earlier methods are now generally discredited whilst assessment of the relative values of others awaits further testing.

Many of the proposed methods involve the development or modification of earlier suggestions so it is possible to group the methods into a number of basic categories. This was done recently by Marcus<sup>6</sup> who outlined the following categories:

- ( i) the determination of 'real' potentials;
- ( ii) the assumption of a negligible liquid junction potential;
- (iii) electrostatic models;
- ( iv) extrapolation methods;
- ( v) the assumption of a constant Gibbs free energy of solvation of a reference ion;

- (vi) the assumption that a reference ion and its uncharged analogue have the same difference in Gibbs free energies of transfer in a given solvent system;
- (vii) the assumption that a reference cation and a reference anion have the same Gibbs free energy of transfer in a given solvent system.

The TATB assumption belongs to the last category in this list. In this assumption tetraphenylarsonium tetraphenylboronate is the reference electrolyte and the transfer chemical potential of the cation,  $\text{Ph}_4\text{As}^+$ , is equated to that of the anion,  $\text{BPh}_4^-$ . Such pairs of reference ions need to be large, symmetrical ions of similar size and structure. The central atom and the charge thereon are buried under large organic residues in order to minimise specific interactions with the solvent and the surface charge density. This method was first proposed by Grunwald *et al.*<sup>7</sup> using tetraphenylphosphonium tetraphenylboronate ( $\text{Ph}_4\text{PPh}_4$ ) as the reference electrolyte. Alternative electrolytes were later suggested, i.e.  $\text{Ph}_4\text{AsBPh}_4$ <sup>8</sup> and  $\text{TABBPh}_4$ <sup>9</sup> (where  $\text{TAB}^+$  is the tri-isoamyl-n-butylammonium cation). This approach to the estimation of single-ion transfer parameters has been used and discussed by a number of authors<sup>8-14</sup> and the use of TATB as the reference electrolyte has been the subject of several critical studies.<sup>15-17</sup> In discussing the relative merits of proposed extrathermodynamic assumptions, Marcus<sup>6</sup> reached the conclusion that the reference electrolyte method has the strongest conceptual basis and that the TATB assumption is the most favourable method available for deriving single-ion transfer parameters.

### 3.1.3 Methods used by other authors

In addition to the single-ion transfer parameters presented here derived using the TATB assumption, corresponding values for ions calculated by authors using different data or a different extrathermo-

dynamic assumption are included, where available, for comparison.

These are most commonly taken from the works of Popovych and Dill,<sup>18</sup> C. F. Wells<sup>19</sup> and Bax, de Ligny and Remijnse.<sup>20</sup>

Popovych and Dill<sup>18</sup> employed the TABTB assumption in the same manner as the TATB assumption used here. Their choice of reference electrolyte was based on the equality of the Stokes radii of its ions in water and in ethanol.

The set of single-ion parameters presented by Wells<sup>19</sup> was derived from experimentally determined values for  $\Delta G_t^\ominus(\text{H}^+)$ . This free energy of transfer of the proton was considered to be the sum of two contributions. Firstly, the free energy of transfer of the aqua-proton from  $\text{H}_2\text{O}$  into the solvent mixture, which was calculated by means of the Born equation. Secondly, the free energy due to rearrangement of the solvent molecules after transference, which was derived using spectroscopic measurements on p-nitroaniline in  $\text{H}_2\text{O} + \text{ethanol}$ . Wells has used this approach in studying ionic solvation in several binary aqueous solvent mixtures other than water + ethanol.<sup>21-25</sup> It appears, however, that this series is marred by certain ambiguities and inconsistencies. These problems, including uncertainty as to the exact nature of the entity being transferred, the non-rigorous approach to the definition of activity coefficients and the lack of precise indication as to extra-thermodynamic assumptions used, have been explored by Blandamer et al.<sup>26</sup> The approach is also restricted by its applicability being limited to water-rich solvent mixtures.<sup>6,21,22</sup> Wells used the  $\Delta G_t^\ominus(\text{H}^+)$  values to obtain single-ion values for anions,  $\text{X}^-$ , using electrochemical data for  $\text{HX}$ , i.e.  $\Delta G_t^\ominus(\text{X}^-) = \Delta G_t^\ominus(\text{HX}) - \Delta G_t^\ominus(\text{H}^+)$ . From these, values for cations,  $\text{M}^+$  and  $\text{M}^{2+}$ , were derived from solubility and electrochemical data for  $\text{MX}$  and  $\text{MX}_2$  salts and so on.

The method used by Bax et al.<sup>20</sup> to estimate single-ion transfer parameters from water into water + ethanol mixtures was first proposed by Alfenaar and de Ligny.<sup>27</sup> This model was based on the supposition that the transfer chemical potential of a dissolved ion,  $\Delta\mu^\ominus$ , can be split into 2 contributions  $\Delta\mu_{\text{neutral}}^\ominus$  and  $\Delta\mu_{\text{el}}^\ominus$ . The former accounts for Van der Waals interactions of the ion with the solvent and for a very large ion is taken to be equal to the chemical potential of an uncharged particle of the same physical properties.  $\Delta\mu_{\text{el}}^\ominus$  accounts for the interactions of the charge of the ion with the two solvents involved and is predicted by the Born equation. Modifications to this method were later introduced<sup>28-31</sup> to account more precisely for specific interactions such as ion-solvent quadrupole and solvent dipole-solvent quadrupole interactions. The model finally proposed concluded that for hypothetical  $M^+$  and  $A^-$  ions of equal radius the following equation holds for the transfer from one solvent to another:

$$\Delta\mu^\ominus(H^+) - \frac{1}{2}\Delta\mu^\ominus(M^+) + \frac{1}{2}\Delta\mu^\ominus(A^-) = \Delta\mu^\ominus(H^+) - C \quad \dots [3.1]$$

where C is a collection of terms describing electrostatic interactions in terms of the dipole and quadrupole moments of the two solvents, the distance between the ion and solvent molecules in the primary solvation layer and the number of coordinated solvent molecules around the  $M^+$  and  $A^-$  ions. Evaluations of the l.h.s. of equation [3.1] and of C for varying radii of component ions, r, were plotted against 1/r. Matching of the two curves and extrapolation to a common intercept yielded a value for  $\Delta\mu^\ominus(H^+)$ .  $\Delta\mu^\ominus(A^-)$  values were calculated from those of  $\Delta\mu^\ominus(H^+) + \Delta\mu^\ominus(A^-)$  and  $\Delta\mu^\ominus(M^+)$  values from  $\Delta\mu^\ominus(H^+) - \Delta\mu^\ominus(M^+)$ .

Where values reported by these and other authors are included they have all been converted to the same solute composition scale (molar) and the same solvent composition scale (weight percentage ethanol).

#### 3.1.4 Ion solvation in binary aqueous mixtures

Investigation of the solvation of ions in binary aqueous mixtures by means of thermodynamic transfer parameters be they free energies, entropies or enthalpies of transfer has been widely practised for many years. Positive values of free energies of transfer indicate that the solute exists in a higher energy state in the solvent mixture than in water. That is to say that the ion is more favourably solvated in water than in the solvent mixture.

Qualitative interpretation of these parameters requires consideration of the solvation pattern of the ions in the solvent mixtures and in the pure solvents. The interactions between the ion and each solvent must be considered as must any modifications to inter- and intra-solvent interactions caused by the presence of the ion.

There are numerous types of solute-solvent and solvent-solvent interactions, the relative importance of which may vary greatly for different ions in different solvent systems depending on the properties of both the solute and the solvent. In the case of the solute, i.e. the ions, important considerations include size, electrical properties (charge, dipole moment, polarizability), H-bonding ability and the size and relative positions of polar and apolar residues. For solvents it is important to consider the degree of association within the solvents and the nature of this association, the relative acidities of the solvents, local charge distributions and dielectric constants amongst other properties.

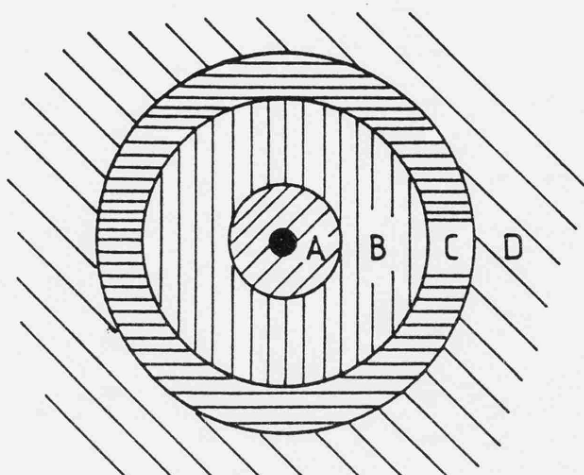
With the existence of so many possible contributory factors, single-ion transfer parameters can be interpreted in several different ways by emphasising different aspects of solvation. Thus, for example, results have been discussed in the literature in terms of Born-charging,

specific solute-solvent interactions, solvation zones and solvent structure. Authors have often described the behaviour of one set of ions in terms of certain solute and/or solvent criteria and then described that of another set of ions by totally different criteria. However, detailed analysis of the solvation of ions in terms of the balance achieved between possible contributory factors must realistically await the proposition of sets of single-ion transfer parameters that are more or less universally accepted.

In discussing specific ion-solvent interactions it is perhaps best to introduce the concept that the solvation energy of an ion is made up of an electrostatic contribution and a neutral contribution.<sup>32</sup> Many authors have used this proposition to calculate the solvation energies of ions.<sup>7,33-35</sup> The electrostatic component consists of contributions due to Born-charging and to short-range specific solute-solvent interactions. These short-range terms include ion-dipole, ion-quadrupole and ion-induced dipole interactions. The neutral component consists of energy contributions that would be present even if the solute molecule was uncharged. This consists of the free energy required to create a cavity of suitable size to accommodate the solute molecule and a contribution due to other specific solute-solvent interactions including dipole-dipole, dipole-quadrupole and dispersion interactions.

The general picture describing the environment of an ion in aqueous solution can be depicted as shown in (I).<sup>10,36,37</sup>

(A) is the primary solvation shell around the ion (●). The water molecules in this solvation zone interact or bond directly with the ion. In this region dielectric saturation occurs. Contributions to the solvation energy in this zone are a function of the coulombic interaction between the ion and the charge on the oxygen atom of the water molecule



(I)

in the case of a cation, or between the ion and the charge on the hydroxyl hydrogen for an anion.<sup>38</sup>

Zone (B) is the region of secondary solvation in which field-induced molecular orientation may be strongly assisted by H-bonded correlation with water molecules in the primary solvation shell. Dielectric saturation may occur in this region. The ion and solvent molecules are far enough apart for the contribution to the solvation energy to be considered as that given for the interaction between a point charge and a structureless dipole.<sup>38</sup>

Zone (C) is a disordered region or 'fault zone' separating the ordered (A) and (B) regions from the differently ordered region (D). The volumes of regions (B) and (C) depend on the nature of the ion involved.

Zone (D) is the bulk solvent and in this region the distance from the centre of the ionic charge is great enough and the ionic field is weak enough for any contribution to the solvation energy to be computed by Born-charging.<sup>38</sup>

Ions that are 'structure-breakers' will have a relatively small structure-making region, i.e. small (A) and (B) zones whereas 'structure-

making' ions will have relatively small (C) zones.

This general picture also holds for the solvation of ions by ethanol. For water + ethanol mixtures the ratio of solvent molecules of each type in regions (A) to (D) must be considered as must the effect on the solvation energy of the ion by replacing water molecules with ethanol molecules in the different zones. For example, for smaller ions in particular there will be a steric effect which will favour the occupation of the primary zone by water molecules rather than bulkier alcohol molecules. This will be more pronounced the larger the alkyl group in the alcohol.

Interpretation of single-ion transfer parameters involving references to solvent structure requires some consideration of the structure of liquid water, ethanol and water + ethanol mixtures.

Water is a highly associated liquid due to its H-bonding ability. A water molecule is able to form four approximately tetrahedrally disposed H-bonds around the oxygen atom.<sup>36</sup> The oxygen atom can act twice as donor (H-bonding from its two hydrogen atoms) and twice as acceptor (H-bonding to its two lone pairs). The co-operative nature of this bonding, i.e. that the mutual polarization of the participating molecules is of a kind to strongly facilitate further bonding, results in the formation of short-lived but tetrahedrally structured H-bonded clusters.

Lumry et al.<sup>39</sup> proposed that water consists of a random network of H-bonded molecules, termed the long bond form, in which are embedded the structured H-bonded units, termed the short bond form. The minimum cluster is the pentamer or tetramic fragment which allows simultaneous bond contraction with increased bond lengths to the central water molecule. These water molecules are linked by short, stiff, linear H-bonds

and this rigid geometry increases the free volume much of which is available to solutes. In the long bond form, molecules are held together by simple H-bonds having the strength associated with water dimers. The increase in bending, librational and rotational freedom means that the free volume decreases and becomes less available to solutes. The fluctuation between the short bond and long bond forms is termed 'geometric relaxation'. Lumry et al.<sup>39</sup> estimated that at 295 K only about 10% of the water molecules are in the short bond form, the rest being part of the long H-bonded network.

Alcohols, like water, are also associated in the liquid state although not to the same extent. Although theoretically each alcohol molecule is capable of forming three H-bonds (twice acting as donor, once as acceptor) it appears to form no more than two (acting once as donor, once as acceptor). Thus the formation of three-dimensional clusters like in water is not possible in alcohols. Instead there is a rapid equilibrium between very short-lived polymeric chains of assorted but finite length having a degree of rigidity due to appreciable hindrance of internal rotation.

The excess Gibbs free energy of mixing for water + ethanol mixtures is positive and nearly symmetrical about  $x_{\text{EtOH}} = 0.5$  being a function of the negative and unsymmetrical excess enthalpy and excess entropy of mixing. It is generally accepted that addition of small quantities of ethanol to water leads to structure enhancement in the mixture relative to that in water. The alcohol molecules are believed to occupy the cavities in the water clusters and to stabilize the structure. This stabilization increases until a point is reached when no more ethanol molecules can be accommodated in the cavities and after this a progressive decrease in structure in the mixture ensues with the continued

addition of alcohol.

## 3.2 METHOD

### 3.2.1 Description of the system and definitions of standard states

Consider a system containing three components, 1, 2 and 3, at equilibrium at temperature  $T$  and ambient pressure  $p$  ( $\approx p^\ominus$ ). The total Gibbs function,  $G$ , of the system is given by equation 3.2, where  $n_x$  and  $\mu_x$  are the number of moles of  $x$  and the chemical potential of  $x$  respectively.

$$G^{\text{eq}}(T) = n_1\mu_1^{\text{eq}}(T) + n_2\mu_2^{\text{eq}}(T) + n_3\mu_3^{\text{eq}}(T) \quad \dots [3.2]$$

The system consists of a solvent, a mixture of components 1 and 2, having constant composition independent of  $n_3$  and a solute, component 3. The chemical potential of  $j$ , where  $j = 1$  or  $2$ , is given by equation 3.3, where  $\text{Limit}(x_j \rightarrow 1.0)$ , the activity coefficient,  $f_j = 1.0$  at all  $T$  and  $p$ .  $\mu_j^*(l)$ , the reference state for the solvent component, is the

$$\mu_j = \mu_j^*(l) + RT \ln(x_j f_j) \quad \dots [3.3]$$

chemical potential of the pure liquid  $j$  at the same  $T$  and  $p$ .

The chemical potential of the solute,  $\mu_3$ , is related to the concentration,  $c_3$ , by equation 3.4, where  $\text{Limit}(c_3 \rightarrow 0)$ , the activity coefficient on the concentration scale,  $\gamma_3 = 1.0$  at all  $T$  and  $p$ . The definition of  $\gamma_3$  requires that the properties of component 3 approach ideal as the system becomes infinitely dilute in component 3.  $\mu_3^\ominus$  is

$$\mu_3 = \mu_3^\ominus + RT \ln\left(\frac{c_3 \gamma_3}{c_r}\right) \quad \dots [3.4]$$

the standard chemical potential of 3 in a solvent "1+2" where  $c_3 = 1$  and  $\gamma_c = 1$  at the same  $T$  and  $p$ .  $c_r$  is a reference molarity ( $1 \text{ mol dm}^{-3}$ ).

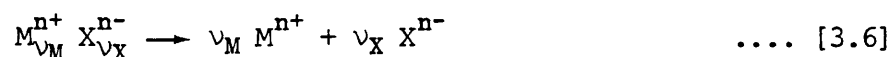
Consider the transfer of solute 3 from water ( $x_2 = 0$ ) into a solvent of mole fraction  $x_2$ . In such a case the transfer chemical potential of the solute,  $\delta_m \mu_3^\ominus$ , is defined as the difference between the standard

chemical potentials of solute 3 in the solvent mixture of composition  $x_2$  and in water, i.e.  $x_2 = 0$  (see equation 3.5). The reference state,

$$\delta_m \mu_3^\ominus ([x_2 = 0] \rightarrow x_2) = \mu_3^\ominus(x_2) - \mu_3^\ominus(x_2 = 0) \quad \dots [3.5]$$

i.e. solvent,  $x_2 = 0$  is taken as comprising solute 3 in solvent 1 and changes in standard chemical potentials of 3 arise as substance 2 is added (i.e.  $x_2 > 0$ ).

Extending the description of the system, let substance 3 be a salt such that, complete dissociation of one mole of the salt yields  $\nu_M$  moles of cations,  $M^{n+}$ , and  $\nu_X$  moles of anions,  $X^{n-}$  (equation 3.6).



The transfer chemical potential of the salt,  $\delta_m \mu_3^\ominus$ , is related to the transfer parameters of the constituent ions,  $\delta_m \mu_+^\ominus$  and  $\delta_m \mu_-^\ominus$ , by equation 3.7.

$$\delta_m \mu_3^\ominus = \nu_M \delta_m \mu_+^\ominus + \nu_X \delta_m \mu_-^\ominus \quad \dots [3.7]$$

### 3.2.2 Calculation of transfer chemical potentials for salts

The data used in this study had been presented in the literature in various forms - solubilities, solubility products, medium effects, free energies of transfer, transfer chemical potentials, etc. Each set of data selected from the literature was systematically processed, where necessary, to yield transfer chemical potentials,  $\delta_m \mu^\ominus$ , for salts in  $\text{kJ mol}^{-1}$  on the molar composition scale for the solute and the weight percentage ethanol composition scale for the solvent. Where both solubilities and solubility products were available for a given salt, the transfer parameters were calculated using the more rigorous solubility products. Transfer chemical potentials were calculated from solubilities (soly) using equation 3.8, from solubility products ( $K_{sp}$ ) using equation 3.9 and from medium effects ( $\log_m \gamma_{\pm}^2$ ) for 1:1 electro-

lytes using equation 3.10.

$$\delta_{m\mu}^{\ominus}(\text{salt}) = -\nu RT \ln \left[ \frac{\text{soly}(\text{mixture})}{\text{soly}(\text{water})} \right] \quad \dots \quad [3.8]$$

$$\delta_{m\mu}^{\ominus}(\text{salt}) = -RT \ln \left[ \frac{K_{sp}(\text{mixture})}{K_{sp}(\text{water})} \right] \quad \dots \quad [3.9]$$

$$\delta_{m\mu}^{\ominus}(\text{salt}) = 2.303 RT (\log_m \gamma_{\pm}^2) \quad \dots \quad [3.10]$$

In equation 3.8,  $\nu$  is the stoichiometry of the salt, i.e. 2 for a 1:1 salt, 3 for a 1:2 salt, etc., and (mixture) refers to the binary solvent.

To produce transfer parameters on the molar scale, only solubilities given in moles per litre of solution could be used in equation 3.8.

For solubilities quoted in grams per gram of solvent or grams per gram of solution, the conversion to solubility in moles per litre of solution was straightforward and accurate if the density of the saturated solution was available. When these densities were not available there were two alternative assumptions that could be made in calculating the solubility in terms of moles per litre of solution and subsequent transfer chemical potentials:

( i) density of solution = density of solvent

(ii) total volume of solution = volume of solvent + volume of solid.

Wherever possible assumption (ii) was used. Obviously, using this assumption, the more soluble the salt the less accurate the resulting transfer parameters were likely to be. In these cases, as with all the solubility data, the calculation of transfer chemical potentials was limited to the solvent composition range in which the composition of the solid phase remained the same as that in water.

For salts whose transfer parameters had been presented in the literature on the molal scale,  $\delta_{m\mu}^{\ominus}(m)$ , or mole fraction scale,  $\delta_{m\mu}^{\ominus}(x)$ , the conversion to the molar scale,  $\delta_{m\mu}^{\ominus}(c)$ , was effected using equations

3.11 and 3.12 respectively.

$$\delta_m \mu^{\ominus}(c) = \delta_m \mu^{\ominus}(m) - \nu RT \ln \left[ \frac{\rho(\text{mixture})}{\rho(\text{water})} \right] \quad \dots [3.11]$$

$$\delta_m \mu^{\ominus}(c) = \delta_m \mu^{\ominus}(x) - \nu RT \ln \left[ \left( \frac{100-w_2}{M_1} + \frac{w_2}{M_2} \right) M_1 \frac{\rho(\text{mixture})}{\rho(\text{water})} \right] \quad \dots [3.12]$$

In equations 3.11 and 3.12,  $\rho(\text{mixture})$  and  $\rho(\text{water})$  are the densities of the solvent mixture and water respectively. In equation 3.12,  $M_1$  is the molar mass of water,  $M_2$  that of ethanol and  $w_2$  is the weight percentage of ethanol in the solvent mixture.

Throughout the study the densities of the ethanol + water mixtures used were those measured by Bruun et al.<sup>40</sup> and the densities of solids were taken from the 'Chemical Rubber Handbook'.<sup>41</sup>

Unless otherwise stated all the data were derived from measurements made at 298.2 K.

### 3.2.3 Application of the TATB assumption

Having calculated sets of transfer chemical potentials for salts all on the molar scale and all on the same solvent composition scale, the TATB assumption was introduced. As this yielded single-ion values for  $\text{Ph}_4\text{As}^+$ ,  $\text{BPh}_4^-$ ,  $\text{K}^+$  and  $\text{Pic}^-$ , ( $\text{Pic}^-$  = picrate ion), from which all other single-ion values were directly or indirectly calculated, the need for accurate transfer chemical potentials of the parent electrolytes  $\text{Ph}_4\text{AsPic}$ ,  $\text{KBPh}_4$  and  $\text{KPic}$  was imperative. These transfer parameters were derived from solubility products that had been calculated for  $\text{Ph}_4\text{AsPic}$  by Berne and Popovych<sup>42</sup> and for  $\text{KBPh}_4$  and  $\text{KPic}$  by Dill and Popovych.<sup>43</sup>

The transfer chemical potentials were calculated for these electrolytes from both solubilities and solubility products using equations

3.8 and 3.9 respectively. Values of  $\delta_{m\mu}^{\ominus}$  from 10 to 100 wt % ethanol at exactly 10 wt % ethanol intervals were interpolated from large scale plots of  $\delta_{m\mu}^{\ominus}$  vs. wt % ethanol for the 3 electrolytes. The  $\delta_{m\mu}^{\ominus}$  values were read from the curve derived from solubility products, the curve derived from the less accurate solubilities being included solely as an aid to drawing the best curve.

Single-ion values for  $\text{Ph}_4\text{As}^+$  and  $\text{Ph}_4\text{B}^-$  were then calculated using equation 3.13.

$$\begin{aligned} \delta_{m\mu}^{\ominus}(\text{Ph}_4\text{As}^+) &= \delta_{m\mu}^{\ominus}(\text{BPh}_4^-) \\ &= \frac{\delta_{m\mu}^{\ominus}(\text{Ph}_4\text{AsPic}) + \delta_{m\mu}^{\ominus}(\text{KBPh}_4) - \delta_{m\mu}^{\ominus}(\text{KPic})}{2} \end{aligned} \quad \dots [3.13]$$

From these values and using equations 3.14 and 3.15,  $\delta_{m\mu}^{\ominus}(\text{Pic}^-)$  and  $\delta_{m\mu}^{\ominus}(\text{K}^+)$  were calculated.

$$\delta_{m\mu}^{\ominus}(\text{Pic}^-) = \delta_{m\mu}^{\ominus}(\text{Ph}_4\text{AsPic}) - \delta_{m\mu}^{\ominus}(\text{Ph}_4\text{As}^+) \quad \dots [3.14]$$

$$\delta_{m\mu}^{\ominus}(\text{K}^+) = \delta_{m\mu}^{\ominus}(\text{KBPh}_4) - \delta_{m\mu}^{\ominus}(\text{BPh}_4^-) \quad \dots [3.15]$$

### 3.2.4 Derivation of single-ion transfer parameters

Using the single-ion values derived in equations 3.13, 3.14 and 3.15 and  $\delta_{m\mu}^{\ominus}$  values calculated for salts containing  $\text{BPh}_4^-$ ,  $\text{Pic}^-$  or  $\text{K}^+$  ions, transfer chemical potentials of the counter ions, Y, were calculated using equations 3.16 or 3.17.

$$\delta_{m\mu}^{\ominus}(\text{Y}^-) = \delta_{m\mu}^{\ominus}(\text{XY}) - \delta_{m\mu}^{\ominus}(\text{X}^+) \quad \dots [3.16]$$

$$\delta_{m\mu}^{\ominus}(\text{Y}^+) = \delta_{m\mu}^{\ominus}(\text{YZ}) - \delta_{m\mu}^{\ominus}(\text{Z}^-) \quad \dots [3.17]$$

where  $\text{X}^+ = \text{K}^+$ , then  $\text{Y}^- = \text{Cl}^-$ ,  $\text{Br}^-$ ,  $\text{I}^-$ ,  $\text{ClO}_4^-$ ,  $\text{NO}_3^-$ ,  $\text{CN}^-$ ,  $\text{IO}_3^-$ ,  $\text{ClO}_3^-$ ,  $\text{OAc}^-$  (acetate),  $\text{H tart}^-$  (hydrogen tartrate),  $\text{Sbtart}^-$  (antimonyl tartrate),  $\text{N2S}^-$  (naphthalene- $\beta$ -sulphonate),  $\text{SO}_4^{2-}$ ,  $[\text{PtCl}_6]^{2-}$ ,  $[\text{SiF}_6]^{2-}$ ,  $\text{cit}^{3-}$  (citrate),  $[\text{Co}(\text{NO}_2)_6]^{3-}$

where  $\text{Z}^- = \text{Pic}^-$ , then  $\text{Y}^+ = \text{Na}^+$ ,  $\text{Ph}_4\text{P}^+$ ,  $\text{TAB}^+$ ,  $\text{Ba}^{2+}$

where  $\text{Z}^- = \text{BPh}_4^-$ , then  $\text{Y}^+ = \text{TAB}^+$ ,  $\text{Hg}^{2+}$ .

References indicating the source of the data for the appropriate salts are given in Section 3.3.2 where the behaviour of each ion is discussed individually.

In cases where the transfer values for the salt had been measured at anything other than 10 wt % ethanol intervals, large scale plots of  $\delta_{m\text{Li}}^{\ominus}$  vs. wt % ethanol for  $\text{K}^+$ ,  $\text{Pic}^-$  and  $\text{BPh}_4^-$  were used to interpolate the transfer chemical potentials at the required ethanol content.

Those counter ions whose transfer parameters could be calculated in one step from those of  $\text{K}^+$ ,  $\text{Pic}^-$  or  $\text{BPh}_4^-$  and the salt were termed 'one-step' derivatives.

From these, values for another set of ions termed 'two-step' derivatives were calculated. These were derived from transfer parameters of salts in which the counter ion was a 'one-step' derivative. Thus two calculations were required in all to obtain these single-ion values using those of the salt, the one-step derivative and of  $\text{K}^+$ ,  $\text{Pic}^-$  or  $\text{BPh}_4^-$ . Such 'two-step' derivations yielded values for  $\text{H}^+$ ,  $\text{Li}^+$ ,  $\text{Na}^+$ ,  $\text{Rb}^+$ ,  $\text{Cs}^+$ ,  $\text{Me}_4\text{N}^+$ ,  $n\text{-Pr}_4\text{N}^+$ ,  $n\text{-Bu}_4\text{N}^+$ ,  $\text{Ag}^+$ ,  $\text{Tl}^+$ ,  $\text{Ca}^{2+}$ ,  $\text{Ba}^{2+}$ ,  $\text{Pb}^{2+}$ ,  $\text{Zn}^{2+}$ ,  $\text{OAc}^-$ ,  $\text{trans-}[\text{Co}(\text{en})_2\text{Cl}_2]^+$ ,  $[\text{Fe}(\text{phen})_3]^{2+}$ ,  $[\text{Fe}(\text{bipy})_3]^{2+}$ ,  $[\text{Co}(\text{NH}_3)_5\text{Cl}]^{2+}$ ,  $\text{cis-}[\text{Co}(\text{NH}_3)\text{Br}(\text{en})_2]^{2+}$  and  $[\text{Fe}(\text{bsb},\text{Ph},\text{Ph};\underline{\text{m}}\text{-OMe})_3]^{2+}$  where (bsb,Ph,Ph;m-OMe) is the bidentate Schiff base made from 2-benzoyl pyridine and m-methoxy-aniline.

'3-Step' derivations gave values for  $\text{A2S}^-$  (anthraquinone-2-sulphonate),  $\text{ox}^{2-}$  (oxalate),  $\text{S}_2\text{O}_3^{2-}$ ,  $\text{S}_2\text{O}_6^{2-}$  and  $[\text{ReCl}_6]^{2-}$ .

Again, the references for the sources of data for the appropriate salts are given in Section 3.3.2.

In some cases more than one route could be used to obtain single-ion transfer parameters for the same ion which could then be compared.

### 3.2.5 Accuracy of results

There are two main sources of error in the transfer chemical potentials derived as outlined earlier. The first concerns the accuracy of the data used, the second results from the introduction of various assumptions in calculating the transfer parameters from these data.

Transfer chemical potentials are a measure of solute-solvent interactions. As such, solute-solute interactions should ideally make no contribution to these parameters. With increased solubility of electrolytes it becomes necessary to take into account such ion-ion interactions in order to maintain this criterion. This means that the accuracy of solubility or electrochemical data depends not only on the experimental procedures but also on the inclusion of such parameters as activity coefficients, ion-pair association constants, etc. The use of data which contain no correction for ion-ion interactions amounts to adoption of the assumption that for a given salt the ratio of the mean ionic activity coefficients in the mixed solvent and in water is unity. This is acceptable for sparingly soluble salts whose solubility decreases with increasing ethanol content of the binary aqueous mixture. In these cases the reduction in validity of the approximation as the dielectric constant of the solvent mixture decreases is accompanied by the compensatory trend of reduced solubility of the electrolyte. For salts whose solubility increases with increasing co-solvent content of the mixture the approximation is still judged to be tenable in water-rich mixtures,<sup>26</sup> at least for moderately soluble salts.

Accuracy in calculating the transfer chemical potentials on the molar scale from data given in the literature is dependent on the solute composition scale of the data. This accuracy varies with the solubility of the electrolyte. For example, calculations of transfer chemical

potentials (molar scale) from basic data (molar scale) is accurate and straightforward. Calculation of transfer parameters (molar scale) from solubility data (molal scale) is accurate if the densities of the saturated solutions are known. For solutions for which no densities are available, the accuracy of conversion to the molar scale is dependent on the solubility of the salt. Calculation of transfer parameters (molar scale) from those on the molal scale is accurate only for sparingly soluble salts.

The wide range of sources used in this study in calculating transfer chemical potentials meant that all these alternative routes were used. Some insight into and assessment of these routes and the assumptions they involve is attempted in the following discussion.

For solubility data given in g/100g soln. it is possible, if the densities of the solution are known, to calculate transfer chemical potentials (molar scale) in several different ways. These values can then be compared to give an indication of the accuracy of the routes used:

- ( i) Transfer parameters (molar scale) can be calculated using equation 3.8 using solubilities in m/l calculated using the densities of solutions. This involves no assumption and thus the values obtained in this way are precise.
- ( ii) The molarity of the solutions can be calculated without the use of the relevant densities of solutions but by introducing the assumption that the volume of the solution is the sum of the volumes of the constituent solvent and solute. The transfer chemical potentials are then calculated using equation 3.8.
- (iii) The solubility of the salt given in g/100g soln. can be converted accurately to give the molality of the solution. Calculation of

transfer chemical potentials using equation 3.8 then yields values on the molal scale. Conversion of these parameters to the molar scale is effected using equation 3.11.

The assumptions involved in method (ii) and equation 3.11 are approximations that will be less accurate the more soluble the electrolyte.

Using the solubility data given for potassium hydrogen tartrate (the saturated aqueous solution of which is given as 0.03 M, reference given in Section 3.3.2) the percentage errors between the transfer chemical potentials derived using methods (i) and (ii) across the solvent composition range are less than  $\pm 0.5\%$ . Those between values calculated by routes (i) and (iii) are even smaller (less than  $\pm 0.2\%$ ).

From the solubility data for potassium antimonyl tartrate given as containing the monomeric anion (0.27 M saturated aqueous solution, reference given in Section 3.3.2) the percentage error in values calculated by method (i) and (ii) and methods (i) and (iii) is no more than  $\pm 2\%$ .

With increasing solubility of the electrolyte not only do the percentage errors in values calculated by different methods increase but it becomes apparent that this increase is greater for method (iii) than method (ii). Solubility data for potassium nitrate and lead acetate yield percentage errors of no more than  $\pm 2\%$  and  $\pm 5\%$  respectively in comparing values obtained by routes (i) and (ii). In contrast, comparison of values derived by routes (i) and (iii) gives percentage errors rising to over  $\pm 10\%$  in water-rich solvent mixtures. Thus whenever the use of both methods (ii) or (iii) was possible the former was used.

It becomes clear that with so many different sources of data measured by many different methods each requiring different conversions to produce transfer chemical potentials (molar scale) quantitative assessment of the

accuracy of the results would be difficult. The weight attached to each set of results must necessarily be partly intuitive. In view of this some of the solubilities of salts in water used in this study are given in Table 3.1. Figures in parentheses indicate the temperature at which the measurements were made if other than 298.2 K. The references for these salts are given in Section 3.3.2.

It should be remembered that any inaccuracies in single-ion transfer parameters will be perpetuated when using these values with those for a salt to derive values for the counter ion. The magnification of inaccuracies in deriving single-ion transfer parameters for ions of charge greater than one can be examined by comparing the single-ion values with those derived by a different route for the same ion.

### 3.3 RESULTS AND DISCUSSION

#### 3.3.1 Introduction

For reasons of clarity the presentation and discussion of the results of this study are given in three parts.

In the first part, Section 3.3.2, the route by which each set of transfer chemical potentials was derived is outlined. For each ion these values are compared with those derived by other authors where available. Unless otherwise stated, measurements for salts had been made at 298.2 K and values had been given on the molar scale.

In cases where alternative routes of derivation were possible for the same ion, one set of transfer chemical potentials for each ion is adopted on the basis of the discussion in Section 3.2.5 (to be discussed in terms of the general solvation pattern of ions in aqueous ethanol in the following section). These 'final' values are tabulated in Appendix A. A number of figures in this section, Section 3.3.2, compare values

TABLE 3.1

Indication of the solubilities in water (298.2 K) of some electrolytes used in this study

Salts for which the molarity of saturated aqueous solution <1		
Ph <sub>4</sub> AsPic	Ca (A2S) <sub>2</sub>	CaSO <sub>4</sub>
KPic	RbClO <sub>4</sub>	Ba (Pic) <sub>2</sub>
KBPh <sub>4</sub>	CsClO <sub>4</sub>	PbSO <sub>4</sub>
KH tart	Me <sub>4</sub> NClO <sub>4</sub>	PbCl <sub>2</sub>
BaS <sub>2</sub> O <sub>3</sub> (288 K)	n-Pr <sub>4</sub> NClO <sub>4</sub>	K <sub>2</sub> PtCl <sub>6</sub> (287 K)
Ph <sub>4</sub> PPic	n-Bu <sub>4</sub> NClO <sub>4</sub>	Cs <sub>2</sub> ReCl <sub>6</sub>
TABBPh <sub>4</sub>	AgOAc	[Co(en) <sub>2</sub> Cl <sub>2</sub> ]ClO <sub>4</sub>
TABPic	AgBrO <sub>3</sub>	[Fe(phen) <sub>3</sub> ](ClO <sub>4</sub> ) <sub>2</sub>
KN2S	AgCl	[Fe(bipy) <sub>3</sub> ](ClO <sub>4</sub> ) <sub>2</sub>
Ca ox (293 K)	TlIO <sub>3</sub>	[Fe(bsb,Ph,Ph:m-OMe)](ClO <sub>4</sub> ) <sub>2</sub>

Salts for which the molarity of saturated aqueous solution is 0.1 - 1	Salts for which the molarity of saturated aqueous solution >1
KSb tart	KNO <sub>3</sub>
KClO <sub>4</sub>	Pb(OAc) <sub>2</sub>
KIO <sub>3</sub>	KCN
KClO <sub>3</sub> (303 K)	K <sub>3</sub> cit
K <sub>2</sub> SO <sub>4</sub>	KOAc
BaS <sub>2</sub> O <sub>6</sub> (303 K)	NaOAc
NaPic	LiCl
Ba(ClO <sub>4</sub> ) <sub>2</sub> (293 K)	Li <sub>2</sub> SO <sub>4</sub> (303 K)
[Co(NH <sub>3</sub> )Br(en) <sub>2</sub> ]Br <sub>2</sub>	Li <sub>3</sub> cit
K <sub>3</sub> [Co(NO <sub>2</sub> ) <sub>6</sub> ] (287 K)	AgNO <sub>3</sub>
	Zn(OAc) <sub>2</sub>
	[Co(NH <sub>3</sub> ) <sub>5</sub> Cl]Cl <sub>2</sub>

given by different sets of authors for a particular ion. In these figures the works of several sets of authors are repeatedly referred to. For ease of reference the symbol used to denote values due to a particular set of authors is retained throughout these figures, i.e. this work (●); Wells<sup>19</sup> (□); Popovych and Dill<sup>18</sup> (○); Bax, de Ligny and Remijnse<sup>20</sup> (Δ); Dill, Itzkowitz and Popovych<sup>44</sup> (∇); Bose, Das, Das and Kundu<sup>45</sup> (◇). The figures referred to in this section (Figs. 3.1 - 3.20) are presented together at the end of the section.

In the second part, Section 3.3.3, the transfer chemical potentials calculated in this work using the TATB assumption are collated. The general solvation pattern in these mixtures is discussed in terms of a variety of factors. The figures referred to in this section (Figs. 3.21 - 3.26) are presented together at the end of the section. In these figures, plots of values for ions that are deemed to be of relatively high uncertainty due to any of the considerations outlined in Section 3.2.5 are indicated by narrower lines.

In the final part, Section 3.3.4, transfer chemical potentials of ions derived using the TATB assumption in aqueous alcohol and aqueous acetone mixtures are compared. The figures referred to in this section (Figs. 3.27 and 3.28) are presented together at the end of the section.

### 3.3.2 Transfer chemical potentials for ions in aqueous ethanol mixtures

#### *The TATB ions*

Transfer chemical potentials for the TATB ions,  $\text{BPh}_4^-$ ,  $\text{Ph}_4\text{As}^+$ ,  $\text{K}^+$  and  $\text{Pic}^-$ , derived from the solubility data of Dill and Popovych<sup>43</sup> and Berne and Popovych<sup>42</sup> directly by application of the TATB assumption are shown in Figs. 3.1, 3.2, 3.3 and 3.4 respectively. The corresponding values for these ions calculated by other authors using different data or different extrathermodynamic assumptions (outlined earlier) are also shown.

Four sets of values for  $\delta_m \mu^\ominus(\text{BPh}_4^-)$  are presented in Fig. 3.1. All indicate that addition of the alcohol has a stabilizing effect on the ion. The closest agreement as to the extent of this stabilization from 0 to 60 wt % EtOH is between the values calculated by Bax et al.<sup>20</sup> and those calculated in this work using the TATB assumption. The degree of stabilization estimated by Wells<sup>19</sup> in this range is somewhat smaller, while the values given by Popovych et al.<sup>18</sup> occupy an intermediate

position between the two. All the authors had made use of Dill and Popovych's solubility data for  $\text{KPh}_4$ <sup>43</sup> in their analyses to calculate transfer parameters for  $\text{BPh}_4^-$ .

Estimations due to both Wells<sup>19</sup> and this work agree that the  $\text{Ph}_4\text{As}^+$  ion is substantially stabilized when ethanol is added to aqueous solutions of these ions. Fig. 3.2 shows that the initial degree of this stabilization is, however, more marked in the predictions of Wells<sup>19</sup> than in those of this work. In both cases the same solubility data for  $\text{Ph}_4\text{AsPic}$  had been used.<sup>42</sup>

That there is a continuous decrease in the transfer chemical potentials of the  $\text{BPh}_4^-$  and  $\text{Ph}_4\text{As}^+$  ions as shown in Figs. 3.1 and 3.2 indicates that the neutral component of the solvation energy outweighs the electrostatic component for these ions in which the charge is shielded by large organic ligands. The hydrophobic nature of these ligands and their bulk lead to a preference for solvation by ethanol and thus greater stabilization in mixtures of increasing ethanol content. The curvature across the composition range also indicates strong preferential solvation by ethanol.

Of the four ions for which transfer parameters were derived directly by means of the TATB in this work,  $\text{K}^+$  provides the most interesting comparison with values derived by other authors. Fig. 3.3 shows five sets of estimations for the transfer chemical potentials of  $\text{K}^+$  in water + ethanol mixtures. All, except Wells,<sup>19</sup> predict that the  $\text{K}^+$  ion is destabilized by the addition of ethanol over the entire ranges studied. This continuous increase in solvation energy with increasing ethanol content and therefore decreasing dielectric constant is as predicted qualitatively by the Born equation. Wells,<sup>19</sup> however, predicts stabilization from 0 to 50 wt % EtOH and then destabilization at higher ethanol

contents. The values given by Popovych et al.<sup>18</sup> and by Dill et al.<sup>44</sup> are in very close agreement up to 50 wt % EtOH and indicate that the addition of ethanol has almost no effect on the chemical potential of  $K^+$  up to this point. In this lower ethanol content range the values derived in this work correspond most closely to those of Bax et al.<sup>20</sup> in predicting a larger destabilization effect than Popovych et al.<sup>18</sup> or Dill et al.<sup>44</sup>. Above 50 wt % EtOH, however, Popovych et al.<sup>18</sup> identify a much more marked increase in the destabilization of the ion than Dill et al.<sup>44</sup>. In this range the values predicted by Popovych et al.<sup>18</sup> increase to almost coincide with those of this work and those of Bax et al.<sup>20</sup>. Bax et al.<sup>20</sup> had used  $\Delta\mu^{\ominus}H^+ - \Delta\mu^{\ominus}K^+$  values calculated from data in the literature with their estimates of  $\Delta\mu^{\ominus}H^+$  to derive transfer parameters for the potassium ion. Wells<sup>19</sup> had also used these  $\Delta\mu^{\ominus}H^+ - \Delta\mu^{\ominus}K^+$  values that had been calculated by Bax et al.<sup>20</sup> but with his own experimentally determined values of  $\Delta G_t^{\ominus}(H^+)$ . He had derived additional values for  $K^+$  from emf data for KCl. Dill et al.<sup>44</sup> had used a model developed by Stokes for the free energy of hydration of ions with a noble gas structure to calculate the electrostatic free energy of  $K^+$  ions in water and water + ethanol mixtures. From these values they had calculated the medium effects. They had omitted the 'neutral' part of the solvation energy thereby adopting the 'zero-energy assumption'. The values of Popovych et al.<sup>18</sup> had been obtained directly from the application of the TABTB assumption to their solubility data for  $KBPh_4$ ,<sup>43</sup>  $KPic$ <sup>43</sup> and  $TABPic$ <sup>43</sup> [cf. in this work, the direct derivation of  $\delta_{m\mu}^{\ominus}(K^+)$  by the application of the TATB assumption to the solubility data<sup>42,43</sup> for  $KBPh_4$ ,  $KPic$  and  $Ph_4AsPic$ ].

For the picrate ion, Fig. 3.4, Wells<sup>19</sup> identifies an initial destabilization on introduction of ethanol into the system compared with

a slight stabilization predicted by this work for this ion. The values given by Popovych et al.<sup>18</sup> at low wt % EtOH lie approximately midway between the two. Above 50 wt % EtOH there is general agreement that the ion is stabilized. All three sets of authors had used the same solubility data for KPic<sup>43</sup> in calculating values of  $\delta_{m\mu}^{\ominus}(\text{Pic}^-)$  but had effected its split into single-ion contributions by different means. This, then, is a direct example of the effect of the incorporation of different extrathermodynamic assumptions on estimations of single-ion transfer parameters. That the picrate ion occupies, as expected, an intermediate position on the graphs between the elemental, inorganic K<sup>+</sup> ion and the large, organic Ph<sub>4</sub>As<sup>+</sup> and BPh<sub>4</sub><sup>-</sup> ions is predicted by all the authors except Wells.<sup>19</sup>

Combinations of values for cations and anions from any set of single-ion transfer parameters should agree with independently measured values for the relevant salt. This Kohlrausch-type condition should be satisfied regardless of the extrathermodynamic assumptions used. Fig. 3.5 shows such ionic combinations for KBPh<sub>4</sub>. The unbroken line shows  $\delta_{m\mu}^{\ominus}(\text{KBPh}_4)$  values calculated from solubility data for the salt measured by Popovych et al.<sup>18</sup> At first sight, the general agreement of these values for KBPh<sub>4</sub> may seem surprising considering the inconsistency of the reported values for its constituent ions. However, this agreement for the salt is to be hoped for, and indeed expected, given that the same solubility data for the salt<sup>43</sup> had been incorporated at some point into all the analyses.

#### *Simple anions*

Estimations of the transfer parameters for the halide ions Cl<sup>-</sup>, Br<sup>-</sup> and I<sup>-</sup> are shown in Figs. 3.6, 3.7 and 3.8 respectively. There is general agreement that all 3 ions experience a destabilizing effect when

ethanol is added to the system in the order  $\text{Cl}^- > \text{Br}^- > \text{I}^-$ . For each of these halide ions the closest agreement of values is between Bax et al.<sup>20</sup> and this work. The initial rate of destabilization predicted by Bose et al.<sup>45</sup> and by Wells<sup>19</sup> is, in all cases, substantially greater than the rest. This is particularly marked in the case of  $\text{Br}^-$  and  $\text{I}^-$ . Wells<sup>19</sup> predicts a levelling off of the transfer chemical potentials for each ion around 40 wt % EtOH whilst a continuing increase is evident in the rest of the estimations. For all 3 ions, Bose et al.<sup>45</sup> had used emf data of the hydrogen halides which had been split into ionic contributions using an extrapolation procedure. For the chloride ion Popovych et al.,<sup>18</sup> Bax et al.,<sup>20</sup> and this work had all made use of the same solubility data for KCl.<sup>18</sup> Wells<sup>19</sup> had used various emf data available for HCl. For the bromide and iodide ions Bax et al.<sup>20</sup> and Wells<sup>19</sup> had both used the former's  $\Delta\mu^{\ominus}\text{H}^+ + \Delta\mu^{\ominus}\text{Br}^-$  and  $\Delta\mu^{\ominus}\text{H}^+ + \Delta\mu^{\ominus}\text{I}^-$  values calculated from emf data. This work had used KBr and KI values of Bax et al.<sup>20</sup>

Fig. 3.9 shows estimations for  $\delta_{\text{m}}\mu^{\ominus}(\text{ClO}_4^-)$  given by Wells,<sup>19</sup> Bax et al.<sup>20</sup> and this work. All had used solubility data for  $\text{KClO}_4$ <sup>46</sup> in their analyses. Again, all three sets of estimations show a destabilizing effect on the ion with the addition of ethanol, although Bax et al.<sup>20</sup> and this work predict a more modest, though consistent, increase throughout the range studied compared with Wells.<sup>19</sup> Scattered about the lines due to Bax et al.<sup>20</sup> and this work are two sets of less accurate estimations of  $\delta_{\text{m}}\mu^{\ominus}(\text{ClO}_4^-)$  calculated in this work. Solubilities of  $\text{KClO}_4$  measured by Pierrat<sup>47</sup> at 287.2 K were used with the TATB  $\delta_{\text{m}}\mu^{\ominus}(\text{K}^+)$  values to give values for the perchlorate ion ( $\nabla$ ). Other solubility values for  $\text{KClO}_4$ ,<sup>48</sup> measured at 298.2 K but given on the molal scale, were converted to m/l using assumption (ii) outlined earlier in Section 3.2.2 and

yielded more values for the anion ( $\diamond$ ). The perchlorate values tabulated in Appendix A are those derived from solubility data for  $\text{KClO}_4$ .<sup>46</sup>

Two sets of solubilities taken from the literature for  $\text{KNO}_3$ , both at 298.2 K, were used to estimate  $\delta_{\text{m}}\mu^{\ominus}(\text{NO}_3^-)$ . In both sets the solubilities had been measured on the molal scale. The values taken from Stephen<sup>49</sup> were accurately converted to the molar scale using the densities of the saturated solutions that had been given. For the values taken from Seidell<sup>50</sup> however, no such densities were available. For comparison, these values were converted to the molar scale using both of the alternative assumptions discussed earlier in Section 3.2.2. Firstly, it was assumed that the density of the solvent equalled that of the solution ( $\circ$ ). Secondly, that the total volume of solution equalled the sum of the volume of the solvent and the volume of the solute ( $\bullet$ ). The two resulting sets of  $\delta_{\text{m}}\mu^{\ominus}(\text{NO}_3^-)$  values are shown along with those calculated from the data taken from Stephen and Stephen<sup>49</sup> ( $\nabla$ ) in Fig. 3.10. It can be seen that the values derived using the second assumption are closer to the 'precise' values derived from data in Stephen and Stephen<sup>49</sup> than are those derived using the first assumption. The values for  $\delta_{\text{m}}\mu^{\ominus}(\text{NO}_3^-)$  tabulated in Appendix A are the average of those derived from the data taken from Seidell<sup>50</sup> and those from Stephen and Stephen<sup>49</sup> which involved incorporation of the more accurate assumption.

The transfer chemical potentials for the cyanide, iodate, chlorate and sulphate ions were derived from the solubility measurements of their respective potassium salts;  $\text{KCN}$ ,<sup>51</sup>  $\text{KIO}_3$ ,  $\text{KClO}_3$ <sup>52</sup> and  $\text{K}_2\text{SO}_4$ .<sup>53</sup> Values for  $\text{KCN}$  and  $\text{KIO}_3$  had been determined at 298.2 K and on the molar scale so estimations of  $\delta_{\text{m}}\mu^{\ominus}(\text{CN}^-)$  and  $\delta_{\text{m}}\mu^{\ominus}(\text{IO}_3^-)$  were straightforward. The solubilities of  $\text{KIO}_3$  in water and water + ethanol mixtures were measured

in this work by titrimetric analysis. The experimental procedure used was described in Chapter 2 (Section 2.6). For  $\text{KClO}_3$  and  $\text{K}_2\text{SO}_4$ , values had been given on the molal scale. Those for  $\text{K}_2\text{SO}_4$  had been measured at 303.2 K.

Values of  $\delta_{\text{m}\mu}^{\ominus}(\text{S}_2\text{O}_3^{2-})$  and  $\delta_{\text{m}\mu}^{\ominus}(\text{S}_2\text{O}_6^{2-})$  were calculated from solubility data of the barium salts of these ions.<sup>54</sup>

The values of the transfer chemical potentials adopted for these anions, derived using the TATB assumption, are shown together in Figs. 3.21 and 3.23 at the end of the next section, Section 3.3.3.

#### *Organic ions*

Fig. 3.11 shows transfer chemical potentials for the triisooamyl-n-butylammonium ion,  $\text{TAB}^+$ , and the tetraphenylphosphonium ion,  $\text{Ph}_4\text{P}^+$ . All estimations show that both these ions exhibit a strong preference for solvation by EtOH as is expected for such large organic ions (cf.  $\text{Ph}_4\text{As}^+$  and  $\text{BPh}_4^-$ ). The values shown had been derived using solubility data for  $\text{TABBPh}_4$ ,<sup>18</sup>  $\text{TABPic}$ <sup>43</sup> and  $\text{Ph}_4\text{PPic}$ .<sup>42</sup>

Data for potassium citrate,<sup>55</sup> potassium antimonyl tartrate<sup>56</sup> and potassium naphthalene- $\beta$ -sulphonate<sup>57</sup> were combined with  $\delta_{\text{m}\mu}^{\ominus}(\text{K}^+)$  values derived in this work to give the transfer chemical potentials for the anions  $\delta_{\text{m}\mu}^{\ominus}(\text{cit}^{3-})$ ,  $\delta_{\text{m}\mu}^{\ominus}(\text{Sb tart}^-)$  and  $\delta_{\text{m}\mu}^{\ominus}(\text{N}_2\text{S}^-)$  respectively. Values for these salts had been measured at 298.2 K and on the molar scale.

The transfer chemical potentials for the oxalate ion,  $\delta_{\text{m}\mu}^{\ominus}(\text{ox}^{2-})$ , and the anthraquinone-2-sulphonate ion,  $\delta_{\text{m}\mu}^{\ominus}(\text{A}_2\text{S}^-)$ , were derived from solubility data of their respective calcium salts<sup>58,59</sup> using the values for  $\delta_{\text{m}\mu}^{\ominus}(\text{Ca}^{2+})$  tabulated in Appendix A. The values for calcium oxalate had been measured at 293.2 K on the molar scale. Those for calcium anthraquinone-2-sulphonate had been measured at 298.2 K on the molal scale.

Two sets of solubility data for potassium hydrogen tartrate were used in conjunction with the  $\delta_{m\mu}^{\ominus}(\text{K}^+)$  values derived in this work to yield the values for  $\delta_{m\mu}^{\ominus}(\text{H tart}^-)$  shown in Fig. 3.12. Both sets of data for the salt had been measured on the molar scale but those of Pierrat<sup>47</sup> had been measured at 287.2 K (o), those taken from Seidell<sup>60</sup> at 298.2 K (●). The latter are the ones tabulated in Appendix A.

Fig. 3.13 shows two sets of estimations for  $\delta_{m\mu}^{\ominus}(\text{OAc}^-)$ . One set was derived from solubility data for potassium acetate<sup>61</sup> (●) using  $\delta_{m\mu}^{\ominus}(\text{K}^+)$  values calculated using the TATB assumption. The other was derived from solubility data for sodium acetate<sup>62</sup> (o) using the  $\delta_{m\mu}^{\ominus}(\text{Na}^+)$  values given in Appendix A. The values for the acetate ion derived from potassium acetate<sup>61</sup> are the ones tabulated in Appendix A.

The values adopted for these organic ions derived using the TATB assumption are shown together in Fig. 3.22 at the end of the next section, Section 3.3.3.

#### Cations

Estimations of the transfer chemical potentials for the proton are shown in Fig. 3.14. At low wt % EtOH, this work predicts a slight destabilization of the ion indicating reduced proton affinity over this range compared to that in water and mixtures of higher ethanol content. This is consistent with the fact that the addition of small amounts of ethanol lead to an increase in water structure thereby decreasing the number of basic sites available on the water molecules for bonding with protons. This effect can also be seen in the results of Popovych et al.<sup>18</sup> and Bax et al.<sup>20</sup> to the extent that in this range the continuous decrease in the transfer chemical potential is relatively small. No such delay in this region can be seen in Wells's<sup>19</sup> prediction. With increasing ethanol content all authors predict a continuing decrease in the transfer para-

meters,  $\delta_{m\mu}^{\ominus}(H^+)$  reaching a minimum in the region of equimolar solvent composition and increasing again at higher wt % EtOH. This minimum in the transfer chemical potential corresponds to the water + ethanol mixture of maximum basicity. It is thought<sup>63</sup> that up to this point increasing ethanol content reduces the degree of water structure (increasing the proton affinity of the solvent) until such time when the higher aqueous solvates,  $H^+(H_2O)_n$ , are replaced by smaller fragments. This maximum in the proton affinity for water + ethanol mixtures occurs in Wells's<sup>19</sup> estimation at about 40 wt % EtOH. In this work and that of Popovych et al.<sup>18</sup> it occurs at about 60 wt % EtOH and at a slightly higher ethanol content in that of Bax et al.<sup>20</sup> The increase in the transfer chemical potentials after this point corresponds to the gradual increase in concentration of the less basic organic oxonium ions,  $C_2H_5OH_2^+$ .

In calculating transfer parameters for  $H^+$ , Popovych et al.<sup>18</sup> and this work had both used electrochemical data for  $HCl$ <sup>18</sup> with their own  $\delta_{m\mu}^{\ominus}(Cl^-)$  values. The values given by Wells<sup>19</sup> were those that he had experimentally determined. Those given by Bax et al.<sup>20</sup> were the average values that had been derived from four different solvation models they had chosen.

Fig. 3.15 shows three sets of estimations derived in this study for  $\delta_{m\mu}^{\ominus}(Li^+)$ . The two sets of estimations showing that the small elemental  $Li^+$  is increasingly stabilized in mixtures of increasing EtOH content are obviously unsatisfactory. These values were derived from solubility data for  $LiCl$ <sup>64</sup> (■) and  $Li_2SO_4$ <sup>65</sup> (▲) and values for the chloride and sulphate ions respectively. Values for both salts had been given on the molal scale and those for  $Li_2SO_4$  had been measured at 303.2 K. The third set of estimations (●) was derived from solubilities of lithium citrate<sup>66</sup>

and  $\delta_{m\mu}^{\ominus}(\text{cit}^{3-})$  values derived as described previously. Quantitatively at least these values are more acceptable in predicting that  $\text{Li}^+$  has a preference for solvation by water. That for 'hard'  $\text{Li}^+$  this preference is so small at higher wt % EtOH is surprising. The values derived from lithium citrate<sup>66</sup> are the ones tabulated in Appendix A.

Two sets of estimations for  $\delta_{m\mu}^{\ominus}(\text{Na}^+)$  are shown in Fig. 3.16. One set was derived from solubility data for sodium picrate<sup>67</sup> (●) using  $\delta_{m\mu}^{\ominus}(\text{Pic}^-)$  values, the other from solubility data for sodium acetate<sup>62</sup> (○) and  $\delta_{m\mu}^{\ominus}(\text{OAc}^-)$  values. There is good agreement between the two sets at lower wt % EtOH content, the average of which is tabulated in Appendix A.

Transfer chemical potentials for  $\text{Rb}^+$ ,  $\text{Cs}^+$ ,  $\text{Me}_4\text{N}^+$ ,  $n\text{-Pr}_4\text{N}^+$  and  $n\text{-Bu}_4\text{N}^+$  are shown in Fig. 3.17. Qualitatively, there is agreement that for this series of ions, all of the same charge, the transfer chemical potentials decrease in the order  $\text{Rb}^+ > \text{Cs}^+ > \text{Me}_4\text{N}^+ > n\text{-Pr}_4\text{N}^+ > n\text{-Bu}_4\text{N}^+$ . This reflects the increase in the size of ion along the series. An increase in preferential solvation by ethanol with increasing size of alkyl group (and therefore increasing hydrophobicity) is also evident. Aside from these general trends there is little quantitative agreement between the estimations of Wells<sup>19</sup> and those of this work and Bax *et al.*<sup>20</sup> for these ions. Wells<sup>19</sup> predicts that throughout the range studied all these ions exist in a lower energy state in water + ethanol mixtures than in pure water. There is a continuous increase in this stabilizing effect for both  $n\text{-Pr}_4\text{N}^+$  and  $n\text{-Bu}_4\text{N}^+$  with increasing EtOH while for  $\text{Rb}^+$ ,  $\text{Cs}^+$  and  $\text{Me}_4\text{N}^+$  the stabilizing effect falls off at higher wt % EtOH. Like Wells,<sup>19</sup> this work and Bax *et al.*<sup>20</sup> predict a stabilizing effect, though less marked, for the  $n\text{-Pr}_4\text{N}^+$  and  $n\text{-Bu}_4\text{N}^+$  ions with the addition of the alcohol. In contrast to Wells,<sup>19</sup> however, for  $\text{Rb}^+$  and  $\text{Cs}^+$  this work and

Bax et al.<sup>20</sup> predict the effect of introduction of alcohol into the system to be a destabilizing one. Little preference for water or ethanol is evident at low wt % EtOH for the  $\text{Me}_4\text{N}^+$  ion though destabilization occurs in solutions of higher ethanol content.

All the authors had made use of the same solubility data for the perchlorate salts of these cations.<sup>46</sup> Again, both Bax et al.<sup>20</sup> and Wells<sup>19</sup> had used the former's calculated values of  $\Delta\mu^{\ominus}\text{H}^+ - \Delta\mu^{\ominus}\text{M}^+$  where  $\text{M} = \text{Rb}^+, \text{Cs}^+, \text{Me}_4\text{N}^+, \text{n-Pr}_4\text{N}^+$  and  $\text{n-Bu}_4\text{N}^+$  with their own values for the proton. In this work, the transfer chemical potentials for the perchlorate salts were combined with those derived as outlined earlier for the perchlorate ion to yield  $\delta_{\text{m}\mu}^{\ominus}$  values for the cations.

Fig. 3.18 shows estimations derived in this study for  $\delta_{\text{m}\mu}^{\ominus}(\text{Ag}^+)$ . The agreement between these estimates, based on measurements made for various silver salts, is unimpressive. Values derived from silver acetate<sup>68</sup> (■) predict a marked destabilization of the ion in contrast to the stabilization shown by values derived from silver bromate<sup>69</sup> (▼). Values for  $\delta_{\text{m}\mu}^{\ominus}(\text{Ag}^+)$  obtained using measurements made for silver chloride<sup>70</sup> (●) and silver nitrate<sup>71</sup> (▲) are intermediate in position between the two. The derivation of  $\delta_{\text{m}\mu}^{\ominus}(\text{Ag}^+)$  values from those for silver chloride and silver acetate are the most accurate of the group as solubilities for both salts had been measured on the molar scale. Values for silver nitrate had been measured on the molal scale and the unavailability of densities of the saturated solutions meant that conversion of these values to the molar scale required the incorporation of an assumption, see Section 3.2.2. These values had been measured at 288.2 K. As no values for the bromate ion were calculated in this study, the transfer chemical potentials of  $\text{Ag}^+$  were derived from values for silver bromate using  $\delta_{\text{m}\mu}^{\ominus}(\text{IO}_3^-)$  values, i.e. by assuming that  $\delta_{\text{m}\mu}^{\ominus}(\text{IO}_3^-)$

$\approx \delta_{m\mu}^{\ominus}(\text{BrO}_3^-)$ . The values for  $\delta_{m\mu}^{\ominus}(\text{Ag}^+)$  at low wt % EtOH tabulated in Appendix A are those derived from AgCl values as both the actual solubility measurements (which had been presented as solubility products) and the route of derivation of  $\delta_{m\mu}^{\ominus}(\text{Ag}^+)$  values were deemed the most accurate of the four alternatives.

The transfer chemical potentials for  $\text{Tl}^+$  were calculated using solubility data for  $\text{TlIO}_3$ <sup>72</sup> and the values for  $\delta_{m\mu}^{\ominus}(\text{IO}_3^-)$  determined experimentally in this work as described in Section 2.6.

The available solubilities of magnesium<sup>73</sup> and strontium salts<sup>74,75</sup> in these solvent mixtures yielded negative transfer chemical potentials for these cations. These unsatisfactory results are perhaps indicative of ion-pairing in the solutions.

Values of  $\delta_{m\mu}^{\ominus}(\text{Ca}^{2+})$  were derived from the solubilities of calcium sulphate,<sup>76</sup> which had been measured on the molal scale, together with  $\delta_{m\mu}^{\ominus}(\text{SO}_4^{2-})$  values.

Fig. 3.19 shows estimations for  $\delta_{m\mu}^{\ominus}(\text{Ba}^{2+})$ . The two sets coincide only at very low wt % EtOH. The values derived using the solubility of barium perchlorate<sup>77</sup> (●) show a continuous increase in the transfer chemical potentials for this ion with increasing ethanol content on the solvent mixtures. The solubility of this salt had been measured at 293.2 K and values had been given on the molal scale. The other set of values in Fig. 3.19 were derived from estimations of the solubility of barium picrate<sup>78</sup> (O) in water + ethanol mixtures. The values derived from  $\text{Ba}(\text{ClO}_4)_2$  are the ones shown in Fig. 3.24 in the next section and tabulated in Appendix A.

$\delta_{m\mu}^{\ominus}(\text{Zn}^{2+})$  values were derived using solubility data for zinc acetate<sup>79</sup> and  $\delta_{m\mu}^{\ominus}(\text{OAc}^-)$  values. The solubility of  $\text{Hg}(\text{BPh}_4)_2$ <sup>80</sup> was used, with  $\delta_{m\mu}^{\ominus}(\text{BPh}_4^-)$  values, to calculate transfer chemical potentials for

for  $\text{Hg}^{2+}$ .

Fig. 3.20 shows estimations for  $\delta_{\text{m}\mu}^{\ominus}(\text{Pb}^{2+})$  derived using the TATB assumption. Values were derived from solubility measurements of lead acetate<sup>81</sup> (●), lead sulphate<sup>82,83</sup> (■) and lead chloride<sup>84,85</sup> (□) and (○). All, except the set of lead chloride values taken from Stephen and Stephen<sup>85</sup> (○), had been measured on the molar scale. All agree that the ion is destabilized with increasing ethanol content of the solvent mixtures and there is good agreement at low wt % EtOH between the values derived from lead chloride and lead acetate. The latter are the values shown in Fig. 3.24 in the next section and tabulated in Appendix A.

The values of the transfer chemical potentials adopted for each of these cations, derived using the TATB assumption, are shown together in Fig. 3.24 in the next section, Section 3.3.3, and are tabulated in Appendix A.

#### *Halogenoanions*

The transfer chemical potentials of  $[\text{PtCl}_6]^{2-}$  and  $[\text{SiF}_6]^{2-}$  were derived from those of their respective potassium containing salts<sup>47</sup> and those for the potassium ion. The solubility of both salts had been measured at 287.2 K. Solubility products of  $\text{Cs}_2\text{ReCl}_6$ <sup>86</sup> were used to calculate transfer chemical potentials for this salt which when combined with those for  $\text{Cs}^+$  yielded  $\delta_{\text{m}\mu}^{\ominus}(\text{ReCl}_6^{2-})$  values. Values for these halogenoanions are shown together in Fig. 3.25 at the end of Section 3.3.3. Also included in Fig. 3.25 are transfer chemical potentials for  $[\text{UCl}_6]^{2+}$  and  $[\text{UO}_2\text{Cl}_4]^{2-}$  derived by Kim *et al.*<sup>87</sup> by extraction equilibrium study.

#### *Co(III) and Fe(II) complexes*

Transfer chemical potentials for four Co(III) complex ions were derived using solubility measurements for  $[\text{Co}(\text{en})_2\text{Cl}_2]\text{ClO}_4$ ,<sup>88</sup>  $[\text{Co}(\text{NH}_3)_5\text{Cl}]\text{Cl}_2$ ,<sup>89</sup>  $[\text{Co}(\text{NH}_3)\text{Br}(\text{en})]\text{Br}_2$ <sup>90</sup> and  $\text{K}_3[\text{Co}(\text{NO}_2)_6]$ <sup>47</sup> with  $\delta_{\text{m}\mu}^{\ominus}$

values for  $\text{ClO}_4^-$ ,  $\text{Cl}^-$ ,  $\text{Br}^-$  and  $\text{K}^+$  respectively. Measurements for all these salts had been made at 298.2 K, except for  $\text{K}_3[\text{Co}(\text{NO}_2)_6]$  which had been measured at 287.2 K. Values for the three Fe(II) complex ions were derived from solubility measurements for the perchlorate salts of the cations,  $[\text{Fe}(\text{phen})_3](\text{ClO}_4)_2$ ,<sup>80</sup>  $[\text{Fe}(\text{bipy})_3](\text{ClO}_4)_2$ <sup>80</sup> and  $[\text{Fe}(\text{bsb},\text{Ph},\text{Ph};\text{m-OMe})_3](\text{ClO}_4)_2$ .<sup>91</sup> These values had all been measured on the molar scale and at 298.2 K.

The values of the transfer chemical potentials for each of these ions, derived using the TATB assumption, are shown together in Fig. 3.26 in the next section.

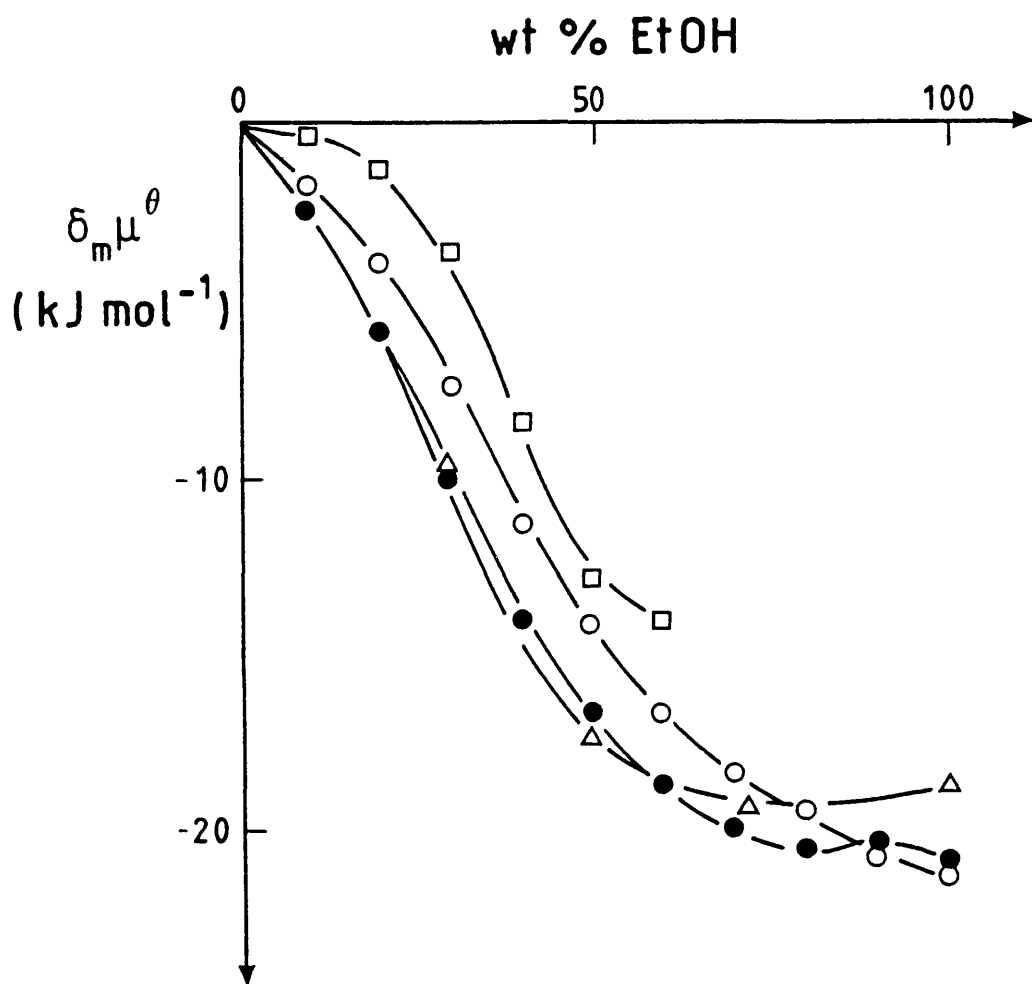


FIGURE 3.1

Transfer chemical potentials for  $\text{BPh}_4^-$  (molar scale, 298.2 K): this work (●); Wells [ref. 19] (□); Bax et al. [ref. 20] (Δ); Popovych et al. [ref. 18] (○).

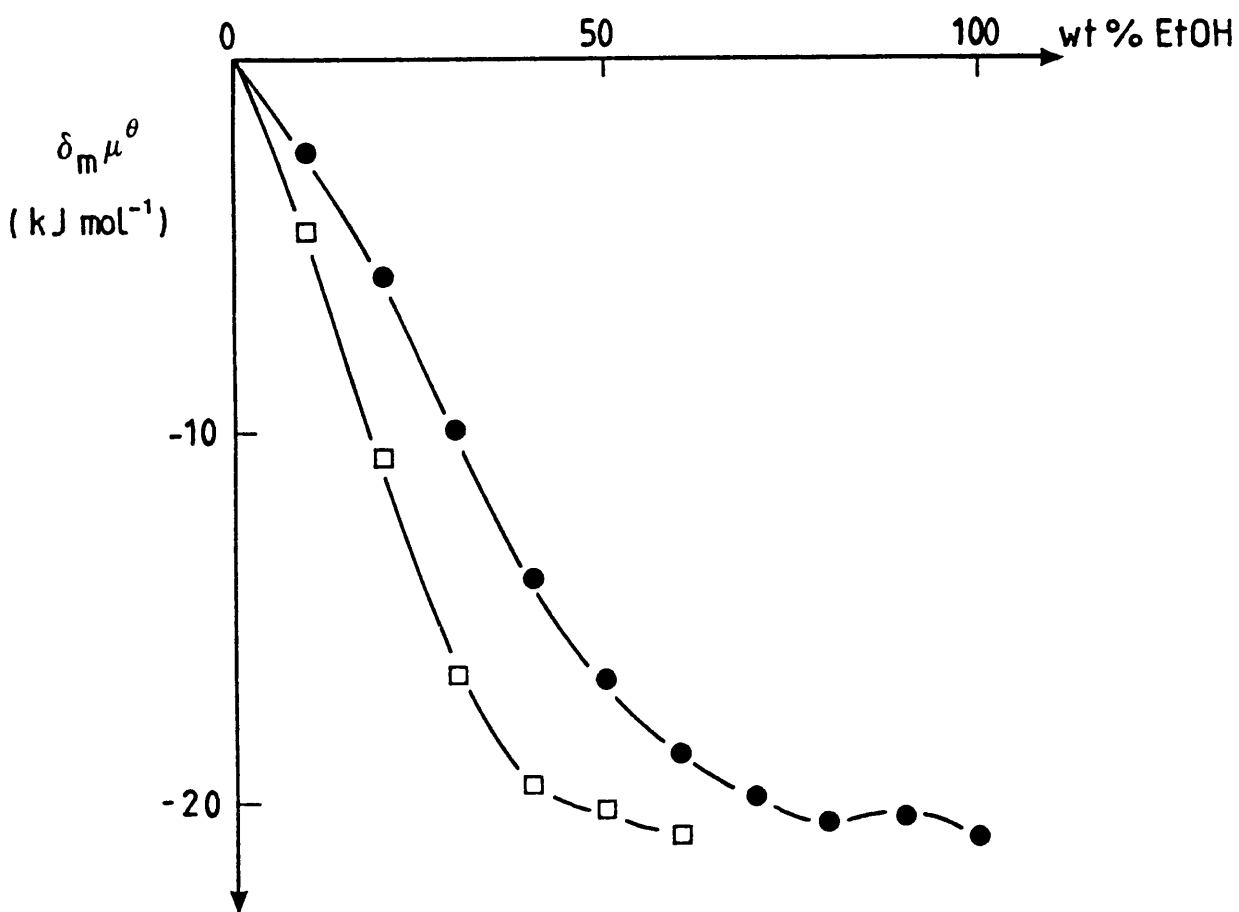


FIGURE 3.2

Transfer chemical potentials for  $\text{Ph}_4\text{As}^+$  (molar scale, 298.2 K):  
 this work (●); Wells [ref. 19] (□).

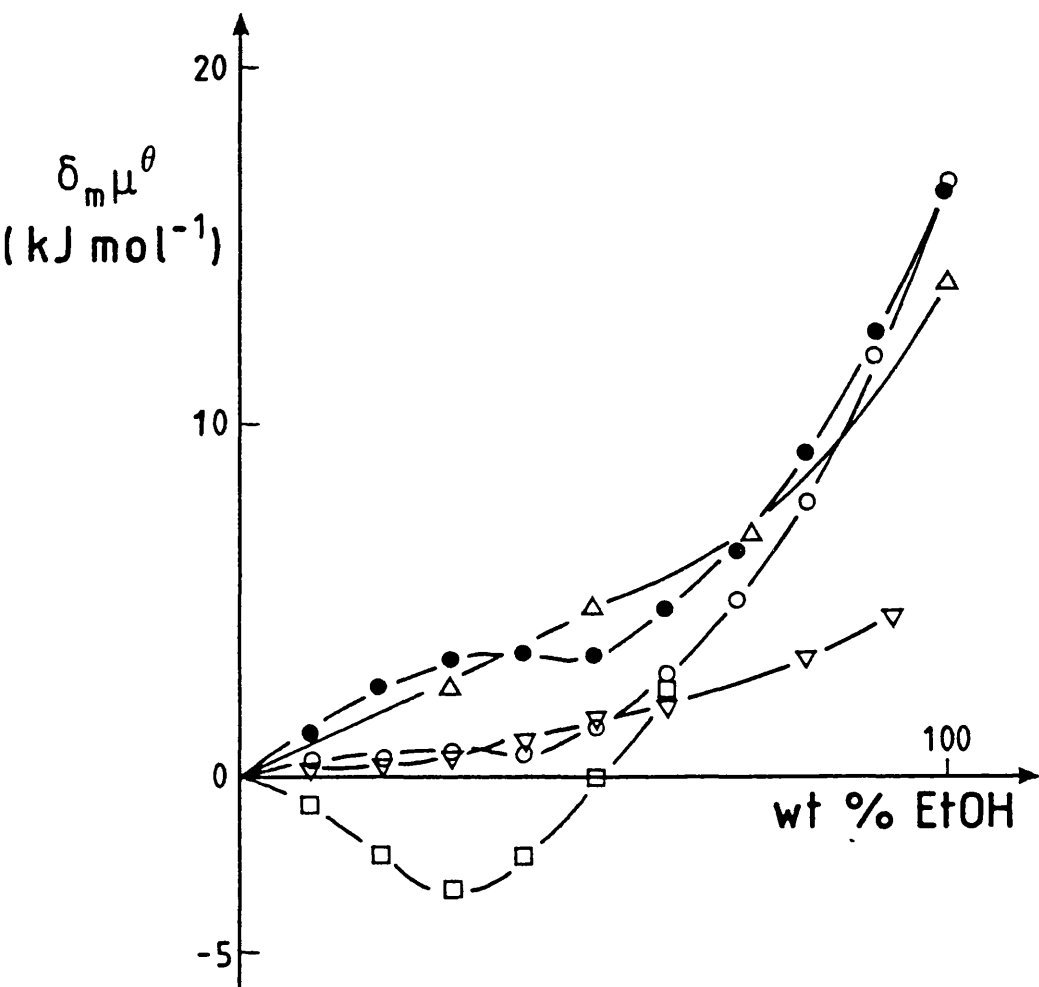
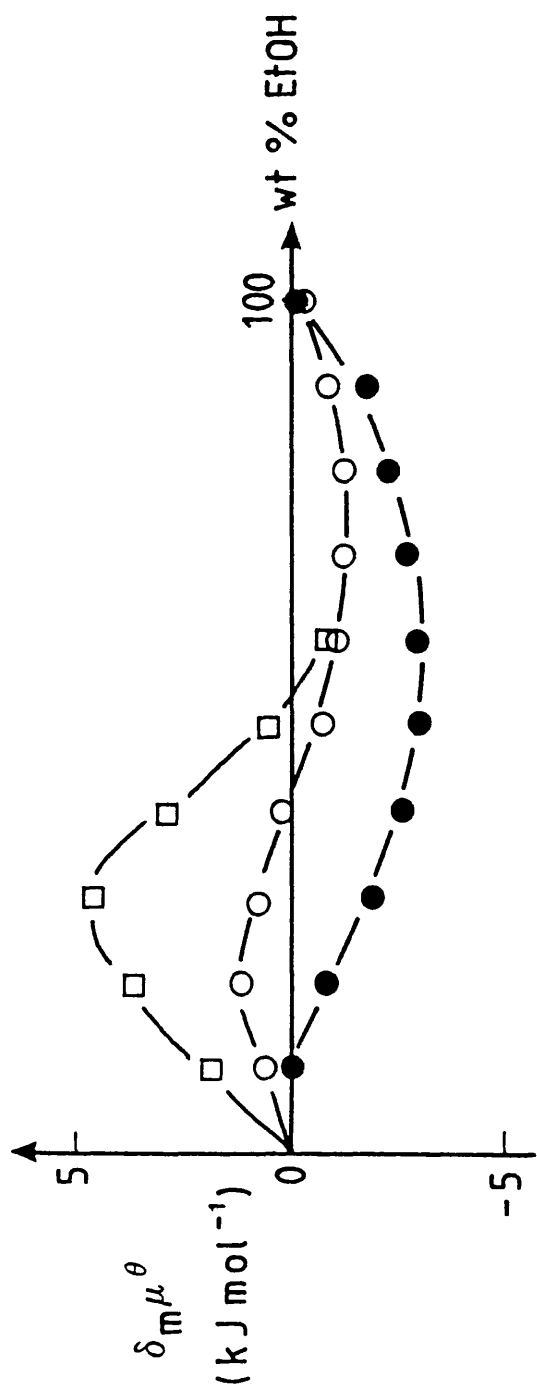


FIGURE 3.3

Transfer chemical potentials for  $\text{K}^+$  (molar scale, 298.2 K):  
 this work (●); Wells [ref. 19] (□); Bax et al. [ref. 20] (△);  
 Popovych et al. [ref. 20] (○); Dill et al. [ref. 44] (▽).



**FIGURE 3.4**  
 Transfer chemical potentials for the picrate ion (molar scale, 298.2 K):  
 this work (●); Wells [ref. 19] (□); Popovych et al. [ref. 18] (○).

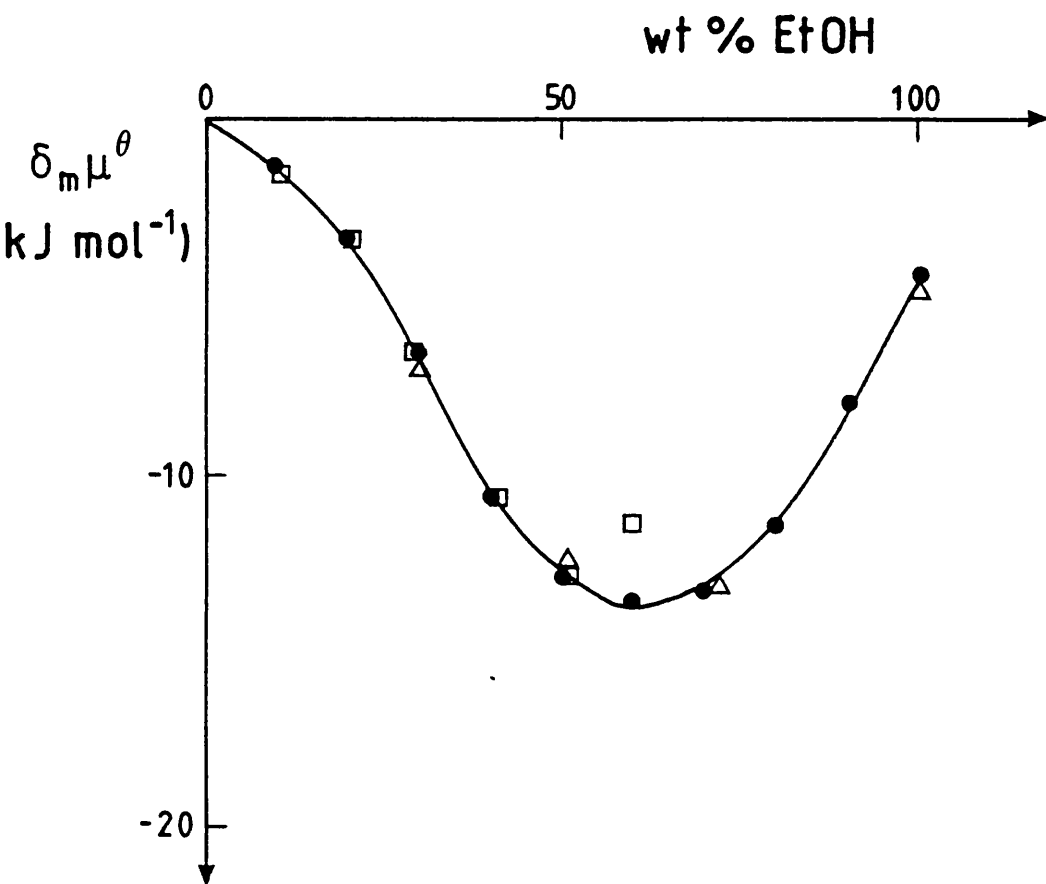


FIGURE 3.5

Transfer chemical potentials for  $\text{KPh}_4$  (molar scale, 298.2 K): this work ( $\bullet$ ); Wells [ref. 19] ( $\square$ ); Bax et al. [ref. 20] ( $\triangle$ ); Popovych et al. [ref. 18] (unbroken line).

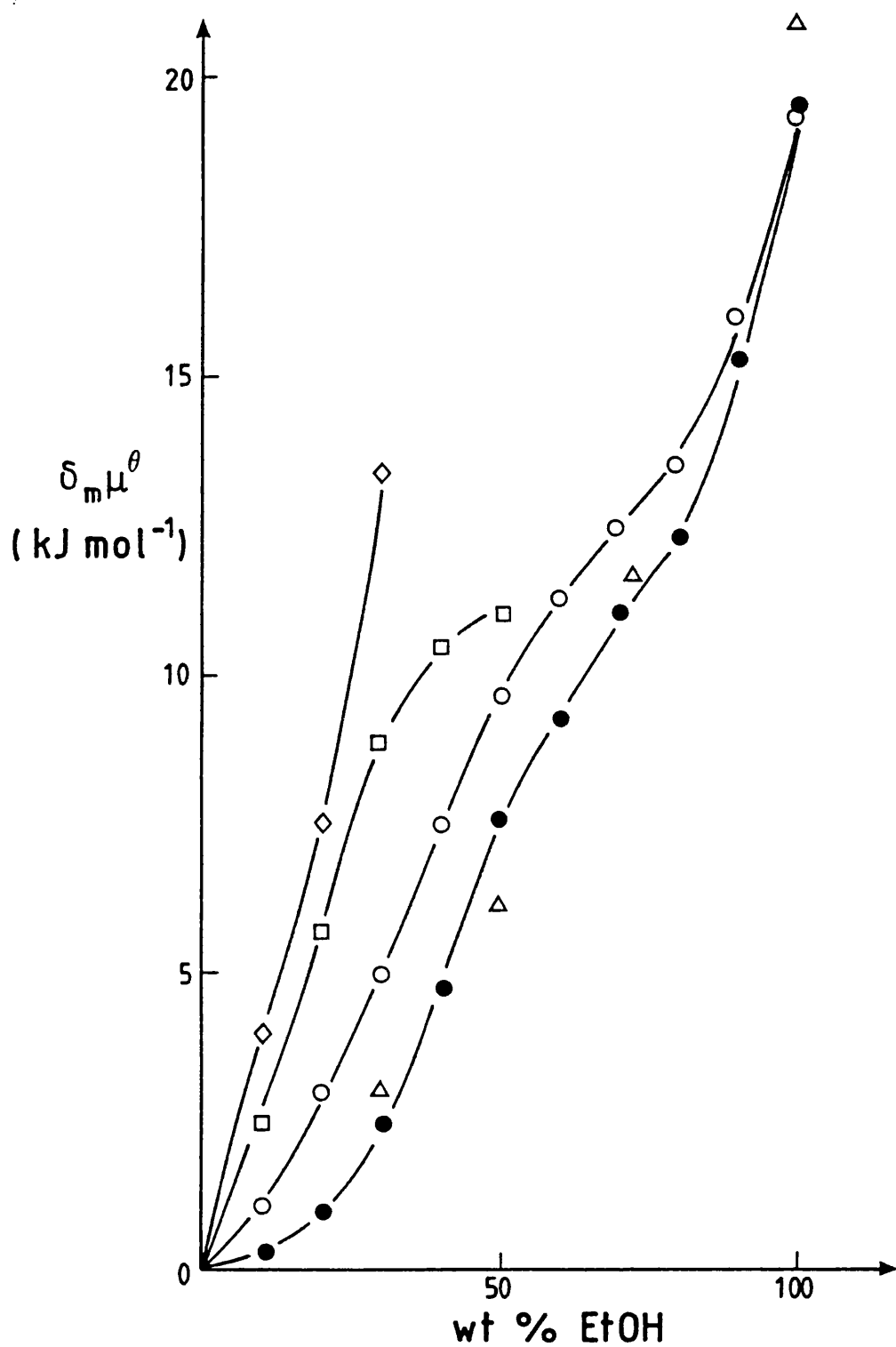


FIGURE 3.6

Transfer chemical potentials for  $\text{Cl}^-$  (molar scale, 298.2 K): this work (●); Wells [ref. 19] (□); Bax *et al.* [ref. 20] (△); Popovych *et al.* [ref. 18] (○); Bose *et al.* [ref. 45] (◇).

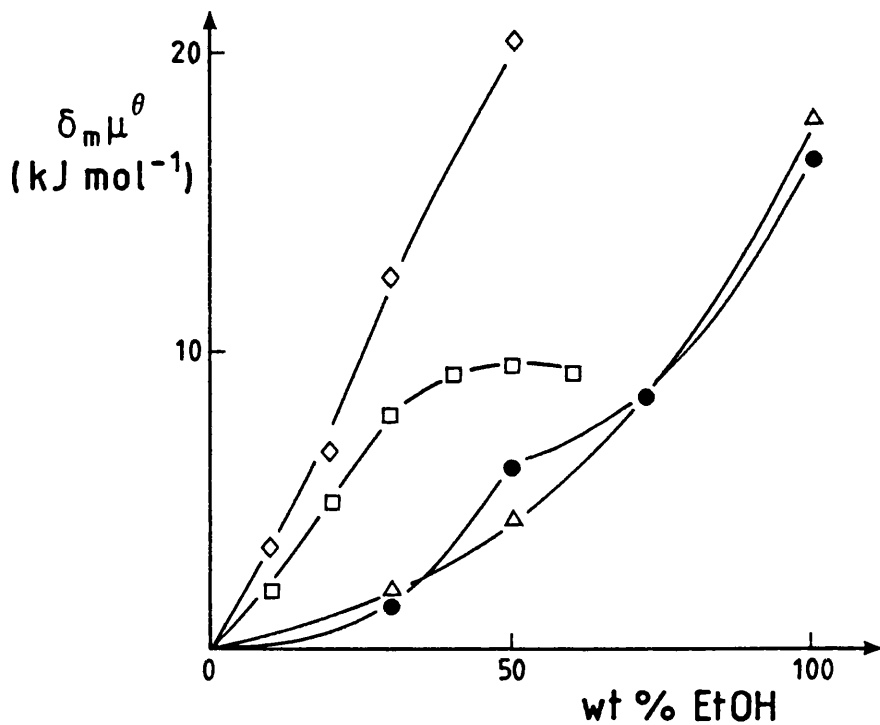


FIGURE 3.7

Transfer chemical potentials for  $\text{Br}^-$  (molar scale, 298.2 K): this work (●); Wells [ref. 19] (□); Bax et al. [ref. 20] (△); Bose et al. [ref. 45] (◇).

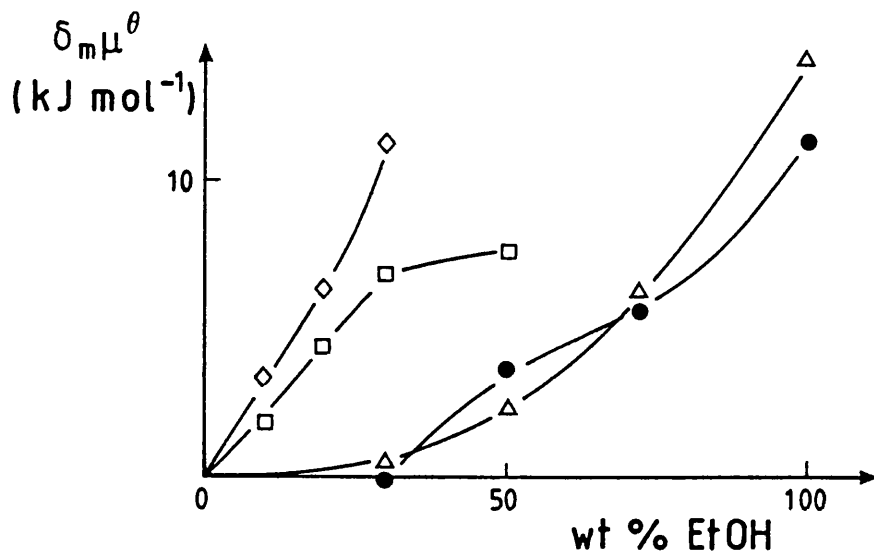


FIGURE 3.8

Transfer chemical potentials for  $\text{I}^-$  (molar scale, 298.2 K): this work (●); Wells [ref. 19] (□); Bax et al. [ref. 20] (△); Bose et al. [ref. 45] (◇).

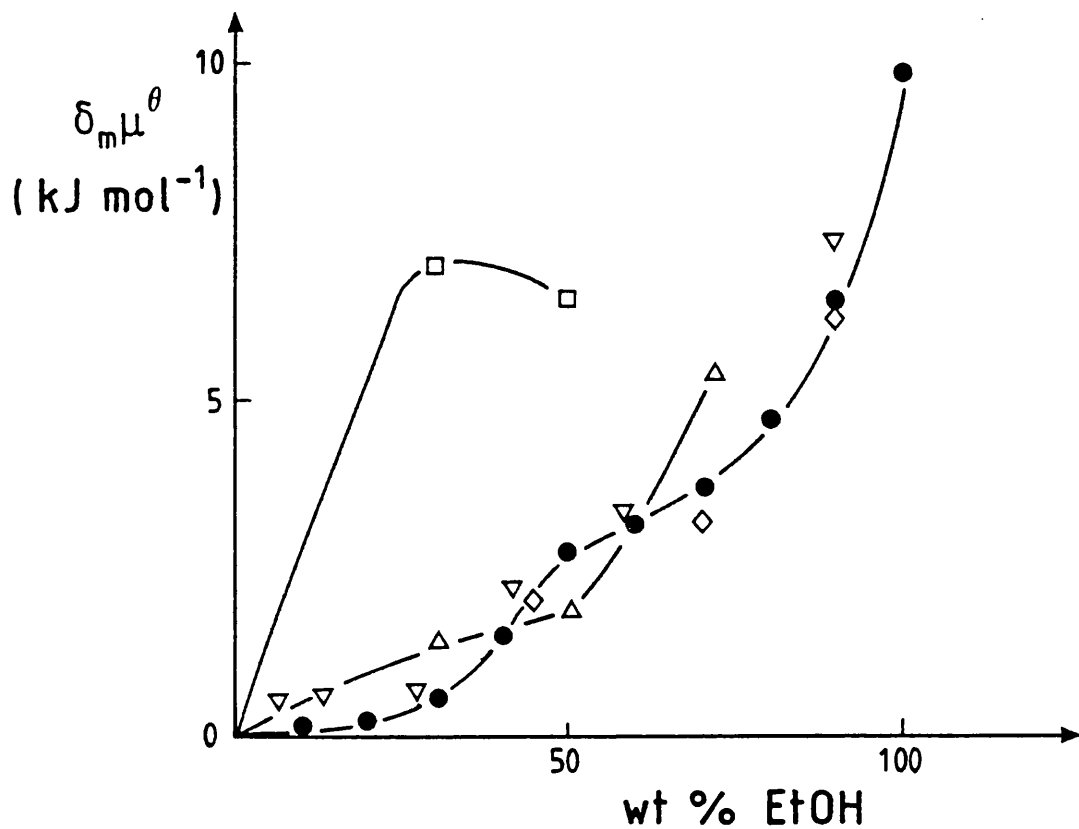


FIGURE 3.9

Transfer chemical potentials for  $\text{ClO}_4^-$  (molar scale):  
 this work, using data for  $\text{KClO}_4$  [ref. 46] (●),  $\text{KClO}_4$  [ref.  
 47] (▽),  $\text{KClO}_4$  [ref. 48] (◇), Wells [ref. 19] (□), Bax et  
al. [ref. 20] (Δ).

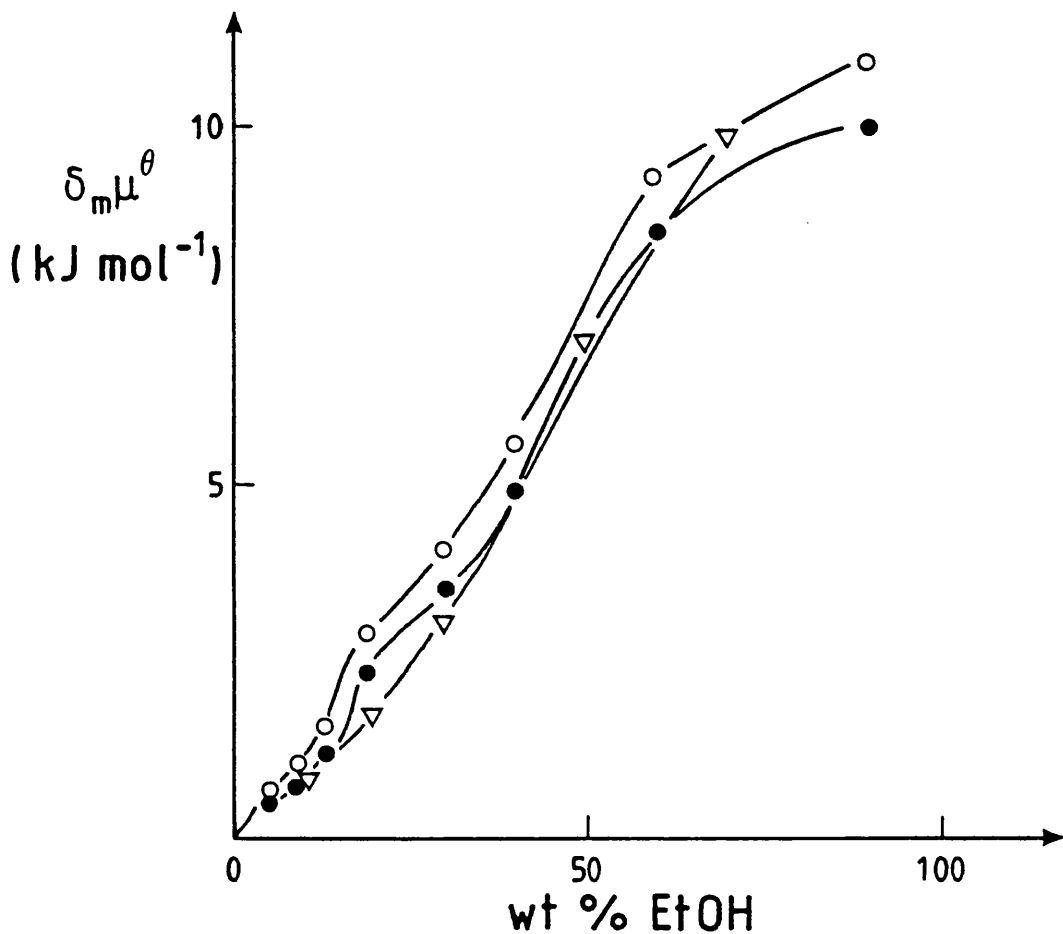


FIGURE 3.10

Transfer chemical potentials for  $\text{NO}_3^-$  (molar scale, 298.2 K, TATB assumption) derived using data for  $\text{KNO}_3$  [ref. 49] ( $\nabla$ ),  $\text{KNO}_3$  [ref. 50] ( $\bullet$ ),  $\text{KNO}_3$  [ref. 50] ( $\circ$ ).

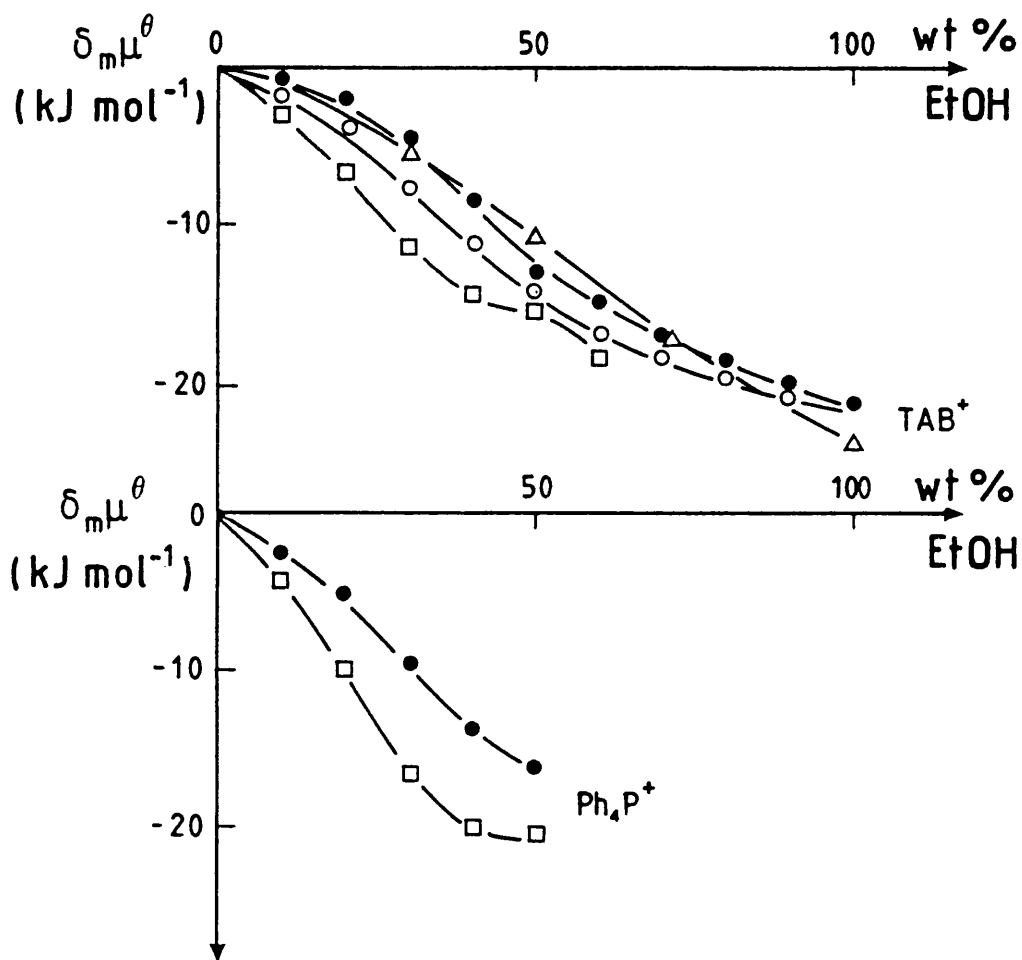


FIGURE 3.11

Transfer chemical potentials for TAB<sup>+</sup> and Ph<sub>4</sub>P<sup>+</sup> (molar scale, 298.2 K): this work (●); Wells [ref. 19] (□); Bax et al. [ref. 20] (Δ); Popovych et al. [ref. 18] (O).

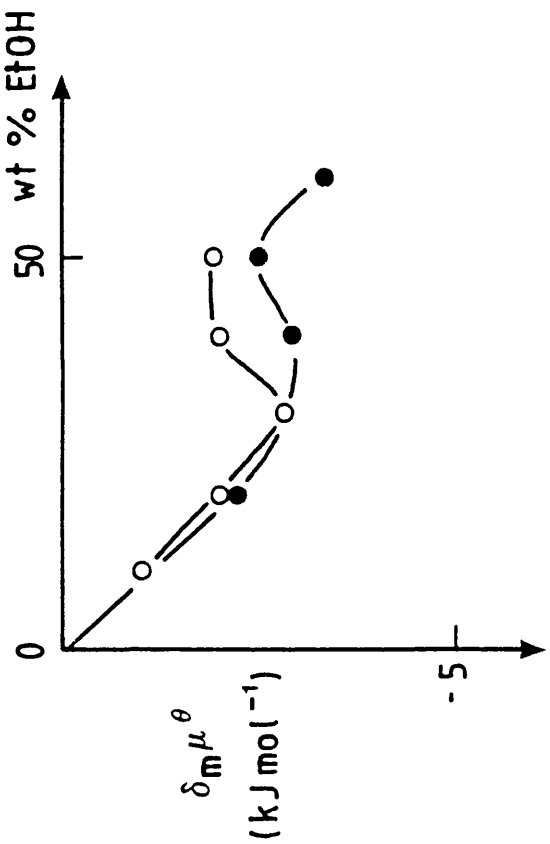


FIGURE 3.13

Transfer chemical potentials for  $\text{OAc}^-$  (molar scale, 298.2 K, TATB assumption) derived using data for KOAc [ref. 61] (●), NaOAc [ref. 62] (O).

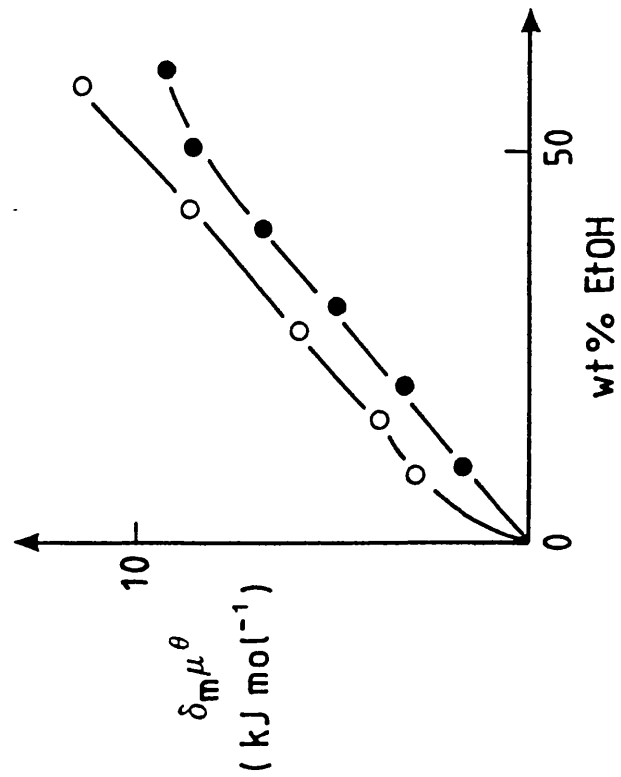


FIGURE 3.12

Transfer chemical potentials for  $\text{H tart}^-$  (molar scale, TATB assumption) derived using data for KH tart [ref. 47] (O), KH tart [ref. 60] (●).

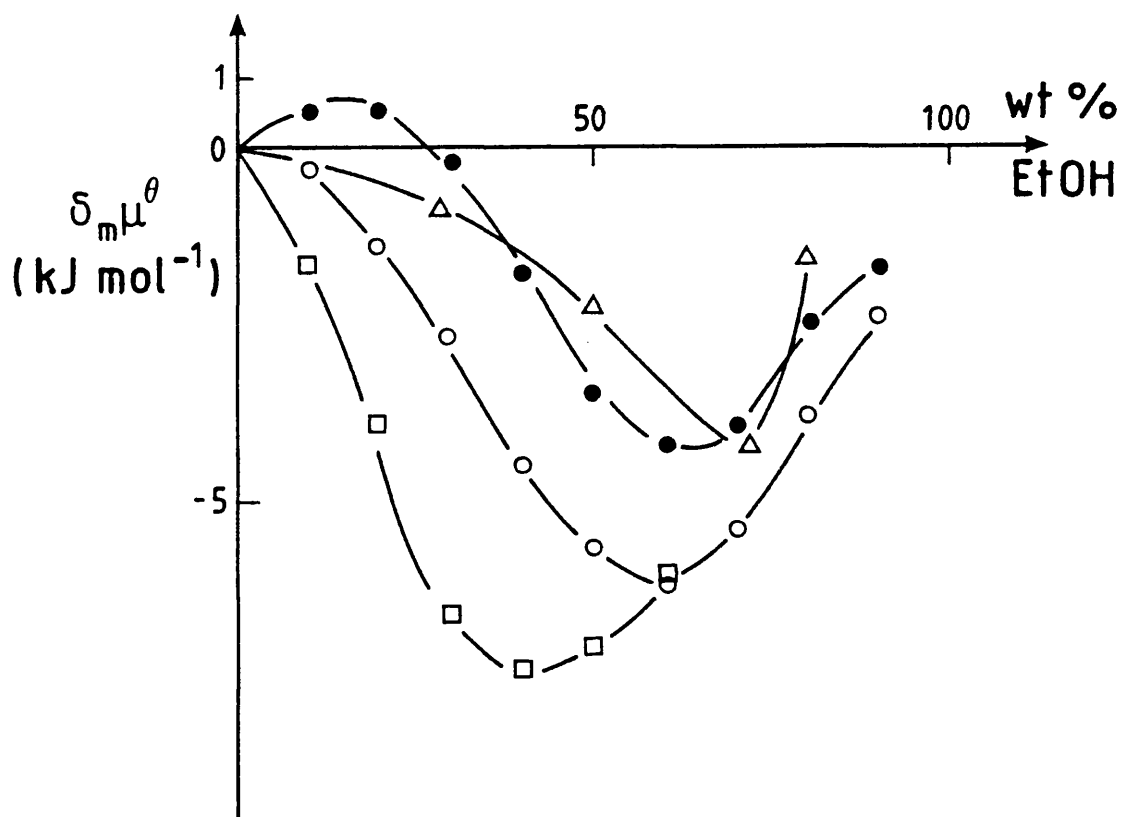


FIGURE 3.14

Transfer chemical potentials for  $\text{H}^+$  (molar scale, 298.2 K):  
 this work (●), Wells [ref. 19] (□), Bax et al. [ref. 20]  
 (Δ), Popovych et al. [ref. 18] (○).

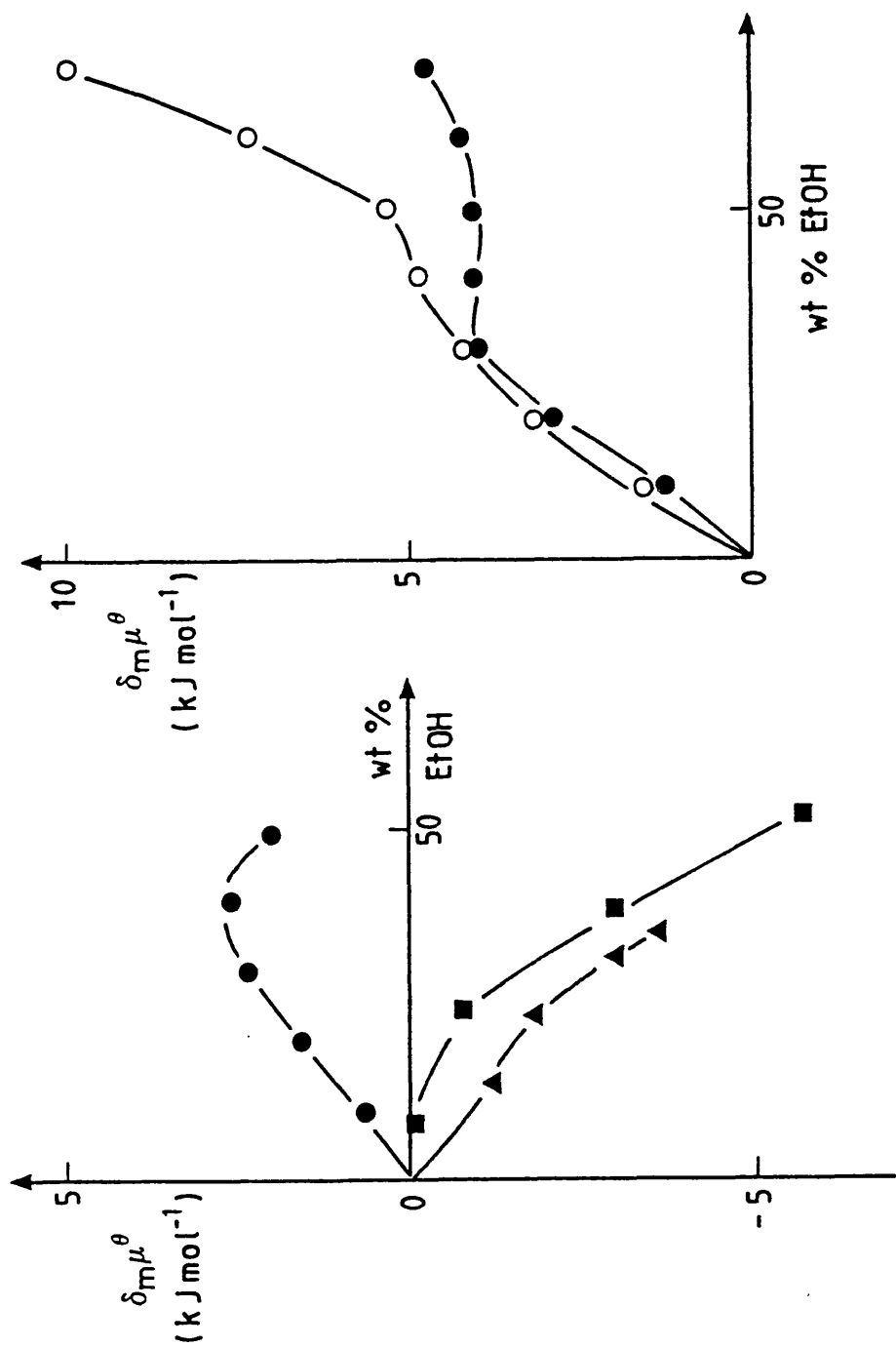


FIGURE 3.15

Transfer chemical potentials for Li<sup>+</sup> (molar scale, TATB assumption) derived using data for LiCl [ref. 64] (■), Li<sub>2</sub>SO<sub>4</sub> [ref. 65] (▲), Li<sub>3</sub>cit [ref. 66] (●).

FIGURE 3.16

Transfer chemical potentials for Na<sup>+</sup> (molar scale, 298.2 K, TATB assumption) derived using data for NaPic [ref. 67] (●), NaOAc [ref. 62] (○).

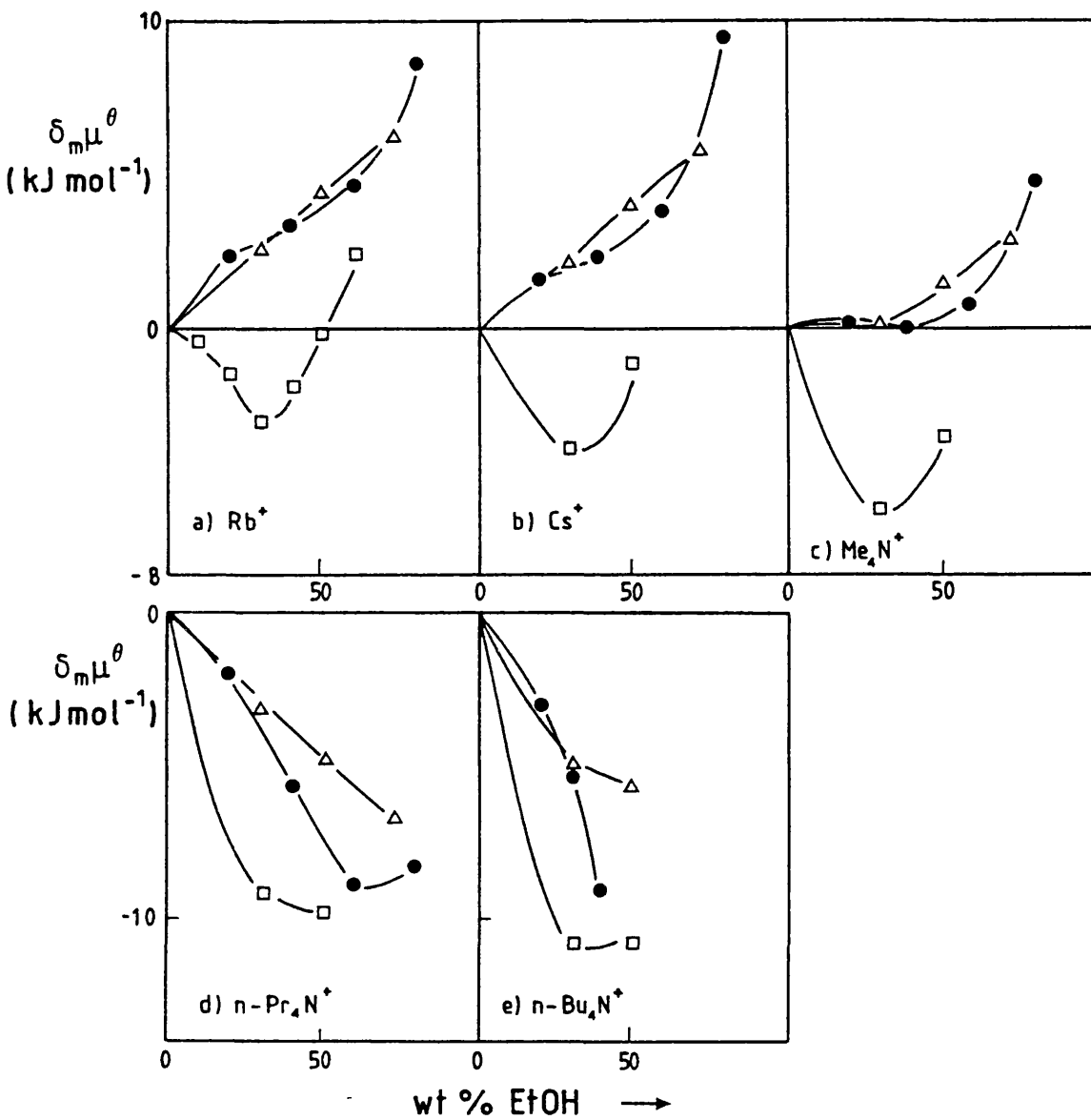


FIGURE 3.17

Transfer chemical potentials for a)  $\text{Rb}^+$ , b)  $\text{Cs}^+$ , c)  $\text{Me}_4\text{N}^+$ ,  
 d)  $n\text{-Pr}_4\text{N}^+$ , e)  $n\text{-Bu}_4\text{N}^+$  (molar scale, 298.2 K):  
 this work (●); Wells [ref. 19] (□); Bax et al. [ref. 20]  
 (Δ).

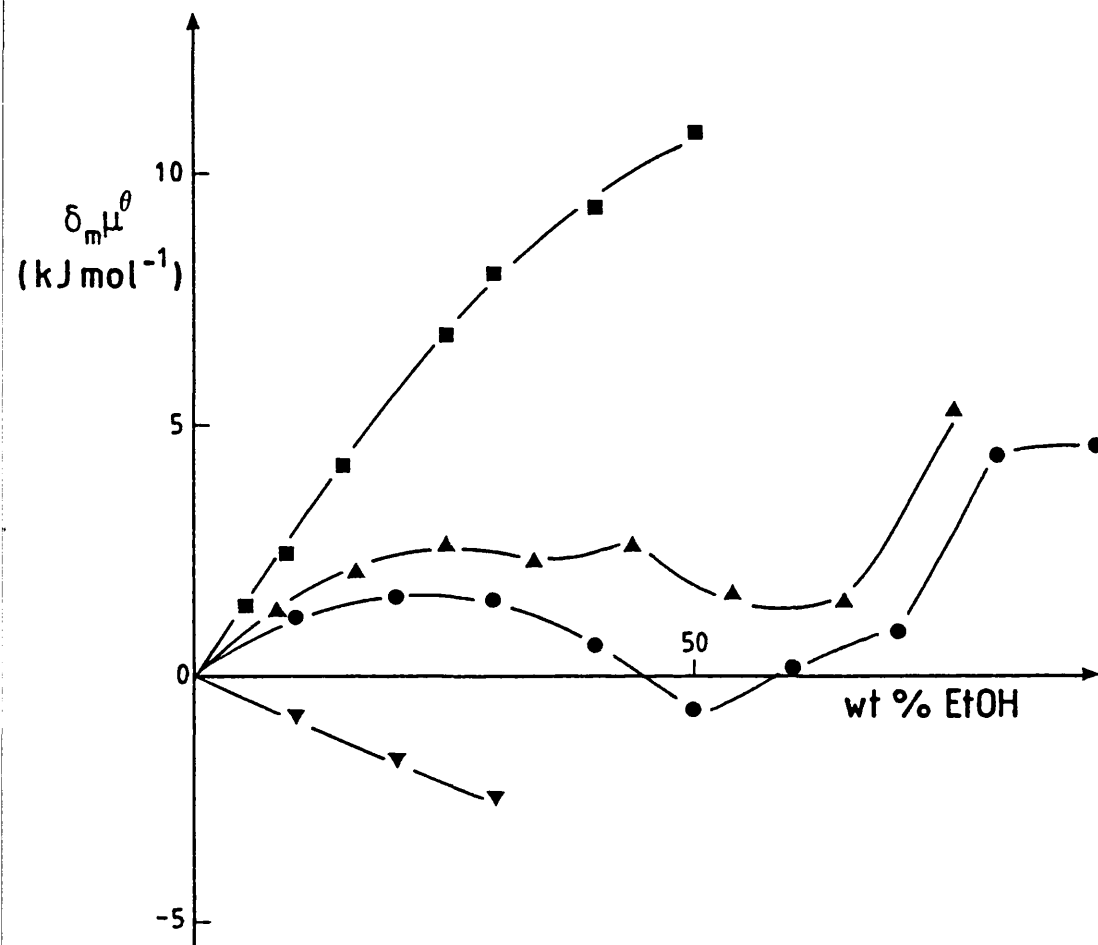


FIGURE 3.18

Transfer chemical potentials for  $\text{Ag}^+$  (molar scale, TATB assumption) derived using data for  $\text{AgOAc}$  [ref. 68] ( $\blacksquare$ ),  $\text{AgBrO}_3$  [ref. 69] ( $\blacktriangledown$ ),  $\text{AgCl}$  [ref. 70] ( $\bullet$ ),  $\text{AgNO}_3$  [ref. 71] ( $\blacktriangle$ ).

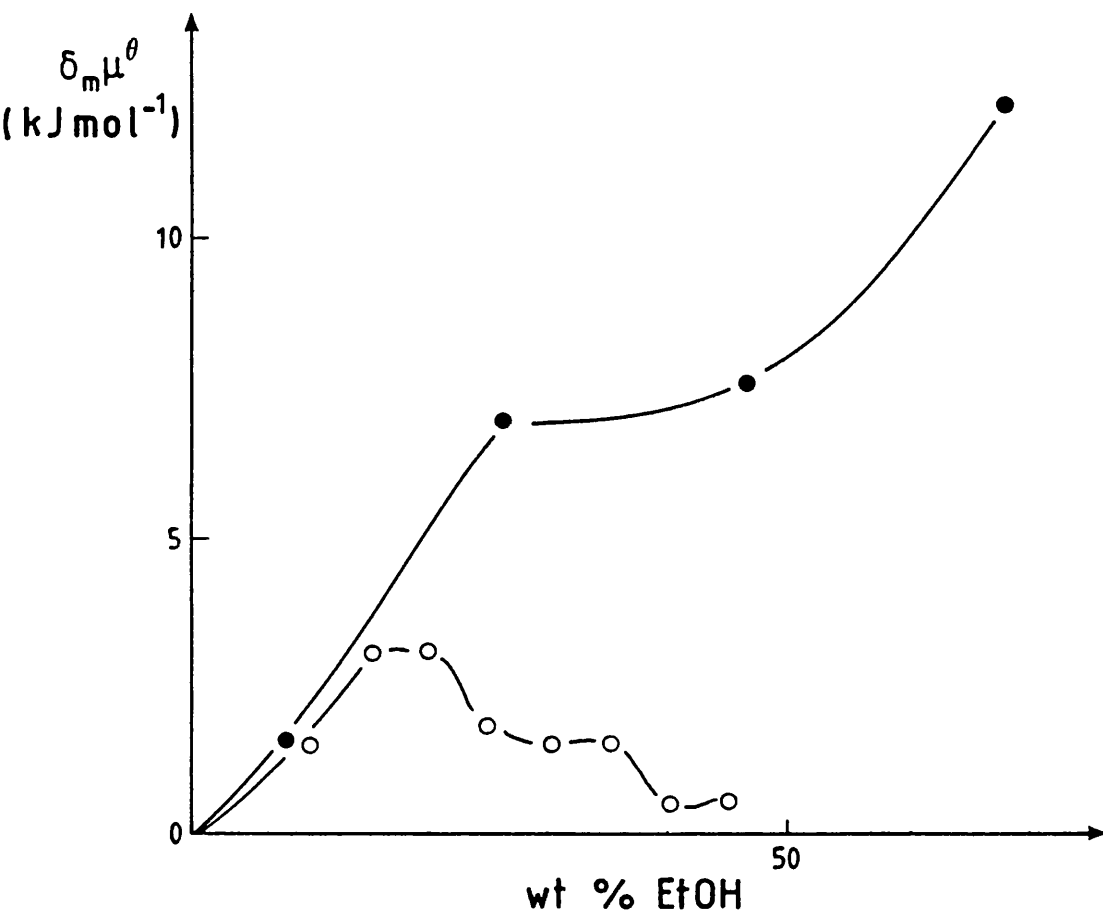


FIGURE 3.19

Transfer chemical potentials for  $\text{Ba}^{2+}$  (molar scale, TATB assumption) derived using data for  $\text{Ba}(\text{ClO}_4)_2$  [ref. 77] (●), BaPic [ref. 78] (○).

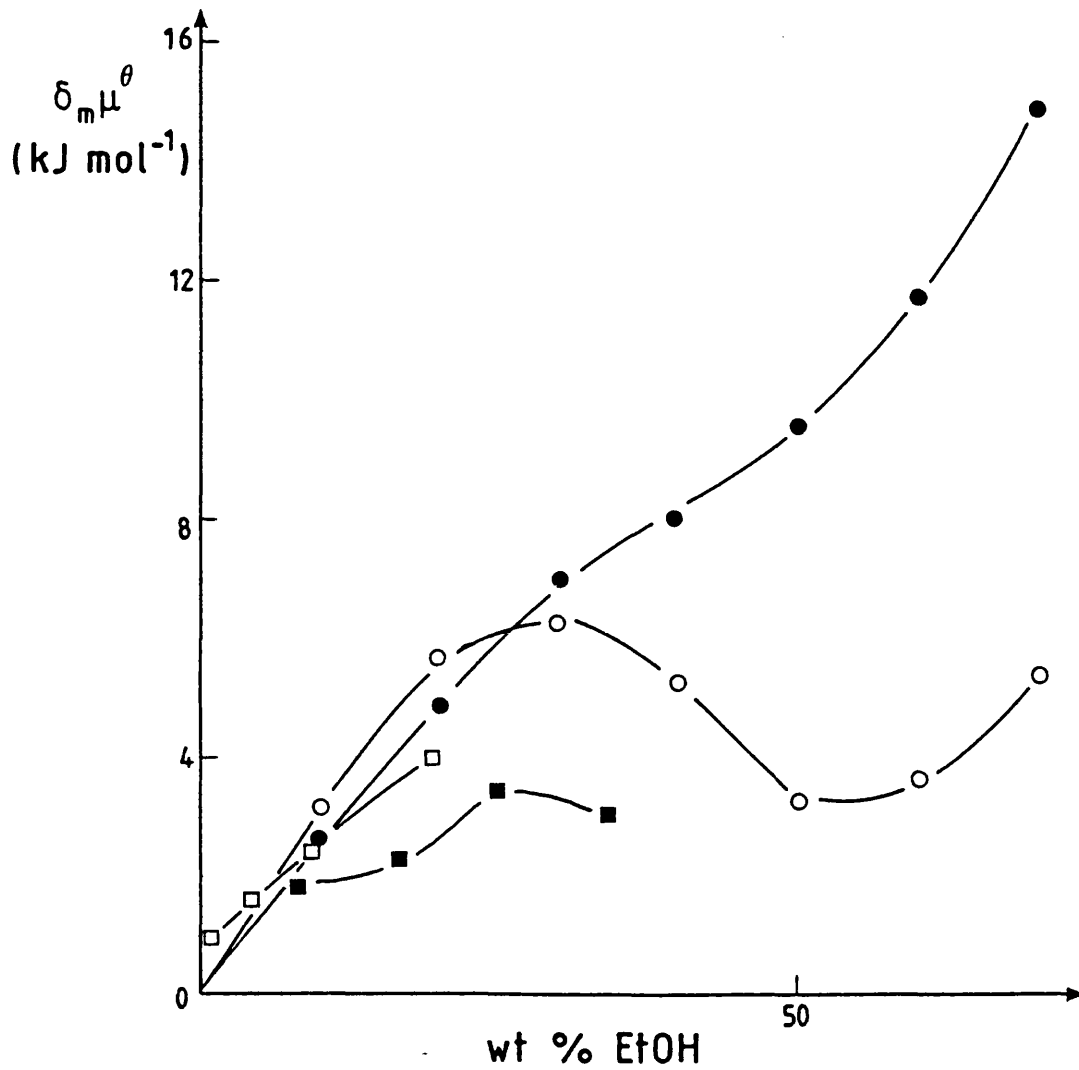


FIGURE 3.20

Transfer chemical potentials for  $\text{Pb}^{2+}$  (molar scale, 298.2 K, TATB assumption) derived using data for  $\text{Pb}(\text{OAc})_2$  [ref. 81] (●);  $\text{PbSO}_4$  [refs. 82, 83] (■);  $\text{PbCl}_2$  [ref. 84] (□);  $\text{PbCl}_2$  [ref. 85] (○).

### 3.3.3 General solvation pattern in aqueous ethanol mixtures

#### *Halide ions*

The  $\delta_m \mu^\ominus$  values for the halide ions calculated using the TATB assumption show, for any given water + ethanol solvent mixture, a decrease in the transfer chemical potentials in the order  $\text{Cl}^- > \text{Br}^- > \text{I}^-$  (Fig. 3.21). With the exception of a negligible negative value at 30 wt % ethanol for the iodide ion, all values for these ions are positive and increase with increasing ethanol content of the solvent mixtures. This trend of decreasing destabilization down the series paralleling increasing ionic size is predicted also by Bax et al.,<sup>20</sup> Wells<sup>19</sup> and Bose et al.<sup>45</sup>

The ions follow a pattern as predicted by the Born equation which is a measure of long-range electrostatic ion-solvent interactions. In this equation the free energy of transfer is estimated to increase with decreasing dielectric constant of the solvent and decreasing ionic radius. Thus for a co-solvent such as ethanol in which the dielectric constants of the mixtures are less than that of water, the Born contribution to the solvation energies of the halide ions should all be positive and decrease in the order  $\text{Cl}^- > \text{Br}^- > \text{I}^-$  as seen.

However, for these ions it is more likely that the solvation energies will be dominated by the effect of the addition of the alcohol on the H-bonding in the primary solvation zone. The small, negatively charged chloride ion is a strong H-bond acceptor and will therefore be destabilized upon transfer from water to a solvent of lower acidity. In water + ethanol mixtures the inductive effect of the ethyl group means that the alcohol molecules have both a more negatively charged O atom and a less positively charged hydroxyl hydrogen atom than in water. The cooperative nature of H-bonding means that ethanol may in turn increase

the basicity and decrease the acidity of the water molecules to which it is bonded. Thus it is proposed that water + ethanol mixtures are more basic than either of the pure liquids. The effect of transferring the chloride ion from water to such mixtures would therefore be one of destabilization. It is interesting that the idea of ethanol conferring increased basicity on water molecules means that speculation as to the exact composition of the first solvation shell is not necessary as the chloride ion will be destabilized relative to water whatever its composition. The decrease in H-bond acceptor ability down the series  $\text{Cl}^- > \text{Br}^- > \text{I}^-$  due to increase in ionic size results in a decrease in the transfer chemical potentials for the ions in the same order.

An alternative explanation of the increased basicity in water + ethanol mixtures relative to the pure liquids has been used to describe the behaviour of the proton in such mixtures (Section 3.3.2). It would be difficult to explain the behaviour of the chloride ion in terms of this model. The destruction of higher aqueous solvates with increasing ethanol content up to 60 wt % EtOH leads to an increase in the number of basic sites and presumably acidic sites. In such a mixture stabilization of the chloride ion would be the expected result.

It is possible that there may be a positive contribution to the solvation energies of these ions resulting from ion-dipole interactions. This is envisaged as being potentially important in the second solvation shell. Favourable contributions to the solvation energies due to dispersion forces in this region are likely to be small. [The effect is proportional to  $\sigma^{-6}$  where  $\sigma$  is the distance between the centres of the ion and the solvent molecule.] The polarizability of the solvent mixtures increases with increasing EtOH content and that of the ions in the order  $\text{Cl}^- < \text{Br}^- < \text{I}^-$  so any contributions of this nature would be greatest for

the iodide ion in higher ethanol content mixtures.

#### *Large organic ions*

For ions such as  $\text{BPh}_4^-$  and  $\text{Ph}_4\text{As}^+$  (Fig. 3.22) stabilization of the ions occurs with transfer from water to water + ethanol mixtures. For these ions the charge is buried under the large organic ligands and the ions behave like neutral molecules showing a marked preference for non-aqueous solvation rather than hydration. Thus the electrostatic contribution to the solvation energy (due mainly to Born-charging and ion-dipole interactions and positive in both cases irrespective of the sign of charge) is very small and the behaviour of these ions is dominated by the neutral contribution. The ions are solvated primarily through dispersion interactions which increase with increasing polarizability of the solvent. The latter increases with increasing ethanol content.

In terms of solvent structure these large ions will fit poorly into highly structured solvents of small molecules such as water. The solvent mixtures are less structured (above the critical region) than pure water and thus transfer to such solvent mixtures is favourable. Thus the structure-breaking ability of the ions is less in the mixtures than in water.

#### *Other anions*

The behaviour of the chloride ion and the tetraphenylborate ion in water + ethanol mixtures explained in terms of electrostatic and neutral contributions to their free energies of transfer provides two extreme cases. The behaviour of  $\text{Cl}^-$  is dominated by electrostatic considerations due to its strong H-bonding interactions and small size resulting in increasing destabilization with increasing ethanol content in the solvent mixtures. The large  $\text{BPh}_4^-$  ion is solvated mainly by dispersion interac-

tions and the neutral contribution to the transfer chemical potential dominates. These favourable interactions increase with increasing ethanol content in the solvent mixtures.

Between these two extremes there are anions for which a balance between these two mutually opposing contributions is achieved.

The transfer chemical potentials of the perchlorate ion (Figs. 3.21 and 3.23) are less than those of the chloride ion though still positive. This reduction may be due to increasing importance of dispersion interactions due to the increased size and polarizability of the perchlorate ion relative to that of the chloride ion. All the quoted authors found the relevant transfer parameters for  $\text{ClO}_4^-$  to be similar to those for  $\text{I}^-$ . For the picrate ion (Fig. 3.22) with increased dispersal of charge, a balance between the electrostatic and neutral contributions to the free energy of transfer is achieved such that only a slight preference for solvation by ethanol is shown. The increasingly negative transfer chemical potentials of the acetate, anthraquinone-2-sulphonate, naphthalene- $\beta$ -sulphonate and  $\text{TAB}^+$  ions (Fig. 3.22) show dispersion interactions becoming increasingly important for these ions.

The preference for solvation by water exhibited by the oxalate and citrate ions presumably reflects the increase in charge (2- and 3- respectively) so that the less favourable electrostatic interactions increasing with increasing basicity of the solvent mixture override favourable interactions between these organic ions and the co-solvent. For the smaller, inorganic, di-negative sulphate ion (Figs. 3.21 and 3.23) the preference for aqueous solvation is even more pronounced.

The transfer chemical potentials for the oxoanions shown in Fig. 3.23 are all positive, i.e. all the ions are destabilized upon transference into ethanol. The order of this destabilization is:-



and is best explained in terms of enhanced basicity in the solvent mixtures. Thus, in less acidic mixtures di-negative ions are more destabilized than uninegative ones. The  $\text{ClO}_4^-$  ion may be less destabilized than  $\text{ClO}_3^-$  due to greater charge dispersal in the former.

#### Cations

Transfer chemical potentials for cations, derived using the TATB assumption, are shown in Fig. 3.24. Disagreement between authors in the estimation of transfer parameters in water + ethanol mixtures is most pronounced for cations (with the exception of the large, organic cations).

The disagreement lies not in the sequence for the cations, in each case the transfer chemical potentials decrease in the order  $\text{K}^+ \approx \text{Rb}^+ > \text{Cs}^+ > \text{Me}_4\text{N}^+ > \text{n-Pr}_4\text{N}^+ > \text{n-Bu}_4\text{N}^+$ , but in whether the ions are preferentially solvated by water or the solvent mixtures. This, in fact, applies only to  $\text{K}^+$ ,  $\text{Rb}^+$ ,  $\text{Cs}^+$  and  $\text{Me}_4\text{N}^+$  as the values for  $\text{n-Pr}_4\text{N}^+$  and  $\text{n-Bu}_4\text{N}^+$  although varied are all negative.

For  $\text{K}^+$ ,  $\text{Rb}^+$ ,  $\text{Cs}^+$  and  $\text{Me}_4\text{N}^+$ , all values predicted in this work using the TATB assumption and those due to Bax *et al.*<sup>20</sup> are positive and increase with increasing ethanol content (the only exception being a very small negative value for  $\text{Me}_4\text{N}^+$  at 50 wt % EtOH calculated in this work). In contrast to this, all values estimated by Wells<sup>19</sup> for these four ions below 50 wt % EtOH are negative. At higher ethanol content, values for  $\text{K}^+$  and  $\text{Rb}^+$  become positive. Thus in lower wt % EtOH mixtures the difference between alternative sets of estimations is not one of degree for an agreed effect (stabilization or destabilization) but of the effect itself.

The behaviour of the sodium ion in water + ethanol mixtures derived

using the TATB assumption follows that predicted by the Born equation, i.e. increasing destabilization with decreasing dielectric constant. In terms of ion-dipole interactions the transfer of this ion from water into ethanol is also unfavourable and so the transfer chemical potentials for this ion would seem to be dominated by unfavourable electrostatic considerations. Along the series  $\text{Na}^+$ ,  $\text{K}^+$ ,  $\text{Rb}^+$ ,  $\text{Cs}^+$ ,  $\text{Me}_4\text{N}^+$ ,  $\text{n-Pr}_4\text{N}^+$ ,  $\text{n-Bu}_4\text{N}^+$  the size of the ion and its polarizability increases and so the contribution to the change in solvation energy made by these electrostatic interactions decreases in the same order. Any favourable contribution due to dispersion interactions will, however, increase along the series and for a given ion will increase with increasing ethanol content of the solvent. These considerations together with the change from hydrophilic to hydrophobic character along the series are consistent with the values obtained for these ions using the TATB assumption.

The order of transfer chemical potentials in the series  $\text{Li}^+ < \text{K}^+ < \text{Na}^+$  has been identified by other authors in water-rich mixtures of aqueous alcohols.<sup>24,92</sup>

It is difficult to explain the behaviour of  $\text{Li}^+$ ,  $\text{Na}^+$ ,  $\text{K}^+$ ,  $\text{Rb}^+$  and  $\text{Cs}^+$  in terms of the modified charge distribution in the mixed solvents as compared to that in water. Increased charge on the oxygen atoms in the mixtures would be expected to have a stabilizing effect on these ions.

The effect of increased charge can be seen by comparing transfer chemical potentials for  $\text{K}^+$  and  $\text{Ba}^{2+}$  which are ions of approximately equal radius.<sup>93</sup> The divalent cation is as expected more destabilized than the univalent cation. All the divalent cations are in fact more destabilized than the univalent cations except for  $\text{Ca}^{2+}$  at low wt % ethanol. The result that 'hard'  $\text{Ca}^{2+}$  is less destabilized than 'soft'  $\text{Pb}^{2+}$  (as was found to be the case in water + methanol mixtures<sup>26</sup>) may at

first seem surprising. Values for  $\delta_{m\mu}^{\ominus}(\text{Ca}^{2+})$ , however, are given only at low wt % ethanol mixtures. It is possible that in ethanol-rich solvent mixtures stronger preferential hydration of  $\text{Ca}^{2+}$  than of  $\text{Pb}^{2+}$  could result in  $\delta_{m\mu}^{\ominus}(\text{Ca}^{2+})$  values being more positive than those for  $\delta_{m\mu}^{\ominus}(\text{Pb}^{2+})$ . The greater destabilization of  $\text{Hg}^{2+}$  than  $\text{Pb}^{2+}$  is surprising. As expected 'soft'  $\text{Ag}^+$  and  $\text{Tl}^+$  are slightly less destabilized than 'hard'  $\text{Cs}^+$  on increasing the ethanol content of the mixture.

#### *Halogenoanions*

All these ions are destabilized upon transfer from water into water + ethanol mixtures (Fig. 3.25) all preferring solvation by water with the exception of  $[\text{UO}_2\text{Cl}_4]^{2-}$  at low wt % EtOH. This is presumably due to the less favourable interactions of the negatively charged halogen atoms in the complexes with alcohol than with water. The destabilization is greatest for  $[\text{SiF}_6]^{2-}$  in which the charge density is greatest and in which the halogen atoms are the highly electronegative fluorine atoms.

#### *Fe(II) and Co(III) complex ions*

The transfer chemical potentials of the Fe(II) complex cations, shown in Fig. 3.26, indicate that all three ions,  $[\text{Fe}(\text{phen})_3]^{2+}$ ,  $[\text{Fe}(\text{bipy})_3]^{2+}$  and  $[\text{Fe}(\text{bsb}, \text{Ph}, \text{Ph}; \text{m-Ome})_3]^{2+}$  are markedly stabilized upon transfer from water into aqueous ethanol mixtures, as is expected considering the large, hydrophobic nature of the ligands. The effect of such transfer on the Co(III) complexes shown in Fig. 3.26 is much less marked. All four Co(III) complexes exhibit a preference for solvation by water. This preference is largest for the triply charged  $[\text{Co}(\text{NO}_2)_6]^{3-}$  ion and least for the singly charged  $[\text{Co}(\text{en})_2\text{Cl}_2]^+$  ion. The two doubly charged Co(III) complexes occupy intermediate positions. The solvation pattern of these Co(III) complexes also reflects the fact that en is more hydrophobic than  $\text{NH}_3$  and that  $\text{NO}_2^-$  and  $\text{Cl}^-$  are both more hydrophilic than either en or  $\text{NH}_3$ .

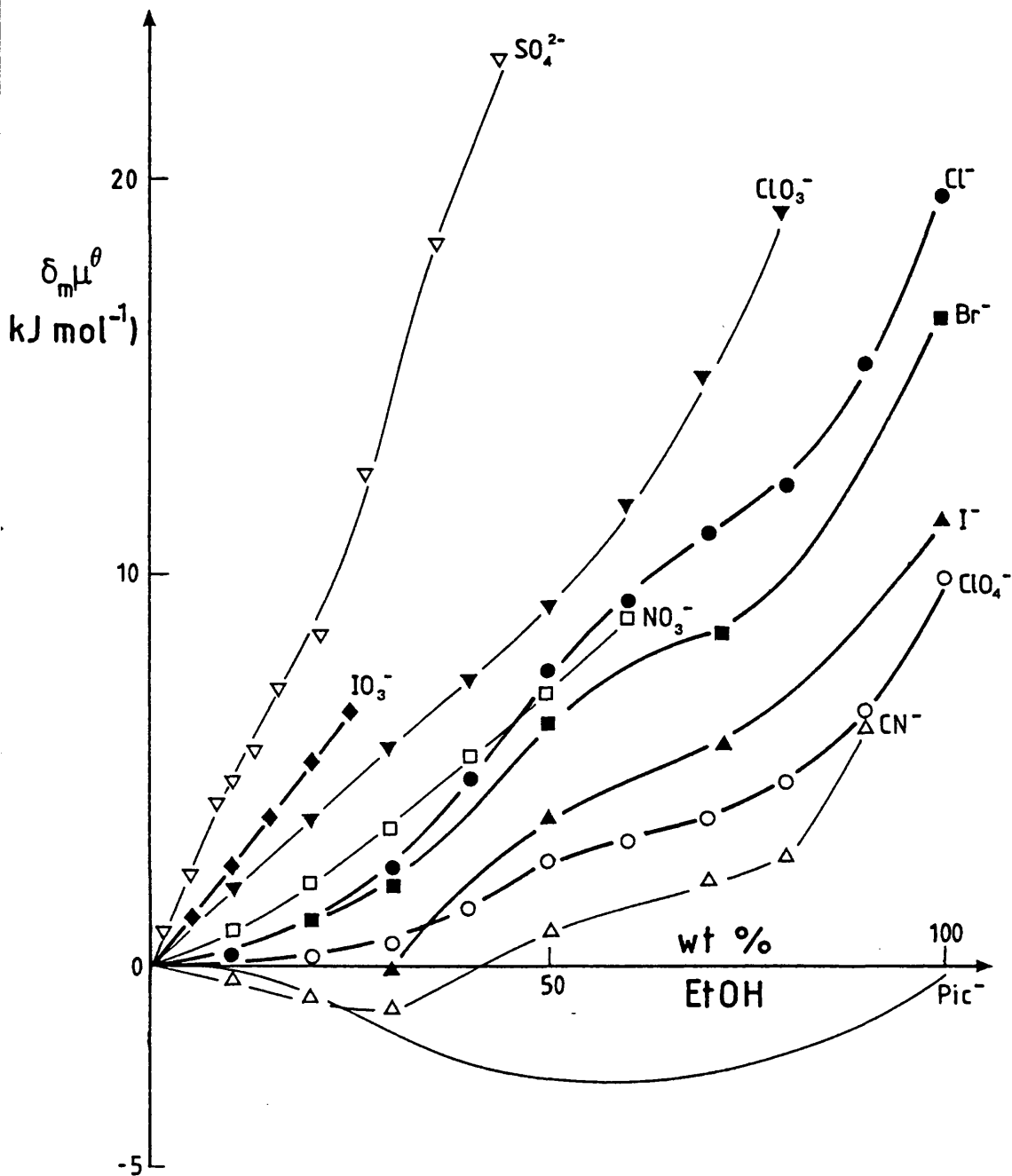


FIGURE 3.21

Transfer chemical potentials for simple anions (molar scale, 298.2 K, TATB assumption) in water + ethanol mixtures.

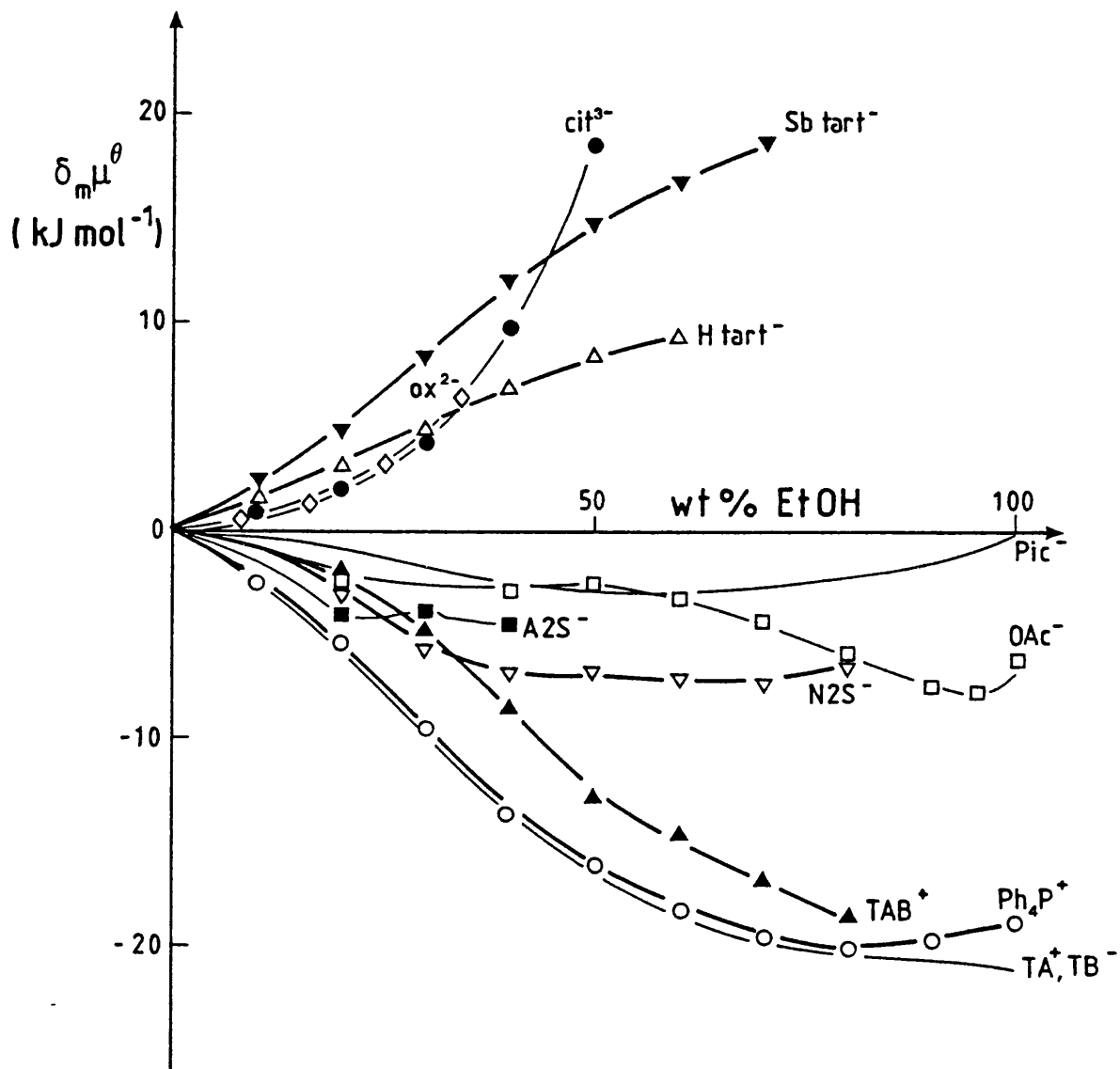


FIGURE 3.22

Transfer chemical potentials for some organic ions (molar scale, 298.2 K, TATB assumption) in water + ethanol mixtures.

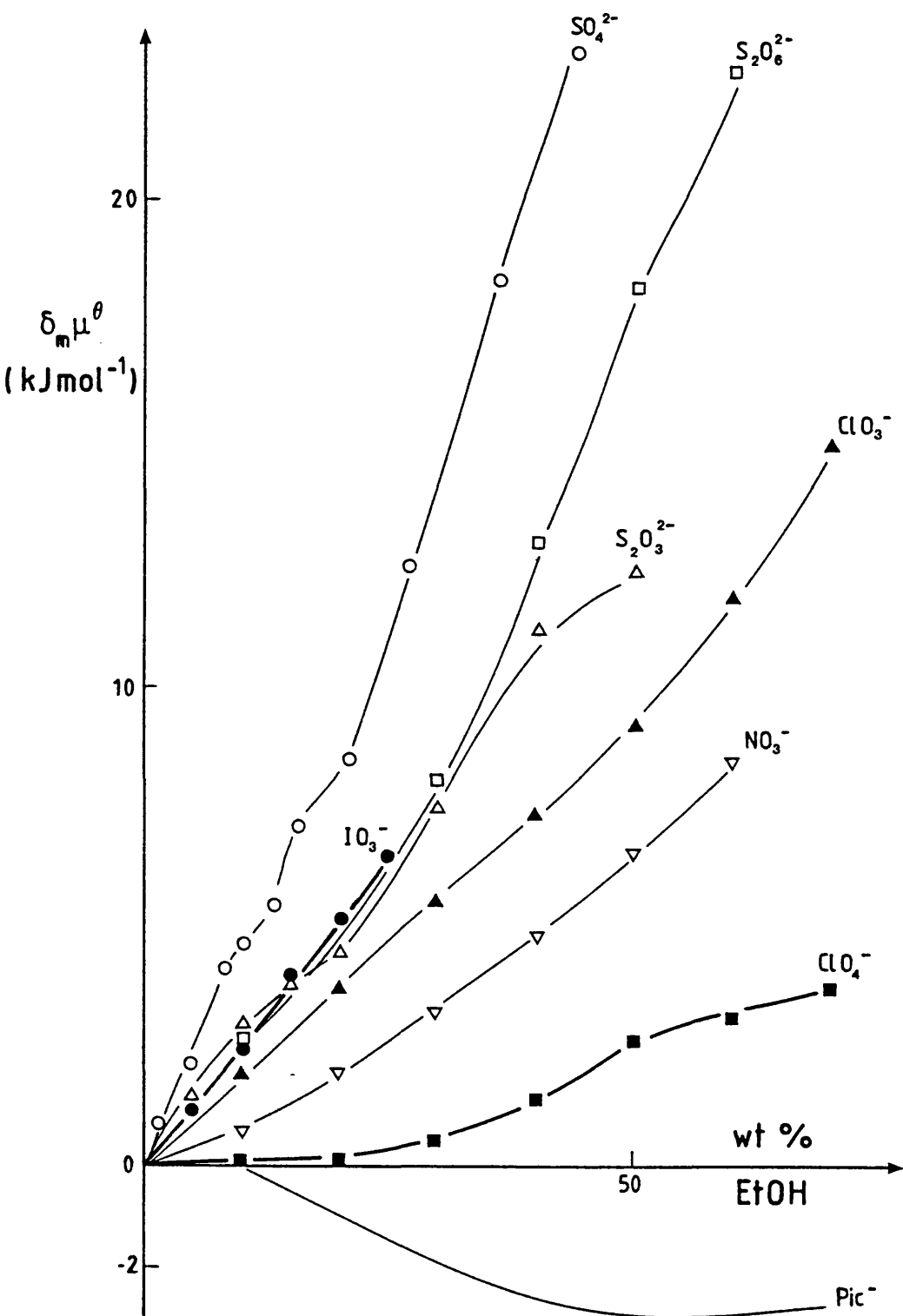


FIGURE 3.23

Transfer chemical potentials for oxoanions (molar scale, 298.2 K, TATB assumption) in water + ethanol mixtures.

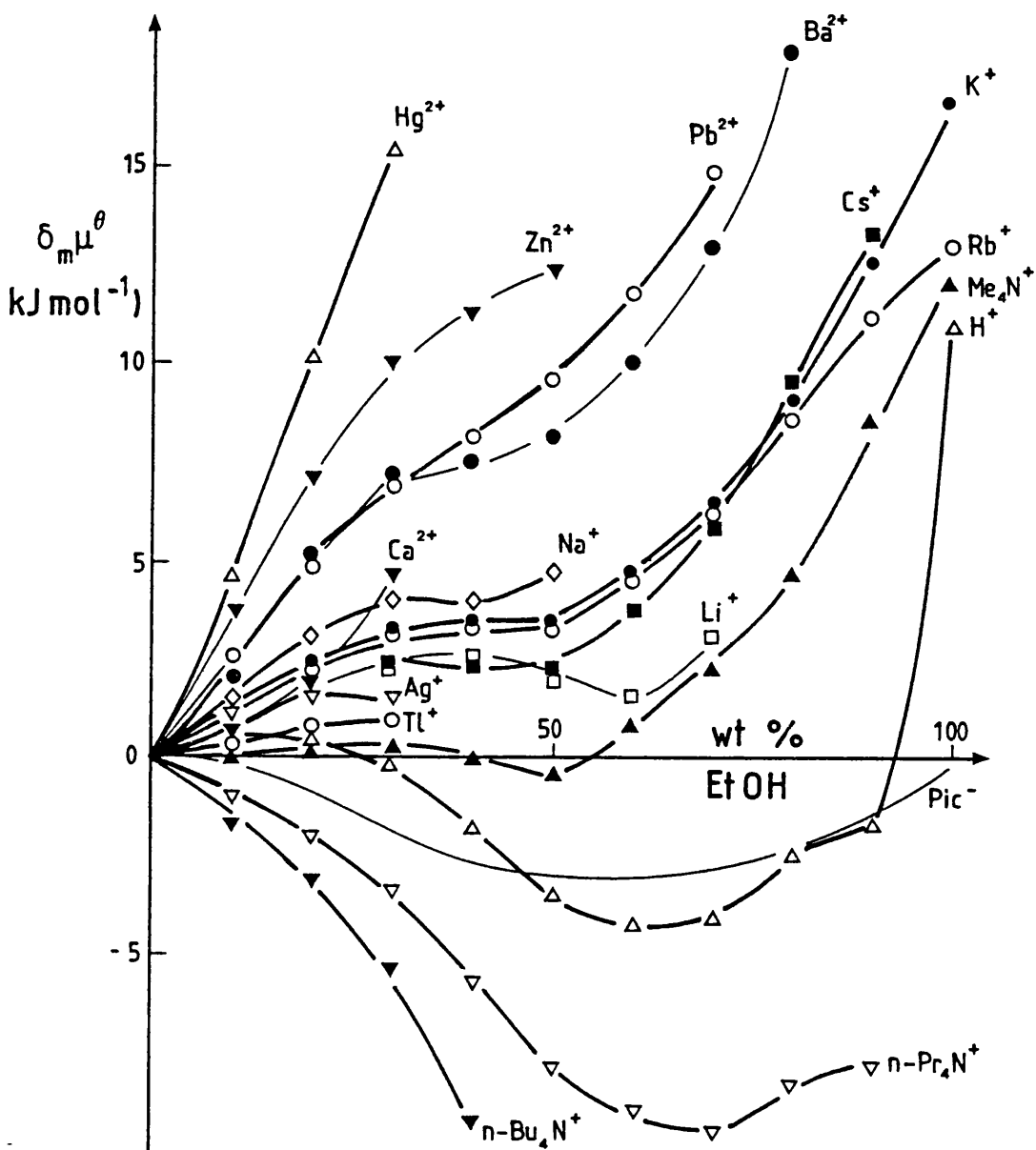


FIGURE 3.24

Transfer chemical potentials for simple cations (molar scale, 298.2 K, TATB assumption) in water + ethanol mixtures.

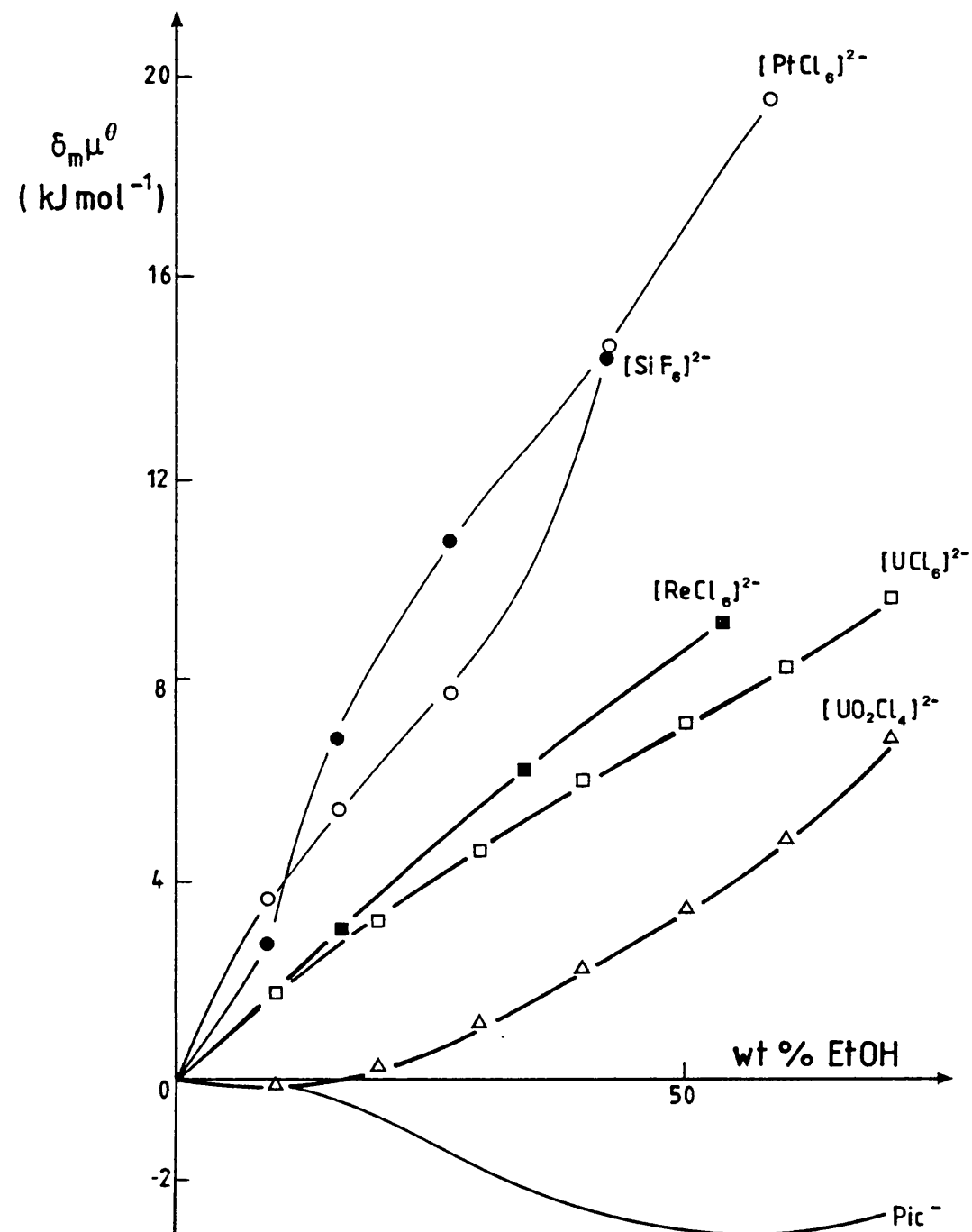


FIGURE 3.25

Transfer chemical potentials for halogenoanions (molar scale, 298.2 K, TATB assumption) in water + ethanol mixtures.

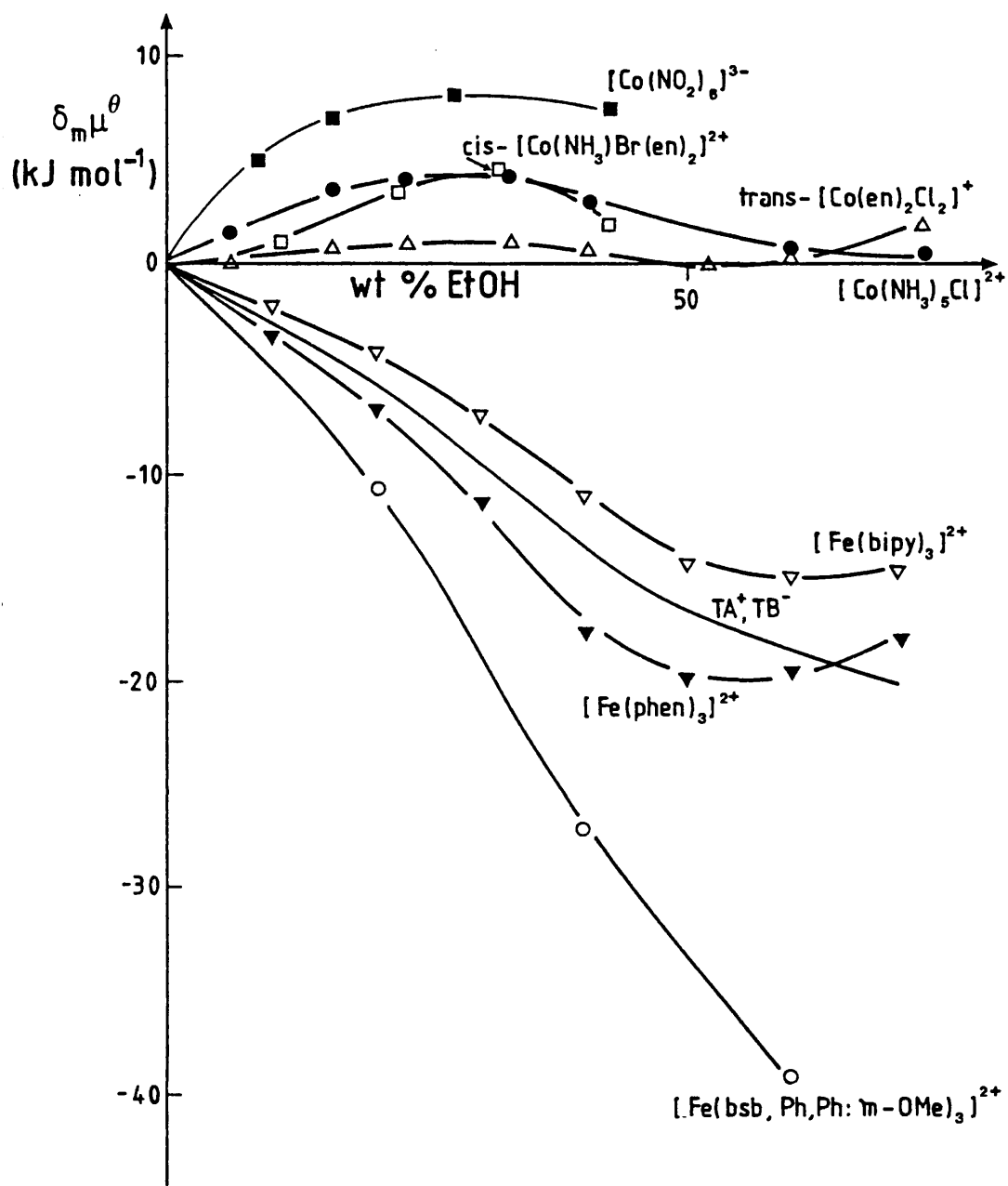


FIGURE 3.26

Transfer chemical potentials for some Fe(II) and Co(III) complexes (molar scale, 298.2 K, TATB assumption) in water + ethanol mixtures.

### 3.3.4 Comparison of solvation patterns in aqueous alcohols and aqueous acetone mixtures

Transfer chemical potentials for a range of ions in various water + co-solvent mixtures are shown in Fig. 3.27. The co-solvents are acetone,<sup>94</sup> methanol,<sup>14</sup> ethanol (this work), isopropanol<sup>94</sup> and t-butyl alcohol.<sup>95</sup> All values are based on the TATB assumption. [In the case of methanol as the co-solvent the TPTB assumption was actually used but this has been proved to be almost identical to the TATB assumption in these solvent mixtures.<sup>92</sup>]

In all five aqueous mixtures the halide ions,  $\text{Cl}^-$ ,  $\text{Br}^-$  and  $\text{I}^-$ , are destabilized and the destabilization increases with increasing co-solvent content in the solvent mixture. In comparing the transfer chemical potentials for each of these ions in the different aqueous alcohol mixtures it can be seen that there is a general increase in destabilization with increasing size of the alkyl group in the alcohol. This trend can be interpreted in terms of the inductive effect of the alkyl residue. This effect, leading to decreased partial positive charge on the hydroxyl hydrogen in the alcohol molecules relative to water, increases in the order  $\text{MeOH} < \text{EtOH} < \text{Pr}^i\text{OH} < \text{Bu}^t\text{OH}$ . Thus, although transfer from water to aqueous mixtures of any of these alcohols is unfavourable for these ions in terms of H-bonding, the effect is most pronounced for aqueous t-butyl alcohol mixtures and decreases in the order  $\text{Bu}^t\text{OH} > \text{Pr}^i\text{OH} > \text{EtOH} > \text{MeOH}$ .

These ions are all markedly more destabilized in water + acetone mixtures than in any of the aqueous alcohol mixtures. This can be explained in terms of the inability of acetone to form H-bonds with these ions.

The destabilization of the perchlorate ion in aqueous alcohols follows a similar pattern to that of the halide ions, i.e. destabilization in

the solvent mixtures decreases in the order  $\text{Pr}^i\text{OH} > \text{EtOH} > \text{MeOH}$ . The destabilization of this ion in aqueous t-butyl alcohol is however slightly less than that in aqueous isopropanol. The similar destabilizing effect of aqueous acetone and aqueous t-butyl alcohol mixtures on the  $\text{ClO}_4^-$  ion, both being less than that in aqueous isopropanol, could indicate the increased importance of dispersion interactions as both the ion and co-solvent become more polarizable.

For the large organic ions  $\text{Ph}_4\text{As}^+$  and  $[\text{Fe}(\text{phen})_3]^{2+}$ , the rapid initial stabilization upon transfer from water into all these solvent mixtures increases in the order  $\text{aq MeOH} < \text{aq EtOH} < \text{aq Pr}^i\text{OH} < \text{aq Bu}^t\text{OH} < \text{aq acetone}$ , paralleling the increasing size in the hydrophobic moiety and increasing polarizability along the series of alcohols and the decrease in structure of the solvent mixtures.

Stabilization of the proton upon transfer from water into aqueous alcohols occurs at progressively lower wt % co-solvent content values for MeOH, EtOH and  $\text{Bu}^t\text{OH}$ . In terms of solvent structure this is expected as the higher the alcohol the greater is the relative degree of breakdown of water structure in aqueous mixtures with the same proportion of co-solvent content. Thus, more basic sites become available for bonding with the proton with the addition of a certain amount of  $\text{Bu}^t\text{OH}$  than addition of the same amount of MeOH.

Fig. 3.28 shows transfer chemical potentials for various cations in the same five water + co-solvent mixtures due to the same authors as in the previous figure.

For the  $\text{K}^+$ ,  $\text{Rb}^+$  and  $\text{Cs}^+$  ions the destabilization observed in aqueous alcohol mixtures decreases in terms of the co-solvent in the order  $\text{MeOH} > \text{EtOH} > \text{Pr}^i\text{OH}$ . In complete contrast to this is the stabilization of these ions in aqueous acetone mixtures.

Addition of any of these co-solvents to water results in mixtures which are less structured than water (above the critical composition range in the case of alcohols). The degree of this structure breakdown will depend partly on the compensatory formation of solvent/co-solvent interactions and will therefore be greater in aqueous acetone than in aqueous alcohols as in the latter both types of solvent molecules can act both as H-bond donors and acceptors. Thus, although in both types of aqueous mixtures an increased number of basic sites are available on the water molecules for interaction with the cation, alcohol molecules can interact more favourably with these basic sites than can acetone molecules and the former are thus in a sense in competition with the cations for such sites. This results in destabilization of the ions in aqueous alcohol mixtures and stabilization in aqueous acetone mixtures relative to water.

Ions behave in much the same way upon transfer from water into aqueous mixtures of any of these alcohols. Observed differences in degree of stabilization or destabilization of the ions has its basis in the effect of the reduced similarity between properties of alcohol and water molecules with increasing size of the alkyl group in the alcohol.

Differences between the structure and behaviour of the two components in aqueous acetone are much more pronounced than in aqueous alcohols. This results in generally more marked behaviour in the former than the latter when the effect on the ions is of the same type but can also result in opposite effects on ions as in the case of alkali-metal cations.

The relative behaviour of given ions in various binary aqueous mixtures is affected by the nature of the extrathermodynamic assumption employed in the analysis. For example, the difference in the behaviour of ions

in aqueous acetone mixtures and in aqueous alcohol mixtures appears to be more pronounced in values derived using the TATB assumption than, say, in the values predicted by Wells.<sup>96</sup>

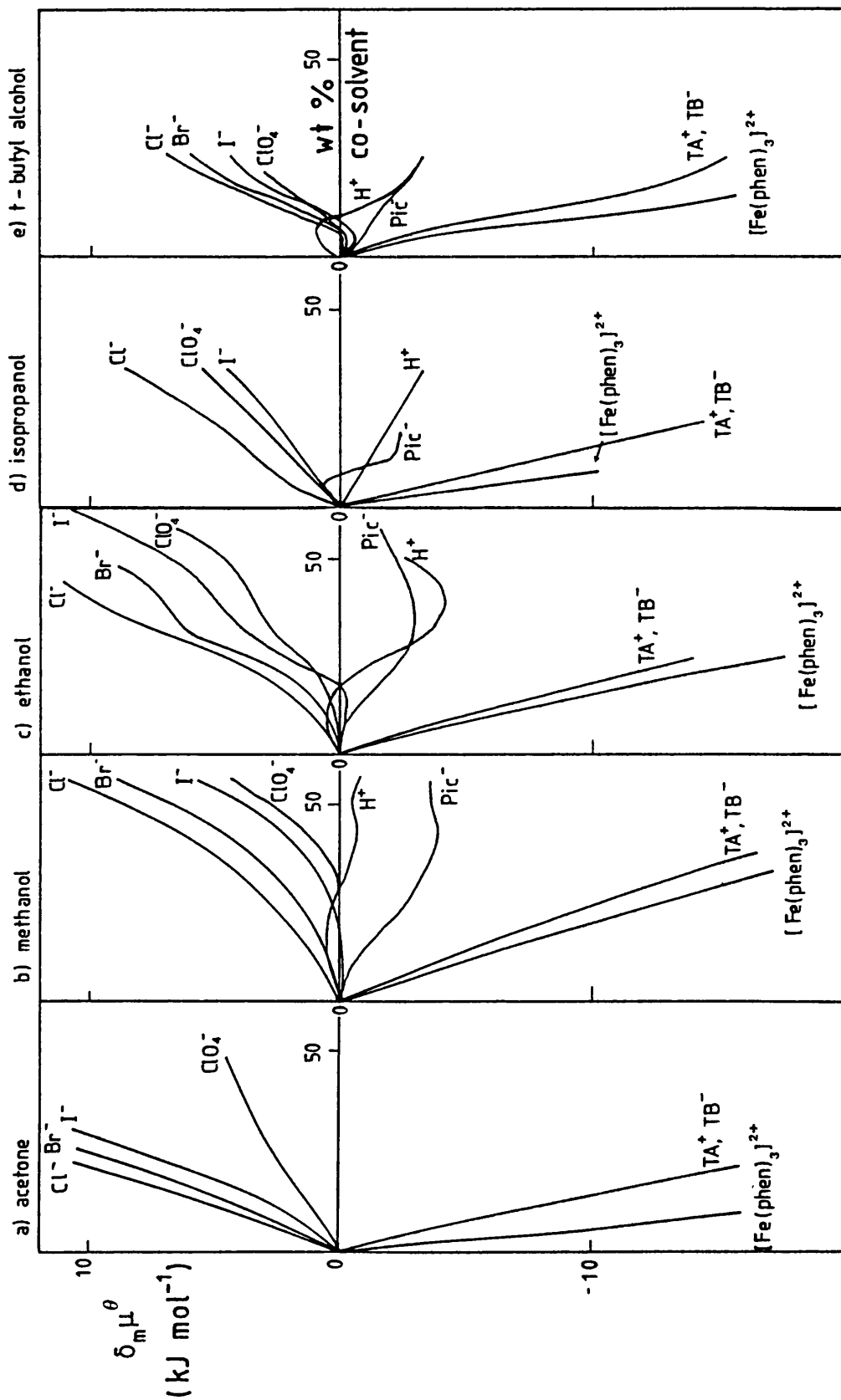


FIGURE 3.27  
 Transfer chemical potentials for ions (molar scale, 298.2 K, TATB assumption) in aqueous mixtures of a) acetone; b) methanol; c) ethanol; d) isopropanol; e) t-butyl alcohol.

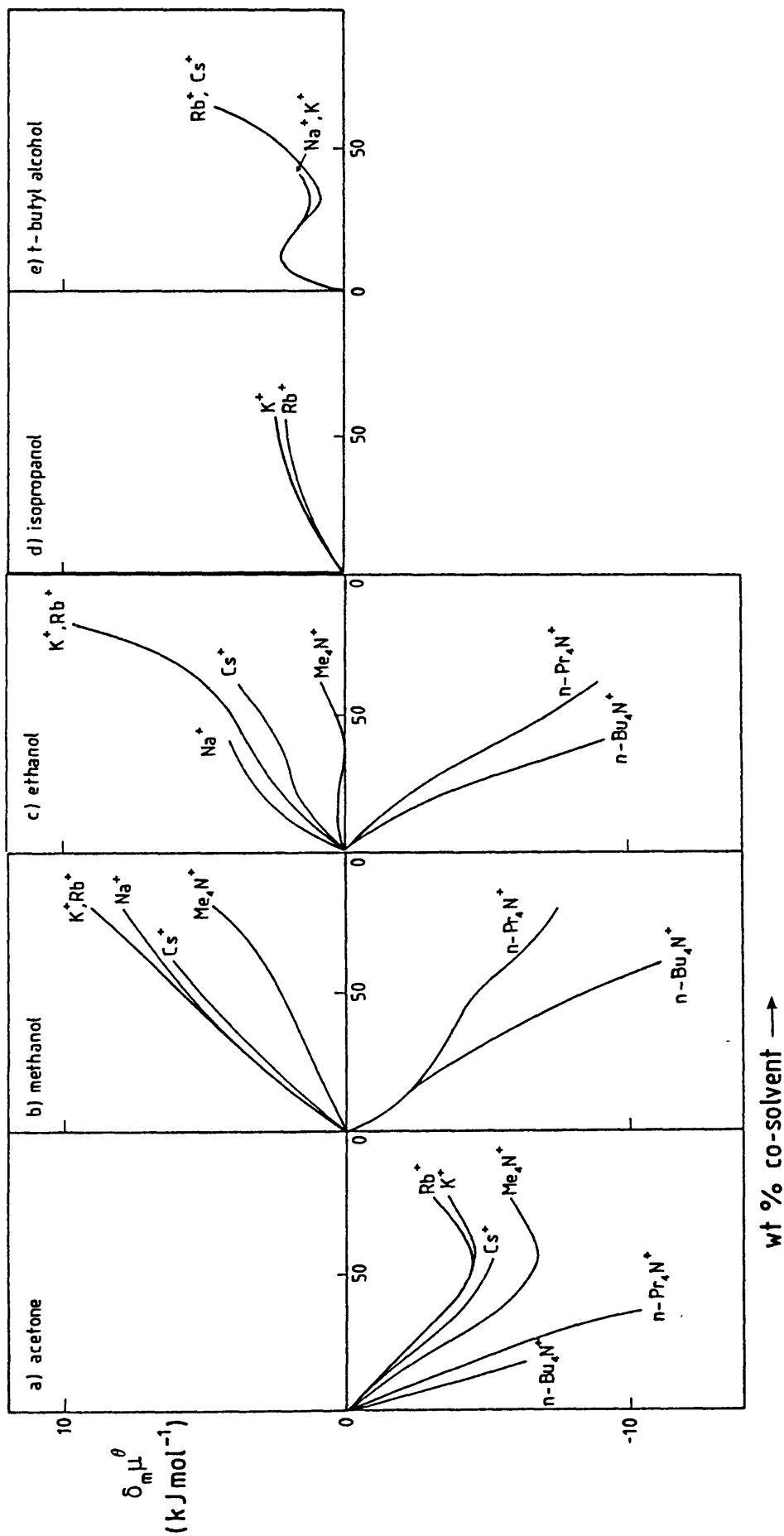


FIGURE 3.28

Transfer chemical potentials for cations (molar scale, 298.2 K, TATB assumption) in aqueous mixtures of a) acetone; b) methanol; c) ethanol; d) isopropanol; e) t-butyl alcohol.

### REFERENCES FOR CHAPTER 3

In the list of references below, the following abbreviations are made.

"Stephen and Stephen" refers to "Solubilities of Inorganic and Organic Compounds", Volume 2, parts 1 and 2, ed. H. Stephen and T. Stephen, Pergamon Press, Oxford, 1963.

"Seidell" refers to "Solubilities of Inorganic and Metal Organic Compounds", 3rd. edn., Volume 1, ed. A. Seidell, D. Van Nostrand Company, New York, 1940.

- 
1. A. Ben-Naim, J. Phys. Chem., 1978, 82, 792.
  2. A. J. Parker and R. Alexander, J. Am. Chem. Soc., 1968, 90, 3313.
  3. A. J. Parker, Chem. Rev., 1969, 69, 1.
  4. O. Popovych, Crit. Rev. Anal. Chem., 1970, 1, 73.
  5. Y. Marcus, Rev. Anal. Chem., 1980, 5, 53.
  6. Y. Marcus, Pure and Appl. Chem., 1986, 58, 1721.
  7. E. Grunwald, G. Baughman and G. Kohnstam, J. Am. Chem. Soc., 1960, 82, 5801.
  8. R. Alexander and A. J. Parker, J. Am. Chem. Soc., 1967, 89, 5549.
  9. O. Popovych, Anal. Chem., 1966, 38, 558.
  10. B. G. Cox, G. R. Hedwig, A. J. Parker and D. W. Watts, Aust. J. Chem., 1974, 27, 477.
  11. I. M. Kolthoff and M. K. Chantooni, J. Phys. Chem., 1972, 76, 2024.
  12. O. Popovych, A. Gibofsky and D. H. Berne, Anal. Chem., 1972, 44, 811.
  13. S. Villiermaux, V. Baudot and J. J. Delpuech, Bull. Soc. Chim. Fr., 1972, 1781.
  14. M. H. Abraham, T. Hill, H. C. Ling, R. A. Schultz and R. A. C. Watt, J. Chem. Soc., Faraday Trans. I, 1984, 80, 489.
  15. J. I. Kim, J. Phys. Chem., 1978, 82, 191.
  16. J. I. Kim, Z. Phys. Chem. (N.F.), 1978, 113, 129.
  17. M. Booiij and G. Somsen, Electrochim. Acta, 1983, 28, 1883.
  18. O. Popovych and A. J. Dill, Anal. Chem., 1969, 41, 456.
  19. C. F. Wells, J. Chem. Soc., Faraday Trans. I, 1984, 80, 2445.
  20. D. Bax, C. L. de Ligny and A. G. Remijnse, Rec. Trav. Chim., 1972, 91, 965.
  21. C. F. Wells, J. Chem. Soc., Faraday Trans. I, 1973, 69, 984.
  22. C. F. Wells, J. Chem. Soc., Faraday Trans. I, 1974, 70, 694.
  23. C. F. Wells, J. Chem. Soc., Faraday Trans. I, 1975, 71, 1868.

REFERENCES (Continued) ....

24. C. F. Wells, J. Chem. Soc., Faraday Trans. I, 1976, 72, 601.
25. C. F. Wells, J. Chem. Soc., Faraday Trans. I, 1978, 74, 636.
26. M. J. Blandamer, J. Burgess, B. Clark, P. P. Duce, A. W. Hakin, N. Gosal, S. Radulovic, P. Guardado, F. Sanchez, C. D. Hubbard and E. A. Abu-Gharib, J. Chem. Soc., Faraday Trans. I, 1986, 82, 1471.
27. M. Alfenaar and C. L. de Ligny, Rec. Trav. Chim., 1967, 86, 929.
28. A. D. Buckingham, Disc. Faraday Soc., 1957, 24, 151.
29. H. F. Halliwell and S. C. Nyburg, Trans. Faraday Soc., 1963, 59, 1126.
30. J. S. Muirhead-Gould and K. J. Laidler, Trans. Faraday Soc., 1963, 59, 1126.
31. D. Bax, C. L. de Ligny and M. Alfenaar, Rec. Trav. Chim., 1972, 91, 452.
32. N. Bjerrum and E. Larsson, Z. Phys. Chem., 1927, 127, 358.
33. D. H. Berne and O. Popovych, Anal. Chem., 1972, 44, 817.
34. R. M. Noyes, J. Am. Chem. Soc., 1962, 84, 513.
35. G. R. Haugen and K. L. Friedman, J. Phys. Chem., 1968, 72, 4549.
36. H. S. Frank and W. Y. Wen, Disc. Faraday Soc., 1957, 24, 133.
37. G. Nemethy and H. A. Scheraga, J. Chem. Phys., 1962, 36, 3382.
38. D. Feakins and P. Watson, J. Chem. Soc., 1963, 4734.
39. R. Lumry, E. Battistel and C. Jolicoeur, Faraday Symp. Chem. Soc., 1982, 17, 93.
40. S. G. Bruun, P. G. Sørensen and A. Hvidt, Acta Chem. Scand., 1974, A28, 1047.
41. "CRC Handbook of Chemistry and Physics", 62nd. edn., ed. R. C. Weast, CRC Press, Boca Raton, Florida, 1981/1982.
42. D. H. Berne and O. Popovych, J. Chem. Eng. Data, 1972, 17, 178.
43. A. J. Dill and O. Popovych, J. Chem. Eng. Data, 1969, 14, 240.
44. A. J. Dill, L. M. Itzkowitz and O. Popovych, J. Phys. Chem., 1968, 72, 4580.
45. K. Bose, K. Das, A. K. Das and K. K. Kundu, J. Chem. Soc., Faraday Trans. I, 1978, 5, 1051.
46. C. L. de Ligny, D. Bax, M. Alfenaar and M. G. L. Elferink, Rec. Trav. Chim., 1969, 88, 1183.
47. M. Pierrat, Compt. Rend., 1921, 172, 1041.
48. Stephen and Stephen, part 1, p.324.
49. Stephen and Stephen, part 1, p.354.
50. Seidell, p.848.

REFERENCES (Continued) ....

51. M. J. Blandamer, J. Burgess and A. J. Duffield, J. Chem. Soc., Dalton Trans., 1980, 1.
52. Stephen and Stephen, part 1, p.321.
53. Seidell, p.875.
54. Seidell, p.600.
55. Seidell, p.709.
56. Stephen and Stephen, part 1, p.361.
57. A. P. Krasnoperova, B. S. German and V. S. Chernyi, Izv. Vyssh. Uchebn. Zaved., Khim. Khim. Tekhnol., 1973, 16, 699.
58. J. A. Molzon, J. M. Lausier and A. N. Paruta, J. Pharm. Sci., 1978, 67, 733.
59. A. P. Krasnoperova, Russ. J. Phys. Chem., 1975, 49, 1838.
60. Seidell, p.705.
61. Seidell, p.700.
62. Seidell, p.1169.
63. E. A. Braude and E. S. Stern, J. Chem. Soc., 1967, 1948.
64. Seidell, p.916.
65. Seidell, p.933.
66. Seidell, p.902.
67. Seidell, p.1175.
68. Seidell, p.17.
69. Seidell, p.13.
70. J. I. Kim and H. Duschner, J. Inorg. Nucl. Chem., 1977, 39, 471.
71. Seidell, p.65.
72. Seidell, p.1554.
73. Stephen and Stephen, part 1, p.517.
74. Stephen and Stephen, part 1, p.572.
75. Seidell, p.1511.
76. Seidell, p.343.
77. Stephen and Stephen, part 1, p.593.
78. Stephen and Stephen, part 1, p.605.
79. Stephen and Stephen, part 1, p.565.
80. R. I. Haines, Ph.D. Thesis, Leicester, 1977.
81. Seidell, p.1375.
82. E. Koizumi, J. Chem. Soc. Japan, Pure Chem. Section, 1948, 69, 40.
83. I. M. Kolthoff, R. W. Perlich and D. Welblen, J. Phys. Chem., 1942, 46, 561.

REFERENCES (Continued) ....

84. Seidell, p.1393.
85. Stephen and Stephen, part 1, p.706.
86. J. Burgess and S. J. Cartwright, J. Chem. Soc., Dalton Trans., 1975, 100.
87. J. I. Kim, H. Duschner, H.-J. Born and T. Hashimoto, Z. Phys. Chem., 1976, 103, 15.
88. E. M. Strel'tsova, N. K. Markova and G. A. Krestov, Russ. J. Phys. Chem., 1974, 48, 992.
89. E. M. Strel'tsova, N. K. Markova and G. A. Krestov, Izvest. Vyssh. Uchebn. Zaved., Khim. Khim. Tekhnol., 1973, 16, 694.
90. O. Grancicova and V. Holba, Trans. Met. Chem., 1984, 9, 322.
91. C. D. Hubbard, personal communication.
92. O. Popovych, J. Phys. Chem., 1984, 88, 4167.
93. F. A. Cotton and G. Wilkinson, "Advanced Inorganic Chemistry", 4th. edn., Wiley, New York, 1980.
94. B. Clark, Ph.D. Thesis, Leicester, 1986.
95. J. Juillard and C. Tissier, Electrochim. Acta, 1982, 27, 123;  
J. Burgess and P. P. Duce, personal communication.
96. C. F. Wells, Aust. J. Chem., 1983, 36, 1739.



## CHAPTER 4

**Solvation of Ions in Water + Ethylene  
Glycol and Water + Glycerol Mixtures**

## 4.1 INTRODUCTION

### 4.1.1 General

In the previous chapter single-ion transfer chemical potentials derived using the tetraphenylarsonium tetraphenylboronate (TATB) assumption were used to probe the nature of ion solvation in several binary aqueous mixtures. Comparisons were made between the solvation patterns for ions in aqueous mixtures of a dipolar aprotic solvent (acetone) and of several lower monohydric alcohols (methanol, ethanol, isopropanol and t-butyl alcohol). The comparison between single-ion transfer parameters for the aqueous alcohol mixtures provided an insight into the effect on ion solvation of the size of the alkyl group in the alcohol. In this chapter the effect due to increased number of hydroxyl groups in the organic co-solvent is investigated by studying transfer parameters of single ions in aqueous mixtures of ethylene glycol (ethane-1,2-diol) and of glycerol (propane-1,2,3-triol).

Transfer chemical potentials for single ions in water + ethylene glycol (EG) and water + glycerol (G) mixtures are derived from available data in the literature in the same way as for water + ethanol mixtures in Chapter 3. Once again the TATB assumption is the extrathermodynamic assumption used. The data are presented on the same solute and solvent composition scales as before (viz. molar and weight percentage co-solvent scales respectively).

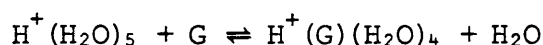
As a result of the close similarity between this chapter and Chapter 3 much of the introductory discussion in the latter (Section 3.1) concerning extrathermodynamic assumptions, composition scales, interpretation of transfer parameters, etc., is equally relevant here.

#### 4.1.2 Methods used by other authors

As in Chapter 3, single-ion transfer parameters derived using the TATB assumption are compared with those derived by other authors using alternative extrathermodynamic assumptions.

For water + EG mixtures, results from the works of Wells,<sup>1</sup> Kundu et al.,<sup>2</sup> and Rao et al.<sup>3</sup> are cited. For water + G mixtures, results due to Wells<sup>4</sup> and Khoo<sup>5</sup> are used. Where such comparisons are made all the data due to the different sets of authors have been converted to the molar solute composition scale and the weight percentage co-solvent composition scale.

The method used by Wells for both of these aqueous solvent mixtures<sup>1,4</sup> was based on the calculation of Gibbs free energies of transfer for the proton,  $\Delta G_t^\ominus(\text{H}^+)$ , from a consideration of the transfer of the spherical entity  $\text{H}^+(\text{H}_2\text{O})_5$ . This is the same method used by Wells for calculating values of  $\Delta G_t^\ominus(\text{H}^+)$  in aqueous ethanol and other binary aqueous mixtures (see Section 3.1.3). In addition to the general criticisms of this method,<sup>6</sup> Basumullick et al.<sup>7</sup> expressed doubt as to its validity specifically in water + G mixtures. Their concern was with the fact that for the reaction



the equilibrium constant,  $K_c$ , is negligibly small for these solvent mixtures. This meant that for water + G mixtures, values of  $\Delta G_t^\ominus(\text{H}^+)$  were calculated by Wells<sup>4</sup> on the basis of Born-type interactions only. In this method all single-ion values are calculated, directly or indirectly, using  $\Delta G_t^\ominus(\text{H}^+)$  so the need for highly accurate values for the proton is essential. Such accuracy in values of  $\Delta G_t^\ominus(\text{H}^+)$  derived from Born-type interactions only is questionable.

For water + G mixtures Khoo<sup>5</sup> used the extrapolation method to derive

single-ion free energies of transfer for the proton. Values of  $\Delta G_t^\ominus(\text{HX})$  where X =  $\text{Cl}^-$ ,  $\text{Br}^-$  and  $\text{I}^-$  were plotted as a function of the inverse anionic radius,  $r_a^{-1}$ . Extrapolation to  $r_a^{-1} = 0$  yielded  $\Delta G_t^\ominus(\text{H}^+)$  values. Kundu et al.<sup>2</sup> used the related simultaneous extrapolation method to derive single-ion values for  $\Delta G_t^\ominus(\text{H}^+)$  and  $\Delta G_t^\ominus(\text{Cl}^-)$  in water + EG mixtures. Criticisms aimed at these methods (which also apply to the extrapolation method of Bax et al.<sup>8</sup> discussed in Section 3.1.3) include invalidity of representing ion-solvent interactions as a linear function of ionic radius and the uncertainty in or omission of estimating a 'neutral' contribution term.

For aqueous water + EG mixtures, Rao et al.<sup>3</sup> calculated transfer parameters for the proton using the reference ion/molecule redox couple assumption. In this assumption, the free energy of transfer for ferrocene is equated to that of the ferricinium ion for transfer between given solvent systems except for an electrostatic interaction term for the ion that is absent for the molecule. Rao et al.<sup>3</sup> estimated values of this electrostatic interaction using the Born equation. Electrochemical measurements for a cell in which the redox couple constituted the reference electrode and the other electrode was reversible to  $\text{H}^+$ , yielded values for  $\Delta G_t^\ominus(\text{H}^+)$ . Criticisms of this 'Foc/Fic<sup>+</sup>' method are usually connected with insufficiently large size of the species involved and the possibility of specific solvent interactions with the iron atom in such a 'sandwich' complex.

All these authors, having derived sets of single-ion transfer parameters by invoking extrathermodynamic assumptions, calculated values for other single ions using the additivity rule applicable to these thermodynamic parameters from data for salts available in the literature.

#### 4.1.3 Structure of aqueous ethylene glycol and aqueous glycerol mixtures

Free energies of transfer provide a measure of the relative affinities of an ion for two solvents. It is thought<sup>9,10</sup> that these quantities are usually dominated by contributions due to ion-solvent interactions rather than those resulting from structural changes in the solvent. Such structural effects mainly appear in compensating contributions to the enthalpies and entropies of transfer having little or no effect on the free energies of transfer. Nevertheless, interpretation of transfer parameters in terms of possible contributory effects requires some consideration of solvent structure and the nature of the interactions therein.

The presence of the hydroxyl groups in both ethylene glycol and glycerol means that, like monohydric alcohols, these liquids are highly associated. Unlike the mono-ols, however, the presence of more than one -OH group means the structures of ethylene glycol and glycerol are modified by the possibility of intra-molecular H-bonding.

It is generally accepted<sup>1,5,7,11</sup> that addition of small amounts of EG or G to water, like addition of alcohols, promotes structure while addition of larger amounts disrupts it. The degree of structure promotion in water-rich aqueous mixtures of EG and of G is similar, and is comparable to that in aqueous methanol mixtures.<sup>7,12</sup> Reduced structure promotion in aqueous mixtures of EG and G compared with that in the analogous mono-ols may be the result of increased specific-site hydration in the former mixtures reducing the effect of hydrophobic hydration.

It has been suggested<sup>13,14</sup> that ethylene glycol can act as a bidentate ligand towards cations forming specific electrostatically bound complexes. Such interactions are likely to be affected by steric and ionic charge

considerations.

The structural compatibility of glycerol with water is high.

Glycerol molecules can adopt a conformation in which the spacing between the oxygen atoms is compatible with second nearest neighbour distance of the oxygen atoms in liquid water.<sup>15</sup> In this sense, glycerol is more 'similar' to water than the alcohols or ethylene glycol. As a result the effect on ion solvation of transfer from water into water + G mixtures might be expected to be less than that for transfer in aqueous alcohols and aqueous EG.

All aqueous mixtures of ethylene glycol and of glycerol have lower dielectric constants than water. Thus, for a given ion, any contributions to the transfer parameters due to Born-type interactions will be positive for these mixtures. However, the effect will be less for transfer into these mixtures than into, say, aqueous methanol mixtures, the latter having lower dielectric constants for mixtures of a given wt % co-solvent content.

In terms of 'acid-base' interactions dominating primary solvation, the negative charges on the oxygen atoms in ethylene glycol, like in alcohols, are judged to be greater than in water molecules. Thus water + EG mixtures are more basic and less acidic than water.<sup>2,3,11,13</sup> Aqueous glycerol mixtures are in contrast less basic and more acidic than water.<sup>4,7</sup> This effect, however, is not universally agreed upon, e.g. Khoo<sup>5</sup> proposed that aqueous glycerol mixtures are more basic than water.

Contributions to transfer parameters due to secondary solvation envisaged in terms of ion-structureless dipole interactions will be negative for transfer into both water + EG and water + G mixtures (cf. aqueous methanol mixtures for which such a contribution is positive).

## 4.2 METHOD

### 4.2.1 Calculation of transfer chemical potentials for salts

The relevant data from the literature for salts in both water + EG and water + G mixtures were processed to yield transfer chemical potentials,  $\delta_{m\mu}^{\ominus}$ , in  $\text{kJ mol}^{-1}$  on the molar scale in varying weight percentage (wt %) co-solvent mixtures.

Transfer chemical potentials for salts were calculated from solubility data (molar scale) using equation 4.1. As in Chapter 3, the calculation

$$\delta_{m\mu}^{\ominus}(\text{salt}) = -\nu RT \ln \left[ \frac{\text{soly}(\text{mixture})}{\text{soly}(\text{water})} \right] \quad \dots [4.1]$$

of transfer chemical potentials was limited to the solvent composition range in which the composition of the solid phase remained the same as that in water. Soly(mixture) and soly(water) are the solubilities of the salt in the solvent mixture and in water respectively;  $\nu$  is the stoichiometry, 2 for a 1:1 salt, 3 for a 1:2 salt, etc.

Solubility data given on the molal scale were converted to the molar scale using the assumption that for a given solution the volume of the solution equals the sum of the volumes of the constituent solute and solvent (see Section 3.2.2). Equation 4.1 was then used to calculate  $\delta_{m\mu}^{\ominus}(\text{salt})$  values.

Equation 4.2 was used to calculate  $\delta_{m\mu}^{\ominus}(\text{salt})$  values from solubility products,  $K_{sp}$ , on the molar scale for salts.

$$\delta_{m\mu}^{\ominus}(\text{salt}) = -RT \ln \left[ \frac{K_{sp}(\text{mixture})}{K_{sp}(\text{water})} \right] \quad \dots [4.2]$$

Transfer chemical potentials for salts (molar scale) were calculated from standard electrode potentials on the molar scale,  $E_c^{\ominus}$ , using equation 4.3. The use of standard electrode potentials on the molal

$$\delta_{m\mu}^{\ominus}(\text{salt}) = F[E_c^{\ominus}(\text{water}) - E_c^{\ominus}(\text{mixture})] \quad \dots [4.3]$$

scale,  $E_m^\ominus$ , or mole fraction scale,  $E_x^\ominus$ , in equation 4.3 yielded  $\delta_{m\mu}^\ominus(\text{salt})$  values on the molal, (m), and mole fraction, (x), scale respectively.

These were converted to the molar scale (c) using equations 4.4 and 4.5.

$$\delta_{m\mu}^\ominus(c) = \delta_{m\mu}^\ominus(m) - \nu RT \ln \left[ \frac{\rho(\text{mixture})}{\rho(\text{water})} \right] \quad \dots [4.4]$$

$$\delta_{m\mu}^\ominus(c) = \delta_{m\mu}^\ominus(x) - \nu RT \ln \left[ \left( \frac{100-w_2}{M_1} + \frac{w_2}{M_2} \right) M_1 \frac{\rho(\text{mixture})}{\rho(\text{water})} \right] \quad \dots [4.5]$$

$\rho(\text{water})$  and  $\rho(\text{mixture})$  are the densities of water and of the solvent mixture respectively.  $M_1$  and  $M_2$  are the molar masses of water and the organic co-solvent;  $w_2$  is the weight percentage of co-solvent in the solvent mixture.

Medium effects (molal scale),  $\log_m \gamma_{\pm}^2$ , for 1:1 electrolytes were used in equation 4.6 to calculate  $\delta_{m\mu}^\ominus(\text{salt})$  values on the molal scale.

Conversion to the molar scale was effected using equation 4.4.

$$\delta_{m\mu}^\ominus(\text{salt}) = 2.303 RT (\log_m \gamma_{\pm}^2) \quad \dots [4.6]$$

For water + EG mixtures, the densities of the solvent mixtures used in calculating transfer chemical potentials were the average of those given by Banerjee *et al.*<sup>16</sup> and Ray *et al.*<sup>17</sup> The density of ethylene glycol was taken to be 1.10982 g/cm<sup>3</sup>.<sup>18</sup> For water + glycerol mixtures, the densities of the solvent mixtures used were those given in "International Critical Tables".<sup>19</sup> In all cases the density of water was taken as 0.99705 g/cm<sup>3</sup>.<sup>20</sup> Specific gravities of the salts were taken from the "Chemical Rubber Handbook".<sup>21</sup>

Unless otherwise stated all the data for the salts had been measured at 298.2 K.

#### 4.2.2 Calculation of single-ion transfer chemical potentials

The TATB assumption was used to produce single-ion transfer parameters for  $\text{Ph}_4\text{As}^+$ ,  $\text{BPh}_4^-$ ,  $\text{K}^+$  and  $\text{Pic}^-$  (Pic = picrate) from those of the parent electrolytes  $\text{Ph}_4\text{AsPic}$ ,  $\text{KBPPh}_4$  and  $\text{KPic}$  in water + EG<sup>13</sup> and in water + G mixtures<sup>7</sup> using equation 4.7.

$$\begin{aligned}\delta_{\text{m}\mu}^{\ominus}(\text{Ph}_4\text{As}^+) &= \delta_{\text{m}\mu}^{\ominus}(\text{BPh}_4^-) \\ &= \frac{\delta_{\text{m}\mu}^{\ominus}(\text{Ph}_4\text{AsPic}) + \delta_{\text{m}\mu}^{\ominus}(\text{KBPPh}_4) - \delta_{\text{m}\mu}^{\ominus}(\text{KPic})}{2} \quad \dots [4.7]\end{aligned}$$

Values of  $\delta_{\text{m}\mu}^{\ominus}(\text{K}^+)$  and  $\delta_{\text{m}\mu}^{\ominus}(\text{Pic}^-)$  were then calculated using equations 4.8 and 4.9.

$$\delta_{\text{m}\mu}^{\ominus}(\text{K}^+) = \delta_{\text{m}\mu}^{\ominus}(\text{KBPPh}_4) - \delta_{\text{m}\mu}^{\ominus}(\text{BPh}_4^-) \quad \dots [4.8]$$

$$\delta_{\text{m}\mu}^{\ominus}(\text{Pic}^-) = \delta_{\text{m}\mu}^{\ominus}(\text{Ph}_4\text{AsPic}) - \delta_{\text{m}\mu}^{\ominus}(\text{Ph}_4\text{As}^+) \quad \dots [4.9]$$

Using these four sets of single-ion transfer chemical potentials,  $\delta_{\text{m}\mu}^{\ominus}$  values for other ions were calculated using the additivity rule as for water + ethanol mixtures (Section 3.2.1).

For water + EG mixtures 'one-step' derivations (Section 3.2.4) yielded transfer chemical potentials for  $\text{Cl}^-$ ,  $\text{Br}^-$ ,  $\text{I}^-$ ,  $\text{ClO}_4^-$ ,  $\text{CO}_3^{2-}$  and  $\text{SO}_4^{2-}$ . 'Two-step' derivations yielded values for  $\text{H}^+$ ,  $\text{Li}^+$ ,  $\text{Na}^+$ ,  $[\text{Fe}(\text{gmi})_3]^{2+}$  and  $[\text{Fe}(\text{bsb,Ph,Ph:3,4-Me}_2)_3]^{2+}$ . gmi is the bidentate Schiff base made from glyoxal and methylamine, (bsb,Ph,Ph:3,4-Me<sub>2</sub>) is the bidentate Schiff base made from 3,4-dimethylaniline and 2-benzoyl pyridine.

In water + glycerol mixtures 'one-step' derivations gave transfer chemical potentials for  $\text{Cl}^-$ ,  $\text{Br}^-$ ,  $\text{ClO}_4^-$  and  $\text{SO}_4^{2-}$ . 'Two-step' derivations yielded values for  $\text{H}^+$ ,  $\text{Li}^+$ ,  $\text{Na}^+$ ,  $\text{Rb}^+$ ,  $\text{Cs}^+$ ,  $\text{NH}_4^+$  and  $[\text{Fe}(\text{bsb,Ph,Ph:3,4-Me}_2)_3]^{2+}$ . Values for  $\text{Br}^-$  and  $\text{I}^-$  were obtained by 'three-step' derivations.

The references indicating the sources of the data for the relevant salts are given in Sections 4.3.2 and 4.3.3 where the derivations of

values for each ion are reported separately. The comments made concerning the accuracy of  $\delta_{m\mu}^{\oplus}$  values for ions in water + ethanol mixtures in Section 3.2.5 apply equally here.

### 4.3 RESULTS

#### 4.3.1 Introduction

In the following two sections the routes by which single-ion transfer chemical potentials for ions in water + EG and water + G mixtures were derived are outlined. For each ion, the sources of the data for the salts used in the calculation of these values are given. Where alternative routes or alternative sets of data were used to derive values for the same ion the results are compared. In such cases, one set of values for each ion is chosen to be used as values for that ion in subsequent derivations. The sets of values thus adopted for each ion are tabulated in Appendix B.

The figures referred to in each section are shown at the end of that section. The sets of values finally adopted for the ions are shown together in Figs. 4.6 and 4.7 (for water + EG mixtures) and Fig. 4.11 (for water + G mixtures) at the end of Sections 4.4.1 and 4.4.2 respectively in which the general solvation patterns are discussed.

#### 4.3.2 Derivation of single-ion transfer parameters for aqueous ethylene glycol mixtures

The transfer chemical potentials for  $\text{Ph}_4\text{As}^+$ ,  $\text{BPh}_4^-$ ,  $\text{K}^+$  and  $\text{Pic}^-$  in water + EG mixtures were derived by application of the TATB assumption using solubility products measured for the parent electrolytes  $\text{Ph}_4\text{AsPic}$ ,  $\text{KPh}_4$  and  $\text{KPic}$  by Das and Kundu.<sup>13</sup> Values of  $\text{BPh}_4^-$  ( $=\text{Ph}_4\text{As}^+$ ) are negative across the composition range and the stabilization of these ions increases with increasing glycol content of the solvent mixture. By comparison, the effect of transfer from water into these solvent

mixtures for both  $K^+$  and  $Pic^-$  is much less marked. In low wt % glycol solvent mixtures the transfer chemical potentials of the picrate ion are positive. However, with increasing glycol content of the solvent mixtures  $\delta_{m\mu}^\ominus(Pic^-)$  becomes negative and this stabilization increases progressively across the remaining solvent composition range. All values for  $\delta_{m\mu}^\ominus(K^+)$  (except at 10 wt % glycol) are relatively small but positive.

Transfer chemical potentials for the halide ions,  $\delta_{m\mu}^\ominus(X^-)$  where  $X^- = Cl^-, Br^-$  and  $I^-$ , were derived from electrochemical measurements<sup>2</sup> and solubility measurements<sup>22,23,24</sup> for  $KX$  using  $\delta_{m\mu}^\ominus(K^+)$  values. The solubility data had been measured at 303.2 K. These alternative sets of  $\delta_{m\mu}^\ominus(X^-)$  values are shown in Fig. 4.1. Both sets of data (electrochemical and solubility) yielded positive values of  $\delta_{m\mu}^\ominus(X^-)$  which decrease in the order  $Cl^- > Br^- > I^-$ . For each ion in a given solvent mixture the transfer chemical potentials calculated using the solubility data are less than those calculated using the electrochemical data. The latter are the ones tabulated in Appendix B.

Electrochemical data<sup>2</sup> for the alkali-metal halides,  $MX$  where  $M = H^+, Li^+$  and  $Na^+$  and  $X^- = Cl^-, Br^-$  and  $I^-$ , were used to derive values for  $\delta_{m\mu}^\ominus(M^+)$ . Three sets of transfer chemical potentials for each of the cations were calculated using values of  $\delta_{m\mu}^\ominus(Cl^-)$ ,  $\delta_{m\mu}^\ominus(Br^-)$  and  $\delta_{m\mu}^\ominus(I^-)$  derived earlier. For each cation, the values were in very good agreement; their average is tabulated in Appendix B.  $Li^+$  and  $Na^+$  are destabilized across the concentration range studied, the former more so than the latter. The proton is slightly stabilized in solvent mixtures containing up to about 80 wt % glycol, after which  $\delta_{m\mu}^\ominus(H^+)$  becomes positive.

A second set of electrochemical data for  $HI$ <sup>11</sup> was used with  $\delta_{m\mu}^\ominus(I^-)$

values to give transfer chemical potentials for the proton. This alternative set of results was in very good agreement with the  $\delta_{m\mu}^{\ominus}(\text{H}^{\oplus})$  values derived from electrochemical measurements of HI.<sup>2</sup>

Solubility data for NaCl<sup>25</sup> measured at 303.2 K was used to calculate transfer chemical potentials for the salt,  $\delta_{m\mu}^{\ominus}(\text{NaCl})^{\text{S}}$  (where superscript S denotes solubility derivation). Combination of these values with the alternative sets for the chloride ion derived from electrochemical data,  $\delta_{m\mu}^{\ominus}(\text{Cl}^{-})^{\text{E}}$  (where superscript E denotes electrochemical derivation), and solubility data,  $\delta_{m\mu}^{\ominus}(\text{Cl}^{-})^{\text{S}}$ , yielded two sets of values for the sodium ions  $\delta_{m\mu}^{\ominus}(\text{Na}^{\oplus})^{\text{SE}}$  and  $\delta_{m\mu}^{\ominus}(\text{Na}^{\oplus})^{\text{SS}}$ . For comparison, transfer chemical potentials for NaCl derived from electrochemical data,<sup>2</sup>  $\delta_{m\mu}^{\ominus}(\text{NaCl})^{\text{E}}$ , were treated in the same way yielding  $\delta_{m\mu}^{\ominus}(\text{Na}^{\oplus})^{\text{EE}}$  and  $\delta_{m\mu}^{\ominus}(\text{Na}^{\oplus})^{\text{ES}}$  values. All these quantities are shown in Fig. 4.2. It is interesting to note that although the spread of values in the four sets of  $\delta_{m\mu}^{\ominus}(\text{Na}^{\oplus})$  values is large the closest agreement is between  $\delta_{m\mu}^{\ominus}(\text{Na}^{\oplus})^{\text{EE}}$  and  $\delta_{m\mu}^{\ominus}(\text{Na}^{\oplus})^{\text{SS}}$  values. This may be a result of the cancelling out of certain terms in the purely 'electrochemical derivation', EE, and again in the purely 'solubility derivation', SS, resulting from non-ideal interactions not corrected for in the basic data given for the salt and the anion. In contrast, in derivations of  $\delta_{m\mu}^{\ominus}(\text{Na}^{\oplus})$  from  $\delta_{m\mu}^{\ominus}(\text{NaCl})$  and  $\delta_{m\mu}^{\ominus}(\text{Cl}^{-})$  using solubility data for one species and electrochemical data for the other, no such cancellation occurs and the resulting values,  $\delta_{m\mu}^{\ominus}(\text{Na}^{\oplus})^{\text{SE}}$  and  $\delta_{m\mu}^{\ominus}(\text{Na}^{\oplus})^{\text{ES}}$ , are vastly different.

Values for  $\delta_{m\mu}^{\ominus}(\text{SO}_4^{2-})$  were derived from solubility data of Na<sub>2</sub>SO<sub>4</sub><sup>26</sup> and K<sub>2</sub>SO<sub>4</sub>.<sup>27,28</sup> The resulting values for SO<sub>4</sub><sup>2-</sup> are shown in Fig. 4.3. One set of solubility data for K<sub>2</sub>SO<sub>4</sub> had been measured at 303.2 K,<sup>27</sup> the other had been measured at 298.2 K but values had been given on the molal scale.<sup>28</sup> Conversion to the molar scale was effected by introduction of

the usual assumption (Section 4.2.1). All the estimates predict that  $\text{SO}_4^{2-}$  is destabilized when ethylene glycol is added to the system. The degree of this destabilization is more pronounced in values derived from solubility data for  $\text{K}_2\text{SO}_4$  than from  $\text{Na}_2\text{SO}_4$ . The values derived for  $\text{SO}_4^{2-}$  using solubility data for  $\text{K}_2\text{SO}_4$  at 298.2 K are the ones tabulated in Appendix B.

Solubility data for  $\text{KClO}_4$ <sup>29</sup> were used with  $\delta_{\text{m}\mu}^{\ominus}(\text{K}^+)$  values to yield  $\delta_{\text{m}\mu}^{\ominus}(\text{ClO}_4^-)$ . These, in turn, in combination with solubility data for  $[\text{Fe}(\text{gmi})_3](\text{ClO}_4)_2$ <sup>29</sup> and  $[\text{Fe}(\text{bsb},\text{Ph},\text{Ph}:3,4\text{-Me}_2)_3](\text{ClO}_4)_2$ <sup>29</sup> yielded transfer chemical potentials for the two complex cations.

Values for  $\delta_{\text{m}\mu}^{\ominus}(\text{CO}_3^{2-})$  were derived from solubility data for  $\text{K}_2\text{CO}_3$ .<sup>30</sup>

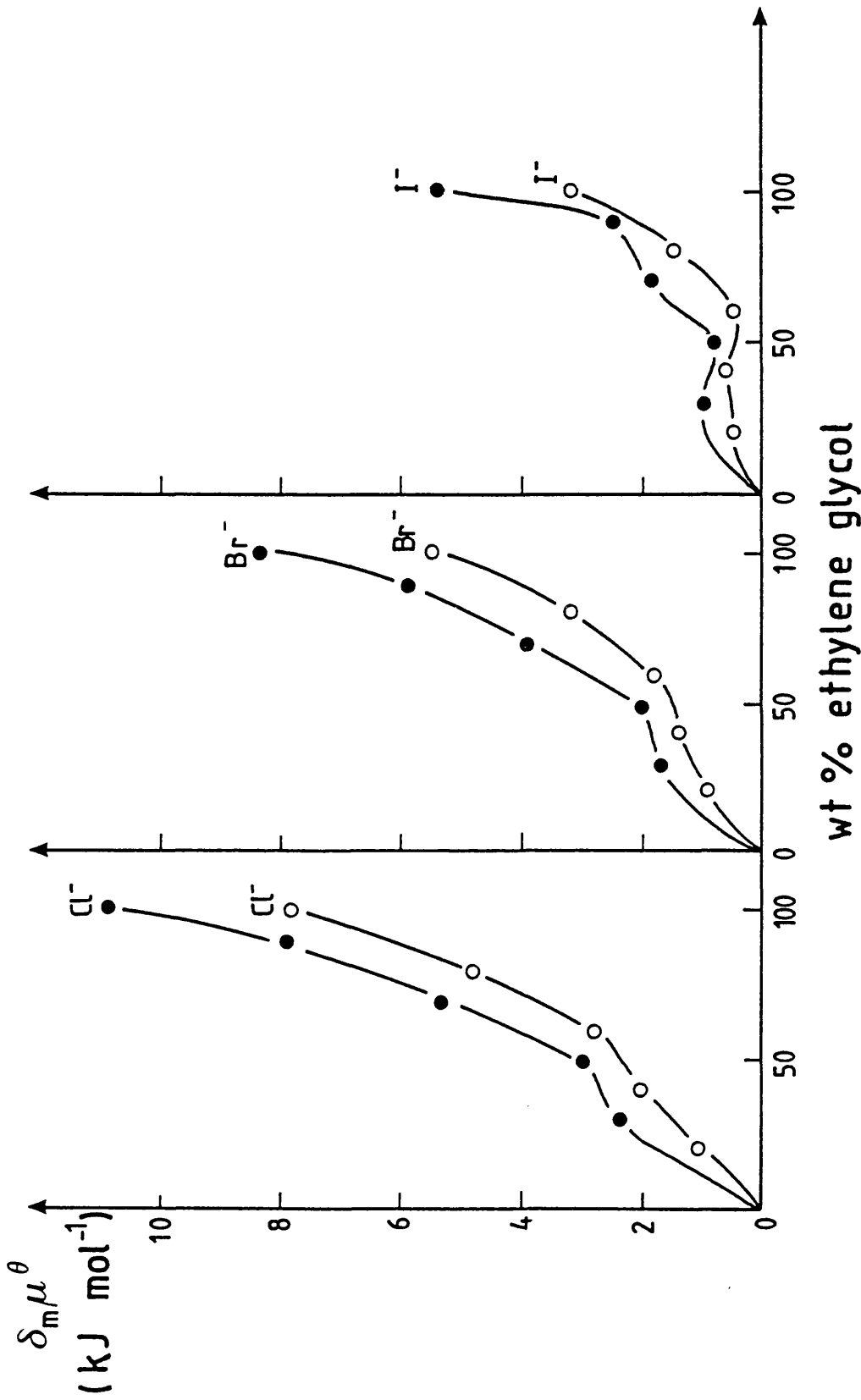


**FIGURE 4.1**

Transfer chemical potentials for Cl<sup>-</sup>, Br<sup>-</sup> and I<sup>-</sup> (molar scale, TATB assumption) derived using electrochemical data [ref. 2] (●) for KX and solubility data at 303.2 K (O) for KCl [ref. 22], KBr [ref. 23] and KI [ref. 24] in water + EG mixtures.

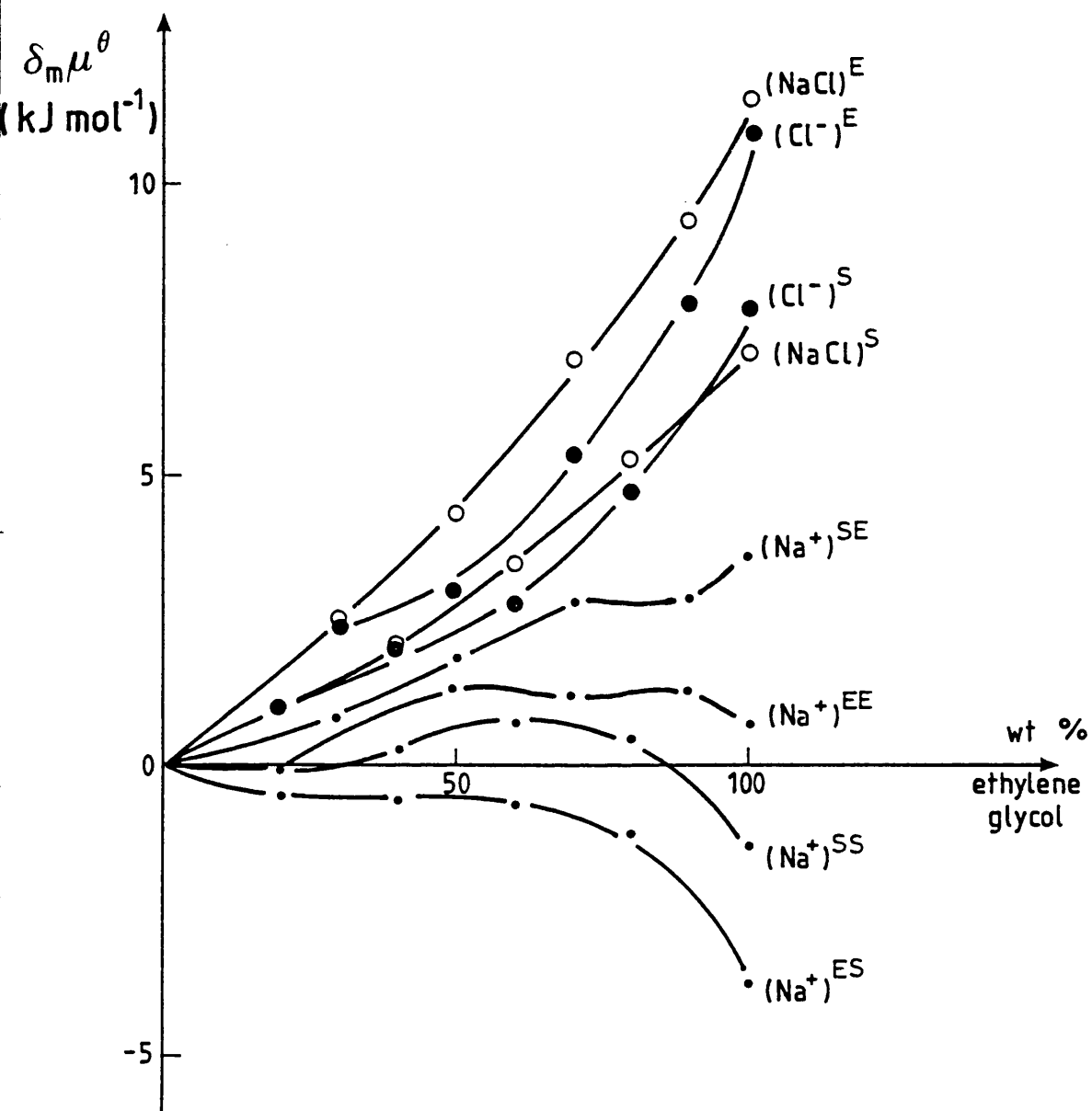
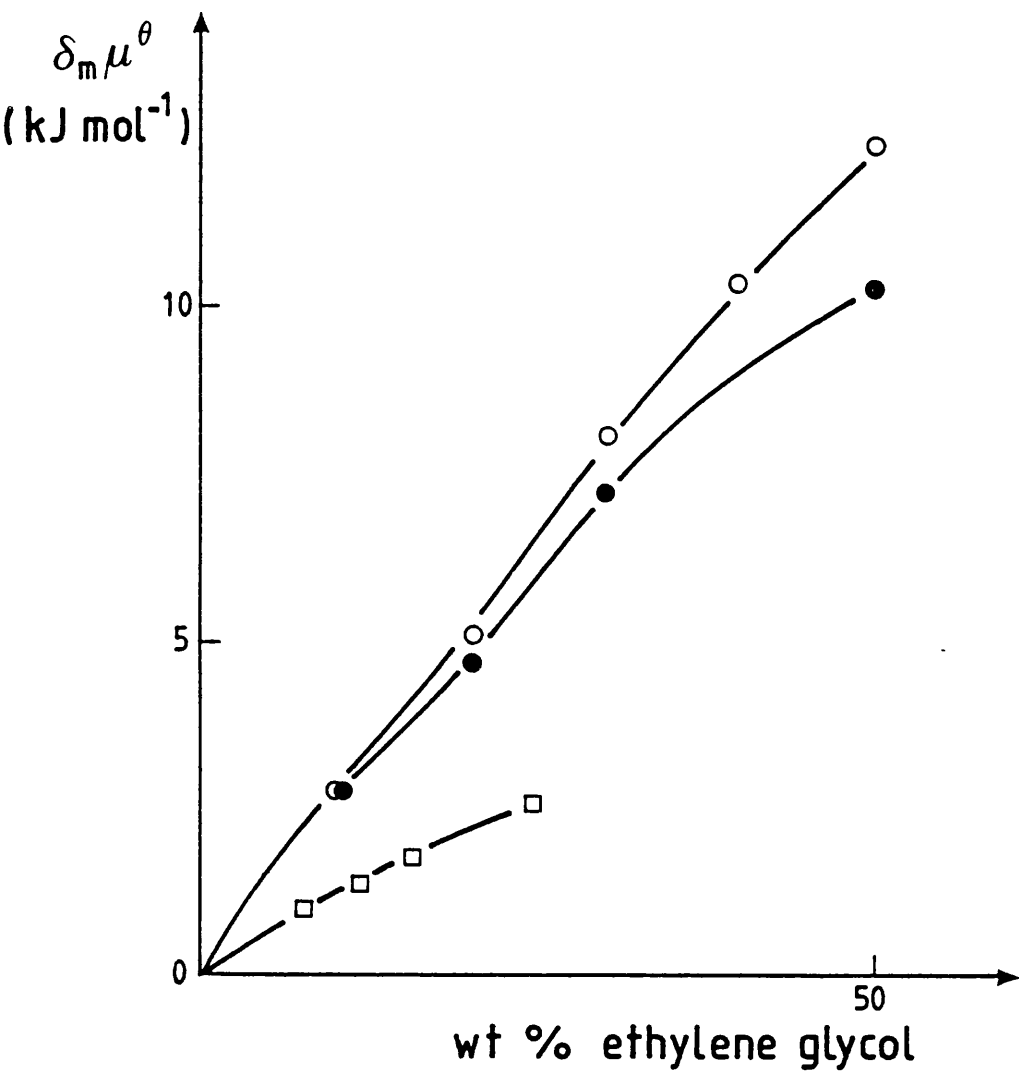


FIGURE 4.2

Transfer chemical potentials for NaCl,  $\text{Cl}^-$  and  $\text{Na}^+$  (molar scale, TATB assumption) derived using solubility data [refs. 22,25] (S), electrochemical data [ref. 2] (E) or combinations of the two types of data (EE), (SS), (ES), (SE) in water + EG mixtures.



**FIGURE 4.3**

Transfer chemical potentials for  $\text{SO}_4^{2-}$  (molar scale, TATB assumption) derived using data for  $\text{K}_2\text{SO}_4$  at 303.2 K [ref. 27] (O),  $\text{K}_2\text{SO}_4$  [ref. 28] (●) and  $\text{Na}_2\text{SO}_4$  [ref. 26] (□) in water + EG mixtures.

#### 4.3.3 Derivation of single-ion transfer parameters for aqueous glycerol mixtures

The values for  $\text{Ph}_4\text{As}^+$ ,  $\text{BPh}_4^-$ ,  $\text{K}^+$  and  $\text{Pic}^-$  tabulated in Appendix B were derived from solubility products for  $\text{Ph}_4\text{AsPic}$ ,  $\text{KBPh}_4$  and  $\text{KPic}$  given by Basumullick and Kundu,<sup>7</sup> using the TATB assumption. The potassium ion is increasingly destabilized in mixtures of increasing glycerol content, whilst  $\text{BPh}_4^-$  ( $=\text{Ph}_4\text{As}^+$ ) and  $\text{Pic}^-$  are increasingly stabilized across the composition range. The stabilization of  $\text{Pic}^-$  is less marked than that of  $\text{BPh}_4^-$ .

The transfer chemical potentials for the chloride ion were derived from two alternative sets of data for  $\text{KCl}$ , one based on solubility<sup>22</sup> the other on electrochemical<sup>7</sup> measurements. Combination of  $\delta_{\text{m}}\mu^\ominus(\text{KCl})$  with  $\delta_{\text{m}}\mu^\ominus(\text{K}^+)$  values derived using the TATB assumption yielded the two sets of  $\delta_{\text{m}}\mu^\ominus(\text{Cl}^-)$  values shown in Fig. 4.4. The transfer of the ion from water into water + glycerol mixtures is shown by both sets of estimates to have little effect on the chemical potential of the ion. The  $\delta_{\text{m}}\mu^\ominus(\text{Cl}^-)$  values are very slightly negative below and very slightly positive above the region of equimolar solvent composition. The averages of these sets were adopted as  $\delta_{\text{m}}\mu^\ominus(\text{Cl}^-)$  values and are tabulated in Appendix B.

Values for  $\delta_{\text{m}}\mu^\ominus(\text{H}^+)$  were derived from two sets of data for  $\text{HCl}$ . Both sets of transfer chemical potentials for the salt were based on electrochemical measurements.<sup>5,7</sup> The resulting  $\delta_{\text{m}}\mu^\ominus(\text{H}^+)$  values obtained using values for the chloride ion are shown in Fig. 4.4. There is good agreement between the two sets of values, the averages of which are tabulated in Appendix B and were used subsequently as  $\delta_{\text{m}}\mu^\ominus(\text{H}^+)$  values. Upon transfer from water into mixtures of water + glycerol the proton is destabilized. This destabilization increases with increasing co-solvent

content of the solvent mixture.

Fig. 4.5 shows three sets of values for  $\delta_{m\mu}^{\ominus}(\text{Br}^-)$ . One set of values was derived using transfer chemical potentials for KBr based on solubility measurements.<sup>23</sup> The other sets were derived from electrochemical measurements for HBr.<sup>5,12</sup> In low wt % glycerol mixtures there is good general agreement between the three sets of estimates for  $\delta_{m\mu}^{\ominus}(\text{Br}^-)$  that the ion is slightly stabilized upon transfer from water into these mixtures. At higher wt % glycerol content, the values derived from electrochemical measurements become increasingly negative. The values derived from solubility measurements, however, become less negative with increasing co-solvent content of the mixtures and become positive in solvent mixtures containing more than 45 wt % glycerol. The values adopted as those for  $\delta_{m\mu}^{\ominus}(\text{Br}^-)$  are the average of the two sets derived from electrochemical measurements.

The values for  $\delta_{m\mu}^{\ominus}(\text{I}^-)$  were calculated from the transfer chemical potentials of HI based on electrochemical measurements.<sup>5,12</sup> Combination of these two sets of values for the salt with those for the proton yielded  $\delta_{m\mu}^{\ominus}(\text{I}^-)$  values shown in Fig. 4.5. The values are negative across the composition range studied and become more negative with increasing glycerol content of the solvent mixtures. The values of  $\delta_{m\mu}^{\ominus}(\text{I}^-)$  tabulated in Appendix B are the average of the two sets.

Values of  $\delta_{m\mu}^{\ominus}(\text{M}^+)$ , where  $\text{M}^+ = \text{Li}^+, \text{Na}^+, \text{Rb}^+, \text{Cs}^+, \text{NH}_4^+$ , were all derived using the transfer chemical potentials for the chloride salts of these cations. Values of  $\delta_{m\mu}^{\ominus}(\text{MCl})$  where  $\text{M}^+ = \text{Li}^+, \text{Na}^+, \text{Rb}^+, \text{Cs}^+$ , were derived from electrochemical measurements<sup>7</sup> and  $\delta_{m\mu}^{\ominus}(\text{NH}_4\text{Cl})$  values were derived from solubility measurements.<sup>31</sup> Combination of values for  $\delta_{m\mu}^{\ominus}(\text{MCl})$  with those for  $\delta_{m\mu}^{\ominus}(\text{Cl}^-)$  yielded values for the cations.

Transfer from water into water + glycerol mixtures has a destabilizing

effect on all these cations which increases with increasing glycerol content of the solvent mixture. The destabilizing effect decreases in the order  $\text{Na}^+ > \text{Rb}^+ > \text{Cs}^+ > \text{NH}_4^+$  across the composition range studied.

Although in solvent mixtures containing 70 wt % glycerol the lithium ion is the most destabilized of these ions, in mixtures of lower wt % glycerol it is less destabilized than all the cations except  $\text{NH}_4^+$ .

$\delta_{\text{m}\mu}^{\ominus}(\text{K}^+)$  values were used with solubility data for  $\text{KClO}_4$ <sup>29</sup> and  $\text{K}_2\text{SO}_4$ <sup>32</sup> to derive transfer chemical potentials for the perchlorate and chloride ions respectively. The solubility data for  $\text{K}_2\text{SO}_4$  were given on the molal scale. These were converted to the molar scale using the usual assumption (Section 4.2.1). Both  $\text{ClO}_4^-$  and  $\text{SO}_4^{2-}$  are destabilized on transfer from water into aqueous glycerol mixtures. The effect on  $\text{ClO}_4^-$  is small in comparison to the destabilization of  $\text{SO}_4^{2-}$ . The latter effect increases steadily across the composition range studied.

Solubility data for  $[\text{Fe}(\text{bsb}, \text{Ph}, \text{Ph}:3,4\text{-Me}_2)_3](\text{ClO}_4)_2$ <sup>29</sup> in combination with  $\delta_{\text{m}\mu}^{\ominus}(\text{ClO}_4^-)$  values yielded transfer parameters for the cation.

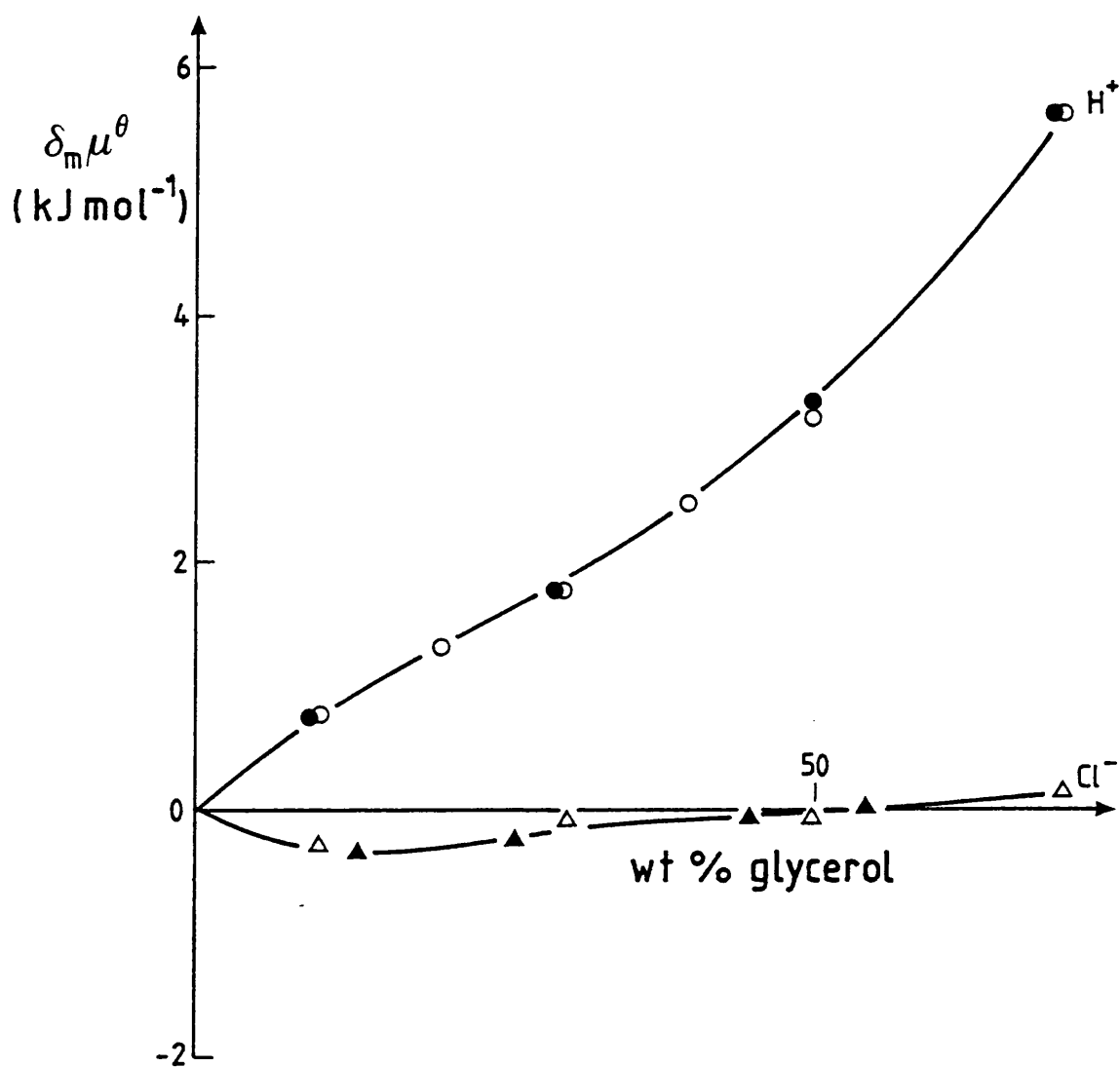


FIGURE 4.4

Transfer chemical potentials for  $\text{Cl}^-$  and  $\text{H}^+$  (molar scale, 298.2 K, TATB assumption) derived using data for KCl [ref. 22] (▲), KCl [ref. 7] (△), HCl [ref. 7] (●) and HCl [ref. 5] (○) in water + G mixtures.

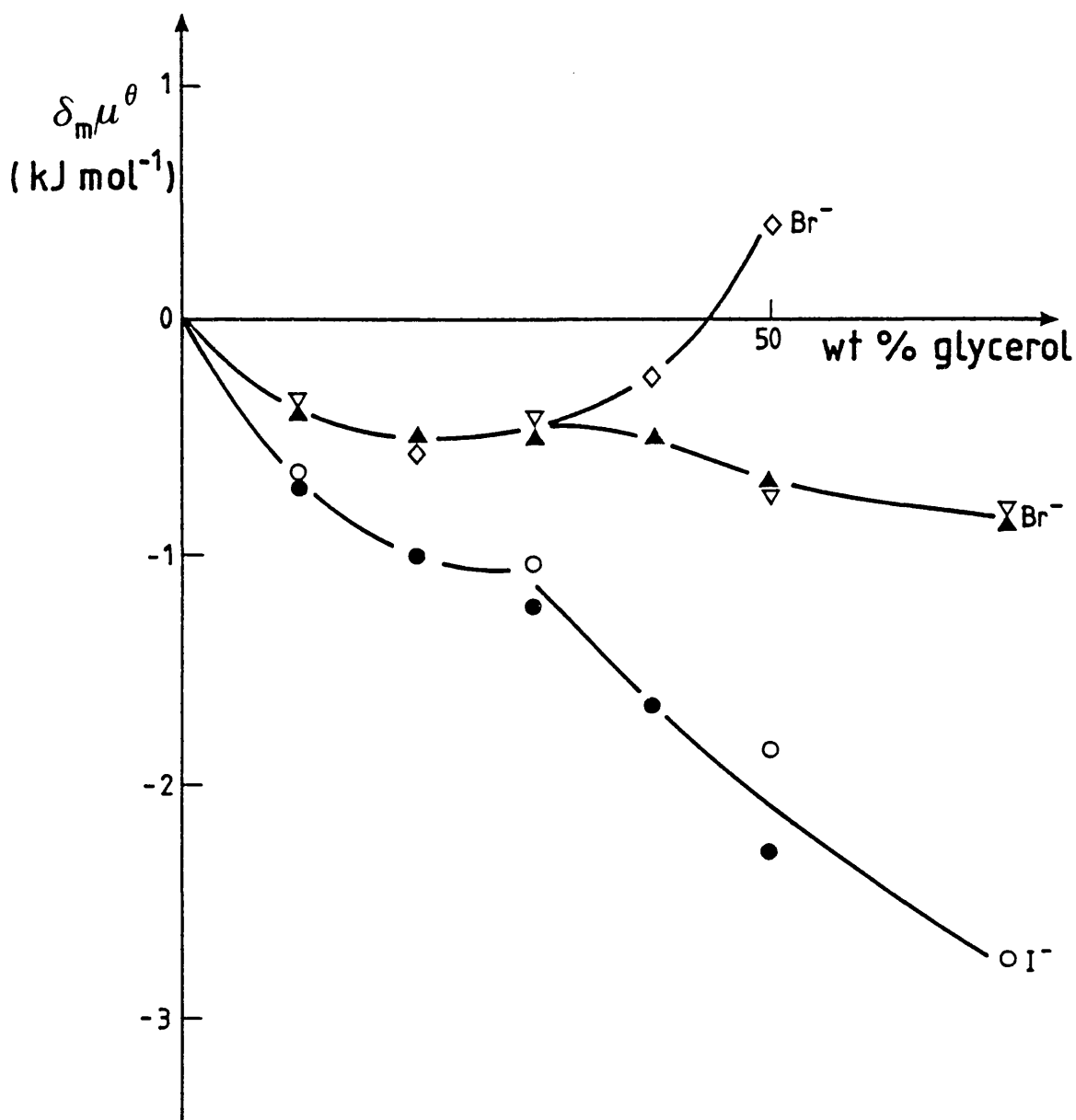


FIGURE 4.5

Transfer chemical potentials for  $\text{Br}^-$  and  $\text{I}^-$  (molar scale, 298.2 K, TATB assumption) derived using data for KBr [ref. 23] ( $\diamond$ ), HBr [ref. 12] ( $\nabla$ ), HBr [ref. 5] ( $\triangle$ ), HI [ref. 12] ( $\circ$ ) and HI [ref. 5] ( $\bullet$ ) in water + G mixtures.

## 4.4 DISCUSSION

### 4.4.1 General solvation pattern in aqueous ethylene glycol mixtures

Figs. 4.6 and 4.7 at the end of this section show the general solvation pattern for ions in water + EG mixtures derived using the TATB assumption. Transfer chemical potentials for  $\text{Cu}^{2+}$  derived using the negligible liquid junction potential assumption,<sup>33,34</sup> are also included. Values for  $\text{CO}_3^{2-}$  and  $\text{SO}_4^{2-}$  are judged to be of lesser accuracy due to solubility considerations (see Section 3.2.5).

One of the most immediately noticeable features in both figures is the less than smooth change in  $\delta_{\text{m}}\mu^{\ominus}$  values across the composition range for most of the ions. Of the ions for which values are given over the majority of the composition range, only  $\text{Ph}_4\text{As}^+$  (=BPh<sub>4</sub><sup>-</sup>) shows a smooth change in  $\delta_{\text{m}}\mu^{\ominus}$ . For the rest of the ions, values for transfer into mixtures of around 50 wt % EG consistently impede such a change. It can be seen that deviations of the observed values in this composition range from 'smoothed-out' plots ignoring these values are in all cases negative for anions and positive for cations. That this is a real phenomenon and not the result of inaccurate data or miscalculation of values is borne out by the fact that this trend is evident also in the results of Wells<sup>1</sup> and Kundu *et al.*<sup>2</sup> for water + EG mixtures. The effect may have its origins in the reversal in magnitudes of  $\Delta H^{\text{E}}$  and  $T\Delta S^{\text{E}}$  (the changes in the excess functions of mixing of the solvent) in solvent mixtures of approximately 50 wt % EG content.<sup>1</sup> Also the onset of solvent structure breakdown, following structure promotion due to addition of small amounts of ethylene glycol to water, occurs around 35 wt % EG in the solvent mixture.<sup>7</sup>

Transfer chemical potentials for anions are shown together in Fig.

4.6. The halide ions,  $\text{Cl}^-$ ,  $\text{Br}^-$  and  $\text{I}^-$ , are all destabilized upon trans-

fer from water into water + EG mixtures. The destabilization decreases in the order  $\text{Cl}^- > \text{Br}^- > \text{I}^-$ . In terms of primary solvation of the ions this behaviour is expected. In ethylene glycol the partial negative charges on the oxygen atoms and the partial positive charges on the hydroxyl hydrogens are greater and smaller respectively than on the corresponding atoms in water. As in water + ethanol mixtures the co-solvent molecules confer greater basicity on the water molecules in the solvent mixtures due to the co-operative nature of H-bonding. Thus hydrogen bonds between the anions and hydroxyl hydrogens of the solvent molecules will be weaker in the solvent mixtures than in water. The observed order,  $\text{Cl}^- > \text{Br}^- > \text{I}^-$ , is the result of decreased H-bonding ability down the series with decreasing charge densities of the ions.

The behaviour of these ions also follows the pattern predicted by the Born equation,  $\delta_{\text{m}\mu}^\ominus$  values increasing with decreasing dielectric constants of the solvent mixtures. The order,  $\text{Cl}^- > \text{Br}^- > \text{I}^-$  parallels the increase in ionic size. Any contribution to the transfer parameters of these ions due to ion-structureless dipole interactions operating outside the primary solvation shell will be negative, the dipole moment of ethylene glycol being greater than that of water. With increasing ionic size, dispersion interactions may become more important in particular for  $\text{I}^-$  making an increasingly favourable contribution to  $\delta_{\text{m}\mu}^\ominus(\text{I}^-)$  with increasing glycol content of the solvent mixtures.

The transfer chemical potentials of the perchlorate and carbonate ions are similar in magnitude to those for the iodide ion. Although this has often been found to be the case for  $\text{ClO}_4^-$ ,<sup>35,36,37</sup> the relatively small  $\delta_{\text{m}\mu}^\ominus(\text{CO}_3^{2-})$  values are surprising. For  $\text{ClO}_4^-$ , positive contributions to the transfer parameters due to Born-type interactions or acid-base considerations will be less than, say, for  $\text{Cl}^-$  due to

decreased charge density in  $\text{ClO}_4^-$ . These factors would lead to expectations that  $\text{CO}_3^{2-}$  would be much more destabilized than  $\text{ClO}_4^-$ .

As in water + ethanol mixtures the doubly charged sulphate ion is more rapidly and more markedly destabilized than the univalent ions being considerably more hydrophilic.

The ionic size and hydrophobic nature of the picrate ion results in stabilization over most of the composition range (values are slightly positive in low wt % EG mixtures). Favourable changes in dispersion interactions become more important for this ion dominating the positive contribution to the transfer parameters due to decreased H-bond interactions upon transfer.

For the large organic  $\text{BPh}_4^-$  ion, the transfer parameters are controlled by dispersion interactions, the values being comparatively large and negative and increasing with increasing wt % EG content of the solvent mixture.

Fig. 4.7 shows the transfer chemical potentials for cations in water + EG mixtures. Values for the large hydrophobic cation  $[\text{Fe}(\text{bsb},\text{Ph},\text{Ph}:-3,4\text{-Me}_2)_3]^{2+}$ , like those for  $\text{Ph}_4\text{As}^+$ , are large and negative. The smaller complex cation,  $[\text{Fe}(\text{gmi})_3]^{2+}$ , follows a similar trend in low wt % EG mixtures but after this becomes less stabilized.

The proton is slightly stabilized in mixtures containing up to 80 wt % EG after which the proton becomes destabilized. The change in sign occurs around 80 wt % EG (cf. water + ethanol mixtures - 90 wt % ethanol) implying that solvent mixtures of lower wt % co-solvent content are more basic than water. Destabilization of the alkali-metal cations is in the order  $\text{Li}^+ > \text{Na}^+ \approx \text{K}^+$  indicating Born-type behaviour and decreasing positive contribution to transfer parameters due to secondary solvation interactions. The levelling off of the plots for  $\text{Na}^+$  and  $\text{K}^+$

at higher wt % EG content mixtures may indicate formation of specific complexes between the ions and the organic co-solvent, with ethylene glycol acting as a bidentate ligand. In the case of  $\text{Li}^+$ , absence of levelling off in  $\delta_{\text{m}}\mu^{\ominus}$  values may be a result of reduced complex formation due to steric limitations. However, as the levelling off is accentuated by values for 50 wt % EG content mixtures, the behaviour could be a reflection of structural changes in the solvent rather than ion-solvent interactions. The downward trend of values from 90 wt % EG to pure EG is indicative of ion-pairing.

The values for  $\text{Cu}^{2+}$  (derived using the negligible liquid junction potential assumption<sup>33</sup>) show the ion to be increasingly stabilized with increasing EG content of the solvent mixture. That the destabilization is comparatively small considering the charge may be due to formation of specific complexes of the type  $[\text{Cu}(\text{EG})_2]^{2+}$ .<sup>13,14</sup>

Figs. 4.8 and 4.9 show comparison of values for a range of ions derived using different extrathermodynamic assumptions in water + EG mixtures. Most obvious for both cations and anions is the much greater magnitude of values derived using the simultaneous extrapolation method (SE method)<sup>2</sup> than by either Wells's method<sup>1</sup> or the TATB assumption. In comparison to the values derived using the SE method,<sup>2</sup> the values derived using Wells's method<sup>1</sup> and the TATB assumption are in fair agreement.

Irrespective of magnitude, the sign of the transfer chemical potentials for the halide ions (Fig. 4.8) are the same for all methods and all decrease in the order  $\text{Cl}^- > \text{Br}^- > \text{I}^-$ . For the proton (Fig. 4.9), all methods predict stabilization in this lower wt % co-solvent content composition range. The value of  $\delta_{\text{m}}\mu^{\ominus}(\text{H}^+)$  at 50 wt % EG from the SE method<sup>2</sup> is almost ten times greater than that derived using the reference

electrolyte assumption. For the alkali-metal cations,  $\delta_{m\mu}^{\ominus}$  values derived using the SE method<sup>2</sup> are large and negative while those derived using the TATB assumption and by Wells's method<sup>1</sup> are positive and relatively small. It is noteworthy that the conversion of Wells's values<sup>1</sup> for the alkali-metal cations in mixtures of less than 50 wt % EG from the mole fraction to the molar solute composition scale resulted in a change of sign, the former being negative.

Fig. 4.10 shows sets of  $\delta_{m\mu}^{\ominus}(H^+)$  values derived using different assumptions. The values derived using the Foc/Fic<sup>+</sup> method, FM, the acidity function method, AFM, and the extrapolation method, EM, are taken from the work of Rao et al.<sup>3</sup> Values derived using the TATB assumption, REM, Wells's method,<sup>1</sup> WM, and the SE method,<sup>2</sup> SEM, are also included. In mixtures of up to 50 wt % EG content the  $\delta_{m\mu}^{\ominus}(H^+)$  values derived using all the methods are negative. The general agreement concerning the degree of this stabilization is, however, poor. The two sets of values derived from extrapolation methods<sup>2,3</sup> show a marked stabilization of  $H^+$ . In this composition range the results of the TATB assumption, the acidity function method<sup>3</sup> and Wells's method<sup>1</sup> are in relatively good agreement predicting little effect on the chemical potential of  $H^+$  on transfer from water into these mixtures. The values derived using the Foc/Fic<sup>+</sup> method<sup>3</sup> are intermediate between these two effects.

In higher wt % EG content mixtures, values for  $H^+$  derived from the TATB and acidity function<sup>3</sup> methods become positive. Those from the Foc/Fic<sup>+</sup><sup>3</sup> and extrapolation methods<sup>2,3</sup> remain negative but the stabilization of  $H^+$  between 90 wt % and 100 wt % EG decreases (not shown for the extrapolation methods).

Thus, values from the Foc/Fic<sup>+</sup><sup>3</sup> and extrapolation methods<sup>2,3</sup> suggest

all the solvent mixtures and ethylene glycol to be more basic than water. The results derived using the reference electrolyte method, the acidity function method<sup>3</sup> and Wells's method<sup>1</sup> indicate water-rich mixtures to be more basic than water. However, with higher co-solvent content the two former methods show the mixtures and ethylene glycol to be less basic than water.

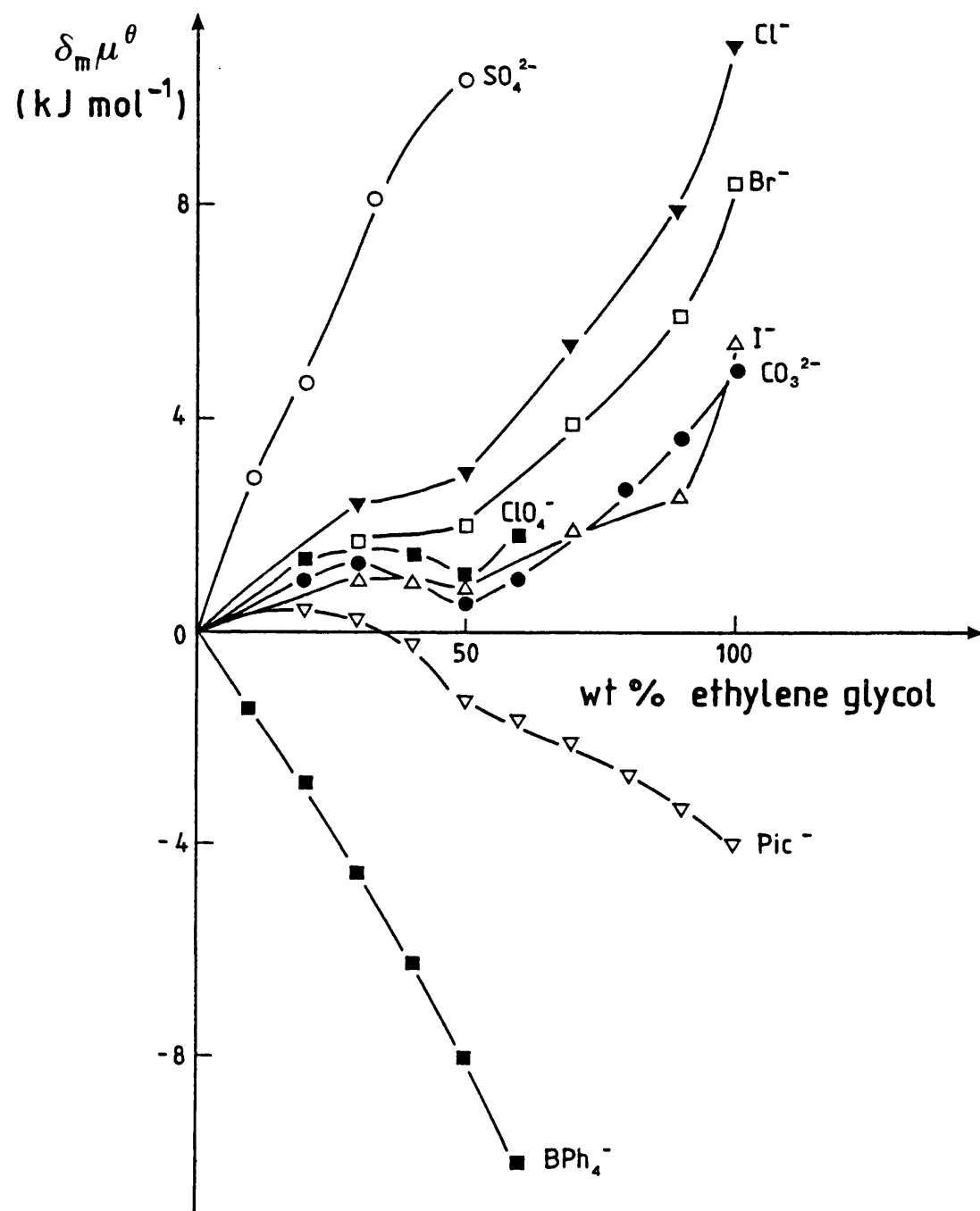


FIGURE 4.6

Transfer chemical potentials for anions (molar scale, 298.2 K, TATB assumption) in water + EG mixtures.

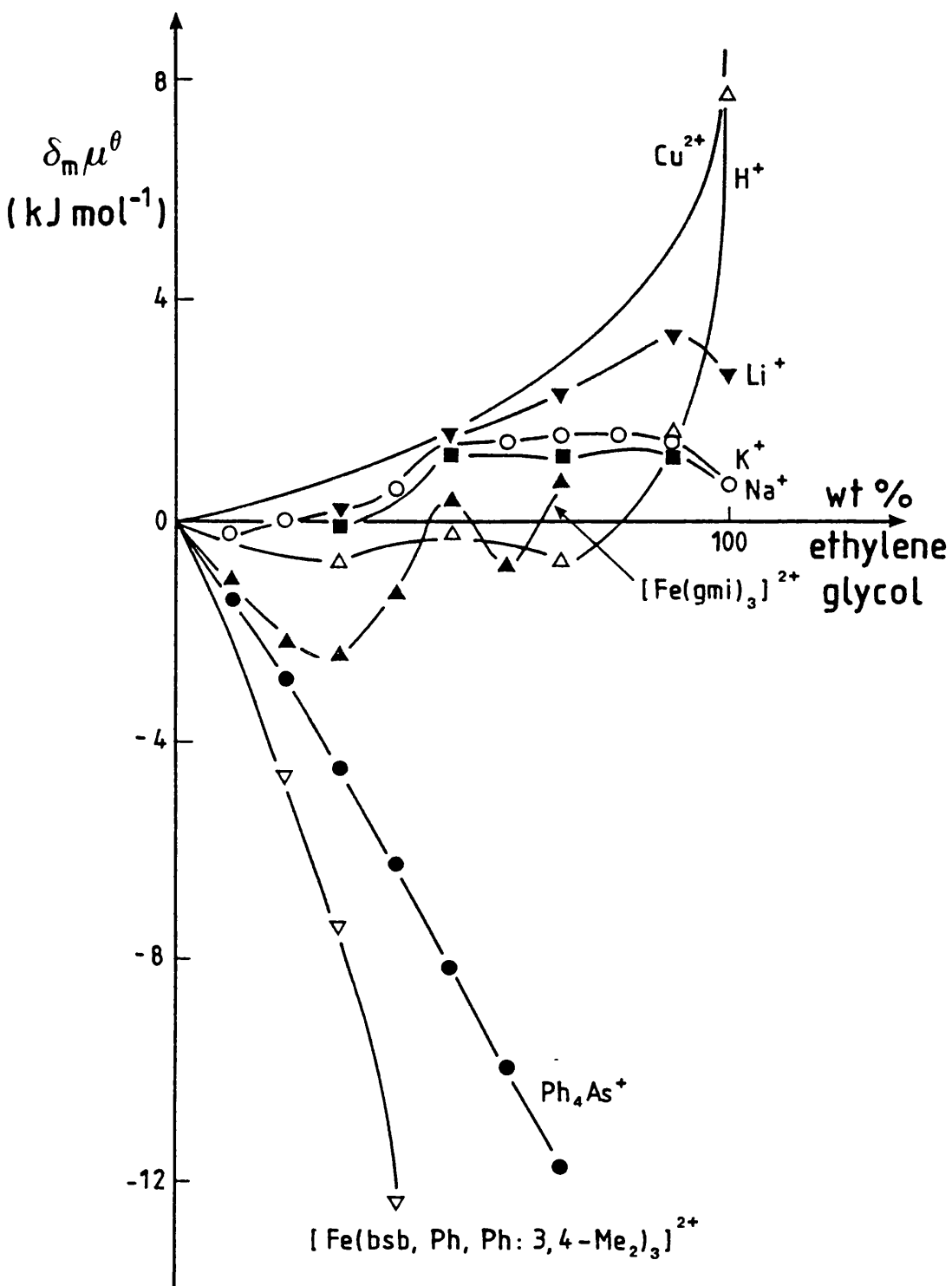
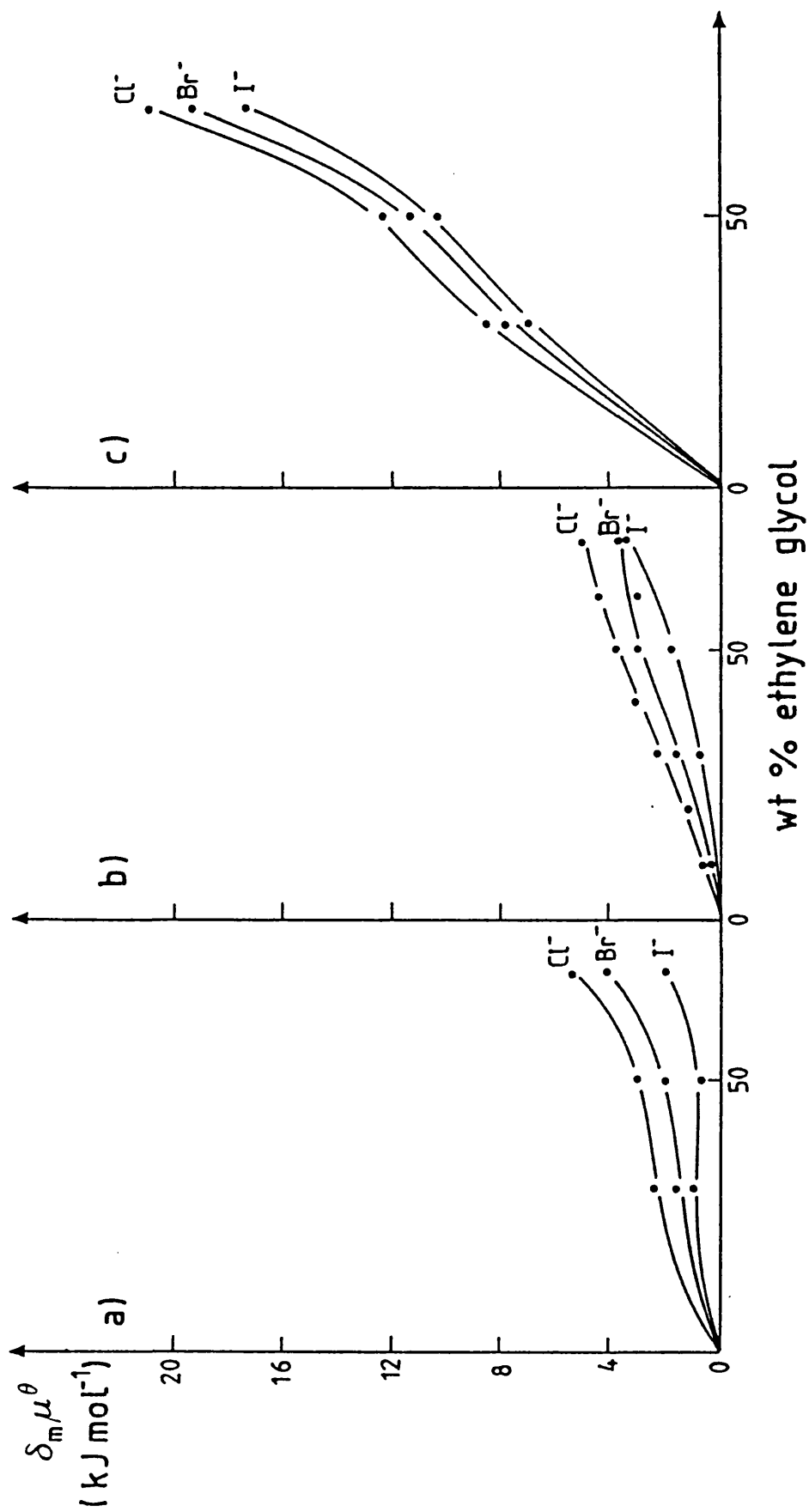


FIGURE 4.7

Transfer chemical potentials for cations (molar scale, 298.2 K, TATB assumption) in water + EG mixtures. [Data for  $\text{Cu}^{2+}$  from refs. 33 and 34.]



**FIGURE 4.8**

Transfer chemical potentials for anions (molar scale, 298.2 K) derived using a) TATB assumption method, b) Wells' method [ref. 1] and c) simultaneous extrapolation method [ref. 2] in water + EG mixtures.

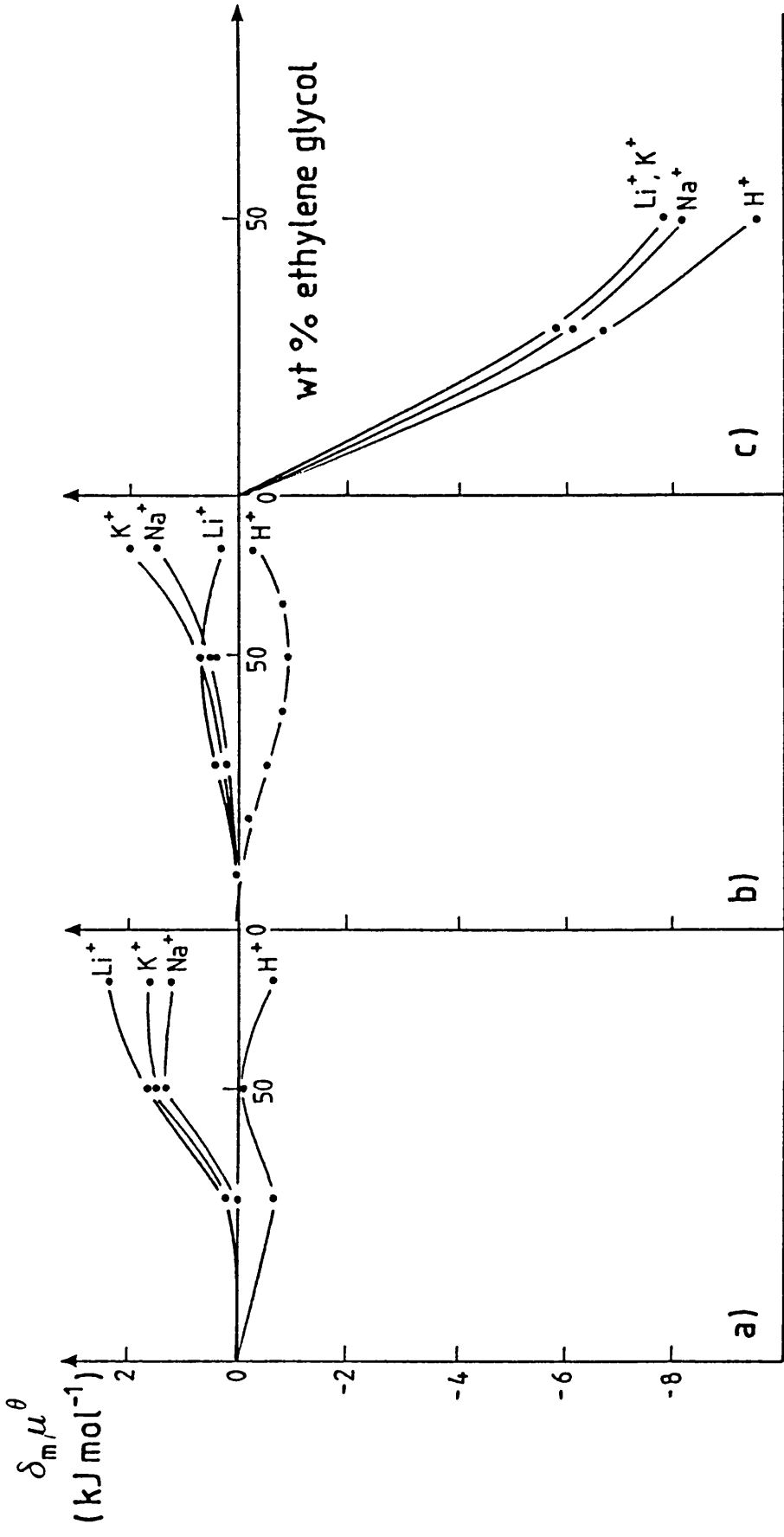


FIGURE 4.9

Transfer chemical potentials for cations (molar scale, 298.2 K) derived using a) TATB assumption method, b) Wells's method [ref. 1] and c) simultaneous extrapolation method [ref. 2] in water + EG mixtures.

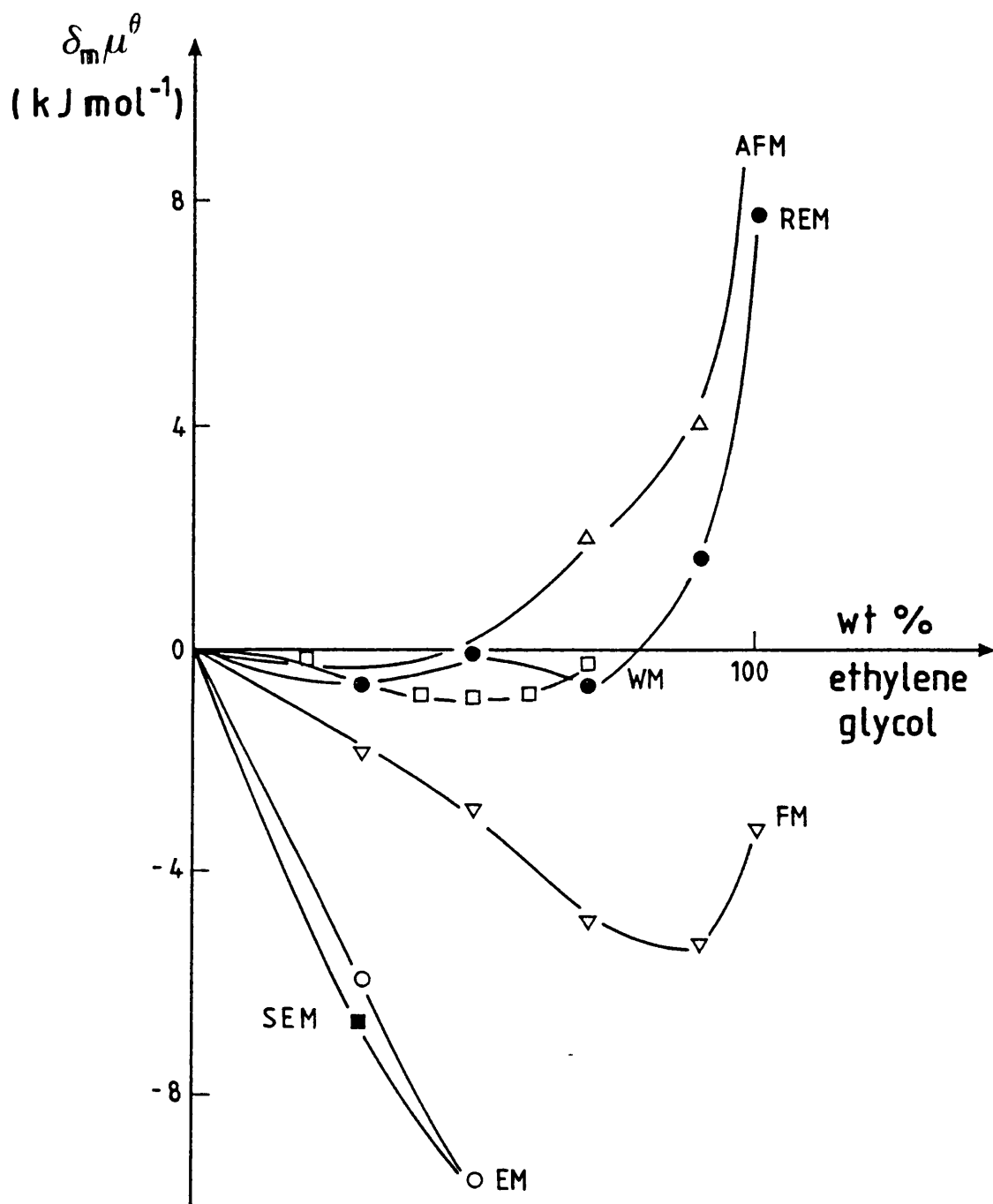


FIGURE 4.10

Transfer chemical potentials for  $\text{H}^+$  (molar scale, 298.2 K) derived using TATB assumption method (REM) ( $\bullet$ ), Wells's Method (WM) [ref. 1] ( $\square$ ), acidity function method (AFM) [ref. 3] ( $\Delta$ ), Foc/Fic<sup>+</sup> assumption method (FM) [ref. 3] ( $\nabla$ ), extrapolation method (EM) [ref. 3] ( $\circ$ ) and simultaneous extrapolation method (SEM) [ref. 2] ( $\blacksquare$ ) in water + EG mixtures.

#### 4.4.2 General solvation pattern in aqueous glycerol mixtures

Fig. 4.11 at the end of this section shows the general solvation pattern for ions in water + glycerol mixtures containing up to 70 wt % G derived using the TATB assumption. Values for  $\text{Cu}^{2+}$  derived using the negligible liquid junction potential assumption<sup>34</sup> are also included. Values for  $\text{SO}_4^{2-}$  and  $\text{NH}_4^+$  are judged to be of lesser accuracy due to solubility or derivation of route considerations (see Section 3.2.5).

For the majority of these ions the effect of transfer from water into these mixtures is much less marked than has been seen for other binary aqueous mixtures in this study. This results from the increased relative structural compatibility of water and glycerol. The general sequence of ions is also different. The only ions which retain their relative positions in the solvation patterns as for aqueous mixtures of the alcohols and EG are the TATB ions and the doubly charged  $\text{Cu}^{2+}$  and  $\text{SO}_4^{2-}$  ions. Their positions in the solvation pattern relative to the other ions can be explained in the same way as their behaviour in the aqueous alcohols (Section 3.3.4) and in aqueous ethylene glycol (Section 4.4.1).

The transfer chemical potentials for the proton are positive for this composition range and increase steadily as the amount of organic co-solvent in the system increases. This implies that these water + glycerol mixtures are less basic than water.

The alkali-metal cations  $\text{Na}^+$ ,  $\text{K}^+$ ,  $\text{Rb}^+$  and  $\text{Cs}^+$  are all destabilized when transferred from water into these mixtures. This destabilization increases with increasing organic co-solvent content of the mixtures. The magnitude of this effect for each of the ions is relatively similar but decreases in the order  $\text{Na}^+ > \text{K}^+ > \text{Rb}^+ > \text{Cs}^+$ . The signs of these transfer chemical potentials and their relative magnitudes are consistent

with these mixtures being less basic than water and with the charge density on the ions decreasing down the series. These ions also show the behavioural pattern expected due to Born-type interactions. The other alkali-metal cation in Fig. 4.11,  $\text{Li}^+$ , is by contrast less destabilized than  $\text{Cs}^+$  in low wt % G mixtures yet more destabilized than  $\text{Na}^+$  in higher wt % G mixtures. This may be due in the former case to the stronger hydration co-sphere of  $\text{Li}^+$  making replacement of water molecules in the primary solvation zone by glycerol more difficult. In the latter case steric considerations may be the cause.

In these mixtures, transfer chemical potentials for the halide ions  $\text{Cl}^-$ ,  $\text{Br}^-$  and  $\text{I}^-$  are all negative (except for  $\text{Cl}^-$  in mixtures of 70 wt % G). The preference for solvation by the mixtures shown by  $\text{Cl}^-$  and  $\text{Br}^-$  is small, that shown by  $\text{I}^-$  is somewhat larger. This stabilization is consistent with acid-base considerations which appear to dominate any positive contribution to the transfer chemical potentials of these ions made by Born-type interactions. The decrease in stabilization of these ions in the order  $\text{I}^- > \text{Br}^- > \text{Cl}^-$  is the opposite of what would be expected if their interactions with the solvent were solely through H-bonding. However, with increasing size of the ion favourable contributions due to dispersion forces increase and approach to the ions by the larger glycerol molecules (or aquo-complexes in the solvent) becomes easier. These factors appear to be significant enough to change the expected sequence of the anions. In the light of these considerations the position of the perchlorate ion in the solvation pattern is anomalous being positive across the composition range.

Fig. 4.12 shows comparison of values for  $\text{Cl}^-$ ,  $\text{Br}^-$ ,  $\text{I}^-$  and  $\text{H}^+$  in water + G mixtures derived using different assumptions. Unlike in the analogous comparison for water + EG mixtures (Section 4.4.1), the values

for the halide ions derived using the reference electrolyte method, Wells's method<sup>4</sup> and the extrapolation method<sup>5</sup> are not all of the same sign. The proposed effect of transfer on these ions from water into water + G mixtures determined by the extrapolation method<sup>5</sup> is one of destabilization. Using the TATB assumption, these ions are shown to be stabilized. Wells's method<sup>4</sup> indicates that  $\text{Cl}^-$  and  $\text{Br}^-$  are destabilized whereas  $\text{I}^-$  is stabilized. As in water + EG mixtures the magnitudes of the calculated transfer chemical potentials irrespective of sign are much larger using the extrapolation method<sup>5</sup> than the other two methods.

Both the reference electrolyte method and Wells's method<sup>4</sup> yield positive values for the proton (greater for the former than the latter) suggesting these water + glycerol mixtures are less basic than water. In direct contrast to this are the negative values of  $\delta_{\text{m}}\mu^{\ominus}(\text{H}^+)$  derived using the extrapolation method<sup>5</sup> indicating the same mixtures to be more basic than water.

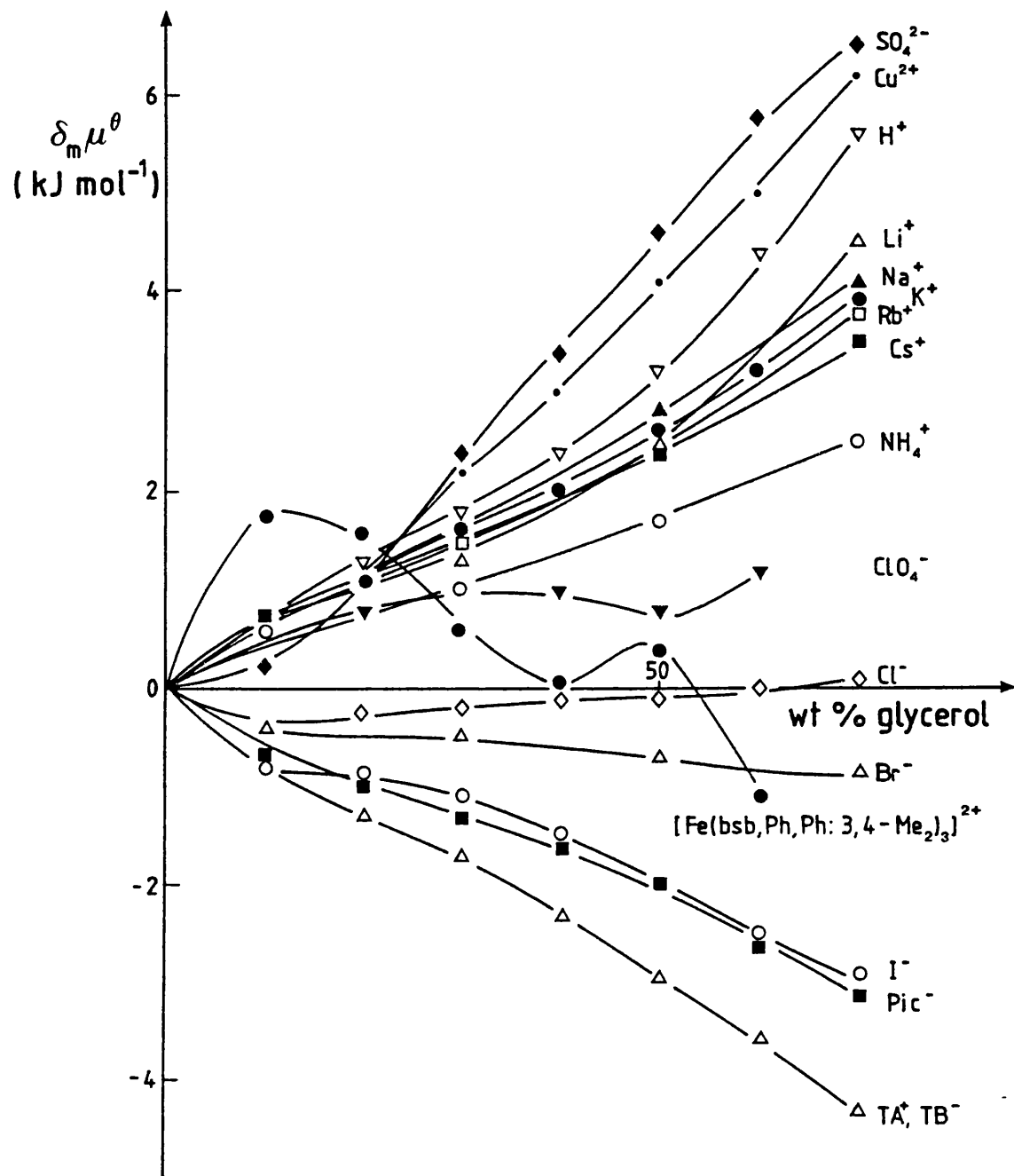
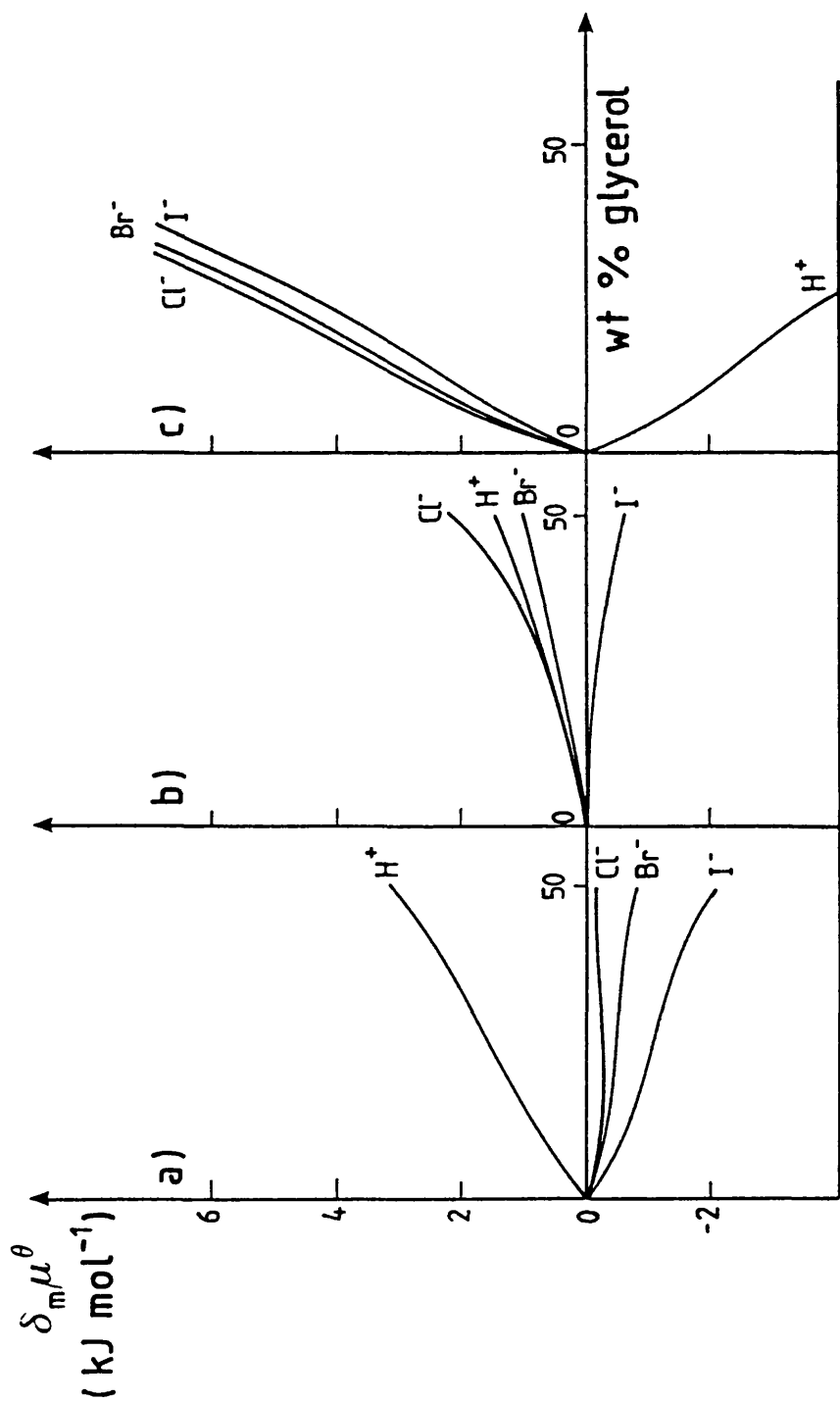


FIGURE 4.11

Transfer chemical potentials for ions (molar scale, 298.2 K, TATB assumption) in water + G mixtures. [Data for  $\text{Cu}^{2+}$  from ref. 34.]



**FIGURE 4.12**  
 Transfer chemical potentials for ions (molar scale, 298.2 K) derived using a) TATB assumption method, b) Wells's method [ref. 4] and c) extrapolation method [ref. 5] in water + G mixtures.

#### 4.4.3 Comparison of solvation of ions in aqueous alcohol, aqueous ethylene glycol and aqueous glycerol mixtures

Figs. 4.13 to 4.16 show the behaviour of a range of ions on transfer from water into aqueous mixtures of methanol,<sup>35</sup> ethanol, isopropanol,<sup>38</sup> ethylene glycol and glycerol, all derived using the TATB assumption.

The comparison between transfer chemical potentials for single ions in water + MeOH, water + EG and water + G mixtures reflects the effect on ion solvation of replacing first one methyl proton in methanol and then two methyl protons with -CH<sub>2</sub>OH groups. Along the series, MeOH, EG, G, the increase in size of the hydrocarbon skeleton in the molecules parallels an increase in the number of hydrophilic -OH groups.

Comparison between values for water + EtOH and water + EG mixtures and between values for water + Pr<sup>1</sup>OH and water + G mixtures reflects the effect on ion solvation of increase in the number of -OH groups in the co-solvent but with retention of the same carbon skeleton length.

Fig. 4.13 shows these comparisons for data for Cl<sup>-</sup>. The values for the ion in mixtures of higher co-solvent content decrease in the order aq MeOH > aq EG > aq G. This parallels the decreasing charge densities on the basic centres of the co-solvent molecules and is consistent with the transfer chemical potentials for Cl<sup>-</sup> being dominated by contributions due to changes in the H-bond primary solvation interactions. That Born-type interactions are relatively unimportant can be seen from the fact that  $\delta_{m\mu}^{\ominus}(\text{Cl}^-)$  in water + MeOH mixtures is closer to  $\delta_{m\mu}^{\ominus}(\text{Cl}^-)$  in water + EG mixtures than to  $\delta_{m\mu}^{\ominus}(\text{Cl}^-)$  in water + G mixtures. Born-type interactions would be most similar for a given ion in aqueous EG and aqueous G mixtures reflecting the similarity of the dielectric constants of these mixtures relative to those of aqueous methanol mixtures.

The results suggest that the basicity of the solvents decreases in the

order  $aq \text{ MeOH} > aq \text{ EG} > aq \text{ G}$  water. This implies that contributions to the transfer chemical potentials for this ion due to secondary solvation described in terms of ion-structureless dipole interactions are also relatively unimportant. Such a contribution would be positive for water + MeOH mixtures but negative for both water + EG and water + G mixtures.

Fig. 4.13 shows that increase in the size of the alkyl group in mono-ols results in increased destabilization of  $\text{Cl}^-$ . Addition of an -OH group to the co-solvent molecule, however, results in reduced destabilization upon transfer from water (adding 2 -OH groups reduces the degree of destabilization even more). Thus comparison of  $\delta_{\text{m}}^{\ominus}(\text{Cl}^-)$  values in water + MeOH, water + EG and water + G mixtures indicates the solvation behaviour of  $\text{Cl}^-$  in these mixtures is dominated more by increasing number of -OH groups in the co-solvents than by increasing carbon skeleton length.

The same effect is seen for  $\text{BPh}_4^-$  in Fig. 4.14. In the aqueous mixtures of MeOH, EG and G the hydrophobicity of the solvents is indicated to decrease in the order  $\text{MeOH} > \text{EG} > \text{glycerol}$ . Although the hydrophobic moiety increases across the series (which fact on its own would be expected to lead to increased stabilization of the large organic ion) reduced stabilization of this ion across the series is observed due to increased number of hydrophilic -OH groups.

Fig. 4.15 shows data for the picrate ion. No discernible regular trends are obvious in the behaviour of this ion on either increasing the carbon skeleton length in the co-solvent or increasing the number of -OH groups, or both. This is probably due to the combined effects of hydrophilic solvation (through the negatively charged O atom and the -NO<sub>2</sub> groups) and dispersion interactions (due to the phenyl group).

Steric effects may also play a part in changing the sequences of the co-solvents if the result of these two effects combined is to yield  $\delta_{m\mu}^{\ominus}(\text{Pic}^-)$  values that are relatively similar in magnitude in all these aqueous co-solvent mixtures.

Transfer chemical potentials for  $\text{K}^+$  are shown in Fig. 4.16. In high wt % co-solvent content mixtures all values of  $\delta_{m\mu}^{\ominus}(\text{K}^+)$  are positive. The destabilization of the ion decreases in the order aq MeOH > aq EtOH > aq Pr<sup>i</sup>OH, i.e. with increasing size of the alkyl chain. The destabilization also decreases on adding an -OH group to a mono-ol, aq EtOH > aq EG. Thus, in comparing the behaviour of the ion in aqueous MeOH, EG and G mixtures it would be expected that these two trends would reinforce each other. The replacement of a methyl proton by a -CH<sub>2</sub>OH group would be expected to cause a substantial decrease in the destabilization of the ion. This is observed in comparing the  $\delta_{m\mu}^{\ominus}(\text{K}^+)$  values in aqueous MeOH and EG mixtures. In comparing the values in aqueous EG and G mixtures, however, there is an increase in destabilization for the latter rather than the expected decrease. Also, the effect of adding two -OH groups to the co-solvent on  $\delta_{m\mu}^{\ominus}(\text{K}^+)$  values (Pr<sup>i</sup>OH → G) is remarkably small given the earlier observations.

These complexities for  $\text{K}^+$  may be due in part to the possibility of formation of specific complexes between the cation and ethylene glycol. Such an occurrence would result in the observed decrease in destabilization seen by comparing values for  $\text{K}^+$  in water + MeOH and water + EG mixtures. Specific complex formation may be less favourable between the cation and glycerol molecules due to steric and 'acid-base' considerations. Thus the destabilization in aqueous glycerol mixtures would be greater than in aqueous ethylene glycol mixtures.

It is clear that the results for this ion cannot be interpreted

wholly in terms of one type of solute-solvent interaction dominating the transfer parameters. The observed values are likely to be the result of an amalgamation of contributions due to several effects.

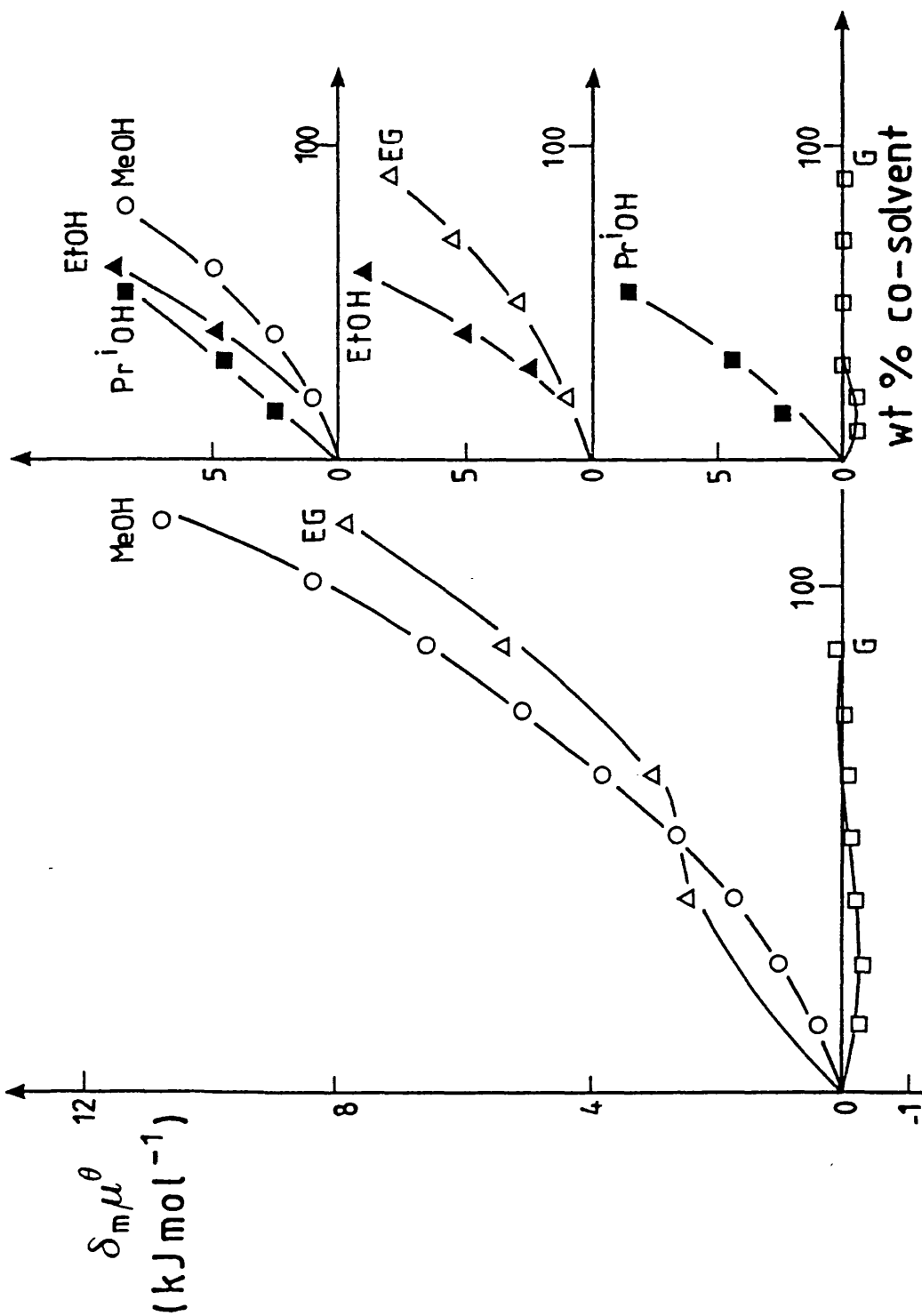


FIGURE 4.13  
Transfer chemical potentials for Cl<sup>-</sup> (molar scale, 298.2 K, TATB assumption) in various water + co-solvent mixtures.

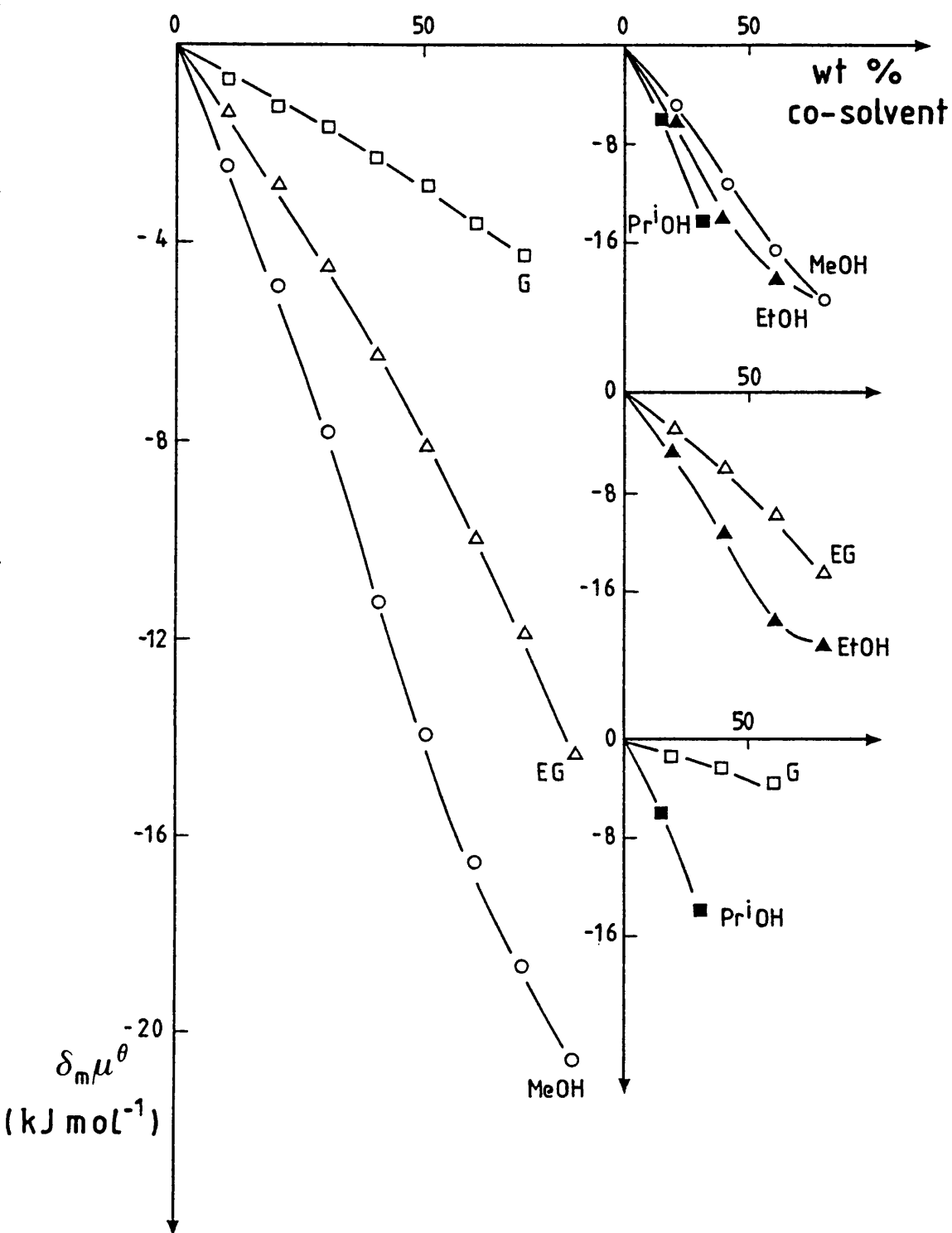
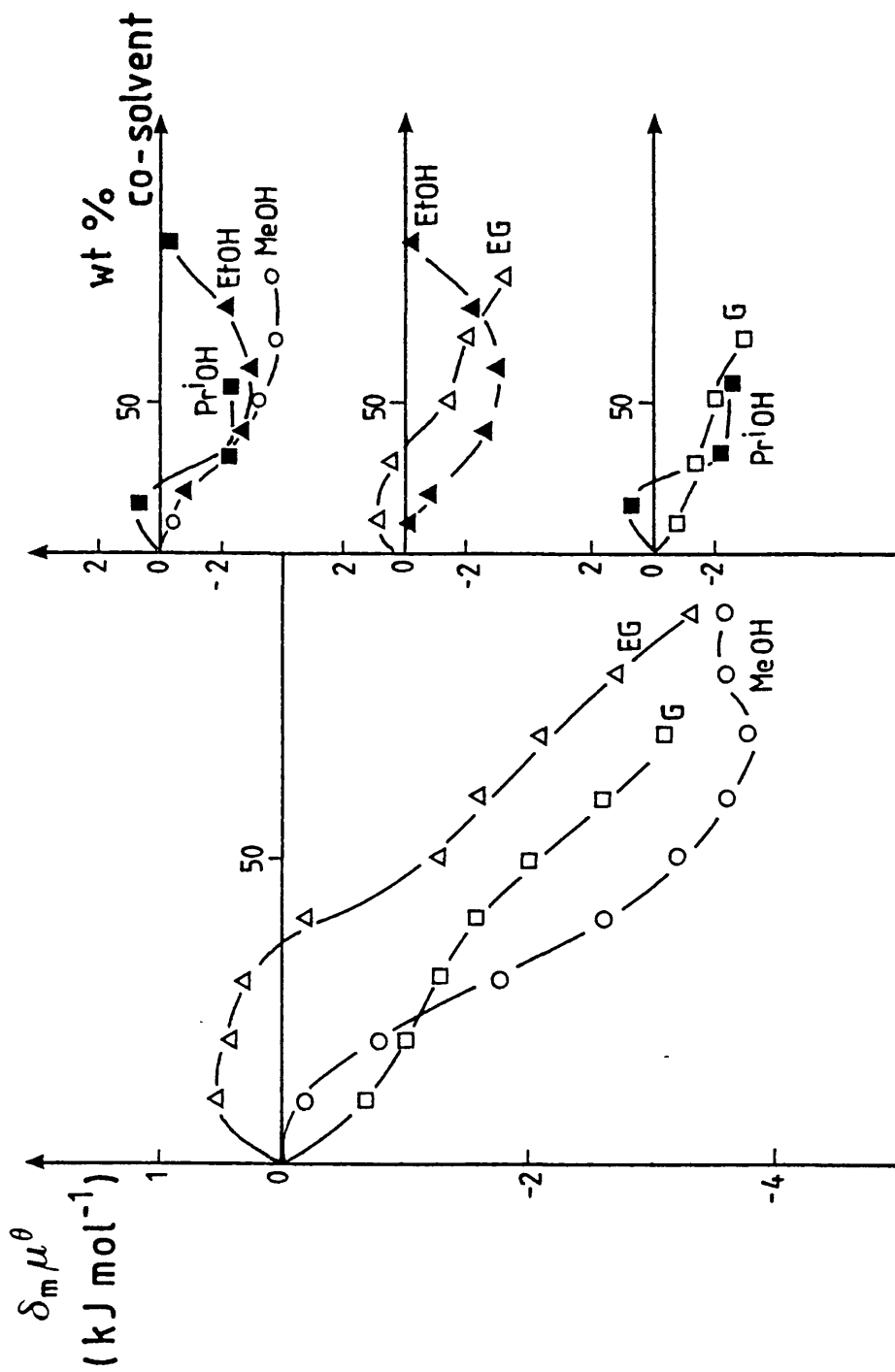


FIGURE 4.14

Transfer chemical potentials for  $\text{BPh}_4^-$  (molar scale, 298.2 K, TATB assumption) in various water + co-solvent mixtures.



**FIGURE 4.15**  
 Transfer chemical potentials for  $\text{Pic}^-$  (molar scale, 298.2 K, TATB assumption)  
 in various water + co-solvent mixtures.

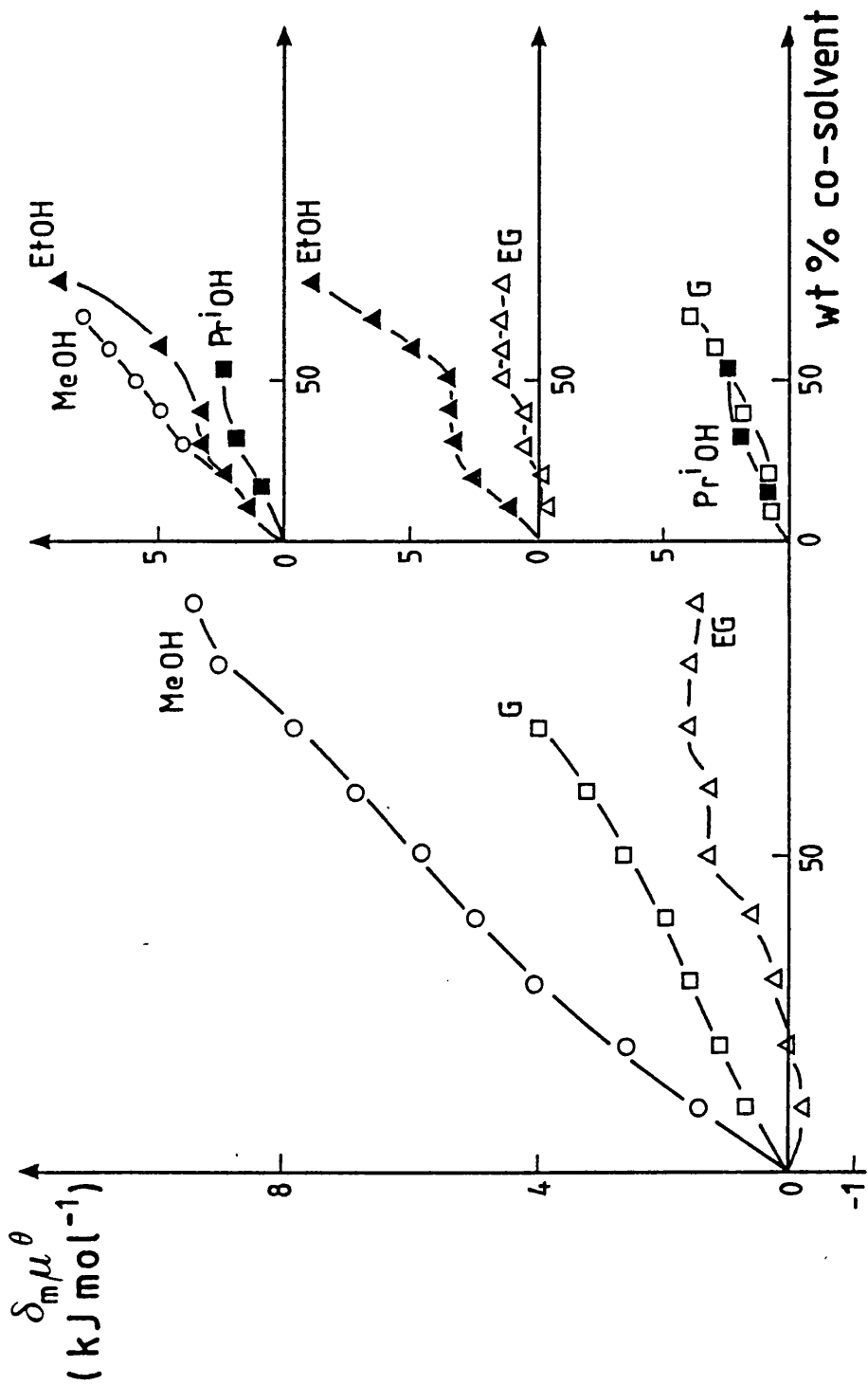


FIGURE 4.16  
 Transfer chemical potentials for  $K^+$  (molar scale, 298.2 K, TATB assumption) in various water + co-solvent mixtures.

#### REFERENCES FOR CHAPTER 4

In the list of references below, the following abbreviations are made.

"Seidell" refers to "Solubilities of Inorganic and Metal Organic Compounds", 3rd. edn., Volume 1, ed. A. Seidell, D. Van Nostrand Company, New York, 1940.

"Stephen and Stephen" refers to "Solubilities of Inorganic and Organic Compounds", Volume 2, part 1, ed. H. Stephen and T. Stephen, Pergamon Press, Oxford, 1963.

- 
1. C. F. Wells, J. Chem. Soc., Faraday Trans. I, 1975, 71, 1868.
  2. K. K. Kundu, A. K. Rakshit and M. N. Das, Electrochim. Acta, 1972, 17, 1921.
  3. S. V. Rao and C. Kalidas, Ind. J. Chem., 1975, 13, 1303.
  4. C. F. Wells, J. Chem. Soc., Faraday Trans. I, 1974, 70, 694.
  5. K. H. Khoo, J. Chem. Soc., Faraday Trans. I, 1972, 68, 554.
  6. Y. Marcus, Pure and Appl. Chem., 1986, 58, 1721.
  7. I. N. Basumullick and K. K. Kundu, Can. J. Chem., 1980, 58, 79.
  8. D. Bax, C. L. de Ligny and M. Alfenaar, Rec. Trav. Chim., 1971, 90, 1265.
  9. D. Feakins and P. Watson, J. Chem. Soc., 1963, 4734.
  10. F. Franks and D. J. G. Ives, Quart. Rev., 1966, 20, 1.
  11. M. M. Elsemongy and A. A. Abdel-Khalek, Monatsh., 1983, 114, 891.
  12. I. N. Basumullick and K. K. Kundu, Can. J. Chem., 1979, 57, 961.
  13. A. K. Das and K. K. Kundu, Ind. J. Chem., 1978, 16A, 467.
  14. J. F. Coetzee and K. Umemoto, Inorg. Chem., 1976, 15, 3109.
  15. D. T. Warner, Nature, 1962, 196, 1055.
  16. S. K. Banerjee, K. K. Kundu and M. N. Das, J. Chem. Soc. (A), 1967, 166.
  17. A. Ray and G. Nemethy, J. Chem. Eng. Data, 1973, 18, 309.
  18. R. L. Blokhra and Y. P. Sehgal, Ind. J. Chem., 1977, 15A, 1035.
  19. "International Critical Tables of Numerical Data, Physics, Chemistry and Technology", 1st. edn., ed. E. W. Washburn, McGraw-Hill Book Company, New York, 1928.
  20. S. G. Bruun, P. G. Sørensen and A. Hvidt, Acta Chem. Scand., 1974, A28, 1047.
  21. "CRC Handbook of Chemistry and Physics", 62nd. edn., ed. R. C. Weast, CRC Press, Boca Raton, Florida, 1981/1982.

REFERENCES (Continued) ....

22. Seidell, p.781.
23. Seidell, p.693.
24. Seidell, p.821.
25. Seidell, p.1240.
26. Stephen and Stephen, p.169.
27. Seidell, p.878.
28. Seidell, p.876.
29. P. Guardado, personal communication.
30. Stephen and Stephen, p.345.
31. Seidell, p.1091.
32. Seidell, p.875.
33. J. F. Coetzee and W. K. Istone, Anal. Chem., 1980, 52, 53.
34. A. Lewandowski, Electrochim. Acta, 1984, 29, 547.
35. M. H. Abraham, T. Hill, H. C. Ling, R. A. Schultz and R. A. C. Watt, J. Chem. Soc., Faraday Trans. I, 1984, 80, 489.
36. C. F. Wells, Aust. J. Chem., 1983, 36, 1739.
37. C. F. Wells, J. Chem. Soc., Faraday Trans. I, 1984, 80, 2445.
38. B. Clark, Ph.D. Thesis, Leicester, 1986.



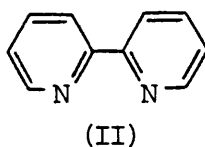
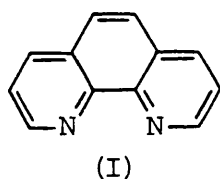
## CHAPTER 5

**Kinetic Investigation into the Existence  
of Geometrical Isomers of Low-Spin Iron(II)  
Schiff Base Di-imine Complexes**

## 5.1 INTRODUCTION

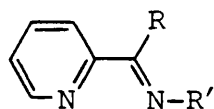
### 5.1.1 Background

The kinetics of reactions of the low-spin iron(II) di-imine complexes  $[\text{Fe}(\text{phen})_3]^{2+}$  and  $[\text{Fe}(\text{bipy})_3]^{2+}$ , where phen and bipy are the bidentate ligands 1,10-phenanthroline (I) and 2,2'-bipyridyl (II) respectively, were first investigated over 30 years ago.<sup>1-3</sup> Since that time kinetic



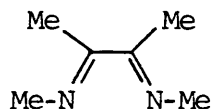
studies involving these complexes, many of their substituted derivatives and other closely related iron(II) tris-(bidentate) complexes have probed the effects of solvents, substituents and added salts on the rates of reactions of these complexes.<sup>4-8</sup> In this way, information concerning the reaction mechanisms, solvent structural properties and solute-solvent interactions involved has been obtained.

One such set of closely related complexes is the series of low-spin iron(II) tris-(bidentate) complexes  $[\text{Fe}(\text{sb})_3]^{2+}$  where sb is a bidentate Schiff base ligand derived from either 2-pyridine carboxaldehyde, 2-acetyl pyridine or 2-benzoyl pyridine and a primary amine (III). The



$R = \text{H}, \text{Me}, \text{Ph}$   
 $R' = \text{alkyl}, \text{aryl}$

(III)



(IV)

reaction kinetics of these complexes were of particular interest in that they provided a structural link between analogous low-spin iron(II) complexes containing aliphatic  $\alpha$ -di-imine ligands, such as the ligand derived from biacetyl and methylamine (IV), and their aromatic counter-

parts  $[\text{Fe}(\text{phen})_3]^{2+}$  and  $[\text{Fe}(\text{bipy})_3]^{2+}$ . They also permitted wider study of substituent effects in terms of the nature, position and number of the substituents on the rates of reactions than was possible for either  $[\text{Fe}(\text{phen})_3]^{2+}$  or  $[\text{Fe}(\text{bipy})_3]^{2+}$  due to the frequent difficulty in preparing substituted derivatives of the latter two ligand molecules. By comparison, preparation of ligands of the type (III), using a range of aliphatic and aromatic amines, is relatively easy. As a result the kinetics of a variety of reactions of these complexes including their reaction with acid,<sup>9,11,14</sup> nucleophiles such as  $\text{OH}^-$ <sup>10,11,13</sup> and  $\text{CN}^-$ ,<sup>12,14</sup> hydrogen peroxide<sup>10</sup> and peroxodisulphate<sup>11</sup> have been studied.

One drawback to the use of these complexes in such investigations has been that the unsymmetrical nature of these Schiff base ligands leads to the possibility of the existence, in theory at least, of two diastereoisomeric species of  $[\text{Fe}(\text{sb})_3]^{2+}$  in samples of the complex (see Section 1.3.3). In the past, findings of unpublished work<sup>15</sup> involving this type of complex have not always been consistent. One feasible explanation for this is the possible existence of such isomers. It would be desirable indeed to know if this could have been the case.

In the investigation of reaction mechanisms by kinetic study, evidence for the existence of geometrical isomers for several complexes of this type has been found. In studying the kinetics of acid aquation for a series of tris-(bidentate) low-spin iron(II) 2-pyridinalalkylimine complexes, Murmann and Healy<sup>16</sup> found evidence for the existence of diastereoisomers in one case only. For the ligand derived from pyridine-2-carboxaldehyde and  $\alpha$ -phenylethylamine two kinetically different species were identified, one reacting nearly 20 times as fast as the other. Krumholz,<sup>17</sup> also investigating rates of acid fission, found kinetic evidence for the existence of isomers of iron(II) complexes of this type containing ligands

derived from either 2-acetyl pyridine or 2-benzoyl pyridine and aniline. The reactivities of the two species were estimated to differ by a factor of about 20. Ultraviolet/visible absorption spectra of the two forms were reported to be almost identical except for the position of  $\lambda_{\max}$ . Estimations of the differences in  $\lambda_{\max}$  of the two species were 3 nm and 10 nm for the complexes containing ligands derived from pyridine-2-carboxaldehyde and 2-benzoyl pyridine respectively. Close to  $\lambda_{\max}$  the molar absorptivities of the two species were found to be very similar. Preparation of solutions of the complexes containing over 50% of the labile form were reported. The presence of isomers in initial preparations of samples exhibiting marked differences in their reactivities towards hydroxide ions has also been reported for some complexes containing ligands derived from 2-benzoyl pyridine and substituted anilines.<sup>11</sup> Thus, although evidence for the existence of such isomers has been found kinetically in some cases, there is relatively little detailed information concerning the two species. For example, for complexes in which isomers have been detected kinetically the relative abundance of the two species has been largely unexplored.

The fact that sets of kinetic results, apparently consistent at the time, have proved later to be irreproducible suggests the possibility that the presence of isomers may have gone without detection. Obviously in terms of kinetic study of reaction mechanisms the undetected presence of a mixture of such isomers is undesirable. As such, it was felt that the existence and detection of diastereoisomers merited further investigation. The reported similarities in the ultraviolet/visible absorption spectral properties of the two species indicated that their detection by these means might be difficult. The reported marked differences in their reactivities, however, were viewed as a potentially more useful, though

possibly not infallible, investigative tool.

With a view to the rationalization of inconsistent results obtained in the past for some complexes of this type the reactions of two complexes with hydroxide were investigated. Initially, the same synthetic and analytical procedures as employed previously were used.

### 5.1.2 Kinetics

The nature of these complexes results in dramatic changes in the absorbance at their  $\lambda_{\max}$  in the ultraviolet/visible region when complexes of this type undergo reaction in solution (see Section 1.3.1). Thus, spectrophotometric measurement of the decrease in absorbance with time at  $\lambda_{\max}$  of the complex, corresponding to disappearance of the complex as it reacts, provides an excellent way to study the kinetics of reactions of these complexes.

By such means, the rates of hydroxide attack at  $[\text{Fe}(\text{sb})_3]^{2+}$  where sb is an unsymmetrical Schiff base ligand of the type (III) for which no isomers have been detected have been shown to follow the rate law given in equation 5.1.<sup>10,11</sup>

$$-\frac{d[\text{complex}]}{dt} = k_1[\text{complex}] + k_2[\text{OH}^-][\text{complex}] \quad \dots [5.1]$$

This rate law for alkaline hydrolysis is followed also by  $[\text{Fe}(\text{phen})_3]^{2+}$ ,  $[\text{Fe}(\text{bipy})_3]^{2+}$  and many of their derivatives as well as by  $[\text{Fe}(\text{sb})_3]^{2+}$  where sb is a variety of symmetrical Schiff base ligands,<sup>8,18,19</sup> except at high hydroxide concentrations. The most satisfactory interpretation of such a rate law is that hydroxide attack at these complexes proceeds by two simultaneously occurring reaction pathways. The first, the rate constant for which is  $k_1$ , is independent of  $[\text{OH}^-]$ . The second reaction pathway, the rate constant for which is  $k_2$ , indicates direct participation of  $\text{OH}^-$  in the rate-determining step, or pre-equilibrium, of this reaction.

Under conditions where  $[\text{OH}^-] \gg [\text{complex}]$  an observed first-order rate constant,  $k_{\text{obs}}$ , is defined by equation 5.2.

$$k_{\text{obs}} = k_1 + k_2 [\text{OH}^-] \quad \dots [5.2]$$

The procedure by which kinetic data were collected and analysed to yield values of  $k_{\text{obs}}$  in this study and others previously was described in Section 2.3.

## 5.2 EXPERIMENTAL

### 5.2.1 Preparation of complexes

In all cases the complexes were prepared by mixing stoichiometric amounts of iron(II) chloride tetrahydrate, the carbonyl compound and the primary amine. The complexes were generated in solution by one of several methods, outlined below, and were then precipitated as salts. The perchlorate, iodide and thiocyanate salts of the complexes were precipitated by the addition of saturated aqueous solutions of sodium perchlorate, potassium iodide and ammonium thiocyanate respectively to portions of the reaction mixtures. The chloride salts were obtained by allowing evaporation of a portion of the solutions of the iron(II) complexes until precipitation occurred. In cases where salts of the complexes were re-crystallized, they were re-crystallized from water + methanol mixtures.

The complexes were first prepared by the general method described in Section 2.2.2. Subsequently, modified versions of this general method were used to prepare samples of the complexes in an attempt to obtain samples containing differing proportions of isomers.

General method. - This involved generation of the 'in situ' Schiff base ligand in solution followed by addition of the  $\text{Fe}^{2+}$  solution. The subsequent treatment of the reaction mixture involved allowing the solu-

tion of the complex to stand for 1 hour at room temperature.

Modified method (i). - Stoichiometric amounts of the reactants were mixed together in the same way as in the preparation of the complex by the general method. Generation of the iron(II) complex in solution, however, was followed by immediate filtration of the solution through 'celite filter-aid' and subsequent precipitation of the complex in the usual way. Thus the solution was not allowed to age as in the general method of preparation. In this way the time lapse between the initial mixing of the reactants and precipitation of the salt was reduced to a minimum.

Modified method (ii). - In this method the order of mixing of the stoichiometric amounts of the reactants was changed. Instead of generation of the 'in situ' Schiff base ligand being followed by addition of the  $\text{Fe}^{2+}$  solution as in the general method, the solutions of the amine and iron(II) chloride tetrahydrate were mixed together first and the solution of the carbonyl compound was added afterwards. Subsequent treatment of the reaction mixture was the same as in the general method.

Modified method (iii). - The reactants were mixed in the same way as in the general method. Instead of allowing the resulting solution to stand at room temperature for 1 hour the reaction mixture was heated to  $40^{\circ}\text{C}$  for the same length of time. Subsequent treatment of the reaction mixture was the same as in the general method.

### 5.2.2 Kinetics

For all the samples the kinetics of reactions of the complexes were investigated using the Unicam SP800 and SP1800 spectrophotometers. In all cases the concentration of sodium hydroxide was in vast excess over

that of the complex, corresponding to typical first-order conditions.

Using the Unicam SP800 spectrophotometer, repeat wavelength scans (from approximately 300 to 715 nm) were used to monitor the reactions of each of the samples with 0.33 M sodium hydroxide in water + methanol mixtures containing up to 40 vol % MeOH. The solvent composition scale used, x vol % co-solvent, was defined in Section 2.2.1. The ultra-violet/visible absorption spectra provided the necessary information to monitor the reactions using the SP1800 spectrophotometer. The reactions in these cases were followed by monitoring the decrease in absorption at  $\lambda_{\max}$  with time. First-order rate constants,  $k_{\text{obs}}$ , for the reactions of the complexes with sodium hydroxide (0.33 M) at 298.15 K in water + methanol mixtures were calculated by the procedure described in Section 2.3.2. Hard copies of the absorbance/time data from all the kinetic runs were obtained from the printer connected to the minicomputer.

Kinetic runs were first carried out using freshly made-up solutions of the complexes. In other words, reactions were initiated as soon as possible after preparation of the solutions of the iron(II) complexes. Subsequently, the dependence of  $k_{\text{obs}}$  on the age of the solutions of the complexes was investigated. In these cases a large portion of the required solution was made. Aliquots taken from this stock solution were reacted with sodium hydroxide under the same conditions on a daily basis.

## 5.3 RESULTS AND DISCUSSION

### 5.3.1 Observed trends in $k_{\text{obs}}$

The investigation began with the preparation of the perchlorate salt of complex A, the unsubstituted N-phenyl complex  $[\text{Fe}(\text{bsb},\text{Ph},\text{Ph})_3]^{2+}$  containing the ligand derived from 2-benzoyl pyridine and aniline, by

the general method (see Section 2.2.2). For a solution of the salt in 6.6 vol % MeOH,  $\lambda_{\max}$  was 580 nm. Krumholz<sup>17</sup> had reported  $\lambda_{\max}$  for the stable isomeric form of this complex to be  $579 \pm 1$  nm. This suggested that the sample prepared by the general method contained predominantly, if not solely, the more stable form. Using this value for  $\lambda_{\max}$  first-order rate constants,  $k_{\text{obs}}$ , were obtained using the SP1800 spectrophotometer for the reaction of freshly made-up solutions of the sample with sodium hydroxide (0.33 M) at 298.15 K in water + methanol mixtures. The values of  $k_{\text{obs}}$ , initial absorbance,  $P_0$ , absorbance at  $t = \infty$ ,  $P_\infty$ , and the standard deviation of the absorbances,  $SD/P$ , calculated by the mini-computer (see Section 2.3.2) for these reactions are given in Table 5.1. [The tables referred to in this chapter are given together at the end of the chapter. The figures referred to are given, in order, at appropriate places throughout the text.] The first-order plots for these reactions appeared to be satisfactory straight lines. The plots were compared with others obtained by the same analytical method for first-order reactions of closely related compounds containing symmetrical bidentate ligands. No significant differences in the shapes of the plots were observed. The results show the expected trend of increase in  $k_{\text{obs}}$  with increasing MeOH content of the solvent mixture.<sup>8,13</sup> At this point the indications were that the solutions of the complex contained only the slow isomer. The kinetic runs were repeated using other sets of freshly made-up solutions of the sample. Reproducibility of the results was found to be very poor, values of  $k_{\text{obs}}$  differing in some cases by as much as 20%. The first-order plots, however, appeared to be in all cases linear. To ensure that the inability to produce consistent results was in no way connected with the use of the perchlorate ion in precipitating the complex, samples of the iodide, thiocyanate and chloride salts of the complex were prepared by

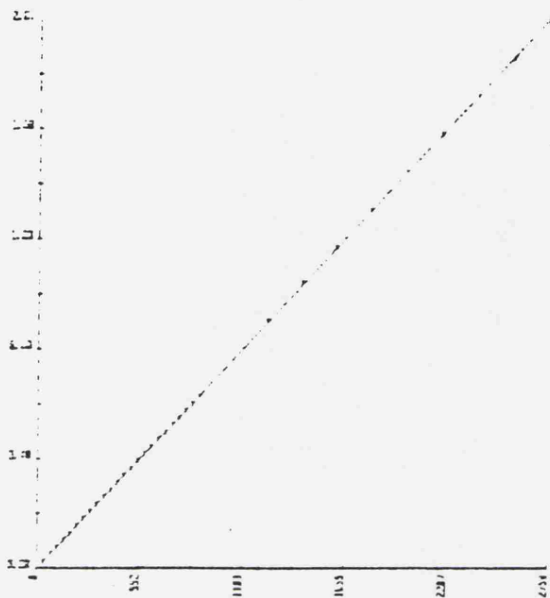
the same general method. The results obtained for the reactions of solutions of these samples with hydroxide under the same conditions as before are shown in Table 5.2. The ranges of values of  $k_{obs}$  obtained using freshly made-up solutions of different salts of the complex were in general even greater than those obtained using different solutions of the same salt for a given solvent mixture. The only one of the samples to produce anywhere near consistent results was the chloride salt. Values of  $k_{obs}$  obtained using this salt were in all cases lower than those obtained for the other salts of complex A prepared in this way. Yet, once again, all the first-order plots appeared to be linear (Fig. 5.1). The results given in Tables 5.1 and 5.2 are shown together in Fig. 5.2.

Preliminary investigation into the kinetics of the analogous reactions involving complex B,  $[Fe(bsb,Ph,Ph:m-Me)_3]^{2+}$ , the *m*-methyl substituted derivative of complex A, revealed the same pattern. Freshly made-up solutions of the complex (using samples prepared by the general method) yielded a range of  $k_{obs}$  values yet linear first-order plots for a given solvent composition.

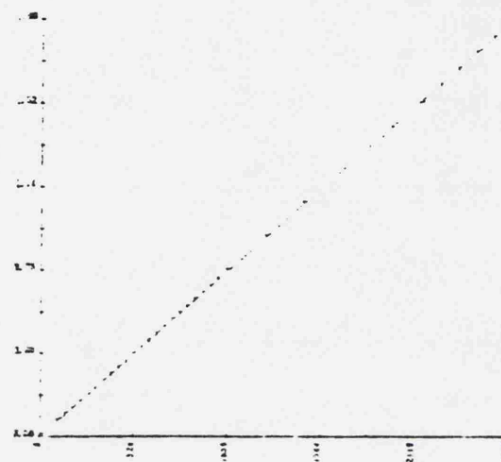
For both complexes it was found that, for freshly made-up solutions, consistent values of  $k_{obs}$  could be obtained only by re-using the same freshly made-up stock solutions of a given sample. Even then identical runs needed to be carried out within a very short time of each other. When the time lapse between identical runs was longer, then values of  $k_{obs}$  obtained using the 'older' stock solutions were always smaller than those obtained using the freshly made-up stock solutions. The space of time within which consistent values of  $k_{obs}$  could be obtained using the same freshly made-up solution appeared to depend on the methanol content of the solvent. For solutions of the complexes in low vol % MeOH mixtures,

FIGURE 5.1

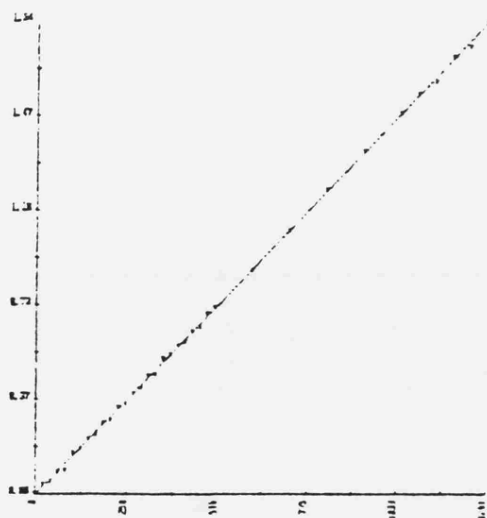
Examples of the first-order plots obtained from the minicomputer for the reactions of the salts of complex A with sodium hydroxide (0.33 M) at 298.15 K.



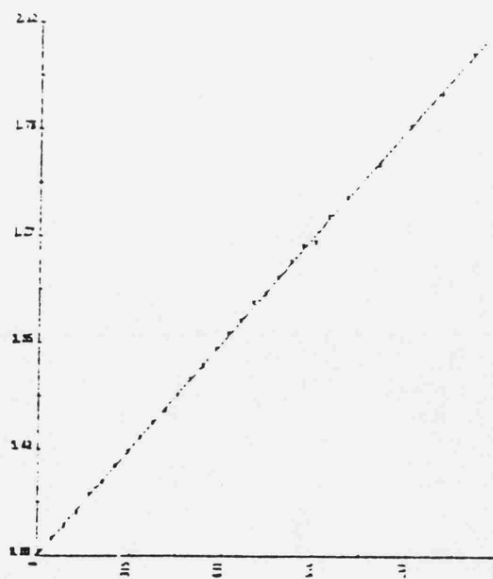
a) perchlorate salt (water)



b) chloride salt (water)



c) thiocyanate salt (30 vol % MeOH)



d) iodide salt (30 vol % MeOH)

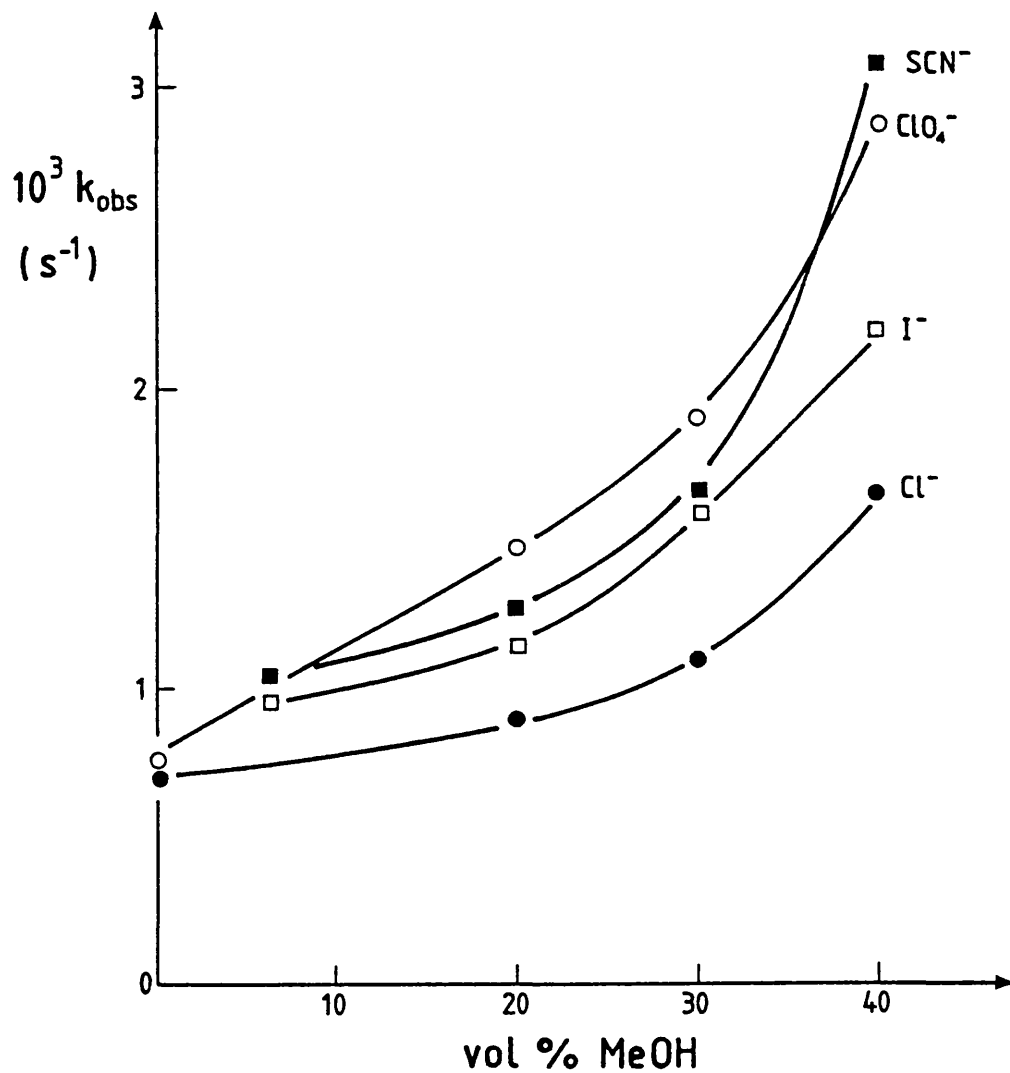
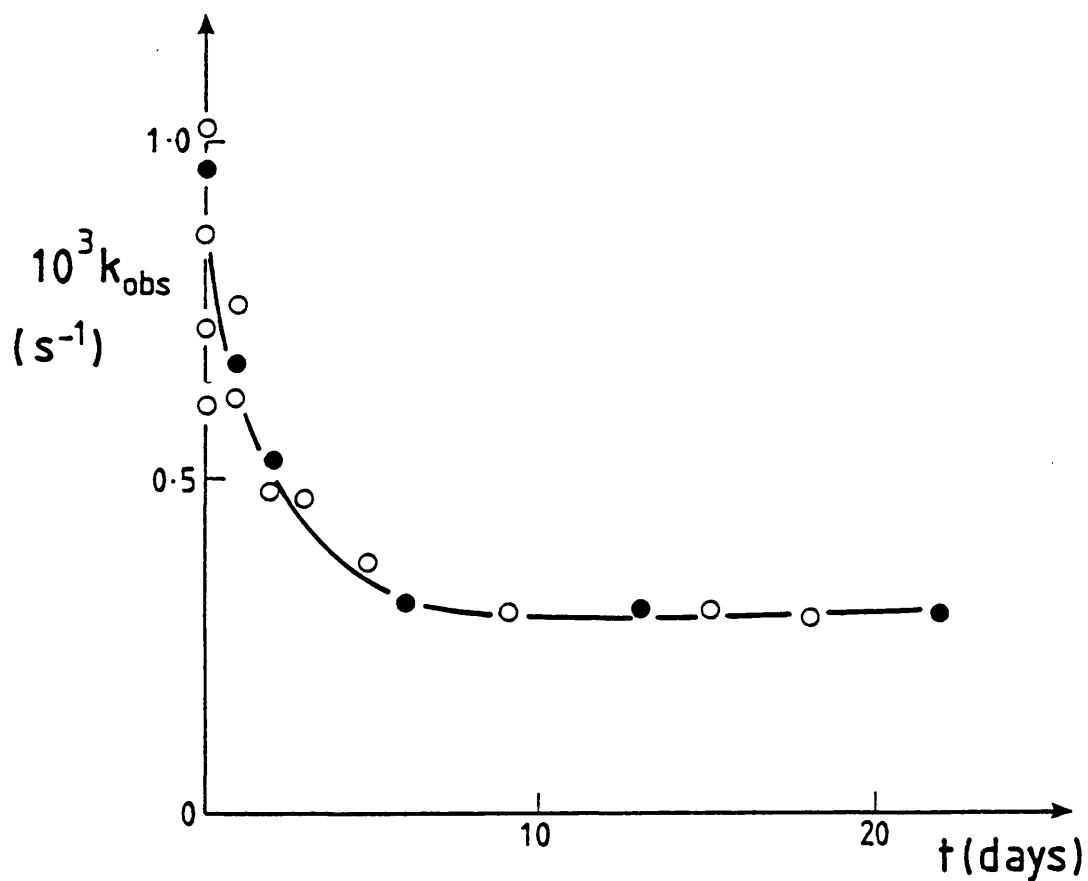


FIGURE 5.2

Observed first-order rate constants,  $k_{\text{obs}}$ , for reactions of salts of complex A with sodium hydroxide (0.33 M) in water + methanol mixtures at 298.15 K.

runs could be repeated after several hours and still produce consistent  $k_{\text{obs}}$  values. For solutions having a greater methanol content, runs needed to be repeated almost immediately to produce consistent  $k_{\text{obs}}$  values. Thus, a consistent set of  $k_{\text{obs}}$  values could be obtained for any one set of freshly made-up solutions provided the runs were repeated soon enough. However, other analogous sets of freshly made-up solutions of the same sample gave different sets of  $k_{\text{obs}}$  values. These seemingly erratic results observed for freshly made-up solutions were in contrast to those obtained for 'older' stock solutions (stock solutions that had been allowed to stand for a certain length of time before  $k_{\text{obs}}$  was measured). In these cases, different stock solutions of the same composition that were above a certain age yielded consistent  $k_{\text{obs}}$  values. The age beyond which such  $k_{\text{obs}}$  values could be obtained appeared to depend on the solvent composition.

An example of the effect of age of stock solutions on  $k_{\text{obs}}$  values is shown in Fig. 5.3. The solid circles represent  $k_{\text{obs}}$  values obtained for the reactions of aliquots of a stock solution of complex B  $[\text{Fe}(\text{bsb}, \text{Ph}, -\text{Ph}:\underline{\text{m}}-\text{Me})_3]^{2+}$ , solution B, with sodium hydroxide (0.33 M) in 6.6 vol % MeOH at 298.15 K. Each point is the average of several  $k_{\text{obs}}$  values obtained for solution B by immediate repetition of runs. These values and the corresponding values of  $P_0$ ,  $P_\infty$  and SD/P are given in Table 5.3. Day 0 corresponds to measurement of  $k_{\text{obs}}$  using the freshly made-up solution of the complex. It can be seen that as the age of solution B increases so  $k_{\text{obs}}$  decreases. The decrease in  $k_{\text{obs}}$  over the first few days is comparatively large. By the end of week 1  $k_{\text{obs}}$  is less than 40% of its value on day 0. By comparison, the decrease in  $k_{\text{obs}}$  after day 6 is very small. The open circles in Fig. 5.3 represent corresponding values of  $k_{\text{obs}}$  obtained for other stock solutions of the same sample. Kinetic



**FIGURE 5.3**

Observed first-order rate constants,  $k_{\text{obs}}$ , for reactions of the thiocyanate salt of complex B with sodium hydroxide (0.33 M) in 6.6 vol % MeOH at 298.15 K: solution B (●); other solutions (○).

measurements involving stock solutions less than one week old produced ranges of  $k_{obs}$  values using different stock solutions of the same age. However, values of  $k_{obs}$  obtained for stock solutions older than one week were, within experimental error, the same. For any given stock solution, successive measurements of  $k_{obs}$  over the first week produced successively lower values of  $k_{obs}$  in all cases. Similar  $k_{obs}/time$  profiles were observed for both complexes A and B in water + methanol mixtures.

For each solution it was observed that the intensity of colour of the stock solutions decreased with time, finally disappearing. This was reflected in the decreasing values of  $P_0$ ,  $P_0$  being the absorbance at  $t=0$ , in successive kinetic runs using the same solution. This raised the possibility that the trend observed in Fig. 5.3 may have been the result of a dependence of  $k_{obs}$  on  $[complex]$ . Two observations, however, indicated this not to be the case. Firstly, rate constants for the reactions of solutions older than one week were the same even though, for a given solution,  $P_0$  continued decreasing during this time period. Secondly, when different solutions of the same age (but less than 1 week old) gave varying values of  $k_{obs}$  no correlation was observed between the absorbance of the solution at  $t=0$  and  $k_{obs}$ . Thus, by comparison of values of  $P_0$  for different solutions of the same age, a smaller  $P_0$  did not necessarily result in a smaller  $k_{obs}$ . This independence of  $k_{obs}$  on  $[complex]$  was expected (see equation 5.2).

The observed trends in  $k_{obs}$  could all be rationalized in terms of the existence of two isomers in the samples, one reacting at a faster rate with hydroxide than the other, and one isomer, or both, aquating relatively slowly. Fig. 5.2 suggested that different salts of the same complex contained differing proportions of the two isomers, reflected in the varying

values of  $k_{obs}$ . Fig. 5.3 suggested that sets of freshly made-up solutions of the same complex also contained differing proportions of the isomers. Perhaps the most interesting trend observed was that concerning the dependence of  $k_{obs}$ , measured using a given stock solution, on the age of the stock solution as shown, for example, for solution B in Fig. 5.3. In this case the implication is that solution B initially contains a mixture of the faster-reacting isomer and the slower-reacting isomer. With increasing age of the solution the ratio of the isomers changes, the proportion of the 'fast' isomer decreasing, until only the 'slow' isomer of complex B remains in the solution. When this point is reached then increase in the age of the solution has no effect on  $k_{obs}$ . It was much more difficult to explain, in terms of the presence of such isomers, the sets of seemingly linear first-order plots obtained for the reactions.

As a result, suspicion as to the presence of isomers in the samples, aroused by the observed trends in  $k_{obs}$ , lead to investigation of the apparent linearity of the observed first-order plots. The hard copies of absorbance/time data produced by the minicomputer provided a means by which this could be done.

### 5.3.2 Re-analysis of kinetic data

Consider a solution in which two geometrical isomers exist. The two species react with hydroxide at different rates, the reactions of both being first-order under the given conditions. The rate of change of the proportion of the two species in the solution is very much less than the rate of reaction of either with hydroxide. The ultraviolet/visible absorption spectra of the two species are almost identical. Close to  $\lambda_{max}$ , the wavelength used to monitor the rates of reactions of the solution by disappearance of the reactants, the extinction coefficients are very similar. The kinetic data obtained from the reaction of such a

solution with hydroxide would then be the result of parallel first-order reactions. It should be possible, provided the reaction was monitored for long enough, to produce a plot of  $\ln(P_t - P_\infty)$  versus  $t$  where  $P_t$  is the absorbance at time  $t$  from the absorbance/time data of the form shown in Fig. 5.4 for some value of  $P_\infty$ . The curved portion of the plot from  $t=0$  to  $t=t_m$  corresponds to the concurrent reactions of the isomers with hydroxide.  $t_m$  is the value of  $t$  at which the reaction of the 'fast' isomer with hydroxide is essentially complete. Beyond this point, the region of the plot where  $t > t_m$ , the plot corresponds to the reaction of the 'slow' isomer with hydroxide. This portion of the plot is a straight line, the slope of which gives the rate constant for the reaction of the

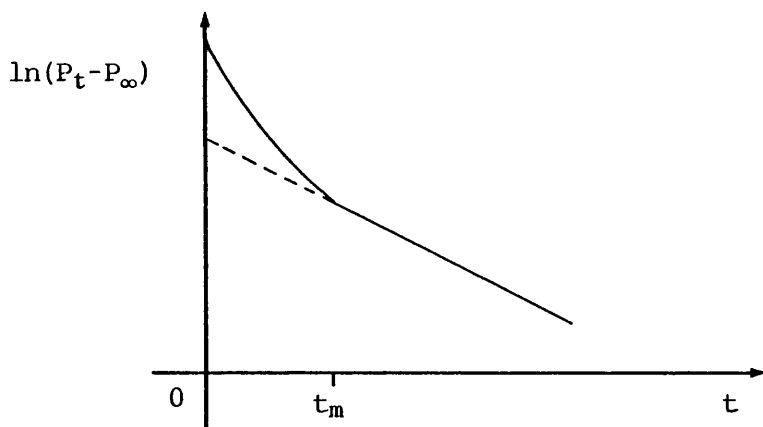


FIGURE 5.4  
Parallel first-order reactions pattern.

'slow' isomer with hydroxide,  $k_s$ . Extrapolation of this line to  $t=0$  yields a value for the absorption of the 'slow' isomer in the solution,  $P_s$ , at  $t=0$ . The absorbance of the 'fast' isomer in the solution,  $P_f$ , at  $t=0$  can then be calculated using the relationship  $P_m = P_f + P_s$  where  $P_m$  is the total absorbance of the solution, in this case at  $t=0$ . By repeating this procedure for other values of  $t$ , absorbance/time data for the reaction of the 'fast' isomer in the solution with hydroxide can be

obtained. A first order plot of  $\ln P_f$  versus time should be a straight line the slope of which is  $k_f$ , the rate constant for the reaction of the 'fast' isomer with hydroxide.

In terms of reactions of complexes A and B with hydroxide (under the conditions described previously) following such a reaction scheme, then from Fig. 5.3 it appears that by day 22 solution B contains only the slow isomer. First-order analysis of the kinetic data from this reaction should therefore produce a first-order fit of low standard deviation for some value of  $P_\infty$ , the slope of which is  $k_s$ . Table 5.4 shows the kinetic data obtained for the reaction of solution B with hydroxide on day 22.

The absorbance data obtained from the printouts were, in all cases,  $1000 \times P$ . Such absorbance values were labelled  $P'$ , i.e.  $P = P'/1000$ , and were used throughout the re-analysis procedure. Thus, for example, if  $P' = 616$ , then  $P = 0.616$ . If  $P'_\infty = 40$ , then  $P_\infty = 0.040$ , etc. Using the data given in Table 5.4, a plot of  $P'$  against time was drawn from which values of  $P'$  at 500s intervals were interpolated. The first-order analysis of the data by the minicomputer had resulted in a value for  $P_\infty$  of 0.042 so this was used as a starting point. Two plots of  $\ln(P'_t - P'_\infty)$  versus  $t$  were drawn where  $P'_\infty = 42$ , one using the interpolated values of  $P'$  the other using the experimentally observed values. Paying particular attention to the region of high  $t$ ,  $P'_\infty$  was changed to see if a better straight line fit could be made. [The region of high  $t$  refers to the part of the plot where  $t > t_m$ . For the reactions of solution B, preliminary plots of the data had shown  $t_m$  to be no more than 2000s so the region of high  $t$  implied is the region for which  $t > 2000$ s.] By changing  $P'_\infty$  in increments of  $\pm 1$  no better fit than when  $P'_\infty = 42$  could be found. For this value of  $P'_\infty$ , values at low  $t$  also lay on the best straight line fitted to the data. Fig. 5.5 shows the first-order plots derived using interpolated values of  $P'$  for

$P'_{\infty} = 42$ . For comparison the analogous plots obtained when  $P'_{\infty} = 0, 20$  and  $60$  are also included. Having adopted  $P'_{\infty}$  as  $42$ , a computer was used to calculate the slope of the line and the error involved. This was done for both the experimental and interpolated absorbance values from  $t = 0$  to  $t = 8000\text{s}$  and also, for both these sets of values, from  $t = 2000\text{s}$  onwards. The results are shown in Table 5.5. The relatively high error of the line derived using  $P'_{\infty} = 42$  with the experimental values of  $P'$  was probably due to the scatter observed in the plot of  $P'$  versus  $t$ . This effect was removed when absorbance values were interpolated and the percentage error of the slope for this  $P'_{\infty}$  over the whole time range was reduced from  $2.3$  in the former case to  $0.5$  using the interpolated values. The first-order rate constant for the reaction of solution B with hydroxide on day 22,  $k_s$ , was  $0.3 \times 10^{-3} \text{ sec}^{-1} \pm 3\%$ . The same re-analysis procedure was carried out using absorbance/time data collected from an identical run. The resulting rate constant was within experimental error of the above value.

Table 5.6 shows absorbance/time data collected during the reaction of solution B with hydroxide on day 13. The data were treated in the same way as those for the reaction on day 22. The best straight lines were obtained when  $P'_{\infty} = 46$ . Table 5.7 shows the rate constants and their percentage errors derived from the observed and interpolated data when  $P'_{\infty} = 46$ . The average of the four values of  $k_s$  is  $0.29 \times 10^{-3} \text{ sec}^{-1}$ . Therefore within experimental error values of  $k_s$  computed from the data for the reaction of solution B with hydroxide on days 13 and 22 are the same. Within the proposed reaction scheme by day 13 only the 'slow' isomer is present in solution B.

Table 5.8 shows absorbance/time data collected for the reaction of solution B with sodium hydroxide on day 6. The data were analysed in the

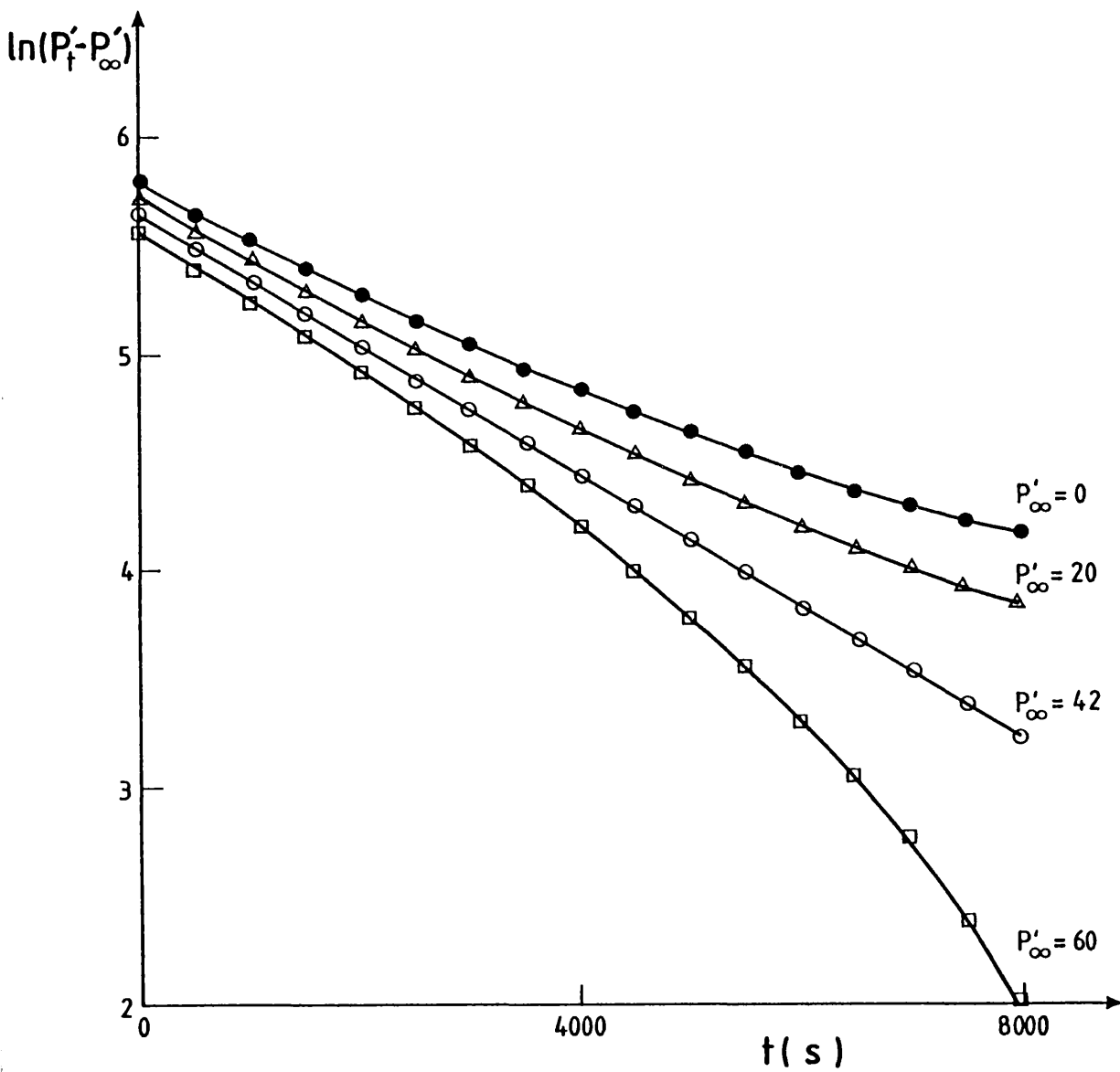


**FIGURE 5.5**

First-order plots of the kinetic data (interpolated values of  $P'$ ) for the reaction of solution B with sodium hydroxide (0.33 M) at 298.15 K on day 22.

same way as for the reactions carried out on days 13 and 22.  $P'_\infty$  was taken to be 39 and the resulting  $k_s$  values derived using the observed and interpolated sets of  $P'$  values are shown in Table 5.9. The average of these four values is  $0.31 \times 10^{-3} \text{ sec}^{-1}$ . It appears that by day 6, also, solution B contains only the 'slow' isomer.

The average of the values obtained thus far for  $k_s$  by analysis of the data from days 6, 13 and 22 is  $0.30 \times 10^{-3} \text{ sec}^{-1}$ . This was taken to be the rate constant for the reaction of the 'slow' isomer of  $[\text{Fe}(\text{bsb}, \text{Ph}, -\text{Ph}; \text{m-Me})_3]^{2+}$  with sodium hydroxide (0.33 M) in 6.6 vol % MeOH at 298.15 K.

Tables 5.10 and 5.11 show the absorbance/time data collected during the reaction of solution B with sodium hydroxide on days 2 and 1 respectively. For both these sets of values, but using values of  $P'$  for  $t > 2000\text{s}$  only,  $P'_\infty$  was adjusted to give the best straight line fit through these values. For day 2,  $P'_\infty = 55$  and for day 1,  $P'_\infty = 58$ . The resulting  $k_s$  values and their percentage errors derived using the respective infinity values are given in Table 5.12.

Fig. 5.6 shows the first-order plots derived from interpolated absorbance/time data as described above for the reaction of solution B with NaOH on days 1, 2, 6, 13 and 22. For days 1 and 2 it can be seen that there is a positive divergence at low  $t$  values from the best straight line drawn through the values for  $t > 2000\text{s}$ . This can be seen more clearly in Fig. 5.7. In this figure, the line through the values at  $t > 2000\text{s}$  in each plot has a slope of  $0.3 \times 10^{-3} \text{ sec}^{-1}$  representing the contribution made to the kinetic data by the reaction of the 'slow' isomer with hydroxide. From large scale first-order plots drawn using the observed and interpolated kinetic data of solution B (analogous to those in Fig. 5.7) absorbance/time data for the reaction of the 'fast' isomer in solu-

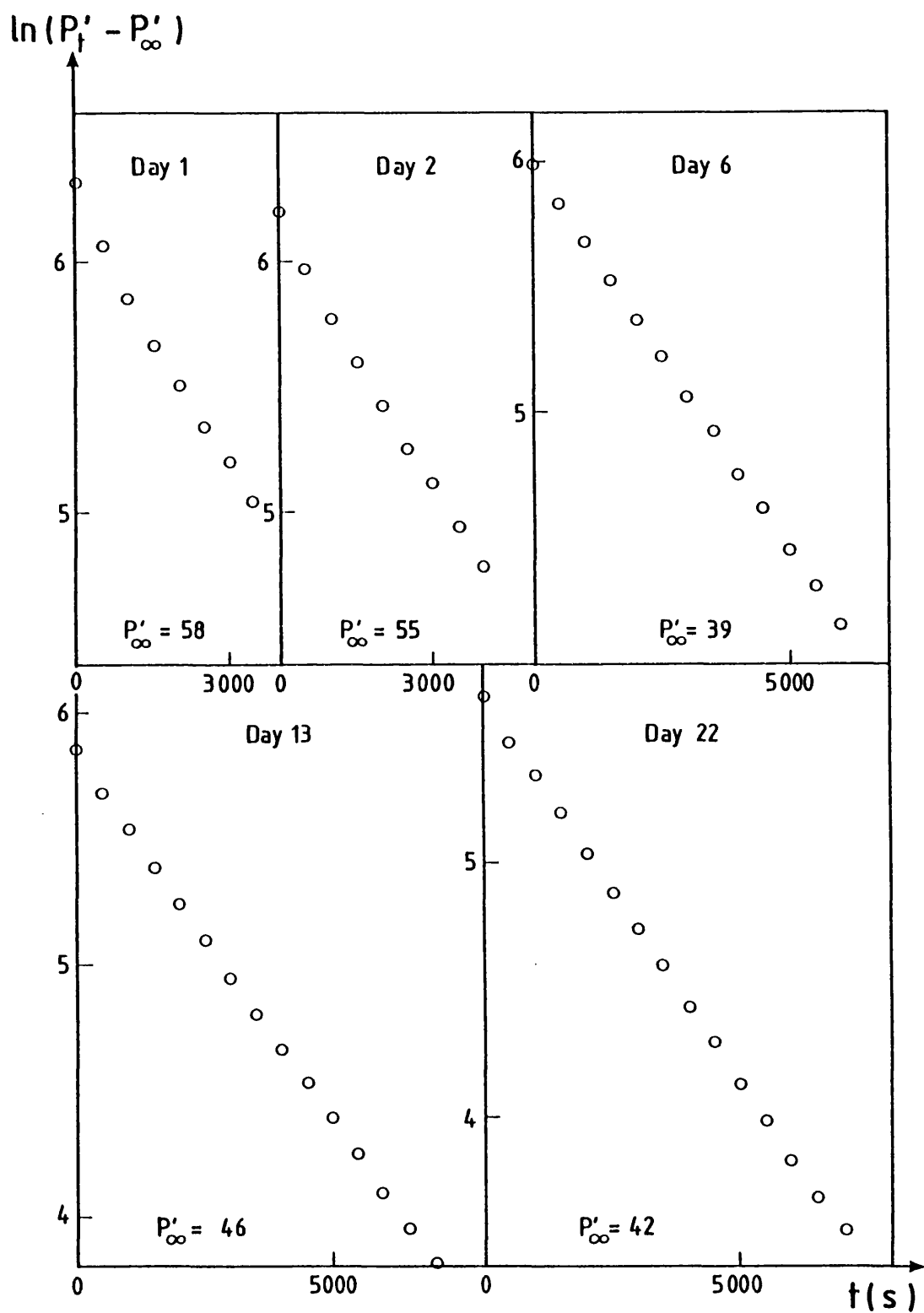
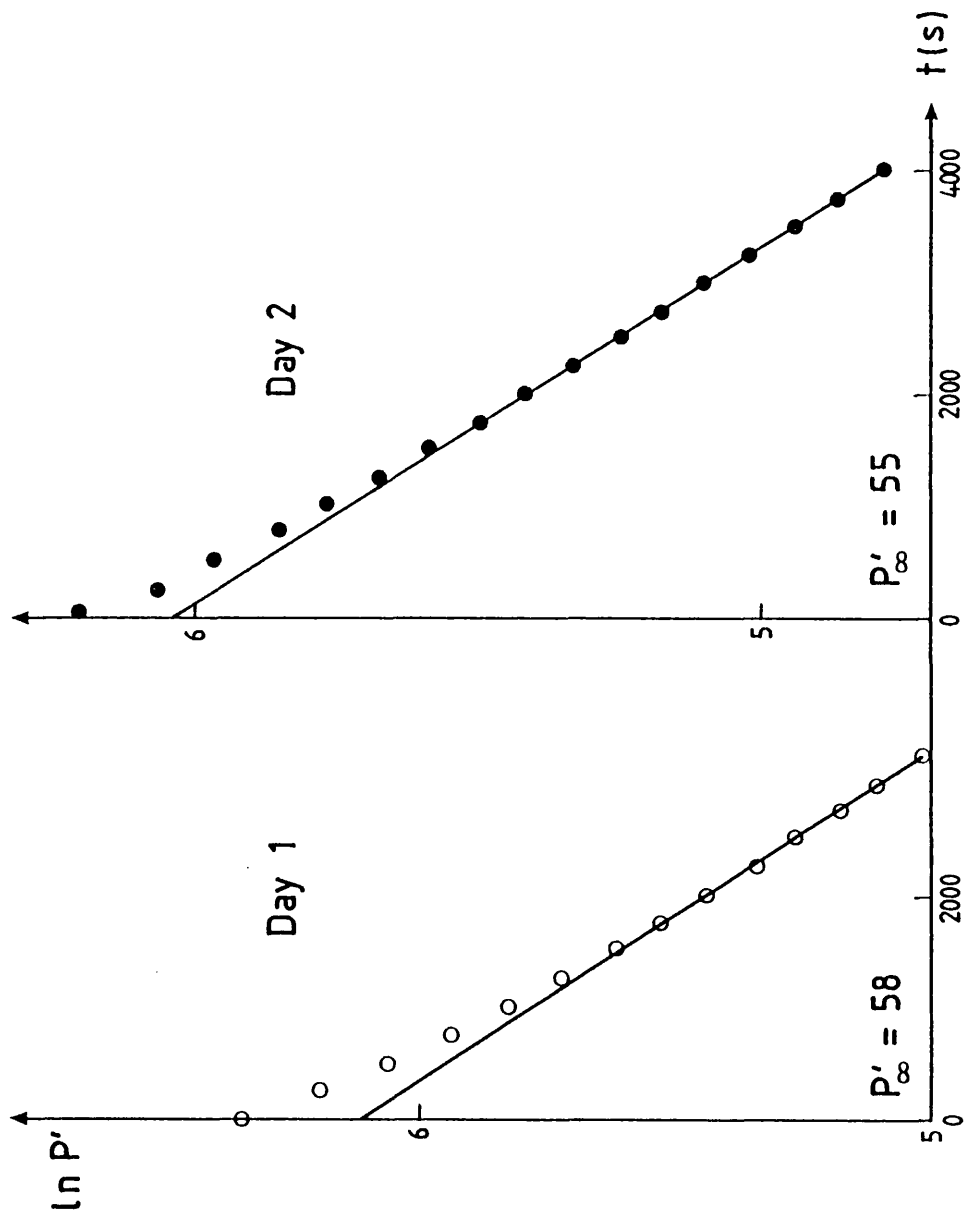


FIGURE 5.6

First-order plots of the kinetic data (interpolated values of  $P'$ ) for the reaction of solution B with sodium hydroxide (0.33 M) at 298.15 K.



**FIGURE 5.7**  
 First-order plots of the kinetic data (interpolated values of  $P'$ ) for the reaction of solution B with sodium hydroxide (0.33 M) at 298.15 K.

tion B with NaOH on days 1 and 2 were calculated using the relationship  $P_m = P_s + P_f$ . These data are shown in Table 5.13. First-order plots for the reaction of the 'fast' isomer with hydroxide are shown in Fig. 5.8. Both are straight lines, the slopes of which correspond to the rate constant for the reaction of the 'fast' isomer with hydroxide. Using the data for day 1  $k_f = 1.82 \times 10^{-3} \text{ sec}^{-1}$ , from those for day 2  $k_f = 1.80 \times 10^{-3} \text{ sec}^{-1}$ . Considering the nature of the analysis resulting in these values and the possible margin of error involved therein, the agreement between these two values of  $k_f$  is excellent.

From large scale plots of the type shown in Fig. 5.7 the relative amounts of the 'fast' and 'slow' isomers were estimated. On day 1 the percentage of the 'fast' isomer in the mixture was approximately 19%. By day 2 this had decreased to 16%. The means by which the proportion of the isomers in solution B changed with time cannot be ascertained from these results. Two limiting possibilities are that the 'fast' isomer isomerized to form the 'slow' isomer or that the rate of decomposition of the 'fast' isomer was greater than that of the 'slow' isomer. Whatever the route, the rate of change in the proportion of the isomers with time was much slower than the rates of reaction of either isomer with hydroxide under the given conditions.

Using the same procedure the absorbance/time data obtained for the reactions of complex B with sodium hydroxide in 30 vol % MeOH were re-analysed. Fig. 5.9 shows the first-order rate constants,  $k_{obs}$ , calculated by the minicomputer for the reactions of solutions of complex B with sodium hydroxide (0.33 M) in 30 vol % MeOH at 298.15 K. The pattern is very similar to that obtained for the same reaction in 6.6 vol % MeOH (Fig. 5.3). Over the first few days  $k_{obs}$  decreases rapidly with time reaching a value of  $k_{obs}$  at time  $t$  beyond which  $k_{obs}$  remains constant.

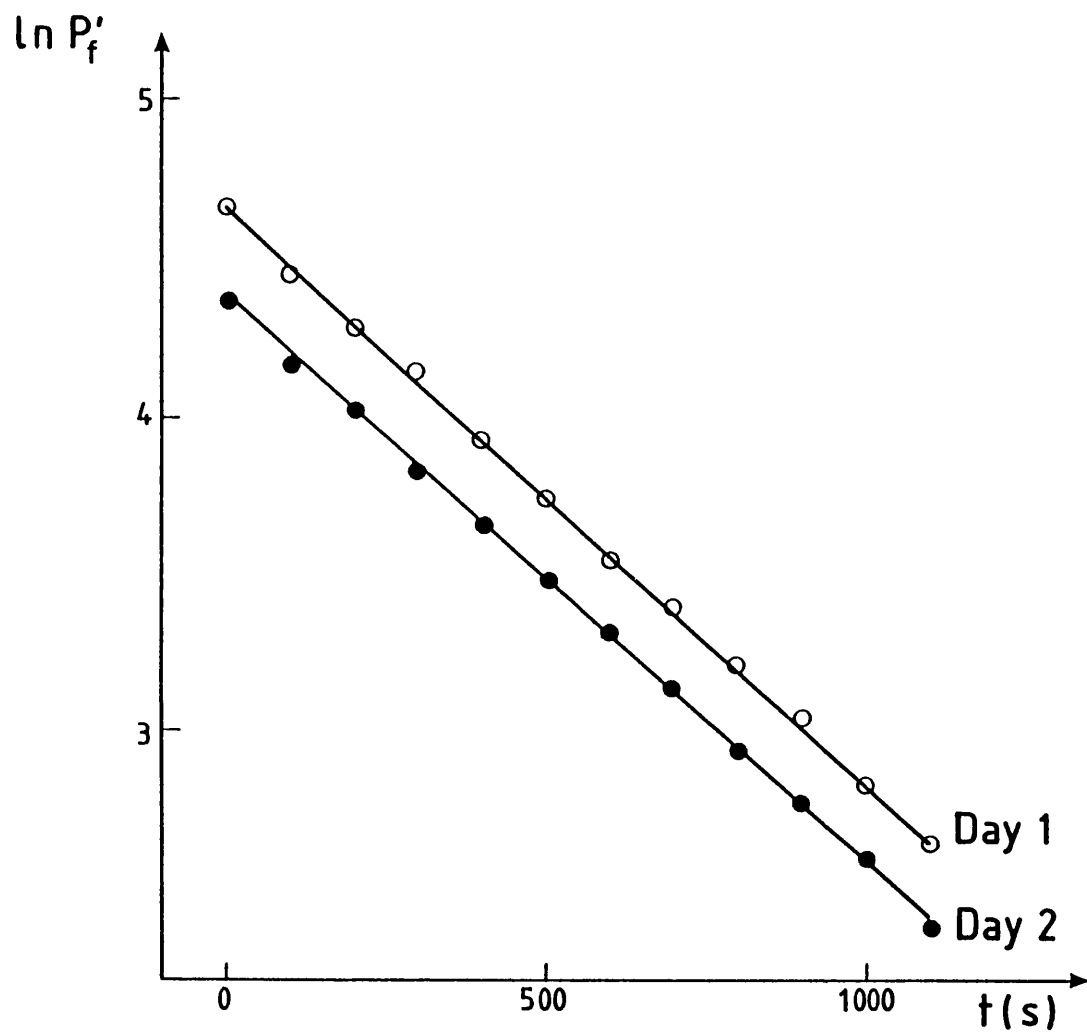


**FIGURE 5.8**

First-order rate plots for the reaction of the 'fast' isomer in solution B with sodium hydroxide (0.33 M) at 298.15 K.

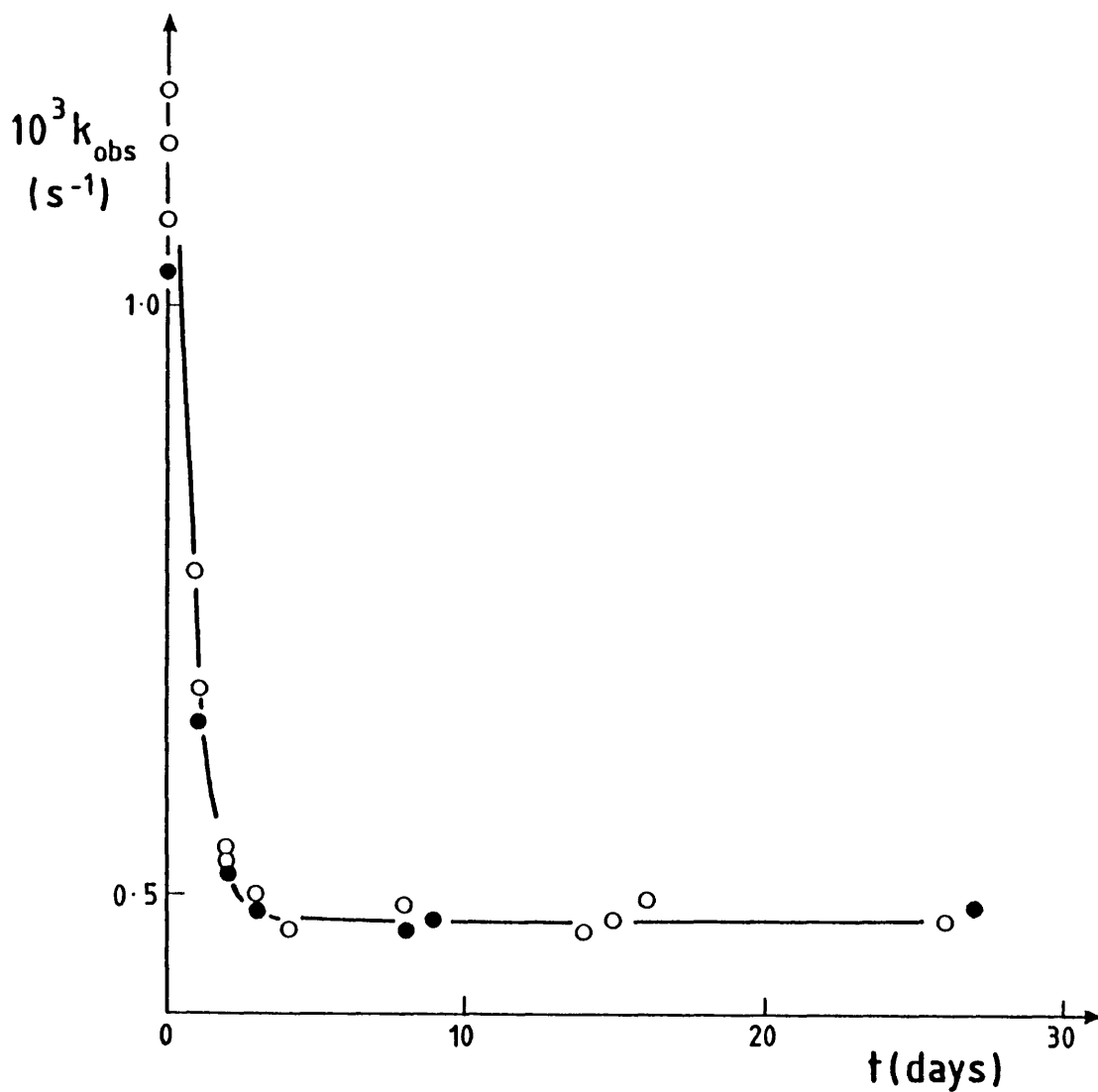


FIGURE 5.9

Observed first-order rate constants,  $k_{\text{obs}}$ , for reactions of the thiocyanate salt of complex B with sodium hydroxide (0.33 M) in 30 vol % MeOH at 298.15 K: solution B' (●); other solutions (○).

The main differences between the patterns observed in 6.6 and 30 vol % MeOH are that in the latter the limiting value of  $k_{obs}$  appears to be attained more rapidly than in the former and that the limiting value of  $k_{obs}$  appears to be greater in 30 vol % MeOH than in 6.6 vol % MeOH. In terms of the proposed reaction scheme, Fig. 5.9 indicates that by day 3 the stock solutions contain only the 'slow' isomer.

Re-analysis of the data was carried out using absorbance/time data collected from individual kinetic runs for the reaction of a solution of complex B with hydroxide in 30 vol % MeOH, solution B'. Values of  $k_{obs}$  obtained using solution B' are denoted in Fig. 5.9 by solid circles. The best linear first-order fits of the data collected from the reactions of solution B' with hydroxide on days 3, 8, 9 and 27 were investigated first. Using experimentally observed values of P' and interpolated values of P' (from plots of P' versus t) over the whole time range studied,  $P'_{\infty}$  was changed to give the best linear first-order plots. The slopes of these lines were taken to represent  $k_s$  the rate constant for the reaction of the 'slow' isomer in solution B' with hydroxide in 30 vol % MeOH under the given conditions. For days 3, 8, 9 and 27,  $k_s = 0.47 \times 10^{-3}$ ,  $0.46 \times 10^{-3}$ ,  $0.47 \times 10^{-3}$  and  $0.48 \times 10^{-3} \text{ sec}^{-1}$  respectively. Reduction of the time range studied (omission of values of t less than 1000s) had no significant effect on the values of  $k_s$ . Thus from day 3 onwards solution B' contained only the 'slow' isomer for which the rate constant for its reaction with hydroxide (0.33 M) in 30 vol % MeOH at 298.15 K was  $0.47 \pm 0.01 \times 10^{-3} \text{ sec}^{-1}$ . Analysis of the data collected from the reaction on day 2, using values of P' for  $t > 1000s$ , yielded a value for  $k_s$  of  $0.46 \times 10^{-3} \text{ sec}^{-1}$ . The slight positive deviations from this first-order plot when  $t < 500s$  indicated that on day 2 solution B' contained a trace of the 'fast' isomer. First-order plots obtained for the

solution B' with hydroxide on days 2, 3, 8, 9 and 27 are shown in Fig. 5.10 for interpolated values of P'.

Fig. 5.11 shows processed data from the reactions carried out on days 0 and 1. The linear extrapolations to  $t=0$  from the points at  $t > 1000s$  represent the first-order plots for the 'slow' isomer in solution B' on these days. From large scale plots of  $\ln(P'_t - P'_\infty)$  versus  $t$  using observed values of P' the changes in the absorbance due to the 'fast' isomer,  $P'_f$ , with time were calculated for both reactions. The resulting plots of  $\ln P'_f$  versus  $t$  are shown in Fig. 5.12. Values of  $k_f$  derived using the data from days 0 and 1 were  $2.5 \times 10^{-3}$  and  $2.6 \times 10^{-3} \text{ sec}^{-1}$  respectively. The proportion of the 'fast' isomer in solution B' on day 0 was approximately 20%. By day 1 this had decreased to approximately 8%.

Thus, re-analysis of the data showed that the samples of complex B contained a mixture of both the possible isomers. The reactivities of the two isomers towards hydroxide were different and the rates of the reactions of both with hydroxide increased with increasing methanol content of the solvent. The rate of change in the proportion of isomers in a solution also increased with increasing methanol content of the solvent. The same pattern emerged when data obtained for the reactions of solutions of complex A,  $[\text{Fe}(\text{bsb}, \text{Ph}, \text{Ph})_3]^{2+}$ , with hydroxide were re-analysed. However for both complexes, the differences in the reactivities of the two isomers with hydroxide were not as great as had been expected. This fact coupled with the nature of the kinetic analysis program and the fact that the samples contained predominantly the more stable isomeric form resulted in deceptively linear first-order plots for the reactions of the complexes.

In monitoring the reactions of complexes A and B with hydroxide the minicomputer controlling the kinetic runs in this study analysed the

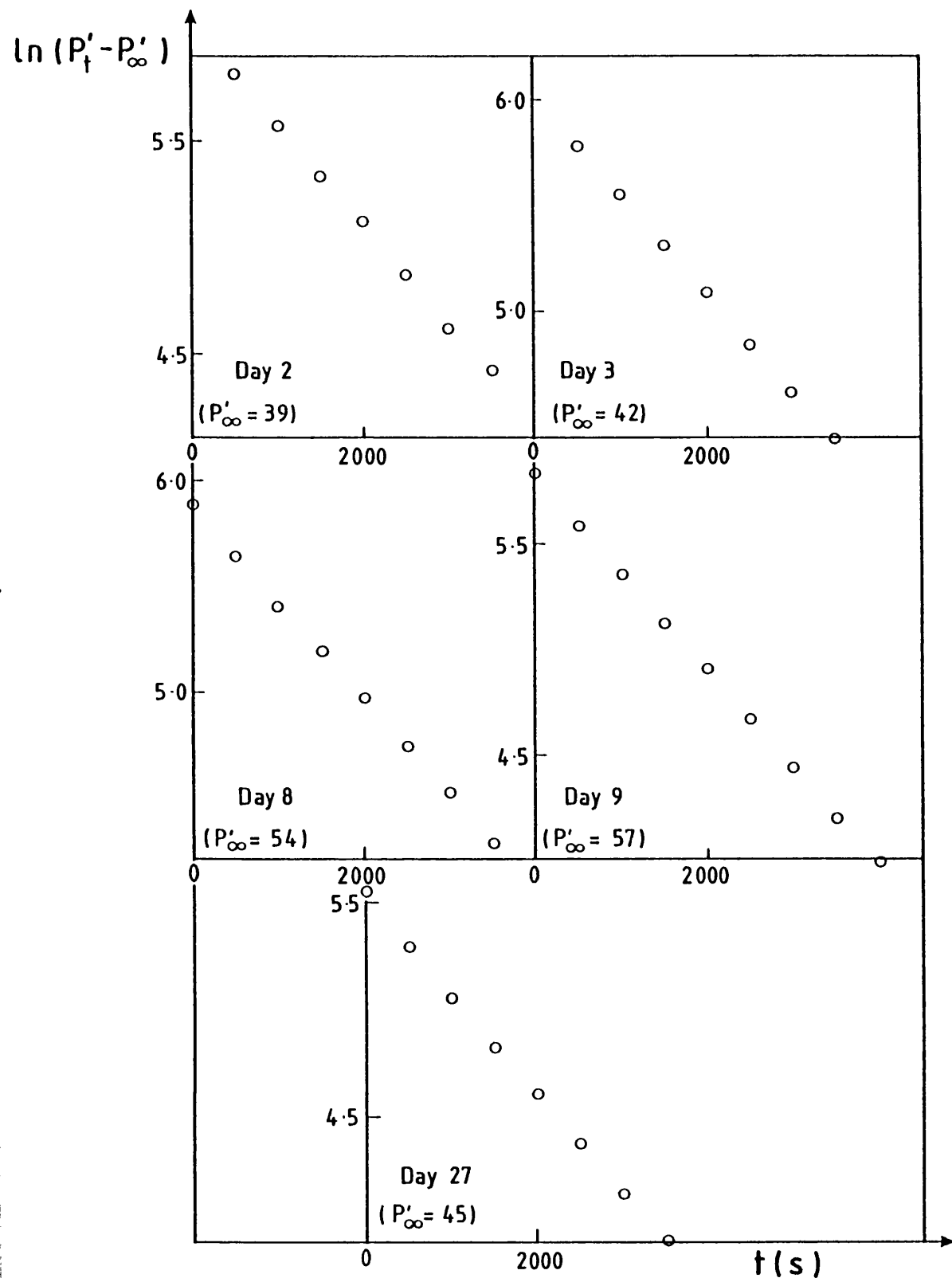
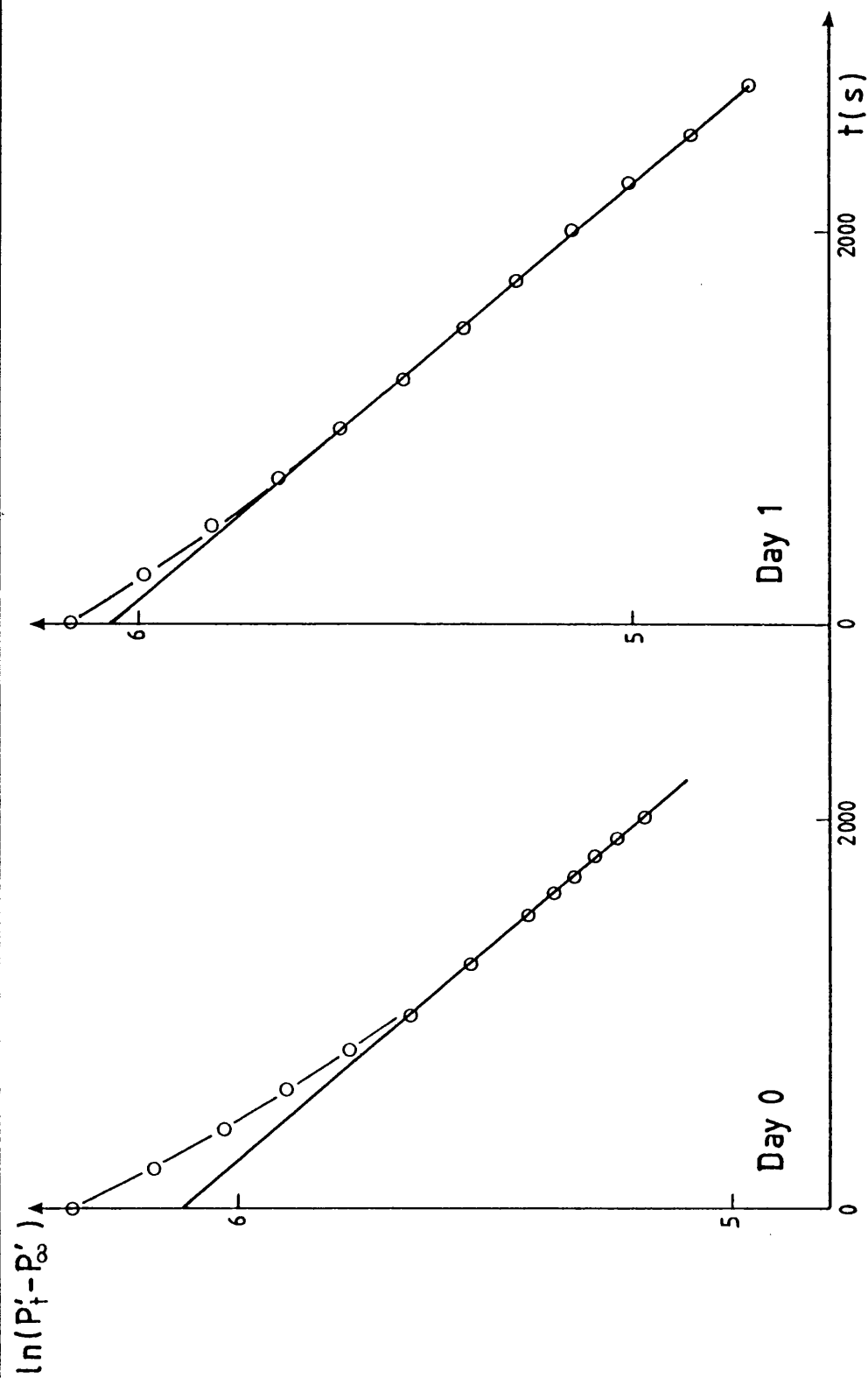


FIGURE 5.10

First-order rate constants of the kinetic data (interpolated values of  $P'$ ) for the reaction of solution B' with sodium hydroxide (0.33 M) at 298.15 K.



**FIGURE 5.11**  
 First-order plots of the kinetic data (interpolated values of  $P'$ ) for the reaction of solution B' with sodium hydroxide (0.33 M) at 298.15 K.

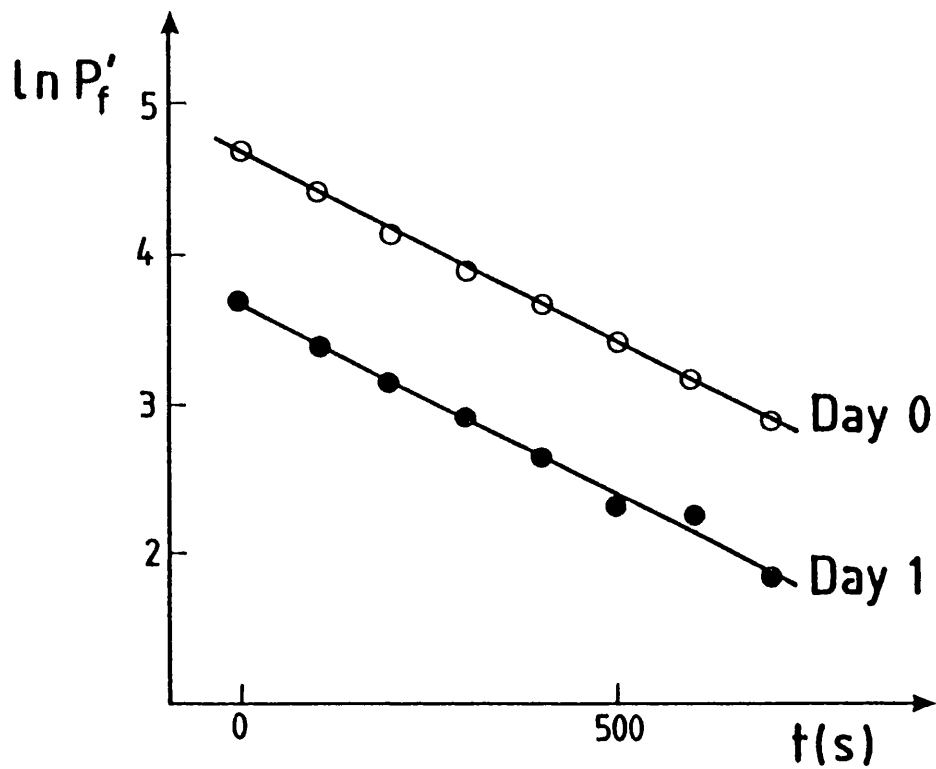


FIGURE 5.12

First-order rate plots for the reaction of the 'fast' isomer in solution B' with sodium hydroxide (0.33 M) at 298.15 K.

collected absorbance/time data for a first-order rate constant,  $k_{obs}$ , by solving equation 5.3. This was done by a non-linear least squares method

$$\ln \left[ \frac{(P_0 - P_\infty)}{(P_t - P_\infty)} \right] = kt \quad \dots [5.3]$$

described in Section 2.3.2. The deviation of observed values of P from a first-order plot over the whole time range studied (i.e. from  $t=0$  to  $t=t_e$  where  $t_e$  is the time when monitoring of the reaction finished) was minimized by the calculation of optimum values for  $P_0$ ,  $P_\infty$  and  $k$ .

Consider the result of such an analysis on absorbance/time data collected during a reaction of the type described earlier involving in the early stages parallel reactions of a 'fast' and 'slow' isomer and in the later stages reaction of the 'slow' isomer only. An attempt to fit the best first-order straight line plot to the observed data would result in a value of  $k_{obs}$  intermediate between the values of the rate constants for the reaction of the 'fast' isomer,  $k_f$ , and the 'slow' isomer,  $k_s$ , with hydroxide. The greater the proportion of fast isomer in the mixture the larger the estimated value of  $k_{obs}$  would be. Similarly, the smaller the proportion of the 'fast' isomer in the mixture the smaller the slope of the best first-order fit of the observed data becomes, values of  $k_{obs}$  approaching  $k_s$ . In the limiting case, for analysis of the reaction of a solution containing only the slow isomer  $k_{obs}$  would be equal to  $k_s$ . The standard deviation of the absorbances from the best first-order fit would also be expected to increase as the proportion of the 'fast' isomer in the solution increases. This would be paralleled by an increase in the estimated value of  $P_\infty$ . This results from the fact that changes in  $P_\infty$  have a greater effect on values of P at high t (lower absorbances) than on values of P at low t (higher absorbances). Thus, for the case in question, increasing  $P_\infty$  would increase the slope of a line in the high t

region considerably more than in the low  $t$  region making a straight line fit over the whole time range more satisfactory. Theoretically then, at least, such analysis of data from successive kinetic runs monitoring the reaction of hydroxide with aliquots of a stock solution containing geometrical isomers, the proportion of which changes at a much slower rate than that of alkaline hydrolysis of either isomer, should produce successively lower values of  $k_{obs}$ ,  $P_{\infty}$  and  $SD/P$ . For the reactions of complexes A and B with hydroxide a decrease in  $k_{obs}$  with time was observed in the period before attainment of a constant  $k_{obs}$  value for every solution without exception. A general decrease in  $P_{\infty}$  and  $SD/P$  with time was also observed.

In observing trends of  $k_{obs}$ , profiles of  $k_{obs}/\text{time}$  had been obtained for the reactions of the complexes with hydroxide in varying water + methanol mixtures. The re-analysis of data showed the constant values of  $k_{obs}$  obtained for a stock solution above a certain age to be the rate constants for the reactions of the 'slow' isomer with hydroxide under the given conditions. These values,  $k_s$ , are given in Table 5.14 and shown in Fig. 5.13. For both complexes A and B the expected increase in  $k_s$  with increasing methanol content of the solvent is observed. For a given solvent composition,  $k_s$  for complex A is larger than  $k_s$  for complex B. The slower rates of reactions for complex B, the *m*-methyl substituted derivative of complex A, can be explained in terms of the electron-releasing effect of the methyl group increasing the electron density in the vicinity of the central iron atom thus making hydroxide attack more difficult. The electron-releasing effect of the methyl group also strengthens the iron-nitrogen  $\sigma$ -bond making the cleavage of this bond more difficult.

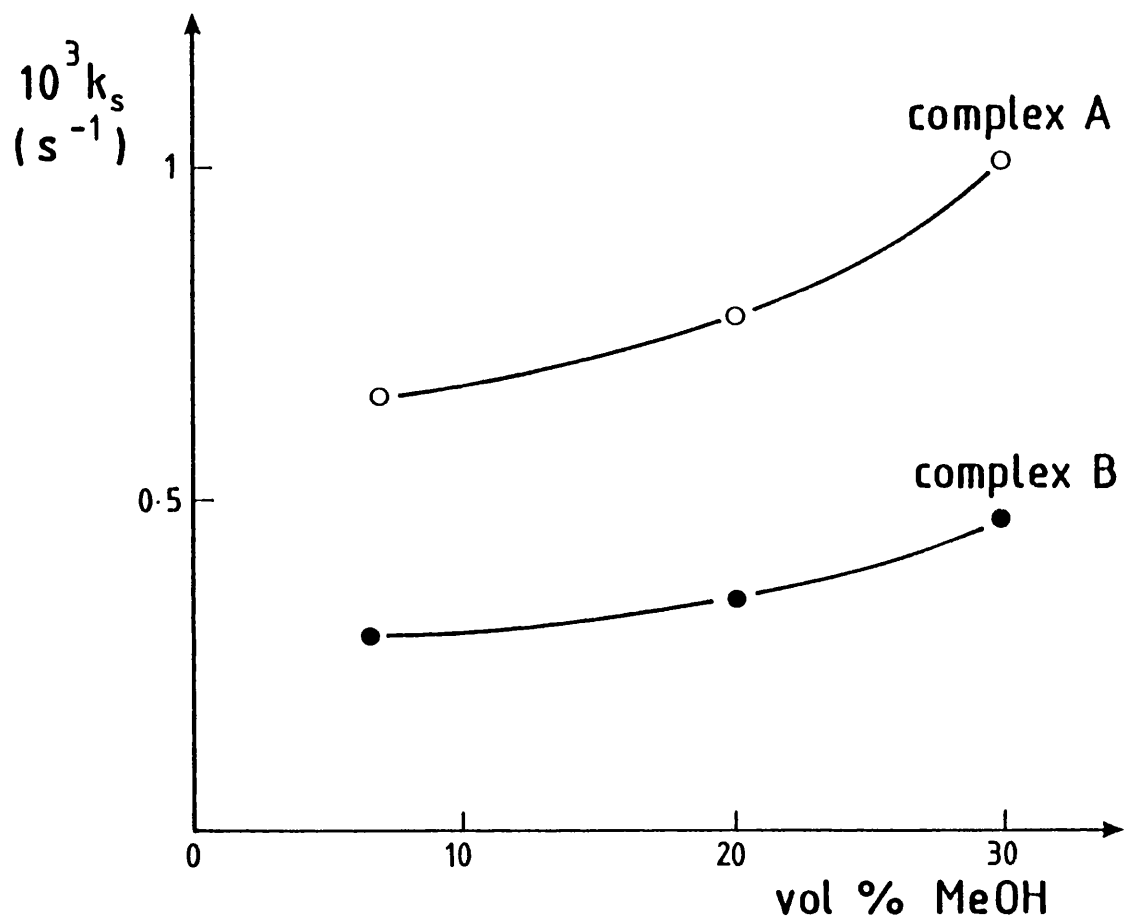


FIGURE 5.13

First-order rate constants for the reactions of the 'slow' isomers of complexes A and B with sodium hydroxide (0.33 M) in water + methanol mixtures at 298.15 K.

### 5.3.3 Ultraviolet/visible absorption spectra

Having found very strong kinetic evidence for the existence of isomers in the samples of complexes A and B, ultraviolet/visible absorption spectra of the reactions of the complexes were examined to see if they also indicated the presence of isomers in the samples. Krumholz<sup>17</sup> had estimated the difference in  $\lambda_{\max}$  of the stable and labile forms of complex A,  $[\text{Fe}(\text{bsb},\text{Ph},\text{Ph})_3]^{2+}$ , to be 10 nm. The absorption maximum of the labile form was shifted towards longer wavelengths as compared with the maximum of the stable form. However, no solutions containing solely the labile form had been prepared and thus  $\lambda_{\max}$  for this isomer had been estimated using solutions in which the labile form had been judged to be the major component. Given that values of  $\lambda_{\max}$  obtained in this study using the SP800 spectrophotometer were accurate to within 3 nm then some indication as to the presence of isomers should be obtainable from positions of  $\lambda_{\max}$  of the solutions. Repeat wavelength scans, monitoring the decrease in absorption due to the complex as the reactions progressed, provided the most satisfactory means of investigation. For these spectra the change in values of  $\lambda_{\max}$  as the reaction proceeds is real and accurate, the uncertainty in values of  $\lambda_{\max}$  being constant throughout each spectrophotometric run. Such spectra were obtained for the reactions of samples of complexes A and B, made by the general method, with sodium hydroxide (0.33 M) in water + methanol mixtures. An example of the type of spectra obtained is given in Fig. 5.14. From these spectra it could be seen that there were small, but distinct, shifts in  $\lambda_{\max}$  towards shorter wavelengths as the reactions proceeded.

Table 5.15 shows this trend as observed for reactions of four salts of complex A with hydroxide in 6.6 vol % MeOH. Values of  $\lambda_{\max}$  at the start of the run,  $P_1$ , at  $P(t_1)$  and  $P(2t_1)$  are shown in each case. For

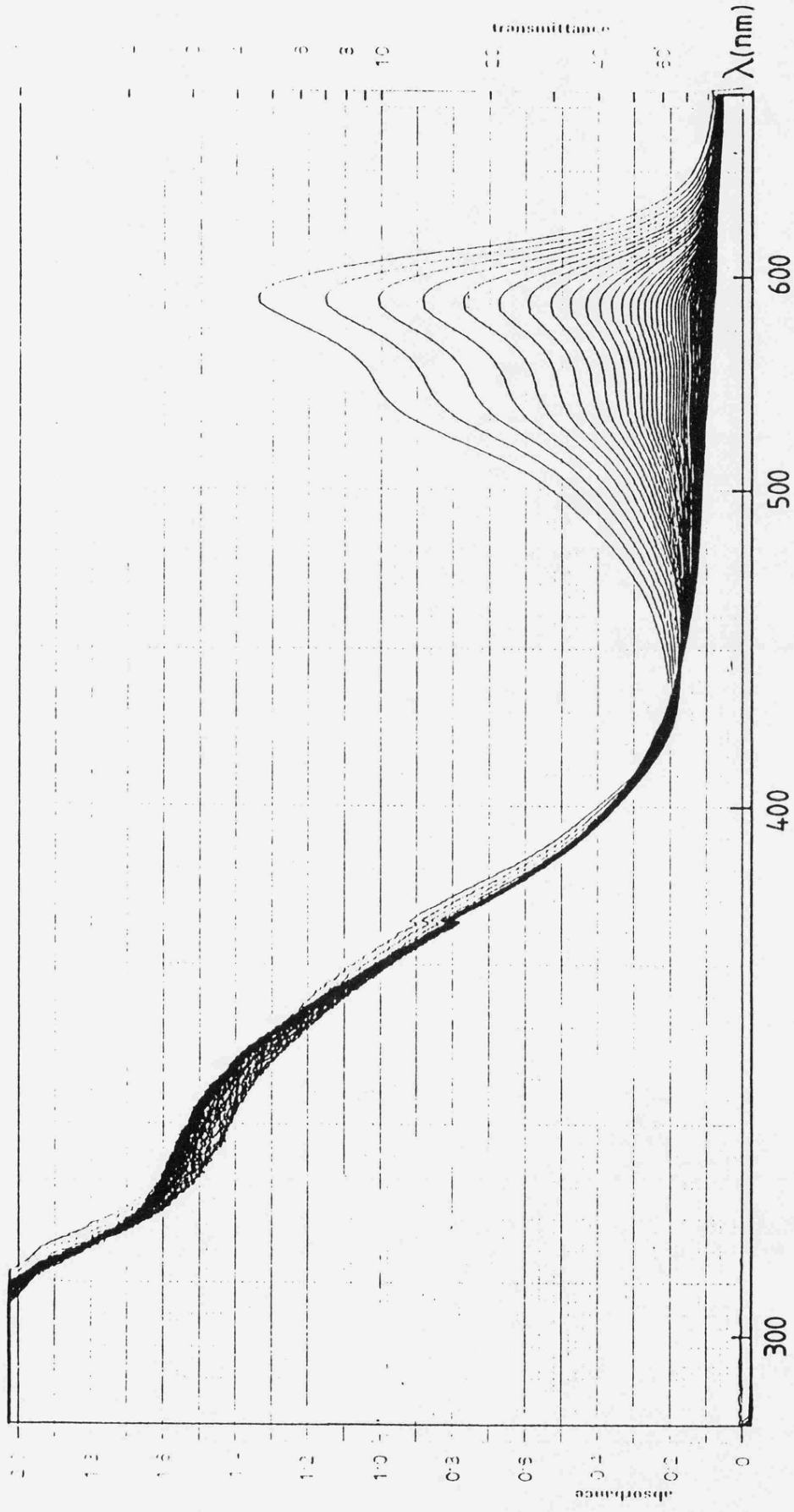


FIGURE 5.14

A typical ultraviolet/visible absorption spectrum obtained using the SP800 spectrophotometer: the reaction of the perchlorate salt of complex A with sodium hydroxide (0.33 M) in 30 vol % MeOH.

different sets of solutions of these salts, values of  $\lambda_{\max}$  at  $P_i$  were always lowest for the chloride salt (cf. Fig. 5.2 where values of  $k_{\text{obs}}$  obtained using freshly made-up solutions of this chloride salt were always lower than those obtained using other salts).

Table 5.16 shows the changes in  $\lambda_{\max}$  as measured for reactions of salts of complex B with hydroxide in varying water + methanol mixtures. The shifts observed from  $\lambda_{\max}$  at  $P_i$  to  $\lambda_{\max}$  at  $P(2t_{1/2})$  appeared to be somewhat greater for complex B than complex A as did the range of values obtained at  $P_i$ .

#### 5.3.4 The effect of modified synthetic methods

Values of  $k_{\text{obs}}$  measured as described earlier using solutions of the complexes containing a mixture of the isomers have no quantitative use individually. However, the nature of the program used to determine first-order rate constants resulted for such solutions in values of  $k_{\text{obs}}$  the magnitude of which reflected the proportion of isomers in the sample. Thus, for a given system values of  $k_{\text{obs}}$  could be used in conjunction with observed shifts in  $\lambda_{\max}$  as a simple, convenient way to probe the effect of synthetic routes of a complex on the resulting proportions of isomers in the samples.

For comparison with the sample of the perchlorate salt of complex A,  $[\text{Fe}(\text{bsb}, \text{Ph}, \text{Ph})_3]^{2+}$ , prepared by the general method, the same compound was prepared by the modified method (i) (see Section 5.2.1). This involved precipitation of the salt as quickly as possible after the complex was generated in solution. The sample prepared by the general method is referred to as sample 1. The sample prepared by the modified method is referred to as sample 2. Two further samples of this compound were obtained by its preparation using the modified method. When the precipitated sample 2 was removed from the reaction mixture by filtration the

filtrate was still intensely coloured. On standing for 24 hours filtration of the mother liquor produced another sample of the compound, sample 3. After a further time lapse of 24 hours filtration of the mother liquor produced a fourth sample of the compound, sample 4.

Fig. 5.15 shows the general trends in values of  $k_{obs}$  obtained for the reactions of samples 1, 2, 3 and 4 with hydroxide (0.33 M) at 298.15 K. It was observed that for any given solvent composition, values of  $k_{obs}$  obtained generally decreased in the order sample 2 > sample 3 > sample 4. The highest  $k_{obs}$  values were always obtained for sample 2.  $k_{obs}$  values for sample 1 were generally most similar to those obtained for sample 3.  $\lambda_{max}$  of the four samples in 6.6 vol % MeOH were 581, 585, 580 and 578 nm respectively. Ultraviolet/visible absorption spectra of the reactions indicated  $\lambda_{max}$  at  $P(2t_{1/2})$  to be in all cases in the range 577-579 nm. Thus it appeared that precipitation of the complex almost immediately after its generation in solution (i.e. sample 2) yielded a sample containing a higher proportion of the 'fast' isomer. The longer the reaction mixture was left standing before precipitation of the complex, the greater was the proportion of the 'slow' isomer in the sample. This latter effect was seen in Fig. 5.2 where the chloride salt of complex A consistently produced the lowest values of  $k_{obs}$  for a series of salts of this complex prepared by the general method. The sample of the chloride salt had been precipitated by allowing a portion of the reaction mixture to evaporate until precipitation occurred. The other salts had been precipitated by the addition of saturated aqueous solutions of salts containing the respective anions. Thus, the reaction mixture had stood for a longer time in obtaining the chloride salt than in obtaining the other salts. The changes in  $k_{obs}$  with the age of stock solutions of samples 2, 3 and 4 were investigated. For all three samples  $k_{obs}$  decreased with

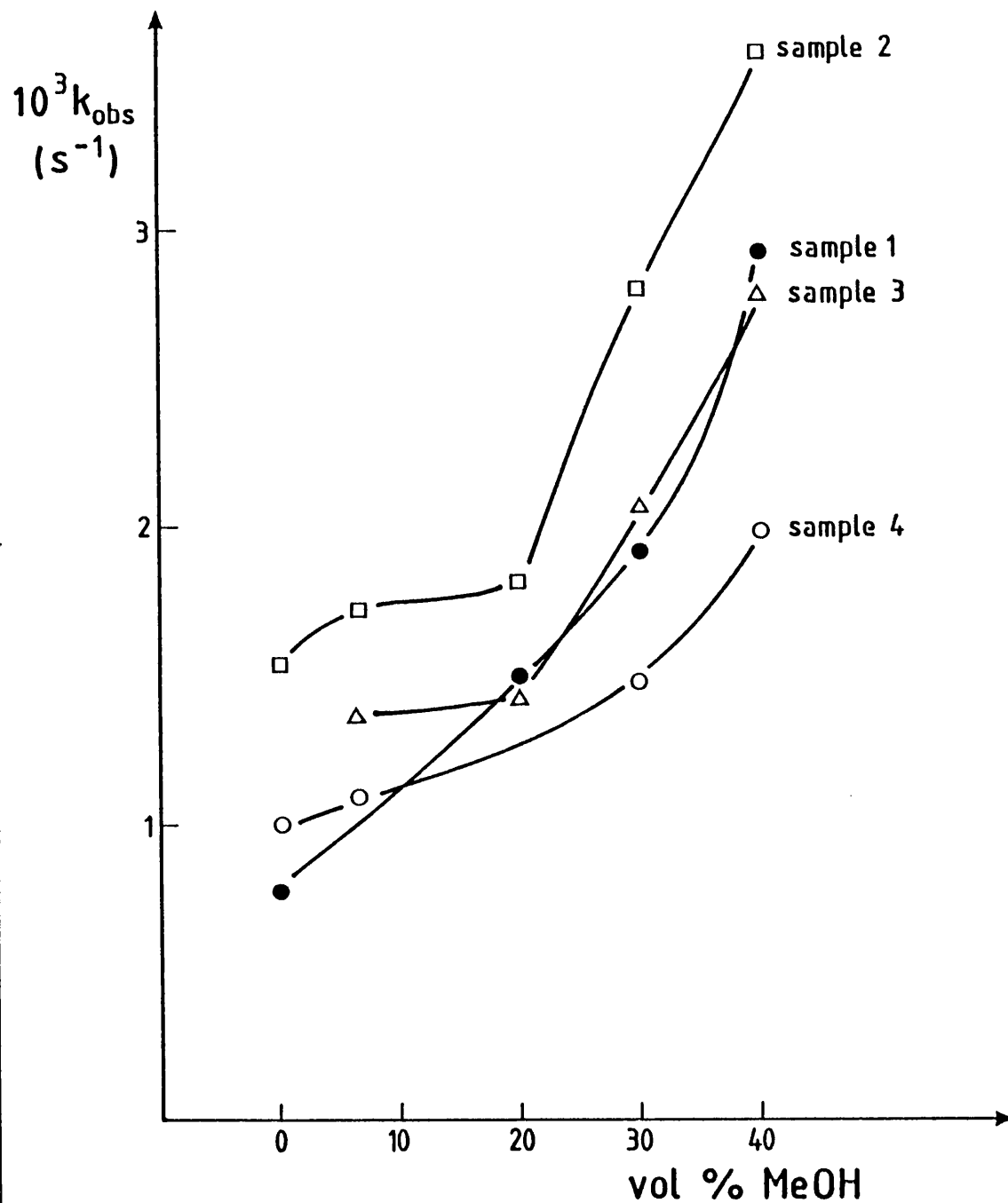


FIGURE 5.15

Observed first-order rate constants,  $k_{obs}$ , for the reactions of samples 1, 2, 3 and 4 of  $[Fe(bsb,Ph,Ph)_3](ClO_4)_2$  with sodium hydroxide (0.33 M) in water + methanol mixtures at 298.15 K.

time, reaching values of  $k_{obs}$  consistent with those given previously (Table 5.14) for the rate constants for the reactions of the 'slow' isomer of the complex with hydroxide in the solvent mixtures.

Measurement of the solubilities of the four samples yielded values that proved to be irreproducible, yet more positive evidence as to the presence of isomers in the samples. Although consistent values for the solubilities of the salts in water + methanol mixtures could not be obtained, the same general trends were observed throughout the results. One such set of values of the absorbances of saturated solutions is given in Table 5.17. Measurements were carried out simultaneously under identical conditions (as described in Section 2.5). The values given in Table 5.17 are those obtained 24 hours after combining solutes and solvents. Solubilities increase in the order sample 2 < sample 3 < sample 4 for all the solvent compositions. The solubilities of sample 1 were never greater than sample 2 but usually intermediate between those of sample 3 and sample 4. Solubilities of each sample also increased in the order water < 20 vol % MeOH < 40 vol % MeOH. The results suggest the perchlorate salt of the 'slow' isomer of complex A to be more soluble than the 'fast' isomer in both water and the water + methanol mixtures. Also, that the solubilities of the perchlorate salts of one or other of the isomers, or both, increases with increasing methanol content of the solvent.

Preparation of the complex by the modified method (ii), involving changing the order of mixing of the reactants, resulted in values of  $k_{obs}$  most similar to those obtained using the sample prepared by the general method. Thus the order of mixing of the reactants seemed to have little effect on the resulting proportions of isomers in the sample. Heating the reaction mixtures [modified method (iii)] produced samples which gave

relatively low values of  $k_{obs}$ . Thus heating the reaction mixtures increased the proportion of the 'slow' isomer in the resulting sample. Re-crystallization of the samples also had the effect of decreasing the proportion of the 'fast' isomer in the samples. Successive re-crystallizations reduced values of both  $k_{obs}$  and  $\lambda_{max}$ . For example,  $\lambda_{max}$  of sample 2 [complex A prepared by modified method (i)] was 585 nm. Re-crystallization of sample 2 resulted in a value for  $\lambda_{max}$  of 581 nm.

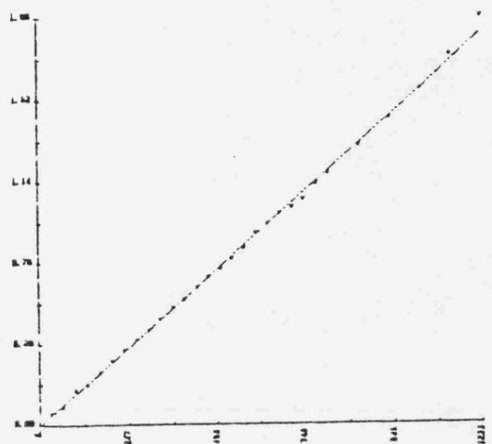
Thus, the main factor in determining the proportion of isomers in the samples appeared to be the length of time for which the reaction mixture stood after generation of the complex in solution before its precipitation. The shorter the time before the complex was precipitated the larger the portion of the 'fast' isomer in the sample. For the salts obtained by almost immediate precipitation of the complex after its generation the proportion of the 'fast' isomer in the samples were estimated to be approximately 40%. These samples were the only ones for which deviations from first-order plots produced by the minicomputer for the reactions of the complex with hydroxide were discernible. All the other methods of preparation produced samples containing lower proportions of the isomers.

#### 5.3.5 Isomers in samples of related complexes

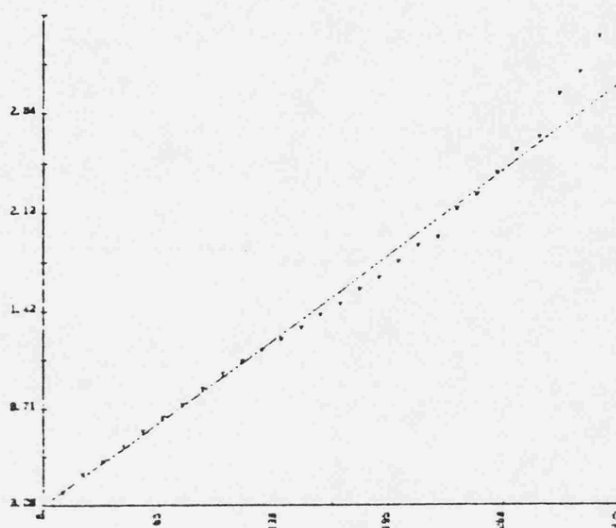
In only a small number of cases was the presence of isomers in the samples of complexes reflected in obvious non-linearity of first-order plots obtained for the reactions of the samples of the complexes with hydroxide. This type of plot obtained using samples of complex A,  $[\text{Fe}(\text{bsb}, \text{Ph}, \text{Ph})_3]^{2+}$ , and of complex B,  $[\text{Fe}(\text{bsb}, \text{Ph}, \text{Ph}:m\text{-Me})_3]^{2+}$ , prepared by the modified method (i) involving almost immediate precipitation of the complex after its generation in solution, is shown in Fig. 5.16. Similar plots were obtained only for the reactions of the samples which

FIGURE 5.16

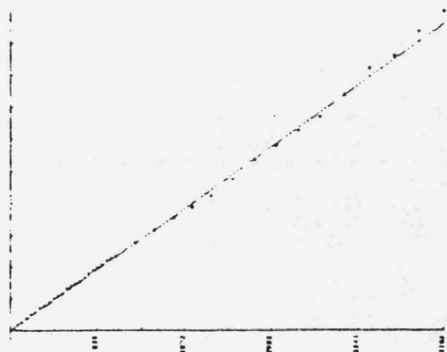
Examples of first-order plots obtained for reactions of salts of complexes A and B prepared by modified method (i) with sodium hydroxide (0.33 M) in water + methanol mixtures at 298.15 K.



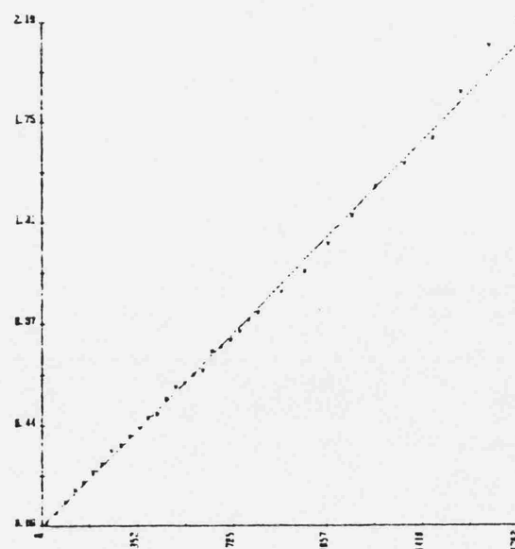
a) complex A:  $\text{ClO}_4^-$  salt (20 vol % MeOH)



b) complex A:  $\text{SCN}^-$  salt (40 vol % MeOH)



c) complex B:  $\text{ClO}_4^-$  salt (6.6 vol % MeOH)



d) complex B:  $\text{SCN}^-$  salt (30 vol % MeOH)

contained the higher proportions of the 'fast' isomer. In a brief investigation into the existence of isomers in samples of other iron(II) di-imine complexes containing unsymmetrical Schiff base ligands the first-order plots obtained for reactions of the complexes were studied.

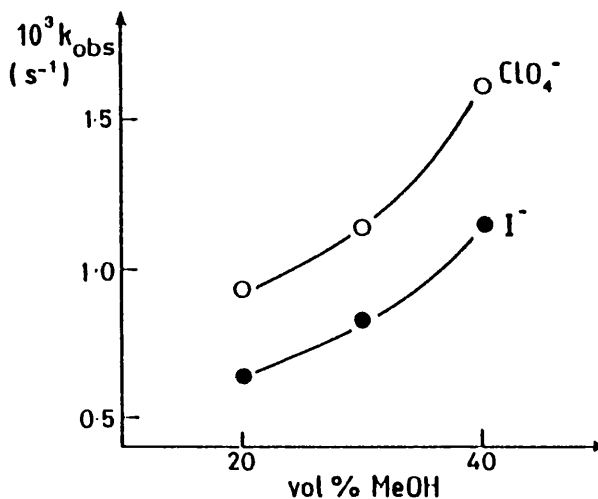
Several complexes of the type  $[\text{Fe}(\text{sb})_3]^{2+}$  where sb is a Schiff base ligand made from 2-benzoyl pyridine and a primary amine were prepared by modified method (i). Fig. 5.17 shows trends observed for the reactions of samples of such an iron(II) tris-(bidentate) complex where the primary amine used was 3,4-dimethylaniline. This complex,  $[\text{Fe}(\text{bsb}, \text{Ph}, \text{Ph}; 3,4\text{-Me}_2)_3]^{2+}$  is the 3,4-dimethyl substituted derivative of complex A. The ultraviolet/visible absorption spectra of reactions of this complex with sodium hydroxide (0.33 M) showed small but distinct shifts in  $\lambda_{\text{max}}$  to shorter wavelengths as the reactions proceeded (Fig. 5.17a). Values of  $k_{\text{obs}}$  (Fig. 5.17b) were found to be smaller than those obtained for the analogous reactions using complex B, the 3-methyl substituted derivative of complex A. This observed decrease in values of  $k_{\text{obs}}$  in the order unsubstituted > m-Me > 3,4-Me<sub>2</sub> complexes reflects the electron-releasing effect of methyl groups making hydroxide attack in the vicinity of the iron atom more difficult. Figs. 5.17c and 5.17d show two examples of first-order plots obtained for reactions of this 3,4-dimethyl substituted complex with hydroxide. Fig. 5.17c is clearly not linear indicating the presence of isomers in the sample. Similar evidence for the existence of isomers in samples of  $[\text{Fe}(\text{sb})_3]^{2+}$  where preparation of the ligand involved the use of the amines p-toluidine, m-anisidine and p-anisidine was found.

For tris-(bidentate) iron(II) complexes of the type  $[\text{Fe}(\text{sb})_3]^{2+}$  kinetic evidence for the existence of isomers for such complexes containing ligands derived from 2-benzoyl pyridine but not their analogues derived using pyridine-2-carboxaldehyde has in the past been attributed to steric

FIGURE 5.17

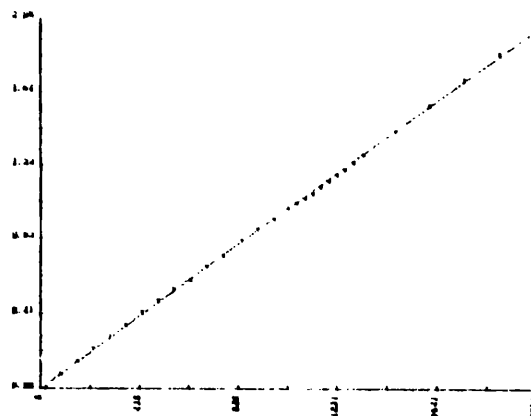
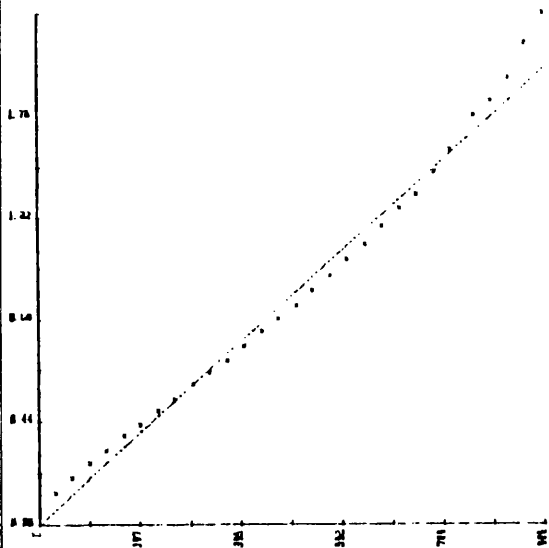
Observed trends for the reactions of salts of  $[\text{Fe}(\text{bsb}, \text{Ph}, \text{Ph}:3,4\text{-Me}_2)_3]^{2+}$  with sodium hydroxide (0.33 M) in water + methanol mixtures at 298.15 K.

Salt	vol % MeOH	$\lambda_{\text{max}}$ in nm	
		$P_1$	$P(2t_{1/2})$
$\text{ClO}_4^-$	20	590	583
$\text{ClO}_4^-$	30	590	585
$\text{ClO}_4^-$	40	587	585
$\text{I}^-$	20	588	583
$\text{I}^-$	30	587	583
$\text{I}^-$	40	587	583



a) shifts in  $\lambda_{\text{max}}$

b) observed first-order rate constants,  $k_{\text{obs}}$  (day 0)



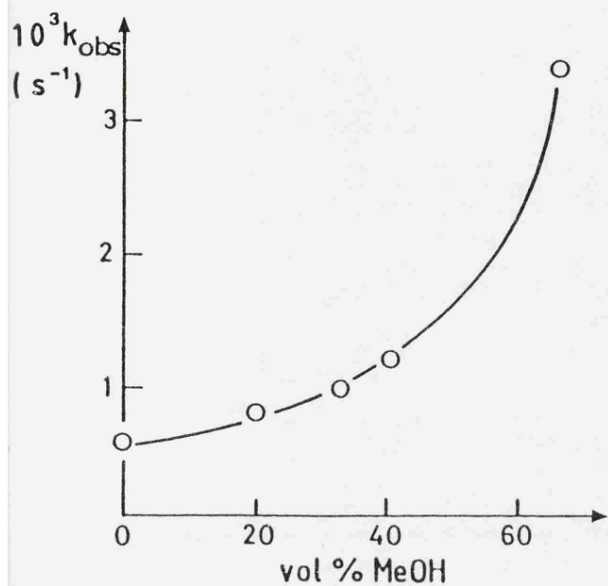
c) first-order plot obtained using a sample of the  $\text{ClO}_4^-$  salt prepared by modified method (i)

d) first-order plot obtained using a sample of the  $\text{ClO}_4^-$  salt prepared by the general method

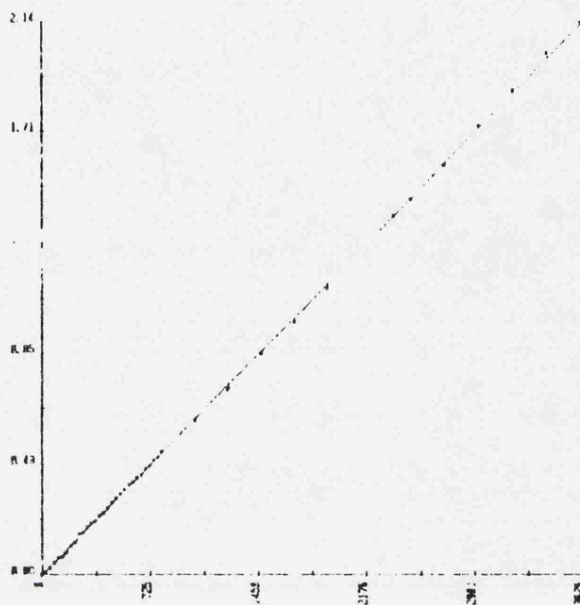
factors, i.e. the replacement of a hydrogen atom in the latter by a bulky phenyl group in the former.<sup>11</sup> Several complexes in which the bidentate ligand was derived from pyridine-2-carboxaldehyde and a primary amine were prepared using modified method (i). For the complexes  $[\text{Fe}(\text{bsb},\text{H},\text{Ph})_3]^{2+}$  and  $[\text{Fe}(\text{bsb},\text{H},\text{Ph};\text{p-Me})_3]^{2+}$  the amines used were aniline and p-toluidine respectively. Under the same conditions as before solutions of these complexes went colourless immediately on addition of the hydroxide solution. Reduction of  $[\text{OH}^-]$  by a factor of 100 produced the same result. For comparison the N-alkyl complex  $[\text{Fe}(\text{bsb},\text{H},\text{Me})_3]^{2+}$  prepared using methylamine was synthesised. From the ultraviolet/visible spectra of reactions of this complex with sodium hydroxide (0.33 M) in water + methanol mixtures there was some indication of a shift in  $\lambda_{\text{max}}$  to shorter wavelengths as the reactions proceeded. On average, shifts of approximately 3 nm were observed,  $\lambda_{\text{max}}$  at  $P_1$  being approximately 555 nm. In measuring values of  $k_{\text{obs}}$  (Fig. 5.18a) it was found that the results obtained appeared to depend on the manner in which solutions of the complex were made up. Figs. 5.18(b-d) show three first-order plots obtained for the reactions of the complex with sodium hydroxide (0.33 M) in 33 vol % MeOH. The solutions of the complex were initially made up in water (Fig. 5.18b), 50 vol % MeOH (Fig. 5.18c) and methanol (Fig. 5.18d). It can be seen that the deviations from linearity of the first-order plots are greatest for the latter. This may have been a result of the differences in the relative reactivities of the two isomers changing with solvent composition or that the rate of change in the proportion of the isomers was slowest in methanol. For the complex  $[\text{Fe}(\text{bsb},\text{H},\text{CH}_2\text{Ph})_3]^{2+}$  derived using benzylamine, deviations from linear first-order plots for its reactions with hydroxide of the same type as in Fig. 5.18d were observed. The analogous reactions of this complex with hydroxide were

FIGURE 5.18

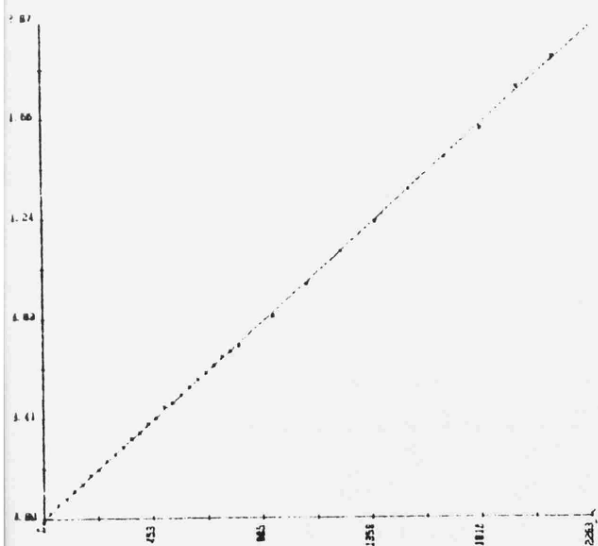
Observed trends for the reactions of  $[\text{Fe}(\text{bsb},\text{H},\text{Me})_3](\text{ClO}_4)_2$  with sodium hydroxide (0.33 M) in water + methanol mixtures at 298.15 K



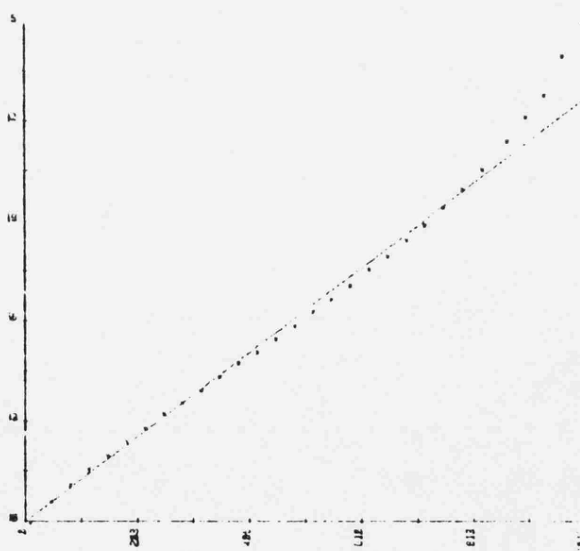
a) observed first-order rate constants,  $k_{\text{obs}}$



b) first-order plot (solution of complex made up in water)



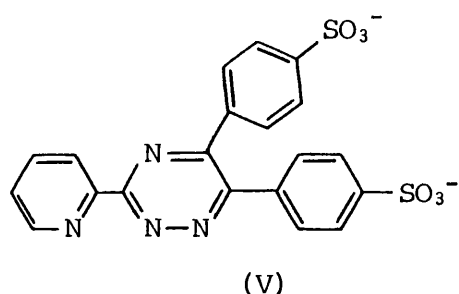
c) first-order plot (solution of complex made up in 50 vol % MeOH)



d) first-order plot (solution of complex made up in methanol)

faster than for  $[\text{Fe}(\text{bsb},\text{H},\text{Me})_3]^{2+}$ . The decrease in the reactivities of the complexes with hydroxide in the order  $\text{N-Ph} > \text{N-CH}_2\text{Ph} > \text{N-Me}$  once again demonstrates the electron-releasing effects of alkyl groups increasing the electron density in the vicinity of the iron atom reducing the ease of  $\text{OH}^-$  attack and also increasing the strength of the Fe-N  $\sigma$ -bond.

Fig. 5.19 shows the ultraviolet/visible absorption spectrum obtained for the reaction of  $[\text{Fe}(\text{bsb},\text{H},\text{CH}_2\text{CH}_2\text{SO}_3^-)_3]^-$  with sodium hydroxide ( $3 \times 10^{-3}$  M) in 40 vol % MeOH.  $[\text{Fe}(\text{bsb},\text{H},\text{CH}_2\text{CH}_2\text{SO}_3^-)_3]^-$  contains the bidentate ligand derived from pyridine-2-carboxaldehyde and taurine. The complex was prepared by modified method (i) and precipitated as the potassium salt. In the spectrum three peaks were discernible, values of  $\lambda_{\text{max}}$  at these peaks being 588, 512 and 415 nm when monitoring of the reaction began. There appear to be three stages involved in the reaction. The first is indicated by the initial increase in absorbance of the 'middle' peak where  $\lambda_{\text{max}} = 512$  nm. This may correspond to the formation of an intermediate of the type  $[\text{Fe}(\text{L}_2\text{LOH})]^{2-}$  where L is the bidentate ligand. Similar intermediates in the reactions of  $[\text{Fe}(\text{L}_3)]^{2+}$  and  $[\text{Fe}(\text{L}')_3]^{4-}$  with hydroxide where L is the 5- $\text{NO}_2$  derivative of 1,10-phenanthroline and L' is (V) have previously been proposed.<sup>20,21</sup> The second stage



corresponds to hydroxide attack at the intermediate complex. The first-order rate constants obtained for this reaction from plots of  $\ln(P_t - P_\infty)$  versus  $t$  using sets of absorbance data measured at the three values of  $\lambda_{\text{max}}$ , are within experimental error, the same. For this reaction  $k = 3.3 \times$

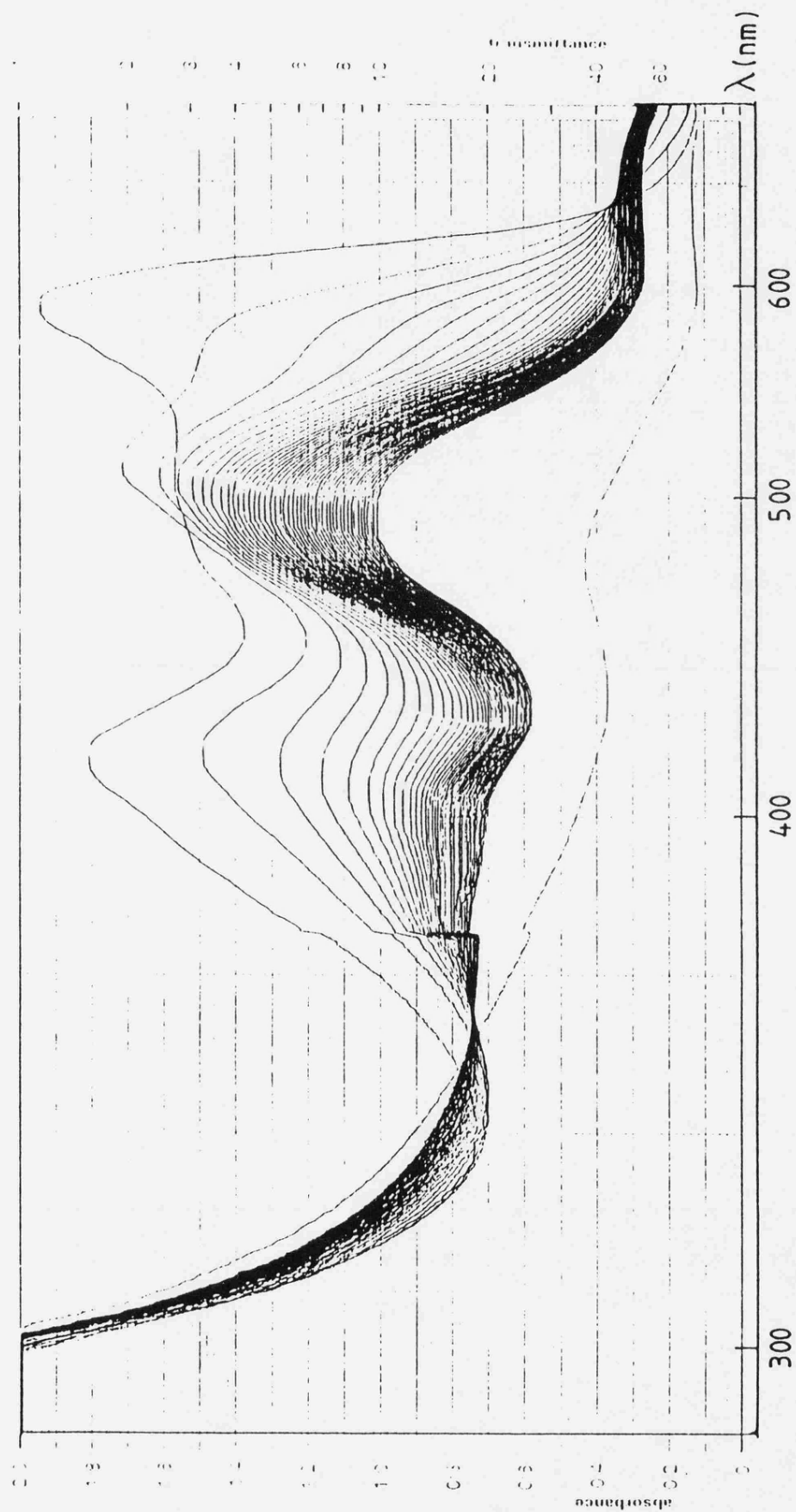


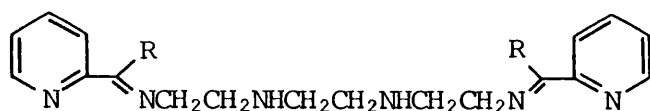
FIGURE 5.19

Ultraviolet/visible absorption spectrum obtained for the reaction of  $[\text{Fe}(\text{bsb}, \text{H}, \text{CH}_2\text{CH}_2\text{SO}_3^-)_3]^-$  with sodium hydroxide ( $3 \times 10^{-3}$  M) in 40 vol % MeOH.

$10^{-3} \text{ sec}^{-1}$ . The first-order plots are shown in Fig. 5.20. The third stage, much slower than the second, may correspond to aquation of the complex or to the interchange of  $\text{OH}^-$  groups bonded to the ligands onto the iron atom. In Fig. 5.20 the positive deviations of the plots from linearity at low values of  $t$  may be indicative of the presence of isomers. However, they may also be the result of concurrent reactions, i.e. the first and second stage reactions occurring simultaneously.

Fig. 5.21, the first-order plot obtained for the reaction of the complex with hydroxide (0.03 M) in 40 vol % MeOH from the minicomputer (monitored at  $\lambda_{\text{max}} = 588 \text{ nm}$ ,  $k_{\text{obs}} = 4.16 \times 10^{-3} \text{ sec}^{-1}$ ), shows deviations similar to those seen earlier which suggested the presence of isomers. In addition, distinct shifts in  $\lambda_{\text{max}}$  can be seen for the middle peak in Fig. 5.19. The same salient features were seen in ultraviolet/visible absorption spectra obtained for the same reaction using a sample of the sodium salt of the complex and also for analogous reactions involving higher hydroxide concentrations.

Low-spin iron(II) di-imine complexes  $[\text{FeL}]^{2+}$  where L is a hexadentate Schiff base of the type (VI) and R is H or Ph were prepared. The ligand



(VI)

where  $\text{R} = \text{H}$ , (hsb,H, trien), was prepared using pyridine-2-carboxaldehyde and triethylenetetramine. The ligand where  $\text{R} = \text{Ph}$ , (hsb,Ph, trien), was prepared using 2-benzoyl pyridine and triethylenetetramine. The nature of such hexadentate ligands means that theoretically there are several ways in which the ligand may be wrapped around the central iron atom resulting in the possibility of several geometrical isomers existing for complexes of this type (see Section 1.3.3). From molecular models it

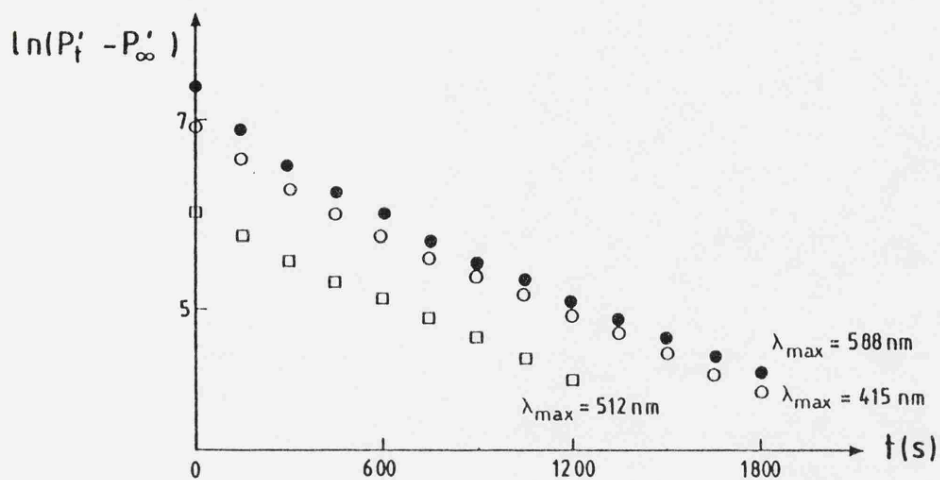


FIGURE 5.20

First-order plots obtained from the ultraviolet/visible absorption spectrum for the reaction of  $[\text{Fe}(\text{bsb}, \text{H}, \text{CH}_2\text{CH}_2\text{SO}_3^-)_3]^-$  with sodium hydroxide ( $3 \times 10^{-3} \text{ M}$ ) in 40 vol % MeOH.

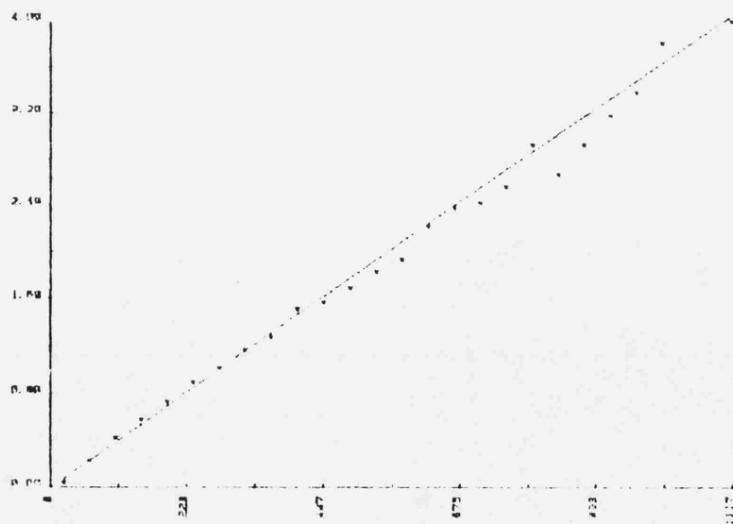
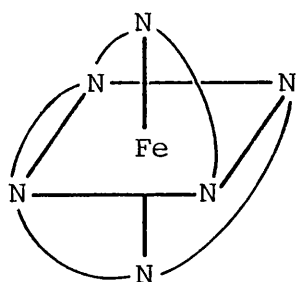


FIGURE 5.21

First-order plot obtained from the minicomputer for the reaction of  $[\text{Fe}(\text{bsb}, \text{H}, \text{CH}_2\text{CH}_2\text{SO}_3^-)_3]^-$  with sodium hydroxide (0.03 M) in 40 vol % MeOH at 298.15 K.

appears that the least-strained stereochemistry is that shown in (VII).



(VII)

X-ray crystallographic determination of the structure of  $[\text{Fe}(\text{hsb},\text{H},\text{-trien})]^{2+}$ <sup>22</sup> indicated the stereochemical disposition of the ligand to be that shown in (VII). The sample of  $[\text{Fe}(\text{hsb},\text{H},\text{trien})](\text{SCN})_2$  used in the structural determination had been prepared by a method similar to the general method used in this study. The compound had then been re-crystallized by allowing evaporation of a saturated aqueous solution of the complex. Thus, although the structural determination had shown the complex to have the stereochemistry shown in (VII) it is possible that the initial mixing of reactants to produce the complex had initially resulted in the formation of other isomers of the complex also. The method of preparation and subsequent re-crystallization may have resulted in the sample used in the X-ray analysis containing only one isomer. No inconsistencies were reported in the study of the kinetics of the reactions of the complex with hydroxide or cyanide at 298.2 K at atmospheric pressure.<sup>22</sup> If this type of complex follows the same trends as observed in the previous pages then the isomer shown in (VII) would appear to be the slowest reacting of any of the isomers with hydroxide.

Ultraviolet/visible absorption spectra of reactions of samples of  $[\text{Fe}(\text{hsb},\text{Ph},\text{trien})](\text{ClO}_4)_2$  prepared in various ways with sodium hydroxide (0.33 M) in 40 vol % MeOH showed definite shifts in  $\lambda_{\text{max}}$  as the reactions proceeded. These shifts are given in Table 5.18. The shifts, in the

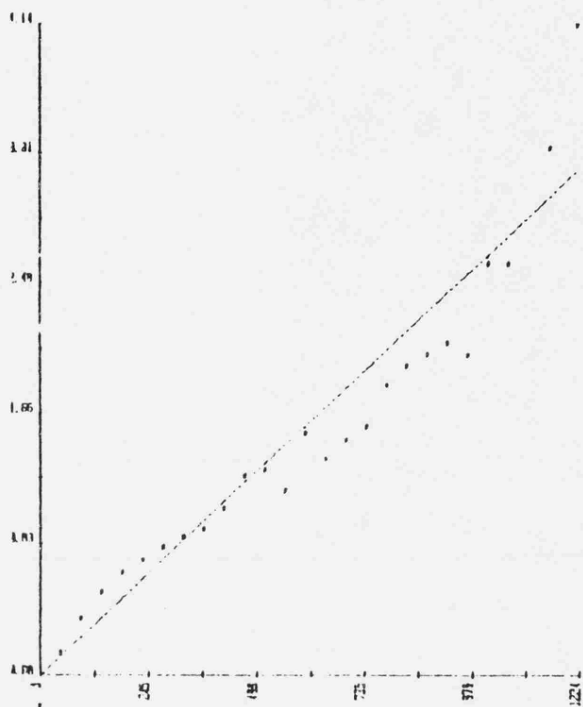
region of 11-13 nm, are much larger than those observed during the analogous reactions of the tris-(bidentate) complexes discussed earlier. Also, the shifts for the hexadentate Schiff base complex are towards shorter wavelengths whereas those observed during the reactions of the tris-(bidentate) complexes were towards longer wavelengths. In comparison to the shifts in  $\lambda_{\max}$  observed for the salts of  $[\text{Fe}(\text{hsb},\text{Ph},\text{trien})]^{2+}$  the range in values of  $\lambda_{\max}$  obtained at  $P_1$  for the complexes is small. This latter observation suggested that if the observed shifts in  $\lambda_{\max}$  were a result of changing proportions of isomers in the samples then the differing methods of preparations appeared to have little effect on the initial proportion of isomers in the sample.

Solubility measurements of the samples of this complex in water + methanol mixtures proved to be once again irreproducible. Table 5.19 shows a set of such values obtained for the perchlorate salt of  $[\text{Fe}(\text{hsb},\text{Ph},\text{trien})]^{2+}$ . As was observed for the tris-(bidentate) complex which contained the ligand derived from 2-benzoyl pyridine and *m*-toluidine the solubilities of the samples in a given solvent mixture increased in the order modified method (i) < general method < modified method (iii). However, unlike the tris-(bidentate) complexes no general trends in the solubilities with respect to solvent composition were observed. Solubility measurements were also carried out using the thiocyanate salt of the complex. These are given in Table 5.20. The method of preparation termed modified method (iv) involved addition of methanol to a sample of the complex prepared by modified method (i). Some of the sample remained undissolved and this was filtered off, washed and dried. For the samples prepared by the general method, modified method (i) and modified method (ii) no trends in solubilities were discernible, relating to either the synthetic routes or the solvent composition. Compared to the analogous

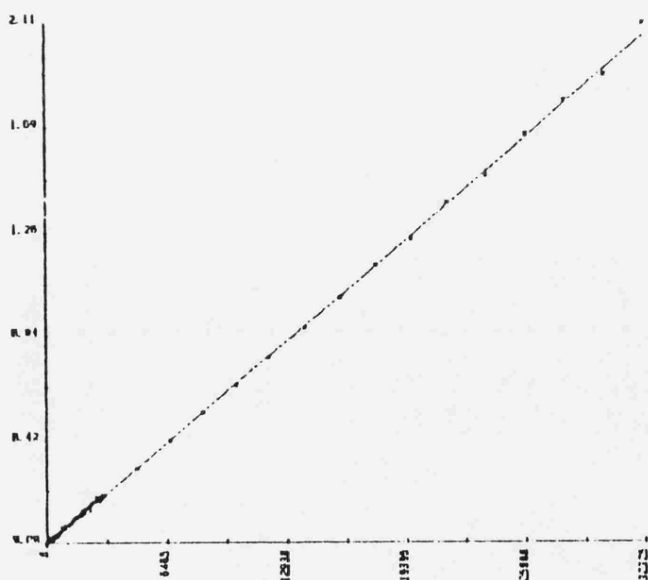
results obtained for the perchlorate salt of the complex, the range of values observed for the thiocyanate salt were much smaller. The sample prepared by modified method (iv), however, was much more soluble in these solvent mixtures than any of the other samples. In a comparison of the solubility results obtained using the samples prepared by modified methods (i) and (iv), values obtained for the latter in water and 20 vol % MeOH were over 10 and 20 times greater respectively than those obtained for the former. Values of  $k_{obs}$  obtained for the reactions of samples of the complex prepared by modified method (i) and by modified method (iv) with sodium hydroxide (0.33 M) in 40 vol % MeOH were  $1.6 \times 10^{-3} \text{ sec}^{-1}$  and  $0.67 \times 10^{-5} \text{ sec}^{-1}$  respectively. The first-order plots obtained for these reactions are shown in Fig. 5.22. Re-analysis of the absorbance/time data from the reaction of the sample prepared by modified method (iv) with hydroxide confirmed the first-order plot to be linear. Re-analysis of the analogous absorbance/time data obtained from the reaction of the other sample with hydroxide indicated the same behaviour as was seen for the tris-(bidentate) complexes described earlier. Values of  $\ln(P_t - P_\infty)$  for higher values of  $t$  could be fitted to a line of slope  $0.67 \times 10^{-5} \text{ sec}^{-1}$ . The corresponding values at lower  $t$ , however, deviated from the line in such a way that as values of  $t$  decreased the deviation (which was always positive) increased. Values of the absorbance of the solution at lower values of  $t$  minus the contribution to the absorbance from the slower reaction did not yield linear first-order plots. This could mean that in the sample of the complex prepared by modified method (i) more than two isomers were initially present. Although the value of  $k_{obs}$  obtained for the reaction of the sample prepared by modified method (iv) with hydroxide correlates favourably with first-order rate constants measured independently for the same reaction in other water + methanol

FIGURE 5.22

First-order plots obtained for the reactions of samples of  $[\text{Fe}(\text{hsb}, \text{Ph}, \text{trien})](\text{SCN})_2$  with sodium hydroxide (0.33 M) in 40 vol % MeOH at 298.15 K.



a) sample prepared by modified method (i)



b) sample prepared by modified method (iv)

mixtures,<sup>13,23</sup> the solubility measurements for the sample do not.<sup>24</sup>

Unpublished results of the kinetics of alkali fission of this complex have also indicated the initial stages of such reactions to be other than first-order at 298 K.<sup>25</sup> This is in contrast to results obtained for the analogous reactions at 308 K for which first-order kinetics were observed.<sup>23</sup>

For the other hexadentate Schiff base complex  $[\text{Fe}(\text{hsb},\text{H},\text{trien})]^{2+}$  containing the ligand derived from pyridine-2-carboxaldehyde and triethylenetetramine, no obvious shifts in  $\lambda_{\text{max}}$  or non-linearity of first-order plots for the reaction of the complex with hydroxide were observed. The absence of isomers in samples of this complex correlates with the fact that no inconsistencies have been reported in previous kinetic and solubility<sup>24</sup> investigations involving this complex.

Attempts at synthesising low-spin iron(II) Schiff base complexes containing ligands derived using pyrrole-2-aldehyde and a primary amine were successful only in the case of preparation of the hexadentate complex. This complex, the ligand in which was derived using pyrrole-2-aldehyde and triethylenetetramine, was prepared by the general method. The sample was very impure but attempted re-crystallization of the compound resulted in decomposition of the complex.  $\lambda_{\text{max}}$  of the complex was 540 nm. Under previously used conditions the rate of reaction of the complex with hydroxide was too fast to be monitored. The first-order rate constant obtained for the reaction of the complex with sodium hydroxide (0.0033 M) at 298.15 K, however, was  $2.37 \times 10^{-3} \text{ sec}^{-1}$ . No indications as to the presence or absence of isomers in the sample could be obtained from the resulting first-order plots of the reaction due to the large scattering of points on the plots. The nature of the ultraviolet/visible absorption spectra of the reaction (Fig. 5.23) made any detection of shifts in  $\lambda_{\text{max}}$

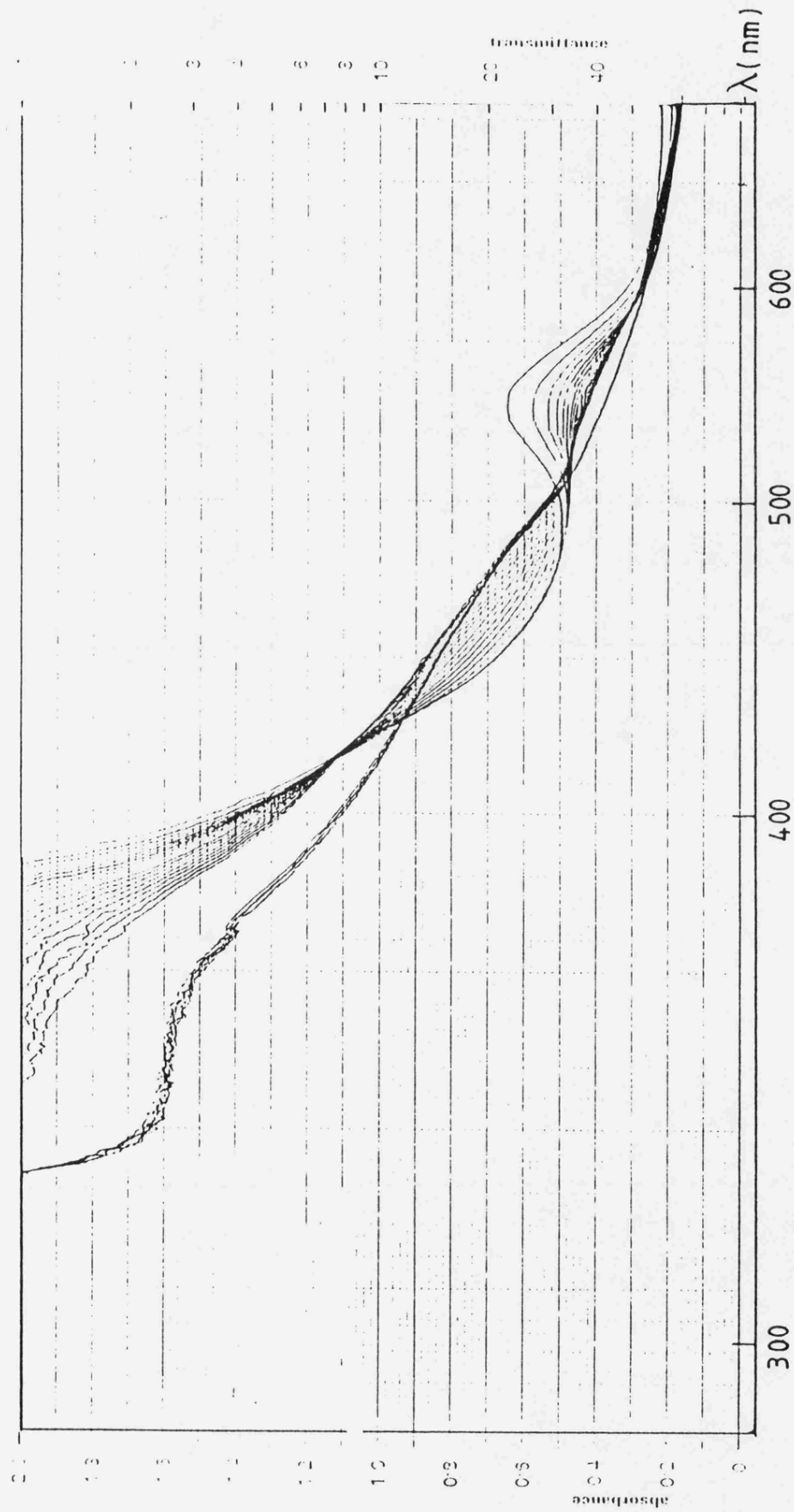


FIGURE 5.23

Ultraviolet/visible absorption spectrum obtained for the reaction of  $[\text{FeL}]^{2+}$ , where L is the ligand derived from pyrrole-2-aldehyde and triethylenetetramine, with sodium hydroxide ( $3 \times 10^{-3}$  M) in 40 vol % MeOH.

during the reaction also very difficult.

#### 5.4 CONCLUSION

The irreproducibility of sets of results obtained in the past that were seemingly consistent at the time for reactions of  $[\text{Fe}(\text{sb})_3]^{2+}$ , where sb is an unsymmetrical Schiff base ligand derived from 2-benzoyl pyridine and a primary amine, with hydroxide can be rationalized in terms of the presence of two geometrical isomers of the complexes in the samples. It was found that under certain conditions apparently consistent values of first-order rate constants and linear first-order plots for the reactions could be obtained for a given set of solutions of the complexes.

However, by re-analysing the absorbance/time data of the kinetic runs it was found that the first-order plots were not in reality in all cases linear. The apparent linearity of the plots resulted from the less than expected differences in the reactivities of the two isomers towards hydroxide and the fact that the synthetic method used resulted in samples of the complexes containing predominantly the slower reacting isomer.

By monitoring the change in observed first-order rate constants obtained for reactions of a given solution of a complex as the age of the solution increased, the proportion of the isomers in the solution was seen to change. The rate of change of the proportion of the isomers in solution was much slower than the rates of reactions of either isomer with hydroxide under the given conditions. This change could also be detected by shifts in  $\lambda_{\text{max}}$  of the complex in the ultraviolet/visible region of several nm.

The proportion of isomers in the samples depended on how the samples were prepared. Different salts of the same complex prepared in the same way contained varying proportions of the isomers. However, the major

factor in determining the proportion of the isomers appeared to be the length of time taken in preparing the samples. The shorter length of time a reaction mixture stood before the complex was precipitated the greater was the proportion of the 'fast' isomer in the sample. Longer preparation times and re-crystallization of the samples both had the effect of reducing the proportion of the 'fast' isomer in the resulting samples. Solutions containing solely the slower-reacting isomers of the complexes could be obtained by either allowing the solutions of the complexes to stand for several days or by repeated re-crystallization of the samples. Repeated measurement of first-order rate constants with time provided a means of checking that solutions contained only one isomer.

By observing trends in  $k_{obs}$  and  $\lambda_{max}$  and by studying first-order plots obtained for reactions with hydroxide, the presence of isomers in samples of other complexes could be detected. Some kinetic evidence for the existence of isomers in iron(II) tris-(bidentate) complexes containing ligands derived using pyridine-2-carboxaldehyde and a primary amine was found. Results consistent with the presence of isomers were also observed for the iron(II) hexadentate Schiff base complex containing the ligand derived from 2-benzoyl pyridine and triethylenetetramine.

In the next chapter, Chapter 6, the occurrence of diastereoisomerism in some low-spin iron(II) Schiff base di-imine complexes containing unsymmetrical ligands is investigated from a different aspect, by the use of  $^1H$  nmr spectroscopy. Some of the pertinent observations made in the two investigations, kinetic and spectroscopic, are collated at the end of Chapter 6 in Section 6.3.3.

TABLE 5.1

Observed first-order rate constants,  $k_{obs}$ , and related parameters for reactions of the perchlorate salt of complex A with sodium hydroxide (0.33 M) in water + methanol mixtures at 298.15 K

vol % MeOH	$10^3 k_{obs}$ ( $s^{-1}$ )	$P_0$	$P_\infty$	SD/P
0	0.77	0.403	0.074	$0.94 \times 10^{-3}$
20	1.47	0.977	0.056	$1.99 \times 10^{-3}$
30	1.91	0.865	0.098	$3.56 \times 10^{-3}$
40	2.89	0.892	0.031	$1.15 \times 10^{-3}$

TABLE 5.3

Observed first-order rate constants,  $k_{obs}$ , for reactions of solution B with sodium hydroxide (0.33 M) at 298.15 K

t (days)	$10^3 k_{obs}$ ( $s^{-1}$ )	$P_0$	$P_\infty$	SD/P
0	0.96	0.756	0.215	$4.9 \times 10^{-3}$
1	0.67	0.615	0.186	$2.3 \times 10^{-3}$
2	0.53	0.538	0.137	$2.1 \times 10^{-3}$
6	0.32	0.449	0.057	$1.1 \times 10^{-3}$
13	0.31	0.390	0.054	$1.7 \times 10^{-3}$
22	0.30	0.328	0.044	$4.3 \times 10^{-3}$

TABLE 5.2

Observed first-order rate constants,  $k_{\text{obs}}$ , and related parameters for reactions of salts of complex A with sodium hydroxide (0.33 M) in water + methanol mixtures at 298.15 K

a) iodide salt

vol % MeOH	$10^3 k_{\text{obs}}$ ( $\text{s}^{-1}$ )	$P_0$	$P_\infty$	SD/P
6.6	0.96	0.403	0.103	$1.26 \times 10^{-3}$
20	1.14	0.977	0.076	$3.29 \times 10^{-3}$
30	1.59	0.865	0.080	$2.91 \times 10^{-3}$
40	2.20	0.892	0.037	$1.11 \times 10^{-3}$

b) thiocyanate salt

vol % MeOH	$10^3 k_{\text{obs}}$ ( $\text{s}^{-1}$ )	$P_0$	$P_\infty$	SD/P
6.6	1.04	0.665	0.099	$1.72 \times 10^{-3}$
20	1.27	1.014	0.108	$2.72 \times 10^{-3}$
30	1.66	0.736	0.060	$3.06 \times 10^{-3}$
40	3.08	0.891	0.045	$1.19 \times 10^{-3}$

c) chloride salt

vol % MeOH	$10^3 k_{\text{obs}}$ ( $\text{s}^{-1}$ )	$P_0$	$P_\infty$	SD/P
0	0.71	1.045	0.095	$1.39 \times 10^{-3}$
20	0.90	0.649	0.045	$2.87 \times 10^{-3}$
30	1.09	0.952	0.047	$1.17 \times 10^{-3}$
40	1.65	0.893	0.043	$1.68 \times 10^{-3}$

TABLE 5.4

Kinetic data for the reaction of solution B with sodium hydroxide (0.33 M) at 298.15 K on day 22

t(s)	P'	t(s)	P'
0	331	1850	202
93	324	1942	199
185	317	2034	203
278	302	2127	193
370	288	2220	184
463	285	2520	174
555	280	2821	159
648	272	3121	158
740	254	3421	151
833	260	3722	134
925	258	4106	129
1017	252	4491	115
1110	246	4876	108
1202	237	5260	94
1295	236	5645	93
1387	228	6098	85
1480	223	6552	81
1572	222	7005	74
1665	213	7458	72
1757	206	7912	69

TABLE 5.5

First-order rate constants,  $k_s$ , for the reaction of solution B with sodium hydroxide (0.33 M) at 298.15 K on day 22 [ $P'_\infty = 42$ ]

Set of P' values	$10^3 k_s$ ( $s^{-1}$ )	time range (s)	% error
observed	0.30	0-8000	2.3
	0.31	2000-8000	1.9
interpolated	0.30	0-8000	0.5
	0.30	2000-8000	0.7

TABLE 5.6

Kinetic data for the reaction of solution B with sodium hydroxide (0.33 M) at 298.15 K on day 13

t(s)	P'	t(s)	P'
0	394	1458	266
139	374	1528	264
208	367	1597	258
278	360	1667	255
347	353	1961	238
416	346	2255	223
486	339	2549	210
555	333	2844	196
624	327	3138	184
695	322	3517	169
765	317	3895	158
834	311	4274	147
903	305	4653	138
972	300	5032	128
1042	295	5454	118
1112	290	5877	110
1181	285	6299	101
1250	280	6722	96
1320	276	7144	90
1389	272		

TABLE 5.7

First-order rate constants,  $k_s$ , for the reaction of solution B with sodium hydroxide (0.33 M) at 298.15 K on day 13 [ $P_\infty = 46$ ]

Set of P' values	$10^3 k_s$ ( $s^{-1}$ )	time range (s)	% error
observed	0.29	0-7000	0.29
	0.29	2000-7000	0.75
interpolated	0.29	0-7000	0.40
	0.29	2000-7000	0.35

TABLE 5.8

Kinetic data for the reaction of solution B with sodium hydroxide (0.33 M) at 298.15 K on day 6

t(s)	P'	t(s)	P'
10	438	1131	321
75	432	1186	314
131	427	1242	310
186	420	1297	305
242	410	1361	302
297	405	1796	268
353	400	2231	240
408	394	2667	215
464	386	3102	193
520	382	3537	175
575	373	3752	162
631	369	3967	158
686	364	4182	149
742	358	4397	142
797	352	4611	135
853	346	5047	123
908	342	5483	113
964	338	5918	102
1019	330	6354	95
1075	325	6789	89

TABLE 5.9

First-order rate constants,  $k_s$ , for the reaction of solution B with sodium hydroxide (0.33 M) at 298.15 K on day 6 [ $P'_\infty = 39$ ]

Set of P' values	$10^3 k_s$ ( $s^{-1}$ )	time range (s)	% error
observed	0.31	0-7000	0.20
	0.31	2000-7000	0.75
interpolated	0.31	0-7000	0.22
	0.30	2000-7000	0.33

TABLE 5.10

Kinetic data for the reaction of solution B with sodium hydroxide (0.33 M) at 298.15 K on day 2

t(s)	P'	t(s)	P'
0	551	926	383
46	535	972	378
93	524	1018	373
139	514	1065	368
185	504	1110	361
231	495	1290	343
278	484	1469	326
324	476	1647	309
370	467	1826	295
417	459	2005	282
463	452	2217	266
509	444	2430	252
556	435	2642	240
602	428	2855	227
648	422	3067	216
694	415	3313	205
741	408	4050	175
833	396	4295	166
880	390		

TABLE 5.11

Kinetic data for the reaction of solution B with sodium hydroxide (0.33 M) at 298.15 K on day 1

t(s)	P'	t(s)	P'
0	616	770	441
40	600	813	433
83	587	856	427
125	576	899	421
168	563	942	414
211	553	985	408
254	541	1028	402
297	532	1187	382
340	521	1346	363
383	512	1505	345
426	504	1664	332
469	495	1822	316
512	486	2009	302
555	477	2196	288
598	469	2382	274
641	462	2569	262
684	453	2756	251
727	446		

TABLE 5.12

First-order rate constants,  $k_s$ , for the reaction of solution B with sodium hydroxide (0.33 M) at 298.15 K on days 1 and 2

day	$P'_\infty$	$10^3 k_s$ ( $s^{-1}$ )	time range	% error
1	58	0.32	2009 - end	1.34
2	55	0.31	2005 - end	0.72
2	55	0.31	2430 - end	0.67

TABLE 5.14

First-order rate constants,  $k_s$ , for the reactions of the 'slow' isomers of complexes A and B with sodium hydroxide (0.33 M) in water + methanol mixtures at 298.15 K

	$10^3 k_s$ ( $s^{-1}$ )		
	vol % MeOH		
	6.6	20	30
complex A	0.66	0.78	1.01
complex B	0.30	0.36	0.47

TABLE 5.13

Calculated absorbance/time data for the reaction of the 'fast' isomer in solution B with sodium hydroxide (0.33 M) at 298.15 K on days 1 and 2

DAY 1			DAY 2		
t (s)	P <sub>f</sub> '	ln P <sub>f</sub> '	t (s)	P <sub>f</sub> '	ln P <sub>f</sub> '
0	105.2	4.66	0	79.1	4.37
100	85.9	4.45	100	65.6	4.18
200	73.2	4.29	200	56.3	4.03
300	63.6	4.15	300	46.1	3.83
400	51.6	3.94	400	39.4	3.67
500	42.7	3.75	500	32.7	3.49
600	34.8	3.55	600	27.6	3.32
700	29.8	3.40	700	23.2	3.14
800	24.7	3.21	800	18.7	2.93
900	21.1	3.05	900	16.1	2.78
1000	16.9	2.83	1000	13.4	2.60
1100	14.1	2.65	1100	10.5	2.36

TABLE 5.15

Changing positions of the absorption maxima,  $\lambda_{\max}$ , during the reactions of salts of complex A with sodium hydroxide (0.33 M) in 6.6 vol % MeOH

salt	$\lambda_{\max}$ in nm		
	$P_i$	$P(t_{1/2})$	$P(2t_{1/2})$
$\text{ClO}_4^-$	581	580	577
$\text{I}^-$	581	579	578
$\text{SCN}^-$	583	581	579
$\text{Cl}^-$	579	578	577

TABLE 5.16

Changing positions of the absorption maxima,  $\lambda_{\max}$ , during the reactions of salts of complex B with sodium hydroxide (0.33 M) in water + methanol mixtures

salt	vol % MeOH	$\lambda_{\max}$ in nm		
		$P_i$	$P(t_{1/2})$	$P(2t_{1/2})$
$\text{ClO}_4^-$	6.6	584	581	578
$\text{ClO}_4^-$	20	583	581	579
$\text{ClO}_4^-$	30	587	585	581
$\text{ClO}_4^-$	40	586	584	580
$\text{SCN}^-$	6.6	581	580	578
$\text{SCN}^-$	20	582	581	579
$\text{SCN}^-$	30	584	581	578
$\text{SCN}^-$	40	587	583	581

TABLE 5.17

Absorbances at  $\lambda_{\max}$  of saturated solutions of samples 1, 2, 3 and 4 of complex A in water + methanol mixtures at 298.2 K

sample	$\lambda_{\max}$	Absorbance, P		
		solvent composition		
		water	20 vol % MeOH	40 vol % MeOH
1	581	0.657	0.873	2.142
2	585	0.131	0.210	1.070
3	580	0.326	0.348	1.212
4	578	0.724	1.728	3.660

TABLE 5.18

Changing positions of the absorption maxima,  $\lambda_{\max}$ , during reactions of samples of the perchlorate salt of  $[\text{Fe}(\text{hsb}, \text{Ph}, \text{trien})]^{2+}$  with sodium hydroxide (0.33 M) in 40 vol % MeOH

method of preparation of $\text{ClO}_4^-$ salt	$\lambda_{\max}$ in nm	
	$P_i$	$P(2t_2)$
general method	613	624
modified method ( i )	613	625
modified method ( ii )	614	627
modified method (iii)	612	625

TABLE 5.19

Absorbances at  $\lambda_{\max}$  of saturated solutions of samples of the perchlorate salt of  $[\text{Fe}(\text{hsb},\text{Ph},\text{trien})]^{2+}$  in water + methanol mixtures

method of preparation of $\text{ClO}_4^-$ salt	Absorbance, P		
	solvent composition, vol % MeOH		
	0	20	40
general method	8.616	4.392	6.072
modified method ( i )	0.969	1.492	4.260
modified method (iii)	16.440	6.732	11.820

TABLE 5.20

Absorbances at  $\lambda_{\max}$  of saturated solutions of samples of the thiocyanate salt of  $[\text{Fe}(\text{hsb},\text{Ph},\text{trien})]^{2+}$  in water + methanol mixtures

method of preparation of $\text{ClO}_4^-$ salt	Absorbance, P		
	solvent composition, vol % MeOH		
	0	20	40
general method	1.812	2.196	4.962
modified method ( i )	5.400	3.960	5.064
modified method (ii)	3.292	1.923	3.828
modified method (iv)	53.732	88.173	72.45

## REFERENCES FOR CHAPTER 5

1. T. S. Lee, I. M. Kolthoff and D. L. Leussing, J. Am. Chem. Soc., 1948, 70, 3596.
2. J. H. Baxendale and P. George, Nature, 1948, 162, 777.
3. J. H. Baxendale and P. George, Trans. Faraday Soc., 1950, 46, 736.
4. J. Burgess, J. Chem. Soc. (A), 1967, 431.
5. J. Burgess, Inorg. Chim. Acta, 1971, 5, 133.
6. N. F. Ashford, M. J. Blandamer, J. Burgess, D. Laycock, M. Waters, P. Wellings, R. Woodhead and F. M. Mekhail, J. Chem. Soc., Dalton Trans., 1979, 869.
7. M. J. Blandamer, J. Burgess, T. Digman, P. P. Duce, J. P. McCann, R. H. Reynolds and D. M. Sweeney, Trans. Met. Chem., 1983, 8, 148.
8. M. J. Blandamer, J. Burgess, B. Clark, P. P. Duce, A. W. Hakin, N. Gosal, S. Radulovic, P. Guardado, F. Sanchez, C. D. Hubbard and E. A. Abu-Gharib, J. Chem. Soc., Faraday Trans. I, 1986, 82, 1471.
9. J. Burgess and R. H. Prince, J. Chem. Soc. (A), 1967, 434.
10. J. Burgess, J. Chem. Soc. (A), 1967, 955.
11. J. Burgess, J. Chem. Soc. (A), 1968, 497.
12. J. Burgess, G. E. Ellis, D. J. Evans, A. Porter, R. Wane and R. D. Wyvill, J. Chem. Soc. (A), 1971, 44.
13. M. J. Blandamer, J. Burgess, P. Cookson, D. L. Roberts, P. Wellings, F. M. Mekhail and P. Askalani, J. Chem. Soc., Dalton Trans., 1978, 996.
14. M. J. Blandamer, J. Burgess, R. I. Haines, F. M. Mekhail and P. Askalani, J. Chem. Soc., Dalton Trans., 1978, 1001.
15. J. Burgess, personal communication.
16. R. K. Murmann and E. A. Healy, J. Am. Chem. Soc., 1961, 83, 2092.
17. P. Krumholz, Inorg. Chem., 1965, 4, 609.
18. J. Burgess and R. H. Prince, J. Chem. Soc., 1965, 4697.
19. J. Burgess and R. H. Prince, J. Chem. Soc., 1965, 6061.
20. R. D. Gillard, C. T. Hughes and P. A. Williams, Trans. Met. Chem., 1976, 1, 51.
21. M. J. Blandamer, J. Burgess and P. Wellings, Trans. Met. Chem., 1979, 4, 95.
22. A. J. Duffield, Ph.D. Thesis, Leicester, 1980.
23. E. R. Gardner, F. M. Mekhail and J. Burgess, Int. J. Chem. Kinetics, 1974, 6, 133.
24. E. A. Abu-Gharib, M. J. Blandamer, J. Burgess, N. Gosal, P. Guardado, F. Sanchez and C. D. Hubbard, Trans. Met. Chem., 1984, 9, 306.
25. C. D. Hubbard, personal communication.

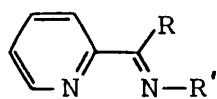


# CHAPTER 6

**<sup>1</sup>H Nmr Study of Low-Spin Iron(II)  
Schiff Base Di-imine Complexes**

## 6.1 INTRODUCTION

In the previous chapter, Chapter 5, kinetic evidence was presented for the existence of geometrical isomers (diastereoisomeric forms) of some low-spin iron(II) Schiff base di-imine complexes containing unsymmetrical multidentate ligands. For the tris-(bidentate) and mono-(hexadentate) complexes discussed,  $[\text{FeL}_3]^{2+}$  and  $[\text{FeL}]^{2+}$  respectively, the ligands L were of the type (I) and (II), being derived from either pyridine-2-carboxaldehyde or 2-benzoyl pyridine and a primary amine.



$R = H, Ph$   
 $R' = \text{alkyl}, \text{aryl}$

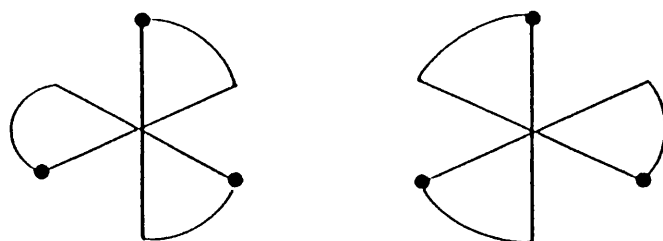
(I)



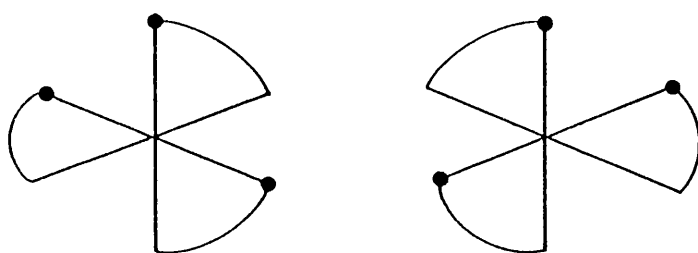
$R = H, Ph$

(II)

For such tris-(bidentate) complexes, the unsymmetrical nature of the ligands results in four possible stereochemical arrangements of the ligands around the central iron atom in forming a six co-ordinate pseudo-octahedral complex (see Section 1.3.3). Of the set of four possible stereoisomeric molecules, two possess a 'fac' configuration with respect to the arrangement of the ligands around the central iron atom, (III), and two a 'mer' configuration, (IV). The two fac isomers (1,2,3-isomers) constitute a pair of enantiomers, as do the two mer isomers (1,2,6-isomers). The relationship between the fac and mer isomers is that of diastereoisomers. It can be seen that the idealized fac isomers each possess a  $C_3$  symmetry axis of rotation which is absent from the mer isomers. This observation has led in the past to the use of the nmr technique in investigating the existence of diastereoisomers of complexes of this type.<sup>1</sup> The rotational element of symmetry present in the fac isomers suggests that, for a molecule of the complex having the fac con-



(III)



(IV)

figuration, the corresponding protons in the three bidentate ligand moieties are equivalent. Thus, for these equivalent ligand protons, one resonance signal would be expected. For the mer isomers, however, owing to the lack of symmetry three separate signals, one for each of the three sets of corresponding protons, would be expected. For example, if in (I),  $R=H$ , then the presence of both diastereoisomeric forms of the complex would be indicated in the  $^1H$  nmr spectrum of the complex by the occurrence of four signals in the low field region associated with the resonance of aldehydic protons.<sup>1</sup> Three of these signals would be attributable to the mer isomeric forms of the complex and one to the fac isomeric forms. Nmr spectroscopic studies have probed the existence of such geometrical isomers of a number of transition metal complexes containing unsymmetrical bidentate ligands including complexes of cobalt(II),<sup>2</sup> cobalt(III),<sup>3,4</sup> vanadium(III),<sup>5</sup> nickel(II)<sup>1</sup> and zinc(II).<sup>1</sup>

Thus, the nmr technique provides a means of detecting the presence of diastereoisomeric forms, i.e. the mer and fac isomers, of such tris-(bidentate) complexes of iron(II) where the ligands are of the type shown

in (I). Different enantiomers of the same diastereoisomeric form, however, cannot be distinguished in this way as enantiomers have identical physical properties except for the direction of rotation of the plane of polarized light. Thus, in this chapter, discussion as to the presence of isomers of complexes relates to diastereoisomeric forms only. The diastereoisomeric forms of a complex are termed the mer isomer and the fac isomer, although it should be remembered that two (enantiomeric) fac isomers and two (enantiomeric) mer isomers may exist for each complex of this type.

In this way it should also be possible, using the  $^1\text{H}$  nmr technique, to investigate the occurrence of diastereoisomeric forms of bis-(terdentate) and mono-(hexadentate) iron(II) complexes of this type. For iron(II) bis-(terdentate) complexes containing unsymmetrical Schiff base ligands, more than one diastereoisomeric form is possible only if the ligands are non-planar (see Section 1.3.3). For the iron(II) mono-(hexadentate) Schiff base complexes of the type shown in (II), the existence of several diastereoisomers is, in theory, possible (see Section 1.3.3). Three of these four diastereoisomers each contain a  $C_2$  rotation axis of symmetry, the other one does not. Thus, elucidation of the isomeric content of a sample of such a complex using the  $^1\text{H}$  nmr technique could be complicated if several isomers were present. However, as it is unlikely that different isomers possessing common symmetry elements would give identical spectra, then an indication as to the existence of either only one isomeric form or more than one isomeric form in a sample should be obtainable from  $^1\text{H}$  nmr spectra.

Having found kinetic evidence (Chapter 5) for the existence of isomers of iron(II) complexes containing ligands of the type (I), particularly strong in the cases where  $R=\text{Ph}$ ,  $^1\text{H}$  nmr spectroscopy was viewed as a com-

plementary method of detection of these diastereoisomeric species. For ligands of the type (I) where  $R=H$ , the resonance of such aldehydic-type protons occurring at lower fields than most protons in organic molecules suggested that, for these complexes in particular, nmr spectra could yield clear, definite information concerning the existence of the mer and fac isomeric forms of such complexes.

## 6.2 EXPERIMENTAL

Pure samples of low-spin iron(II) Schiff base di-imine complexes have often been found difficult to prepare. For an nmr investigation, contamination of the samples by the presence of traces of iron(III) and organic residues is obviously undesirable in terms of a resultant possible reduction in the quality of the spectra and the appearance of additional resonance signals.

$^1\text{H}$  nmr spectra were first obtained from a Varian EM 390 spectrometer using the same samples of iron(II) Schiff base di-imine complexes that had been used in the kinetic study probing the existence of isomers (Chapter 5). These samples of the iron(II) complexes had been prepared by either the general method of preparation or by various modified methods (see Section 5.2.1). The complexes had been precipitated as either the perchlorate, iodide, thiocyanate or chloride salts. The  $^1\text{H}$  nmr spectra of these samples in  $\text{d}_3$ -acetonitrile were of poor quality. Preparation of the complexes under an inert atmosphere of nitrogen did little to improve the quality of the spectra.

As a result, the analogous hexafluorophosphate salts of the complexes, which were more soluble in  $\text{d}_3$ -acetonitrile than the other salts previously used, were synthesised by various methods. It was found in the previous chapter (Chapter 5) that the longer the complexes were left in the

preparative solutions before their precipitation, the smaller were the proportions of one of the isomers in the resulting samples of the complexes. Re-crystallization of the samples had the same effect. In contrast, the longer the preparative time scales involved, the greater were the resulting yields and purities (in terms of reduced amounts of organic contaminants) of the samples. Thus, an optimum balance of these two opposing factors was sought by preparing the samples of the complexes by various modified methods. It was hoped in this way, to produce samples of the complexes pure enough to yield satisfactory spectra yet containing proportions of the two isomers such that the presence of both isomeric species could be detected. The most satisfactory spectra were obtained using samples of the hexafluorophosphate salts of the complexes prepared by a modified version of the general method of synthesis, modified method (V), outlined below. All the samples of the complexes used in the nmr study were prepared by this modified method except those of the tris-(bidentate) complex containing the ligand derived from 2-acetyl pyridine and hydroxylamine hydrochloride. In the case of this complex, complex I (see Section 6.3.1.1), the bidentate Schiff base ligand, methyl-2-pyridyl ketoxime, was prepared, isolated and then purified prior to its combination with iron(II) under acidic conditions. The preparative procedure followed was described in Section 2.2.3. This procedure was adopted in the hope of obtaining samples of the complex containing predominantly the least stable isomeric form of the complex.<sup>6</sup>

<sup>1</sup>H nmr spectra of the samples of the complexes in deuterated solvents were obtained from Varian EM 390 and Bruker AM 300 spectrometers.

#### Modified method (V)

The preparation of each complex involved the combination of iron(II), a primary amine and a carbonyl compound. The carbonyl compound used in

the preparation was either pyridine-2-carboxaldehyde, 2-acetyl pyridine or 2-benzoyl pyridine.

Methanolic solutions containing stoichiometric amounts of the appropriate carbonyl compound and primary amine were combined to generate the 'in situ' Schiff base ligand. This solution was allowed to stand for 15 minutes. A solution of iron(II) chloride tetrahydrate (containing a stoichiometric amount of the iron(II) salt) was added and after addition of a small quantity of sodium dithionite the solution was allowed to age at room temperature for 30 minutes. The reaction mixture was then filtered through 'celite filter-aid' and the hexafluorophosphate salt of the complex was precipitated by the addition of a saturated aqueous solution of potassium hexafluorophosphate to the filtrate. The precipitate was removed from solution and washed successively with water, ether, toluene and cold methanol. The product was then dried in vacuo over phosphorus pentoxide.

### 6.3 RESULTS AND DISCUSSION

#### 6.3.1 Assignment of spectra measured in d<sub>3</sub>-acetonitrile at 298 K

##### 6.3.1.1 General

<sup>1</sup>H nmr spectra were obtained for a series of low-spin iron(II) Schiff base di-imine complexes in d<sub>3</sub>-acetonitrile at 298 K with TMS as the internal reference. The complexes studied were of the type [FeL<sub>3</sub>]<sup>2+</sup> where L is a bidentate ligand, [FeL<sub>2</sub>]<sup>2+</sup> where L is a terdentate ligand or [FeL]<sup>2+</sup> where L is a hexadentate ligand. The structure of the ligands in these complexes, complexes A to U, are given in Schemes 6.1, 6.2 and 6.3. The ligand notations given follow the system used to abbreviate the names of ligands outlined in Section 1.3.4. Complexes A to O are of the type [FeL<sub>3</sub>]<sup>2+</sup> where L is a bidentate ligand. Complexes P, Q and R

SCHEME 6.1

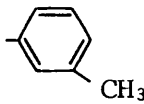
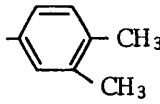
The nature of R and R' in the iron(II) tris-(bidentate) complexes of the type  $[\text{Fe}(\text{bsb},\text{R},\text{R}')_3]^{2+}$  studied by  $^1\text{H}$  nmr spectroscopy where (bsb,R,R') is an unsymmetrical bidentate Schiff base di-imine ligand.



(bsb,R,R')

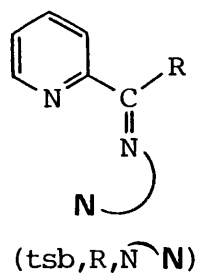
Complex	R	R'	Ligand notation
A	H	-CH <sub>3</sub>	(bsb,H,Me)
B	H		(bsb,H,Ph)
C	H		(bsb,H,Ph:p-Me)
D	H		(bsb,H,Ph:3,4-Me <sub>2</sub> )
E	H	-CH <sub>2</sub> -	(bsb,H,CH <sub>2</sub> Ph)
F	H		(bsb,H,Ph:m-Me)
G	H		(bsb,H,Ph:m-OMe)
H	H		(bsb,H,Ph:p-OMe)
I	CH <sub>3</sub>	-OH	(bsb,Me,OH)
J	CH <sub>3</sub>	-CH	(bsb,Me,Me)
K	CH <sub>3</sub>		(bsb,Me,Ph)
L		-CH <sub>3</sub>	(bsb,Ph,Me)
M			(bsb,Ph,Ph)

SCHEME 6.1 (Continued) ....

Complex	R	R'	Ligand notation
N			(bsb,Ph,Ph:m-Me)
O			(bsb,Ph,Ph:3,4-Me <sub>2</sub> )

SCHEME 6.2

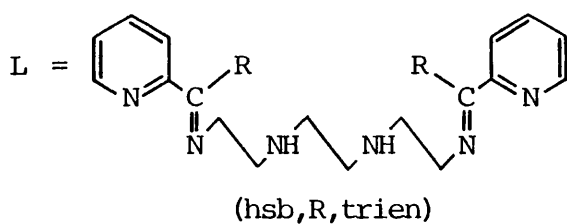
The nature of R and  $\widehat{N-N}$  in the iron(II) bis-(terdentate) complexes of the type  $[\text{Fe}(\text{tsb},\text{R},\widehat{N-N})_2]^{2+}$  studied by  $^1\text{H}$  nmr spectroscopy where  $(\text{tsb},\text{R},\widehat{N-N})$  is an unsymmetrical terdentate Schiff base di-imine ligand.



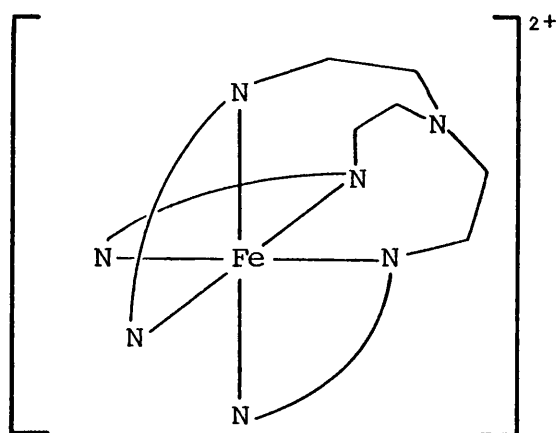
Complex	R	$\widehat{N-N}$	Ligand notation
P	H		$(\text{tsb},\text{H},8\text{amq})$
Q	$\text{CH}_3$		$(\text{tsb},\text{Me},8\text{amq})$
R	H		$(\text{tsb},\text{H},2\text{pa})$

SCHEME 6.3

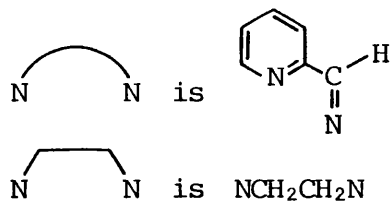
The nature of the ligand L in the iron(II) complexes of the type  $[\text{FeL}]^{2+}$  studied by  $^1\text{H}$  nmr spectroscopy where L is a hexadentate Schiff base di-imine ligand.



Complex	R	Ligand notation
S	H	(hsb,H, trien)
T		(hsb,Ph, trien)



complex U :  $[\text{Fe}(\text{hsb,H,t2a})]^{2+}$



are of the type  $[\text{FeL}_2]^{2+}$  where L is a terdentate ligand. Complexes S, T and U are of the type  $[\text{FeL}]^{2+}$  where L is a hexadentate ligand. All spectra were measured initially using a Varian EM 390 (90 MHz) spectrometer. The spectra of some complexes were also obtained using a Bruker AM 300 (300 MHz) spectrometer. The figures referred to in the following sections are shown together at the end of the chapter. In these figures, the labelling of the protons in the ligand insets, e.g.  $\text{H}_A$ ,  $\text{H}_B$ ,  $\text{H}_C$ , etc., does not reflect the equivalence, or otherwise, of the protons. Thus, for example, two protons both labelled  $\text{H}_B$  in a ligand inset does not necessarily mean that these protons are equivalent. Such labelling is adopted only in an effort to eliminate tedious repetition when indicating which proton, or set of protons, is being referred to in the text.

#### 6.3.1.2 Tris-(bidentate) complexes

Fig. 6.1 shows the  $^1\text{H}$  nmr spectrum of complex A,  $[\text{Fe}(\text{bsb},\text{H},\text{Me})_3]^{2+}$ , in  $\text{d}_3$ -acetonitrile measured at 300 MHz. Complex A contains the bidentate ligand derived from pyridine-2-carboxaldehyde and methylamine. In this ligand (see ligand inset in Fig. 6.1) there are three substantially different types of protons labelled  $\text{H}_A$ ,  $\text{H}_B$  and  $\text{H}_C$ .  $\text{H}_A$  is an aldehydic-type proton. This proton is attached directly to the di-imine moiety of the ligand and as such will be de-shielded. The proton also lies in the magnetically anisotropic de-shielding zone of the aromatic pyridine ring. This proton will therefore be expected to absorb at a relatively low field. In most simple organic molecules, resonances due to aldehydic protons appear in the region 8-10 ppm.<sup>7-9</sup> The protons labelled  $\text{H}_B$  are the four pyridyl protons. These protons are not equivalent and each should absorb at a different frequency. For unsubstituted (and uncomplexed) pyridine these protons absorb in the region 7-8.5 ppm.<sup>7-9</sup> The

protons labelled  $H_C$  are methyl protons. Provided there is no restriction to rotation about the N-C single bond, then the three protons in each methyl group are equivalent and will absorb at the same frequency. This applies to the methyl groups in both the mer and fac isomeric forms of the complex. However, although the three protons of each methyl group are equivalent, their chemical shift may be different from that of another set of three methyl protons. For the mer isomeric form of this tris-(bidentate) complex, the three methyl groups (one in each bidentate ligand) will not be equivalent and each set of methyl protons will absorb at a different frequency. In contrast, for the fac isomeric form of the complex, the three methyl groups are equivalent and only one signal due to methyl protons will be seen. In saturated alkyl molecules, methyl protons absorb in the region of 0.9 ppm.<sup>7-9</sup> However, in this case, the close proximity of the methyl group to the di-imine moiety would be expected to result in the appearance of resonance peaks due to these protons at relatively lower fields.

In the spectrum shown in Fig. 6.1 three distinct sets of signals are discernible. The set of signals occurring at lowest field strengths, in the region of 8.9 to 9.2 ppm, consists of four resonance signals. A second set of signals occurring at slightly higher field strengths, in the region of 7.0 to 8.3 ppm, consists of three unresolved multiplets. A third set of signals occurring at relatively high field strengths, in the region of 2.9 to 3.5 ppm, consists of four signals. From the integration, the ratio of the areas under these three sets of peaks can be seen to be 1:4:3 respectively. The peaks between 8.9 and 9.2 ppm are due to the resonance of aldehydic-type protons,  $H_A$ , in the ligands of the complex. The existence of four peaks of very similar shape in this region, three being of equal intensity, the fourth less intense, is

indicative of the presence of both the mer and the fac isomeric forms in the solution of the complex. These signals appear as (poorly resolved) quartets due to the coupling of the aldehydic-type proton with the three equivalent methyl protons in each bidentate ligand, H<sub>C</sub>. Each of the four signals in the higher field region, 2.9 to 3.5 ppm, is due to the resonance of the three equivalent methyl protons in the ligand, H<sub>C</sub>. Again, the three signals of equal intensity are due to the resonance of the three sets of methyl protons in the mer isomeric form of the complex. In this isomeric form the three N-methyl groups are not equivalent and thus each set of methyl protons resonates at a different frequency. The fourth signal, less intense than the other three, is due to the resonance of the three equivalent sets of methyl protons in the fac isomeric form. All these four signals appear as doublets due to the coupling of these protons with the aldehydic-type protons in the ligands, H<sub>A</sub>. The signals in the region of 7.0 to 8.3 ppm are due to the resonance of the pyridyl protons in the complex, H<sub>B</sub>. This set of signals should consist of sixteen resonances, each pyridyl proton being responsible for, in total, four peaks. However, the overlapping of the signals in this region makes detailed assignment of the peaks difficult. From the integration of the signals due to the aldehydic-type protons and the methyl protons, the ratio of the mer and fac isomeric forms in the sample is approximately 4.4:1 (approximately 19% of the sample is in the fac isomeric form).

Fig. 6.2 shows the <sup>1</sup>H nmr spectrum of complex B, [Fe(bsb,H,Ph)<sub>3</sub>]<sup>2+</sup>, in d<sub>3</sub>-acetonitrile at 300 MHz. Complex B contains the bidentate ligand derived from pyridine-2-carboxaldehyde and aniline. Thus, this complex corresponds to the replacement of the methyl group in complex A by a phenyl group. This ligand, see ligand inset in Fig. 6.2, contains three significantly different types of protons, labelled H<sub>A</sub>, H<sub>B</sub> and H<sub>C</sub>. As for

complex A,  $H_A$  and  $H_B$  are the aldehydic-type proton and the pyridyl protons respectively. For complex B, however,  $H_C$  refers to the five phenyl protons. These phenyl protons would be expected to absorb at generally higher fields than the pyridyl protons, being further removed from the di-imine group and considering the absence of a nitrogen atom in the phenyl aromatic ring. Fig. 6.2 clearly shows four resonance peaks, in the region of 8.8 to 9.4 ppm, due to the aldehydic-type protons,  $H_A$ . From the integration of these peaks, the sample of complex B contains the mer and fac isomers in the ratio 4:1 (approximately 20% of the sample is in the fac isomeric form). The peaks in the region 5.3 to 8.7 ppm are due to the resonance of the phenyl and pyridyl protons. The detailed assignment of these peaks would, at this stage, be difficult. The broad peak at 2.68 ppm disappears on shaking with  $D_2O$  and is therefore most probably due to the presence of water in the sample.

Fig. 6.3 shows the spectrum of complex C,  $[Fe(bsb,H,Ph:p-Me)_3]^{2+}$ , in  $d_3$ -acetonitrile measured at 300 MHz. Complex C is the (N-phenyl) p-methyl derivative of complex B. This ligand, derived from pyridine-2-carboxaldehyde and p-toluidine, contains four significantly different types of protons, labelled  $H_A$ ,  $H_B$ ,  $H_C$  and  $H_D$  [see ligand inset in Fig. 6.3]. As for complex B,  $H_A$ ,  $H_B$  and  $H_C$  refer to the aldehydic-type proton, the pyridyl protons and the phenyl protons respectively.  $H_D$  refers to the methyl protons. The set of signals consisting of four peaks in the expected region of absorption of the  $H_A$  protons indicates the presence of the two isomeric forms in the sample. However, in the region of 2.1 to 2.5 ppm, the expected region of absorption of the methyl protons  $H_D$ , there are at least six peaks [see enlargement of this region of the spectrum in Fig. 6.3]. From  $^1H$  nmr spectra obtained using different samples of complex C, it was found that the peaks labelled 2, 3 and 4 in

Fig. 6.3 are those due to the methyl protons in the mer isomeric form of the complex. The resonance due to the methyl protons in the fac isomer forms part of the signal labelled 1. Thus, a portion of signal 1 and signal 5 are due to impurities in the sample. In the region of the resonance of the aromatic (phenyl and pyridyl) protons there are two discernible sets of peaks. In the region 5.3 to 7.3 ppm there are eight doublets, the coupling constant in which is the same in all cases ( $J = 8.25$  Hz). From the integration of these peaks, six of the signals are equally intense and two are less intense, but equally so. In the lower field region 7.3 to 8.7 ppm there is a group of more complex signals of variable intensities. The total intensities of these two sets of signals (one set appearing between 5.3 and 7.3 ppm, the other between 7.3 and 8.7 ppm) is 4:4 when the total intensity of the  $H_A$  resonance peaks is taken to be 1. The position and multiplicities of these two sets of peaks indicates the lower field set to be due to the four pyridyl protons,  $H_B$ , and the higher field set to be due to the four phenyl protons,  $H_C$ . The observed pattern of the resonances due to the phenyl protons, eight doublets, is consistent with relatively fast flipping of the phenyl group due to rotation about the N-phenyl single bond. In such a case the protons attached to the two carbon atoms 'ortho' to the methyl group will be equivalent. Similarly, the protons attached to the two carbon atoms 'meta' to the methyl group will be equivalent. However, the two ortho protons will not be equivalent with the two meta protons. Signals due to the ortho protons appear as doublets due to splitting by the neighbouring meta protons and vice versa, the coupling constant being the same in both cases. Further splitting due to the coupling of protons across the ring is too small to be apparent. Due to the presence of both isomeric forms there are four doublet resonances due to the ortho protons

and the same number due to the meta protons. In both instances, three of the four doublets are attributable to the mer isomeric form, the fourth to the fac isomer. A series of spin decoupling experiments supported the assignment of these eight doublets to the resonance of the phenyl protons. This technique involves the application of a second radio-frequency field equal to the resonance frequency of one group of nuclei. This leads to saturation and effectively decouples the set of nuclei from the remaining nuclei. Systematic double irradiation by the application of a decoupling field set exactly on the centre of one of the doublets lead, in each case, to the collapse of one of the other doublets to a singlet. For example, the application of a decoupling field of frequency corresponding to the chemical shift of the doublet at 6.61 ppm lead to the collapse of the doublet at 7.21 ppm to a singlet. The rest of the spectrum was unchanged. The doublets found to be coupled by such experiments are indicated in Fig. 6.3. From the symmetry and intensity of this pattern it appears that the four doublets appearing at relatively high fields (5.38, 6.12, 6.61 and 6.69 ppm) are due to one type of proton, i.e. either those meta or ortho to the methyl group, and the four doublets appearing at relatively lower fields (6.84, 7.03, 7.07 and 7.21 ppm) are due to the other type of proton. From correlation tables of chemical shifts<sup>7-9</sup> it appears that the former set are due to the meta protons, the latter set to the ortho protons.

Thus the indications are that the phenyl ring is rotating sufficiently fast for the two protons ortho to the methyl group to be equivalent, and for the two protons meta to the methyl group to be equivalent. From the signals due to the H<sub>A</sub> and H<sub>C</sub> protons, the ratio of the mer and fac isomeric forms in the sample is 4.7:1 (the sample contains approximately 18% of the fac isomeric form).

These observations concerning complex C make further assignment of signals in the spectrum of complex B [Fig. 6.2] possible, complex B being the unsubstituted derivative of complex C. In the spectrum of complex B, shown in Fig. 6.2, four doublets can be seen at higher fields in the region of phenyl proton absorption, at 5.40, 6.18, 6.71 and 6.84 ppm. These chemical shifts are very close to those observed for a similar set of peaks due to the resonance of phenyl protons in complex C [see Fig. 6.3]. These latter resonances were due to one set of equivalent phenyl protons, probably the protons meta to the methyl group in the complex, at 5.38, 6.12, 6.61 and 6.69 ppm. For both complexes the doublet appearing at highest field is less intense than the other three resonances. The four doublets in the spectrum of complex B would therefore appear to be due to the protons attached to the carbon atoms ortho to the C-N single bond. Indeed, if these signals were due to the resonance of the protons attached to the carbon atoms meta to the C-N single bond in complex B, they would be expected to have the appearance of triplets. In a comparison of the phenyl proton absorption regions in the spectra shown in Fig. 6.2 (complex B) and Fig. 6.3 (complex C) there is an increased complexity of the signals in the region 6.9 to 7.5 ppm in the former spectrum as compared with the latter. This is due to the presence of a fifth phenyl proton in complex B, para to the C-N bond, which is replaced by a methyl group in complex C.

Fig. 6.4 shows the  $^1\text{H}$  nmr spectrum of complex D,  $[\text{Fe}(\text{bsb},\text{H},\text{Ph}:3,4\text{-Me}_2)_3]^{2+}$ , in  $\text{d}_3$ -acetonitrile measured at 300 MHz. Complex D contains the bidentate ligand derived from pyridine-2-carboxaldehyde and 3,4-dimethylaniline. The presence of isomers in this sample can be seen immediately by the existence of four peaks in the region 8.6 to 9.3 ppm due to the absorption of the aldehydic-type protons (labelled  $\text{H}_A$  in the

ligand inset in Fig. 6.4). From these signals the ratio of the mer and fac isomeric forms present in the sample is 3:1 (the sample contains approximately 25% of the fac isomeric form). The existence of isomeric forms in the sample is reflected in the appearance of a number of singlets in the region 1.8 to 2.3 ppm due to the resonance of the two methyl groups in each bidentate ligand. Unfortunately, assignment of these peaks is complicated by the presence in this region of a quintet due to undeuterated solvent. Also, there is the possibility that one (or maybe even more than one) of these peaks is due to the presence of impurities in the sample. The broad peak around 2.7 ppm disappears upon shaking the sample with D<sub>2</sub>O and is thus most probably due to water. Signals due to the absorption of the pyridyl protons, labelled H<sub>B</sub> in the ligand inset, appear in the region 7.2 to 8.6 ppm. Those due to the phenyl protons H<sub>E</sub>, H<sub>F</sub> and H<sub>G</sub> appear in the region 4.8 to 7.2 ppm. Three types of signals can be seen in this latter region. At lower field strengths there are four doublets due to the resonance of the proton H<sub>E</sub> at 6.80, 6.96, 6.99 and 7.05 ppm (the middle two doublets are overlapped giving the signal the appearance of a triplet). Three of these peaks are attributable to the presence of the mer isomeric form, the fourth to the fac isomeric form. These signals appear as doublets due to the coupling of H<sub>E</sub> with H<sub>F</sub> ( $J_{EF} = 8.25$  Hz). The resonances due to H<sub>F</sub> appear as doublets of doublets. There are four of these signals at 5.23, 6.16, 6.26 and 6.57 ppm (the latter being partially obscured by another signal of similar chemical shift). The observed multiplicities of these signals arise from the coupling of H<sub>F</sub> with H<sub>E</sub> and H<sub>F</sub> with H<sub>G</sub> ( $J_{FG} = 2.25$  Hz). The absorption of H<sub>G</sub> appears as four doublets at 4.85, 5.54, 6.36 and 6.60 ppm. The splitting of the signals into doublets is a result of the coupling of H<sub>G</sub> with H<sub>F</sub>. Such an interpretation of this spectrum

indicates that, as for complexes B and C, the N-phenyl ring is rotating rapidly enough for all possible conformations of the ring to be equally populated so that for each proton (or set of equivalent protons) a single time-averaged set of resonances is observed.

Fig. 6.5 shows the  $^1\text{H}$  nmr spectrum of complex E,  $[\text{Fe}(\text{bsb},\text{H},\text{CH}_2\text{Ph})_3]^{2+}$ , in  $\text{d}_3$ -acetonitrile at 300 MHz. Complex E contains the bidentate ligand derived from pyridine-2-carboxaldehyde and benzylamine [see ligand inset in Fig. 6.5]. There is no isolated group of four resonance signals at low fields due to the  $\text{H}_\text{A}$  protons in the complex as seen in the previous spectra. However, the presence of isomers in this sample is evident from the pattern of the signals at high fields in the region 3.9 to 5.5 ppm. These signals are due to the methylene protons,  $\text{H}_\text{C}$ , and appear as eight doublets, the splitting in all cases being the same ( $J = 15$  Hz). Six of the doublets are equally intense, the remaining two are relatively more intense, but equally so. The methylene protons,  $\text{H}_\text{C}$ , are evidently not equivalent and thus four of the doublets are due to one of the methylene protons, the remaining four doublets being due to the other. Each of these sets of four doublets consists of three signals of equal intensity, due to the mer isomeric form and one signal, of greater relative intensity, due to the fac isomeric form. The ratio of the mer and fac isomeric forms in the sample is 1.4:1. Thus, 42% of the sample is in the fac isomeric form - a considerably higher proportion than seen for the samples of complexes A, B, C and D. The resonances in the lower field region, 6.6 to 9.1 ppm, are due to the protons  $\text{H}_\text{A}$ ,  $\text{H}_\text{B}$  and  $\text{H}_\text{D}$ . The signals due to the aromatic protons and those due to  $\text{H}_\text{A}$  appear to overlap to some extent. The two lowest field resonances, signals at 8.46 and 9.05 ppm, are presumably two of the expected set of four signals due to the  $\text{H}_\text{A}$  protons. From the integration, the signal at 8.46 ppm is that due

to the fac isomeric form. The other, at 9.05 ppm, is one of the three  $H_A$  signals due to the mer isomeric form. From the integration, the other two 'mer  $H_A$  signals' may be those at 8.26 and 8.30 ppm.

$^1H$  nmr spectra were obtained for other iron(II) tris-(bidentate) complexes of this type (where  $R = H$ ) in  $d_3$ -acetonitrile using the Varian EM 390 spectrometer. These complexes contained ligands derived from pyridine-2-carboxaldehyde and either *m*-toluidine (complex F), *m*-anisidine (complex G) or *p*-anisidine (complex H) [see Scheme 6.1]. Although these spectra were not resolved to such an extent as to allow detailed assignment of peaks, the signals due to the aldehydic-type protons (and certain other groups) were clear enough to permit the detection of isomeric forms in the samples. In all cases, the presence of both isomeric forms was evident, the samples containing predominantly the mer isomers. No satisfactory  $^1H$  nmr spectra could be obtained for the complexes in which ligands were derived from pyridine-2-carboxaldehyde and either taurine or  $\alpha$ -phenylethylamine.

$^1H$  nmr spectra of complexes containing bidentate ligands derived from 2-acetyl pyridine and a primary amine revealed the presence of two isomeric forms in the samples of the complexes. Spectra of the complexes were measured at 298 K in  $d_3$ -acetonitrile using the 90 MHz or 300 MHz spectrophotometers. Three such spectra measured at 300 MHz are shown in Figs. 6.6, 6.7 and 6.8.

The  $^1H$  nmr spectrum of complex I,  $[Fe(bsb,Me,OH)_3]^{2+}$ , in  $d_3$ -acetonitrile measured at 300 MHz is shown in Fig. 6.6. In this spectrum there are four signals in the region of 2.6 to 2.9 ppm due to the resonance of the methyl protons,  $H_A$ , indicating the existence of both isomeric forms in the sample. The ratio of the mer and fac isomeric forms in the sample is approximately 4.3:1 (approximately 19% of the

sample is in the fac isomeric form). The signals in the region of 7 to 9 ppm are due to the resonance of the aromatic pyridyl protons, H<sub>B</sub>. This set of signals may also contain a peak due to the resonance of the hydroxyl proton, H<sub>C</sub>.

Fig. 6.7 shows the <sup>1</sup>H nmr spectrum of complex J, [Fe(bsb,Me,Me)<sub>3</sub>]<sup>2+</sup>, measured in d<sub>3</sub>-acetonitrile at 300 MHz. Complex J contains the bidentate ligand derived from 2-acetyl pyridine and methylamine. Although the spectrum is not particularly well resolved, resonance absorption signals in the low field region due to the pyridyl protons and in the higher field region due to the methyl protons can easily be discerned. Each bidentate ligand in this complex contains two methyl groups. Thus, if both the possible diastereoisomeric forms of the complex are present in the sample then eight signals, having the appearance of singlets, should be evident in the expected region of methyl proton absorption. In the spectrum, there appear to be more than eight signals in the region of 1.4 to 2.3 ppm, some of which must be due to the presence of impurities in the sample. However, the appearance of the spectrum as a whole, taking into account the complex signals due to the pyridyl protons, suggests the presence of isomeric forms in the sample.

The <sup>1</sup>H nmr spectrum of complex K, [Fe(bsb,Me,Ph)<sub>3</sub>]<sup>2+</sup>, in d<sub>3</sub>-acetonitrile measured at 300 MHz is shown in Fig. 6.8. Complex K contains the bidentate ligand derived from 2-acetyl pyridine and aniline. In Fig. 6.8, the four singlets in the region of 2.3 to 2.9 ppm, at 2.30, 2.33, 2.59 and 2.83 ppm, are due to the resonance of the methyl protons labelled H<sub>A</sub> in the ligand inset. From these signals, the ratio of the mer and fac isomeric forms in the sample is 3.9:1 (approximately 20% of the sample is in the fac isomeric form). The remaining signals, at lower fields, are due to the pyridyl protons, H<sub>B</sub>, and the phenyl protons,

H<sub>C</sub> and H<sub>D</sub>. It was seen in the previous spectra that pyridyl protons in complexes of this type generally absorbed at lower fields than N-phenyl protons. The seven signals occurring at higher fields, in the region of 4.5 to 6.7 ppm, are therefore most likely to be due to the latter type of protons. The resonances due to the protons labelled H<sub>C</sub> in the ligand inset would be expected to appear as doublets (or some pattern of doublets, possibly doublets of doublets, depending on the resolution). In contrast, the resonances due to the protons labelled H<sub>D</sub> would be expected to have the appearance of triplets. These seven signals, then, appear to be due to the protons labelled H<sub>C</sub>. It is most likely that the seven signals are part of a set of eight signals, the eighth signal appearing at lower field and being masked by other signals. Four of the set of eight signals (three equally intense, the fourth relatively less intense) are due to one of the H<sub>C</sub> protons. The remaining four signals (again, three equally intense, the fourth less so) are due to the other H<sub>C</sub> proton. Thus, rotation about the N-C single bond appears to be restricted and as a result the two H<sub>C</sub> protons are not equivalent. Previously it was seen that in the complexes where R=H and R' was either Ph, Ph:p-Me or Ph:3,4-Me<sub>2</sub> (complexes B, C and D respectively) there was essentially free rotation of the phenyl group. Replacement of H (i.e. R) by a methyl group appears to restrict this rotation.

<sup>1</sup>H nmr spectra of several complexes where R=Ph were obtained in d<sub>3</sub>-acetonitrile. Three of these spectra measured at 300 MHz are shown in Figs. 6.9, 6.10 and 6.11.

The <sup>1</sup>H nmr spectrum of complex L, [Fe(bsb,Ph,Me)<sub>3</sub>]<sup>2+</sup>, is shown in Fig. 6.9. Complex L contains the bidentate ligand derived from 2-benzoyl pyridine and methylamine. The four singlets of greatest intensity in the region of 3.0 to 3.6 ppm, three of equal intensity and the fourth

relatively more intense, are due to the methyl protons in the complex and indicate the presence of both isomeric forms in the sample of the complex. From the integration of these peaks, the ratio of the mer and fac isomeric forms in the sample is 2.3:1. Thus, approximately 30% of the sample is in the fac isomeric form. [The signal of small intensity at 3.35 ppm is due to the presence of diethyl ether used to wash the complex after its preparation. This signal appears as a quartet being due to the resonance of the methylene protons. The signal due to the methyl protons appears as a triplet at 1.05 ppm. These signals, and the small peak at 3.25 ppm, were absent from other spectra obtained for different samples of this complex.] The signals due to the aromatic protons in complex L, both pyridyl and phenyl protons, appear downfield in the region of 7.1 to 8.7 ppm.

Fig. 6.10 shows the  $^1\text{H}$  nmr spectra of complex M,  $[\text{Fe}(\text{bsb},\text{Ph},\text{Ph})_3]^{2+}$ , in  $\text{d}_3$ -acetonitrile measured at 300 MHz. Complex M contains the ligand derived from 2-benzoyl pyridine and aniline. As all the protons in complex M are aromatic, all the resonance signals occur in the low field region and the spectrum is somewhat complex. [The broad peak at approximately 2.35 ppm disappears on shaking the sample with  $\text{D}_2\text{O}$ . This signal, then, is most probably due to water in the sample.] However, two relatively intense doublets can be seen in the higher field region at 5.05 and 5.42 ppm. There are also four less intense signals downfield of these doublets at 5.83, 6.14, 6.57 and 6.71 ppm. These appear to be doublets also. These six doublets are likely to be part of a set of eight doublets which consists of six doublets of relatively low, but equal, intensity and two more intense doublets, the latter doublets being those at 5.05 and 5.42 ppm. The 'missing' two doublets are then taken to be masked by other signals in the region above 6.75 ppm. The

assignment of these signals to the ortho protons in the N-phenyl group, labelled  $H_A$  and  $H_B$  in the ligand inset, is consistent with there being restricted rotation of the phenyl group around the N-C single bond with the result that the  $H_A$  and  $H_B$  protons are not equivalent. [If these signals were due to the resonance of either the meta or para protons in the ring, then they would be expected to have the appearance of triplets.] In such a case, the existence of both of the possible isomeric forms of the complex is indicated. The two more intense doublets at 5.05 and 5.42 ppm are due to the resonance of the  $H_A$  and  $H_B$  protons in the fac isomeric form of the complex. The six doublets at lower fields are due to the resonance of the ortho protons in the mer isomeric form of the complex, i.e. three of the six doublets are due to the  $H_A$  proton and the other three are due to the  $H_B$  proton. Interestingly, the proportion of the fac isomer in the sample appears to be relatively high, as much as 50% of the sample may be in this form.

Fig. 6.11 shows the  $^1H$  nmr spectrum of complex N measured in  $d_3$ -acetonitrile at 300 MHz. Complex N contains the bidentate ligands derived from 2-benzoyl pyridine and *m*-toluidine. There are a number of signals occurring in the region of 1.8 to 2.4 ppm due to the resonance of the methyl protons in the complex. It appeared, however, that none of the samples of complex N were totally free of impurities as the number of peaks in this region differed with the samples of the complex used. By comparison, the position and number of peaks in the lower field region of 4.4 to 8.4 ppm did not change significantly in the spectra of the different samples. For spectra of related compounds (N-phenyl derivatives) discussed previously, signals appearing between approximately 4.0 and 6.7 ppm have consistently been assigned to the resonance of phenyl protons attached to carbon atoms adjacent to the

N-phenyl ring single bond, i.e. ortho protons. Such resonances appeared as either singlets or patterns of doublets depending on whether the constituent attached to the adjacent meta carbon atom was a proton or a methyl group. The same types of signals can be seen in the spectrum of complex N in the region of 4.4 to 6.7 ppm shown in Fig. 6.11. This pattern of signals, however, is less readily interpreted than those previously seen for other complexes. The added complexity presumably arises as a result of restricted rotation about the N-C single bond so that all possible conformations of the N-phenyl ring are not equally populated. This possibility, together with the fact that the complex may exist in mer and fac isomeric forms and that the methyl group attached to the ring is meta substituted thereby removing any possibility of the ortho protons being equivalent, could well account for the increased complexity of the spectrum of complex N. The spectrum of this complex is further discussed in Section 6.3.2.3.

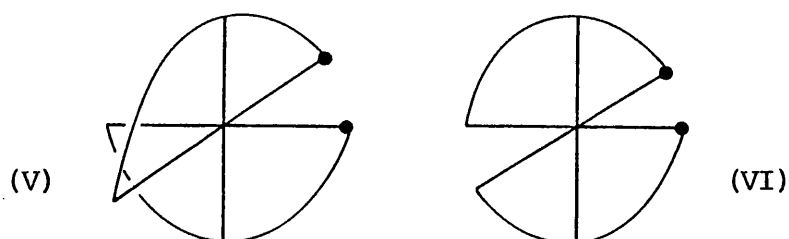
The spectra obtained for complex O were not sufficiently well-resolved to allow useful comparison of the spectra with that of complex N. Although the peaks in the spectra were rather broad, the increased number of the peaks in the region of 4.0 to 6.7 ppm relative to that in the spectrum of complex D, the R=H analogue of complex O, suggested that, as for complexes M and N in which R=Ph, there is restricted rotation of the N-phenyl ring.

#### 6.3.1.3 Bis-(terdentate) and mono-(hexadentate) complexes

$^1\text{H}$  nmr spectra were obtained for three complexes containing unsymmetrical terdentate Schiff base ligands, complexes P, Q and R. Figs. 6.12 and 6.13 show the  $^1\text{H}$  nmr spectra of complexes P,  $[\text{Fe}(\text{tsb},\text{H},8\text{amq})_2]^{2+}$ , and Q,  $[\text{Fe}(\text{tsb},\text{H},8\text{amq})_2]^{2+}$ , respectively, both measured in  $\text{d}_3$ -acetonitrile at 300 MHz. These complexes contain the terdentate ligands derived from

8-aminoquinoline and either pyridine-2-carboxaldehyde (complex P) or 2-acetyl pyridine (complex Q). For both complexes, the presence of only one isomeric form in each sample is evident. In the spectrum of complex P, there is a singlet at 11.06 ppm due to the resonance of the aldehydic-type protons in the complex which are labelled  $H_A$  in the ligand inset in Fig. 6.12. In the spectrum of complex Q, there is a singlet at 3.92 ppm due to the resonance of the methyl protons in the complex which are labelled  $H_A$  in the ligand inset in Fig. 6.13. As both complexes P and Q are of the type  $[FeL_2]^{2+}$  with two terdentate ligands per iron atom, then the singlet nature of these signals indicates that the two isomeric forms detected, one for complex P and one for complex Q, both possess a  $C_2$  rotation axis of symmetry. The  $^1H$  nmr spectrum of complex R, containing the terdentate ligand derived from pyridine-2-carboxaldehyde and 2-picolyamine, measured at 90 MHz also showed a single resonance peak due to the aldehydic-type proton in the expected region of low fields.

Two of the four theoretically possible diastereoisomeric forms of complexes of this type [see Section 1.3.3] possess a  $C_2$  rotation axis of symmetry, those shown in (V) and (VI). In (V), each terdentate



ligand is essentially co-planar, in (VI) the ligands are 'bent'. Formation of complexes of this type in which each terdentate ligand is essentially co-planar is likely to be more favourable, in terms of reduced strain and greater delocalization in the complexes, than that

of complexes in which the terdentate ligands are significantly 'bent'. If, however, the ligands were non-planar then the existence of several diastereoisomeric forms of the complexes would be possible. Having detected the presence of both of the possible diastereoisomeric forms in the related tris-(bidentate) complexes, there is no obvious reason why, if the terdentate ligands were non-planar, that only one of the three possible diastereoisomeric forms would exist in solution. Thus, the indications are that, as expected, these complexes do not exist in more than one diastereoisomeric form due to the essentially co-planar nature of the terdentate ligands.

$^1\text{H}$  nmr spectra of the two hexadentate Schiff base complexes, complexes S and T [see Scheme 6.3], were obtained in  $\text{d}_3$ -acetonitrile at 300 MHz. These spectra of complex S where  $\text{R} = \text{H}$ ,  $[\text{Fe}(\text{hsb}, \text{H}, \text{trien})]^{2+}$ , and complex T where  $\text{R} = \text{Ph}$ ,  $[\text{Fe}(\text{hsb}, \text{Ph}, \text{trien})]^{2+}$ , are shown in Fig. 6.14 and Fig. 6.15 respectively.

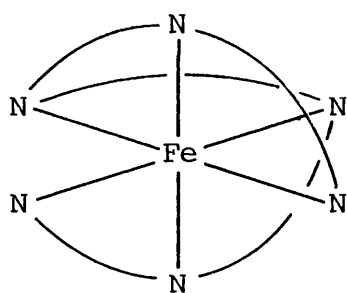
In the spectrum of complex S [Fig. 6.14] four sets of signals are discernible. These signals occur at 9.95 ppm and in the regions 7.1 to 8.2 ppm, 4.7 to 5.3 ppm and 2.6 to 3.1 ppm. From the integration, the ratio of the areas under these sets of peaks is 1:4:4:8. The first two sets of peaks are attributable to the aldehydic-type protons,  $\text{H}_\text{A}$ , and the pyridyl protons,  $\text{H}_\text{B}$ ,  $\text{H}_\text{C}$ ,  $\text{H}_\text{D}$  and  $\text{H}_\text{E}$  respectively. The second two sets are due to the methylene protons, twelve in all, of the types labelled  $\text{H}_\text{F}$  and  $\text{H}_\text{G}$ . The appearance of the four sets of peaks indicates that these signals are due to a single isomeric form of the complex which possesses a two-fold symmetry axis of rotation. Thus, for this isomeric form, the corresponding protons in the two halves of the ligand are equivalent, e.g. the two  $\text{H}_\text{A}$  protons in each ligand molecule are equivalent and absorb at the same field. The same applies to the two  $\text{H}_\text{B}$  protons, the

two H<sub>C</sub> protons, etc.

The signal at 9.95 ppm is due to the resonance of the aldehydic-type protons labelled H<sub>A</sub> in the ligand inset. This signal appears as a doublet of doublets due to the coupling of H<sub>A</sub> with the methylene protons, H<sub>F</sub>. The resonances due to the eight pyridyl protons appear as four signals in the region 7.1 to 8.2 ppm. From the integration, each of these signals corresponds to the resonance of two (equivalent) protons. From correlation tables,<sup>7-9</sup> the signals at 8.14, 7.22, 7.86 and 7.51 ppm can be attributed to the resonances of the H<sub>B</sub>, H<sub>C</sub>, H<sub>D</sub> and H<sub>E</sub> protons respectively. The two sets of peaks in the relatively higher field regions are due to the methylene protons. The signals in the region, 4.7 to 5.3 ppm, are due to the two sets of protons of the type labelled H<sub>F</sub>. The two H<sub>F</sub> protons attached to the same carbon atom are not equivalent. The signals in the region 2.6 to 3.1 ppm are due to the eight methylene protons of the type labelled H<sub>G</sub>. The broad peak at 2.25 ppm disappears upon shaking of the sample with D<sub>2</sub>O. This signal could therefore be due to water. The broad signal at the low field end of the unresolved multiplet around 2.9 ppm also disappears on shaking with D<sub>2</sub>O. This signal, at 3.02 ppm, may be due to the resonance of the N-H protons.

Of the four possible stereoisomers of this complex [see Section 1.3.3] three possess a C<sub>2</sub> rotation axis of symmetry. However, from molecular models, it appears that two of these isomeric configurations possess a relatively high degree of strain as compared with the other possible configuration. This latter isomeric form, shown in (VII), is most likely to be the isomeric form in this sample of complex S. The disposition of the ligand around the central iron atom as shown in (VII) is that found previously in an X-ray crystallographic structural determination of a

sample of this complex.<sup>10</sup> It is interesting to note the similarity of this stereochemical arrangement of the hexadentate ligand around the iron atom with that in the related bis-(terdentate) complexes in which each terdentate ligand is planar (V). In the hexadentate complex, the arrangement of the ligand is the same as in a terdentate complex in which one set of adjacent ends of the two ligands are connected. The presence of several small bumps in the baseline of the spectrum shown



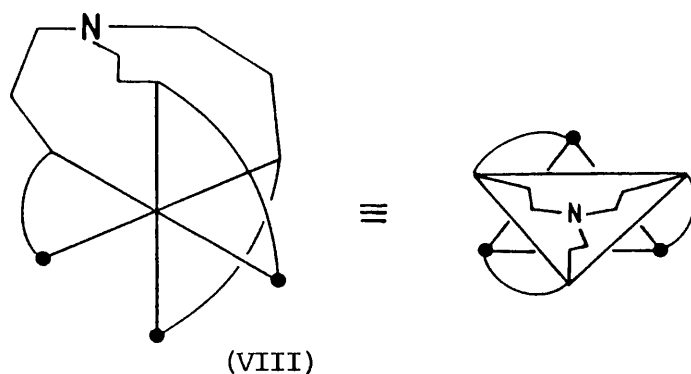
(VII)

in Fig. 6.14, e.g. at 9.15, 8.27, 7.07, 3.62, 3.49 and 3.14 ppm may be due to the presence of a very small amount of another possible isomeric form of the complex. These signals were, however, absent from other spectra of this complex.

The <sup>1</sup>H nmr spectrum of complex T in d<sub>3</sub>-acetonitrile at 300 MHz is shown in Fig. 6.15. The resonance signals due to the aromatic protons, both phenyl, H<sub>A</sub>, and pyridyl, H<sub>B</sub>, appear in the region 7.2 to 8.0 ppm. The chemical shifts of the methylene protons of this complex, 4.5 to 4.9 ppm and 2.6 to 3.1 ppm, are very similar to those of the corresponding protons in the related complex, complex S [Fig. 6.14]. For the complex T, the former peaks are due to the methylene protons labelled H<sub>C</sub>, the latter due to those labelled H<sub>D</sub> in the ligand inset. In the spectrum of complex T, the reduced complexity of the signal due to one of the H<sub>C</sub> protons around 4.65 ppm as compared with the corresponding signal in the spectrum of complex S (at approximately 4.8 ppm in Fig. 6.14) supports

the assignment of these signals to  $H_C$  rather than  $H_D$  in complex T and to  $H_F$  rather than  $H_G$  in complex S. The fine structure of the signal due to the  $H_F$  protons in the spectrum of complex S results from the coupling of the aldehydic-type protons,  $H_A$ , with  $H_F$ . In complex T these aldehydic-type protons are replaced by phenyl groups and, thus, such coupling is absent. In the spectrum of complex T the peak at 3.45 ppm, the integration of which corresponds to two protons, may be due to the two N-H protons. This signal disappears upon shaking the sample with  $D_2O$ . Thus, the spectrum in Fig. 6.15 of complex T is consistent with the presence of one isomeric form only in the sample of the complex. The configuration of this isomeric species is likely to be the same as that of the predominant isomer in the sample of complex S (VII).

The  $^1H$  nmr spectrum of complex U,  $[Fe(hsb,H,t2a)]^{2+}$ , measured in  $d_3$ -acetonitrile at 90 MHz is shown in Fig. 6.16. Complex U contains the hexadentate Schiff base ligand derived from pyridine-2-carboxaldehyde and tris(2-aminoethyl)amine. The nature of this primary amine means that in this complex the three unsymmetrical bidentate di-imine groups must adopt a fac configuration about the central iron atom (VIII). The



resulting complex can possess a three-fold rotation axis of symmetry analogous to those of the tris-(bidentate) complexes. This complex, therefore, provides a possible means of confirming the equivalence of

corresponding protons in the three ligands in the fac isomeric form of this type of complex. In Fig. 6.16, the lone singlet at 9.2 ppm indicates the equivalence of the three aldehydic-type protons in the complex, H<sub>A</sub>. The signals in the region of 7.0 to 8.4 ppm are due to the resonance of the pyridyl protons. The two signals in this group at higher fields, 7.1 and 7.5 ppm, resemble those seen for pyridyl protons in the spectrum of complex S shown in Fig. 6.14 which contained only one isomeric form which possessed a two-fold axis of symmetry. The lower field signal in this region of the spectrum of complex U, around 8.2 ppm, is due to the resonance of two different sets of pyridyl protons and is most likely an amalgamation of two signals similar to those at 7.1 and 7.5 ppm. The resonances due to the twelve methylene protons appear in the region of 2.6 to 3.9 ppm.

### 6.3.2 Further observations

#### 6.3.2.1 General

From <sup>1</sup>H nmr spectra of the tris-(bidentate) complexes mentioned earlier, measured at 90 MHz, it was seen that different samples of the same complex contained differing proportions of the isomers. In the vast majority of cases the complexes existed predominantly in the mer isomeric form. In general, the samples of the complexes prepared by modified method (V) [see Section 6.2] contained in the region of 20% of the fac isomeric form. However, in a small number of cases, the proportions of the fac isomeric form in the samples of the complexes were significantly higher. For complexes E, K and M, spectra were obtained showing that the samples contained approximately equal proportions of the two isomers.

In Chapter 5 it was seen that, for some complexes of this type, the proportion of isomers in a solution of a complex in water + methanol

mixtures appeared to change with time. Unfortunately, the insufficient degree of solubility of these complexes in such solvent mixtures made it impossible to monitor any such change in these solvent mixtures by  $^1\text{H}$  nmr spectroscopy. For some spectra of the complexes measured in deuterated methanol, peaks were discernible in the same resonance absorption regions as in spectra of the complexes measured in  $\text{d}_3$ -acetonitrile. Such spectra were, however, generally very poorly resolved and very noisy. For all the complexes,  $^1\text{H}$  nmr spectra obtained for a given sample of a complex in  $\text{d}_3$ -acetonitrile over a period of time showed no significant changes in the proportion of isomers in the sample. For example, the nmr spectrum of complex A,  $[\text{Fe}(\text{bsb},\text{H},\text{Me})_3]^{2+}$ , was measured immediately after being made-up and then again several weeks later. From the integration of the aldehydic-type proton and methyl proton peaks, the sample contained 20% and 18% of the fac isomeric form respectively.

It was also related in Chapter 5 how the preparative method of the complexes appeared to affect the proportion of isomers in the resulting samples of the complexes. For example, the longer the preparative solution of a complex was left to stand before the complex was precipitated as a salt, the more unequal was the proportion of isomers in the resulting sample. This was confirmed using nmr spectroscopy in the following way. Several of the tris-(bidentate)iron(II) complexes, namely complexes A, K, L and M, were generated in solution using modified method (V) [see Section 6.2]. These preparative solutions of the complexes were then split into several portions. The hexafluorophosphate salts of the complexes were precipitated immediately from one portion of the preparative solutions of each of the complexes. The following day another set of hexafluorophosphate salts of the complexes were precipitated from a second set of portions of the preparative solutions. This procedure was repeated for

several days. For each complex,  $^1\text{H}$  nmr spectra showed that the longer the preparative solution of a complex was left before precipitation of the salt, the smaller was the proportion of the fac isomeric form in the resulting sample of the complex. This was observed in all cases. Thus, it appears that the fac isomeric form of these complexes is less stable than the mer isomeric form in water + methanol mixtures.

It was found that the complexes were soluble enough in  $\text{d}_6$ -acetone to, in general, produce satisfactory spectra of these complexes. It was difficult to assess any effect on the proportion of isomers in the samples of the two solvents as even for different portions of the same sample, spectra measured in  $\text{d}_3$ -acetonitrile gave values for the proportion of the isomers in the sample which differed by several percent. However, the values obtained for the complexes in  $\text{d}_6$ -acetone were in the same region (on average around 20% of each sample was in the fac isomer form) as those obtained for the complexes in  $\text{d}_3$ -acetonitrile. In terms of the appearance of the spectra of complexes in  $\text{d}_3$ -acetonitrile and  $\text{d}_6$ -acetone, the number and multiplicities of the signals were not significantly different. In some cases shifts in the positions of peaks of up to 0.2 ppm when comparing spectra of the same complex measured in the two solvents were observed.

#### 6.3.2.2 Temperature effects

The  $^1\text{H}$  nmr spectra obtained for the tris-(bidentate) complexes measured at 300 MHz in  $\text{d}_3$ -acetonitrile at 298 K indicated that, for the complexes in which R' is a phenyl or substituted phenyl group, there was essentially free rotation of the N-phenyl rings when R was H. For the related complexes in which R was Me, rotation of the N-phenyl rings was restricted. With this in mind,  $^1\text{H}$  nmr spectra for complexes K and C were measured at temperatures other than 298 K.

The effect of temperature on the appearance of signals occurring in the region of 4.4 to 9.0 ppm in a  $^1\text{H}$  nmr spectrum obtained for a sample of complex K measured in  $\text{d}_6$ -acetone at 300 MHz is shown in Fig. 6.17. This complex,  $[\text{Fe}(\text{bsb},\text{Me},\text{Ph})_3]^{2+}$ , contains the bidentate ligand derived from 2-acetyl pyridine and aniline. By comparison of this spectrum measured at 298 K with that shown for the complex measured in  $\text{d}_3$ -acetonitrile at 298 K, shown in Fig. 6.8, it can be seen that the sample used to obtain the former spectrum contained significantly more of the fac isomer. In Fig. 6.17, the spectra obtained for the sample at 298, 303, 313 and 323 K are shown. In these spectra, the relatively intense peaks at 4.67 and 5.46 ppm are due to the resonance of the ortho protons, labelled  $\text{H}_A$  in the ligand inset, in the fac isomeric form of the complex. The relatively weak peaks at 4.98, 5.40, 6.42, 6.76 and 6.88 ppm are five of a set of six signals due to the resonance of the  $\text{H}_A$  protons in the mer isomeric form. Two signals appear due to the  $\text{H}_A$  protons in the fac isomer and six signals appear due to the  $\text{H}_A$  protons in the mer isomer because of restricted rotation of the N-phenyl rings. With increasing temperature, there is obvious broadening of the peaks at 4.98, 6.42, 6.76 and 6.88 ppm indicating increased rate of rotation of the N-phenyl rings. The energy barrier to flipping appears to be different for each of the three N-phenyl rings in the mer isomeric form. The peaks due to the  $\text{H}_A$  protons in the fac isomeric form have broadened only slightly in the spectrum measured at 323 K indicating that the barrier to flipping for the N-phenyl rings in the fac isomeric form is greater than those in the mer isomeric form. With increasing temperature, the resolution of the signals in the spectra due to undeuterated solvent, the methyl protons in the complex and the pyridyl protons (low field region in the spectra shown in Fig. 6.17) remained unchanged.

Fig. 6.18 shows the effect of reduced temperature on the signals due to the ortho and meta phenyl protons, labelled  $H_A$  and  $H_B$  respectively in the ligand inset, in complex C. This complex,  $[\text{Fe}(\text{bsb}, \text{H}, \text{Ph}: \text{p-Me})_3]^{2+}$ , contains the bidentate ligand derived from pyridine-2-carboxaldehyde and *p*-toluidine. Fig. 6.18 shows the appearance of spectra obtained for a sample of the complex in  $d_3$ -acetonitrile measured at 300 MHz at 298 and 273 K. From the spectra measured at 298 K, it can be seen that the *N*-phenyl rings in the *fac* isomeric form of the complex are rotating fast enough for only one signal to be apparent for the two  $H_A$  protons and for only one signal to be apparent for the two  $H_B$  protons (i.e. the signals at 5.38 and 7.07 ppm). Similarly, the *N*-phenyl rings in the *mer* isomeric form of the complex are rotating fast enough for one signal due to the two  $H_A$  protons and one signal due to the two  $H_B$  protons to be apparent for each of the three bidentate ligands (i.e. the signals at 6.12, 6.61, 6.69, 6.84, 7.03 and 7.21 ppm). In the spectrum measured at 273 K, there is a noticeable loss of resolution for the signals due to the  $H_A$  and  $H_B$  protons in the *mer* isomeric form. Any change in the corresponding signals due to the  $H_A$  and  $H_B$  protons in the *fac* isomeric form is less evident. The other signals in the two spectra, those appearing at lower fields (pyridyl protons) and those appearing at higher fields (methyl protons and undeuterated solvent) were identical. Thus, it appears that lowering the temperature of a sample of this complex results in a slowing down of the rotation of the phenyl rings. As was seen in the spectra of complex K measured at higher temperatures, the effect of temperature on the rate of rotation of the phenyl rings in the *fac* isomeric form of the complex appears to be less than that observed for the corresponding rings in the *mer* isomeric form of the complex.

### 6.3.2.3 Two-dimensional spectrum of complex N

The  $^1\text{H}$  nmr spectrum of the tris-(bidentate) complex, complex N, containing the bidentate ligand derived from 2-benzoyl pyridine and *m*-toluidine that was shown in Fig. 6.11, proved to be less readily interpretable than spectra of related complexes presented prior to that of complex N. The probable existence of two isomeric forms in the sample and the possibility of the N-phenyl ring existing in two, or maybe more, conformations was presumed to be the reason. For this complex, in which R' is a meta-methyl substituted phenyl group (meta substituted relative to the N-C single bond), the nature and chemical shifts of the signals due to the two ortho protons in the N-phenyl group would be expected to be different. The chemical shifts of the same ortho proton in different conformeric environments would also not be expected to be the same. In an attempt to gain more information concerning the nature of the complex species in the samples of this complex, a two-dimensional  $^1\text{H}$  nmr spectrum was obtained for this complex in  $\text{d}_6$ -acetone measured at 300 MHz by a 'COSY' experiment. The one- and two-dimensional spectra obtained for this sample are shown together in Fig. 6.19. Unfortunately, the resolution in the spectrum of the sample used in this experiment was not as good as that observed in the spectrum shown in Fig. 6.11. However, as far as could be seen, the two spectra were very similar in appearance in the region of interest, 4 to 7 ppm. Using the two-dimensional spectrum, the following observations were made, chemical shifts of signals quoted referring to those in the one-dimensional spectra shown in Fig. 6.19. Taking into account the degree of resolution observed in this spectrum, resonances due to protons labelled  $\text{H}_\text{A}$  in the ligand inset in Fig. 6.19 would be expected to have the appearance of singlets and those due to the  $\text{H}_\text{B}$  protons to have the appearance of doublets. In the

region of 4.5 to 5.7 ppm there are three peaks of the former type of similar intensities, those at 4.65, 4.90 and 4.95 ppm. The signal centred around 4.93 ppm, although having the appearance of a doublet, was judged from the two-dimensional spectrum to be two singlets. From the two-dimensional spectrum, these three signals can be seen to be coupled to the doublets occurring at 5.55, 5.35 and 5.40 ppm respectively. These latter two signals are partially masked by other signals having very similar chemical shifts. There are singlets of smaller, but very similar, intensities at 4.85, 5.10 and 5.15 ppm which are coupled with doublets occurring at 6.05, 5.35 and 5.20 ppm respectively. There also appears to be coupling between another signal in the complex signal around 5.35 ppm and one in the signal around 5.25 ppm. The three singlets of greater intensity may be due to the resonance of the  $H_A$  protons in the mer isomeric form of the complex when the N-phenyl rings exist in the more favourable conformeric state, each signal being due to one of the three  $H_A$  protons in the mer isomer. The three singlets of smaller intensity may be due to the resonance of the  $H_A$  protons when the N-phenyl rings exist in another conformation, i.e. the rings have 'flipped'. As it is unlikely that all three N-phenyl rings will always be the same conformeric state at the same time, then, this assignment requires the flipping of the N-phenyl ring in one of the ligands to have no effect on chemical shifts of the protons in the other two ligands. Then, the six signals can be viewed as three sets of two signals, each pair of signals due to one  $H_A$  proton corresponding to the chemical shifts of  $H_A$  in two different conformeric states. The partially masked signals in the region of 4.5 to 6.2 ppm may be due to the presence of the fac isomeric form in the sample.

The doublets occurring at 6.38, 6.60 and 6.65 ppm in the spectrum

shown in Fig. 6.19 appear to be coupled only with protons whose resonance occurs downfield of these signals. In the spectrum shown in Fig. 6.11, four of these types of doublets can be seen (at 6.25, 6.47, 6.53 and 6.65 ppm). These signals may be due to the ortho protons of the second phenyl ring in the complex labelled H<sub>C</sub> in the ligand inset of Fig. 6.19. If these four doublets are taken to be due to the H<sub>C</sub> protons in the mer isomeric form of complex N, then the implications are that the two H<sub>C</sub> protons are not equivalent and that there is restricted rotation of this phenyl ring also.

### 6.3.3 The occurrence and nature of the diastereoisomeric forms

This chapter, Chapter 6, and the previous chapter, Chapter 5, have both been concerned with the detection of isomeric forms of some low-spin iron(II) Schiff base complexes containing unsymmetrical ligands. In Chapter 5, the emphasis in effecting such a detection lay with the expected different reactivities of the possible isomeric species, i.e. the subject was approached from a kinetic aspect. In this chapter, Chapter 6, the more fundamental aspect of the differing spatial orientations of the constituent atoms in the possible isomeric forms of the complexes was utilized in detecting the isomers, i.e. <sup>1</sup>H nmr spectroscopy was used as a probe to detect the presence of isomers. Thus information concerning the existence of isomeric forms of the complexes was obtained using two complementary techniques.

For all the tris-(bidentate) complexes studied using the <sup>1</sup>H nmr technique in this chapter, whether R was H, Me or Ph and R' was an alkyl or aryl group, the presence of diastereoisomeric forms of the complexes was evident. This supports the attribution of the seemingly erratic kinetic behaviour of the complexes, as discussed in Chapter 5, to the existence of diastereoisomeric forms of the complexes having different

reactivities. The results of the kinetic investigation pointed to the existence of such isomers and for complexes where R = Ph it proved possible, by re-analysis of the raw kinetic data, to rationalize the observed kinetic trends in terms of the existence of such isomers. The reactions of the complexes where R = H were too fast to permit similar re-analysis of the relevant data, although the deviations from the first-order plots and the ultraviolet/visible absorption spectra of the reactions suggested the existence of isomers of these complexes also. The existence of such isomers for complexes where R = H has not always been universally agreed upon in the past.<sup>11,12</sup> By using the nmr technique, however, all the complexes of this type studied here, whether R = H, Me or Ph, were shown to exist in diastereoisomeric forms. Sparse kinetic evidence in the literature for the existence of isomers in complexes of this type where R = H may be, amongst other things, the result of the preparative methods used in obtaining samples of the complexes. If the time scales of the synthetic procedures used were relatively long, and samples were re-crystallized once or more than once, then the samples may have indeed been isomerically pure. Alternatively, reactivities, ultraviolet/visible absorption spectra, etc., of the diastereoisomers may not have been sufficiently different to permit detection. There is also the possibility that the relative solubilities and/or stabilities of the diastereoisomers may have been different enough, in the solvents used, to result in the solutions of the complexes used in the experiments being isomerically pure.

From the kinetic investigation, the proportion of isomers in a solution of a complex in water + methanol mixtures was seen to change over a period of time, both for the preparative solutions and the solutions of the complexes used in the kinetic determinations. This was affirmed by

$^1\text{H}$  nmr spectroscopy by which means the proportion of the fac isomers in the preparative solutions of several complexes was seen to decrease with time. Thus, the fac isomeric forms of these complexes appear to be less stable in aqueous solutions and water + methanol solutions than the mer isomeric forms of the complexes. Although this appears to be the case for the tris-(bidentate) complexes in which R' is either an uncharged alkyl or aryl group, there is evidence presented and discussed in Section 7.4 in the next chapter, that for complexes in which R' is OH the reverse may be true. From the kinetic studies, the solutions were seen to become richer in the slower reacting isomeric species and thus it appears that, for the complexes concerned, the mer isomer is the slower reacting isomer in terms of base hydrolysis and the fac isomer is the faster reacting isomer.

Solutions of the tris-(bidentate) complexes in acetone and in acetonitrile were more stable than those of the complexes in water or in aqueous alcohol mixtures. In general, stoppered vessels containing the former types of solutions retained their intense colours for months. For the latter solutions, the colour of the complexes disappeared in a matter of a few weeks, sometimes days. The increased stability of the complexes in acetonitrile was evident from  $^1\text{H}$  nmr spectra in which the proportion of the isomers in samples of the complexes remained the same over a period of time. Interestingly, in water + methanol mixtures, the rate of change of the proportion of isomers in samples of the complexes appeared to be dependent on the concentration of the solution. From the kinetic investigation, weak solutions of the complexes ( $10^{-4}$  to  $10^{-5}$  M) initially containing both isomers were found to contain the slower reacting isomers, evidently the mer isomeric forms, after a period of days. For the preparative solutions, vastly more concentrated, this

process appeared to take much longer. For example, for the complex in which  $R=H$  and  $R'=Me$ , a preparative solution of the complex found initially to contain 19% of the fac isomeric form, still contained 12% of the fac isomeric form after approximately one week. If the change in the proportion of the isomers proceeds, partly or wholly, by relatively fast decomposition of the fac isomeric form of the complex then the observed effect may be the result of the presence of unreacted ligand molecules in the preparative solutions retarding the rates of decomposition of the complexes.

The mechanism by which the proportions of the isomers change in aqueous and in aqueous methanol solutions is not clear. Differing rates of decomposition of the isomers and isomerization of the fac into the mer isomer (intramolecularly and/or involving bond breaking) are limiting possibilities. More likely, though, is that the changes in the proportions of the isomers in these solutions are a result of an amalgamation of these effects. The unchanging nature of the proportions of the isomers in solutions of the complexes in acetonitrile being paralleled by the relatively high stability of the complexes in this solvent would suggest this to be the case. This in turn implies that, in acetonitrile at least, conversion of the fac to the mer isomer by intramolecular isomerization is unimportant.

The proportion of the isomers in a sample of the complex appeared to depend mostly on the method of preparation of the complex. There did not seem to be any correlation between the size and nature of the groups  $R$  and  $R'$  in the complexes, see (I), and the proportion of isomers in the samples. Although the general predominance of the mer isomeric form over the fac isomer may be in some way a result of steric effects, there are likely to be other factors involved also. The reason for the predominance

may be in part statistical as, if three bidentate ligands are arranged randomly round an iron atom in an octahedral fashion one by one, then a greater percentage of the resulting complex ions will have the mer configuration than will have the fac configuration. There may also be electronic effects and solvent effects making the formation of the mer isomeric forms of the complexes the more favourable of the two.

For the tris-(bidentate) complexes in which  $R = H$  and  $R' = Ph$  or a substituted phenyl group, it was found that in  $d_3$ -acetonitrile and  $d_6$ -acetone the N-phenyl ring was rotating relatively fast such that for each phenyl proton, a single time-averaged set of signals was observed in the  $^1H$  nmr spectra of the complexes. Replacement of a proton by a methyl or phenyl group, i.e.  $R = Me$  or  $Ph$  instead of  $H$ , led to restricted rotation of the N-phenyl rings such that resonance absorption of the phenyl protons in different conformeric positions was observed.

For the bis-(terdentate) complexes studied by  $^1H$  nmr spectroscopy, only one stereoisomeric form was present in each of the samples. From molecular models, it is likely that this form is that in which the two terdentate ligands are both coplanar. In such a case, no diastereoisomers of the complex exist.

For the mono-(hexadentate) complexes,  $^1H$  nmr spectra did not reveal the presence of isomeric forms of the complexes in the samples of the complexes (although for complex S,  $[Fe(hsb,H, trien)]^{2+}$ , containing the ligand derived from pyridine-2-carboxaldehyde and triethylenetetramine, there was a slight possibility that a second isomeric form may have been present in a very small amount in one sample of the complex). In contrast, kinetic investigations have repeatedly suggested the presence of isomeric forms in samples of complex T,  $[Fe(hsb, Ph, trien)]^{2+}$ , containing the ligand derived from 2-benzoyl pyridine and triethylenetetramine, but

not in samples of complex S, the R = H analogue of complex T. It could be that for complex T, the deviations from first-order kinetics observed in the study of alkali fission of the complex were a result of something other than the existence of diastereoisomeric forms of the complex. This could also apply to the observed shifts in  $\lambda_{\max}$  towards longer wavelengths during alkali fission of the complex. These observations could, for instance, reflect the existence of intermediates of reduced coordination numbers having relatively high stabilities. Alternatively, the samples of complex T used in the nmr study could have contained isomers in which the corresponding protons used to characterise the spectrum had, coincidentally, the same chemical shifts.

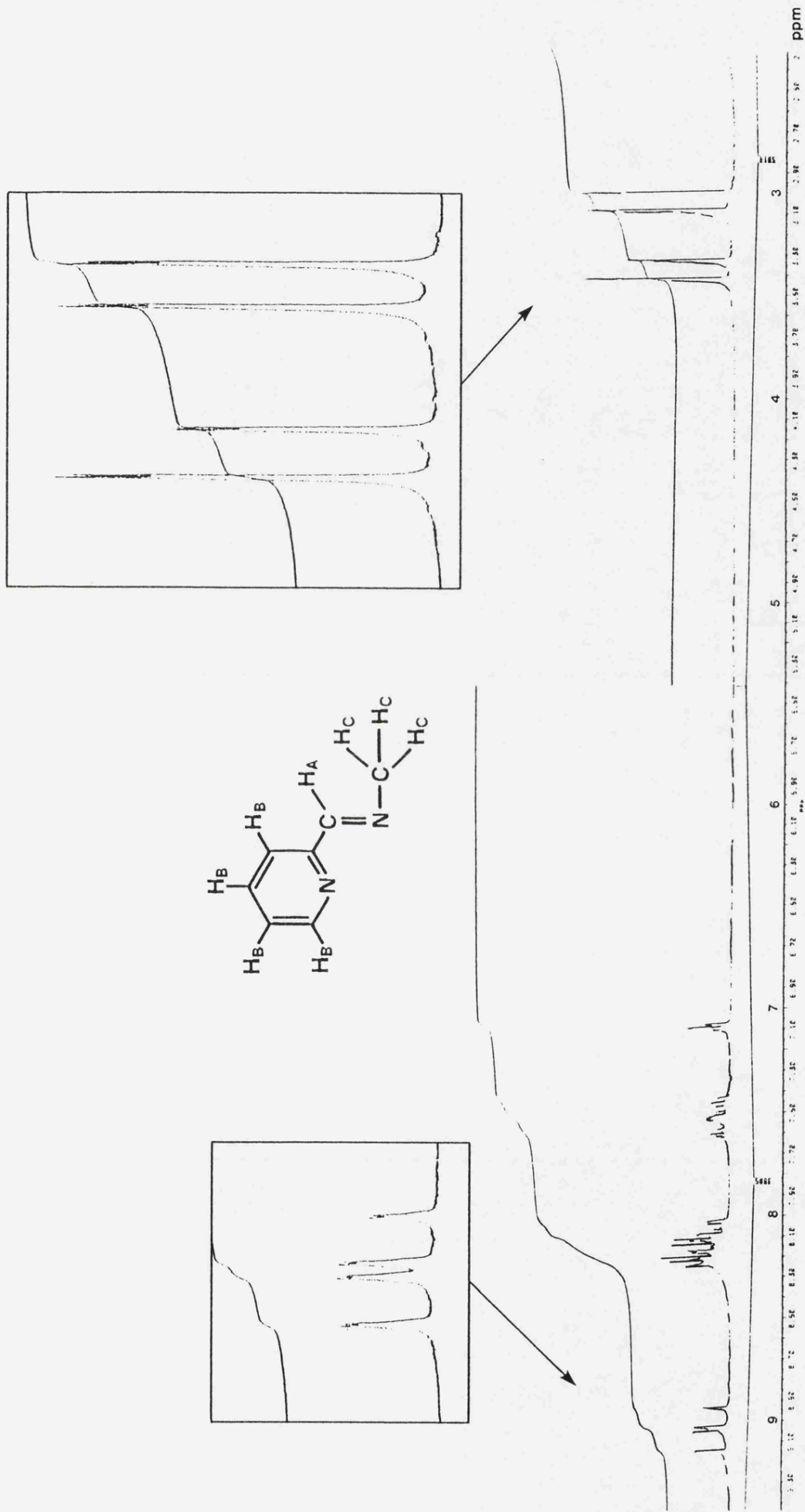
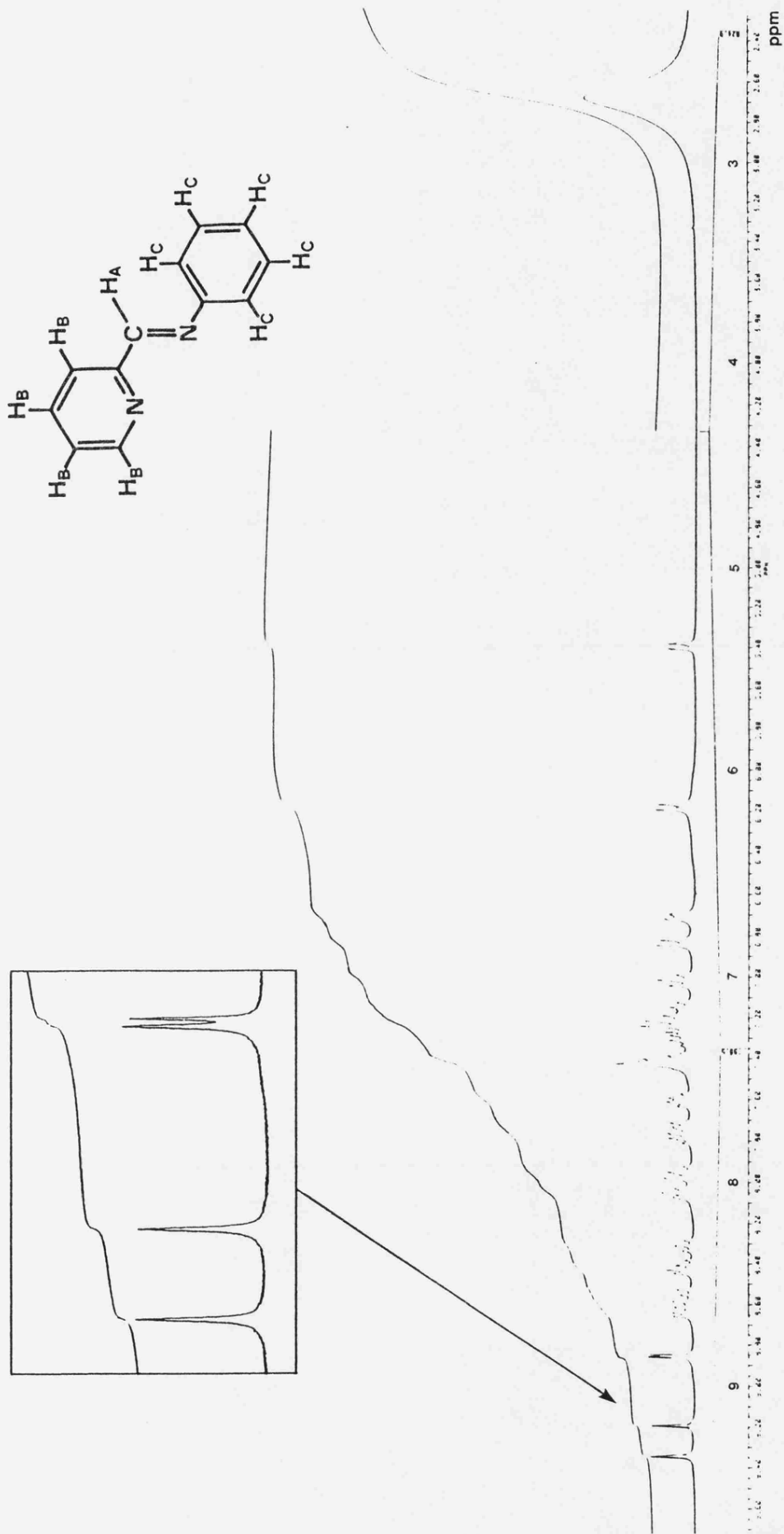


FIGURE 6.1  
<sup>1</sup>H nmr spectrum of complex A, [Fe(bsb,H,Me)<sub>3</sub>]<sup>2+</sup>, in d<sub>3</sub>-acetonitrile.



**FIGURE 6.2**  
 $^1\text{H}$  nmr spectrum of complex B,  $[\text{Fe}(\text{bsb}, \text{H}, \text{Ph})_3]^{2+}$ , in  $\text{d}_3$ -acetonitrile.

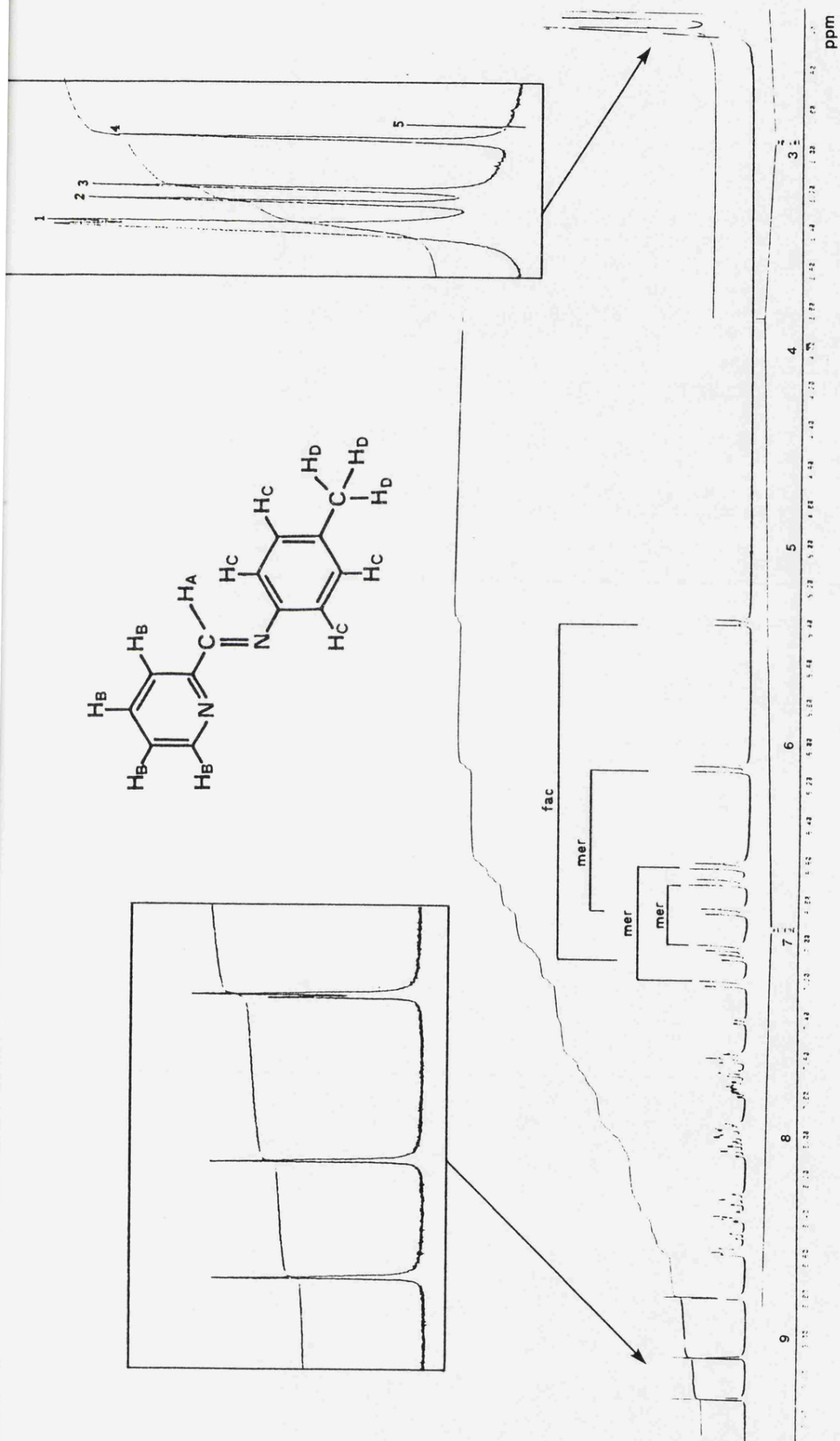


FIGURE 6.3  
 $^1H$  nmr spectrum of complex C,  $[Fe(bsb, H, Ph:p-Me)_3]^{2+}$ , in  $d_3$ -acetonitrile.

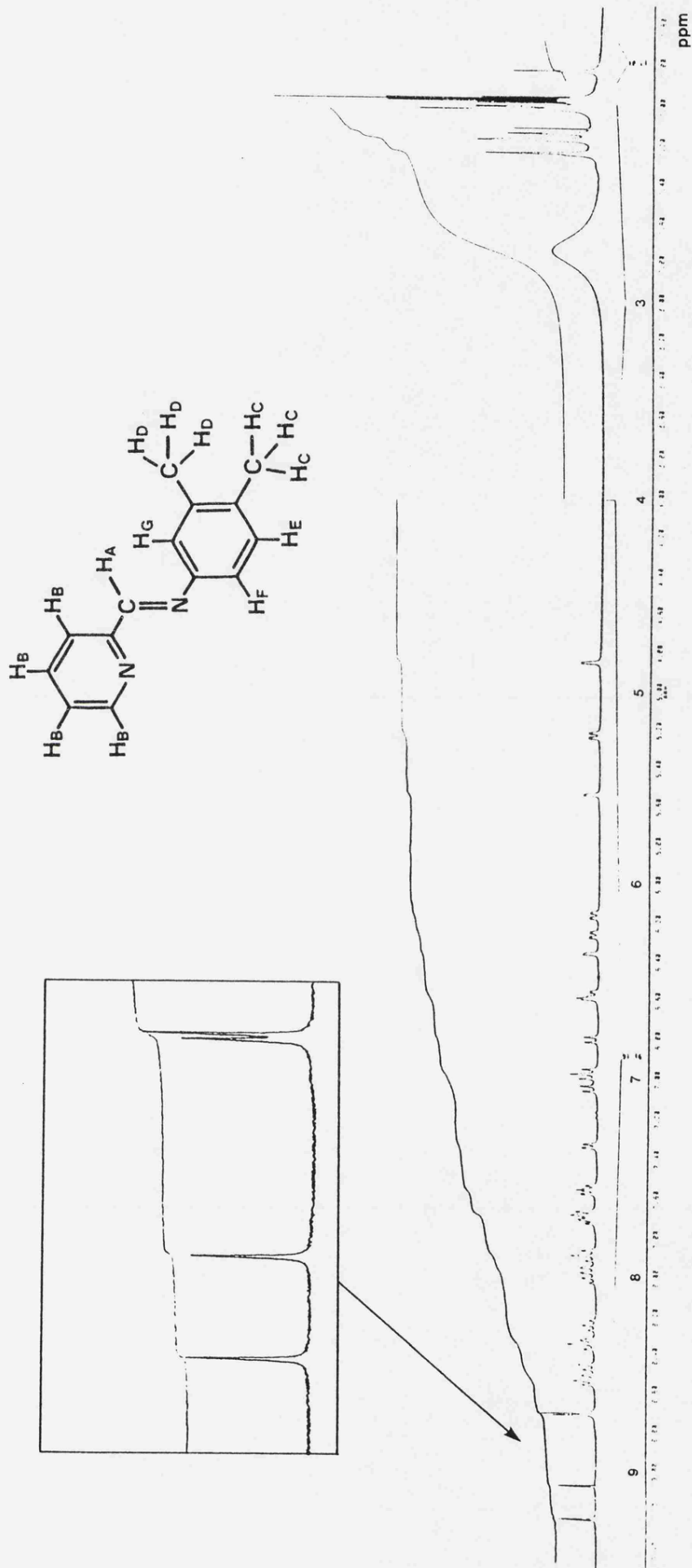
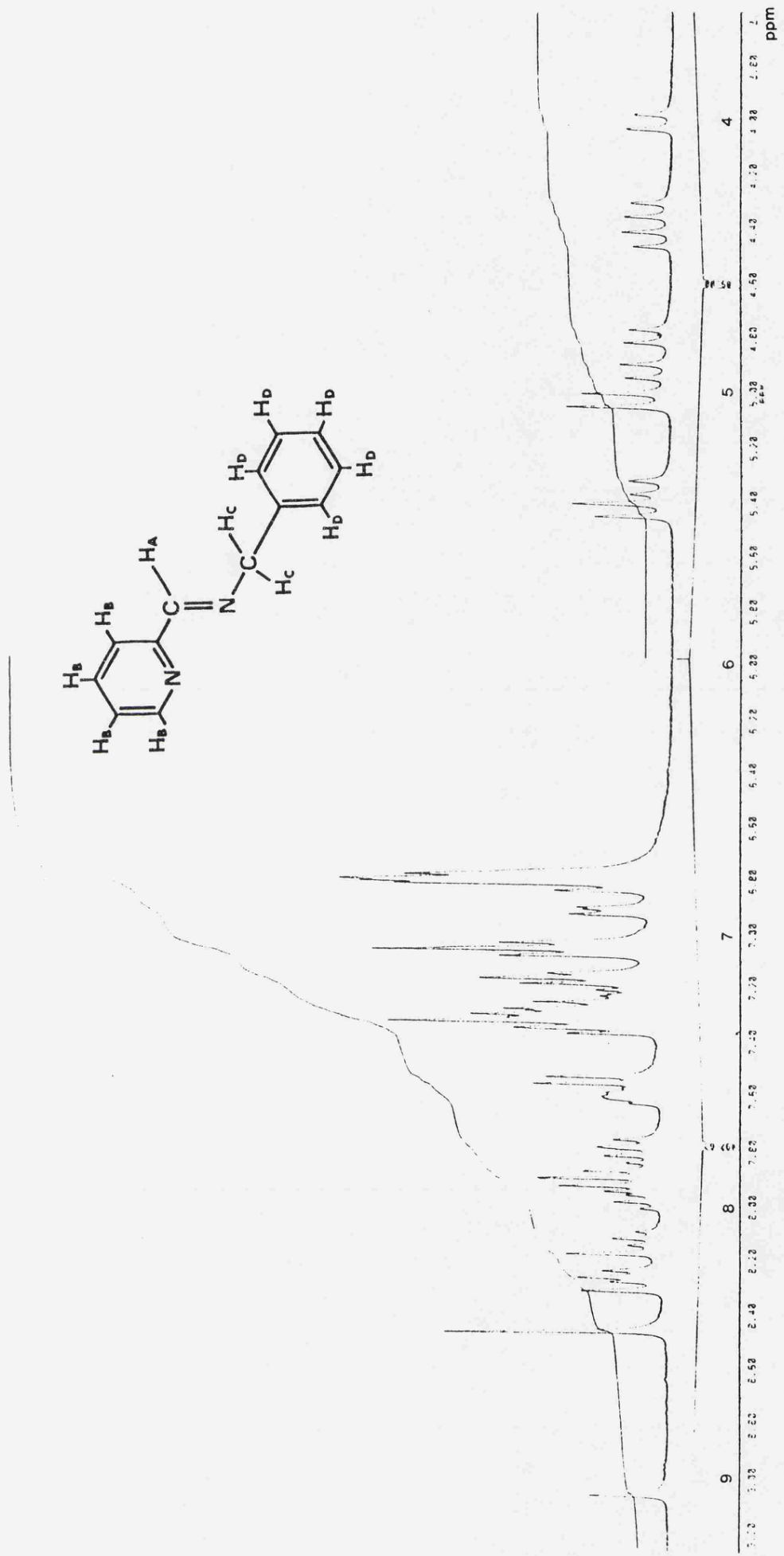


FIGURE 6.4

$^1\text{H}$  nmr spectrum of complex D,  $[\text{Fe}(\text{bsb}, \text{H}, \text{Ph}:3,4\text{-Me}_2)_3]^{2+}$ , in  $\text{d}_3$ -acetonitrile.



**FIGURE 6.5**  
 $^1\text{H}$  nmr spectrum of complex E,  $[\text{Fe}(\text{bsb},\text{H},\text{CH}_2\text{Ph})_3]^{2+}$ , in  $\text{d}_3$ -acetonitrile.

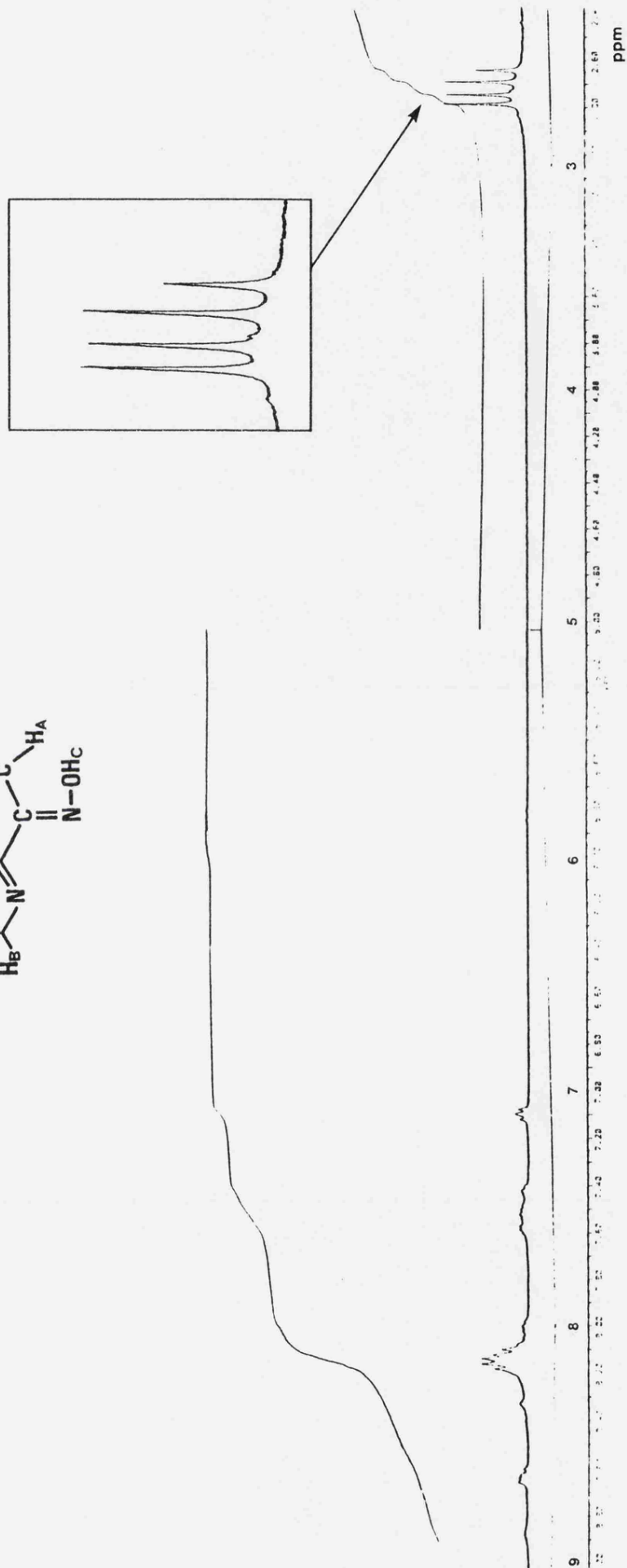
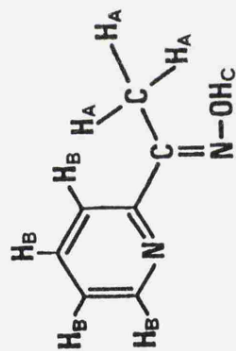
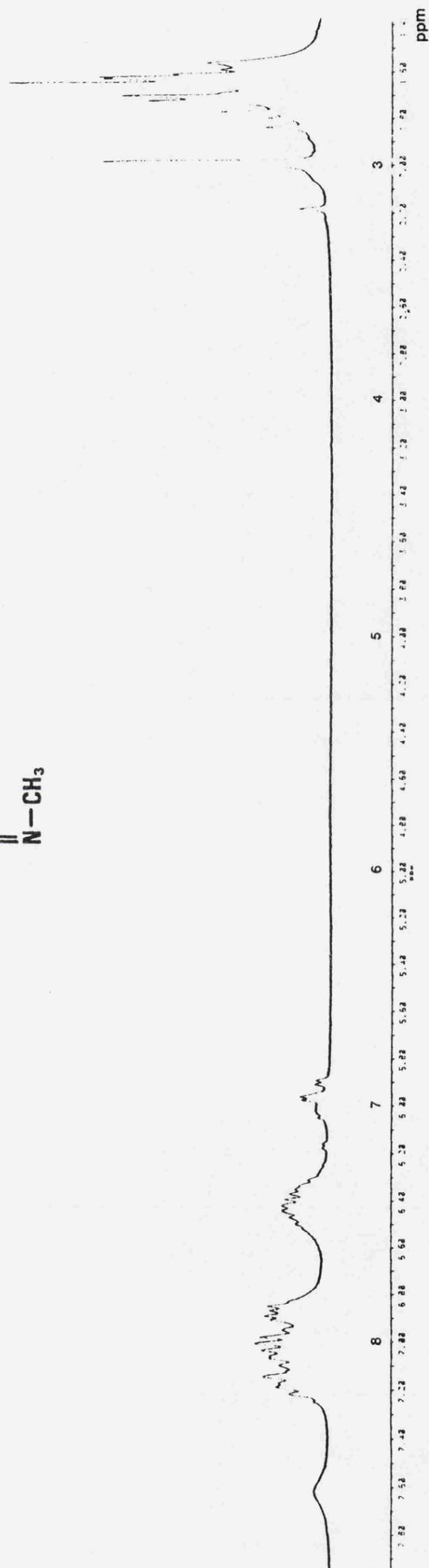
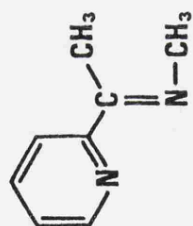


FIGURE 6.6

$^1H$  nmr spectrum of complex I,  $[Fe(bsb, Me, OH)_3]^{2+}$ , in  $d_3$ -acetonitrile.



**FIGURE 6.7**  
<sup>1</sup>H nmr spectrum of complex J, [Fe(bsb,Me,Me)<sub>3</sub>]<sup>2+</sup>, in d<sub>3</sub>-acetonitrile.

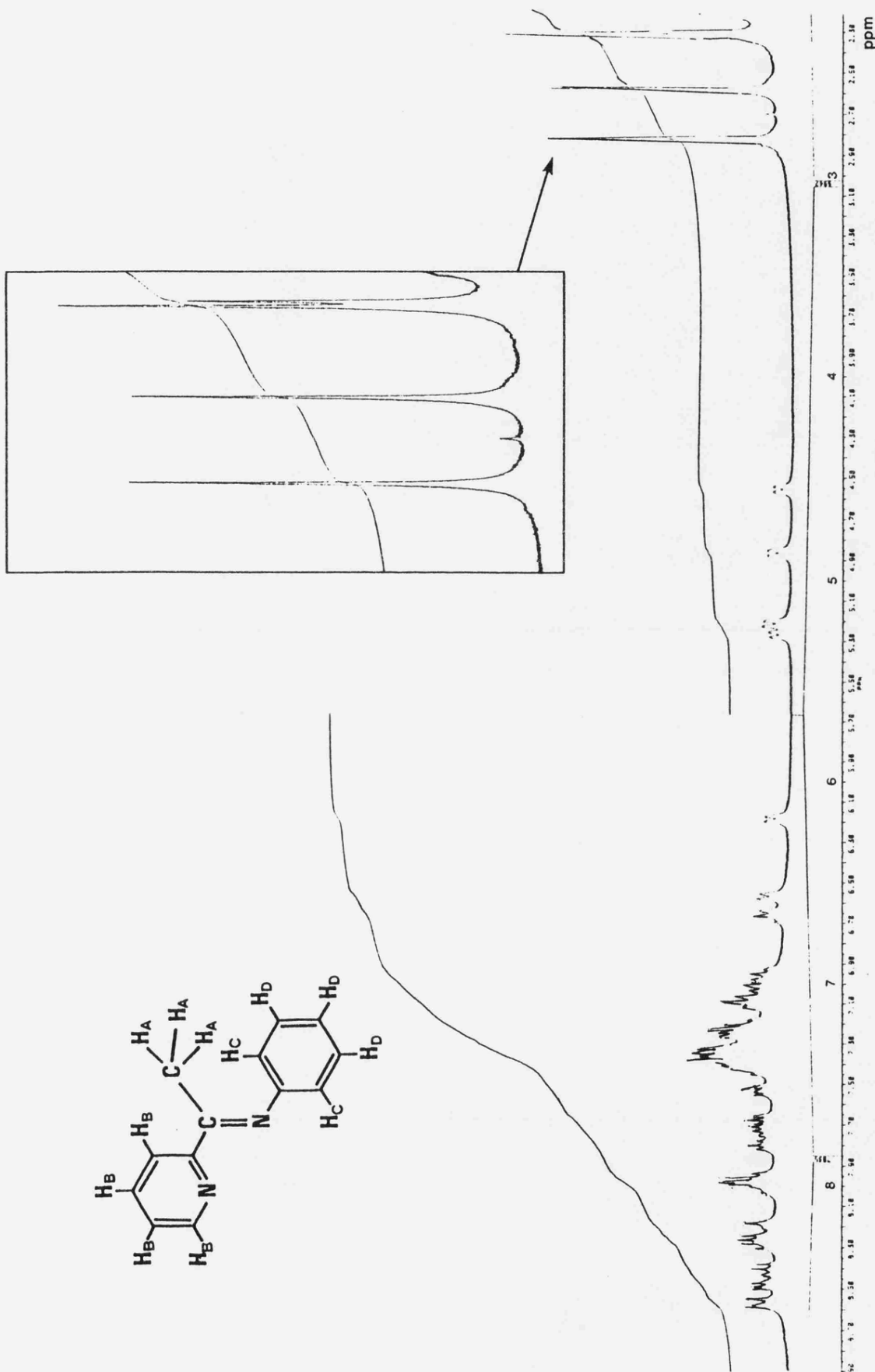
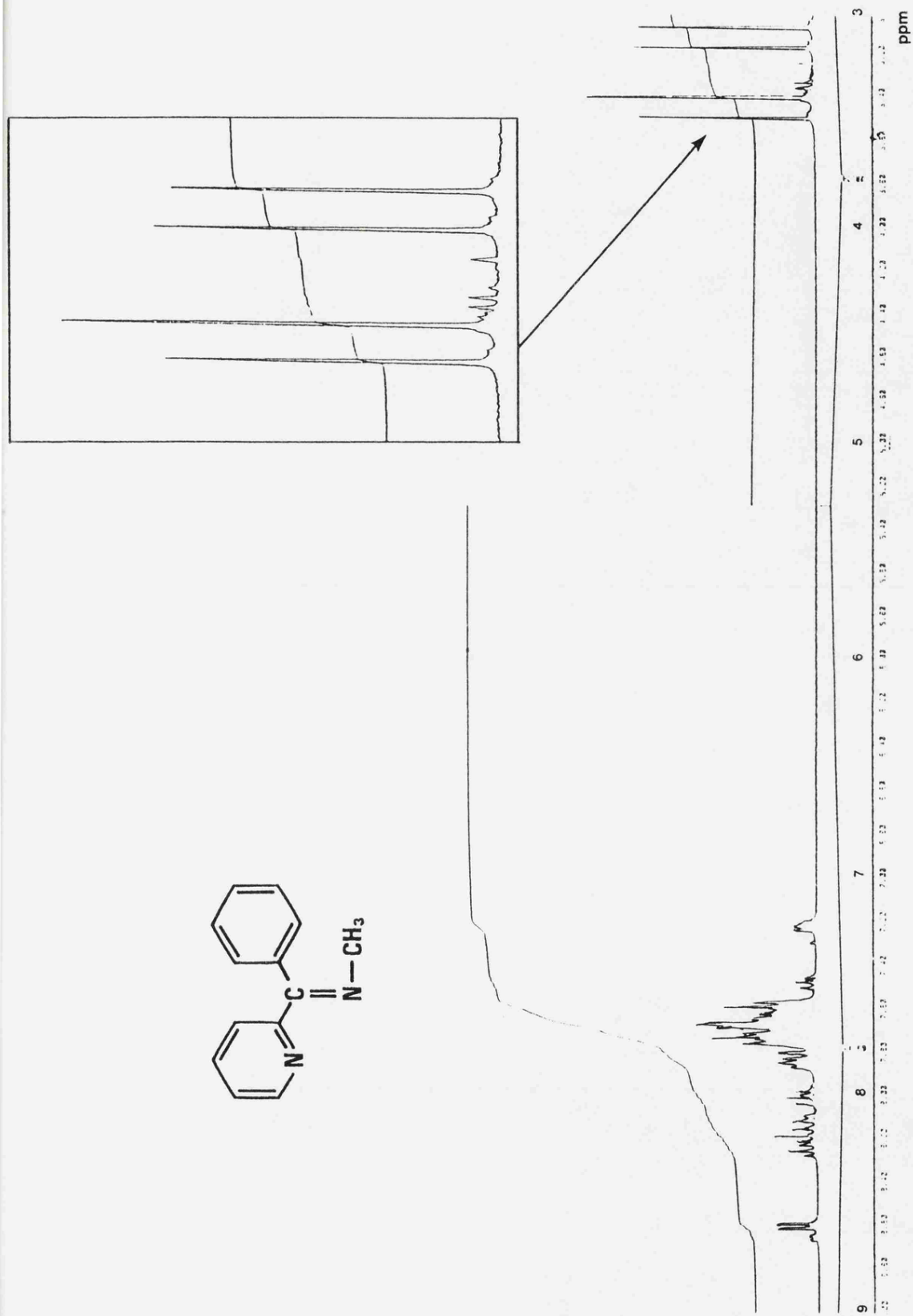
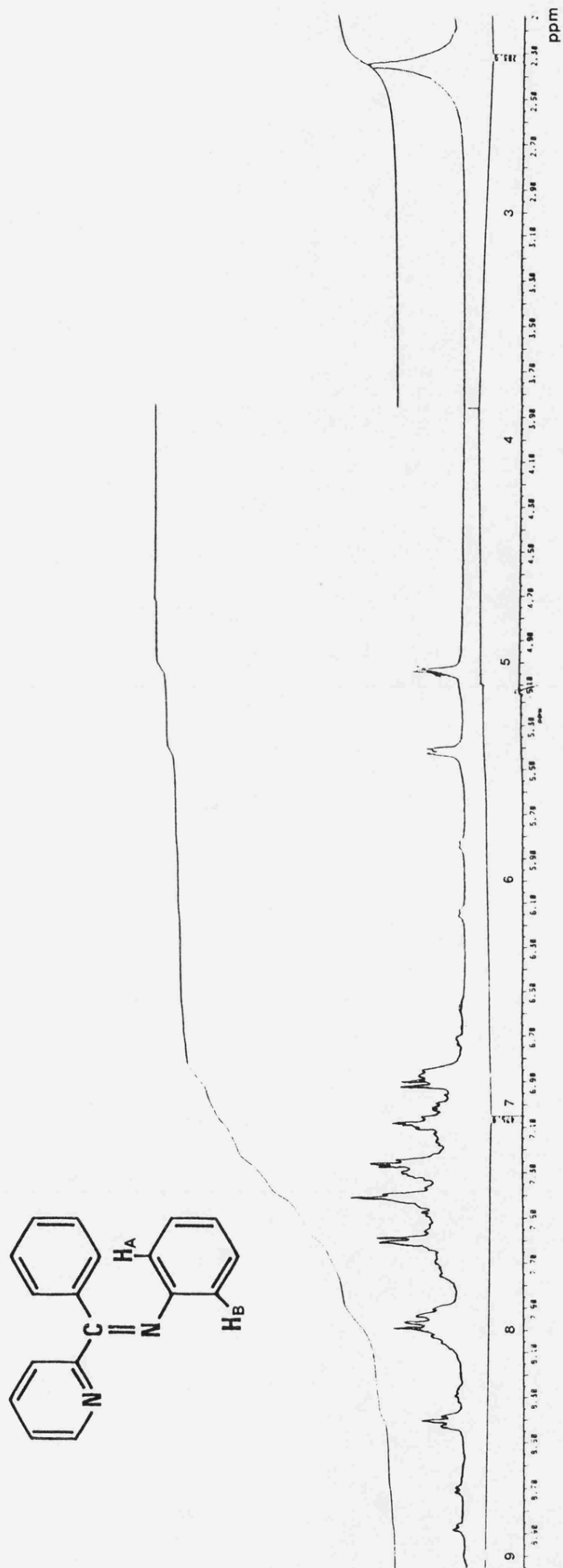


FIGURE 6.8  
 $^1\text{H}$  nmr spectrum of complex K,  $[\text{Fe}(\text{bsb}, \text{Me}, \text{Ph})_3]^{2+}$ , in  $\text{d}_3$ -acetonitrile.



**FIGURE 6.9**  
 $^1\text{H}$  nmr spectrum of complex L,  $[\text{Fe}(\text{bsb}, \text{Ph}, \text{Me})_3]^{2+}$ , in  $\text{d}_3$ -acetonitrile.



**FIGURE 6.10**  
<sup>1</sup>H nmr spectrum of complex M, [Fe(bsb,Ph,Ph)<sub>3</sub>]<sup>2+</sup>, in d<sub>3</sub>-acetonitrile.

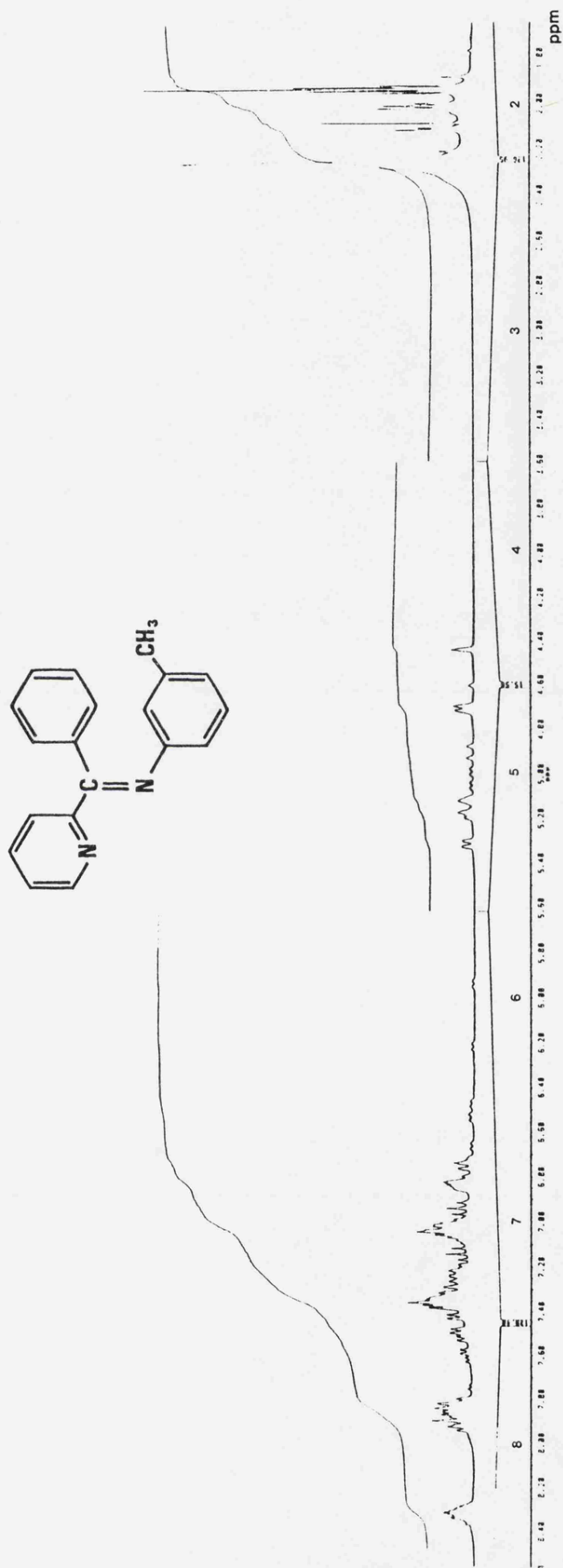


**FIGURE 6.11**  
<sup>1</sup>H nmr spectrum of complex N, [Fe(bsb, Ph, Ph: m-Me)<sub>3</sub>]<sup>2+</sup>, in d<sub>3</sub>-acetonitrile.

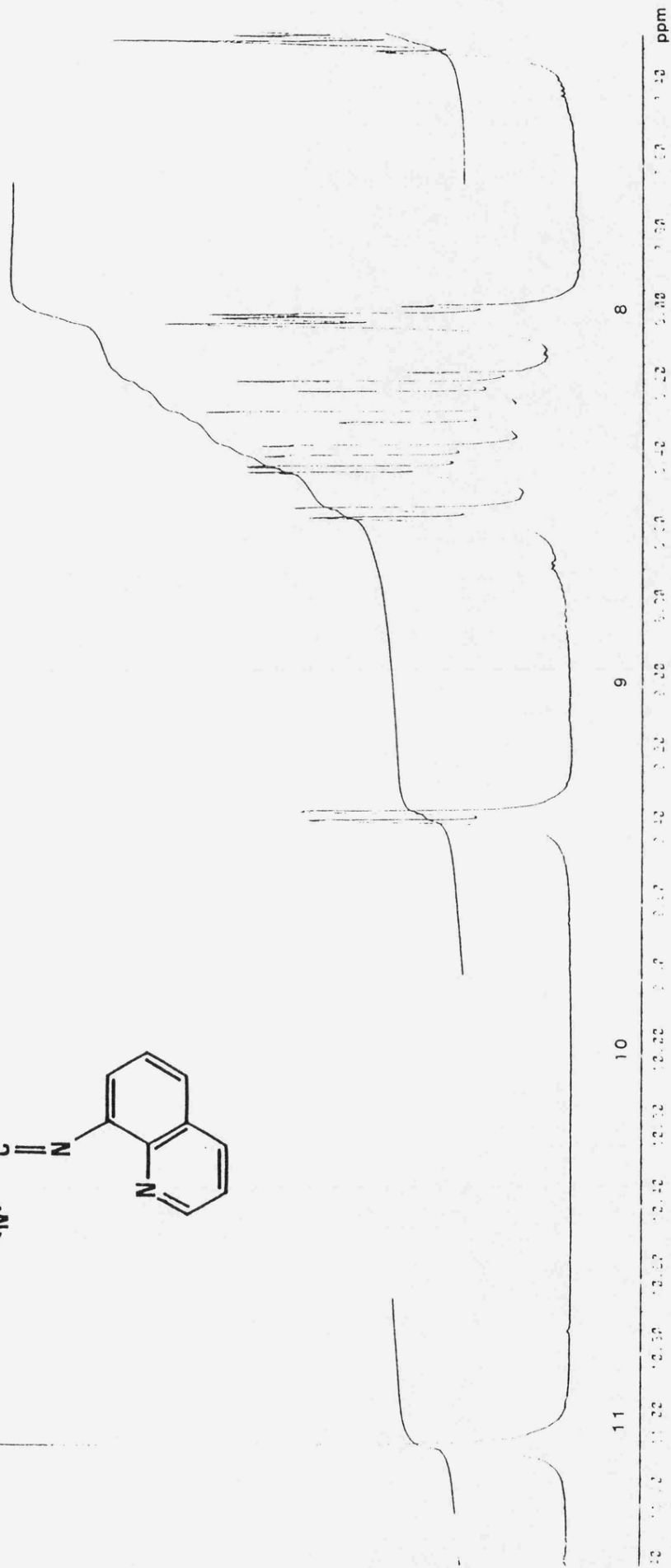
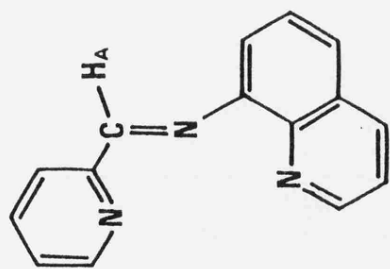


**FIGURE 6.12**  
<sup>1</sup>H nmr spectrum of complex P, [Fe(tsb,H,8amq)<sub>2</sub>]<sup>2+</sup>, in d<sub>3</sub>-acetonitrile.

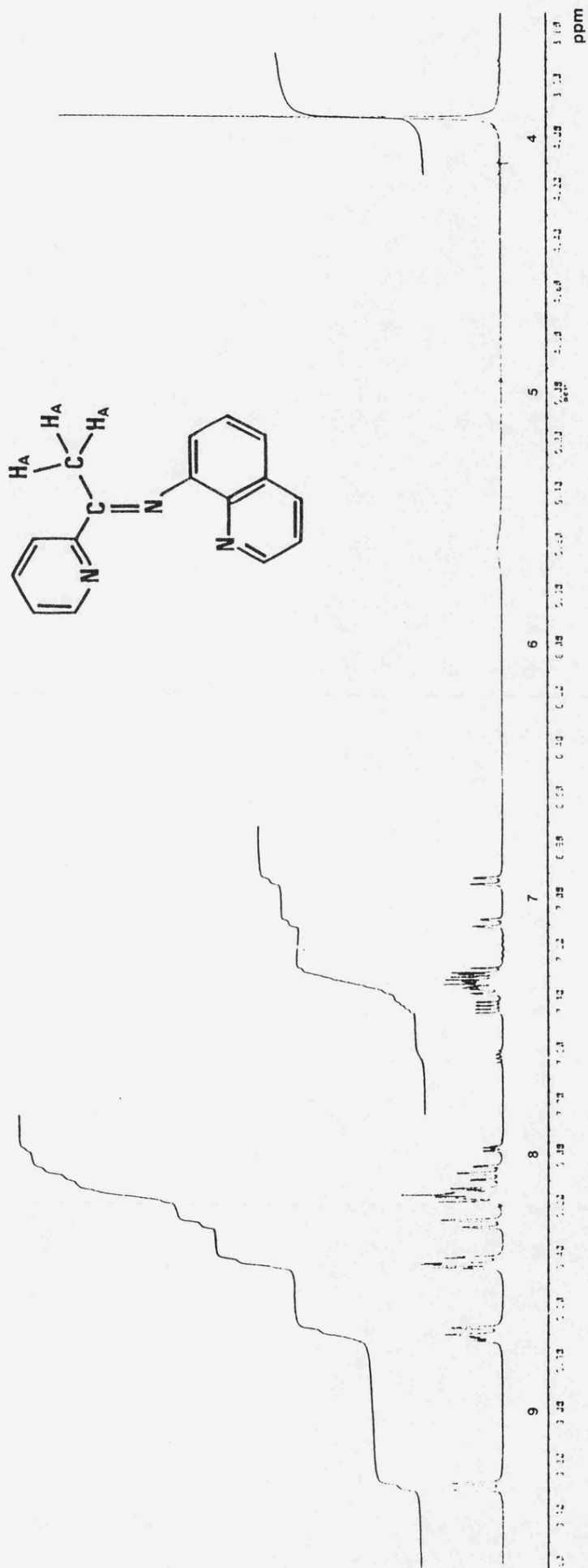
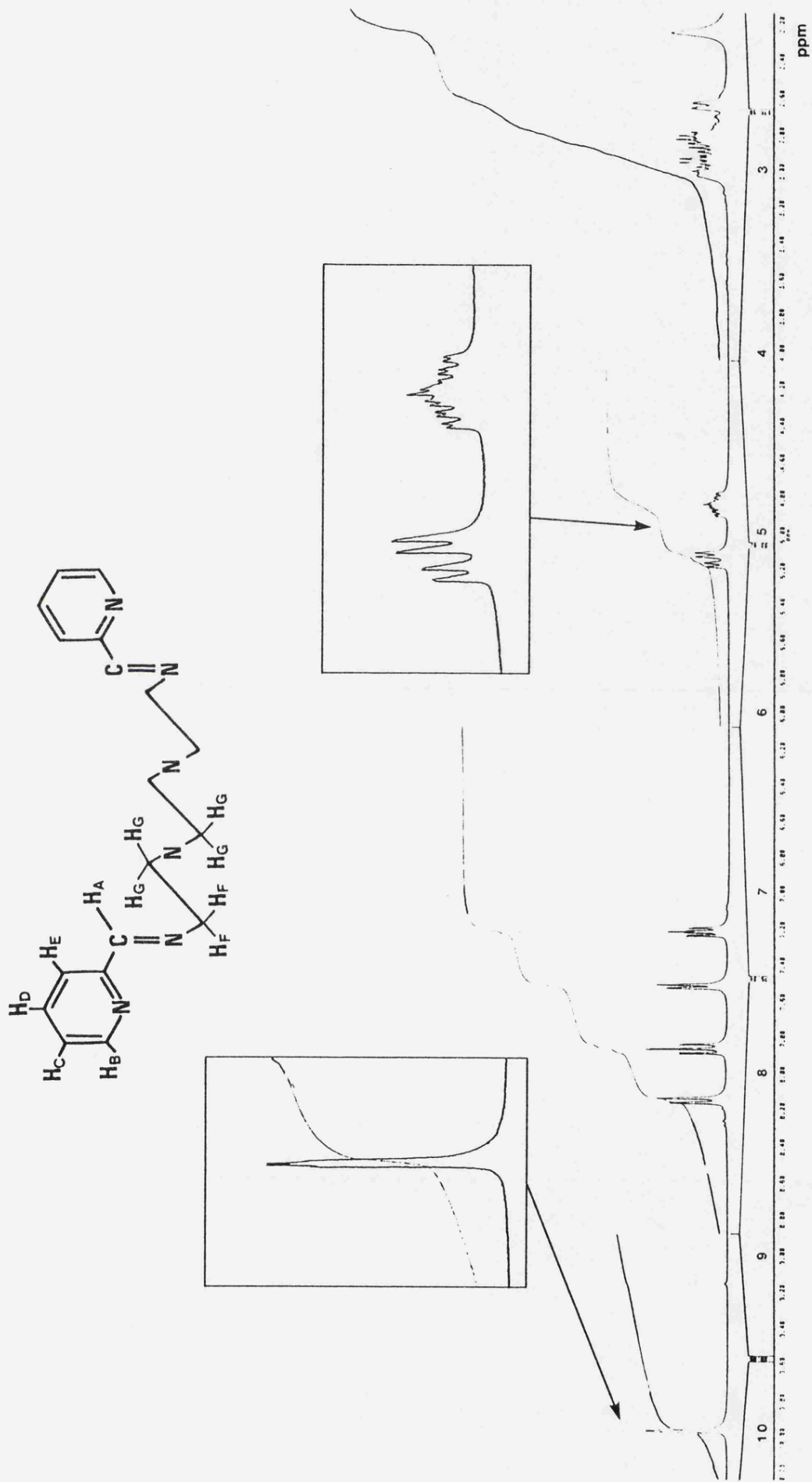
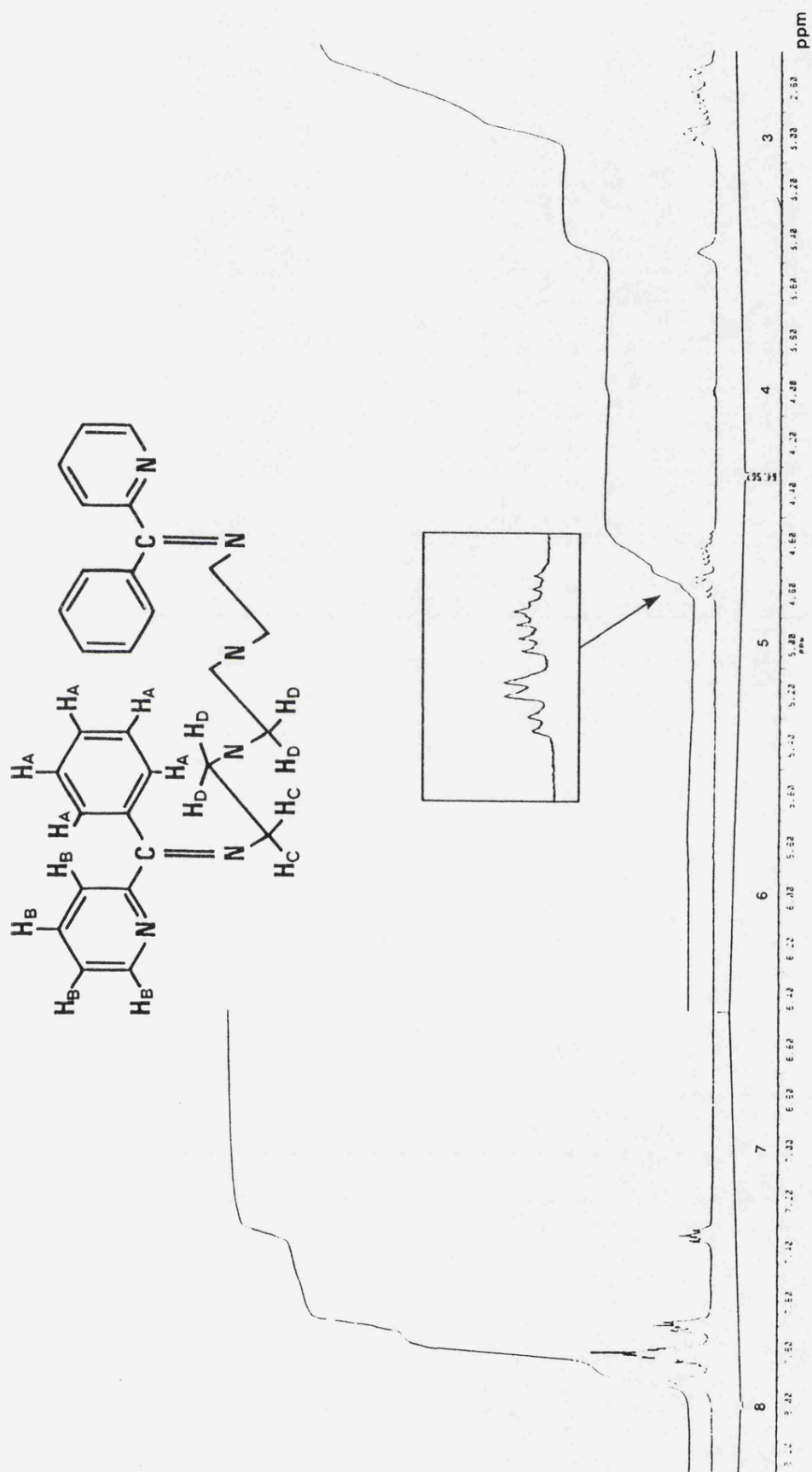


FIGURE 6.13

$^1\text{H}$  nmr spectrum of complex Q,  $[\text{Fe}(\text{tsb},\text{Me},8\text{amq})_2]^{2+}$ , in  $\text{d}_3$ -acetonitrile.



**FIGURE 6.14**  
 $^1\text{H}$  nmr spectrum of complex S,  $[\text{Fe}(\text{hsb}, \text{H}, \text{trien})]^{2+}$ , in  $\text{d}_3$ -acetonitrile.



**FIGURE 6.15**  
 $^1\text{H}$  nmr spectrum of complex T,  $[\text{Fe}(\text{hsb}, \text{Ph}, \text{trien})]^{2+}$ , in  $\text{d}_3$ -acetonitrile.

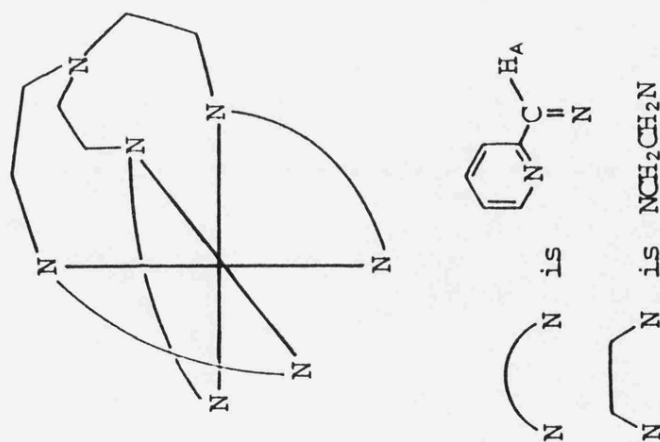
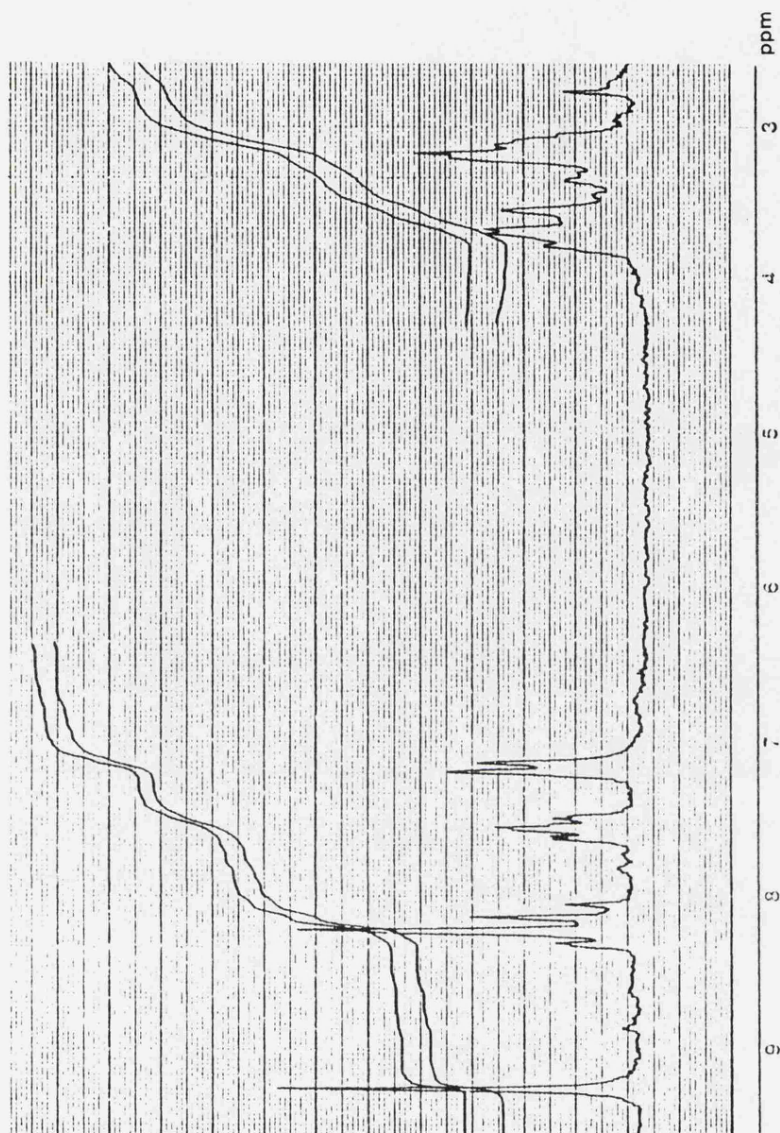
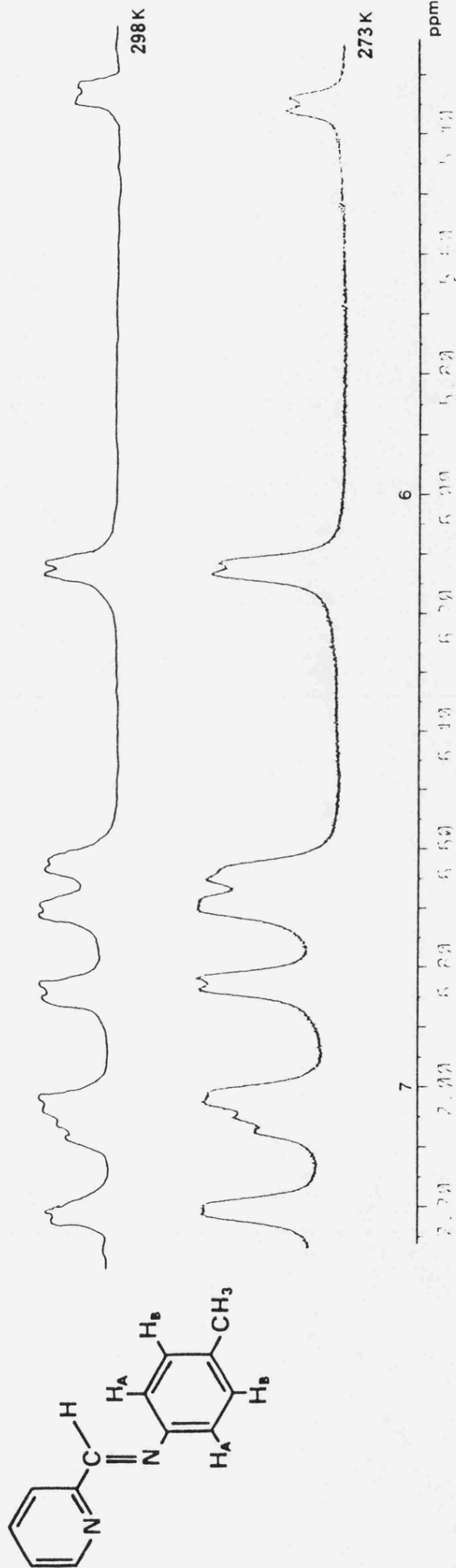


FIGURE 6.16  
 $^1\text{H}$  nmr spectrum of complex U,  $[\text{Fe}(\text{hsb},\text{H},\text{t}2\text{a})]^{2+}$ , in  $\text{d}_3$ -acetonitrile.



**FIGURE 6.17**  
The effect of temperature on the <sup>1</sup>H nmr spectrum of complex K,  $[\text{Fe}(\text{bsb}, \text{Me}, \text{Ph})_3]^{2+}$ , in  $d_6$ -acetone.



**FIGURE 6.18**

$^1\text{H}$  nmr spectra of complex C,  $[\text{Fe}(\text{bsb}, \text{H}, \text{Ph}; \text{p-Me})_3]^{2+}$ , in  $\text{d}_3$ -acetonitrile measured at 298 and 273 K.

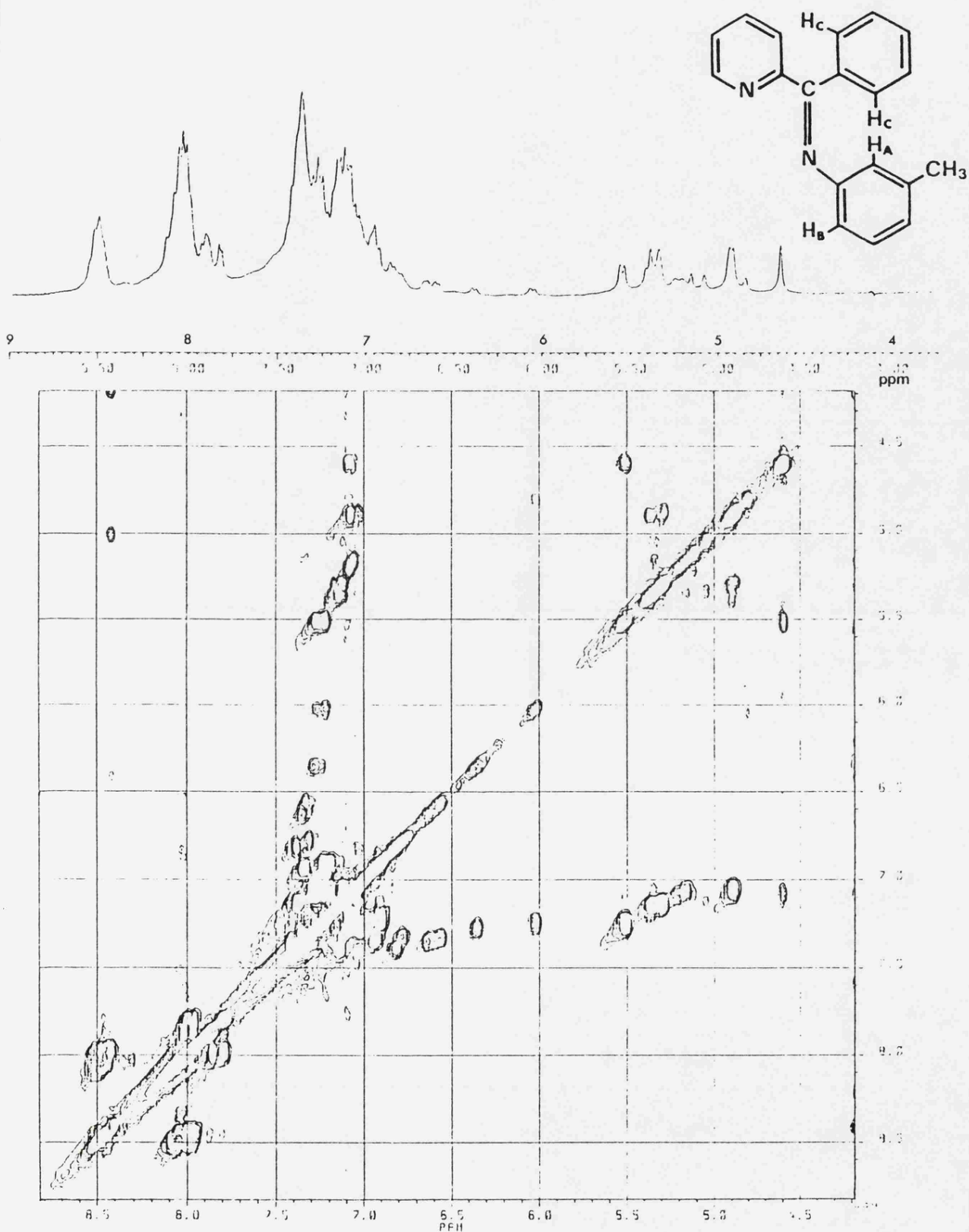


FIGURE 6.19

$^1\text{H}$  nmr spectra of complex N,  $[\text{Fe}(\text{bsb}, \text{Ph}, \text{Ph}-m\text{-Me})_3]^{2+}$ , in  $\text{d}_6$ -acetone: one-dimensional spectrum (top) and two-dimensional spectrum.

## REFERENCES FOR CHAPTER 6

1. L. J. Wilson and I. Bertini, J. Coord. Chem., 1971, 1, 237.
2. L. J. Wilson and I. Bertini, J. Chem. Soc., Chem. Comm., 1970, 1589.
3. A. Chakravorty and R. H. Holm, Inorg. Chem., 1964, 3, 1521.
4. A. Chakravorty and C. Kalia, Inorg. Chem., 1967, 6, 690.
5. F. Rohrscheid, R. E. Ernst and R. H. Holm, Inorg. Chem., 1967, 6, 1607.
6. D. K. Banerjea and K. K. Tripathi, Anal. Chem., 1960, 32, 1196.
7. D. Chapman and P. D. Magnus, "Introduction to Practical High Resolution Nuclear Magnetic Resonance Spectroscopy", Academic Press Inc., London, 1966.
8. S. F. Dyke, A. J. Floyd, M. Sainsbury and R. S. Theobald, "Organic Spectroscopy: An Introduction", Longman, London, 1978.
9. L. M. Jackman and S. Sternhell, "Applications of Nuclear Magnetic Resonance Spectroscopy in Organic Chemistry", 2nd. edn., Pergamon, Oxford, 1969.
10. A. J. Duffield, Ph.D. Thesis, Leicester, 1980.
11. R. K. Murmann and E. A. Healy, J. Am. Chem. Soc., 1961, 83, 2092.
12. J. Burgess, J. Chem. Soc. (A), 1968, 497.



# CHAPTER 7

**Iron(II) Schiff Base Di-imine  
Complexes: Further Studies**

## 7.1 GENERAL INTRODUCTION

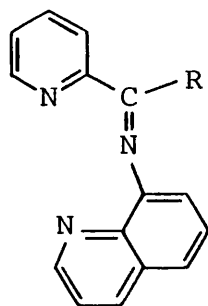
In this chapter the results of three studies, each involving a different type of iron(II) Schiff base complex, are reported. In the first study, in Section 7.2, solubility and kinetic data for a series of bis-(terdentate) iron(II) complexes are reported and discussed. In the second study, in Section 7.3, the crystal structure of a mono-(hexadentate) iron(II) Schiff base complex is reported and some structural features are compared with those observed in related complexes. In the third study, in Section 7.4, the nature of complex species formed when iron(II) is combined with two Schiff base ketoxime ligands under various conditions is investigated.

For each study, the tables referred to therein are given together at the end of the relevant study. The figures referred to occur in appropriate places throughout the text.

## 7.2 BIS-(TERDENTATE) IRON(II) SCHIFF BASE COMPLEXES

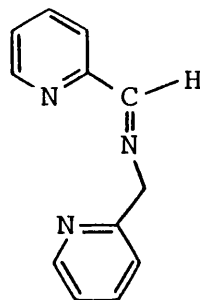
### 7.2.1 Introduction

It was confirmed in Chapter 6 from  $^1\text{H}$  nmr spectra obtained for low-spin iron(II) bis-(terdentate) complexes containing ligands of the type (I) or (II), that samples of the complexes contained only one diastereoisomeric form in each case. The configuration of this stereoisomer is



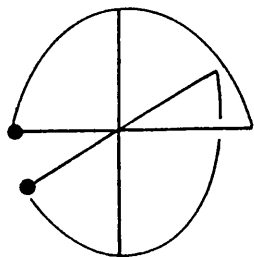
(R = H, Me)

(I)



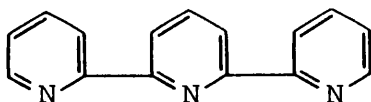
(II)

presumed to be that shown in (III) where the unsymmetrical ligands are planar (or nearly so).



(III)

Compared with the extensive work that has been done concerning the kinetics of reactions of low-spin iron(II) tris-(bidentate) di-imine complexes, the kinetics of reactions of related bis-(terdentate) complexes have not been widely studied. This is mainly as a result of the complicated kinetics observed for reactions of complexes of this type such as have been reported for aquation<sup>1</sup> and base hydrolysis<sup>2</sup> of  $[\text{Fe}(\text{terpy})_2]^{2+}$ , where terpy is the ligand 2,2';6',2''-terpyridyl (IV), the terdentate analogue of bipy. Complicated rate laws for the reactions of such bis-



(IV)

(terdentate) complexes arise from the existence of several possible intermediates of reduced co-ordination (with one or two of the three iron-nitrogen bonds per ligand ruptured) having significant lifetimes. In particular, intermediates in which one of the iron-nitrogen bonds is ruptured, so that the ligand is still bound to the iron atom via a bidentate chelating unit, may be of sufficient stability to give complicated consecutive-reaction-type kinetics. Solubility data and the results of kinetic studies, acid and base hydrolysis, involving a series of low-spin iron(II) bis-(terdentate) complexes containing Schiff base ligands

are presented and discussed in this chapter.

## 7.2.2 Experimental

### 7.2.2.1 Preparation of complexes

The low-spin iron(II) complexes were synthesised by the general method of preparation detailed in Section 2.2.2. Stoichiometric amounts of iron(II) chloride tetrahydrate, the appropriate carbonyl compound and primary amine were used in generating the complexes in solution. The complexes  $[\text{Fe}(\text{tsb},\text{H},8\text{amq})_2]^{2+}$ ,  $[\text{Fe}(\text{tsb},\text{Me},8\text{amq})_2]^{2+}$  and  $[\text{Fe}(\text{tsb},\text{Ph},8\text{amq})_2]^{2+}$  contain ligands of the type shown in (I), the primary amine used in their synthesis being 8-aminoquinoline. The carbonyl compounds used in the preparation of these complexes were pyridine-2-carboxaldehyde, 2-acetyl pyridine and 2-benzoyl pyridine respectively. The complexes  $[\text{Fe}(\text{tsb},\text{Me},2\text{pa})_2]^{2+}$  and  $[\text{Fe}(\text{tsb},\text{Ph},2\text{pa})_2]^{2+}$  contain ligands of the type shown in (II), the primary amine used in their synthesis being 2-picolyamine. The carbonyl compounds used in the preparation of these complexes were 2-acetyl pyridine and 2-benzoyl pyridine respectively. Once generated in solution, the complexes were precipitated as the perchlorate, iodide or thiocyanate salts of the complexes in the usual way.

### 7.2.2.2 Solubility measurements

Measurements of the solubilities of the perchlorate salts of the iron(II) bis-(terdentate) complexes in water + methanol mixtures were obtained from the absorbances of saturated solutions of the complexes in solvent mixtures of given composition. These absorbances were obtained spectrophotometrically as described in Section 2.5.

The absorbances of the saturated solutions were used to calculate the changes in the transfer chemical potentials of the complex ions upon their transference from water into water + methanol mixtures, i.e. the

transfer chemical potentials of the ions,  $\delta_{m\mu}^{\ominus}(\text{complex}^{2+})$ . This was done by first calculating the transfer chemical potentials of each salt in water + methanol mixtures using equation 7.1.  $\nu$  is the stoichiometry of the salt (for the salts in question,  $\nu = 3$ ),  $P(\text{water})$  and  $P(\text{mixture})$  are the absorbances of the saturated solutions of the complex in water and in the water + methanol solvent mixture respectively. Then, using

$$\delta_{m\mu}^{\ominus}(\text{salt}) = -\nu RT \ln \left[ \frac{P(\text{mixture})}{P(\text{water})} \right] \quad \dots [7.1]$$

the  $\delta_{m\mu}^{\ominus}(\text{salt})$  values and values for the transfer chemical potentials of the anion,  $\delta_{m\mu}^{\ominus}(\text{ClO}_4^-)$ , the values of  $\delta_{m\mu}^{\ominus}(\text{complex}^{2+})$  were calculated using equation 7.2. The values used for  $\delta_{m\mu}^{\ominus}(\text{ClO}_4^-)$  were those calculated

$$\delta_{m\mu}^{\ominus}(\text{complex}^{2+}) = \delta_{m\mu}^{\ominus}(\text{salt}) - 2 \delta_{m\mu}^{\ominus}(\text{ClO}_4^-) \quad \dots [7.2]$$

using the TPTB (tetraphenylphosphonium tetraphenylboronate) assumption.<sup>3</sup>

### 7.2.2.3 Kinetics

Kinetic investigations were carried out using the SP 800 and SP 1800 spectrophotometers [see Section 2.3.3] by monitoring the decrease in absorbance with time at  $\lambda_{\text{max}}$  of the complexes. In all cases reactions were carried out under first-order conditions, i.e. the amounts of either acid or alkali used were in excess of those of the complexes. First-order rate constants,  $k_{\text{obs}}$ , were calculated by the minicomputer as described in Section 2.3.2. In the study of acid fission of the complexes in aqueous solutions, hydrochloric acid was used and ionic strengths were maintained by the use of sodium chloride. In the study of alkali fission of the complexes in aqueous solutions and in 40 vol % water + methanol mixtures, freshly made-up solutions of sodium hydroxide were used. The definition of the solvent composition scale  $x$  vol % co-solvent was given in Section 2.2.1. Reported values of  $k_{\text{obs}}$  were measured at 298.15 K and are the average of three individual determinations. For the complexes containing

the terdentate ligands of the type shown in (I), where R = H, Me or Ph,  $\lambda_{\max}$  used in monitoring the reactions was 660, 674 and 681 nm respectively.

### 7.2.3 Results and discussion

#### 7.2.3.1 Transfer chemical potentials

The transfer chemical potentials in water + methanol mixtures at 298.2 K calculated for the three bis-(terdentate) complexes of the type  $[\text{Fe}(\text{tsb},\text{R},\text{8amq})_2]^{2+}$ , where R is either H, Me or Ph, are given in Table 7.1 and shown diagrammatically in Fig. 7.1. As expected for such complexes containing hydrophobic ligands, the complexes are increasingly stabilized upon their transference from water into water + methanol mixtures as the methanol content of the solvent mixtures increases (cf. transfer chemical potentials of related complexes in water + methanol mixtures discussed in Section 3.3.4). This trend reflects the increasing capacity for hydrophobic solvation of water + methanol mixtures as the methanol content of the solvent mixtures increases (this was also discussed in Chapter 3). The observed stabilizing effect, not surprisingly, is greatest for the bis-(terdentate) complex in which R = Ph, i.e. for the complex containing the most hydrophobic of the three ligands. On these grounds it would have perhaps been expected that the complex in which R = Me would have experienced a greater stabilizing effect than the complex in which R = H upon their transference from water into a water + methanol mixture of given composition. This, however, appears only to be the case for solvent mixtures of low vol % MeOH content, i.e. up to approximately 20 vol % MeOH. For solvent mixtures of higher methanol content, the complex in which R = H is more stabilized than that in which R = Me for a given solvent composition over the range studied.

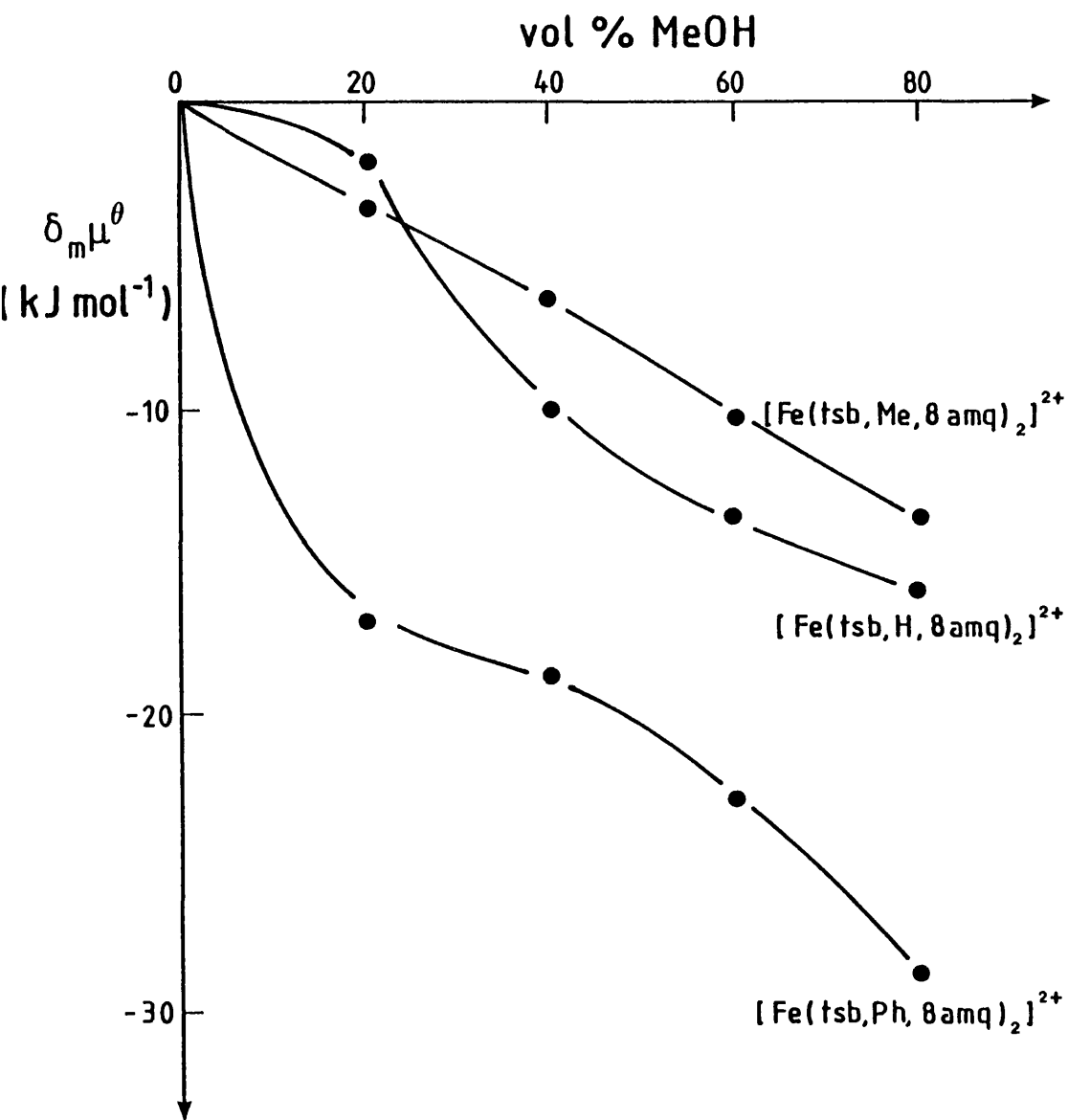


FIGURE 7.1

Transfer chemical potentials for three bis-(terdentate) iron(II) complexes in water + methanol mixtures at 298.2 K.

Fig. 7.2 shows comparisons between the observed trends of transfer chemical potentials in water + methanol mixtures for the bis-(terdentate) complexes of the type  $[\text{Fe}(\text{tsb},\text{R},8\text{amq})_2]^{2+}$  where R is either H, Me or Ph, and those for some other low-spin iron(II) di-imine complexes.<sup>3,4</sup> Included in Fig. 7.2 are the transfer chemical potentials for two mono-(hexadentate) iron(II) Schiff base complexes,  $[\text{Fe}(\text{hsb},\text{H},\text{trien})]^{2+}$ <sup>4</sup> and  $[\text{Fe}(\text{hsb},\text{Ph},\text{trien})]^{2+}$ .<sup>4</sup> These complexes contain the hexadentate ligands derived by the combination of triethylenetetramine with, in the case of the former complex, pyridine-2-carboxaldehyde and, in the case of the latter complex, 2-benzoyl pyridine. In Chapters 5 and 6, it was seen that, in general, the evidence for the existence of diastereoisomeric forms of these mono-(hexadentate) complexes was much more sparse than that indicating the occurrence of diastereoisomerism in the related tris-(bidentate) complexes. No inconsistencies were reported in the monitoring of data used in calculating the values for the transfer chemical potentials of the mono-(hexadentate) complexes depicted in Fig. 7.2. This suggests that the samples used contained only one diastereoisomeric form which, as related in Chapters 5 and 6, is considered here to possess the stereochemical arrangement shown in (V). The similarity of the arrangement of the ligand about the iron atom in (V) with that in (VI), the assumed arrangement in the bis-(terdentate) complexes, is apparent. In Fig. 7.2, for both the pairs of bis-(terdentate) complexes and mono-(hexadentate) complexes in which R is either H or Ph, the stabilization of the ions as the methanol content of the solvent mixtures increases is greater for the Ph derivative than the H derivative over the range studied, reflecting the relatively greater hydrophobicity of the ligands when R is Ph. Comparison of the transfer chemical potentials for the mono-(hexadentate) complex and the bis-(terdentate) complex in which

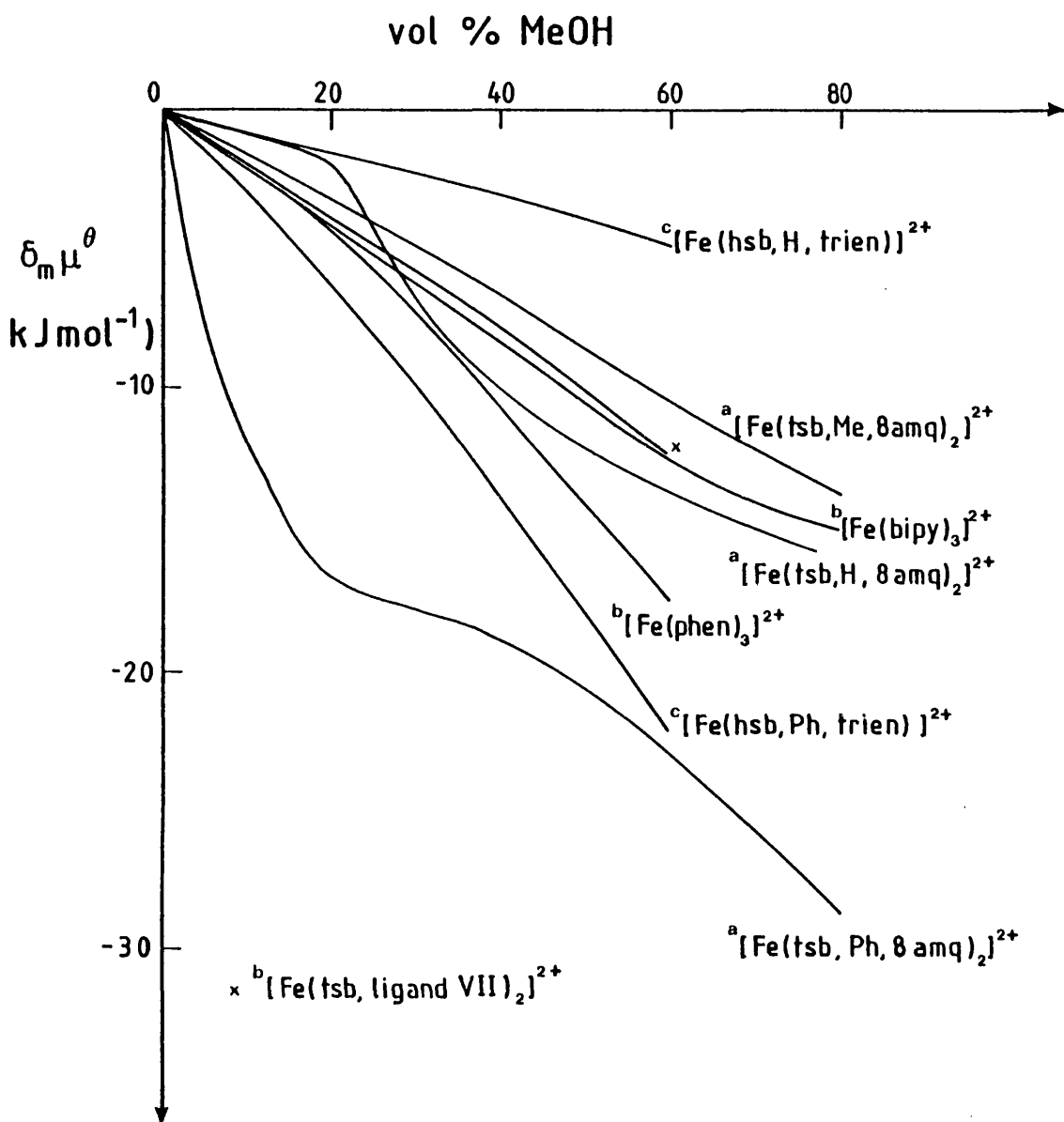
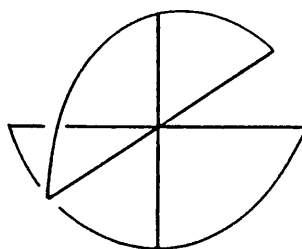
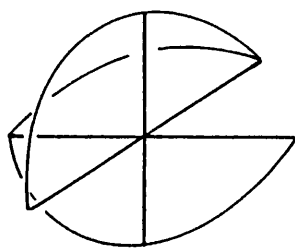
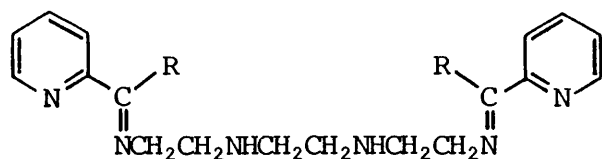


FIGURE 7.2

Transfer chemical potentials for some iron(II) di-imine complexes in water + methanol mixtures at 298.2 K; a, this work; b, ref. 3; c, ref. 4.



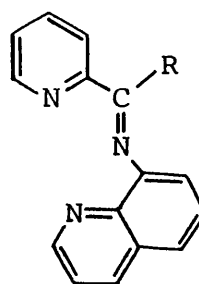
ligand:



$R = H, Ph$

(V)

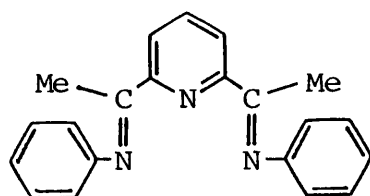
ligand:



$R = H, Ph$  (VI)

R are the same, shows the bis-(terdentate) complex containing ligands derived from 8-aminoquinoline to be generally significantly more stabilized than the mono-(hexadentate) complex containing the ligand derived from triethylenetetramine. This occurs both in the case when  $R = H$  and when  $R = Ph$ , reflecting the greater hydrophobicity of the quinoline residues in the former type of complex than the alkyl residues in the latter type of complex.

For the bis-(terdentate) complex in which  $R = Me$ , the stabilizing effect on the ion in solution resulting from increased methanol content of the solvent mixtures is similar to that depicted for another bis-(terdentate) complex, that containing the ligand shown in (VII).<sup>3</sup> The values of the



(VII)

transfer chemical potentials for this complex shown in Fig. 7.2 are labelled  $[Fe(tsb, \text{ligand VII})_2]^{2+}$ . The stabilizing effect seen for this

complex upon its transference from water into water + methanol mixtures is slightly greater than for the complex  $[\text{Fe}(\text{tsb},\text{Me},8\text{amq})_2]^{2+}$ . This is most likely due to the fact that, although both complexes contain the same number of aromatic rings, the complex  $[\text{Fe}(\text{tsb},\text{Me},8\text{amq})_2]^{2+}$  contains two methyl groups whereas the complex  $[\text{Fe}(\text{tsb},\text{ligand VII})_2]^{2+}$  contains four. The (N-phenyl) p-methyl derivative of the complex  $[\text{Fe}(\text{tsb},\text{ligand VII})_2]^{2+}$ , containing four additional methyl groups per molecule of complex is even more stabilized upon its transference from water into water + methanol mixtures<sup>3</sup> than the unsubstituted derivative. This trend, then, once again reflects increasing preferential solvation of complexes of this type by methanol as the hydrophobicity of the ligands increases.

#### 7.2.3.2 Reaction with acid

The observed first-order rate constants,  $k_{\text{obs}}$ , for acid hydrolysis (hydrochloric acid) of the three bis-(terdentate) complexes,  $[\text{Fe}(\text{tsb},\text{H},8\text{amq})_2]^{2+}$ ,  $[\text{Fe}(\text{tsb},\text{Me},8\text{amq})_2]^{2+}$  and  $[\text{Fe}(\text{tsb},\text{Ph},8\text{amq})_2]^{2+}$ , measured under the conditions where  $[\text{acid}] \gg [\text{complex}]$ , are given in Table 7.2. The ligands in these complexes are derived from 8-aminoquinoline and either pyridine-2-carboxaldehyde, 2-acetyl pyridine or 2-benzoyl pyridine respectively. All first-order plots obtained for these reactions were linear.

In general, values of  $k_{\text{obs}}$  for acid fission of iron(II) di-imine complexes are dependent on  $[\text{H}^+]$  if the leaving ligand is flexible, e.g. when the ligand is 2,2'-bipyridyl. In such cases, the reactions may proceed via pathways involving unidentate protonated ligands. For complexes containing rigid ligands such as 1,10-phenanthroline,  $k_{\text{obs}}$  is independent of  $[\text{H}^+]$  as it is not possible to protonate the ligand whilst it is still bonded to the iron atom. As can be seen in Table 7.2, values of  $k_{\text{obs}}$  for the three bis-(terdentate) complexes containing Schiff base

ligands increase with increasing  $[H^+]$ , as expected from the flexible nature of the ligands. This is shown diagrammatically in Fig. 7.3 in which the patterns of dependence of  $k_{obs}$  on  $[H^+]$  for several other low-spin iron(II) di-imine complexes are also included for comparison.

$[Fe(bipy)_3]^{2+5}$  is the tris-(bidentate) complex which contains the bidentate ligand 2,2'-bipyridyl.  $[Fe(terpy)_2]^{2+1}$  is the bis-(terdentate) complex which contains the terdentate ligand 2,2';6',2''-terpyridyl (IV).  $[Fe(hsb,Ph, trien)]^{2+6}$  is the mono-(hexadentate) complex which contains the hexadentate ligand derived from 2-benzoyl pyridine and triethylene-tetramine.

In Fig. 7.3 it can be seen that the actual form of the dependences of  $k_{obs}$  on  $[H^+]$  are most similar for the four bis-(terdentate) complexes and the mono-(hexadentate) complex. Thus, the patterns of dependence for the three bis-(terdentate) complexes of the type  $[Fe(tsb,R,8amq)_2]^{2+}$ , where R is either H, Me or Ph, resemble those observed for the complexes  $[Fe(terpy)_2]^{2+}$  and  $[Fe(hsb,Ph, trien)]^{2+}$  rather than that observed for the tris-(bidentate) complex  $[Fe(bipy)_3]^{2+}$ . The similarities observed in the patterns of behaviour obtained for the bis-(terdentate) and the mono-(hexadentate) complexes reflect the possible intermediacy in each case of several ligand species of denticity greater than one and their protonated derivatives. For  $[Fe(bipy)_3]^{2+}$ , only intermediates containing monodentate and monodentate monoprotonated ligands are possible.

In Fig. 7.3 it appears that, for the three bis-(terdentate) complexes of the type  $[Fe(tsb,R,8amq)_2]^{2+}$ , for a given value of  $[H^+]$   $k_{obs}$  decreases in the order  $R = H > R = Me > R = Ph$ . This is the general pattern observed for reactions of many iron(II) Schiff base di-imine complexes.<sup>7-9</sup> The observation may be a result of both steric and electronic factors. Replacement of H by a bulky Ph group in the ligands may increase the

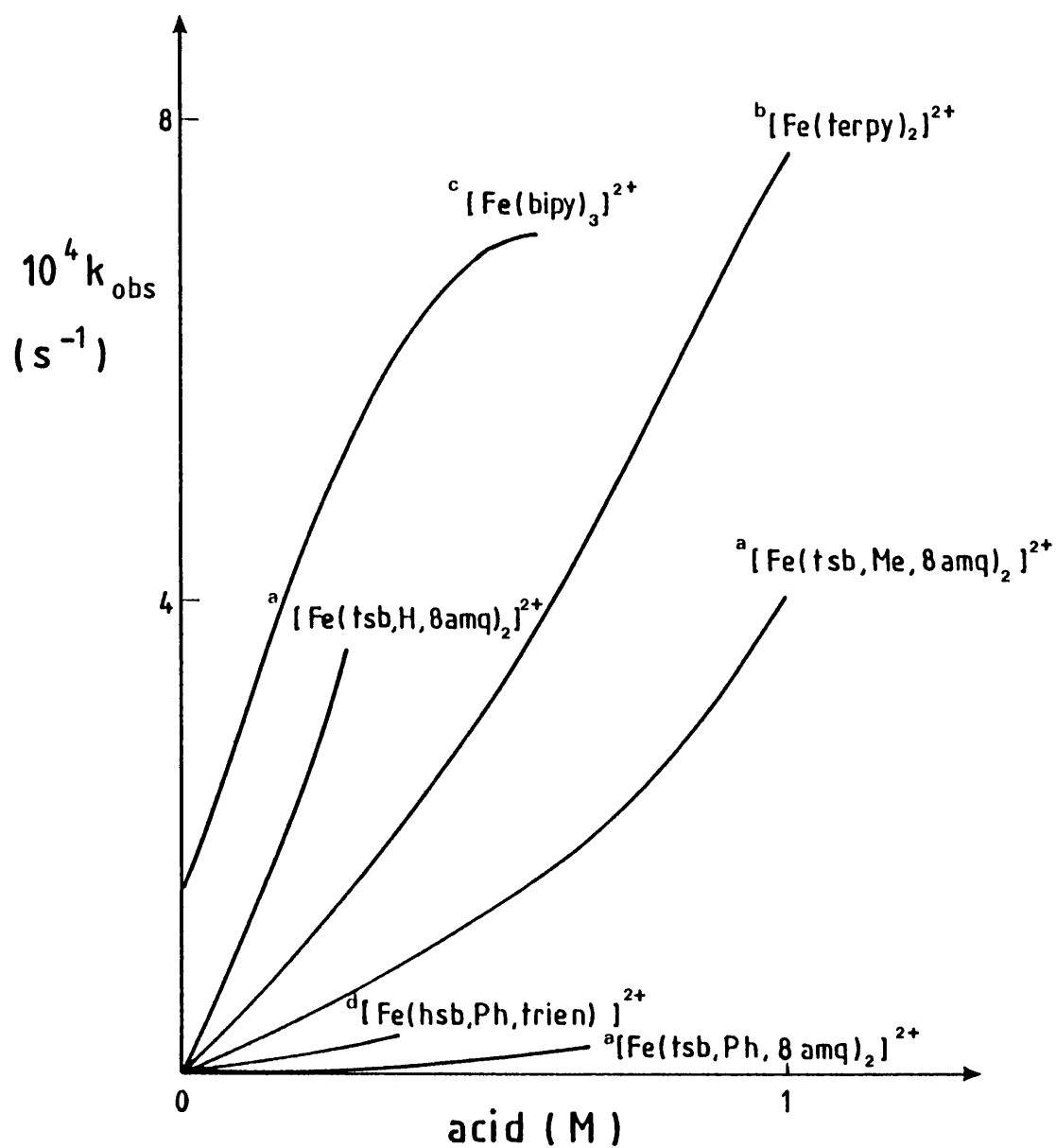


FIGURE 7.3

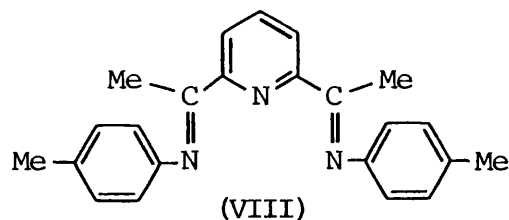
Comparison of the dependences of first-order rate constants for acid hydrolysis,  $k_{\text{obs}}$ , on acid concentration for some flexible multidentate di-imine ligand complexes of iron(II); a, this work; b, ref. 1; c, refs. 2, 5; d, ref. 6.

likelihood of steric interference occurring upon the formation of intermediates in which the co-ordination number in the complex is reduced. If these intermediates are involved in one of the possible reaction pathways, then the relevant rate constant may be smaller for the complex in which R = Ph than for that in which R = H. The presence of an additional aromatic ring in the complex where R = Ph compared to that in which R = H may result in the former complex being less reactive than the latter under the same conditions. The iron to nitrogen back-bonding occurring in complexes of this type has a stabilizing effect on the complexes. Presumably, for the complex in which R = Ph, this back-bonding can be more extensively delocalized than in the complex in which R = H. Thus, smaller values of  $k_{\text{obs}}$  for the complex in which R = Ph may reflect stronger iron-nitrogen bonding in this complex as compared to that in the complex for which R = H.

Such factors may also be pertinent to the observation that acid attack at the bis-(terdentate) complex in which R = Ph is much slower than for  $[\text{Fe}(\text{terpy})_2]^{2+}$  under the same conditions. At higher values of  $[\text{H}^+]$ ,  $k_{\text{obs}}$  for  $[\text{Fe}(\text{terpy})_2]^{2+}$  becomes independent of  $[\text{H}^+]$ .<sup>1</sup> If the behaviour of the complex  $[\text{Fe}(\text{tsb,Ph,8amq})_2]^{2+}$  follows the same pattern then the value of  $[\text{H}^+]$  beyond which  $k_{\text{obs}}$  remains constant is greater than 6.8 M. For this complex, values of  $k_{\text{obs}}$  in the region of  $[\text{H}^+] = 4.8 - 6.8$  M were still increasing with increasing acid concentration. For acid concentrations of 4.8, 6.0, 6.4 and 6.8 M HCl,  $k_{\text{obs}}$  for this complex was  $0.68 \times 10^{-3}$ ,  $1.04 \times 10^{-3}$ ,  $1.52 \times 10^{-3}$  and  $2.37 \times 10^{-3} \text{ sec}^{-1}$  respectively. For the bis-(terdentate) complexes in which R = H and R = Me, values of  $k_{\text{obs}}$  were too great to be determined at higher concentrations of acid. For the complexes in which R = Me and R = Ph, extrapolation to  $[\text{H}^+] = 0$  shows the rate constants for the dissociation of both complexes in water to be very

small. This may also be true of the complex in which R = H. Solutions of this latter complex certainly remained intensely coloured for a period of days. A more definite indication as to the magnitude of the rate constant for rate-determining dissociation of this complex would, however, require more points on the relevant line in Fig. 7.3 in the region of low acid concentration. From ultraviolet/visible absorption spectra of the reactions of the complexes where R = Me and R = Ph with acid, the presence of intermediates was not discernible in terms of the appearance of additional peaks or shifts in peaks when acid was added to the solutions of the complexes. However, the absence of isosbestic points in the spectra indicated the reactions to involve more than one step. The observed peaks (at 578 and 674 nm for the complex where R = Me and at 582 and 681 nm for the complex where R = Ph) decayed in a regular first-order manner.

The stability of the complexes of the type  $[\text{Fe}(\text{tsb},\text{R},8\text{amq})_2]^{2+}$ , where R is either H, Me or Ph, is in contrast to that of the iron(II) bis-(terdentate) complex containing the Schiff base ligand (VIII).<sup>10</sup> The rate of aquation of this complex at 298 K is  $1.5 \times 10^{-3} \text{ sec}^{-1}$ . This complex undergoes rapid hydrolysis in acidic media, which suggests comparatively weak iron-nitrogen bonding. This may be the result of the



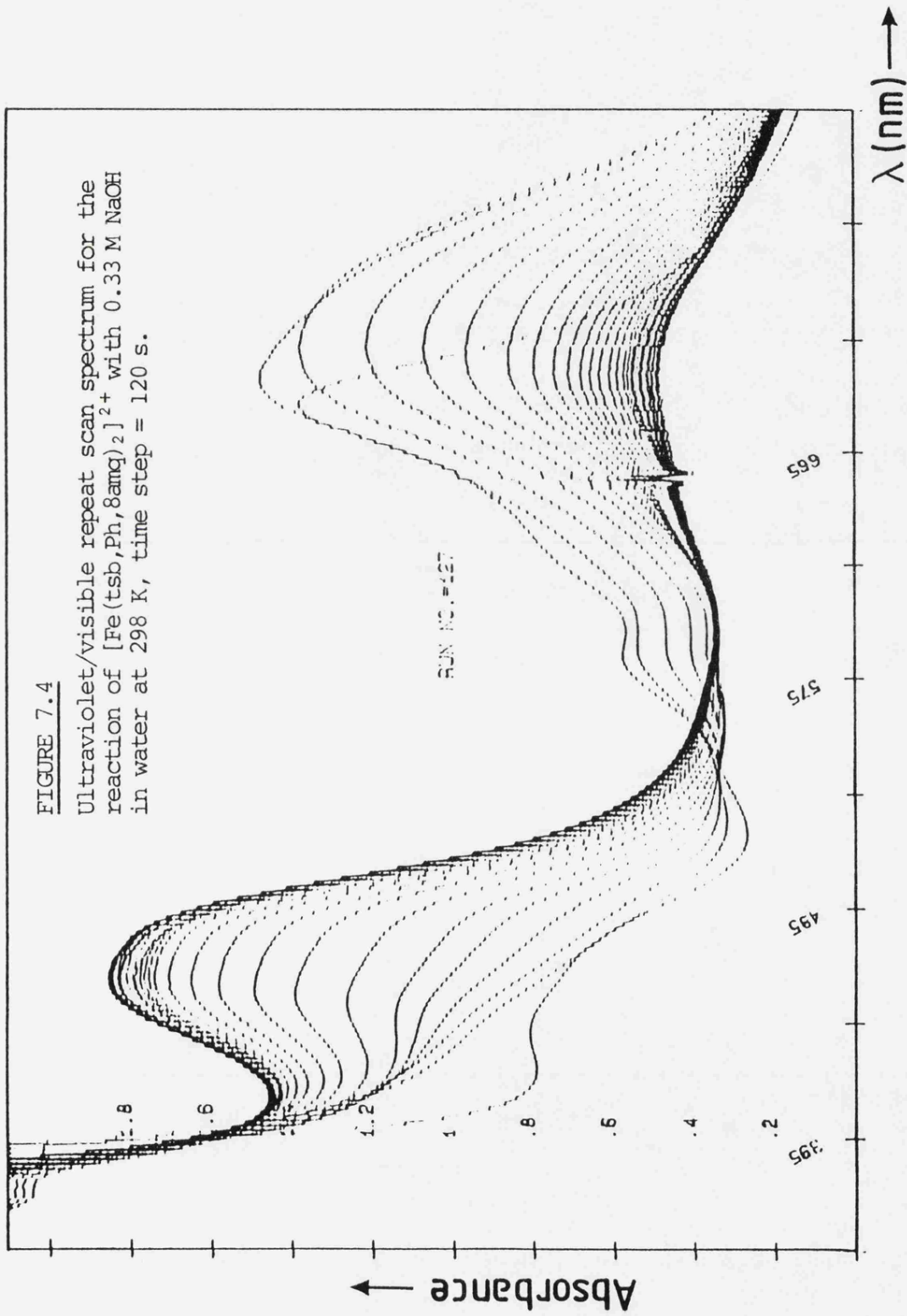
electron-releasing effect of the methyl groups in the complex containing ligand (VIII) decreasing the strength of the back-bonding from the iron to the nitrogens in the complex to a greater extent than strengthening the iron-nitrogen  $\sigma$  bonds.

### 7.2.3.3 Reaction with hydroxide

For the complex  $[\text{Fe}(\text{tsb},\text{Ph},8\text{amq})_2]^{2+}$ , values of  $k_{\text{obs}}$  were obtained using the SP 1800 spectrophotometer, monitoring at 681 nm. For the reaction with 0.33 M NaOH in aqueous solution at 298.15 K, values of  $k_{\text{obs}}$  were in the order of  $10^{-3} \text{ s}^{-1}$ . However, there were small but distinct deviations from linearity, particularly for the early stages of the reactions, in the first-order plots obtained for the reactions from the minicomputer. Under the same conditions, the reactions of the analogous complexes in which R=H and R=Me ( $\lambda_{\text{max}} = 660$  and 674 nm respectively) were too fast to be monitored. Repeat scans of the ultraviolet/visible absorption region for the reaction of  $[\text{Fe}(\text{tsb},\text{Ph},8\text{amq})_2]^{2+}$  with hydroxide confirmed that the reactions were not first-order. One such spectrum, typical of those obtained, is shown in Fig. 7.4. The first scan was identical to that before the hydroxide was added,  $\lambda_{\text{max}} = 682$  nm. The second scan (the time step being 120 s in each case) showed  $\lambda_{\text{max}}$  had shifted towards longer wavelengths, 691 nm. This shift was accompanied by an increase in absorbance at  $\lambda_{\text{max}}$ . In subsequent scans the absorbance in the region of  $\lambda_{\text{max}}$  gradually decayed, the value of  $\lambda_{\text{max}}$  first shifting towards longer wavelengths then back towards shorter wavelengths. The greatest value of  $\lambda_{\text{max}}$  observed was 707 nm. The most plausible explanation for such a spectrum is that the formation of an intermediate species, or probably more than one, for which values of  $\lambda_{\text{max}}$  are towards longer wavelengths compared to that for the initial complex, is being observed. The number or nature of such intermediates cannot be discerned, only that the reaction scheme is not simple. For comparison, an analogous spectrum in which the alkali concentration was reduced by a factor of 5 is shown in Fig. 7.5. As can be seen, the pattern observed in this case is somewhat different. The values of  $\lambda_{\text{max}}$ , initially the same as in the starting

**FIGURE 7.4**

Ultraviolet/visible repeat scan spectrum for the reaction of  $[\text{Fe}(\text{tsb}, \text{Ph}, 8\text{amg})_2]^{2+}$  with 0.33 M NaOH in water at 298 K, time step = 120 s.



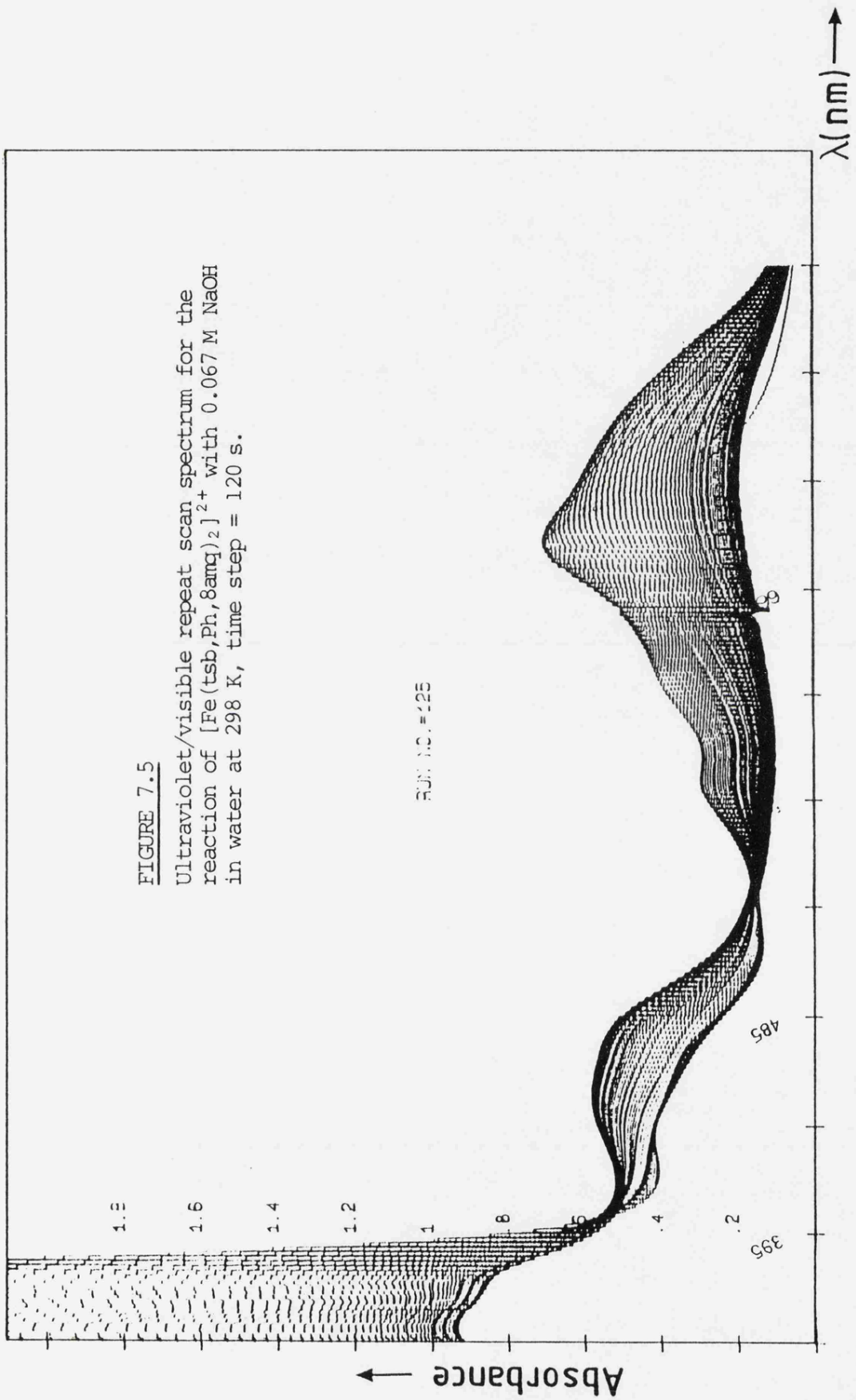


**FIGURE 7.5**

Ultraviolet/visible repeat scan spectrum for the reaction of  $[\text{Fe}(\text{tsb}, \text{Ph}, 8\text{amq})_2]^{2+}$  with 0.067 M NaOH in water at 298 K, time step = 120 s.

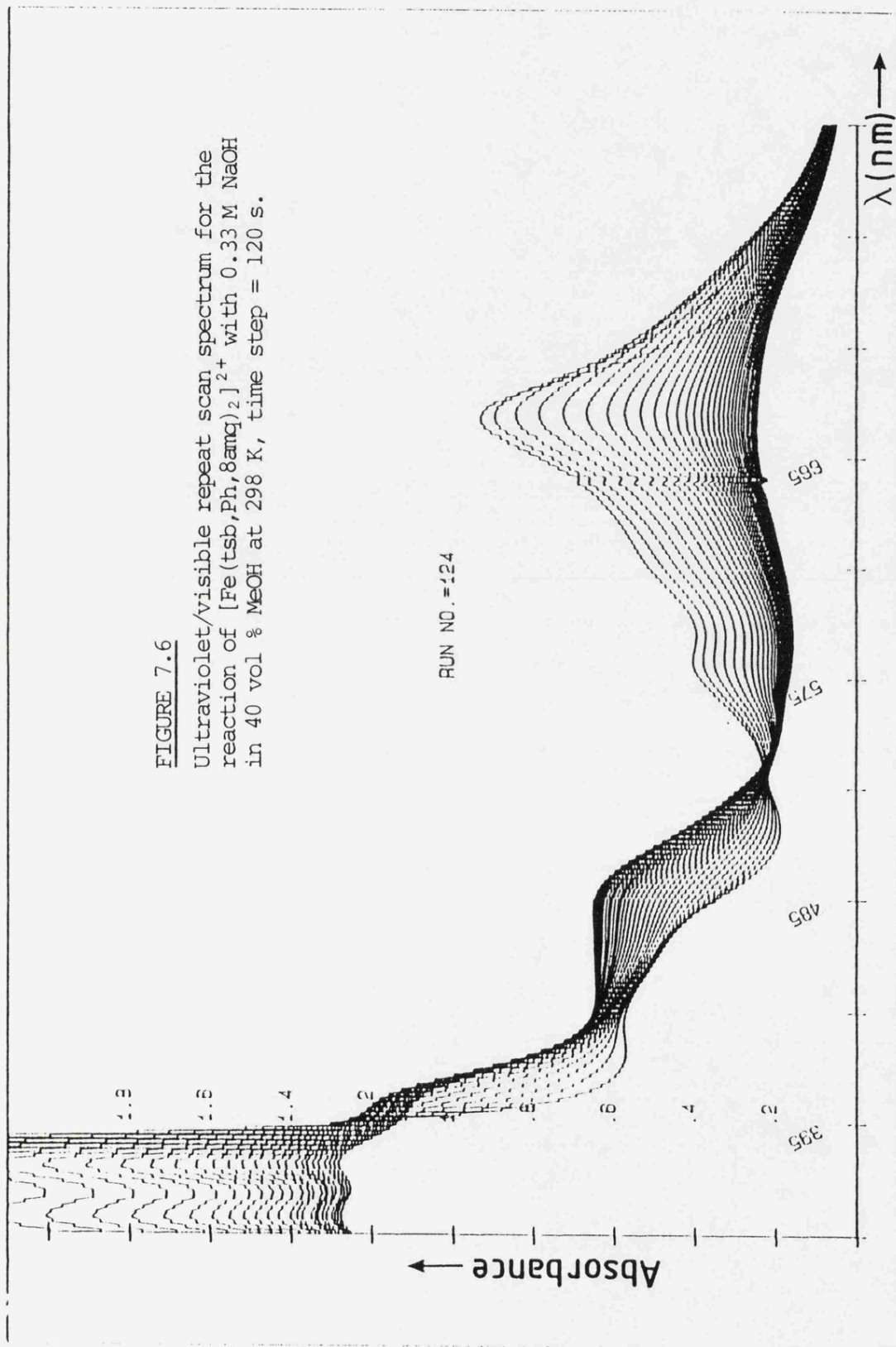
material, move consistently toward longer wavelength as the reaction proceeds. However, the early stages of the reaction appear to be similar, though slower, to those at higher alkali concentrations. It is possible that the effect of hydroxide concentration may be connected with the formation of mono hydroxy- and di hydroxy- intermediates as well as those of reduced co-ordination number.

The possibility of intermediate species having reduced co-ordination numbers suggested that shifts in  $\lambda_{\max}$  could be more pronounced in water + methanol mixtures if solvation of the partially detached hydrophobic ligands by methanol affected  $\lambda_{\max}$ . The repeat scan patterns were indeed different for analogous reactions in aqueous solutions and in 40 vol % MeOH, though not, perhaps, in the manner expected. A typical spectrum observed for the reaction of the complex  $[\text{Fe}(\text{tsb},\text{H},8\text{amq})_2]^{2+}$  with 0.33 M NaOH in 40 vol % MeOH is shown in Fig. 7.6. This pattern was the same when the sodium hydroxide concentration was reduced by a factor of 5. It can be seen that changes in  $\lambda_{\max}$  as the reaction proceeds are much less pronounced than in aqueous solutions. There is a slight shift in  $\lambda_{\max}$  towards longer wavelengths initially, then a gradual shift towards shorter wavelengths. If the same types of intermediates are formed in these solvent mixtures as in water, then, either their values of  $\lambda_{\max}$  are very similar to that of the initial complex or they appear to be formed in much smaller amounts.

Repeat scan spectra of the reactions of  $[\text{Fe}(\text{tsb},\text{Me},8\text{amq})_2]^{2+}$  with sodium hydroxide exhibited similar complicated patterns. For alkali fission (0.05 M NaOH) of the complex  $[\text{Fe}(\text{tsb},\text{H},8\text{amq})_2]^{2+}$  in aqueous solution, studied by stopped-flow experiments,<sup>11</sup> an 'induction' period followed by a rapid process ( $t_x \approx 0.5$  s), then a very slow reaction were observed. The 'induction' and fast steps accounted for about one half of

**FIGURE 7.6**

Ultraviolet/visible repeat scan spectrum for the reaction of  $[\text{Fe}(\text{tsb},\text{Ph},8\text{amq})_2]^{2+}$  with 0.33 M NaOH in 40 vol % MeOH at 298 K, time step = 120 s.



absorbance change of the solution at the initial value of  $\lambda_{\max}$  of the complex, 660 nm.

The complexes derived from either 2-acetyl pyridine or 2-benzoyl pyridine and 2-picolyamine,  $[\text{Fe}(\text{tsb},\text{Me},2\text{pa})_2]^{2+}$  and  $[\text{Fe}(\text{tsb},\text{Ph},2\text{pa})_2]^{2+}$  respectively, were unstable in both aqueous and water + methanol solutions. Loss of absorbance of the solutions was accompanied by a gradual shift in  $\lambda_{\max}$  towards longer wavelengths in all cases. For the R=Me derivative in 0, 20, 40, 60 and 80 vol % MeOH, initial values of  $\lambda_{\max}$  were approximately 575 nm. With time,  $\lambda_{\max}$  shifted to upwards of 594 nm, the rate of shift in  $\lambda_{\max}$  increasing with increasing methanol content of the solvent mixtures. For the R=Ph derivative, the same pattern of shifts in  $\lambda_{\max}$  was observed,  $\lambda_{\max}$  being initially approximately 586 nm and increasing to over 610 nm with time.

TABLE 7.1

Transfer chemical potentials,  $\delta_m \mu^\ominus(\text{complex}^{2+})$  in  $\text{kJ mol}^{-1}$ , of bis-(terdentate) complexes of the type  $[\text{Fe}(\text{tsb}, \text{R}, 8\text{amq})_2]^{2+}$  where  $\text{R} = \text{H}, \text{Me}$  or  $\text{Ph}$  calculated from absorbances of saturated solutions of the perchlorate salts of the complexes,  $\text{P}(\text{salt})$ , in water + methanol mixtures.

$[\text{Fe}(\text{tsb}, \text{H}, 8\text{amq})_2] (\text{ClO}_4)_2$ ,  $\lambda_{\text{max}} = 660 \text{ nm}$

	solvent composition, vol % MeOH				
	0	20	40	60	80
P(salt)	1.560	2.025	6.230	9.190	8.70
$\delta_m \mu^\ominus(\text{salt})$		-1.94	-10.30	-13.19	-12.78
$2 \delta_m \mu^\ominus(\text{ClO}_4^-)$		0.10	-0.20	0.30	3.20
$\delta_m \mu^\ominus(\text{complex}^{2+})$		-2.04	-10.10	-13.49	-15.98

$[\text{Fe}(\text{tsb}, \text{Me}, 8\text{amq})_2] (\text{ClO}_4)_2$ ,  $\lambda_{\text{max}} = 674 \text{ nm}$

	solvent composition, vol % MeOH				
	0	20	40	60	80
P(salt)	0.544	0.871	1.343	2.06	2.188
$\delta_m \mu^\ominus(\text{salt})$		-3.50	-6.72	-9.90	-10.35
$2 \delta_m \mu^\ominus(\text{ClO}_4^-)$		0.10	-0.20	0.30	3.20
$\delta_m \mu^\ominus(\text{complex}^{2+})$		-3.40	-6.52	-10.20	-13.55

$[\text{Fe}(\text{tsb}, \text{Ph}, 8\text{amq})_2] (\text{ClO}_4)_2$ ,  $\lambda_{\text{max}} = 681 \text{ nm}$

	solvent composition, vol % MeOH				
	0	20	40	60	80
P(salt)	0.039	0.377	0.499	0.800	1.219
$\delta_m \mu^\ominus(\text{salt})$		-16.87	-18.96	-22.47	-25.60
$2 \delta_m \mu^\ominus(\text{ClO}_4^-)$		0.10	-0.20	0.30	3.20
$\delta_m \mu^\ominus(\text{complex}^{2+})$		-16.97	-18.76	-22.77	-28.80

TABLE 7.2

Observed first-order rate constants,  $k_{\text{obs}}$ , for acid hydrolysis of three bis-(terdentate) complexes of the type  $[\text{Fe}(\text{tsb},\text{R},8\text{amq})_2]^{2+}$  where R = H, Me or Ph in aqueous hydrochloric acid at 298.15 K [ionic strength maintained at 1M with NaCl].

HCl (M)	$10^4 k_{\text{obs}} (\text{s}^{-1})$		
	R = H	R = Me	R = Ph
1.00		4.40	
0.80		2.61	
0.73		2.23	
0.67		2.04	0.23
0.53		1.54	0.17
0.40		1.13	0.11
0.27	3.57	0.76	0.07
0.13	1.52	0.37	0.04
0.10		0.29	
0.07		0.22	
0.03		0.10	

### 7.3 CRYSTAL STRUCTURE OF A MONO-(HEXADENTATE) IRON(II) SCHIFF BASE COMPLEX: A COMPARATIVE STUDY

#### 7.3.1 Introduction

In Chapter 6, the  $^1\text{H}$  nmr spectrum of the mono-(hexadentate) iron(II) Schiff base complex  $[\text{Fe}(\text{hsb},\text{H},\text{t2a})]^{2+}$  measured in  $\text{d}_3$ -acetonitrile was shown [Fig. 6.16]. This complex contains the half-encapsulating hexadentate ligand derived from pyridine-2-carboxaldehyde and tris(2-aminoethyl)amine. Only one isomeric form of the complex was evident and this form possessed a  $\text{C}_3$  symmetry axis of rotation. Crystals of the perchlorate salt of this complex, prepared by the author, were used in an X-ray crystallographic study to determine the crystal structure of the complex carried out by Lesley Prouse. In this chapter, the resulting crystal structure data are compared with those for some related complexes. The complexes used in the comparison include related tris-(bidentate), bis-(terdentate) and mono-(hexadentate) metal di-imine complexes and complexes containing encapsulating hexadentate ligands.

#### 7.3.2 Experimental

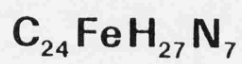
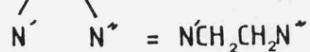
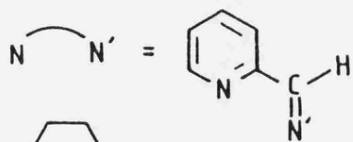
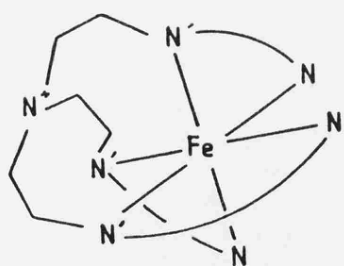
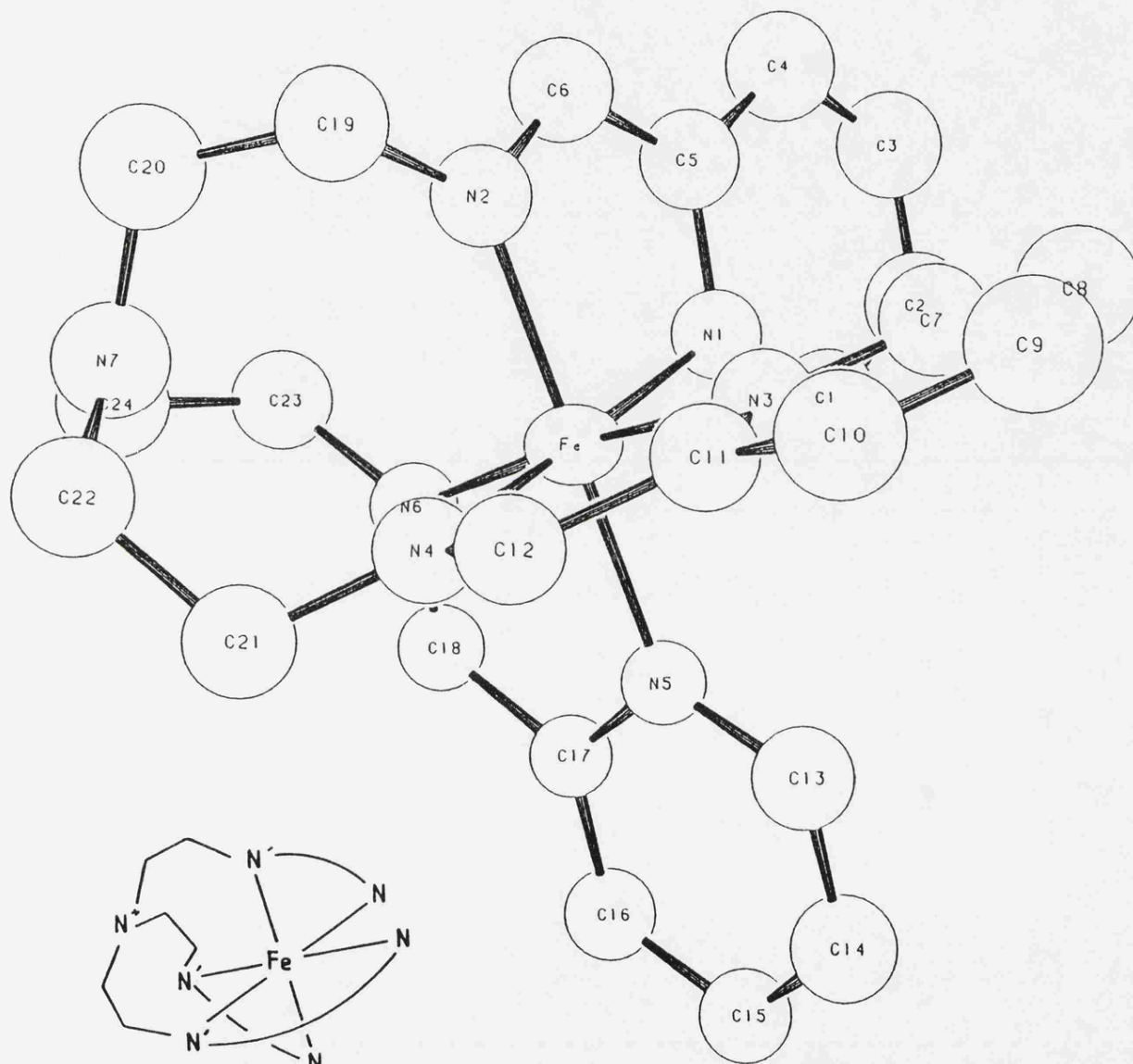
The low-spin iron(II) complex containing the hexadentate ligand derived from pyridine-2-carboxaldehyde and tris(2-aminoethyl)amine was synthesised by the general method of preparation detailed in Section 2.2.2. The complex was precipitated as the perchlorate salt. Precipitation did not occur immediately upon the addition of a saturated aqueous solution of sodium perchlorate to the reaction mixture. After two days, however, filtering of the solution produced a batch of deep purple crystals.

#### 7.3.3 Results and Discussion

The crystal structure of  $[\text{Fe}(\text{hsb},\text{H},\text{t2a})]^{2+}$  is illustrated in Fig. 7.7. Bond lengths and bond angles in the complex cation together with the

FIGURE 7.7

A perspective view of the  $[\text{Fe}(\text{hsb},\text{H},\text{t}2\text{a})]^{2+}$  cation.



those of the  $\text{ClO}_4^-$  units are shown in Tables 7.3 and 7.4 respectively. Fractional atomic co-ordinates are given in Table 7.5.

From Fig. 7.7 it can be seen that the six nitrogen atoms attached directly to the iron atom are arranged around the central iron atom in an approximately octahedral fashion. The arrangement, however, is slightly distorted from octahedral as the N-Fe-N bond angles are not  $90^\circ$ . The twist angle,  $\alpha$ , for the complex, defined in Fig. 7.8(a), is  $54^\circ$ . As such, the co-ordination geometry of these six nitrogen atoms about the central iron atom is much closer to being octahedral than trigonal prismatic. For an octahedron and a trigonal prism,  $\alpha$  is  $60^\circ$  and  $0^\circ$  respectively as illustrated in Fig. 7.8(b) and (c). The distortion of the half-encapsulated complex  $[\text{Fe}(\text{hsb},\text{H},\text{t}2\text{a})]^{2+}$  from octahedral geometry is similar to that in low-spin iron(II) tris-(bidentate) complexes. For example, in  $[\text{Fe}(\text{phen})_3]^{2+}$ , where phen is 1,10-phenanthroline,  $\alpha = 53^\circ$ <sup>15</sup> for the iodide dihydrate salt of the complex and  $\alpha = 55^\circ$ <sup>16</sup> for the bis-(antimony(III)*d*-tartrate) octahydrate salt of the complex. In  $[\text{Fe}(\text{bipy})_3]^{2+}$ , where bipy is 2,2'-bipyridyl,  $\alpha = 55^\circ$ .<sup>17,18</sup> For the mer isomeric form of the complex  $[\text{Fe}(\text{bsb},\text{Me},\text{Me})_3]^{2+}$ ,  $\alpha = 54^\circ$ .<sup>19</sup> Despite the high crystal field stabilization energy of  $t_{2g}^6$  Fe(II), and also  $t_{2g}^6$  Co(III), not all low-spin mono-(hexadentate) complexes of these ions possess approximately octahedral co-ordination geometries. In some cases the steric constraints imposed by ligands may outweigh, to varying degrees, the crystal field effects of the metal ions. This has been found to be the case for several encapsulated complexes of these ions<sup>12</sup> such as the Fe(II) complex shown in Fig. 7.9(a) in which  $\alpha$  is approximately  $22^\circ$ .<sup>13</sup> Even for the half-encapsulated iron(II) complex shown in Fig. 7.9(b) there is significant distortion from octahedral geometry,  $\alpha$  for this complex being  $49^\circ$ .<sup>14</sup> However, in the half-encapsulated complex

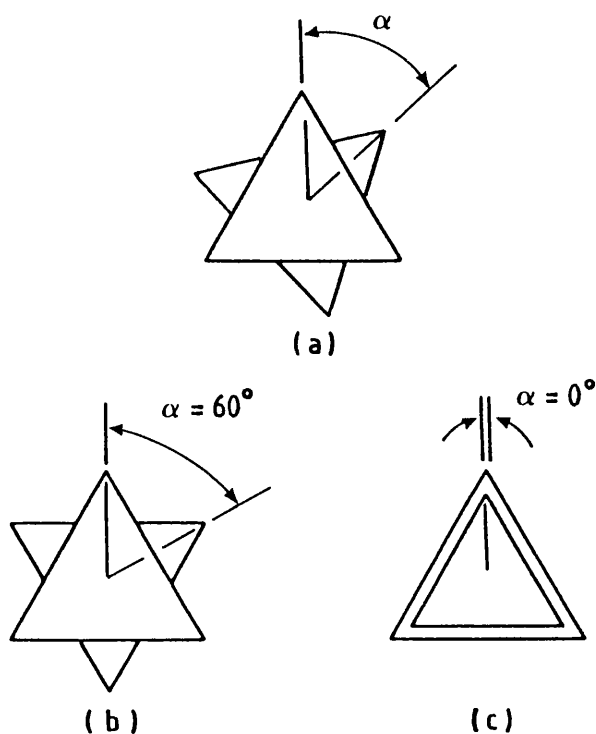


**FIGURE 7.8**

The twist angle,  $\alpha$ , in an octahedron (b), a trigonal prism (c) and an intermediate case (a).

$[\text{Fe}(\text{hsb}, \text{H}, \text{t}2\text{a})]^{2+}$  the ligand is flexible enough to allow the adoption of almost octahedral geometry. In this complex, the presence of a seventh nitrogen in the ligand, which forms the hub of the encapsulating moiety and is not bonded directly to the iron, and the flexible  $\text{CH}_2$  groups to which this atom is attached presumably confer a degree of flexibility on the ligand sufficient for the resulting iron(II) complex of the ligand to adopt a geometry close to that most favoured by the metal ion. By comparison, the half-encapsulating ligand shown in Fig. 7.9(b) appears to be more rigid and is thus more demanding in terms of the structural constraints it imposes in the formation of a complex  $[\text{ML}]^{n+}$  with a metal ion  $\text{M}^{n+}$ . When  $\text{M}^{n+} = \text{Fe}^{2+}$ , these constraints are apparently not completely overcome by the large preference for octahedral geometry of the metal ion. From this point of view, the crystal structures in the fully encapsulated

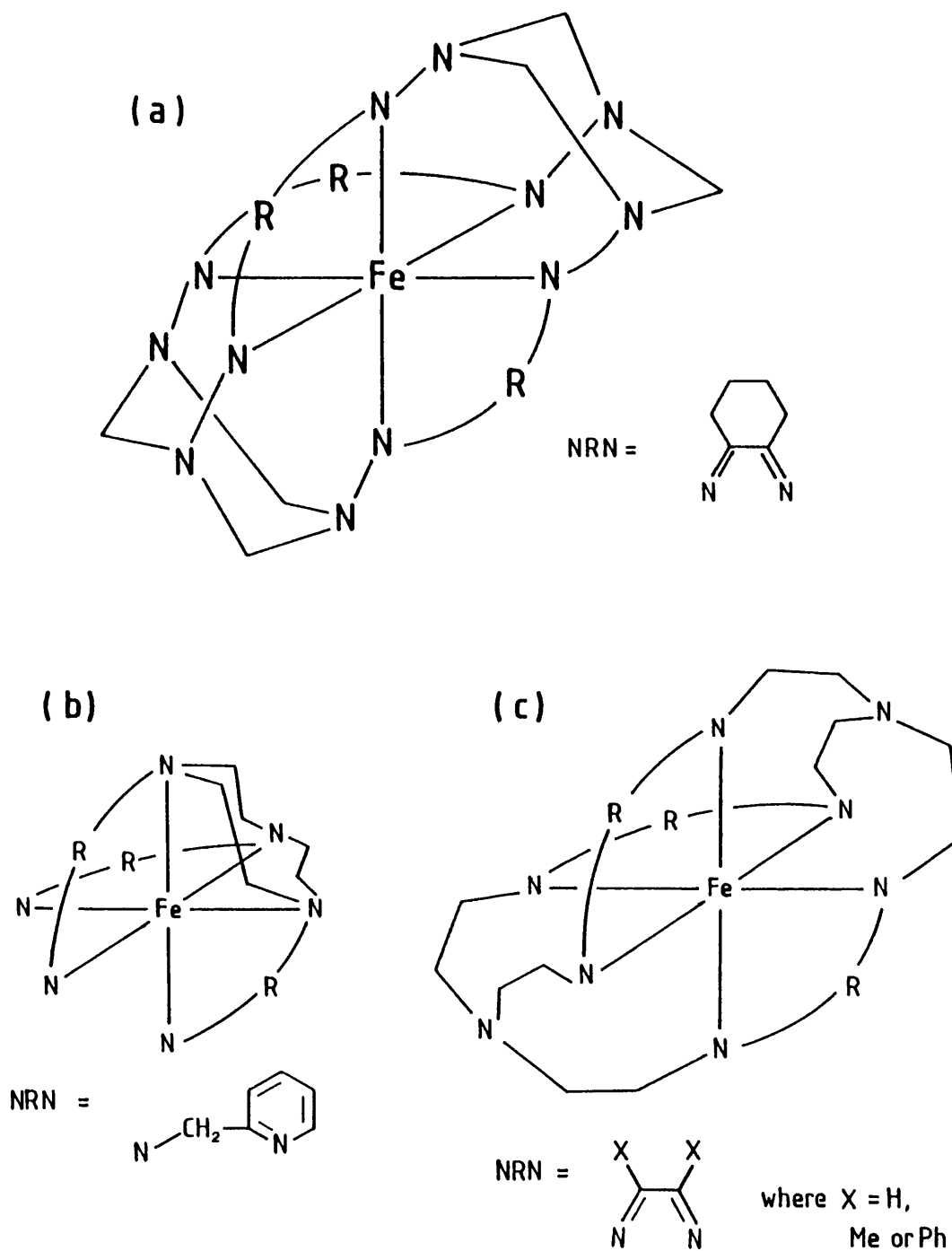


FIGURE 7.9

Six-co-ordinate low-spin iron(II) complexes: (a) and (c) fully encapsulated, (b) half-encapsulated.

analogues of  $[\text{Fe}(\text{hsb},\text{H},\text{t2a})]^{2+}$ , i.e. complexes containing a ligand of the type shown in Fig. 7.9(c) where R=H, Me or Ph would be of interest. Attempts to obtain crystals of the perchlorate salts of these iron(II) complexes using the general method of preparation [see Section 2.2.2] and modified methods [see Section 5.2.1] were unsuccessful. Preparative solutions of the complex in which R=H were purple, though not as intensely coloured as expected. No intense colour formation was observed in preparative solutions of the complex in which R=Ph. A blue powdered sample was precipitated from the preparative solution of the complex in which R=Me but no crystals could be obtained.

Although in solution the  $[\text{Fe}(\text{hsb},\text{H},\text{t2a})]^{2+}$  cation possesses a three-fold symmetry axis of rotation (as seen in the  $^1\text{H}$  nmr spectrum of this complex measured in  $\text{d}_3$ -acetonitrile shown in Fig. 6.16), in the solid state the crystal data parameters for each of the three identical ligand moieties are slightly different. This is in contrast to the mono-(hexadentate) iron(II) Schiff base complex  $[\text{Fe}(\text{hsb},\text{H},\text{trien})]^{2+}$  which possesses a two-fold symmetry axis of rotation both in solution (see nmr spectrum shown in Fig. 6.14) and in the solid state.<sup>20</sup>

The structure of the hexadentate ligand in the complex  $[\text{Fe}(\text{hsb},\text{H},\text{t2a})]^{2+}$  and its approximate stereochemical arrangement around the central iron atom, as determined by the X-ray crystallographic study, are shown in Fig. 7.10(a). For comparison, this figure also includes the corresponding arrangements in some related complexes as determined by X-ray crystallographic studies. The complex shown in Fig. 7.10(b) is the mono-(hexadentate) iron(II) Schiff base complex  $[\text{Fe}(\text{hsb},\text{H},\text{trien})]^{2+}$ .<sup>20</sup> The arrangement shown in Fig. 7.10(c) is typical of that in bis-(terpy) complexes, where terpy is 2,2';6',2''-terpyridyl, such as  $[\text{Co}(\text{terpy})_2]^{2+}$ ,<sup>21,22</sup>  $[\text{Co}(\text{terpy})_2]^{3+}$ ,<sup>23</sup> and  $[\text{Cr}(\text{terpy})_2]^{3+}$ .<sup>24</sup> The complex shown in Fig. 7.10(d)

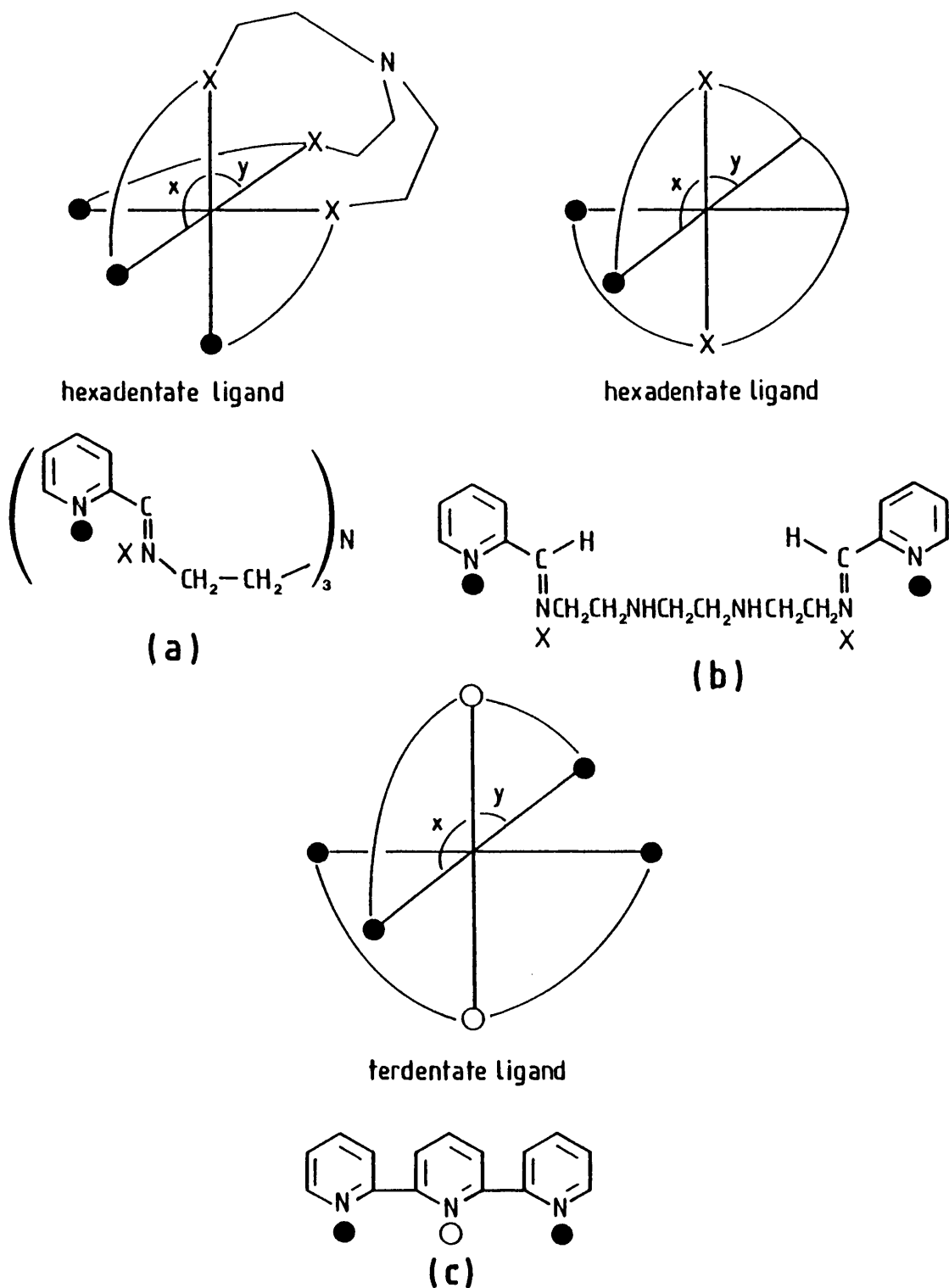
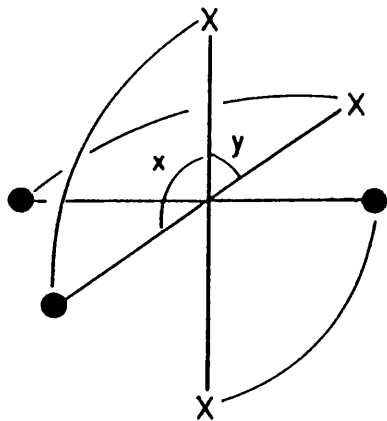
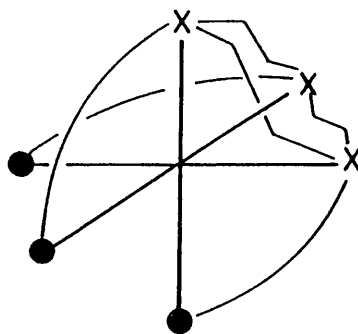


FIGURE 7.10

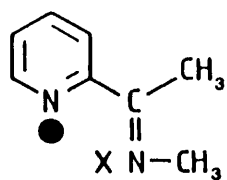
Approximate stereochemical arrangements in five metal complexes containing multidentate ligands in which six nitrogen atoms are bonded directly to the central metal atom.



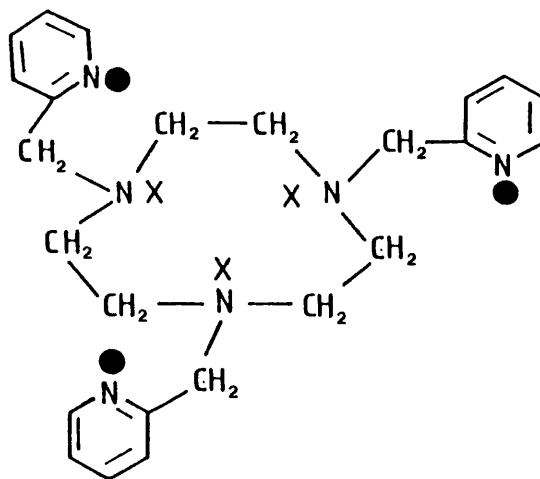
bidentate ligand



hexadentate ligand



(d)



(e)

is the mer isomeric form of the tris-(bidentate) iron(II) Schiff base complex  $[\text{Fe}(\text{bsb},\text{Me},\text{Me})_3]^{2+}$ , containing the unsymmetrical bidentate ligand derived from 2-acetyl pyridine and methylamine.<sup>19</sup> Thus, the complexes depicted in Fig. 7.10(a), (b), (c) and (d) all contain di-imine ligands. Those in Fig. 7.10(a), (b) and (d) contain, more specifically, Schiff base di-imine ligands. For ease of reference, the nitrogen atoms referred to specifically in the following discussion are labelled by symbols in Fig. 7.10. Solid circles indicate pyridyl nitrogen atoms, N (pyridyl). In the case of the complex depicted in Fig. 7.10(c), open circles are used to distinguish the central pyridyl nitrogen atoms from the distal pyridyl nitrogen atoms. Crosses indicate alkyl nitrogen atoms, N (alkyl). For the complex shown in Fig. 7.10(b), the N (alkyl) atoms thus labelled are those that form bidentate chelating units with the N (pyridyl) atoms.

For the complex  $[\text{Fe}(\text{hsb},\text{H},\text{t2a})]^{2+}$ , the Fe-N bond lengths are all different, covering the range 1.948 - 1.991 Å. Inequality of Fe-N bond lengths is a feature in many crystal structures of complexes of this type, for example,  $[\text{Fe}(\text{phen})_3]^{2+}$ ,<sup>15,16</sup>  $[\text{Fe}(\text{bipy})_3]^{2+}$ ,<sup>17,18</sup>  $[\text{Co}(\text{terpy})_2]^{3+}$ ,<sup>23</sup> and  $[\text{Fe}(\text{bsb},\text{Me},\text{Me})_3]^{2+}$ ,<sup>19</sup> although the range is slightly greater for this mono-(hexadentate) complex than for the other iron(II) complexes mentioned. For the three iron(II) Schiff base di-imine complexes depicted in Fig. 7.10(a), (b) and (d), the average iron to pyridyl nitrogen bond lengths, pyridyl nitrogen atoms being depicted by solid circles in Fig. 7.10, are 1.977, 1.969<sup>20</sup> and 1.939<sup>19</sup> Å respectively. Initial comparison of these three values suggests that the comparatively longer bond lengths in the two mono-(hexadentate) complexes may be a result of increased structural constraints due to higher denticity of these ligands as compared with those in the tris-(bidentate) complex. However, comparison of these

values with the corresponding value for  $[\text{Fe}(\text{phen})_3]^{2+}$ , which is  $1.973 \overset{\circ}{\text{A}}$ ,<sup>15</sup> shows those for the hexadentate complexes and  $[\text{Fe}(\text{phen})_3]^{2+}$  to be comparable, whilst those for the tris-(bidentate) complex are shorter.

The average Fe-N (alkyl) bond lengths for the nitrogen atoms denoted by crosses in the complexes shown in Fig. 7.10(a), (b) and (d) are 1.956, 1.868<sup>20</sup> and 1.962<sup>19</sup>  $\overset{\circ}{\text{A}}$  respectively. Thus, for the two mono-(hexadentate) complexes, Fe-N (pyridyl) bond lengths are greater than Fe-N (alkyl) bond lengths. For the tris-(bidentate) complex the reverse is true, i.e. Fe-N (alkyl) bond lengths are greater than Fe-N (pyridyl) bond lengths. In the latter case, this is explicable in terms of the overall weakening of the Fe-N (alkyl) bond due to the electron releasing effect of the methyl group attached directly to the nitrogen atom. For the two mono-(hexadentate) complexes, the comparative shortness of the Fe-N (alkyl) bonds may be the result of the constraints of these hexadentate ligands. The similarity of the co-ordination arrangements in the mono-(hexadentate) complex shown in Fig. 7.10(b) and in bis-(terdentate) complexes such as  $[\text{M}(\text{terpy})_2]^{n+}$  [Fig. 7.10(c)] has already been noted. In these latter complexes such as  $[\text{Co}(\text{terpy})_2]^{2+}$ ,<sup>21,22</sup>  $[\text{Co}(\text{terpy})_2]^{3+}$ ,<sup>23</sup> and  $[\text{Cr}(\text{terpy})_2]^{3+}$ ,<sup>24</sup> the central Fe-N bond in each terdentate ligand is shorter than the two distal Fe-N bonds. Thus in the types of complexes shown in Fig. 7.10(a), (b) and (c), the terminal Fe-N (pyridyl) bonds are, in all cases, longer than the adjacent Fe-Nitrogen bonds, the former nitrogens being depicted by solid circles in Fig. 7.10 and the latter nitrogen atoms by open circles or crosses. That the average Fe-N (pyridyl) bond length in the complex shown in Fig. 7.10(e),  $1.979 \overset{\circ}{\text{A}}$ ,<sup>14</sup> is less than that of the adjacent Fe-N (alkyl) bond,  $2.001 \overset{\circ}{\text{A}}$ ,<sup>14</sup> is most likely due to the nature of this bidentate chelating unit. Delocalization of iron to

nitrogen back-bonding is not possible in this complex unlike in the complexes in which the N (alkyl) atoms form part of the di-imine chelating unit.

The angles subtended by the di-imine chelating units at the iron atoms in the complexes shown in Fig. 7.10(a), (b), (c) and (d), labelled  $x$ , are in the ranges  $81.2$  to  $82.0^\circ$ ,  $81.2^\circ$ ,<sup>20</sup>  $81.7$  to  $82.5^\circ$  and  $80.1$  to  $80.9^\circ$ <sup>19</sup> respectively. The values given for the bis-(terdentate) complexes are those in  $[\text{Co}(\text{terpy})_2]^{3+}$ .<sup>23</sup> The values are comparable to those observed in  $[\text{Fe}(\text{bipy})_3]^{2+}$  which are in the range  $81.3$  to  $81.9^\circ$ .<sup>18</sup> The values of the angles labelled  $y$  are, for the complexes shown in Fig. 7.10(b), (c) and (d),  $84.7^\circ$ ,<sup>20</sup>  $81.7$  to  $82.5^\circ$ ,<sup>23</sup> and  $95.1$  to  $96.1^\circ$ <sup>19</sup> respectively. The comparatively smaller values of  $y$  for the mono-(hexadentate) and bis-(terdentate) complexes compared with those in the tris-(bidentate) complex are presumably due to the constraints of the ligands of higher denticity in the former two complexes. It is interesting, then, to note that the values for angle  $y$  in the complex shown in Fig. 7.10(a) range from  $94.6$  to  $96.1^\circ$ . These values are much closer to the corresponding values in the tris-(bidentate) complex than those in the mono-(hexadentate) or bis-(terdentate) complexes shown in Fig. 7.10(b) and (c) respectively, indicating the relatively undemanding nature of the ligand shown in Fig. 7.10(a) in terms of steric constraints.

Comparisons can also be made of C-N and C-C bond lengths in the di-imine moieties in the complexes shown in Fig. 7.10(a), (b) and (d). For these complexes, the average C-N bond lengths in the di-imine moieties which form part of a pyridyl ring are  $1.37$ ,  $1.36$ ,<sup>20</sup> and  $1.36$ <sup>19</sup> Å respectively, close to that of  $1.37$  Å in pyridine.<sup>25</sup> The average length of the corresponding bonds in the complex shown in Fig. 7.10(e) is also close to this value being  $1.36$ <sup>14</sup> Å. The average lengths of the C-N bonds for the

nitrogen atoms depicted by crosses in Fig. 7.10(a), (b) and (d) are 1.28, 1.31,<sup>20</sup> and 1.28<sup>19</sup> Å. These values are thus intermediate between those for a full C=N double bond (1.27 Å<sup>25</sup>) and a C-N (pyridyl) bond. In contrast, the average length for the corresponding bond in the complex shown in Fig. 7.10(e) is 1.48<sup>14</sup> Å. The increased length of this bond reflects the reduction in delocalization in the bidentate chelating unit in this complex compared with the corresponding di-imine chelating units in the other complexes. For the same reason, the C-C bonds in the di-imine chelating units are shorter than those in the N (pyridyl) CCH<sub>2</sub>N (alkyl) chelating units in the complex shown in Fig. 7.10(e).<sup>14</sup>

For the three complexes containing NCH<sub>2</sub>CH<sub>2</sub>N groups, those shown in Fig. 7.10(a), (b) and (e), the lengths of the C-C and C-N bonds in these moieties may be compared. The average C-C bond lengths for the three complexes, 1.53, 1.50,<sup>20</sup> and 1.52<sup>14</sup> Å respectively are comparable, though slightly shorter, than that in ethane, 1.54 Å.<sup>25</sup> Taking the value of C-N in RNH<sub>2</sub> to be 1.47 Å,<sup>25</sup> then again the average C-N bond lengths in the three complexes, 1.46, 1.50,<sup>20</sup> and 1.50<sup>14</sup> Å, are comparable.

For the complexes mentioned here, any assessment of 'trans' effects, e.g. lengths of Fe-N (pyridyl) bonds when the pyridyl nitrogen atoms are trans to other pyridyl nitrogen atoms or to alkyl nitrogen atoms etc., would be difficult considering the different natures and denticities of the ligands in the complexes. In the case of crystal structures of different diastereoisomeric forms of the same complex, such a study could prove most interesting.

TABLE 7.3

Bond lengths (Å) in [Fe(hsb,H,t2a)](ClO<sub>4</sub>)<sub>2</sub>

N(1)-Fe	1.962(7)	N(2)-Fe	1.969(7)
N(3)-Fe	1.991(8)	N(4)-Fe	1.948(7)
N(5)-Fe	1.977(6)	N(6)-Fe	1.950(7)
C(1)-N(1)	1.329(14)	C(5)-N(1)	1.383(14)
C(6)-N(2)	1.276(13)	C(19)-N(2)	1.456(12)
C(7)-N(3)	1.340(14)	C(11)-N(3)	1.366(12)
C(12)-N(4)	1.292(14)	C(21)-N(4)	1.472(12)
C(13)-N(5)	1.342(12)	C(17)-N(5)	1.371(11)
C(18)-N(6)	1.283(11)	C(23)-N(6)	1.486(12)
C(24)-N(7)	1.428(14)	C(22)-N(7)	1.457(13)
C(20)-N(7)	1.434(14)	H(1)-C(1)	1.080(17)
C(2)-C(1)	1.387(14)	H(2)-C(2)	1.080(20)
C(3)-C(2)	1.378(22)	H(3)-C(3)	1.080(15)
C(4)-C(3)	1.346(21)	H(4)-C(4)	1.080(20)
C(5)-C(4)	1.365(15)	C(6)-C(5)	1.437(15)
H(6)-C(6)	1.080(15)	H(7)-C(7)	1.080(14)
C(8)-C(7)	1.393(17)	H(8)-C(8)	1.080(16)
C(9)-C(8)	1.365(18)	H(9)-C(9)	1.080(21)
C(10)-C(9)	1.381(20)	H(10)-C(10)	1.080(15)
C(11)-C(10)	1.384(16)	C(12)-C(11)	1.441(16)
H(12)-C(12)	0.98(8)	H(13)-C(13)	1.080(13)
C(14)-C(13)	1.363(15)	H(14)-C(14)	1.080(15)
C(15)-C(14)	1.387(14)	H(15)-C(15)	1.080(14)
C(16)-C(15)	1.406(14)	H(16)-C(16)	1.080(14)
C(17)-C(16)	1.394(13)	C(18)-C(17)	1.441(13)
H(18)-C(18)	1.03(8)	H(23)-C(23)	1.080(15)
H(231)-C(23)	1.080(15)	C(24)-C(23)	1.542(15)
H(24)-C(24)	1.080(17)	H(241)-C(24)	1.080(15)
H(22)-C(22)	1.080(15)	H(221)-C(22)	1.080(17)
C(21)-C(22)	1.519(14)	H(20)-C(20)	1.080(17)
H(201)-C(20)	1.080(15)	C(19)-C(20)	1.531(17)
H(21)-C(21)	1.080(15)	H(211)-C(21)	1.080(15)
H(19)-C(19)	1.080(14)	H(191)-C(19)	1.080(14)
O(1)-Cl(1)	1.384(9)	O(2)-Cl(1)	1.411(8)
O(3)-Cl(1)	1.407(10)	O(4)-Cl(1)	1.380(9)
O(5)-Cl(2)	1.318(14)	O(6)-Cl(2)	1.349(14)
O(7)-Cl(2)	1.366(10)	O(8)-Cl(2)	1.350(14)

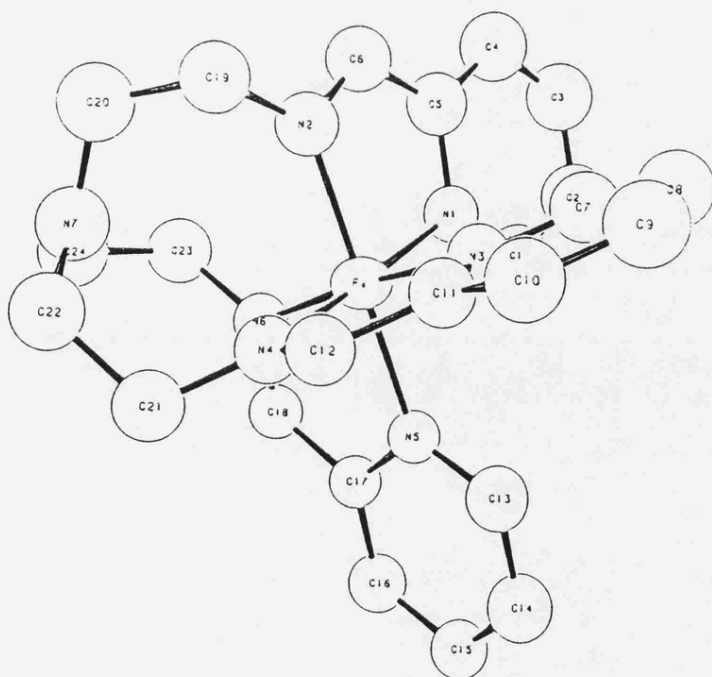
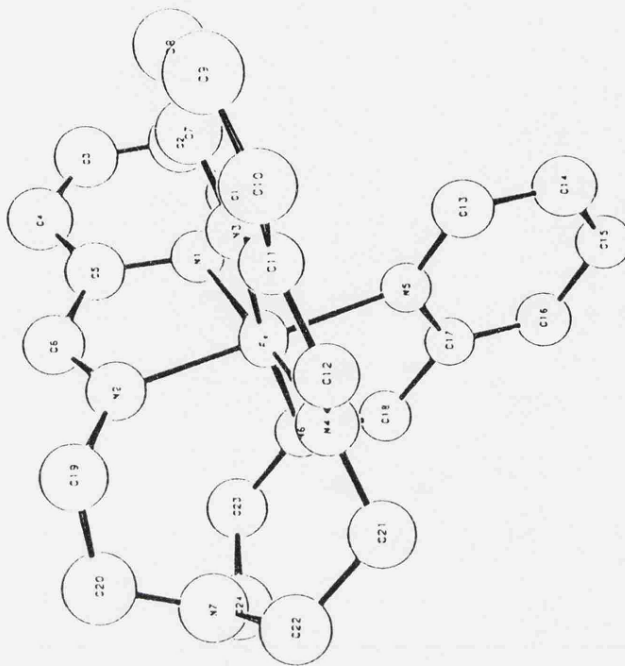


TABLE 7.4

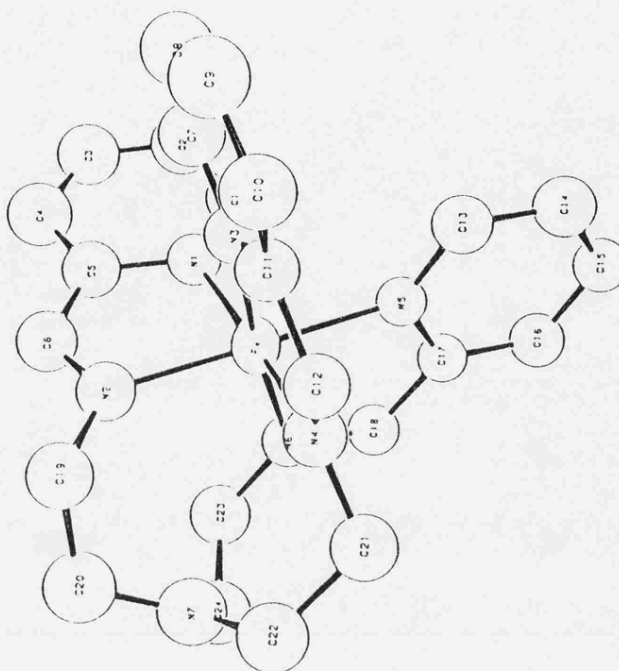
Bond angles (°) in [Fe(hsb,H,t2a)](ClO<sub>4</sub>)<sub>2</sub>

N(2)-Fe-N(1)	82.0(3)	N(3)-Fe-N(1)	93.1(3)	H(21)-C(21)-C(22)	108.8(10)	H(211)-C(21)-N(4)	108.5(10)
N(3)-Fe-N(2)	89.2(3)	N(4)-Fe-N(1)	173.9(3)	H(211)-C(21)-C(22)	108.5(10)	H(211)-C(21)-H(21)	109.5(11)
N(4)-Fe-N(2)	94.6(3)	N(4)-Fe-N(3)	81.8(3)	C(20)-C(19)-N(2)	112.4(9)	H(19)-C(19)-N(2)	109.0(9)
N(5)-Fe-N(1)	94.9(3)	N(5)-Fe-N(2)	175.9(3)	H(19)-C(19)-C(20)	108.8(11)	H(191)-C(19)-N(2)	108.5(10)
N(5)-Fe-N(3)	93.6(3)	N(5)-Fe-N(4)	88.7(3)	H(191)-C(19)-C(20)	108.7(10)	H(191)-C(19)-H(19)	109.5(12)
N(6)-Fe-N(1)	89.4(3)	N(6)-Fe-N(2)	96.1(3)	O(2)-Cl(1)-O(1)	108.5(5)	O(3)-Cl(1)-O(1)	106.2(6)
N(6)-Fe-N(3)	174.4(3)	N(6)-Fe-N(4)	96.1(3)	O(3)-Cl(1)-O(2)	108.5(6)	O(4)-Cl(1)-O(1)	111.9(6)
N(6)-Fe-N(5)	81.2(3)	C(1)-N(1)-Fe	130.3(7)	O(4)-Cl(1)-O(2)	110.3(5)	O(7)-Cl(2)-O(5)	112.6(9)
C(5)-N(1)-Fe	113.2(6)	C(5)-N(1)-C(11)	116.3(8)	O(6)-Cl(2)-O(5)	107.0(9)	O(7)-Cl(2)-O(5)	112.1(9)
C(6)-N(2)-Fe	113.8(7)	C(19)-N(2)-Fe	125.9(6)	O(8)-Cl(2)-O(5)	108.7(8)	O(8)-Cl(2)-O(7)	111.3(8)
C(19)-N(2)-C(6)	120.2(8)	C(7)-N(3)-Fe	128.0(6)	O(8)-Cl(2)-O(6)	104.8(8)		
C(11)-N(3)-Fe	113.4(7)	C(11)-N(3)-C(7)	118.5(9)				
C(12)-N(4)-Fe	114.0(7)	C(21)-N(4)-Fe	126.6(6)				
C(21)-N(4)-C(12)	119.3(8)	C(13)-N(5)-Fe	129.0(6)				
C(17)-N(5)-Fe	113.5(5)	C(17)-N(5)-C(13)	117.5(7)				
C(18)-N(6)-Fe	115.6(6)	C(23)-N(6)-Fe	126.5(6)				
C(23)-N(6)-C(18)	117.8(8)	C(22)-N(7)-C(24)	120.4(8)				
C(20)-N(7)-C(24)	119.3(9)	C(20)-N(7)-C(22)	120.2(9)				
H(1)-C(1)-N(1)	118.3(10)	C(2)-C(1)-N(1)	123.2(11)				
C(2)-C(1)-H(1)	118.5(13)	H(2)-C(2)-C(1)	120.7(14)				
C(3)-C(2)-C(1)	118.4(12)	C(3)-C(2)-H(2)	120.9(12)				
H(3)-C(3)-C(2)	119.9(17)	C(4)-C(3)-C(2)	120.0(11)				
C(4)-C(3)-H(3)	120.1(18)	H(4)-C(4)-C(3)	120.2(13)				
C(5)-C(4)-C(3)	119.4(13)	C(5)-C(4)-H(4)	120.4(14)				
C(4)-C(5)-N(1)	122.6(11)	C(6)-C(5)-N(1)	112.4(8)				
C(6)-C(5)-C(4)	124.9(11)	C(5)-C(6)-N(2)	118.5(9)				
H(6)-C(6)-N(2)	120.7(11)	H(6)-C(6)-C(5)	120.8(11)				
H(7)-C(7)-N(3)	119.3(12)	C(8)-C(7)-N(3)	121.4(9)				
C(8)-C(7)-H(7)	119.3(12)	H(8)-C(8)-C(7)	119.9(12)				
C(9)-C(8)-C(7)	120.2(11)	H(9)-C(8)-H(8)	119.9(14)				
H(9)-C(9)-C(8)	120.6(15)	C(10)-C(9)-C(8)	118.8(12)				
C(10)-C(9)-H(9)	120.5(14)	H(10)-C(10)-C(9)	120.2(14)				
C(11)-C(10)-C(9)	119.4(10)	C(11)-C(10)-H(10)	120.4(14)				
C(12)-C(11)-N(3)	121.6(10)	C(12)-C(11)-N(3)	111.9(9)				
H(12)-C(12)-N(4)	126.4(9)	C(11)-C(12)-N(4)	118.8(9)				
H(13)-C(13)-N(5)	115(5)	H(12)-C(12)-C(11)	126(5)				
C(14)-C(13)-H(13)	118.5(11)	C(14)-C(13)-N(5)	122.7(9)				
C(15)-C(14)-C(13)	118.7(11)	H(14)-C(14)-C(13)	119.4(11)				
H(15)-C(15)-C(14)	121.1(10)	C(15)-C(14)-H(14)	119.5(11)				
C(16)-C(15)-H(15)	121.3(10)	C(16)-C(15)-C(14)	117.4(9)				
C(17)-C(16)-C(15)	121.3(10)	H(16)-C(16)-C(15)	120.7(10)				
C(17)-C(16)-H(16)	118.7(9)	C(17)-C(16)-H(16)	120.7(10)				
C(16)-C(17)-N(5)	122.5(8)	C(18)-C(17)-N(5)	112.7(8)				
C(18)-C(17)-C(16)	124.8(8)	C(17)-C(18)-N(6)	116.9(8)				
H(18)-C(18)-N(6)	116(4)	H(18)-C(18)-C(17)	127(4)				
H(23)-C(23)-N(6)	109.1(11)	H(231)-C(23)-N(6)	109.1(10)				
H(231)-C(23)-H(23)	109.5(12)	C(24)-C(23)-N(6)	111.0(8)				
C(24)-C(23)-H(23)	109.0(10)	C(24)-C(23)-H(231)	109.1(11)				
C(23)-C(24)-N(7)	115.3(10)	H(24)-C(24)-N(7)	108.1(11)				
H(24)-C(24)-C(23)	107.8(10)	H(241)-C(24)-N(7)	108.1(10)				
H(241)-C(24)-C(23)	108.0(11)	H(241)-C(24)-H(24)	109.5(14)				
H(22)-C(22)-N(7)	108.0(10)	H(221)-C(22)-N(7)	108.2(10)				
H(221)-C(22)-H(22)	109.5(12)	C(21)-C(22)-N(7)	114.9(8)				
C(21)-C(22)-H(22)	108.2(11)	C(21)-C(22)-H(221)	108.0(10)				
H(20)-C(20)-N(7)	108.1(12)	H(201)-C(20)-N(7)	108.4(11)				
H(201)-C(20)-H(20)	109.5(12)	C(19)-C(20)-N(7)	114.5(8)				
C(19)-C(20)-H(20)	108.3(11)	C(19)-C(20)-H(201)	108.0(12)				
C(22)-C(21)-N(4)	112.7(9)	H(21)-C(21)-N(4)	108.7(9)				



Atom	x	y	z
Fe	0.20798(11)	0.11303(8)	0.19653(7)
N(1)	0.3524(6)	0.1017(6)	0.2738(4)
N(2)	0.2281(7)	0.2345(4)	0.2234(5)
N(3)	0.0815(7)	0.1023(5)	0.2744(5)
N(4)	0.0550(7)	0.1301(5)	0.1283(4)
N(5)	0.2011(6)	-0.0095(4)	0.1700(4)
N(6)	0.3252(6)	0.1133(4)	0.1160(4)
N(7)	0.1937(8)	0.2681(5)	0.0563(5)
C(1)	0.4138(9)	0.0327(8)	0.3007(6)
C(2)	0.5065(9)	0.0346(10)	0.3617(7)
C(3)	0.5404(10)	0.1125(12)	0.3938(7)
C(4)	0.4823(10)	0.1839(10)	0.3667(7)
C(5)	0.3896(9)	0.1784(8)	0.3078(6)
C(6)	0.3161(10)	0.2491(7)	0.2763(7)
C(7)	0.1031(10)	0.0879(6)	0.3500(7)
C(8)	0.0041(11)	0.0819(6)	0.3976(7)
C(9)	-0.1181(13)	0.0931(7)	0.3679(9)
C(10)	-0.1415(10)	0.1073(6)	0.2899(8)
C(11)	-0.0407(9)	0.1130(6)	0.2444(6)
C(12)	-0.0486(10)	0.1258(6)	0.1623(7)
C(13)	0.1315(9)	-0.0717(7)	0.1985(5)
C(14)	0.1311(9)	-0.1533(7)	0.1717(6)
C(15)	0.2072(9)	-0.1774(6)	0.1444(5)
C(16)	0.2831(9)	-0.1140(6)	0.0844(6)
C(17)	0.2760(8)	-0.0311(6)	0.1125(5)
C(18)	0.3478(8)	0.0401(6)	0.0871(6)
C(19)	0.1503(9)	0.3042(6)	0.1908(7)
C(20)	0.1917(12)	0.3340(6)	0.1132(7)
C(21)	0.0482(10)	0.1418(6)	0.0443(6)
C(22)	0.0754(10)	0.2329(7)	0.0212(7)
C(23)	0.3959(10)	0.1879(6)	0.0892(7)
C(24)	0.3122(11)	0.2414(7)	0.0309(7)
O(1)	0.1978(8)	0.0619(6)	0.8762(6)
O(2)	0.4084(7)	0.0884(4)	0.9047(4)
O(3)	0.3343(10)	0.0290(6)	0.7899(5)
O(4)	0.3356(8)	-0.0492(5)	0.9007(6)
O(5)	0.8298(14)	0.3191(11)	0.1448(7)
O(6)	0.7610(13)	0.4122(8)	0.0616(8)
O(7)	0.7265(11)	0.2764(6)	0.0347(5)
O(8)	0.6248(11)	0.3462(8)	0.1234(9)
H(1)	0.3903(9)	-0.0279(8)	0.2738(6)
H(2)	0.5509(9)	-0.0235(10)	0.3834(7)
H(3)	0.6136(10)	0.1160(12)	0.4405(7)
H(4)	0.5090(10)	0.2451(10)	0.3914(7)
H(6)	0.3349(10)	0.3132(7)	0.2968(7)
H(7)	0.1995(10)	0.0811(6)	0.3748(7)
H(8)	0.0238(11)	0.0681(6)	0.4580(7)
H(9)	-0.1952(13)	0.0908(7)	0.4047(9)
H(10)	-0.2376(10)	0.1140(6)	0.2647(8)
H(12)	-0.127(8)	0.128(5)	0.128(5)
H(13)	0.0737(9)	-0.0562(7)	0.2448(5)
H(14)	0.0701(9)	-0.2000(7)	0.1954(6)
H(15)	0.2083(9)	-0.2423(6)	0.0937(5)
H(16)	0.3454(9)	-0.1292(6)	0.0403(6)
H(18)	0.411(7)	0.040(4)	0.045(4)

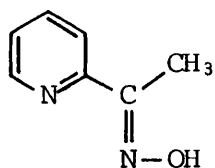
TABLE 7.5  
Fractional atomic co-ordinates for  
[Fe(hsb,H,t2a)](ClO<sub>4</sub>)<sub>2</sub>



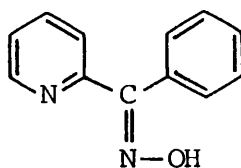
## 7.4 REACTION OF IRON(II) WITH SCHIFF BASE KETOXIME LIGANDS

### 7.4.1 Introduction

Iron(II) forms intensely coloured low-spin complexes with methyl-2-pyridyl ketoxime (IX)<sup>26</sup> and phenyl-2-pyridyl ketoxime (X).<sup>27,28</sup> The nature of these complex species depends on the conditions under which



(IX)



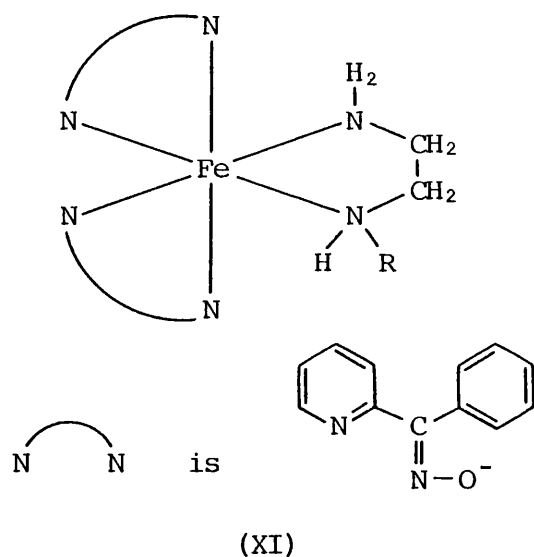
(X)

the preparations are carried out. When iron(II) is combined with imino-oxime ligands of this type in the ratio 1:3 or in the presence of an excess of ligand in aqueous solution, then the complex species formed are low-spin iron(II) tris-(bidentate) complexes.<sup>26,27,29,30</sup> Despite complex species having metal to ligand ratios of 1:3 being generated in all such cases, species formed in acidic aqueous media are different from those formed in aqueous solutions made alkaline by the addition of hydroxide.<sup>26,27,29,30</sup> For example, for the complex formed by the reaction of iron(II) with methyl-2-pyridyl ketoxime in aqueous solution (1:3 ratio of metal to ligand or excess of ligand), Banerjea and Tripathi<sup>26</sup> reported the existence of two different species of the complex, one formed in acidic aqueous solutions (pH < 5.0) and the other in aqueous solutions made alkaline by the addition of hydroxide (pH > 7.0). The acidic species,  $\lambda_{\max} = 475 \text{ nm}$ , was reported to be relatively unstable and the colour of a solution containing this species was seen gradually to change. This change resulted in a shift of  $\lambda_{\max}$  of the solution from 475 to 525 nm. This latter value of  $\lambda_{\max}$  was that of the species formed under alkaline conditions, the more stable of the two species. The shift in  $\lambda_{\max}$  was attributed to a fac (unstable) to mer (stable) isomeric conversion. This

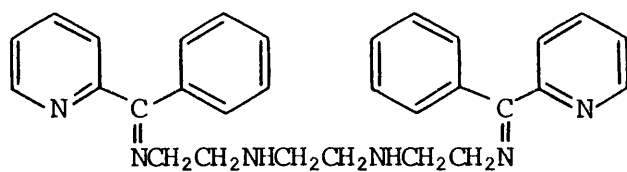
is in contrast to the observations made in Chapter 6 of this study concerning a sample of this complex which had been made under acidic conditions. The  $^1\text{H}$  nmr spectrum of this sample measured in  $\text{d}_3$ -acetonitrile at 300 MHz, which was shown in Fig. 6.6, indicated the sample to contain predominantly the mer isomeric form of the complex. [That the proportions of the isomers as observed in the nmr spectra shown in Chapter 6 reflected the proportions in the solid samples was suggested by the following observations. On many occasions, different samples of the same complex yielded spectra in  $\text{d}_3$ -acetonitrile which indicated the existence of differing proportions of isomers in the samples. Yet, for a given sample, the proportion of the isomers in  $\text{d}_3$ -acetonitrile as indicated by the nmr spectra did not change with time.] In this section,  $^1\text{H}$  nmr spectra obtained for samples of the complexes formed by combination of iron(II) with either methyl-2-pyridyl ketoxime or phenyl-2-pyridyl ketoxime (1:3 metal to ligand ratio) in aqueous solutions under acidic and alkaline conditions are used in conjunction with ultraviolet/visible absorption spectra in an attempt to resolve these conflicting observations.

There is some work in the literature concerned with the use of Schiff base ketoxime ligands as analytical reagents for determining amounts of iron(II) in aqueous solutions made alkaline by the addition of primary amines, rather than by the addition of hydroxide.<sup>28</sup> In such cases, the possibility arises of the amines themselves being involved in the formation of iron(II) complex species as opposed to their solely providing a strongly alkaline medium in which to combine iron(II) and the ketoxime ligands. [The use of different alkaline solvent media was investigated as alkaline media permitted the extraction of complex species formed in solution into isoamyl alcohol (3-methyl-1-butanol) + ethanol mixtures.]

Chernin and Simonsen<sup>28</sup> reported that iron(II) formed bluish-purple complexes with phenyl-2-pyridyl ketoxime in aqueous ethylenediamine,  $\text{NH}_2(\text{CH}_2)_2\text{NH}_2$ , and in aqueous triethylenetetramine,  $\text{NH}_2(\text{CH}_2)_2\text{NH}(\text{CH}_2)_2\text{NH}(\text{CH}_2)_2\text{NH}_2$  mixtures. The complex species formed in each case were reported to have identical ultraviolet/visible absorption spectra ( $\lambda_{\text{max}} = 588, 509$  and  $405$  nm for solutions of the complexes in 15:2 isoamyl alcohol : ethanol mixtures). A 2:1 mole ratio of oxime to iron was established and the complex species were found to be uncharged. Structures of the complex species of the type shown in (XI) were suggested, where R is H and  $(\text{CH}_2)_2\text{NH}(\text{CH}_2)_2\text{NH}_2$  for the species formed in aqueous ethylenediamine and in aqueous triethylenetetramine mixtures respectively. The complex of the type (XI) where R is  $(\text{CH}_2)_2\text{NH}(\text{CH}_2)_2\text{NH}_2$ , i.e. the complex



produced when the amine is triethylenetetramine; is related to the mono- (hexadentate) iron(II) Schiff base di-imine complex  $[\text{Fe}(\text{hsb}, \text{Ph}, \text{trien})]^{2+}$  which appeared in Chapters 5 and 6. This complex contains the hexadentate ligand derived from 2-benzoyl pyridine and triethylenetetramine (XII). Both of these complexes contain related bidentate di-imine moieties and the same amine moiety in the ratio 2:1. In the hexadentate complex, the



(XII)

bidentate ligands are directly attached to each end of the amine moiety while in the complex of the type (XI) they are not. Attempts were made to prepare the complex of the type (XI) in aqueous triethylenetetramine media and, subsequently, in aqueous ethylenediamine media. As a comparison (cf. XI and XII) iron(II) was also combined with 2-benzoyl pyridine in aqueous triethylenetetramine mixtures and in aqueous ethylenediamine mixtures under the same conditions. It was hoped that any complex species isolated from these preparations could be characterised from  $^1\text{H}$  nmr spectra by utilizing information gained thus far from spectra of related complexes.

In the following sections, when complex species formed under acidic and alkaline conditions are referred to, then 'alkaline' indicates only aqueous solutions made alkaline by the addition of sodium hydroxide. When complex species formed in aqueous amine mixtures are referred to, which are also alkaline, then they are referred to specifically as being formed in aqueous amine mixtures, i.e. aqueous triethylenetetramine or aqueous ethylenediamine mixtures.

## 7.4.2 Experimental

### 7.4.2.1 General

Methyl-2-pyridyl ketoxime and phenyl-2-pyridyl ketoxime were prepared as described in Section 2.2.3 by the combination of hydroxylamine hydrochloride with 2-acetyl pyridine and 2-benzoyl pyridine respectively. These Schiff base ketoxime ligands were combined with iron(II) under the various conditions outlined below.

Ultraviolet/visible repeat scan spectra were obtained using an SP 800 spectrophotometer (see Section 2.3.3).  $^1\text{H}$  nmr spectra of samples were measured in deuterated solvents with TMS as the internal reference using Varian EM 390 and Bruker AM 300 spectrometers.

#### 7.4.2.2 Generation of complex species in acidic and alkaline aqueous solutions

The experimental procedure used for combining iron(II) with the Schiff base ketoxime ligands (1:3 metal to ligand ratio) under acidic conditions in aqueous solutions was described in Section 2.2.3. In the preparation of the complexes under alkaline conditions, the procedure used was initially the same as in the generation of complexes under acidic conditions. However, after the reactants had been combined in solution, the pH of the solution was adjusted to over 10 by the addition of aqueous sodium hydroxide. It was noted that for both the ketoxime ligands, the acidic preparative solutions were red whereas the alkaline preparative solutions were more purple in colour. Solid samples were obtained from the acidic preparative solutions by the addition of saturated solutions of either sodium perchlorate or potassium hexafluorophosphate to the reaction mixtures. For the alkaline preparative solutions, precipitation occurred without subsequent addition of any salt solutions. Precipitates were removed from solution by filtration, washed with water, ethanol and ether and dried in vacuo over phosphorus pentoxide.

#### 7.4.2.3 Generation of complex species in water + amine mixtures

In these preparations, iron(II) chloride tetrahydrate and either 2-benzoyl pyridine or phenyl-2-pyridyl ketoxime were combined in a metal to ligand ratio of 1:3. 0.1g of iron(II) chloride tetrahydrate was dissolved in 10  $\text{cm}^3$  of water and to this solution were added either 5  $\text{cm}^3$  of ethylenediamine or 10  $\text{cm}^3$  of triethylenetetramine. After addition of

a small amount of sodium dithionite, the solution was allowed to stand for several minutes. The pyridyl derivative (i.e. either 2-benzoyl pyridine or phenyl-2-pyridyl ketoxime), dissolved in a minimum amount of hot ethanol, was then added to the solution. The solution was heated on a steam bath for 10 minutes and then allowed to cool. It was noted that in the two cases where the pyridyl derivative used was phenyl-2-pyridyl ketoxime, the deep blue colour of the complex species generated in solution developed instantaneously. When the pyridyl derivative was 2-benzoyl pyridine then the colour developed more slowly, in about 10-15 minutes.  $\lambda_{\max}$  for the two preparative solutions containing ethylenediamine was 613 nm. For the solutions containing triethylenetetramine,  $\lambda_{\max} = 615$  nm. Values of  $\lambda_{\max}$  for the complex species extracted into 15:2 isoamyl alcohol : ethanol mixtures were 628 and 629 nm respectively. Complex species were precipitated from all the four types of preparative solutions by the addition of saturated aqueous solutions of either sodium perchlorate or potassium hexafluorophosphate to portions of the reaction mixtures. These solids, deep blue in colour, were removed from the solutions by filtration, washed with water, ethanol and ether and dried in vacuo over phosphorus pentoxide. For the remaining filtrates (still coloured) diluted with water,  $\lambda_{\max}$  remained unchanged except in the case of the preparative solutions in which iron(II) had been combined with phenyl-2-pyridyl ketoxime in aqueous ethylenediamine mixtures.  $\lambda_{\max}$  for these filtrate solutions, which were more purple than blue in colour, was 587 nm. Complex species in a solution of the latter type were extracted into 15:2 isoamyl alcohol : ethanol mixtures and the layers separated. The purple solution of the complex species in the alcohol mixtures was allowed to evaporate. The resulting viscous paste was taken up in water. Solids were obtained from this solution by the addition of saturated

aqueous solutions of either sodium perchlorate or potassium hexafluorophosphate to portions of the solution. The solids were removed by filtration and washed and dried as above.

### 7.4.3 Results and Discussion

#### 7.4.3.1 Complex species formed in acidic and alkaline aqueous solutions

The complex species generated in, and precipitated from, acidic and alkaline aqueous solutions are henceforth referred to as the acidic and alkaline species respectively.

As reported in the literature,<sup>26</sup> the acidic species was unstable in aqueous solutions. In strongly acidic aqueous solution, pH = 1.0, the intense colour of the complex species disappeared within a matter of minutes. No changes in  $\lambda_{\max}$  for the solution, 474 nm, were discernible in the ultraviolet/visible repeat scan spectrum of the solution. In less acidic, neutral and alkaline aqueous solutions, pH = 4.0, 7.0 and 9.2 respectively, a different pattern was observed. The initial values of  $\lambda_{\max}$  for solutions of these types containing the acidic species varied between 474 and 485 nm. With time,  $\lambda_{\max}$  for the solutions shifted towards longer wavelengths. In all cases, the final value of  $\lambda_{\max}$  for solutions of these types was in the region of 528-531 nm. A typical ultraviolet/visible repeat scan spectrum for a solution of the acidic species in water is shown in Fig. 7.11. The lapse of time from the start of monitoring ( $\lambda_{\max} = 484$  nm) to the end ( $\lambda_{\max} = 531$  nm) was approximately 130 minutes. After this time there was a further increase in the absorbance at 531 nm of approximately 0.02 absorbance units. The peak at 531 nm then gradually decayed with no discernible shifts in  $\lambda_{\max}$  and at a much slower rate than it appeared. The half-life for this reaction, i.e. the time taken for the peak at 531 nm to diminish to half its maximum absorbance was approximately

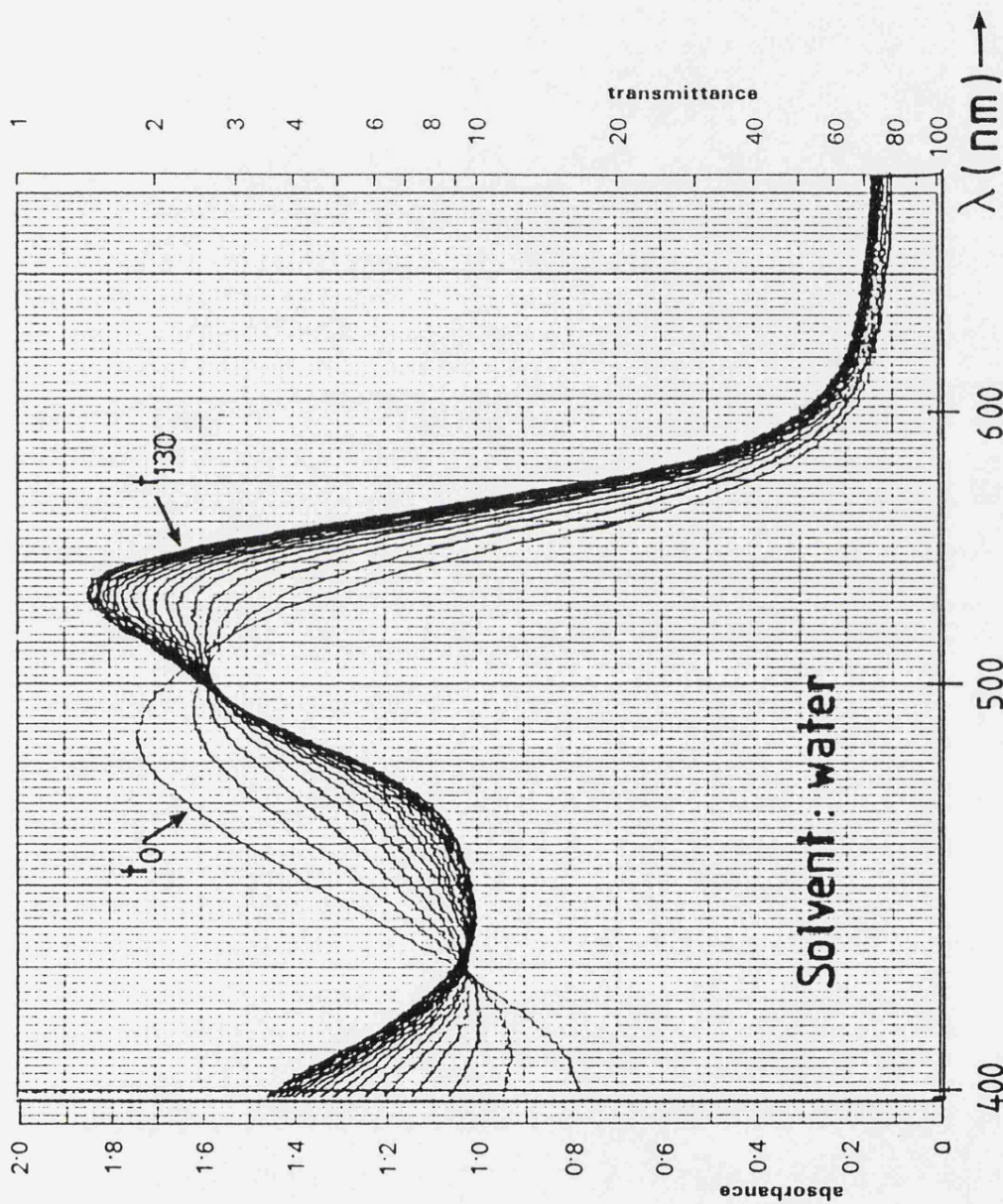


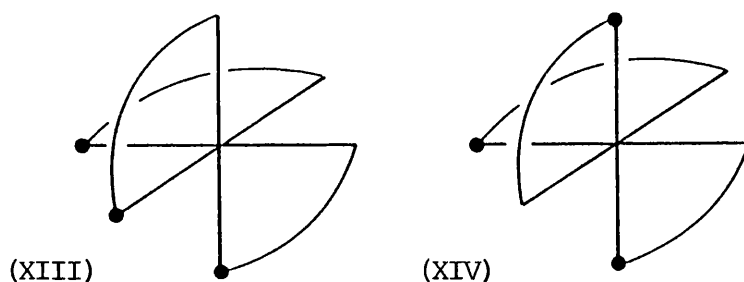
FIGURE 7.11

Repeat scan of the ultraviolet/visible absorption region of  $[\text{Fe}(\text{bsb},\text{Me},\text{OH})_3]^{2+}$  made under acidic conditions:  $t_0$  = spectrum when monitoring began,  $t_{130}$  = spectrum after approximately 130 minutes of monitoring.

10 days. The same pattern of change as shown in Fig. 7.11 was also observed for solutions of the acidic species in buffered aqueous solutions (pH = 4.0, 7.0 or 9.2) and in methanolic solutions. For these solutions, the time taken for the final values of  $\lambda_{\max}$  to be attained (528-531 nm) decreased in the order pH = 4.0 > pH = 7.0 > pH = 9.2. By comparison with solutions of the acidic species, aqueous solutions of the alkaline species were relatively stable. Values of  $\lambda_{\max}$  for these solutions were  $530 \pm 1$  nm in all cases. Aquation of the alkaline species ( $t_{1/2} \approx 10$  days) occurred with no discernible shifts in  $\lambda_{\max}$  of the solutions.

Thus, the simultaneous disappearance of the peak in the region of 474-485 nm and appearance of the peak in the region of 530 nm as observed in the ultraviolet/visible repeat scan spectra of the acidic species in aqueous solutions and in methanolic solutions is consistent with the conversion of the acidic species into the alkaline species. As both the acidic and alkaline species are tris-(bidentate) complexes,<sup>26-30</sup> then the observed conversion could be that of one diastereoisomeric form of the complex into the other. From  $^1\text{H}$  nmr spectra (Chapter 6), samples of the acidic species of this complex,  $[\text{Fe}(\text{bsb},\text{Me},\text{OH})_3]^{2+}$ , like samples of the related complexes  $[\text{Fe}(\text{bsb},\text{R},\text{R}')_3]^{2+}$  where R = H, Me or Ph and R' = uncharged alkyl or aryl group, were indicated to contain predominantly the mer diastereoisomeric forms of the complexes. For the latter type of complexes (R' = alkyl or aryl group), the fac isomers in solutions of the complexes in water and in aqueous methanol mixtures decreased even further with time (Chapters 5 and 6). In some cases, such a change was accompanied by shifts in  $\lambda_{\max}$  of the solutions towards shorter wavelengths of up to 10 nm. These shifts occurred over a period of days. In other cases, no shifts in  $\lambda_{\max}$  were observed. By comparison,  $\lambda_{\max}$  for aqueous solutions of the acidic species of the ketoxime complex,  $[\text{Fe}(\text{bsb},\text{Me},\text{OH})_3]^{2+}$ ,

shifted approximately 50 nm towards longer wavelengths in a matter of hours. Thus, the direction of the shift in values of  $\lambda_{\max}$  for aqueous solutions of the acidic complex species, if not the magnitude of this shift, would be consistent with a mer to fac isomeric conversion. The magnitude of this shift may be connected with the nature of  $R'$  in this complex, i.e. hydroxyl groups. In the fac isomeric arrangement of the complex [see (XIII)], the hydrophilic OH groups all lie in the same face of the octahedron. The relatively close proximity of these groups to each other in this arrangement, compared with that in the mer isomeric arrangement [see (XIV)], may result in enhanced hydrogen bonding interactions, intramolecular and/or solute-solvent, for the former isomeric form. The differing degrees of such interactions for the two isomeric forms of this complex could result in a relatively large difference in



$\lambda_{\max}$  for the two isomeric forms of the complex in aqueous solutions. By the same token, the seemingly anomalous behaviour of this complex in which  $R' = \text{OH}$  (mer to fac conversion in aqueous solutions) compared with related complexes in which  $R' = \text{alkyl}$  or aryl group (fac to mer conversion) may be rationalized. Confirmation of a fac to mer isomeric conversion occurring for the complex derived from iron(II) and methyl-2-pyridyl ketoxime was sought from  $^1\text{H}$  nmr spectra obtained for the acidic and alkaline species of the complex.

The  $^1\text{H}$  nmr spectra obtained for samples of the acidic and alkaline species, measured at 300 MHz in  $d_6$ -acetone and in  $d_4$ -methanol respectively,

are shown in Fig. 7.12. Unfortunately, due to solubility difficulties, no satisfactory spectrum of the alkaline species in  $d_6$ -acetone could be obtained. As no satisfactory spectra of the acidic species could be obtained in  $d_4$ -methanol, a direct comparison of the  $^1H$  nmr spectra of the two samples in the same solvent could not be made. In Fig. 7.12(a), the pattern of four signals in the higher field region due to the resonance of the methyl protons in the complex, three signals of equal intensity and a fourth less intense, is indicative of diastereoisomeric forms in the sample (cf. methyl proton resonance patterns in nmr spectra obtained for tris-(bidentate) complexes shown in Chapter 6). The sample of the acidic species contains predominantly the mer isomeric form of the complex, 21% of the sample is in the fac isomeric form. From the low field region of the two spectra shown in Fig. 7.12, it is obvious that the chemical shifts of the aromatic protons in the complex are significantly different in the two solvents. Despite this, there does appear to be a reduction in the number of signals in the spectrum of the sample precipitated from alkaline solutions shown in Fig. 7.12(b). In the higher field region of this latter spectrum, there is one relatively intense signal, at 2.28 ppm, which may correspond to the resonance of the methyl protons in the fac isomeric form of the complex. The three smaller signals at 1.92, 2.33 and 2.68 ppm may be due to the methyl protons in the mer isomeric form of the complex. As can be seen, the relative chemical shifts of these four signals in  $d_4$ -methanol are significantly different from those observed for the methyl protons of the complex in  $d_6$ -acetone.

A similar pattern of behaviour was observed for the related complex  $[Fe(bsb,Ph,OH)_3]^{2+}$ . This complex contains the bidentate ligand phenyl-2-pyridyl ketoxime derived from 2-benzoyl pyridine and hydroxylamine

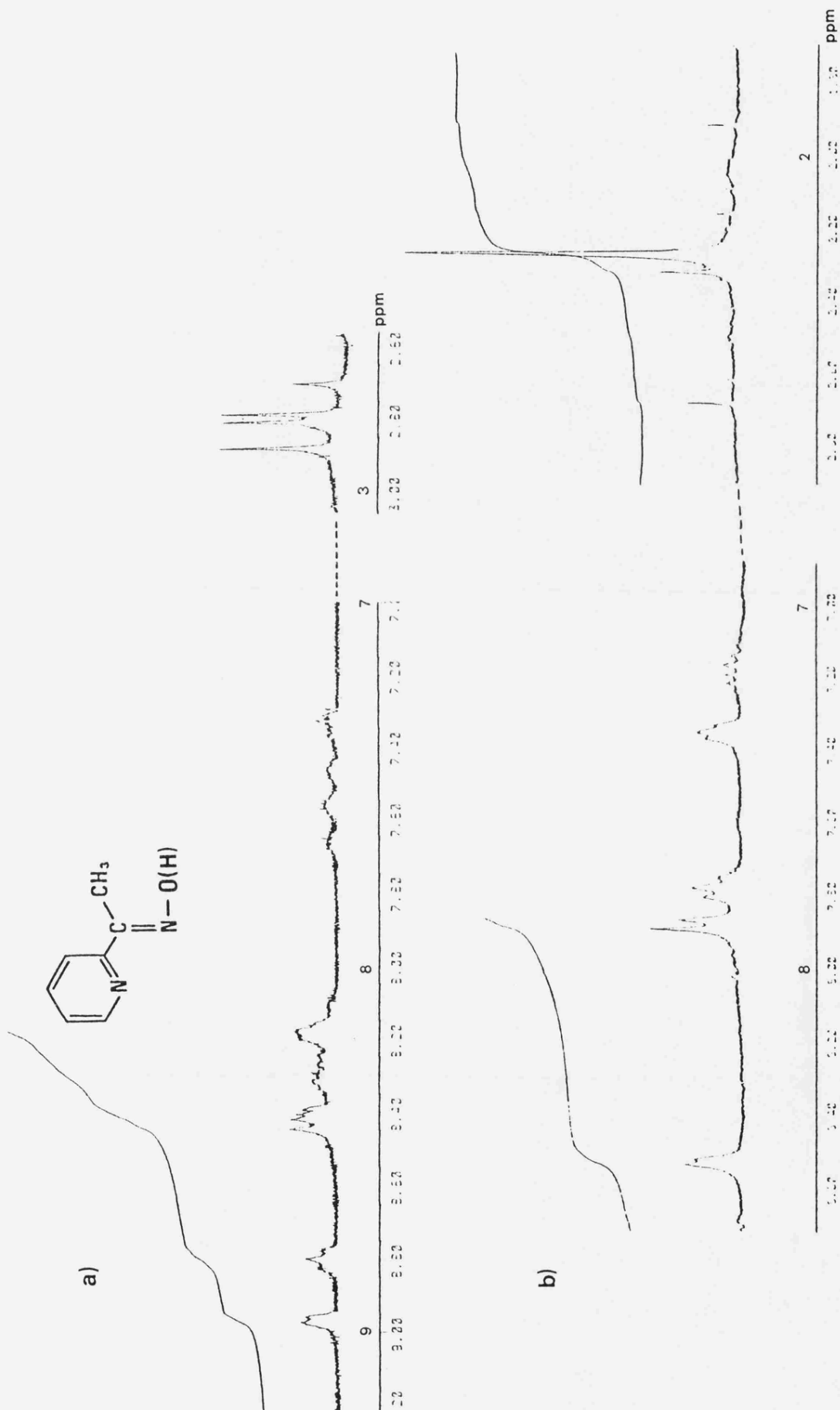


**FIGURE 7.12**

$^1\text{H}$  nmr spectra of samples of  $[\text{Fe}(\text{bsb},\text{Me},\text{OH})_3]^{2+}$  measured under acidic conditions, spectrum measured in  $d_6$ -acetone; b) sample made under alkaline conditions, spectrum measured in  $d_4$ -methanol.

hydrochloride. For the complex species prepared under acidic conditions,  $\lambda_{\max}$  in 5 vol % MeOH was 508 nm. The value of  $\lambda_{\max}$  shifted from 508 to 556 nm in approximately 30 minutes. However, at no time did the absorbance at 556 nm exceed the initial absorbance at 508 nm (cf. Fig. 7.11). For complex species prepared under alkaline conditions,  $\lambda_{\max}$  in water was 557 nm. The low field regions, 7.3 to 9.0 ppm, of the  $^1\text{H}$  nmr spectra obtained for both the samples, one prepared under acidic conditions, the other under alkaline conditions, measured in  $\text{d}_3$ -acetonitrile at 300 MHz are shown in Fig. 7.13. The resonances in these spectra are due to the pyridyl and phenyl protons in the ligands of the complex and, possibly, to hydroxyl protons. Despite the very poor resolution in the spectrum of the sample prepared under acidic conditions, there do appear to be differences in the two spectra. In the regions of 7.85 and 8.05 ppm there certainly appear to be additional signals in the spectrum of the sample prepared under acidic conditions as compared with that of the sample prepared under alkaline conditions. In the former spectrum there is also relatively more signal intensity in the region of 7.70 ppm. Such differences in the spectra would be more consistent with the sample prepared under acidic conditions containing predominantly the mer isomer and the sample prepared under alkaline conditions containing predominantly the fac isomer than vice versa.

Thus, the available evidence for the two complexes  $[\text{Fe}(\text{bsb},\text{Me},\text{OH})_3]^{2+}$  and  $[\text{Fe}(\text{bsb},\text{Ph},\text{OH})_3]^{2+}$  containing the ligands methyl-2-pyridyl ketoxime and phenyl-2-pyridyl ketoxime respectively suggests that it is the mer isomeric form which is formed predominantly in acidic aqueous solutions and the fac isomeric form which is formed predominantly in aqueous solutions made alkaline with hydroxide. In aqueous solutions, acidic or alkaline, and in methanolic solutions, conversion of the mer to the fac

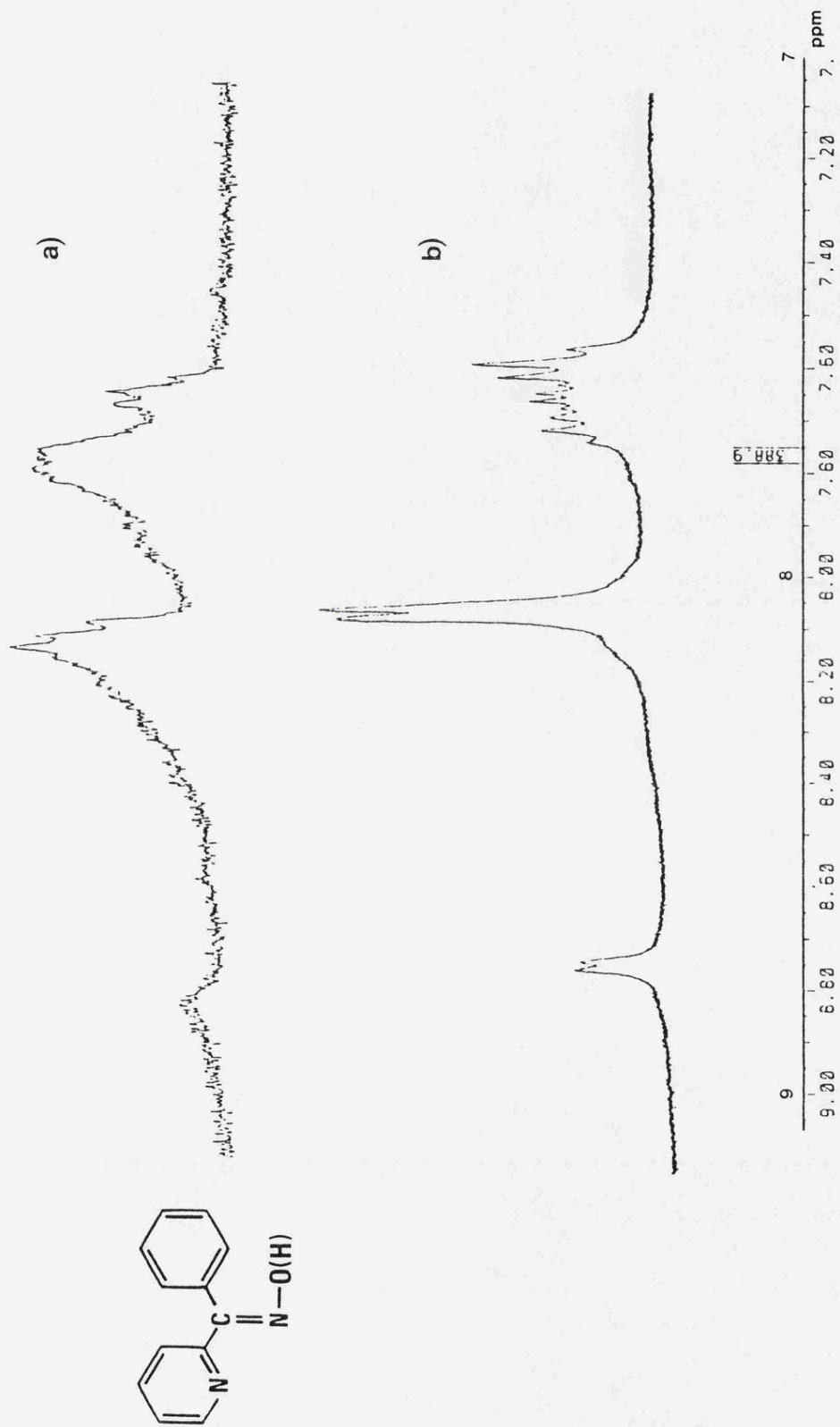


**FIGURE 7.13**  
<sup>1</sup>H nmr spectra of samples of [Fe(bsb,Ph,OH)<sub>3</sub>]<sup>2+</sup> made under a) acidic conditions and b) alkaline conditions, measured in d<sub>3</sub>-acetonitrile at 300 MHz.

isomer occurs. If this is indeed the case, then it is possible that, with further work, this system could provide a means of obtaining essentially pure samples of each diastereoisomeric form. This would obviously facilitate further study concerning such isomeric species. Perhaps, even, crystals of both the fac and mer isomeric form of a complex of this type could be obtained. Then it would be possible, as suggested at the end of Section 7.3, to study the effect of the different stereochemical arrangements in the diastereoisomers on parameters such as bond lengths, bond angles, etc.

#### 7.4.3.2 Complex species formed in water + amine mixtures

The ultraviolet/visible absorption spectra of the four solid samples initially obtained from each type of preparative solution, iron(II) combined with either 2-benzoyl pyridine or phenyl-2-pyridyl ketoxime in aqueous triethylenetetramine and iron(II) combined with either 2-benzoyl pyridine or phenyl-2-pyridyl ketoxime in aqueous ethylenediamine, in water are shown in Fig. 7.14. In this section, these complex species are referred to as (Fe,ketone, trien), (Fe,oxime, trien), (Fe,ketone, en) and (Fe,oxime, en) respectively. For aqueous solutions of (Fe,ketone, trien) and (Fe,oxime, trien),  $\lambda_{\max} = 615$  nm. For aqueous solutions of (Fe,ketone, en) and (Fe,oxime, en),  $\lambda_{\max} = 613$  nm. Values of  $\lambda_{\max}$  for (Fe,oxime, trien) and (Fe,oxime, en) in 15:2 isoamyl alcohol : water mixtures, 629 and 628 nm respectively, do not compare favourably with that reported in the literature, 588 nm, for complex species generated using the same reactants under analogous conditions.<sup>28</sup>

The  $^1\text{H}$  nmr spectra of (Fe,ketone, trien) and (Fe,oxime, trien) were measured in  $\text{d}_3$ -acetonitrile at 300 MHz. Both these spectra were identical to that obtained for the mono-(hexadentate) iron(II) Schiff base di-imine complex,  $[\text{Fe}(\text{hsb}, \text{Ph}, \text{trien})]^{2+}$ , shown in Fig. 6.15 in Chapter 6. This

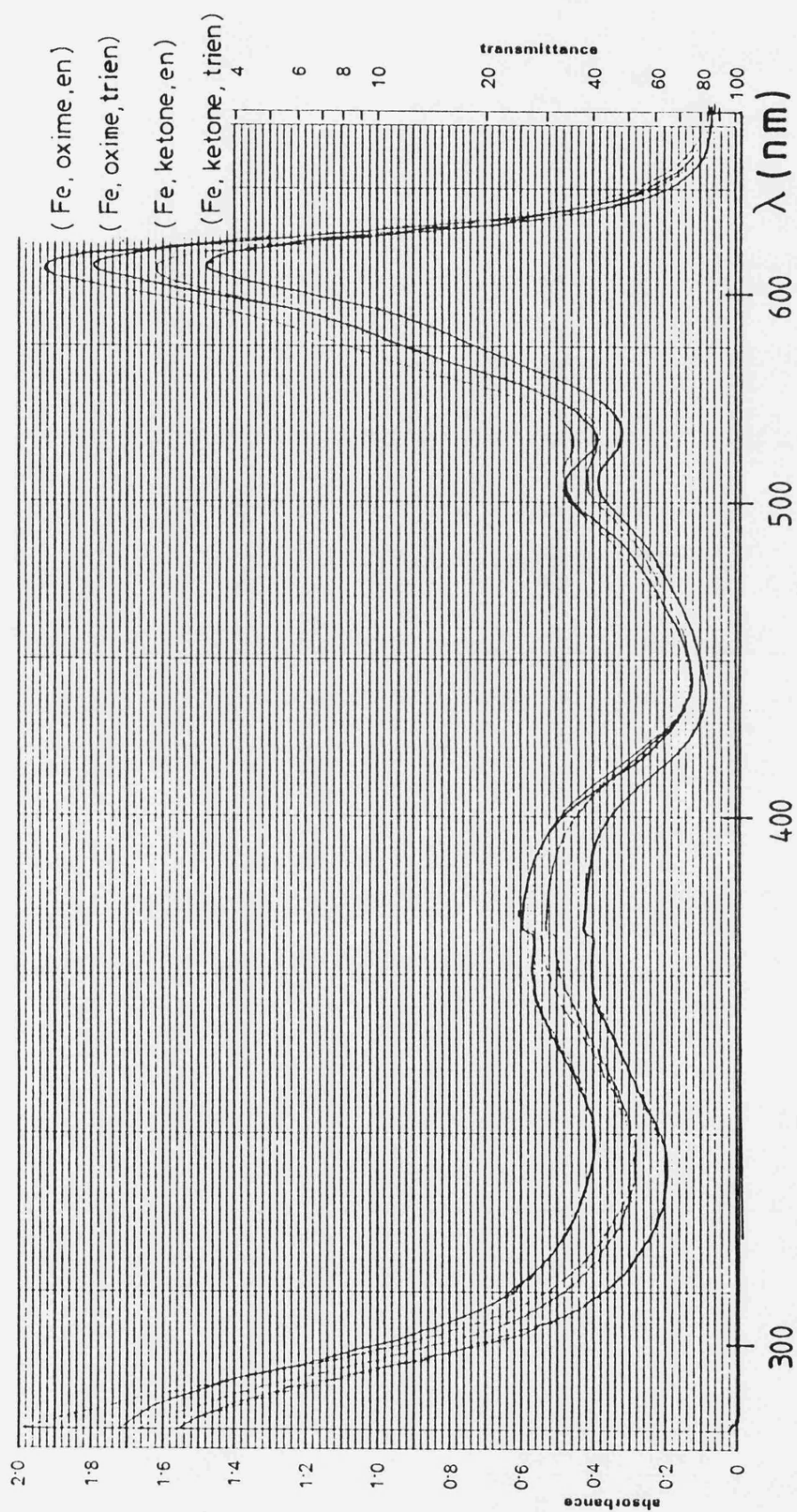


FIGURE 7.14

Ultraviolet/visible absorption spectra of complex species formed when iron(II) was combined with either phenyl-2-pyridyl ketoxime (oxime) or 2-benzoyl pyridine (ketone) in either aqueous ethylenediamine (en) or aqueous triethylenetetramine (trien) mixtures.

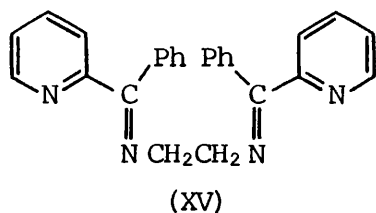
complex contains the ligand derived from 2-benzoyl pyridine and triethylenetetramine shown in (XII). Thus, it appears that in aqueous triethylenetetramine mixtures, phenyl-2-pyridyl ketoxime was hydrolysed forming 2-benzoyl pyridine and hydroxylamine hydrochloride (from which it was originally synthesised) with the result that the complex  $[\text{Fe}(\text{hsb}, \text{Ph}, \text{trien})]^{2+}$  was formed when either 2-benzoyl pyridine or phenyl-2-pyridyl ketoxime were combined with iron(II) in aqueous triethylenetetramine mixtures. Related hydrolysis reactions for other Schiff base ligands in alkaline solutions have been observed.<sup>31</sup> In the spectrum obtained for (Fe,oxime, trien), no evidence for the presence of a species of the type  $\text{Fe}(\text{oxime})_3$  [cf. analogous preparation in aqueous solution made alkaline by the addition of hydroxide discussed in Section 7.4.3.1] was seen.

The  $^1\text{H}$  nmr spectra of (Fe, ketone, en) and (Fe, oxime, en) measured in  $\text{d}_3$ -acetonitrile at 300 MHz are shown in Fig. 7.15(a) and (b) respectively. By analogy with the observations made concerning the complex species formed in aqueous triethylenetetramine mixtures, the two species (Fe, ketone, en) and (Fe, oxime, en) should be identical. The spectra shown in Fig. 7.15 indicate this to be the case. Thus, the species (Fe, ketone, en) and (Fe, oxime, en) are likely to contain the quadridentate Schiff base ligand formed by combination of 2-benzoyl pyridine and ethylenediamine shown in (XV). The ratio of the intensities of the signals in the low field region of 7.0 to 8.3 ppm and those in the region of 4.8 ppm is 18:4. This is the ratio of pyridyl protons to methylene protons in the ligand shown in (XV) [cf. signals due to the corresponding methylene protons in the related hexadentate ligand, (XII), occurring in the region of 4.7 ppm as shown in Fig. 6.15 in Chapter 6]. In both of the spectra shown in Fig. 7.15, however, there are a considerable number of signals

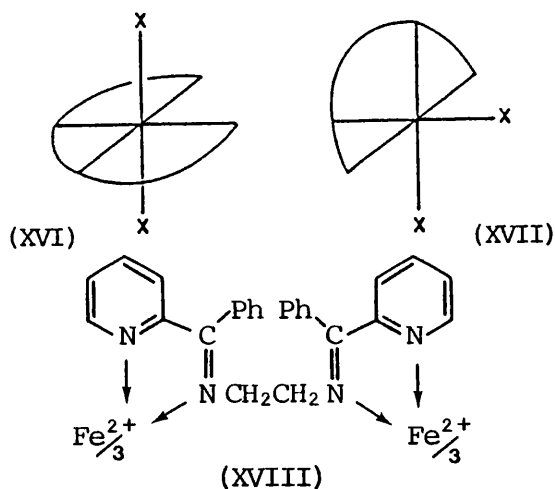


FIGURE 7.15

<sup>1</sup>H nmr spectra of samples ( $\lambda_{\max} = 613$  nm in water) obtained when iron(II) was combined in aqueous ethylenediamine mixtures with a) 2-benzoyl pyridine and b) phenyl-2-pyridyl ketoxime, measured in  $d_3$ -acetonitrile at 90 MHz.



in the high field regions. Whether these are due to ethylenediamine in other complex species, uncomplexed ethylenediamine or other impurities is not clear. Re-crystallization of the samples from water + methanol mixtures did not remove these signals but served only to reduce the quality of the spectra. Several complex species containing the ligand shown in (XV) are feasible. These include those shown in (XVI) and (XVII) where X is a monodentate entity such as water, and also binuclear iron(II) complex species in which three quadridentate ligands are arranged around



two iron atoms. In this latter complex species, each quadridentate ligand is envisaged as forming two bonds with one iron atom and two with the other, as shown in (XVIII).

The  $^1\text{H}$  nmr spectrum obtained for the sample for which  $\lambda_{\text{max}}$  in aqueous solution was 587 nm is shown in Fig. 7.16. This is the sample obtained from the residual preparative solution in which iron(II) had been combined with phenyl-2-pyridyl ketoxime in aqueous ethylenediamine mixtures,  $\lambda_{\text{max}} = 587$  nm, after the solid for which  $\lambda_{\text{max}} = 613$  nm had been precipitated.

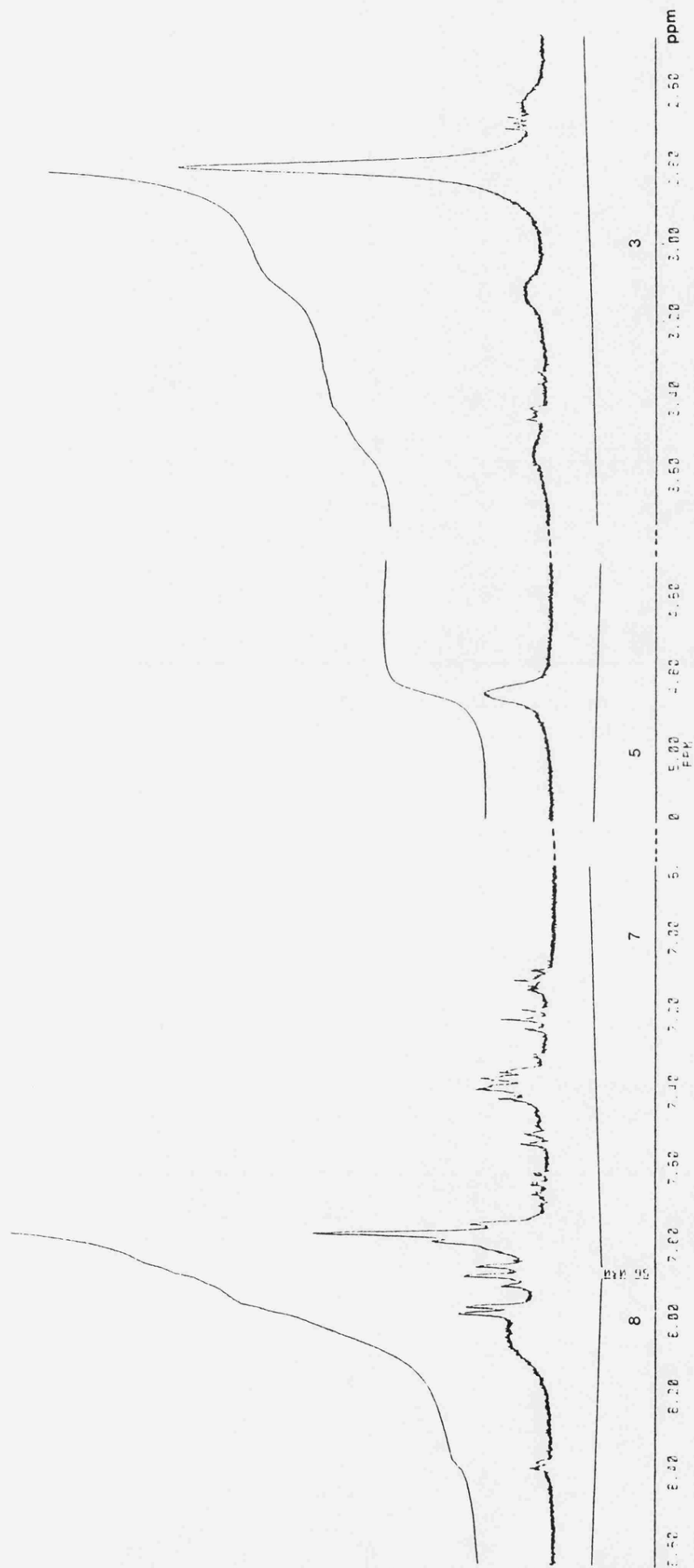


**FIGURE 7.16**

<sup>1</sup>H nmr spectrum of a sample ( $\lambda_{\text{max}} = 587 \text{ nm}$  in water) obtained when iron(II) was combined with phenyl-2-pyridyl ketoxime in aqueous ethylenediamine mixtures, measured in  $\text{d}_3$ -acetonitrile at 300 MHz.

From the spectrum of this former sample, it was clear that the complex species was neither that containing the quadridentate ligand (XV) nor the complex  $[\text{Fe}(\text{bsb}, \text{Ph}, \text{OH})_3]^{2+}$ . The latter complex is that formed when iron(II) and phenyl-2-pyridyl ketoxime are combined in acidic and alkaline (hydroxide) aqueous media. The ratio of the integration of the signals in the region of 7.0 to 8.5 ppm and of the broad signal at 4.85 ppm is 18:2.

It is clear that the products formed when iron(II) reacts with Schiff base ketoxime ligands such as methyl-2-pyridyl ketoxime and phenyl-2-pyridyl ketoxime are dependent to no small degree on the conditions employed. This is particularly true of systems in which other species which can react with the ketoxime ligands, such as primary amines, are present. In these cases, further characterization of the complex species formed could perhaps be achieved by observing the effects of combining differing relative quantities of reactants. For example, the effects of adding different stoichiometric quantities of a primary amine to a solution containing a known quantity of a tris-(bidentate) iron(II) ketoxime complex, such that the ratio of metal to amine in the solution is 1:1, 1:2 or 1:3, etc., could be examined. It should be remembered that the unsymmetrical nature of the Schiff base ketoxime ligands means that not only is the formation of complex species containing different ligands possible, but also that such species may, in some cases, exist in more than one diastereoisomeric form.

## REFERENCES FOR CHAPTER 7

1. J. Burgess and M. V. Twigg, J. Chem. Soc., Dalton Trans., 1974, 2032.
2. J. Burgess and R. H. Prince, J. Chem. Soc., 1965, 6061.
3. M. J. Blandamer, J. Burgess, B. Clark, P. P. Duce, A. W. Hakin, N. Gosal, S. Radulovic, P. Guardado, F. Sanchez, C. D. Hubbard and E. A. Abu-Gharib, J. Chem. Soc., Faraday Trans. I, 1986, **82**, 1471.
4. E. A. Abu-Gharib, M. J. Blandamer, J. Burgess, N. Gosal, P. Guardado, F. Sanchez and C. D. Hubbard, Trans. Met. Chem., 1984, **9**, 306.
5. F. Basolo, J. C. Hayes and H. M. Neumann, J. Am. Chem. Soc., 1954, **76**, 3807.
6. E. R. Gardner, F. M. Mekhail and J. Burgess, Int. J. Chem. Kinetics, 1974, **6**, 133.
7. J. Burgess and R. H. Prince, J. Chem. Soc. (A), 1967, 434.
8. J. Burgess, J. Chem. Soc. (A), 1967, 955.
9. J. Burgess, J. Chem. Soc. (A), 1968, 497.
10. M. J. Blandamer, J. Burgess, R. I. Haines, F. M. Mekhail and P. Askalani, J. Chem. Soc., Dalton Trans., 1978, 1001.
11. C. D. Hubbard, personal communication.
12. G. A. Zakrzewski, C. Ghilardi and E. C. Lingafelter, J. Am. Chem. Soc., 1971, **93**, 4411.
13. M. J. Blandamer, J. Burgess, J. Fawcett, S. Radulovic and D. R. Russell, Trans. Met. Chem., in press.
14. L. Christiansen, D. N. Hendrickson, H. Toftlund, S. R. Wilson and C. L. Xie, Inorg. Chem., 1986, **25**, 2813.
15. L. Johansson, M. Molund and A. Oskarsson, Inorg. Chim. Acta, 1978, **31**, 117.
16. A. Zalkin, D. H. Templeton and T. Ueki, Inorg. Chem., 1973, **12**, 1641.
17. P. C. Healy, B. W. Skelton and A. H. White, Aust. J. Chem., 1983, **36**, 2057.
18. M. E. Garcia Posse, M. A. Juri, P. J. Aymonino, O. E. Piro, H. A. Negri and E. E. Castellano, Inorg. Chem., 1984, **23**, 948.
19. P. Guardado, personal communication.
20. A. J. Duffield, Ph.D. Thesis, Leicester, 1980.
21. B. N. Figgis, E. S. Kucharski and A. H. White, Aust. J. Chem., 1983, **36**, 1537.
22. B. N. Figgis, E. S. Kucharski and A. H. White, Aust. J. Chem., 1983, **36**, 1563.
23. B. N. Figgis, E. S. Kucharski and A. H. White, Aust. J. Chem., 1983, **36**, 1527.

REFERENCES (Continued) ....

24. W. A. Wickramasinghe, P. H. Bird and N. Serpone, Inorg. Chem., 1982, 21, 2694.
25. "CRC Handbook of Chemistry and Physics", 62nd. edn., ed. R. C. Weast, CRC Press, Boca Raton, Florida, 1981/1982.
26. D. K. Banerjea and K. K. Tripathi, Anal. Chem., 1960, 32, 1196.
27. F. Trusell and H. Diehl, Anal. Chem., 1959, 31, 1978.
28. R. Chernin and E. R. Simonsen, Anal. Chem., 1964, 36, 1093.
29. G. I. H. Hanania and D. H. Irvine, J. Chem. Soc., 1962, 2745.
30. K. Burger, I. Egyed and I. Ruff, J. Inorg. Nucl. Chem., 1966, 28, 139.
31. M. D. Luque de Castro, M. Silva and M. Valcárcel, Analyst, 1984, 109, 1375.



# APPENDIX A

**Tables of transfer chemical potentials  
for ions in water + ethanol mixtures**

## A1 INTRODUCTION

The following tables show transfer chemical potentials for ions in water + ethanol mixtures at 298.2 K derived using the TATB assumption in Chapter 3. All the values are given on the molar solute composition scale. An asterisk (\*) indicates ions for which the reported values are considered to be of lesser accuracy. This may be due to solubility or temperature considerations or to the route by which the values were derived (see Sections 3.2.5 and 3.3.2).

TABLE A1

Transfer chemical potentials for  $\text{Ph}_4\text{AsPic}$ ,  $\text{KBPh}_4$ , and  $\text{KPic}$  in water + ethanol mixtures

wt % ethanol	$\delta_{\text{m}}\mu^{\ominus}$ (kJ mol <sup>-1</sup> )		
	$\text{Ph}_4\text{AsPic}$	$\text{KBPh}_4$	$\text{KPic}$
10	- 2.5	- 1.1	1.3
20	- 6.6	- 3.3	1.7
30	-11.8	- 6.6	1.4
40	-16.5	-10.4	0.9
50	-19.6	-13.2	0.5
60	-21.5	-13.8	1.9
70	-22.6	-13.4	3.9
80	-22.7	-11.4	7.0
90	-22.1	- 7.8	11.0
100	-21.1	- 4.3	16.4

TABLE A2

Transfer chemical potentials for  $\text{BPh}_4^-$ ,  $\text{Ph}_4\text{As}^+$ ,  $\text{K}^+$  and  $\text{Pic}^-$  in water + ethanol mixtures

wt % ethanol	$\delta_{\text{m}}\mu^{\ominus}$ (kJ mol <sup>-1</sup> )		
	$\text{BPh}_4^- = \text{Ph}_4\text{As}^+$	$\text{K}^+$	$\text{Pic}^-$
10	- 2.5	1.3	0
20	- 5.8	2.5	-0.8
30	- 9.9	3.3	-1.9
40	-13.9	3.5	-2.6
50	-16.6	3.5	-3.0
60	-18.6	4.8	-2.9
70	-19.9	6.5	-2.7
80	-20.5	9.2	-2.2
90	-20.4	12.6	-1.7
100	-20.9	16.6	-0.2

TABLE A3

Transfer chemical potentials for simple anions in water + ethanol mixtures

wt % ethanol	$\delta_m^\ominus$ (kJ mol <sup>-1</sup> )									
	Cl <sup>-</sup>	Br <sup>-</sup>	I <sup>-</sup>	ClO <sub>4</sub> <sup>-</sup>	*NO <sub>3</sub> <sup>-</sup>	*CN <sup>-</sup>	IO <sub>3</sub> <sup>-</sup>	*ClO <sub>3</sub> <sup>-</sup>	*SO <sub>4</sub> <sup>2-</sup>	
10	0.3			0.2	0.9	-0.4	2.6	2.0	4.7	
20	1.1			0.2	2.1	-0.8	5.3	3.8	8.3	
30	2.5	1.5	-0.1	0.6	3.5	-0.7	7.8	5.6	14.3	
40	4.8	6.2	3.7	1.5	5.3	0.5		7.3	20.9	
50	7.5			2.7	7.0	1.4		9.2		
60	9.3	7.7	5.5	3.2	8.9	2.0		11.8		
70	11.1			3.8		2.4		15.0		
80	12.3			4.7		3.7		19.2		
90	15.3	16.4	11.4	6.5				26.2		
100	19.5			9.9						

TABLE A4

Transfer chemical potentials for organic ions in water + ethanol mixtures

wt % ethanol	Ph <sub>4</sub> P <sup>+</sup>	TAB <sup>+</sup>	*OAc <sup>-</sup>	H tart <sup>-</sup>	Sb tart <sup>-</sup>	*ox <sup>2-</sup>	*cit <sup>3-</sup>	N2S <sup>-</sup>	*A2S <sup>-</sup>
10	- 2.5	- 1.0	-1.3	1.7	2.3	0.7	1.0	-0.9	0.1
20	- 5.4	- 2.0	-2.3	3.2	4.8	1.9	2.1	-2.9	-0.6
30	- 9.6	- 4.7	-3.1	4.9	8.3	4.7	4.4	-5.7	-1.4
40	-13.7	- 8.5	-2.9	6.8	12.1		9.9	-6.9	-2.5
50	-16.3	-12.8	-2.5	8.5	14.7		18.5	-6.6	-3.6
60	-18.3	-14.7	-3.3	9.3	16.8		27.5	-7.1	-3.2
70	-19.6	-16.8	-4.3	8.2	18.6		36.4	-7.3	-1.8
80	-20.1	-18.6	-5.9				51.6	-6.5	2.2
90	-19.7	-19.8	-7.4	5.3				-1.7	10.2
100	-18.9	-21.3	-6.2					8.0	21.0

TABLE A5

Transfer chemical potentials for oxoanions in  
water + ethanol mixtures

wt % ethanol	$\delta_m \mu^\ominus$ (kJ mol <sup>-1</sup> )	
	*S <sub>2</sub> O <sub>3</sub> <sup>2-</sup>	*S <sub>2</sub> O <sub>6</sub> <sup>2-</sup>
10	3.0	2.8
20	4.5	4.5
30	7.5	8.0
40	11.2	13.0
50	12.4	18.2
60	11.2	22.7
70		24.6
80		21.7

TABLE A7

Transfer chemical potentials for divalent cations  
in water + ethanol mixtures

wt % ethanol	$\delta_m \mu^\ominus$ (kJ mol <sup>-1</sup> )				
	*Ca <sup>2+</sup>	*Ba <sup>2+</sup>	Hg <sup>2+</sup>	Pb <sup>2+</sup>	*Zn <sup>2+</sup>
10	0.7	2.1	4.6	2.6	3.8
20	1.9	5.2	10.1	4.9	7.1
30	4.7	7.2	15.4	7.0	10.0
40		7.5	20.6	8.1	11.3
50		8.2		9.6	12.4
60		10.1		11.8	16.3
70		13.0		14.9	20.9
80		18.1		18.9	
90		25.8			
100					

TABLE A6

Transfer chemical potentials for univalent cations in water + ethanol mixtures

wt % ethanol	$\delta_{m\mu}^{\ominus}$ (kJ mol <sup>-1</sup> )										
	H <sup>+</sup>	*Li <sup>+</sup>	Na <sup>+</sup>	K <sup>+</sup>	Rb <sup>+</sup>	Cs <sup>+</sup>	Me <sub>4</sub> N <sup>+</sup>	n-Pr <sub>4</sub> N <sup>+</sup>	n-Bu <sub>4</sub> N <sup>+</sup>	Ag <sup>+</sup>	Tl <sup>+</sup>
10	0.5	0.7	1.5	1.3	1.1	0.7	0	-1.0	-1.6	1.2	0.3
20	0.5	1.6	3.1	2.5	2.3	1.7	0.2	-2.0	-3.1	1.6	0.8
30	-0.2	2.4	4.1	3.3	3.2	2.5	0.3	-3.4	-5.3	1.5	1.0
40	-1.8	2.6	4.0	3.5	3.4	2.4	0	-5.6	-9.1		
50	-3.5	2.0	4.7	3.5	3.3	2.3	-0.4	-7.8	-13.9		
60	-4.2	1.6		4.8	4.6	3.8	0.8	-8.9			
70	-4.0	3.1		6.5	6.2	5.9	2.3	-9.4			
80	-2.5	0.43		9.2	8.6	9.5	4.7	-8.2			
90	-1.7			12.6	11.2	13.3	8.5	-7.7			
100	11.0			16.6	13.0	16.2	12.0	-11.6			

TABLE A8

Transfer chemical potentials for halogenoanions in  
water + ethanol mixtures

wt % ethanol	$\delta_m \mu^\ominus$ (kJ mol <sup>-1</sup> )	
	*SiF <sub>6</sub> <sup>2-</sup>	*PtCl <sub>6</sub> <sup>2-</sup>
8.7	2.8	3.7
15.9	6.9	5.5
27.3	10.8	7.8
42.4	14.4	14.7
58.5		19.6
94.7		16.6

wt % ethanol	$\delta_m \mu^\ominus$ (kJ mol <sup>-1</sup> )
	ReCl <sub>6</sub> <sup>2-</sup>
20	3.0
40	6.2
60	9.2

TABLE A9

Transfer chemical potentials for Fe(II) and Co(III) complexes in water + ethanol mixtures

wt % ethanol	Fe(bipy) <sub>3</sub> <sup>2+</sup>	Fe(phen) <sub>3</sub> <sup>2+</sup>	$\delta_{m\mu}^{\ominus}$ (kJ mol <sup>-1</sup> ) [Fe(bsb,Ph,Ph:m-OMe) <sub>3</sub> ] <sup>2+</sup>
10	- 2.1	- 3.5	
20	- 4.1	- 6.8	-10.6
30	- 7.1	-11.3	
40	-11.0	-17.6	-27.2
50	-14.3	-20.0	
60	-14.8	-19.4	-39.2
70	-14.6	-18.0	

wt % ethanol	$\delta_{m\mu}^{\ominus}$ (kJ mol <sup>-1</sup> ) [Co(en) <sub>2</sub> Cl <sub>2</sub> ] <sup>+</sup>	$\delta_{m\mu}^{\ominus}$ (kJ mol <sup>-1</sup> ) [Co(NH <sub>3</sub> ) <sub>5</sub> Cl] <sup>2+</sup>
6.1	0.2	1.6
15.9	0.7	3.6
22.7	1.1	4.4
33.2	0.9	4.2
40.5	0.1	3.0
51.9	-0.1	0.1
60.0	0.3	0.7
72.5	1.8	0.5

wt % ethanol	$\delta_{m\mu}^{\ominus}$ (kJ mol <sup>-1</sup> ) *[CoNH <sub>3</sub> Br(en) <sub>2</sub> ] <sup>2+</sup>	wt % ethanol	$\delta_{m\mu}^{\ominus}$ (kJ mol <sup>-1</sup> ) *[Co(NO <sub>2</sub> ) <sub>6</sub> ] <sup>3-</sup>
11.0	1.0	8.7	5.1
21.8	3.6	15.9	7.1
32.3	4.6	27.3	8.1
42.5	2.2	42.4	7.8



# APPENDIX B

**Tables of transfer chemical potentials for  
ions in water + ethylene glycol and in  
water + glycerol mixtures**

## B1 INTRODUCTION

The following tables show transfer chemical potentials for ions in water + ethylene glycol mixtures (tables B1-B4) and in water + glycerol mixtures (tables B5-B8) derived using the TATB assumption in Chapter 4. All the values are given on the molar solute composition scale and are derived from measurements made at 298.2 K. An asterisk (\*) indicates that due to solubility considerations the reported values for the ion are considered to be of lesser accuracy.

TABLE B1

Transfer chemical potentials for  $\text{Ph}_4\text{AsPic}$ ,  $\text{KPh}_4$ , and  $\text{KPic}$  in water + ethylene glycol mixtures

wt % ethylene glycol	$\delta_m \mu^\ominus$ (kJ mol <sup>-1</sup> )		
	$\text{Ph}_4\text{AsPic}$	$\text{KPh}_4$	$\text{KPic}$
10	- 1.0	- 1.6	0.3
20	- 2.4	- 2.7	0.4
30	- 4.2	- 4.3	0.5
40	- 6.4	- 5.6	0.4
50	- 9.4	- 6.7	0.2
60	-11.5	- 8.5	-0.1
70	-13.9	-10.2	-0.5
80	-17.0	-12.7	-1.1
90	-20.4	-15.6	-1.8
100	-22.3	-17.7	-3.3

TABLE B2

Transfer chemical potentials for  $\text{BPh}_4^-$ ,  $\text{Ph}_4\text{As}^+$ ,  $\text{K}^+$  and  $\text{Pic}^-$  in water + ethylene glycol mixtures

wt % ethylene glycol	$\delta_m \mu^\ominus$ (kJ mol <sup>-1</sup> )		
	$\text{BPh}_4^- = \text{Ph}_4\text{As}^+$	$\text{K}^+$	$\text{Pic}^-$
10	- 1.4	-0.2	0.5
20	- 2.8	0.0	0.4
30	- 4.5	0.2	0.3
40	- 6.2	0.6	-0.2
50	- 8.1	1.5	-1.3
60	- 9.9	1.5	-1.6
70	-11.8	1.6	-2.1
80	-14.3	1.6	-2.7
90	-17.2	1.5	-3.3
100	-18.4	0.7	-4.0

TABLE B3

Transfer chemical potentials for anions in water + ethylene glycol mixtures

wt % ethylene glycol	$\delta_{\text{m}}^{\oplus}$ (kJ mol <sup>-1</sup> )									
	Cl <sup>-</sup>	Br <sup>-</sup>	I <sup>-</sup>	ClO <sub>4</sub> <sup>-</sup>	*CO <sub>3</sub> <sup>2-</sup>	Pic <sup>-</sup>	BPh <sub>4</sub> <sup>-</sup>	*SO <sub>4</sub> <sup>2-</sup>		
10				0.7	0.4	0.5	- 1.4	2.9		
20				1.4	1.0	0.4	- 2.8	4.7		
30	2.4	1.7	1.0	1.7	1.3	0.3	- 4.5	7.3		
40				1.5	1.0	-0.2	- 6.2	9.0		
50	3.0	2.0	0.8	1.0	0.6	-1.3	- 8.1	10.3		
60				1.8	1.0	-1.6	- 9.9			
70	5.4	3.9	1.9	1.8	1.9	-2.1	-11.8			
80					2.7	-2.7	-14.3			
90	7.9	5.9	2.5		3.6	-3.3	-17.2			
100	10.9	8.4	5.4		4.9	-4.0	-18.4			

TABLE B4

Transfer chemical potentials for cations in water + ethylene glycol mixtures

wt % ethylene glycol	$\delta_{m\mu}^{\ominus}$ (kJ mol <sup>-1</sup> )										
	H <sup>+</sup>	Li <sup>+</sup>	Na <sup>+</sup>	K <sup>+</sup>	Ph <sub>4</sub> As <sup>+</sup>	[Fe(gmi) <sub>3</sub> ] <sup>2+</sup>	[Fe(bsb,Ph,Ph:3,4-Me <sub>2</sub> ) <sub>3</sub> ] <sup>2+</sup>				
10				-0.2	-1.4	-1.1	1.6				
20				0.0	-2.8	-2.2	-4.6				
30	-0.7	0.2	0.0	0.2	-4.5	-2.4	-7.4				
40				0.6	-6.2	-1.3	-12.4				
50	-0.1	1.6	1.3	1.5	-8.1	0.4	-14.1				
60				1.5	-9.9	-0.8	-18.6				
70	-0.7	2.3	1.2	1.6	-11.8	0.7	-21.5				
80				1.6	-14.3						
90	1.6	3.4	1.3	1.5	-17.2						
100	7.7	2.7	0.7	0.7	-18.4						

TABLE B5

Transfer chemical potentials for  $\text{Ph}_4\text{AsPic}$ ,  $\text{KPh}_4$ , and  $\text{KPic}$  in water + glycerol mixtures

wt % glycerol	$\delta_{\text{m}}\mu^{\ominus} (\text{kJ mol}^{-1})$		
	$\text{Ph}_4\text{AsPic}$	$\text{KPh}_4$	$\text{KPic}$
10	-0.1	-1.5	0.1
20	-0.1	-2.2	0.2
30	-0.2	-3.0	0.3
40	-0.3	-3.9	0.4
50	-0.3	-4.9	0.6
60	-0.4	-6.2	0.7
70	-0.4	-7.4	0.8

TABLE B6

Transfer chemical potentials for  $\text{BPh}_4^-$ ,  $\text{Ph}_4\text{As}^+$ ,  $\text{K}^+$  and  $\text{Pic}^-$  in water + glycerol mixtures

wt % glycerol	$\delta_{\text{m}}\mu^{\ominus} (\text{kJ mol}^{-1})$		
	$\text{BPh}_4^- = \text{Ph}_4\text{As}^+$	$\text{K}^+$	$\text{Pic}^-$
10	-0.8	0.7	-0.7
20	-1.3	1.1	-1.0
30	-1.7	1.6	-1.3
40	-2.3	2.0	-1.6
50	-2.9	2.6	-2.0
60	-3.6	3.2	-2.6
70	-4.3	3.9	-3.1

TABLE B7  
 Transfer chemical potentials for anions in water + glycerol mixtures

wt % glycerol	$\delta_m \mu^\ominus$ (kJ mol <sup>-1</sup> )							
	Cl <sup>-</sup>	Br <sup>-</sup>	I <sup>-</sup>	ClO <sub>4</sub> <sup>-</sup>	Pic <sup>-</sup>	BPh <sub>4</sub> <sup>-</sup>	*SO <sub>4</sub> <sup>2-</sup>	
10	-0.3	-0.4	-0.7	0.7	-0.7	-0.8	0.3	
20	-0.3	-0.5	-0.9	0.8	-1.0	-1.3	1.3	
30	-0.2	-0.5	-1.1	1.0	-1.3	-1.7	2.4	
40	-0.1	-0.4	-1.5	1.0	-1.6	-2.3	3.4	
50	-0.1	-0.7	-2.1	0.8	-2.0	-2.9	4.6	
60	0.0		-2.5	1.2	-2.6	-3.6	5.8	
70	0.1	-0.8	-2.9		-3.1	-4.3	6.5	

TABLE B8

Transfer chemical potentials for cations in water + glycerol mixtures

wt % glycerol	$\delta_{m\mu}^{\ominus}$ (kJ mol <sup>-1</sup> )										
	H <sup>+</sup>	Li <sup>+</sup>	Na <sup>+</sup>	K <sup>+</sup>	Rb <sup>+</sup>	Cs <sup>+</sup>	*NH <sub>4</sub> <sup>+</sup>	Ph <sub>4</sub> As <sup>+</sup>	[Fe (bsb, Ph, Ph:3, 4-Me <sub>2</sub> ) <sub>3</sub> ] <sup>2+</sup>		
10	0.8	0.7	0.6	0.7	0.8	0.7	0.6	-0.8	1.7		
20	1.3			1.1			0.9	-1.3	1.3		
30	1.8	1.3	1.3	1.6	1.5	1.4	1.1	-1.7	0.6		
40	2.4			2.0			1.4	-2.3	0.1		
50	3.1	2.4	2.3	2.6	2.3	2.3	1.7	-2.9	0.4		
60	4.3			3.2			2.0	-3.6	-1.1		
70	5.6	4.5	4.0	3.9	3.8	3.5	2.5	-4.3			

# Structure and Solvation of Iron(II) Schiff Base Complexes and Other Ions

by

Diane Lesley Elvidge

## ABSTRACT

The structure and solvation of ions are studied from different aspects using various kinetic, spectroscopic and thermodynamic techniques. The solvation of a wide range of ions, both simple and complex, is investigated by calculation of sets of single-ion transfer chemical potentials for a series of binary aqueous solvent mixtures. Observed trends are discussed in terms of the effects on ion solvation of solute and solvent structure and solute-solvent interactions. Structure, solvation and also reactivity of some low-spin iron(II) di-imine complexes containing unsymmetrical Schiff base ligands are investigated using a variety of techniques. The occurrence of diastereoisomerism in complexes of this type is probed using complementary techniques which highlight different aspects of this phenomenon. Thus, the differing reactivities of, and the differing spatial orientations in, possible diastereoisomeric forms are utilized in detecting diastereoisomers by kinetic and  $^1\text{H}$  nmr spectroscopic methods respectively. In addition, for complexes of this type, links between structure, solvation and reactivity are investigated using kinetic data, solubility data, ultraviolet/visible absorption spectra and  $^1\text{H}$  nmr spectra obtained for the complex species.